INSIGHTS IN MICROBE AND VIRUS INTERACTIONS WITH PLANTS: 2021

EDITED BY: Marco Scortichini and Elvira Fiallo-Olivé
PUBLISHED IN: Frontiers in Microbiology

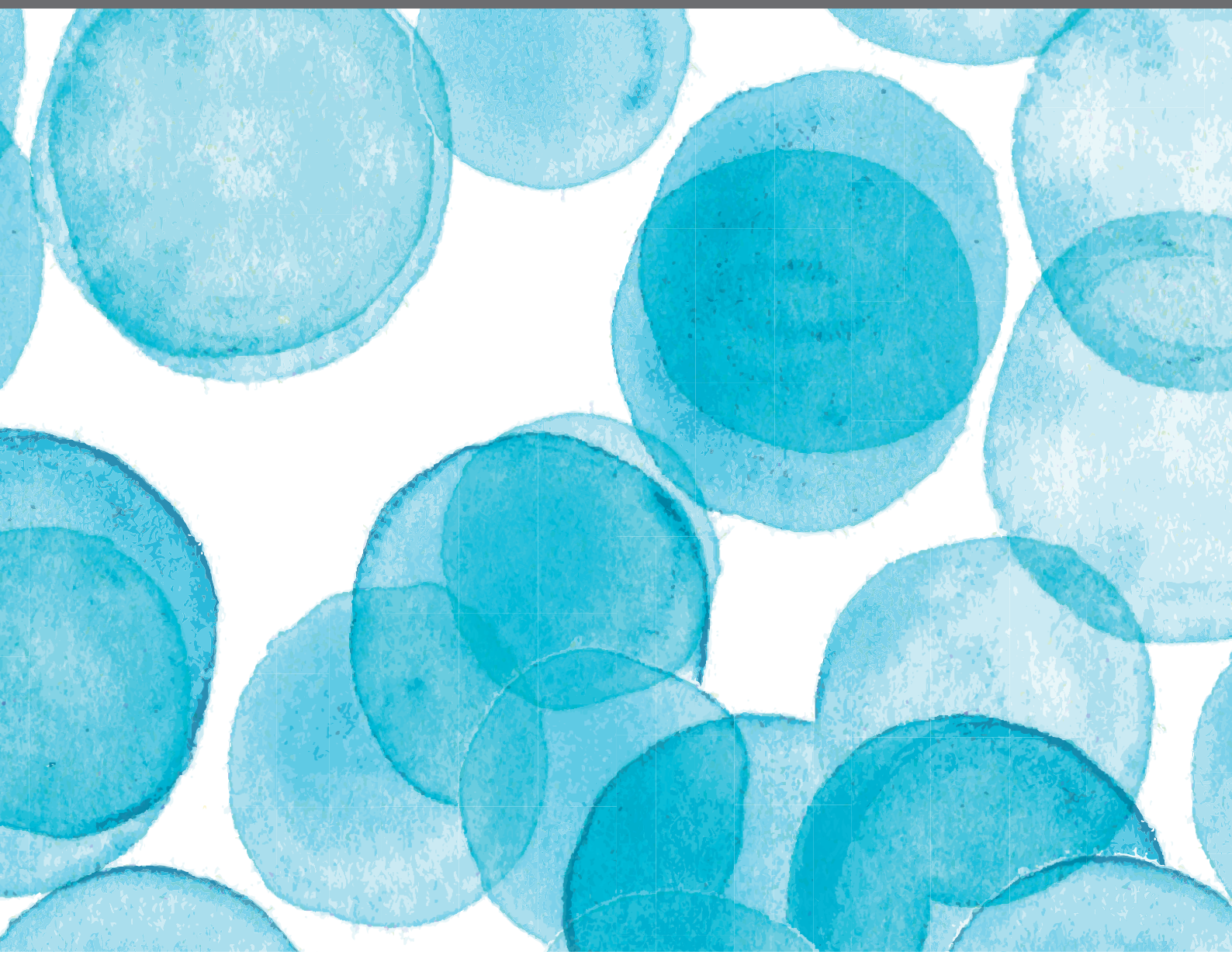

frontiers Research Topics

frontiers

ISSN 1664-8714
ISBN 978-2-88976-936-0
DOI 10.3389/978-2-88976-936-0

About Frontiers

Frontiers is more than just an open-access publisher of scholarly articles: it is a pioneering approach to the world of academia, radically improving the way scholarly research is managed. The grand vision of Frontiers is a world where all people have an equal opportunity to seek, share and generate knowledge. Frontiers provides immediate and permanent online open access to all its publications, but this alone is not enough to realize our grand goals.

Frontiers Journal Series

The Frontiers Journal Series is a multi-tier and interdisciplinary set of open-access, online journals, promising a paradigm shift from the current review, selection and dissemination processes in academic publishing. All Frontiers journals are driven by researchers for researchers; therefore, they constitute a service to the scholarly community. At the same time, the Frontiers Journal Series operates on a revolutionary invention, the tiered publishing system, initially addressing specific communities of scholars, and gradually climbing up to broader public understanding, thus serving the interests of the lay society, too.

Dedication to Quality

Each Frontiers article is a landmark of the highest quality, thanks to genuinely collaborative interactions between authors and review editors, who include some of the world's best academicians. Research must be certified by peers before entering a stream of knowledge that may eventually reach the public - and shape society; therefore, Frontiers only applies the most rigorous and unbiased reviews.
Frontiers revolutionizes research publishing by freely delivering the most outstanding research, evaluated with no bias from both the academic and social point of view. By applying the most advanced information technologies, Frontiers is catapulting scholarly publishing into a new generation.

What are Frontiers Research Topics?

Frontiers Research Topics are very popular trademarks of the Frontiers Journals Series: they are collections of at least ten articles, all centered on a particular subject. With their unique mix of varied contributions from Original Research to Review Articles, Frontiers Research Topics unify the most influential researchers, the latest key findings and historical advances in a hot research area! Find out more on how to host your own Frontiers Research Topic or contribute to one as an author by contacting the Frontiers Editorial Office: frontiersin.org/about/contact

INSIGHTS IN MICROBE AND VIRUS INTERACTIONS WITH PLANTS: 2021

Topic Editors:
Marco Scortichini, Council for Agricultural and Economics Research (CREA), Italy
Elvira Fiallo-Olivé, La Mayora Experimental Station, Spanish National Research Council (CSIC), Spain

Citation: Scortichini, M., Fiallo-Olivé, E., eds. (2022). Insights in Microbe and Virus Interactions With Plants: 2021. Lausanne: Frontiers Media SA.
doi: 10.3389/978-2-88976-936-0

Table of Contents

frontiers | Frontiers in Microbiology

EDITORIAL
published: 02 August 2022
doi: 10.3389/fmicb.2022.947163

Editorial: Insights in Microbe and Virus Interactions With Plants: 2021

Marco Scortichini[1]* *and Elvira Fiallo-Olivé*[2]*

[1] Council for Agricultural and Economics Research (CREA)-Research Centre for Olive, Fruit and Citrus Crops, Rome, Italy, [2] Instituto de Hortofruticultura Subtropical y Mediterránea "La Mayora" (IHSM-UMA-CSIC), Consejo Superior de Investigaciones Científicas Algarrobo-Costa, Málaga, Spain

Keywords: plant-microbe interaction, plant colonization, detection, climate change, disease control

Editorial on the Research Topic

Insights in Microbe and Virus Interactions with Plants: 2021

Both aerial and underground plant organs and tissues are colonized by a composite microbiota that continuously interacts with the host and the surrounding environment. Phytopathogens, beneficial, symbionts, and commensal microbes and viruses are all members of a network that communicate either with the plant or between different microbial taxa through refined molecular mechanisms (Venturi and Bez, 2021). These interactions shape microbial communities according to plant organ/tissue, climatic parameters, and edaphic features (Chaudry et al., 2021). Currently, these interactions should be also assessed considering the climate change scenario (Chaloner et al., 2021). The knowledge of the basic interactions that rule out each specific pathosystem is a fundamental prerequisite to achieving a sustainable control of plant diseases (Leung et al., 2020). Different and complementary techniques can assist such a purpose. Apart from the "omics", computational software can provide genome-scale metabolic models related to the interplays occurring between co-occurring microbes and viruses, and plants (Lam et al., 2020), whereas detection techniques can benefit from targeted genome sequencing (Maina et al., 2021).

The objective of this Research Topic was to publish high-quality research papers and review articles focusing on the following aspects: (a) new insights on plant-microbes/virus molecular interaction; (b) plant colonization; (c) detection; (d) sustainable control.

This Research Topic contains 12 research papers that cover different aspects of viral, bacterial, and fungal pathogens in relation to plant-microbe molecular interaction, plant colonization, detection, or disease control. In addition, it contains a meta-analysis review that concerns the microbe-mediated thermotolerance in plants.

PLANT-MICROBE/VIRUS MOLECULAR INTERACTION

The study by Zhang et al. analyzed the function of nuclear export signals (NESs) and nuclear localization signals (NLSs) of the NIb protein of turnip mosaic virus. NES and NLS are key signatures of proteins for controlling nuclear import and export. Two functional NESs and one functional NLS were identified in the NIb protein. Mutation of the identified functional NESs or NLS inhibited viral RNA accumulation and systemic infection. Exportin 1 (XPO1), a nuclear export receptor that binds directly to cargo proteins harboring a leucine-rich NES and translocates them to the cytoplasm, was found to contain two NIb-binding domains, which recognize the NLS and NES of NIb, respectively, to mediate the nucleocytoplasmic transport of NIb and promote viral infection.

The expression of miRNAs in *Nicotiana benthamiana* in response to the infection of tobacco curly shoot virus (TbCSV) *via* small RNAs sequencing was studied by Wu et al. The results showed that 15 up-regulated miRNAs and 12 down-regulated miRNAs were differentially expressed,

OPEN ACCESS

Edited and reviewed by:
Trevor Carlos Charles,
University of Waterloo, Canada

***Correspondence:**
Marco Scortichini
marco.scortichini@crea.gov.it
Elvira Fiallo-Olivé
efiallo@eelm.csic.es

Specialty section:
This article was submitted to Microbe and Virus Interactions with Plants, a section of the journal Frontiers in Microbiology

Received: *18 May 2022*
Accepted: *02 June 2022*
Published: *02 August 2022*

Citation:
Scortichini M and Fiallo-Olivé E (2022) Editorial: Insights in Microbe and Virus Interactions With Plants: 2021. Front. Microbiol. 13:947163. doi: 10.3389/fmicb.2022.947163

and nbe-miR167b-3p was down-regulated. The overexpression of nbe-miR167b-3p attenuated leaf curling symptoms of TbCSV and decreased viral DNA accumulation. However, suppression of nbe-miR167b-3p expression enhanced the symptoms and accumulation of the virus. The silencing of PRCP, the target gene of nbe-miR167b-3p caused weakened viral symptoms and DNA accumulation of TbCSV in the plants. Overall, this study clarified the effect of nbe-miR167b-3p on plant defense during TbCSV infection.

A new spectroscopic fluorescence non-destructive method for the *in vivo* detection of the early events in the interaction between compatible and incompatible bacterial pathogens and host plants was provided by Agati et al. It is based on the elaboration of the fluorescence excitation spectra recorded at different times during the elicitation process. The phytoalexin scopoletin $F_{385-460}$ fluorescence has been proven as a marker for plant-bacteria interaction. The outcome of the present study can be exploited to define a screening technique for the early diagnosis of plant diseases, even in the field by using suitable portable fluorescence sensors.

The compatible and incompatible interaction between *Phytopthora infestans* and potato was studied by Zhu et al. through a metabolomic approach and a resistant and a susceptible cultivar. A total of 819 metabolites were identified and quantified. Resistant and sensitive potato cultivars had different metabolomic responses toward *P. infestans*, and the metabolic differences were mainly observed after 48 hpi. The resistant potato cultivar had higher levels of salicylic acid and several upstream phenylpropanoid biosynthesis metabolites, triterpenoids, and hydroxycinnamic acids and their derivatives, such as sakuranetin, ferulic acid, ganoderic acid Mi, lucidenic acid D2, and caffeoylmalic acid.

Transcriptomic analyses and resistance and susceptible non-maize cultivars were utilized to assess the pathogenicity behavior of *Bipolaris maydis* that causes "maize leaf blight" (Meshram et al.). The majority of highly differentially expressed genes were associated with mitochondria, cell wall and chitin synthesis, sugar metabolism, peroxidase activity, mitogen-activated protein kinase activity, and shikimate dehydrogenase. The biosynthetic pathways for secondary metabolism, antibiotics, and carbon metabolism of fungus were highly enriched in the susceptible cultivar during infection. Cell wall synthesis genes related to the synthesis of polyketides, toxins, and putative candidate effector genes were found to be the key compounds underlying the pathogenesis of the *B. maydis* race "O" pathogen.

PLANT COLONIZATION

The bacterial community inhabiting the fruiting body of the saprotrophic and necrotrophic Basidiomycetes *Heterobasidium* species complex, and the associated wood, have been analyzed through the functional annotation of the 16S sequence data (Ren et al.). The study showed that bacteria communities in both substrates experienced a process of a new community reconstruction through the various decay stages. *Sphingomonas* spp. was significantly higher in the fruiting body, and phylum Firmicutes was more dominant in wood tissue. The bacteria community was highly dynamic, and the microbiota activeness, community stability, and functions changed with the decay process. Bacteria appear to spread from the wood tissue of the standing living tree to the fruiting body, but after the tree is killed, bacteria moved from the fruiting body to the wood.

Della Rocca et al. have studied, by means of transmission electron microscope, light and fluorescence microscope combined with histochemical analyses staining, in a time-course approach the induction and the ultrastructure of terpenes and polyphenol synthesis in *Cupressus sempervirens* twigs upon *Seiridium cardinale* infection. The study highlighted the involvement of plastids and endoplasmic reticulum in the production of terpenoids and the consequent secretion of terpenoids directly through the plasma membrane, without exhibiting vesicle formation. Plastids are also involved in the polyphenol production that accumulates in the vacuole.

DETECTION

A comparison of the most established high-throughput sequencing (HTS) platform (MiSeq benchtop sequencer-Illumina) with the MinION sequencer (Oxford Nanopore Technologies) for the detection of plant viruses and viroids was carried out (Pecman et al.). Method comparisons were performed on five selected samples, containing two viroids, which were sequenced using nanopore technology for the first time, and 11 plant viruses with different genome organizations. The results obtained in this work showed that when an appropriate sample and library preparation are selected, nanopore MinION sequencing could be used for the detection of plant viruses and viroids with similar performance as Illumina sequencing.

DISEASE CONTROL

The work carried out by Taglienti et al. evaluates the antiphytoviral effectiveness of treatments with three essential oils and corresponding hydrosols extracted from *Origanum vulgare*, *Thymus vulgaris*, and *Rosmarinus officinalis* on *Cucurbita pepo* plants infected by zucchini yellow mosaic virus or tomato leaf curl New Delhi virus (ToLCNDV). Treatments were applied either concurrently or after virus inoculation to ascertain an inhibition or curative activity, respectively. Treatments were effective against ToLCNDV whether applied simultaneously with the inoculation or after and the major inhibition was observed with *O. vulgare* essential oil and hydrosol. The curative activity gave maximum results with all three essential oils and *T. vulgaris* and *R. officinalis* hydrosols.

The effects of biochar (a rich carbon product obtained by pyrolysis of biomass under a limited supply of oxygen) obtained from olive pruning, have been evaluated on tomato seedling growth and response to systemic agents' infection alone or added with the beneficial microorganisms *Bacillus* spp. and *Trichoderma* spp. (Luigi et al.). Biochar seems to promote the development of tomato seedlings without showing any antimicrobial effects on the beneficial soil bacteria at the tomato

rhizosphere level and even improving their growth. Biochar at 10–15% and when added with *Trichoderma* spp. caused a reduction of the replication and symptoms of potato spindle tuber viroid. Also, results obtained showed that biochar could contribute to reducing both infection rate and virus replication of tomato spotted wilt virus.

A study regarded the isolation and characterization of bacteriophages obtained from melon and watermelon infected by the destructive bacterium *Acidovorax citrulli*, and the further genomic characterization and evaluation of the systemic persistence and translocation of a phage from the roots to the upper parts of watermelon plants (Gasic et al.). The persistence of the phages in the plant environment upon their release is one of the critical points for their successful utilization in plant disease control, being that UV light is one of the most adverse factors. The study ascertained a persistence and survival of 10 days within the plant post distribution of the phage in the soil, allowing a relevant decrease in the severity of the disease and the survival of the plants. These findings corroborate previous studies on the possibility to control endophytic bacterial pathogens through phages distributed to the root system.

Fusarium oxysporum is one of the most dangerous soilborne fungal pathogens, capable of infecting many crops worldwide. Iida et al. assessed the biocontrol activity of non-pathogenic mutants of *F. oxysporum* ff. spp. *melonis* and *lycopersici,* which infect melon and tomato, respectively. The mutants were obtained by disruption of the FOW_2 gene. The pre-inoculation of melon and tomato roots with the mutants allowed to reduce the disease incidence. The study indicated that the ability to reduce the pathogen activity was due to the relevant capability showed by the non-pathogenic mutants to colonize the root system and compete for nutrients with the pathogens.

CLIMATE CHANGE AND PLANT SYMBIONTS

A meta-analysis review performed by Dastogeer et al. investigated the interaction of microbial symbionts and plants within a climate change scenario. One of their main conclusions is the lack of experiments that demonstrate how microbes influence plant responses to high temperature stress in the natural environment. Moreover, the Authors indicated that microbial colonization influenced plant growth and physiology, but their effects were more noticeable when the host plants were exposed to high-temperature stress than when they grew under ambient temperature conditions. Another relevant conclusion of the meta-analysis is that, in addition to microbe-plant interaction, microbe-microbe and microbe-environment interaction should be taken into account to understand the stable functions of a particular microbe in its potential application in agricultural settings.

AUTHOR CONTRIBUTIONS

All authors listed have made a substantial, direct, and intellectual contribution to the work and approved it for publication.

ACKNOWLEDGMENTS

The Topic Editors are thankful to all authors who participated in this Research Topic. Special thank are due to the reviewers, Editors, and staff of Frontiers for their time and assistance in the articles' production.

REFERENCES

Chaloner, T. M., Gurr, S. J., and Bebber, D. P. (2021). Plant pathogen infection risk tracks global crop yields under climate change. *Nat. Clim. Chang.* 11, 710–715. doi: 10.1038/s41558-021-01104-8

Chaudry, V., Runge, P., Sengupta, P., Doehlemann, G., Parker, J. E., and Kemen, E. (2021). Shaping the leaf microbiota: plant-microbe-microbe interactions. *J. Exp. Bot.* 72, 36–56. doi: 10.1093/jxb/eraa417

Lam, T. J., Stamboulian, M., Han, W., and Ye, Y. (2020). Model-based and phylogenetically adjusted quantification of metabolic interaction between microbial species. *PLoS Comp. Biol.* 16, e1007951. doi: 10.1371/journal.pcbi.1007951

Leung, K., Ras, E., Ferguson, K. B., Ariens, S., Babendreier, D., Bijma, P., et al. (2020). A. Next-generation biological control: the need for integration genetics and genomics. *Biol. Rev.* 95, 1838–1854. doi: 10.1111/brv.12641

Maina, S., Zheng, L., and Rodoni, B. C. (2021). Targeted genome sequencing (TG-Seq) approaches to detect plant viruses. *Viruses* 13, 583. doi: 10.3390/v13040583

Venturi, V., and Bez, C. (2021). A call to arms for cell-cell interactions between bacteria in the plant microbiome. *Trends Plant Sci.* 26, 11. doi: 10.1016/j.tplants.2021.07.007

Conflict of Interest: The authors declare that the research was conducted in the absence of any commercial or financial relationships that could be construed as a potential conflict of interest.

frontiers in Microbiology

ORIGINAL RESEARCH
published: 16 December 2021
doi: 10.3389/fmicb.2021.791561

Tobacco curly shoot virus Down-Regulated the Expression of nbe-miR167b-3p to Facilitate Its Infection in *Nicotiana benthamiana*

Rui Wu[1†], Gentu Wu[1†], Lyuxin Wang[1], Xu Wang[1], Zhuoying Liu[1], Mingjun Li[1], Wanzhong Tan[2] and Ling Qing[1]*

[1] Chongqing Key Laboratory of Plant Disease Biology, College of Plant Protection, Southwest University, Chongqing, China, [2] College of Tropical Crops Sciences, Yunnan Agricultural University, Kunming, China

OPEN ACCESS

Edited by:
Elvira Fiallo-Olivé, Institute of Subtropical and Mediterranean Horticulture La Mayora, Spain

Reviewed by:
Fangfang Li, Institute of Plant Protection, Chinese Academy of Agricultural Sciences (CAAS), China
Yongliang Zhang, China Agricultural University, China

***Correspondence:**
Ling Qing
qling@swu.edu.cn

[†] These authors have contributed equally to this work and share first authorship

Specialty section:
This article was submitted to Microbe and Virus Interactions with Plants, a section of the journal Frontiers in Microbiology

Received: 08 October 2021
Accepted: 09 November 2021
Published: 16 December 2021

Citation:
Wu R, Wu G, Wang L, Wang X, Liu Z, Li M, Tan W and Qing L (2021) Tobacco curly shoot virus Down-Regulated the Expression of nbe-miR167b-3p to Facilitate Its Infection in Nicotiana benthamiana. Front. Microbiol. 12:791561. doi: 10.3389/fmicb.2021.791561

Tobacco curly shoot virus (TbCSV) belongs to the genus *Begomovirus* of the family *Geminiviridae*, and causes leaf curling and curly shoot symptoms in tobacco and tomato crops. MicroRNAs (miRNAs) are pivotal modulators of plant development and host-virus interactions. However, the relationship between TbCSV infection and miRNAs accumulation has not been well investigated. The present study was conducted to analyze different expressions of miRNAs in *Nicotiana benthamiana* in response to the infection of TbCSV via small RNAs sequencing. The results showed that 15 up-regulated miRNAs and 12 down-regulated miRNAs were differentially expressed in TbCSV infected *N. benthamiana*, and nbe-miR167b-3p was down-regulated. To decipher the relationship between nbe-miR167b-3p expression and the accumulations of TbCSV DNA, pCVA mediation of miRNA overexpression and PVX based short tandem target mimic (STTM) were used in this study. It was found that overexpression of nbe-miR167b-3p attenuated leaf curling symptom of TbCSV and decreased viral DNA accumulation, but suppression of nbe-miR167b-3p expression enhanced the symptoms and accumulation of TbCSV. *PRCP*, the target gene of nbe-miR167b-3p, was silenced in plants using VIGS and this weakened the viral symptoms and DNA accumulation of TbCSV in the plants. Overall, this study clarified the effect of nbe-miR167b-3p on plant defense during TbCSV infection, and provided a framework to reveal the molecular mechanisms of miRNAs between plants and viruses.

Keywords: nbe-miR167b-3p, *Tobacco curly shoot virus*, viral DNA accumulation, miRNA expression, target gene

INTRODUCTION

MicroRNAs (miRNAs) are small RNAs with 20–25 nucleotides that play essential roles in plant biological processes by targeting complementary mRNAs for degradation or translation expression (Bologna and Voinnet, 2014; Cui et al., 2016). In plants, miRNAs regulate leaf morphogenesis, roots and flowers developments, and other key processes (Palatnik et al., 2003; Guo et al., 2005;

Zhang et al., 2007). They also function in the response of plants to biotic and abiotic stresses (Wang et al., 2014; Tong et al., 2017), such as inducible expression of miR164 in *Arabidopsis thaliana* led to decreased NAC1 mRNA levels and reduced lateral root emergence (Guo et al., 2005); miRNA guided cleavage of TCP4 mRNA to control the morphogenesis of the leaves (Palatnik et al., 2003); Plants overexpressing osa-miR171b were less susceptible to *Rice stripe virus* (RSV) and virus symptoms were attenuated (Tong et al., 2017); In rice, osa-miR319b played an important role in plant response to cold stress possibly by targeting OsPCF6 and OsTCP21 (Wang et al., 2014).

Viruses cause a variety of symptoms on their host plants, including dwarf, wrinkle, curl, and yellowing, which indicates that plant viruses interfere with the normal growth and development of plants (Maghuly et al., 2014). In recent years, studies have shown that miRNAs participate in the interaction between plants and pathogens (Finnegan and Matzke, 2003; Kidner and Martienssen, 2005; Voinnet, 2005; Du et al., 2011, 2014; Xu et al., 2014; Wang et al., 2016; Zhang et al., 2016; Xia et al., 2019), and viruses change the expression of endogenous miRNAs in plants. For example, RSV enhanced the accumulation of some miRNAs in rice (Du et al., 2011), *Cucumber mosaic virus* (CMV) FNY2b protein suppressed the function of miR159, inducing disease-like symptoms in host plants (Du et al., 2014); The synergistic infection of *Maize chlorotic mottle virus* (MCMV) and *Sugarcane mosaic virus* (SCMV) caused maize lethal necrosis, meanwhile the down-regulation of miR159, miR393, and miR394 was involved in antiviral defense to synergistic infection (Xia et al., 2019). Moreover, different miRNAs participated in anti-virus defense pathways in various plant (Amin et al., 2011). It was also found by our laboratory that different miRNAs can manipulated infected plants to show varied severity of disease symptoms (Du et al., 2020).

It was reported that the suppression of nbe-miR166h-p5 in plants caused leaves to turn dark green with increased chlorophyll, attenuated leaf yellowing symptom of PVX and decreased viral accumulation (Wang et al., 2018). Inhibition of osa-miR171b caused stunting with reduced chlorophyll content in leaves similar to viral symptoms. However, plants overexpressing osa-miR171b were shown less susceptible to RSV and the viral symptoms were attenuated (Tong et al., 2017). When the expression of miR319 was inhibited, the enrichment of endogenous jasmonic acid (JA) was increased in rice, and the resistance of rice was enhanced to *Rice ragged stunt virus* (RRSV) infection (Zhang et al., 2016). These results indicate that miRNAs play an important role in the processes of plant defense and virus infection.

However, the roles and action modes of specific miRNAs involved in viral infection and host susceptibility remain unclear in most cases (Romanel et al., 2012; Gao et al., 2013; Lian et al., 2016). *Tobacco curly shoot virus* (TbCSV) belongs to *Begomovirus*, with a genome of circular single-stranded DNA. TbCSV is transmitted by whitefly (*Bemisia tabaci*) and causes significant losses of tobacco and tomato frequently in China (Li et al., 2005; Xu et al., 2019). Previous studies have shown that inhibiting the expression of nbe-miR1919c-5p can enhance the infection of TbCSV to *N. benthamiana* (Du et al., 2020). At the same time, nbe-miR167b-3p may also respond to the infection of TbCSV (Du et al., 2019). But, there had no experimental evidences to demonstrate the effect of nbe-miR167b-3p on TbCSV infecting host plants. In this study, it was disclosed that the infection of TbCSV could be enhanced by suppressed nbe-miR167b-3p expression and nbe-miR167b-3p responded to the infection of TbCSV by regulating the expression of its target gene *PRCP*.

MATERIALS AND METHODS

Small RNA Library Construction

The leaves of TbCSV inoculated *N. benthamiana* and control plants were collected, and RNA was extracted to construct a small RNA library. Small RNAs sequencing were performed by the Novogene Bioinformatics Technology Company, Beijing, China, using IlluminaHiseq^{TM}2500 instrument.

Vectors Construction

Plasmids for nbe-miR167b-3p expression were constructed with the methods described by Tang et al. (2010): *Cabbage leaf curl virus* (CaLCuV)-based miRNA expression system was developed and the CaLCuV vectors (pCVA and pCVB) used in this study were provided kindly by Dr. Yule Liu of Tsinghua University. The pCVA and pCVB were used for expressing amiRNA of nbe-miR167b-3p. Firstly, the nbe-miR167b-3p and nbe-miR167b-3p* sequences were inserted into Arabidopsis miR319a precursor gene to construct an amiRNA of nbe-miR167b-3p. Then, amiRNA sequence containing two restriction enzyme sites (*Xba*I and *Kpn*I) was synthesized at Beijing Genomics Institute. Next, this amiRNA sequence and pCVA vector were digested with the restriction enzymes *Xba*I and *Kpn*I (TAKARA Bio, 1093S and 1068S) and the amiRNA and pCVA vector were ligated with a ligase (TOYOBO Bio, LGK-101). The recombinated vector pCVA-miR167b-3p was used to overexpress nbe-miR167b-3p.

Virus-based miRNA suppression (VbMS) system was used for miRNA function analysis in *N. benthamiana*. The PVX-miR167b-3p vector was created to mediate nbe-miR167b-3p down-regulation with the technique described and applied by Du et al. (2020). The target mimic was designed to sequester nbe-miR167b-3p using the method of Yan et al. (2014). Then a sequence containing four copies of target mimic and two restriction enzyme sites (*Cla*I and *Sal*I) was synthesized and the copies were separated by a 48 bp nucleotide sequence. This sequence and PVX vector were digested with the restriction enzymes *Cla*I and *Sal*I (TAKARA Bio, 1034S and 1080S), and finally the target mimic of nbe-miR167b-3p and PVX vector were ligated with a ligase (TOYOBO Bio, LGK-101).

By using the psRNA Target tool, the potential target gene of nbe-miR167b-3p was predicted online at http://plantgrn.noble.org/psRNATarget/*Nicotiana benthamiana*, transcript, Niben101 (Dai et al., 2018). The maximum expected value parameter, length of the complementarity score and target accessibility (range 0–100, as small as possible) were set to 2.5, 23 bp and 20.0, respectively. The *Tobacco rattle virus* (TRV)-based virus-induced gene silencing (VIGS) was used to

silence target gene of nbe-miR167b-3p in *N. benthamiana* and the target gene was cloned from *N. benthamiana* cDNA. PCR amplification was performed using the HiFi DNA polymerase (TransGen Biotech, Beijing, AP131) and the 300 bp PCR product was gel purified using DNA purification and a recovery kit (TIANGEN Biotech, Beijing, DP201) and combined with the T-vector. The primers used were listed in the **Supplementary Table 1**. The positive plasmid was digested with the enzymes *Bam*HI and *Sac*I (TAKARA Bio, 1010S and 1078S) and fragment was purified using a DNA purification and recovery kit. Then, it was cloned into the pTRV-RNA2 and digested with the same restriction enzyme site; the recombinant plasmid was transferred into EHA105 strain of *Agrobacterium tumefaciens*.

All of the sequences described above were verified by Sanger sequencing and their sequencing was performed at Beijing Genomics Institute.

Virus Inoculation and Agrobacterium Infiltration

N. benthamiana plants were grown in a greenhouse with settings of 25°C, 16 h of light/day. The virus infectious clones of TbCSV, relative vectors pCVA, pCVB, and pCVA-miR167b-3p, PVX, PVX-miR167b-3p, TRV:GUS, and TRV:PRCP(s) were transformed, respectively, into *A. tumefaciens*. These transformed *A. tumefaciens* were then infiltrated into *N. benthamina* using the treatments described here: (1) *N. benthamiana* plants were infiltrated with the infectious clone of TbCSV at the five-leaf stage and mock-inoculated were used as control. (2) *N. benthamiana* plants were infiltrated with pCVA-miR167b-3p plus pCVB to overexpress nbe-miR167b-3p at the fourth-leaf stage. The plants infiltrated with pCVA plus pCVB were used as control. Symptoms of TbCSV were shown on these plants 11 days post inoculation (dpi). (3) *N. benthamiana* plants were infiltrated with PVX-miR167b-3p to down-regulate the expression of nbe-miR167b-3p at the five-leaf stage and PVX inoculated plants were used as control. At 7 dpi, these plants were infiltrated with TbCSV. (4) For co-infection, equal concentrations and volumes of individual *A. tumefaciens* cultures were mixed. Twenty plants were used for each treatment and the control. The symptoms on diseased plants were observed and photographed. The leaves at the same position were harvested, and virus accumulation and gene expression in the leaves were further detected with qPCR and qRT-PCR.

DNA Extraction and Virus Accumulation Detection

The DNAs of *N. benthamiana* were extracted using the cetyl trimethylammonium bromide (CTAB) method. To determine whether *N. benthamiana* plants were infected by TbCSV, specific primers of TbCSV were used to amplify the virus DNA in the diseased leaves with PCR. To detect virus accumulation in the leaves, the qRCR technique (Zorzatto et al., 2015) was applied and the result of qRCR was calculated according to the absolute method (Schmittgen and Livak, 2008; Rodríguez-Negrete et al., 2014). The 20 μL reaction solution system of qPCR contained 10 μL NovoStart®SYBR qPCR Super Mix Plus, 8 μL RNase free water, 0.5 μL AV1-qF (10 μM), 0.5 μL AV1-qR (10 μM), and 50 ng DNA template. The linear standard curve of TbCSV was automatically generated by Origin 9.0 software based on the lg (log10) value of the copy number of TbCSV in each sample. Each qPCR reaction was repeated three times (batches) with 24 plants of *N. benthamiana* in each repeated batch.

Quantitative Reverse Transcriptase PCR Analysis

The total RNA of *N. benthamiana* was extracted using TRIzol reagent (Invitrogen, California, United States). The qRT-PCR for nbe-miR167b-3p was based on previous reports (Guo et al., 2012). The specific RT stem-loop primers in the Prime Script RT reagent Kit (TAKARA Bio, Kusatsu, Shiga, Japan) were used to reverse the RNA and the final reverse transcribed products from qRT-PCR was analyzed using the SYBR green kit supplied by Novoprotein, Shanghai, China. The qRT-PCR parameters were set as 95°C pre-denaturation 3 min, 32 cycles of 95°C denaturation 25 s and 60°C annealing 30 s, and a final extension at 72°C for 30 s, using the action gene (XM_033660572.1) of *N. benthamiana* as the internal reference. The $2^{-\Delta\Delta CT}$ method (Du et al., 2020) was used for qRT-PCR analysis. For statistical analysis, three fully independent biological replicates were designed and subjected to qRT-PCR tests.

For detecting expression level of the target gene, NovoStart ®SYBR qPCR Super Mix Plus kit (NovoProtein) was employed to perform qRT-PCR on the CFX 96 real-time system (Bio-Rad). Three biological samples for each qRT-PCR reaction were processed and each biological sample was repeated three times. The experimental results were computed from data of three biological repeats.

RESULTS

Effect of *Tobacco curly shoot virus* on the Expression of MicroRNAs in *Nicotiana benthamiana*

Typical disease symptoms with leaf curling and shrinking developed on inoculated *N. benthamiana* plants 21 days after TbCSV inoculation while the control plants remained symptomless and healthy (**Figure 1A**). Through sequencing analysis of the small RNAs from leaves collected at 21 dpi, 5,982,433 and 5,675,863 specific small RNA sequences were detected in, and a small RNA library was constructed for, the inoculated and healthy plants, respectively. Of the unique reads, 4,762,789 (45.63%) were from the control plants and 4,456,219 (42.69%) from the inoculated plants (**Table 1**). Statistical analysis of the data showed that the content of 21nt sRNA was more than that of 22 nt sRNA in control plants, while in TbCSV-infected samples, the content of 21nt sRNA was less than the content of 22 nt sRNA in TbCSV-infected plants (**Figure 1B**). Compared with miRNA in control plants, there were 21 miRNAs expressed differentially in TbCSV-infected plants, including 12 up-regulated and 9 down-regulated miRNAs (**Figure 1C**).

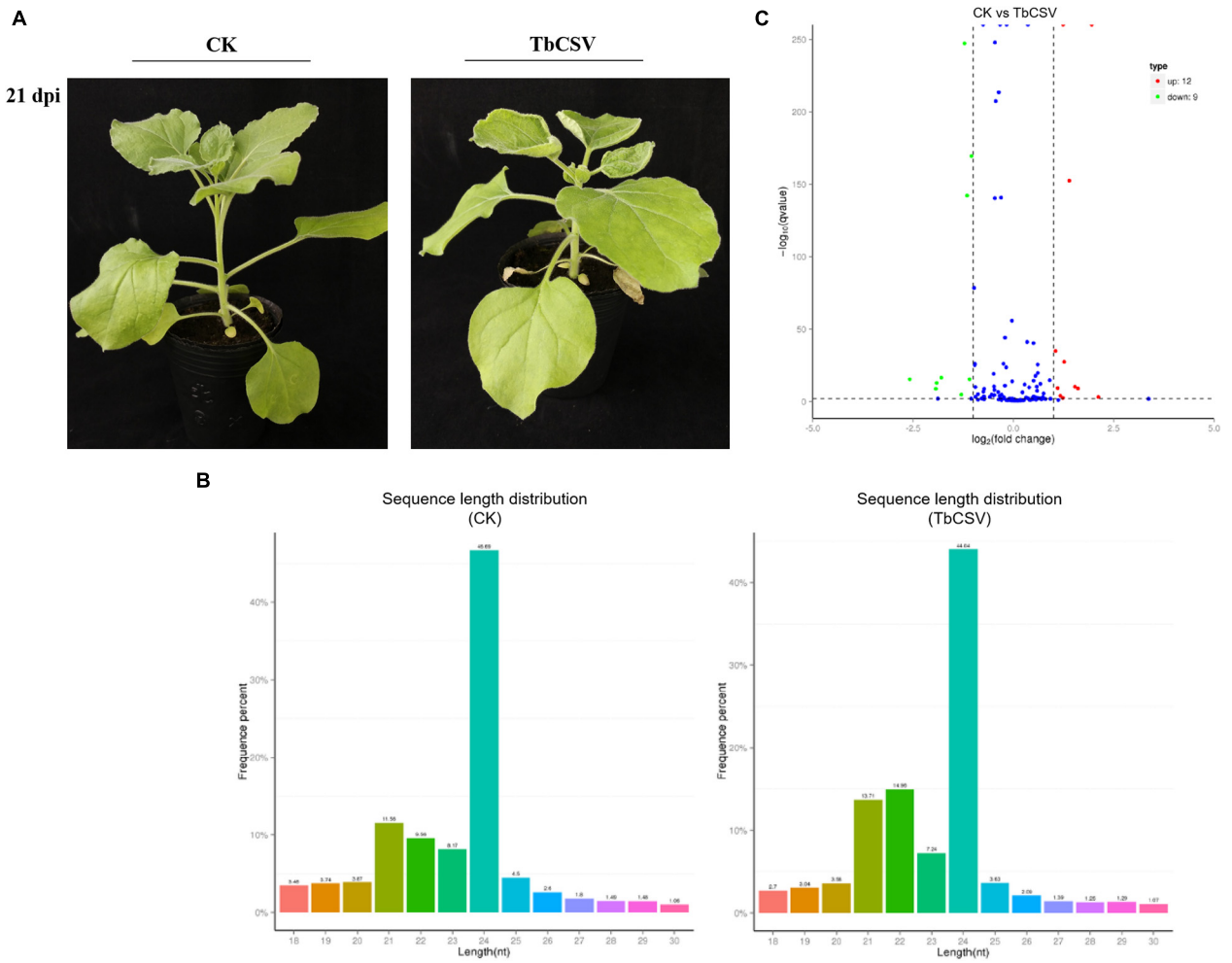

FIGURE 1 | Analysis of small RNA sequencing data. **(A)** TbCSV symptoms on systemic leaves of *N. benthamiana* plants at 21 dpi with leaf curling and shrinking. **(B)** The length distribution of small RNAs after TbCSV infecting *N. benthamiana*. The abscissa shows the size of miRNAs and vertical axis shows percentage of total small RNAs. **(C)** Volcano map of differential expression miRNAs in TbCSV infiltrated *N. benthamiana*. The abscissa shows the fold change difference in the expression of miRNAs in different treatments and control plants, and the vertical axis indicates the adjusted p-adj for the differences in expression. MiRNAs without significant differences are indicated by blue dots, the up-regulated genes by red dots and the down-regulated genes by green dots.

TABLE 1 | Distribution of small RNA sequences among the two constructed libraries.

Small RNA library	Specific sRNAs reads	Unique sRNAs reads	% in specific
CK	5,982,433	4,762,789	45.63%
TbCSV	5,675,863	4,456,219	42.69%

Tobacco curly shoot virus Induced Leaves Curling Symptom and Down-Regulated Expression of nbe-miR167b-3p

Significant and typical systematic curling symptom developed on leaves of *N. benthamiana* plants, at 7 dpi with the infectious clone of TbCSV, but no symptom was observed on the control plant (**Figure 2A**). PCR tests showed that the DNA of TbCSV existed in the leaves showing symptoms but not in the control plants (**Figure 2B**).

According to the results of small RNA sequencing, it was found that TbCSV infection down-regulated the expression of nbe-miR167b-3p in *N. benthamiana*. qRT-PCR tests illustrated that the expression level of nbe-miR167b-3p in the infected *N. benthamiana* plants was down-regulated to about 65%, compared with that in the control plant leaves (**Figure 2C**).

Silencing nbe-miR167b-3p Expression Aggravated Disease Symptoms and DNA Accumulation of *Tobacco curly shoot virus*

For exploring specific function of nbe-miR167b-3p in TbCSV infecting *N. benthamiana*, a vector was constructed to silence

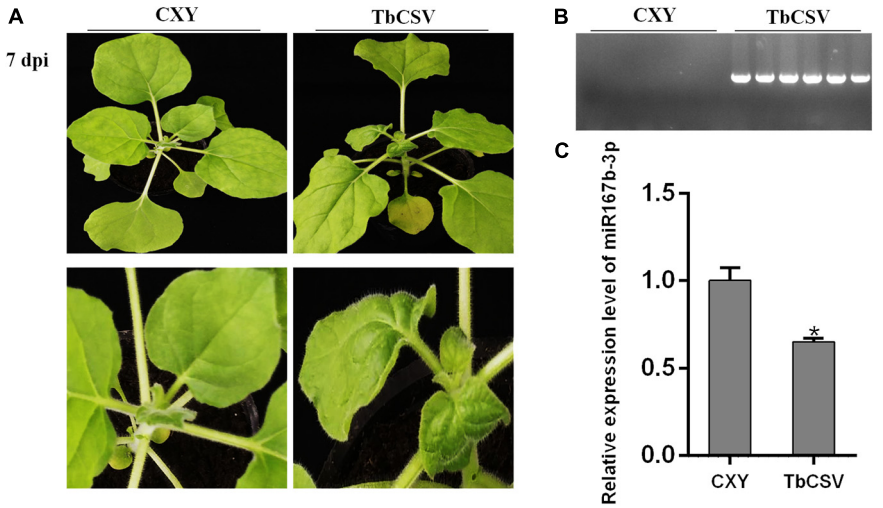

FIGURE 2 | TbCSV symptoms at 7 dpi and differential expression of nbe-miR167b-3p in TbCSV-infected *N. benthamiana*. **(A)** Leaf curling symptom caused by TbCSV in *N. benthamiana* leaves. **(B)** Analysis of TbCSV DNA through PCR. **(C)** Quantitative RT-PCR demonstrating the expression of nbe-miR167b-3p in TbCSV-infected in *N. benthamiana* plants. Significance of difference (*$p < 0.05$) was between the treatments was determined by the Student's *t*-test.

nbe-miR167b-3p (PVX-miR167b-3p) using *Potato virus X* (PVX) infectious clone. Then, *A. tumeficiens* GV3101 transformed with PVX and PVX-miR167b-3p was resuspended and the suspensions (OD_{600} = 1.0) were infiltrated into *N. benthamiana*, respectively. At 7 dpi, the upper leaves showed significant curling symptom on the PVX-miR167b-3p treated plants, while only the mosaic symptom was observed on leaves of control plants (**Figure 3A**). Compared with the PVX-inoculated plants, the expression level of nbe-miR167b-3p in the PVX-miR167b-3p was significantly suppressed and the expression was down-regulated to only 27.4% of that in the control plants (**Figure 3B**).

When inoculated with TbCSV by agroinfiltration, all plants of the above two treatments showed leaf curling symptom at 7 dpi, and the symptom on the PVX-miR167b-3p plus TbCSV-inoculated plants were more severe than that on the control (PVX plus TbCSV) plants (**Figure 3C**). Results from qRT-PCR analysis showed that the relative expression level of nbe-miR167b-3p in the plants inoculated with PVX-miR167b-3p plus TbCSV was down-regulated significantly, compared with that in the plants inoculated with PVX plus TbCSV (**Figure 3D**). Detection of DNA accumulation with qPCR at 7 dpi showed that the amount of viral DNA in the systematically infected leaves of the plants inoculated with PVX-miR167b-3p plus TbCSV treatment was higher than that of the plants inoculated with PVX plus TbCSV (**Figure 3E**). These results suggested that silencing of nbe-miR167b-3p in *N. benthamiana* was beneficial to TbCSV infection.

Overexpression of nbe-miR167b-3p Alleviated Symptoms and *Tobacco curly shoot virus* DNA Accumulation

CaLCuV (pCVA) vector was used to investigate the effect of nbe-miR167b-3p up-expression on TbCSV infection of *N. benthamiana*. Through DNA recombination, pCVA-miR167b-3p plasmid was constructed and transformed into *A. tumeficiens* EHA105 strain. Nbe-miR167b-3p was expressed in *N. benthamiana* plants with pCVA-miR167b-3p plus pCVB through agroinfiltration and the control plants were inoculated with pCVA plus pCVB. The expression level of nbe-miR167b-3p was detected in the upper leaves at 11 dpi. The result showed that there was no significant difference in symptoms between the treated and the control plants (**Figure 4A**). However, compared with that in the pCVA plus pCVB-inoculated plants, the expression level of nbe-miR167b-3p in the pCVA-miR167b-3p plus pCVB-inoculated plants was up-regulated significantly and this overexpression was 3.3 times of that in the control plants (**Figure 4B**).

All plants inoculated with pCVA plus pCVB or pCVA-miR167b-3p plus pCVB were infiltrated at 11 dpi with TbCSV by agroinfiltration. At 13 dpi, the upper leaves in both of the treated and control plants showed upward leaf curling symptom, and the symptom in pCVA-miR167b-3p plus pCVB and TbCSV plants was less severe than that on the control plants (**Figure 4C**). At this stage, qRT-PCR showed that the relative expression level of nbe-miR167b-3p in the plants inoculated with pCVA-miR167b-3p plus pCVB and TbCSV was still up-regulated significantly, compared with that in the control plants (**Figure 4D**). Leaves of the plants were harvested to detect the accumulation of TbCSV DNA with qPCR and the results showed that the accumulation of TbCSV DNA in the leaves of pCVA-miR167b-3p plus pCVB and TbCSV infiltrated plants was significantly lower than that in the control plant leaves (**Figure 4E**). These results indicated that overexpression of nbe-miR167b-3p in *N. benthamiana* inhibited TbCSV infection.

The Expression of nbe-miR167b-3p Target Gene

To explore how nbe-miR167b-3p regulates the infection of TbCSV in *N. benthamiana*, the potential target genes were

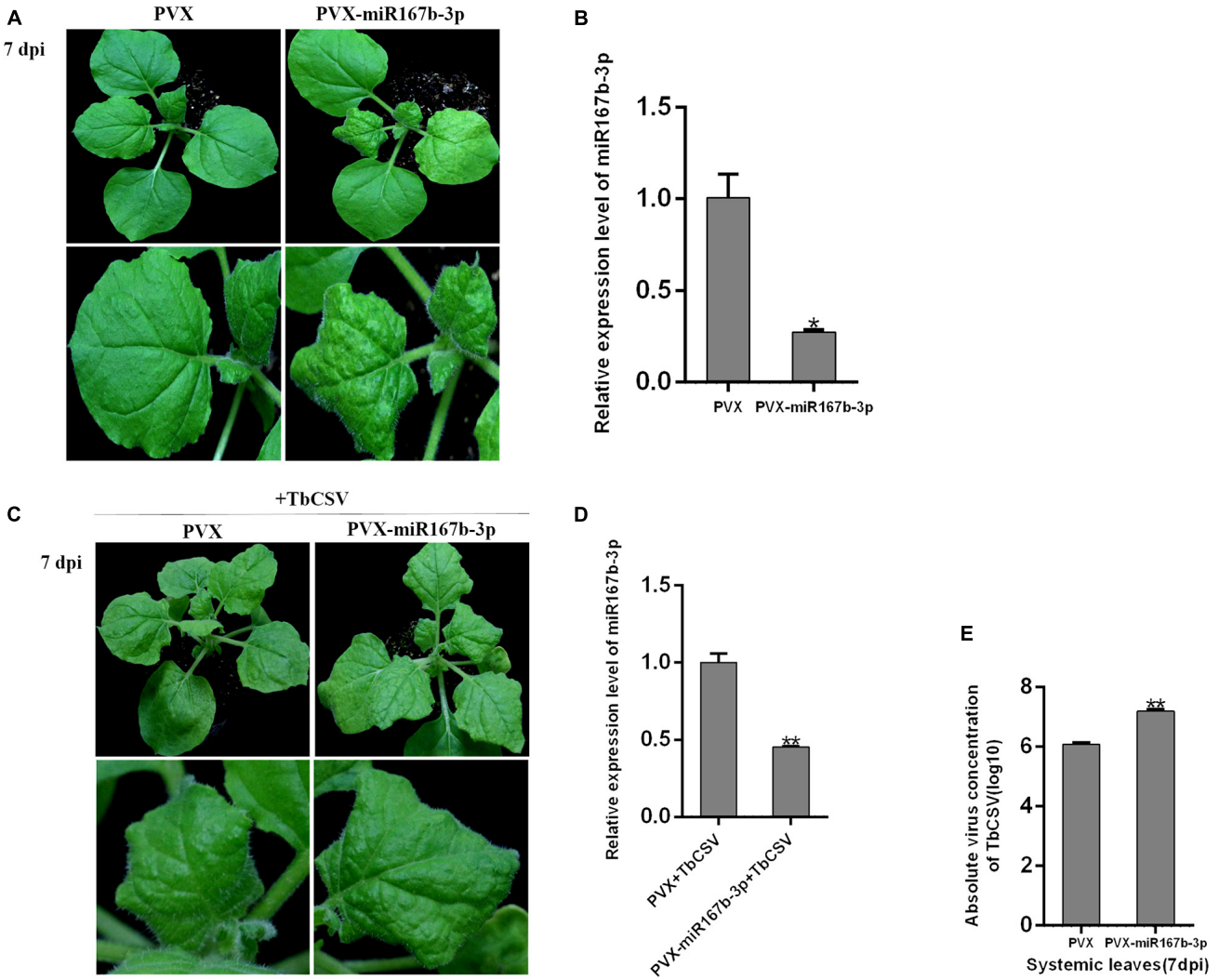

FIGURE 3 | Suppression of nbe-miR167b-3p enhanced leaf curling symptom induced by TbCSV and increased viral DNA accumulation. **(A)** PVX-based miRNA suppression (VbMS) system was used to down-regulate the expression of nbe-miR167b-3p. **(B)** Expression level of nbe-miR167b-3p in PVX-miR167b-3p-treated plants was significantly reduced compared with that in the control plants by qRT-PCR. **(C)** TbCSV was infiltrated into PVX-miR167b-3p-treated and control plants 7 days after VbMS treatment. **(D)** Relative expression level of nbe-miR167b-3p in TbCSV-infected and PVX-miR167b-3p-treated plants using qRT-PCR. **(E)** TbCSV DNA copy numbers in the systemic leaves harvested from the PVX plus TbCSV-inoculated plants or the PVX-miR167b-3p plus TbCSV-inoculated plants. Significance of difference between treatments (*$p < 0.05$; **$p < 0.01$) was determined by the Student's *t*-test.

analyzed using psRNA Target online at http://plantgrn.noble.org/psRNATarget/ and the results were given in **Supplementary Table 2**. Specific primers were designed with the sequences of target genes and qRT-PCR was performed to detect the expression level of these genes. The results showed that, compared with the mock-inoculated plants (CXY), the expression level of the target gene pentatricopeptide repeat-containing protein (PCRP) (**Figure 5A**) in the TbCSV-infected plants was significantly up-regulated (**Figure 5B**). This indicated that the expression level of *PRCP* was up-regulated significantly in the PVX-miR167b-3p infiltrated plants; this was 1.9 times of that in the PVX-inoculated plants (**Figure 5C**). Furthermore, the relative expression of *PRCP* in the pCVA-miR167b-3p plus pCVB inoculated plants was also detected by qRT-PCR and the results showed that the expression of *PRCP* was down-regulated and this was 61.4% of that in the control plants (**Figure 5D**).

Silencing of *PRCP* Reduced Infection of *Tobacco curly shoot virus* in *Nicotiana benthamiana*

To investigate the function of nbe-miR167b-3p target gene *PRCP* in the process of TbCSV infection, *Tobacco rattle virus* (TRV)-induced VIGS was used and recombinant vector (TRV-PRCP) was created to silence *PRCP* in *N. benthamiana*. TRV-PRCP was transformed into *A. tumeficiens* EHA105 and 12 *N. benthamiana* plants were inoculated through the transformants; the control plants were inoculated with TRV-GUS. At 10 dpi, there was

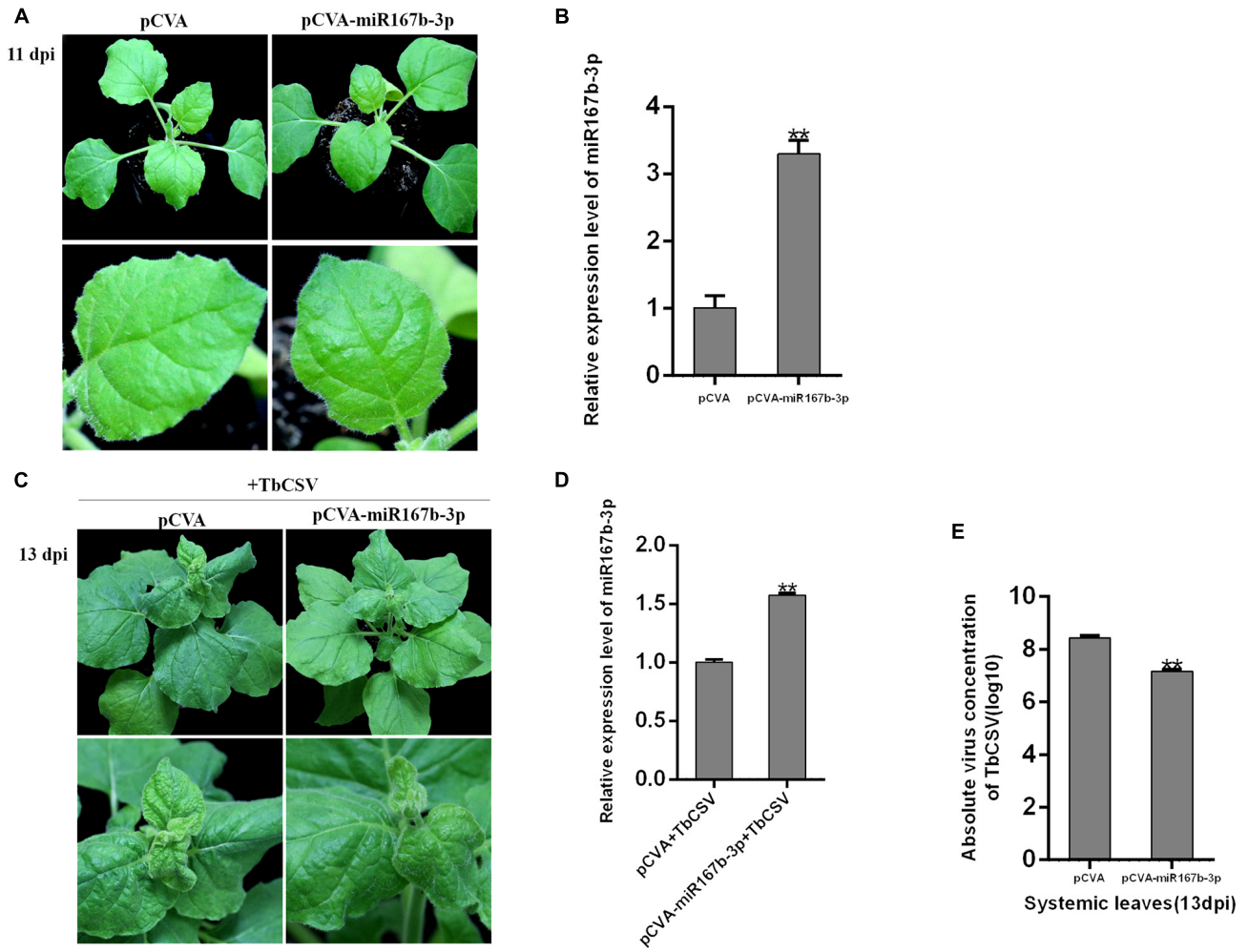

FIGURE 4 | Overexpression of nbe-miR167b-3p attenuated leaf curling symptom induced by TbCSV and reduced viral DNA accumulation. **(A)** pCVA-based miRNA vector (pCVA-miR167b-3p) was used to increase expression of nbe-miR167b-3p. **(B)** Result of qRT-PCR showed that expression of nbe-miR167b-3p in the pCVA-miR167b-3p-inoculated plants was significantly increased compared with that of the control plants (pCVA). **(C)** TbCSV was inoculated onto pCVA-miR167b-3p -treated and control plants. **(D)** qRT-PCR showed that the level of nbe-miR167b-3p in TbCSV-infected and pCVA-miR167b-3p-treated plants was significantly increased compared with that of the TbCSV-infected pCVA-treated plants. **(E)** TbCSV DNA copy numbers in the systemic leaves harvested from the pCVA plus TbCSV-inoculated plants or the pCVA-miR167b-3p plus TbCSV-inoculated plants. Significance of difference between treatments (*$p < 0.05$; **$p < 0.01$) was determined by the Student's *t*-test.

not significantly difference of the growth and development between TRV-PRCP-infiltrated and control plants (**Figure 6A**). qRT-PCR tests showed that the expression of *PRCP* in the TRV-PRCP infected plants was significantly decreased, to 43% of the expression level in the control plants (**Figure 6B**).

When all the plants were inoculated with TbCSV, the *N. benthamiana* plants inoculated with TRV-PRCP plus TbCSV developed little leaf curling symptom, which was similar to the leaf curling symptom induced by TbCSV. In contrast, severe leaf curling symptom was observed on the control plants (**Figure 6C**). The result of qRT-PCR illustrated that the expression of *PRCP* was suppressed significantly in the TRV-PRCP plus TbCSV-inoculated plants, compared with that in the control plants (**Figure 6D**). qPCR detection also found that the viral DNA accumulation in TRV-PRCP plus TbCSV-inoculated plants was down-regulated compared with that in the control plants (**Figure 6E**). These results suggested that silencing of nbe-miR167b-3p target gene *PRCP* in *N. benthamiana* inhibited the TbCSV infection.

DISCUSSION

A number of studies reported that miRNAs played important roles in plant growth and resistance to pathogen infections. It was verified that miRNA-triggered changes in gene expression were essential for controlling plant development and for modulating the adaptation of plants to pathogen infection and the infection by different viruses changed the level of certain miRNAs in plants. For example, studies of Yang et al. (2016)

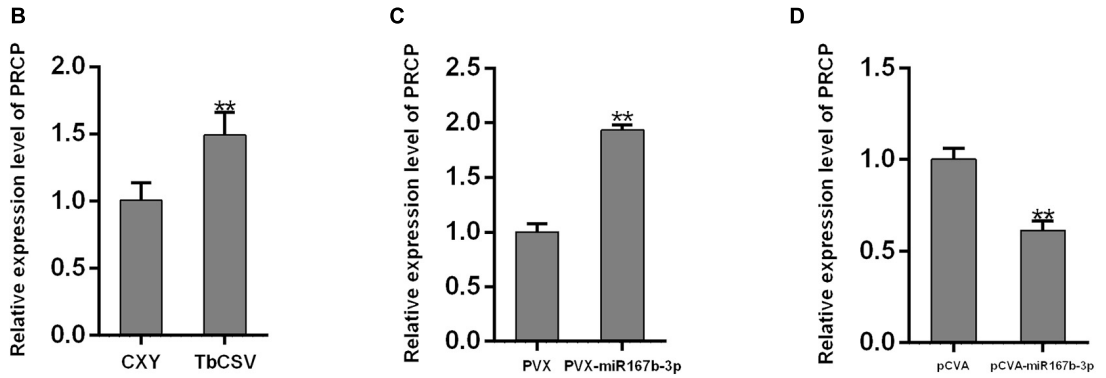

FIGURE 5 | Analyses of the expression of nbe-miR167b-3p target gene *PRCP* through qRT-PCR. **(A)** The binding site of nbe-miR167b-3p on the mRNAs of potential target was localized at the encoding sequence. **(B)** The mRNA levels of *PRCP* were up-regulated in TbCSV-infected *N. benthamiana* plants. **(C)** The mRNA levels of *PRCP* were up-regulated in nbe-miR167b-3p-suppressed leaves. **(D)** The mRNA levels of *PRCP* were down-regulated in nbe-miR167b-3p-overexpressed leaves. Significance of difference between treatments (*$p < 0.05$; **$p < 0.01$) was determined by the Student's *t*-test.

showed that 56 miRNAs were up-regulated and 13 miRNAs were down-regulated by RSV infection, providing new insights into the mechanisms of RSV pathogenicity. In transgenic *A. thaliana* plants, expression of *Cucumber mosaic virus* (CMV) 2b silencing suppressor protein from the severe strain Fny of subgroup IA disrupted miRNA159a-regulated development, which caused severe symptoms on the plants (Du et al., 2014). After infection of Chinese cabbage by *Turnip mosaic virus* (TuMV), the expression of bra-miR1885 and bra-miR158 was significantly up-regulated (He et al., 2008). The change of microRNA expression was considered as the main factor inducing symptoms after virus infection (Yang et al., 2016). Meanwhile, some changes in the expression level of miRNAs may also lead to leaf yellowing, curling, wrinkling, and dwarfing. In our previous experiment, different expressions of miRNAs in *N. benthamiana* during the TbCSV infection were analyzed (Du et al., 2019), but only limited examples of specific virus-inducible miRNAs that were directly involved in viral infection or host susceptibility existed (Zhang et al., 2016). Results from the present study showed that nbe-miR167b-3p expression was suppressed by TbCSV infection and that nbe-miR167b-3p target gene *PRCP* changed plant growth and susceptibility of *N. benthamian* to TbCSV.

Some studies indicated that miR167 was involved in plant development, biostress and abiostress. MiR167a was shown to affect the expression of auxin response factors (ARF6 and ARF8) and to induce flower defection and female sterility in tomato (Liu et al., 2014). MiR167 also induced certain changes in leaf shape, stomatal closure and relative water content by regulating differential expressions of its target genes *MesARF6* and *MesARF8*, thus resulting in response to cassava water deficiency (Phookaew et al., 2014). MiR167b inhibited the infection of PVY and PVX by targeting RNA silencing suppressor HC-Pro of PVY and the TGBp1/p25 (p25) of PVX; this improved tobacco resistance to PVY and PVX (Ai et al., 2011). In our study, the expression level of nbe-miR167b-3p was down-regulated in TbCSV-infected plants. Because nbe-miR167b-3p was inhibited in the process of TbCSV infection, it was speculated that nbe-miR167b-3p played an active role in resistance of *N. benthamiana* to TbCSV infection.

RRSV infection was indicated to increase the accumulation of miR319 in rice plants and simultaneously suppressed the JA-mediated defense against virus infection and symptom development (Zhang et al., 2016). The studies of Wu et al. (2015) revealed that the antiviral function of AGO18 depended on its activity to sequester miR168 to alleviate repression of rice; AGO1 essential for antiviral RNAi increased rice antiviral activity miR528 and negatively regulated viral resistance in rice by cleaving L-ascorbate oxidase (AO) messenger RNA, and thereby reduced AO-mediated accumulation of reactive oxygen. Upon viral infection, AGO18 isolated miR528 leading to elevated AO activity, higher basal reactive oxygen accumulation and enhanced antiviral defense (Wu et al., 2017). In the present study, nbe-miR167b-3p was found to down-regulate the expression by PVX-induced gene silencing system, and these caused downward leaf curling on *N. benthamiana* plants. The silencing of nbe-miR167b-3p aggravated the symptoms of TbCSV infection and increased the accumulation of TbCSV DNA in *N. benthamiana*. Then an expression vector overexpressing nbe-miR167b-3p (pCVA-miR167b-3p) was constructed using the pCVA vector and after inoculating *N. benthamiana* plants with this expression vector, it was found that the up-regulated expression of nbe-miR167b-3p in *N. benthamiana* not only alleviated symptoms of TbCSV infection, but also reduced the accumulation of TbCSV in *N. benthamiana* plants.

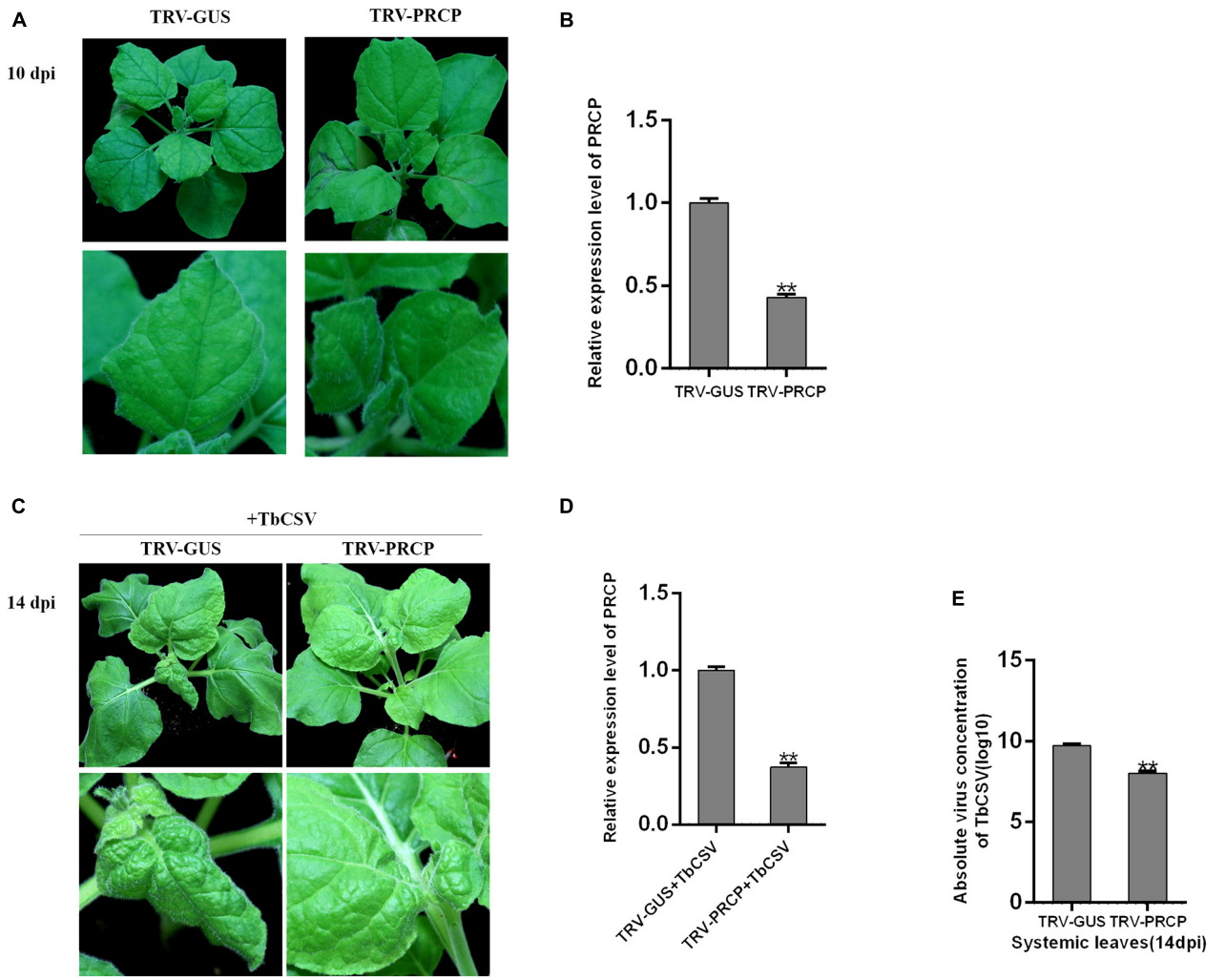

FIGURE 6 | Effect of *PRCP* on TbCSV pathogenicity. **(A)** *Tobacco rattle virus* (TRV)-based vector (TRV-PRCP) was used to down-regulate the expression of *PRCP*. **(B)** The expression level of *PRCP* in TRV-PRCP-treated plants was significantly reduced compared with that in control plants. **(C)** TbCSV was inoculated onto TRV-PRCP-treated and control plants 10 days after VIGS treatment. **(D)** The level of *PRCP* in TbCSV-infected and TRV-PRCP-treated plants was significantly down-regulated compared with that in TbCSV-infected and TRV-GUS-treated plants. **(E)** Detections of TbCSV DNA copy numbers in the systemic leaves harvested from the TRV-GUS plus TbCSV-inoculated plants or the TRV-PRCP plus TbCSV-inoculated plants. Significance of difference between treatments (*$p < 0.05$; **$p < 0.01$) was determined by the Student's *t*-test.

Experimental results of our study showed that the change in expression level of the target gene *PRCP* predicted by nbe-miR167b-3p was regulated by TbCSV infection. The gene mainly encodes a PRCP. PRCP proteins are defined by tandem repeats of a degenerated 35 amino acid motif (Small and Peeters, 2000). The PRCP family is one of the largest protein families in plants and there are 450 and 477 PRCP proteins in *Arabidopsis* and rice, respectively. PRCP proteins were found to play a central and broad role in modulating the expression of organelle genes. For example, delayed greening1 (*DG1*) and yellow seedling1 (*YS1*) mutants in *Arabidopsis* displayed seedling-stage-specific albino and yellow seedling phenotypes, respectively. Both *DG1* and *YS1* encode chloroplast-targeted PRCP proteins (Zhou et al., 2009; Chi et al., 2010). However, the functions of the *PRCP* gene in plant responses to virus infection still remain unknown. In this study, it was found that inhibiting expression of nbe-miR167b-3p in plants induced the up-regulation of *PRCP*, while overexpression of nbe-miR167b-3p induced *PRCP* down-regulation. Further, the knockdown of *PRCP* gene did not affect normal growth of tobacco plants, but reduced TbCSV DNA accumulation in and disease symptom development on the plants. In summary, it was demonstrated that TbCSV infection in *N. benthamiana* reduced the expression of nbe-miR167b-3p, which targeted *PRCP* genes to regulate plant development and enhanced defense of the plants against virus infection. The study did not determine the mechanism by which expression of nbe-miR167b-3p was down-regulated by TbCSV infection, or how *PRCP* affected the pathogenic mechanism of TbCSV. Further studies are necessary to examine and illustrate these mechanisms.

CONCLUSION

To conclude, results from this study showed that TbCSV down-regulated the expression of nbe-miR167b-3p in *N. benthamiana*. The silencing of nbe-miR167b-3p not only affected normal development of *N. benthamiana* plants and induced downward leaf curling, but also aggravated the viral symptoms and increased the accumulation of TbCSV in *N. benthamiana* plants. On the contrary, the overexpression of nbe-miR167b-3p alleviated the symptoms of TbCSV, and reduced the accumulation of TbCSV in *N. benthamiana*. It was also proved that nbe-miR167b-3p responded to the infection of TbCSV by regulating the expression of its target gene *PRCP*. So far, there has been no report on the action of nbe-miR167b-3p on TbCSV infection.

DATA AVAILABILITY STATEMENT

The original contributions presented in the study are included in the article/**Supplementary Material**, further inquiries can be directed to the corresponding author/s.

AUTHOR CONTRIBUTIONS

RW and GW performed the vector constructions and the main experiments, data processing and analysis, and developed the research program. LW participated small RNA library construction. XW and ZL carried out the sampling and the sample processing. ML participated throughout the investigations. WT advised on the research program and revised the manuscript. LQ conceived the study and revised the manuscript. All authors contributed to the article and approved the submitted version.

FUNDING

This study was supported financially by the National Natural Science Founding of China (Grant No. 32072380) and the Fundamental Research Funds for the Central Universities (Grant No. XDJK2020B063).

ACKNOWLEDGMENTS

We are grateful to Xueping Zhou of the Plant Protection Institute, Chinese Academy of Agricultural Sciences for providing infectious clones of TbCSV isolate and to Yule Liu of the School of Life Sciences, Tsinghua University for providing PVX, TRV, pCVA, and pCVB vectors.

SUPPLEMENTARY MATERIAL

The Supplementary Material for this article can be found online at: https://www.frontiersin.org/articles/10.3389/fmicb.2021.791561/full#supplementary-material

REFERENCES

Ai, T., Zhang, L., Gao, Z., Zhu, C. X., and Guo, X. (2011). Highly efficient virus resistance mediated by artificial microRNAs that target the suppressor of PVX and PVY in plants. *Plant Biol. (Stuttg)* 13, 304–316. doi: 10.1111/j.1438-8677.2010.00374.x

Amin, I., Patil, B. L., Briddon, R. W., Mansoor, S., and Fauquet, C. M. (2011). A common set of developmental miRNAs are upregulated in *Nicotiana benthamiana* by diverse Begomoviruses. *Virol. J.* 8, 143. doi: 10.1186/1743-422X-8-143

Bologna, N. G., and Voinnet, O. (2014). The diversity, biogenesis, and activities of endogenous silencing small RNAs in Arabidopsis. *Annu. Rev. Plant Biol.* 65, 473–503. doi: 10.1146/annurev-arplant-050213-035728

Chi, W., Mao, J., Li, Q., Ji, D., Zou, M., Lu, C., et al. (2010). Interaction of the pentatricopeptide-repeat protein delayed greening 1 with sigma factor SIG6 in the regulation of chloroplast gene expression in *Arabidopsis* cotyledons. *Plant J.* 64, 14–25. doi: 10.1111/j.1365-313X.2010.04304.x

Cui, J., You, C., and Chen, X. (2016). The evolution of microRNAs in plants. *Curr. Opin. Plant Biol.* 35, 61–67. doi: 10.1016/j.pbi.2016.11.006

Dai, X., Zhuang, Z., and Zhao, P. X. (2018). PsRNATarget: a plant small RNA target analysis server. *Nucleic Acids Res.* 46, W49–W54. doi: 10.1093/nar/gky316

Du, J., Wu, G., Zhou, Z., Zhang, J., Li, M., Sun, M., et al. (2019). Identification of microRNAs regulated by *Tobacco curly shoot virus* co-infection with its betasatellite in *Nicotiana benthamiana*. *Virol. J.* 16:130. doi: 10.1186/s12985-019-1234-5

Du, J., Wu, R., Liu, Z., Sun, M., Ghanem, H., Li, M., et al. (2020). Suppression of nbe-miR1919c-5p expression in *Nicotiana benthamiana* enhances *Tobacco curly shoot virus* and its beta satellite co-infection. *Viruses* 12:392. doi: 10.3390/v12040392

Du, P., Wu, J., Zhang, J., Zhao, S., Zheng, H., Gao, G., et al. (2011). Viral infection induces expression of novel phased microRNAs from conserved cellular microRNA precursors. *PLoS Pathog.* 7:e1002176. doi: 10.1371/journal.ppat.1002176

Du, Z., Chen, A., Chen, W., Westwood, J. H., Baulcombe, D. C., and Carr, J. P. (2014). Using a viral vector to reveal the role of microRNA159 in disease symptom induction by a severe strain of *Cucumber mosaic virus*. *Plant Physiol.* 164, 1378–1388. doi: 10.1104/pp.113.232090

Finnegan, E. J., and Matzke, M. A. (2003). The small RNA world. *J. Cell Sci.* 116, 4689–4693. doi: 10.1242/jcs.00838

Gao, R., Wan, Z. Y., and Wong, S. M. (2013). Plant growth retardation and conserved miRNAs are correlated to Hibiscus chlorotic ringspot virus infection. *PLoS One* 8:e85476. doi: 10.1371/journal.pone.0085476

Guo, H. S., Xie, Q., Fei, J. F., and Chua, N. H. (2005). MicroRNA directs mRNA cleavage of the transcription factor NAC1 to downregulate auxin signals for Arabidopsis lateral root development. *Plant Cell* 17, 1376–1386. doi: 10.1105/tpc.105.030841

Guo, W., Wu, G., Yan, F., Lu, Y., Zheng, H., Lin, L., et al. (2012). Identification of novel *Oryza sativa* miRNAs in deep sequencing-based small RNA libraries of rice infected with *Rice stripe virus*. *PLoS One* 7:e46443. doi: 10.1371/journal.pone.0046443

He, X. F., Fang, Y. Y., Feng, L., and Guo, H. S. (2008). Characterization of conserved and novel microRNAs and their targets, including a TuMV-induced TIR-NBS-LRR class R gene-derived novel miRNA in *Brassica*. *FEBS. Lett.* 582, 2445–2452. doi: 10.1016/j.febslet.2008.06.011

Kidner, C. A., and Martienssen, R. A. (2005). The developmental role of microRNA in plants. *Curr. Opin. Plant Biol.* 8, 38–44. doi: 10.1016/j.pbi

Li, Z., Xie, Y., and Zhou, X. (2005). *Tobacco curly shoot virus* DNA beta is not necessary for infection but intensifies symptoms in a host-dependent manner. *Phytopathology* 95, 902–908. doi: 10.1094/PHYTO-95-0902

Lian, S., Cho, W. K., Kim, S. M., Choi, H., and Kim, K. H. (2016). Time-ocurse small RNA profiling reveals rice miRNAs and their target genes in response to *Rice stripe virus* infection. *PLoS One* 11:e0162319. doi: 10.1371/journal.pone.0162319

Liu, N., Wu, S., Van, Houten, J., Wang, Y., Ding, B., et al. (2014). Down-regulation of auxin response factors 6 and 8 by microRNA167 leads to floral development defects and female sterility in tomato. *J. Exp. Bot.* 65, 2507–2520. doi: 10.1093/jxb/eru141

Maghuly, F., Ramkat, R. C., and Laimer, M. (2014). Virus versus host plant microRNAs: who determines the outcome of the interaction? *PLoS One* 4:e98263. doi: 10.1371/journal.pone.0098263

Palatnik, J. F., Allen, E., Wu, X., Schommer, C., Schwab, R., Carrington, J. C., et al. (2003). Control of leaf morphogenesis by microRNAs. *Nature* 425, 257–263. doi: 10.1038/nature01958

Phookaew, P., Netrphan, S., Sojikul, P., and Narangajavana, J. (2014). Involvement of miR164- and miR167-mediated target gene expressions in responses to water deficit in cassava. *Biol. Plant.* 58, 469–478. doi: 10.1007/s10535-014-0410-0

Rodríguez-Negrete, E. A., Sánchez-Campos, S., Cañizares, M. C., Navas-Castillo, J., Moriones, E., Bejarano, E. R., et al. (2014). A sensitive method for the quantification of virion-sense and complementary-sense DNA strands of circular single-stranded DNA viruses. *Sci. Rep.* 4:6438. doi: 10.1038/srep06438

Romanel, E., Silva, T. F., Corrêa, R. L., Farinelli, L., Hawkins, J. S., Schrago, C. E., et al. (2012). Global alteration of microRNAs and transposon-derived small RNAs in cotton (*Gossypium hirsutum*) during Cotton leafroll dwarf polerovirus (CLRDV) infection. *Plant Mol. Biol.* 80, 443–460. doi: 10.1007/s11103-012-9959-1

Schmittgen, T. D., and Livak, K. J. (2008). Analyzing real-time PCR data by the comparative C(T) method. *Nat. Protoc.* 3, 1101–1108. doi: 10.1038/nprot.2008.73

Small, I. D., and Peeters, N. (2000). The PPR motif- a TPR-related motif prevalent in plant organellar proteins. *Trends Biochem. Sci.* 25, 46–47. doi: 10.1016/s0968-0004(99)01520-0

Tang, Y., Wang, F., Zhao, J., Xie, K., Hong, Y., and Liu, Y. (2010). Virus-based microRNA expression for gene functional analysis in plants. *Plant Physiol.* 153, 632–641. doi: 10.1104/pp.110.155796

Tong, A., Yuan, Q., Wang, S., Peng, J., Lu, Y., Zheng, H., et al. (2017). Altered accumulation of osa-miR171b contributes to *Rice stripe virus* infection by regulating disease symptoms. *J. Exp. Bot.* 68, 4357–4367. doi: 10.1093/jxb/erx230

Voinnet, O. (2005). Non-cell autonomous RNA silencing. *FEBS Lett.* 579, 5858–5871. doi: 10.1016/j.febslet

Wang, B., Wang, L., Chen, F., Yang, X., Ding, M., Zhang, Z., et al. (2016). MicroRNA profiling of the whitefly *Bemisia tabaci* Middle East-Aisa Minor I following the acquisition of *Tomato yellow leaf curl China virus*. *Virol. J.* 13:20. doi: 10.1186/s12985-016-0469-7

Wang, S., Cui, W., Wu, X., Yuan, Q., Zhao, J., Zheng, H., et al. (2018). Suppression of nbe-miR166h-p5 attenuates leaf yellowing symptoms of *Potato virus X* on *Nicotiana benthamiana* and reduces virus accumulation. *Mol. Plant Pathol.* 19, 2384–2396. doi: 10.1111/mpp.12717

Wang, S. T., Sun, X. L., Hoshino, Y., Yu, Y., Jia, B., Sun, Z. W., et al. (2014). MicroRNA319 positively regulates cold tolerance by targeting OsPCF6 and OsTCP21 in rice (*Oryza sativa* L.). *PLoS One* 9:e91357. doi: 10.1371/journal.pone.0091357

Wu, J., Yang, R., Yang, Z., Yao, S., Zhao, S., Wang, Y., et al. (2017). ROS accumulation and antiviral defence control by microRNA528 in rice. *Nat. Plants* 3:16203. doi: 10.1038/nplants

Wu, J., Yang, Z., Wang, Y., Zheng, L., Ye, R., Ji, Y., et al. (2015). Viral-inducible Argonaute18 confers broad-spectrum virus resistance in rice by sequestering a host microRNA. *eLife* 4:e05733. doi: 10.7554/eLife.05733

Xia, Z., Zhao, Z., Gao, X., Jiao, Z., Wu, Y., Zhou, T., et al. (2019). Characterization of maize miRNAs in response to synergistic infection of *Maize chlorotic mottle virus* and *Sugarcane mosaic virus*. *Int. J. Mol. Sci.* 20:3146. doi: 10.3390/ijms20133146

Xu, D., Mou, G., Wang, K., and Zhou, G. (2014). MicroRNAs responding to *Southern rice black-streaked dwarf virus* infection and their target genes associated with symptom development in rice. *Virus Res.* 190, 60–68. doi: 10.1016/j.virusres

Xu, X., Zhang, Q., Hong, J., Li, Z., Zhang, X., and Zhou, X. (2019). Cryo-EM structure of a Begomovirus geminate particle. *Int. J. Mol. Sci.* 20:1738. doi: 10.3390/ijms20071738

Yan, F., Guo, W., Wu, G., Lu, Y., Peng, J., Zheng, H., et al. (2014). A virus-based miRNA suppression (VbMS) system for miRNA loss-of-function analysis in plants. *Biotechnol. J.* 9, 702–708. doi: 10.1002/biot.201300523

Yang, J., Zhang, F., Li, J., Chen, J. P., and Zhang, H. M. (2016). Integrative Analysis of the microRNAome and transcriptome illuminates the response of susceptible rice Plants to *Rice rtripe virus*. *PLoS One* 11:e0146946. doi: 10.1371/journal.pone.0146946

Zhang, B., Wang, Q., and Pan, X. (2007). MicroRNAs and their regulatory roles in animals and plants. *J. Cell Physiol.* 210, 279–289. doi: 10.1002/jcp.20869

Zhang, C., Ding, Z., Wu, K., Yang, L., Li, Y., Yang, Z., et al. (2016). Suppression of jasmonic acid-mediated defense by viral-inducible microRNA319 facilitates virus infection in rice. *Mol. Plant.* 9, 1302–1314. doi: 10.1016/j.molp.2016.06.014

Zhou, W., Cheng, Y., Yap, A., Chateigner-Boutin, A. L., Delannoy, E., Hammani, K., et al. (2009). The Arabidopsis gene YS1 encoding a DYW protein is required for editing of rpoB transcripts and the rapid development of chloroplasts during early growth. *Plant J.* 58, 82–96. doi: 10.1111/j.1365-313X.2008.03766.x

Zorzatto, C., Machado, J. P., Lopes, K. V., Nascimento, K. J., Pereira, W. A., Brustolini, O. J., et al. (2015). NIK1-mediated translation suppression functions as a plant antiviral immunity mechanism. *Nature* 520, 679–682. doi: 10.1038/nature14171

Conflict of Interest: The authors declare that the research was conducted in the absence of any commercial or financial relationships that could be construed as a potential conflict of interest.

Publisher's Note: All claims expressed in this article are solely those of the authors and do not necessarily represent those of their affiliated organizations, or those of the publisher, the editors and the reviewers. Any product that may be evaluated in this article, or claim that may be made by its manufacturer, is not guaranteed or endorsed by the publisher.

frontiers in Microbiology

ORIGINAL RESEARCH
published: 04 January 2022
doi: 10.3389/fmicb.2021.780724

Nuclear Exportin 1 (XPO1) Binds to the Nuclear Localization/Export Signal of the Turnip Mosaic Virus NIb to Promote Viral Infection

Mingzhen Zhang[1†], Pan Gong[1†], Linhao Ge[1†], Yinzi Li[2,3], Zhaoyang Chang[1], Rui Qiao[1], Xueping Zhou[1,4], Aiming Wang[2,3] and Fangfang Li[1]**

[1] State Key Laboratory for Biology of Plant Diseases and Insect Pests, Institute of Plant Protection, Chinese Academy of Agricultural Sciences, Beijing, China, [2] London Research and Development Centre, Agriculture and Agri-Food Canada, London, ON, Canada, [3] Department of Biology, Western University, London, ON, Canada, [4] State Key Laboratory of Rice Biology, Institute of Biotechnology, Zhejiang University, Hangzhou, China

The nuclear localization signal (NLS) and nuclear export signal (NES) are key signatures of proteins for controlling nuclear import and export. The NIb protein of turnip mosaic virus (TuMV) is an RNA-dependent RNA polymerase (RdRP) that is absolutely required for viral genome replication. Previous studies have shown that NIb is a nucleocytoplasmic shuttling protein and contains four putative NES and four putative NLS motifs. Here, we analyzed the function of these NESs and NLSs, and identified two functional NESs and one functional NLS. Mutation of the identified functional NESs or NLS inhibited viral RNA accumulation and systemic infection. Exportin 1 (XPO1) is a nuclear export receptor that binds directly to cargo proteins harboring a leucine-rich NES and translocates them to the cytoplasm. We found that XPO1 contains two NIb-binding domains, which recognize the NLS and NES of NIb, respectively, to mediate the nucleocytoplasmic transport of NIb and promote viral infection. Taken together, these data suggest that the nucleocytoplasmic transport of NIb is modulated by XPO1 through its interactions with the functional NLS and NES of NIb to promote viral infection.

Keywords: nuclear localization signal (NLS), nuclear export signal (NES), NIb, turnip mosaic virus (TuMV), exportin 1 (XPO1)

OPEN ACCESS

Edited by:
Elvira Fiallo-Olivé, Institute of Subtropical and Mediterranean Horticulture La Mayora, Spain

Reviewed by:
Fernando Ponz, Instituto Nacional de Investigación y Tecnología Agroalimentaria (INIA), Spain
Jared May, University of Missouri–Kansas City, United States

****Correspondence:***
Aiming Wang
aiming.wang@AGR.GC.CA
Fangfang Li
lifangfang@caas.cn

[†] These authors have contributed equally to this work

Specialty section:
This article was submitted to Microbe and Virus Interactions with Plants, a section of the journal Frontiers in Microbiology

Received: *21 September 2021*
Accepted: *08 November 2021*
Published: *04 January 2022*

Citation:
Zhang M, Gong P, Ge L, Li Y, Chang Z, Qiao R, Zhou X, Wang A and Li F (2022) Nuclear Exportin 1 (XPO1) Binds to the Nuclear Localization/Export Signal of the Turnip Mosaic Virus NIb to Promote Viral Infection. Front. Microbiol. 12:780724. doi: 10.3389/fmicb.2021.780724

INTRODUCTION

Nuclear import and export that govern substrate exchange between the nucleus and the cytoplasm are crucial processes in any eukaryotic cell. The nucleocytoplasmic transport depends on a network of proteins that shuttle between the nucleus and cytoplasm, allowing substrate exchange through the nuclear pore complex (NPC). The NPC is a large, multi-subunit structure of ∼110–125 MDa in metazoans and consists of 8–64 copies of about 34 different nuclear pore proteins (Knockenhauer and Thomas, 2016; Lin et al., 2016; Ungricht and Ulrike, 2017; Shen et al., 2021). The plant NPC has similar structure and components to metazoans or yeast (Tamura et al., 2010; Tamura and Hara-Nishimura, 2013). The NPC permits passive diffusion of ions and small molecules up to 9 nm in diameter or up to 70 kDa for globular proteins to gain access to the nucleus (Görlich and Kutay, 1999). However, this diffusion is reasonably fast only for proteins of up to 20–30 kDa, and molecules

and multimolecular complexes larger than 60 kDa must rely exclusively on energy-driven (active) mechanisms that are facilitated by a nuclear localization signal (NLS) or a nuclear export signal (NES) (Görlich and Kutay, 1999; Weis, 2003; Merkle, 2011).

The "classical" active nuclear import pathway begins with a pair of nuclear import receptors importin α and importin β and is ferried across the pore (Meier, 2005; Shen et al., 2021). In the cytoplasm, the importin α/β heterodimer using the NLS-binding region of importin α binds to a protein containing NLS. This trimeric complex is docked to the cytoplasmic face of the NPC and targeted to its core through the affinity of importin β for the NPC components (Nigg, 1997). Translocation into the nucleus requires recruitment of the GTP-bound small GTPase Ran (Ran-GTP) to importin β, which causes the disassembly of the import complex and releases the cargo. Furthermore, the complex of importin β and Ran-GTP is transported back to the cytoplasm, whereas importin α is recycled (Shen et al., 2021). In addition to the members of the importin (Imp) superfamily, an ever-expanding repertoire of Imp-independent nuclear import pathways/mechanisms such as the calcium-binding protein calmodulin or through direct binding to the components of the NPC has been found (Wagstaff and Jans, 2009). For nuclear export, nuclear export receptors such as exportin 1 (XPO1) [also known as chromosome maintenance region 1 (CRM1)] have been identified in different eukaryotic organisms to export substrates from the nucleus to the cytoplasm by targeting the cargo's NES. During the export process, Ran-GTP in the nucleus stimulates binding of XPO1 to the export substrate. After translocation through the NPC, the XPO1/Ran-GTP/cargo protein complex is disassembled following dissociation of Ran-GTP that is hydrolyzed to Ran-GDP (Krichevsky et al., 2006). The exported molecule is released into the cytoplasm, XPO1 is recycled back to the nucleus and Ran-GDP is directed to the nuclear import cycle (Meier, 2005). Although the XPO1-dependent nucleocytoplasmic shuttling is the best-characterized nuclear export pathway, XPO1-independent pathways have been proposed for the nuclear export of various proteins. For example, the nuclear export of the African swine fever virus p37 protein is mediated by both the XPO1-dependent and XPO1-independent nuclear export pathways. Two signals responsible for the XPO1-mediated nuclear export of p37 protein were identified at the N terminus of the protein, and an additional signal was identified at the C-terminal region, which mediates the XPO1-independent nuclear export (Eulálio et al., 2006).

The nucleocytoplasmic shuttling of viral proteins is implicated in virus infections of metazoans (Weidman et al., 2003). The phosphoprotein (P) of human parainfluenza virus type 2 containing a functional NLS and an XPO1-dependent NES is a nucleocytoplasmic shuttling protein and its nucleocytoplasmic transport appears important for efficient viral polymerase activity (Ohtsuka et al., 2019). Many plant virus proteins also contain NLS and NES motifs that usually play multiple functional roles during infection (Krichevsky et al., 2006). For example, the N-terminal basic amino acid cluster $_4$KRNKGGKKSR$_{13}$ in the beet black scorch virus (BBSV) capsid protein (CP) is essential for its nuclear localization. The BBSV CP interacts with the nuclear import factor importin α, raising the possibility that the nuclear import of CP is mediated by importin α (Zhang et al., 2011). It has been postulated that nuclear-cytosolic transport pathways may be exploited by diverse viruses to facilitate replication and systemic infection (Weidman et al., 2003; Krichevsky et al., 2006). For instance, the monopartite geminivirus, tomato yellow leaf curl Java virus (ToLCJAV) encodes the nuclear shuttle protein V1, which could transport the genomic DNA between the nucleoplasm and the cytoplasm (Sharma and Ikegami, 2009). The P20 protein of bamboo mosaic potexvirus satRNA (satBaMV) interacts with the nucleolar protein fibrillarin and the interaction prompts the movement of satBaMV via the fibrillarin-satBaMV-P20 ribonucleoprotein complex in phloem-mediated systemic trafficking (Chang et al., 2016).

Potyviruses adopt polyprotein processing and RNA polymerase slippage-derived viral subpopulation as their genome expression strategy (Yang et al., 2021). Among the 11 known viral proteins, the nuclear inclusion protein b (NIb) is a well-established nuclear-located protein and contains the RNA-dependent RNA polymerase domain absolutely required for viral genome replication (Shen et al., 2020). Potyviral replication is a complex and sophisticated process that occurs in cytoplasmic membrane-bound virus replication complexes (VRCs), which consists of several viral proteins such as NIb and many host factors. To date, many nucleus-localized viral proteins and host factors have been also identified to play essential functional roles in VRCs of other plant RNA viruses, and interestingly, these VRCs are often present in dense masses adjacent to the nucleus (Krichevsky et al., 2006; Nagy and Pogany, 2011; Wang, 2015). Recently, we have shown that XPO1 is involved in the formation of the VRCs of TuMV by interacting with NIb to facilitate nuclear export of viral and host proteins to the VRCs and promote viral RNA replication (Zhang et al., 2021). In this study, we further identified the functional NLS and NES motifs of NIb, which enable NIb shuttling between the nucleus and the cytoplasm. We found that the NLS and NES motifs of NIb could directly bind to the N-terminal importin-beta and C-terminal CRM1 domain of NbXPO1a to regulate the nuclear import and export of NIb and viral RNA accumulation. Our data suggest that XPO1 has an important role in the nucleocytoplasmic transport of NIb by recognizing its NLS and NES to support potyviral infection.

RESULTS

Functional Analysis of the Putative Nuclear Export Signal of NIb

To characterize the nuclear export activity of TuMV NIb, we employed "LocNES"[1] and "NESmapper"[2] to predict its potential NES (Kosugi et al., 2014; Xu et al., 2015). The analysis resulted in the identification of four putative NIb NES motifs, and the four putative NIb NES motifs were named NESa-d (**Figure 1**). We then cloned each of them into the vector that contains YFP tag

[1]http://prodata.swmed.edu/LocNES/LocNES.php

[2]http://sourceforge.net/projects/nesmapper

A

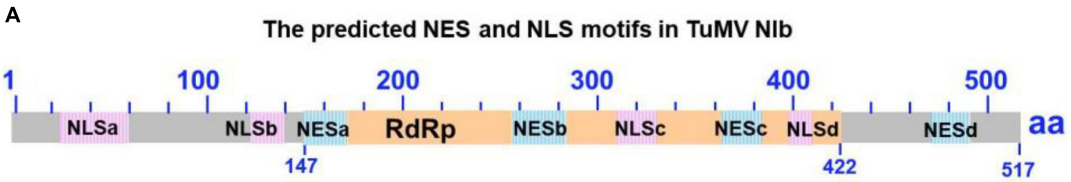

B

Name	Predicted sequences	Position (aa)	Cloned sequence position (aa)
NIb-NESa	LKQSCERLFLGKMGV	153-167	153-195
NIb-NESb	SPYLINAVLNIRLGF	258-272	258-297
NIb-NESc	YEYILDTMADNFREL	363-377	363-402
NIb-NESd	KAPYIAETALRKLYL	473-487	473-518
NIb-NLSa	KHTVKGKCQMFDLYLKLHDEAREYFQ PMLGQY	29-60	29-60
NIb-NLSb	YKGKKK	133-138	133-160
NIb-NLSc	KKFK	304-307	304-337
NIb-NLSd	HKRE	401-404	401-434
NIb-mNESb	SPYWWNAVWNIRWGW	258-272	258-297
NIb-mNESc	YEYWWDTWADNWREW	363-377	363-402
NIb-mNLSc	AAFA	304-307	304-337

FIGURE 1 | Sequence analysis of the turnip mosaic virus (TuMV) NIb protein. **(A)** Predicted TuMV NIb nuclear export signal (NES) and nuclear import signal (NLS) motifs are indicated by blue boxes and pink boxes in the NIb sequence. The RNA-dependent RNA polymerase (RdRP) domain is highlighted by the yellow box. **(B)** Detailed sequence information of the putative NIb NES and NLS motifs. For the mutation of NESs, mNESb or mNESc, tryptophan (Trp, W) was instead of Φ (L, I, V, M, or F) (These mutations are indicated in red). For the mNLSc, the three basic amino acids lysine (K) were replaced with alanine (A) (red).

and conducted an agroinfiltration-mediated transient expression assay in the transgenic *Nicotiana benthamiana* plants that stably express red fluorescent proteins fused to histone 2B (RFP-H2B) to evaluate their nuclear export ability (Martin et al., 2009; Anderson et al., 2018). Upon translation, RFP-H2B targets the nucleus and serves as a nuclear marker. The estimated molecular weight of NES (a, b, c and d)-YFP fusions is 36.47, 36.32, 36.5, 36.8 KDa, respectively, and protein expression of the above fused constructs was confirmed by Western blot (**Supplementary Figure 1**). The fluorescence (green) emitted by NES-YFP fusion proteins was visualized under a confocal microscope at 32 h post infiltration (hpi). Since NPC permits passage of ions and small molecules (usually 20 to 30 kDa) with a maximal size of ∼60 kDa (Nigg, 1997; Eibauer et al., 2015), YFP (∼26 kDa) alone (which does not contain any known NLS or NES) was distributed in both the nucleus and the cytoplasm (**Figure 2A**). NIb-YFP (∼84 kDa) containing potential NES and NLS was also distributed in both the nucleus and cytoplasm (**Figure 2A**), suggesting active nuclear-cytoplasmic transport does exist for NIb. NESa- and NESd- YFP fusions were also found in the nucleus and cytoplasm. In contrast, NESb- and NESc- YFP fusions were predominantly present in the cytoplasm and did not accumulate in the nucleus. Based on these data, we conclude that the putative NIb NESb and NESc are authentic NESs.

It is known that the proteins are produced in the cytoplasm, and many small proteins (usually 20–30 kDa) are often incorporated in the nucleus, and afterward they are translocated back to the cytoplasm under the guidance of NES. To demonstrate whether NESb- and NESc-YFP fusions do also enter the nucleus and then shuttle back to the cytoplasm, we applied the inhibitor of nuclear export, leptomycin B (LMB) (Sun et al., 2013), to analyze the dynamic subcellular localization of NESb-YFP and NESc-YFP. The treatment of LMB inhibited the nuclear export of NESb- and NESc-YFP (**Supplementary Figures 2A,B**) and significantly increased the fluorescence intensity of NESb-YFP and NESc-YFP in the nucleus (**Supplementary Figure 2C**), confirming the nuclear export function of NES2 and NES3.

The putative NESb sequence of TuMV NIb is consistent with the "classical NES consensus amino acid sequence": Φ–X2,3–Φ–X2,3–Φ–X–Φ, where Φ represents leucine (Leu, L), isoleucine (Ile, I), valine (Val, V), methionine (Met, M), or phenylalanine (Phe, F), and X2,3 represents any two or three amino acids (Dong et al., 2009). The putative NESc sequence of TuMV NIb is consistent with the "Class 3 NESs pattern" (Kosugi et al., 2008): Φ–X2–Φ–X3–Φ–X2–Φ (Φ: L, I, V, M, or F, X2: any two amino acids, X3: any three amino acids). We created point mutations to further characterize the nuclear export function of NESb and NESc. Mutants mNESb and mNESc were generated to

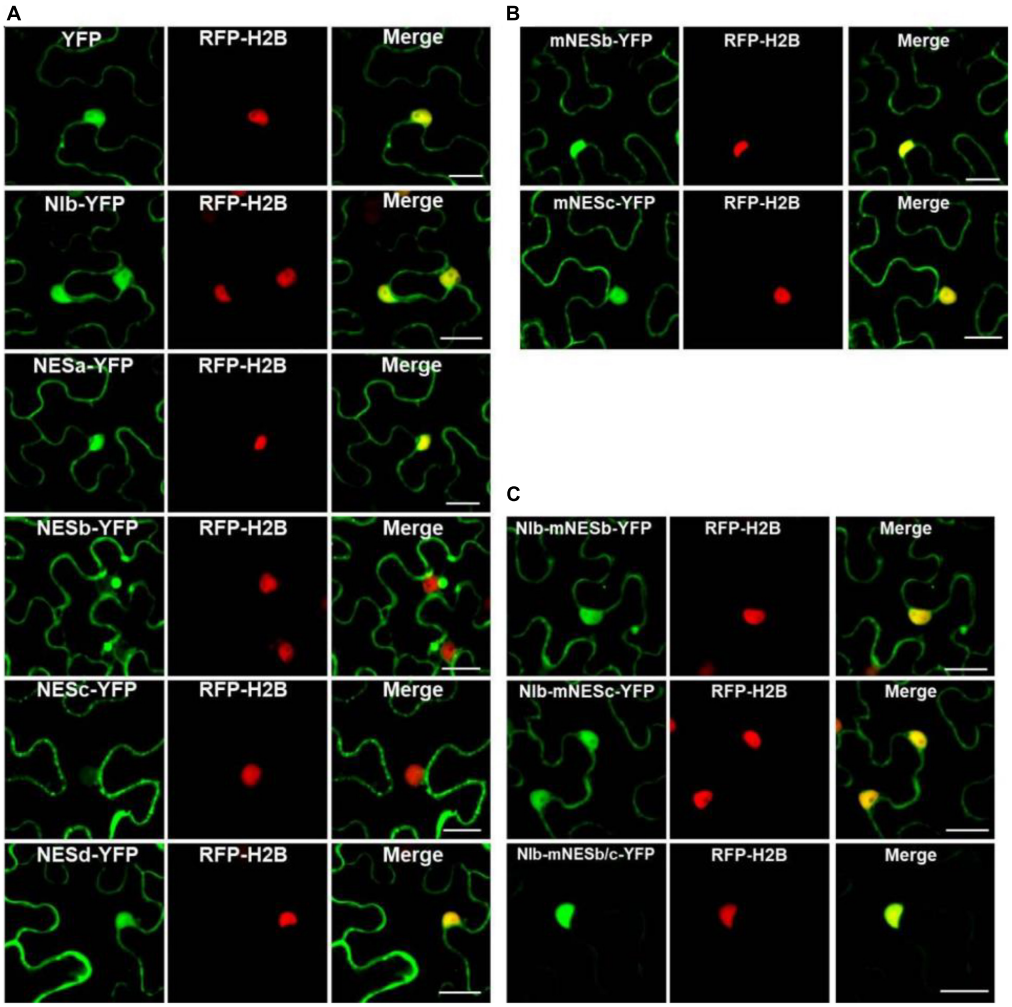

FIGURE 2 | Analyses of the putative NESs of NIb. **(A,B)** Localization of the four putative NIb NESs. Four predicted sequences of the NIb NES (NESa, NESb, NESc, and NESd) domains and the mutated NESb (mNESb) and NESc (mNESc) sequences (**Figure 1B**) were fused to the YFP tagged vector. *Agrobacterium* cultures carrying YFP (as a control), NESa-YFP, NESb-YFP, NESc-YFP, NESd-YFP, mNESb-YFP or mNESc-YFP and NIb-YFP were infiltrated onto RFP-H2B (as a nuclear marker, red) transgenic *Nicotiana benthamiana* plants, and fluorescence (green) was visualized at 32 h post infiltration (hpi). YFP and NIb-YFP were distributed in both the nucleus and cytoplasm, and the putative NESa and NESd that fused with YFP had subcellular localizations similar to YFP. The putative NESb and NESc domains that fused YFP were able to export YFP from the nucleus to the cytoplasm, but the mutated NESb and NESc domains failed to function in nuclear export. **(C)** Localization of NIb carrying the NESb mutation (NIb-mNESb), NESc mutation (NIb-mNESc), or NESb and NESc (NIb-mNESb/c). These full-length NIb mutants were fused to the YFP tagged vector and fluorescence (green) was examined at 32 hpi. The single NES mutation on NIb-YFP failed to alter the fluorescence distribution, but the double NES mutations on NIb-YFP lost its nuclear export activity. Images represent single plain micrographs and bars = 25 μm **(A–C)**.

substitute the residue Φ (L, I, V, M, or F) with tryptophan (Trp, W) (**Figure 2B**) and the resulting mutants were cloned to the vector that contains YFP tag. Confocal microscopy data showed that mNESb or mNESc lost the ability to be exported from the nucleus. Furthermore, full-length NIb derivatives harboring the corresponding NESb or NESc mutations in which residue Φ (L, I, V, M, or F) are replaced by tryptophan (Trp, W) (named NIb-mNESb or NIb-mNESc, respectively), or double mutations of NESb and NESc (NIb-mNESb/c) were engineered by overlapping PCR and specific primers (**Supplementary Table 1**). These NIb derivatives were then cloned into a YFP vector to enable fluorescence observations of their subcellular localization. As shown in **Figure 2C**, NIb-mNESb-YFP and NIb-mNESc-YFP localized in the nucleus and cytoplasm, similar to NIb-YFP, which indicated NESb and NESc can function independently. In contrast, NIb-mNESb/c-YFP only localized in the nucleus, supporting that NIb contains two functional NESs.

Functional Analysis of the Putative Nuclear Localization Signal Motifs of NIb

The NIb NLS motifs were predicted by "cNLS Mapper"[3] and "NLStradamus"[4] (Kosugi et al., 2009; Nguyen Ba et al., 2009), and the four potential NLSs (NLSa-d) were obtained (**Figure 1**).

[3]http://nls-mapper.iab.keio.ac.jp/cgi-bin/NLS_Mapper_form.cgi

[4]http://www.moseslab.csb.utoronto.ca/NLStradamus/

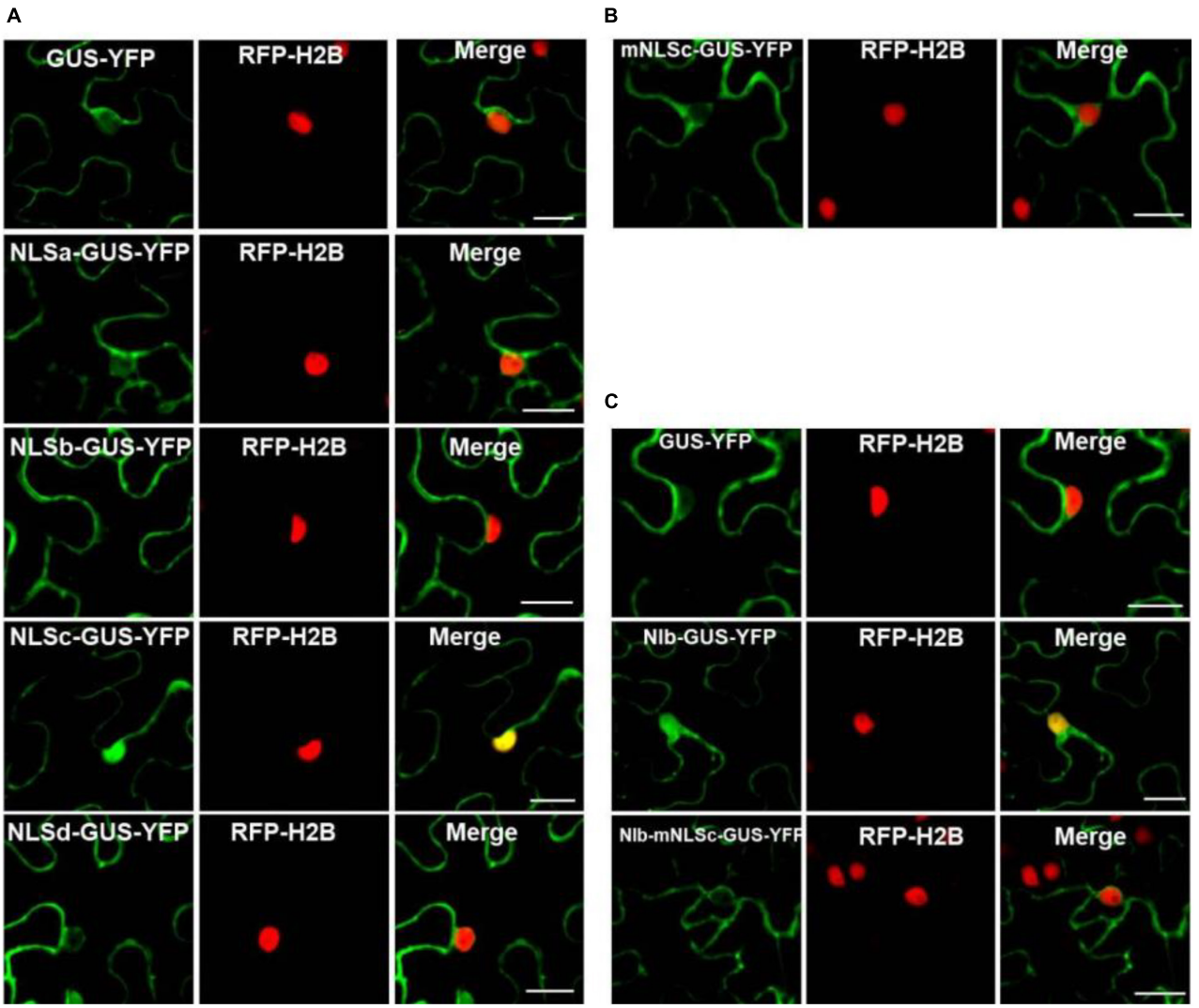

FIGURE 3 | Analyses of the putative NLSs of NIb. **(A,B)** Localization of the putative NIb NLSs. Four putative NIb NLS (NLSa, NLSb, NLSc and NLSd) sequences and the mutated NLSc (mNLSc) were fused to the GUS-YFP vector. *Agrobacterium* cultures carrying the GUS-YFP (as a control), Green fluorescence shows the localization of each protein, and fluorescence was examined at 32 hpi. **(C)** Localization of NIb and the NIb carrying NLS mutation (NIb-mNLS) fused to GUS-YFP fluorescence at 32 hpi. RFP-H2B as a nucleus marker (red). Images represent single plain micrographs and bars = 25 μm **(A–C)**.

To assess these putative NLSs, we constructed a plant expression vector to express β-glucuronidase (GUS) tagged by YFP (GUS-YFP) (∼93 kDa). As expected, GUS-YFP alone failed to localize in the nucleus because either GUS or YFP sequence lacks an efficient NLS (**Figure 3A**). Each of the four putative NLS motifs was cloned into the GUS-YFP vector for transient expression in RFP-H2B transgenic *N. benthamiana* plants and subsequent confocal microscopy analyses of nuclear import activity at 32 hpi. The GUS-YFP vector, NLSa-GUS-YFP, NLSb-GUS-YFP and NLSd-GUS-YFP all localized predominantly in the cytoplasm whereas NLSc-GUS-YFP accumulated clearly in the nucleus and cytoplasm (**Figure 3A**). These data suggest that the putative NLSa, NLSb or NLSd domain alone is not sufficient to exert the NLS function and the putative NLSc alone has strong nuclear import activity.

Classical NLSs are a short, basic amino acid-rich sequence that includes two types of NLSs. One type NLS includes 3–5 consecutive basic amino acid residues, as to K-K/R-X-K/R (K, R represents lysine, arginine respectively, X represents any amino acid), which is called monopartite NLS. The other type NLS consists of K/RK/R-X_{10-12}-K/$R_{3/5}$ (3/5 represents that three of the five consecutive amino acids are lysine or arginine), which is called bipartite NLS (Lange et al., 2007; Xu et al., 2010). The putative NLSc sequence of TuMV NIb (KKFK) is consistent with the monopartite NLS: K-K/R-X-K/R, where X represents phenylalanine (Phe, F). We further generated an NLSc mutant for a lost-function assay. Substitution of the three basic lysines (K) in NLSc with alanines (A) abolished its nuclear localization capacity (**Figure 3B**), further supporting that NIb NLSc is an authentic NLS. The expression

of NLSa-GUS-YFP, NLSb-GUS-YFP, NLSc-GUS-YFP, NLSd-GUS-YFP, and mNLSc-GUS-YFP was confirmed by Western blot assay (**Supplementary Figure 3**). Consistently, the full-length NIb derivative harboring the NLS mutations (NIb-mNLSc) only accumulated in the cytoplasm, in contrast to the nuclear and cytoplasm localization of NIb-GUS-YFP (**Figure 3C**). Therefore, we conclude that NIb has only one functional NLS.

Mapping the Nuclear Export Signals and Nuclear Localization Signal of NIb and Its Interaction Motif With XPO1

Our recent study showed that the N-terminal importin-beta (IBN_N) and the C-terminal CRM1 (CRM1_C) domain of XPO1 interacts with TuMV NIb (Zhang et al., 2021). To map the interaction motifs of NIb and XPO1, we performed yeast two-hybrid (Y2H) and bimolecular fluorescence complementation (BiFC) assays. The four putative NIb NESs, the four putative NIb NLSs and their mutants were examined for their possible interactions with NbXPO1a and two NbXPO1a truncated mutants NbXPO1a-a1 and NbXPO1a-a4 that contain the IBN_N domain and the CRM1_C domain of NbXPO1a, respectively. We found that NbXPO1a and NbXPO1a-a4 bound to NIb by interacting with one of its two NESs (NESb and NESc) but not with the NESa, NESd, mNESb or mNESc of NIb in the cytoplasm (**Figures 4A,B**). In the nucleus, NbXPO1a and NbXPO1a-a1 bound to the NIb NLSc but not to the NLSa, NLSb, NESd, mNLSc of NIb (**Figures 4A,B**). These assays revealed that the CRM1_C domain of NbXPO1a (NbXPO1a-a4) bound to the NIb NESb and NESc motifs and that the interacting pairs localized in the cytoplasm. However, only NbXPO1a and its a1 fragment including the IBN_N domain (NbXPO1a-a1) were associated with NIb NLSc in the nucleus. Together these results suggest that the two functional NESs and one functional NLS in NIb are responsible for nuclear export and import of NIb by binding to the CRM1_C domain and IBN_N domain of XPO1, respectively.

The Mutation of Functional Nuclear Export Signals and Nuclear Localization Signal of NIb Impairs Viral Infection

Based on the above findings, we renamed the putative NESb and NESc to functional NES1 and NES2, and the putative NLSc to functional NLS, respectively (**Figure 5A**). We introduced the above mutations of functional NES1, NES2, NES1 + NES2 and NLS into a TuMV-GFP infectious clone. The resulting TuMV-GFP mutants were agroinfiltrated onto *N. benthamiana* leaves, and the accumulation of viral RNA and protein was then subjected to RT-qPCR and immunoblotting analyses. At 60 hpi, in the plants agroinfiltrated with the mutant clones harboring the mutation of functional NES1, NES2, NLS, or NES1 and NES2 (mNES1 + 2) of NIb, viral RNA and protein accumulation were significantly inhibited compared to the wild type TuMV-GFP infectious clone (**Figures 5B,C**). Moreover, at 7 days post infiltration (dpi) and 20 dpi, the plants agroinfiltrated with the TuMV mutants did not display any obvious viral symptoms, and no viral RNA and protein accumulation was detectable in the systemic leaves of these plants (**Figures 5B,D,E** and **Supplementary Figure 4**). These data indicated that the functional NES1, NES2 and NLS of NIb are important for viral RNA accumulation and systemic infection.

The Interaction Domains of XPO1 With the Nuclear Export Signals and Nuclear Localization Signal of NIb Promote Viral RNA Accumulation and Infection

NbXPO1a interacts with NIb NESs and NLSs by its IBN_N domain, and CRM1_C domain, which promoted us to further investigate their functions in the context of the formation of VRCs, viral RNA accumulation and systemic infection. We conducted an agroinfiltration assay in *N. benthamiana* plants to transiently co-express the viral infectious clone TuMV-6K2-mCherry-CFP-NIb that encodes 6K2-mCherry and CFP-tagged NIb (Cheng et al., 2015) and the full-length NbXPO1a (FL) or each of the four truncated NbXPO1a including a1 (the IBN_N domain), a2 (the exportin 1-like domain, XPO1-L), a3 (an unknown function fragment downstream of a2) and a4 (the CRM1_C domain). NbXPO1a and the truncated fragments were fused with YFP at their C-terminals (**Figure 6A**). The infiltrated leaves were examined for confocal analysis, and microscope images were captured at 70 hpi. It was obvious that NbXPO1a-YFP co-localized with the VRCs which were associated with CFP-NIb- and 6K2-mCherry-stained aggregates shown as irregular structures around the nuclear periphery (**Figure 6B**). NbXPO1a-a1-YFP primarily co-localized with CFP-NIb in the nucleus, NbXPO1a-a4-YFP co-localized with CFP-NIb at the periphery of the nucleus, while no obvious co-localization was found between NbXPO1a-a2-YFP or NbXPO1a-a3-YFP with CFP-NIb. The transient over-expression of NbXPO1a-a1 and NbXPO1a-a4 increased TuMV-6K2-mCherry-CFP-NIb RNA accumulation at 70 hpi (**Figure 6C**). Consistently, transient over-expression of NbXPO1a, NbXPO1a-a1 and NbXPO1a-a4 also promoted the systemic infection and the protein accumulation of TuMV-6K2-mCherry-CFP-NIb at 16 dpi (**Figures 6D,E**). These data suggest that the IBN_N domain and the CRM1_C domain of NbXPO1a facilitate viral accumulation and systemic infection.

DISCUSSION

The potyviral RNA polymerase, NIb, is a nuclear targeting protein (Restrepo et al., 1990; Li et al., 1997; Revers and García, 2015). We functionally identified that the TuMV NIb protein contains one strong NLS and two NESs in the middle domain (**Figures 1–3**) that mediate the nucleocytoplasmic shuttling of NIb. A previous report showed that the NPC size exclusion limit is far larger than 60 kDa and depends on the structure, charges and hydrophobicity of transported molecules (Wang and Brattain, 2007). However, numerous smaller proteins are regulated via active mechanisms during nuclear entry or exit, rather than by passive diffusion through the NPC channel (Rajamäki and Valkonen, 2009). NIb is approximately 60 kDa, but its nuclear-cytosolic shuttling depends on both viral proteins and host

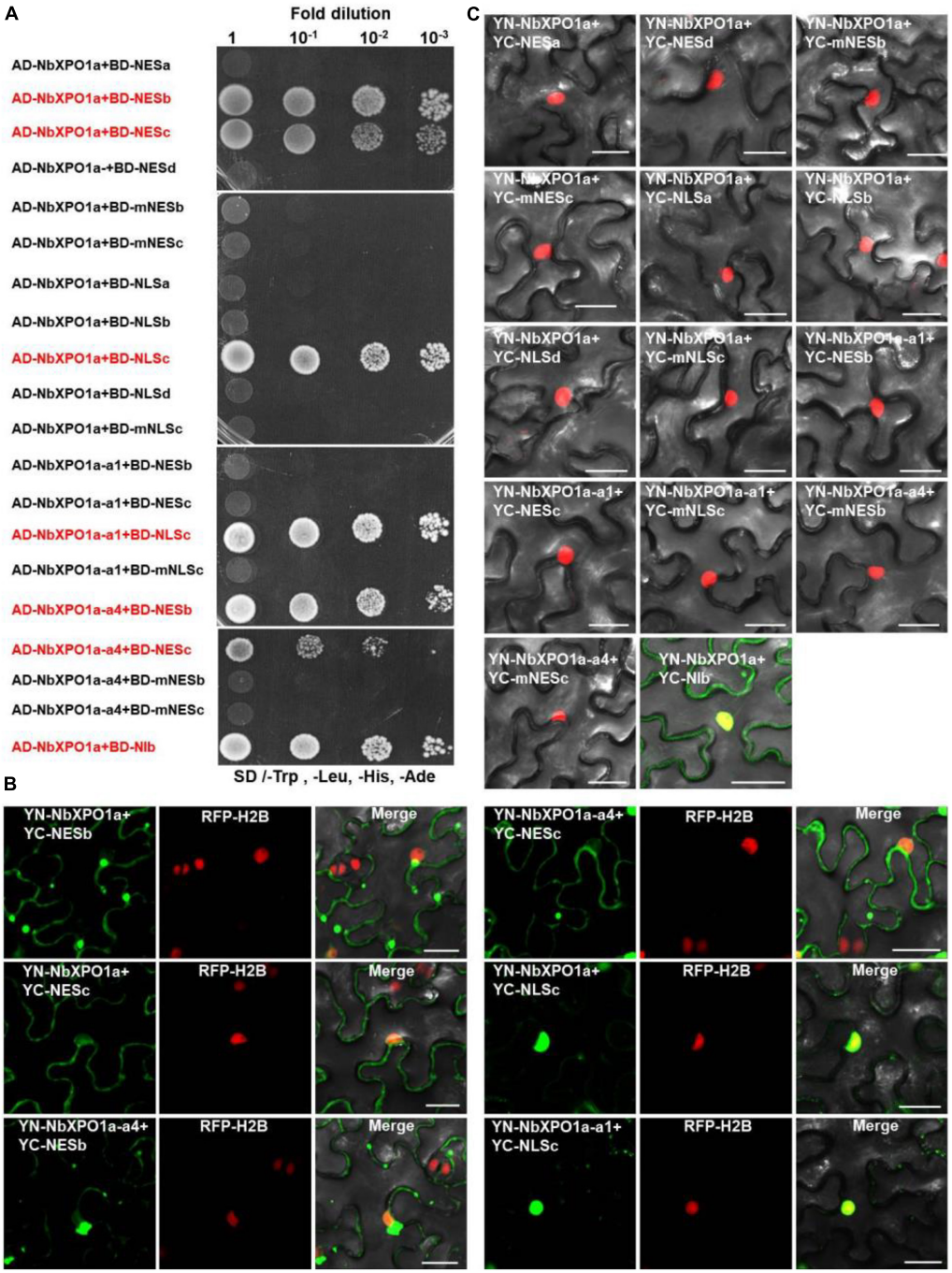

FIGURE 4 | NbXPO1a interacts with Nlb NES and NLS domains. **(A)** Y2H assays to detect interactions between NbXPO1a, the a1 and a4 fragments of NbXPO1a with the Nlb NES and NLS domains and their respective mutant sequences. NbXPO1a-a1 and NbXPO1a-a4 are two NbXPO1a deletion mutants that contain the IBN_N domain and the CRM1_C domain, respectively. Y2H Gold yeast cells harboring the indicated plasmids were co-expressed, subjected to 10-fold serial dilutions and plated on synthetic dextrose (SD)/-Trp, -Leu, -His, -Ade agar to identify protein interactions. **(B,C)** BiFC assays in RFP-H2B transgenic *N. benthamiana* (red) leaves at 32 hpi. Green fluorescence was observed as a consequence of the complementation of YN tagged NbXPO1a, and the a1 (NbXPO1a-a1) and a4 (NbXPO1a-a4) fragments of NbXPO1a with the YC tagged Nlb NES or NLS sequences and their respective mutants shown in **Figure 1B**. The yellow fluorescence results from overlapping of the green BiFC and the red RFP-H2B fluorescence. Bars = 25 μm.

receptors (**Figures 1–4**; Zhang et al., 2021). The functional NESs and NLS of Nlb are located in the RdRP domain, which is the most conservative structural domain of viral RdRPs containing the palm subdomain (Bruenn, 2003; Ferrer-Orta et al., 2015). This subdomain is comprised of five structural conservative motifs that are extremely important for viral RNA replication, such as

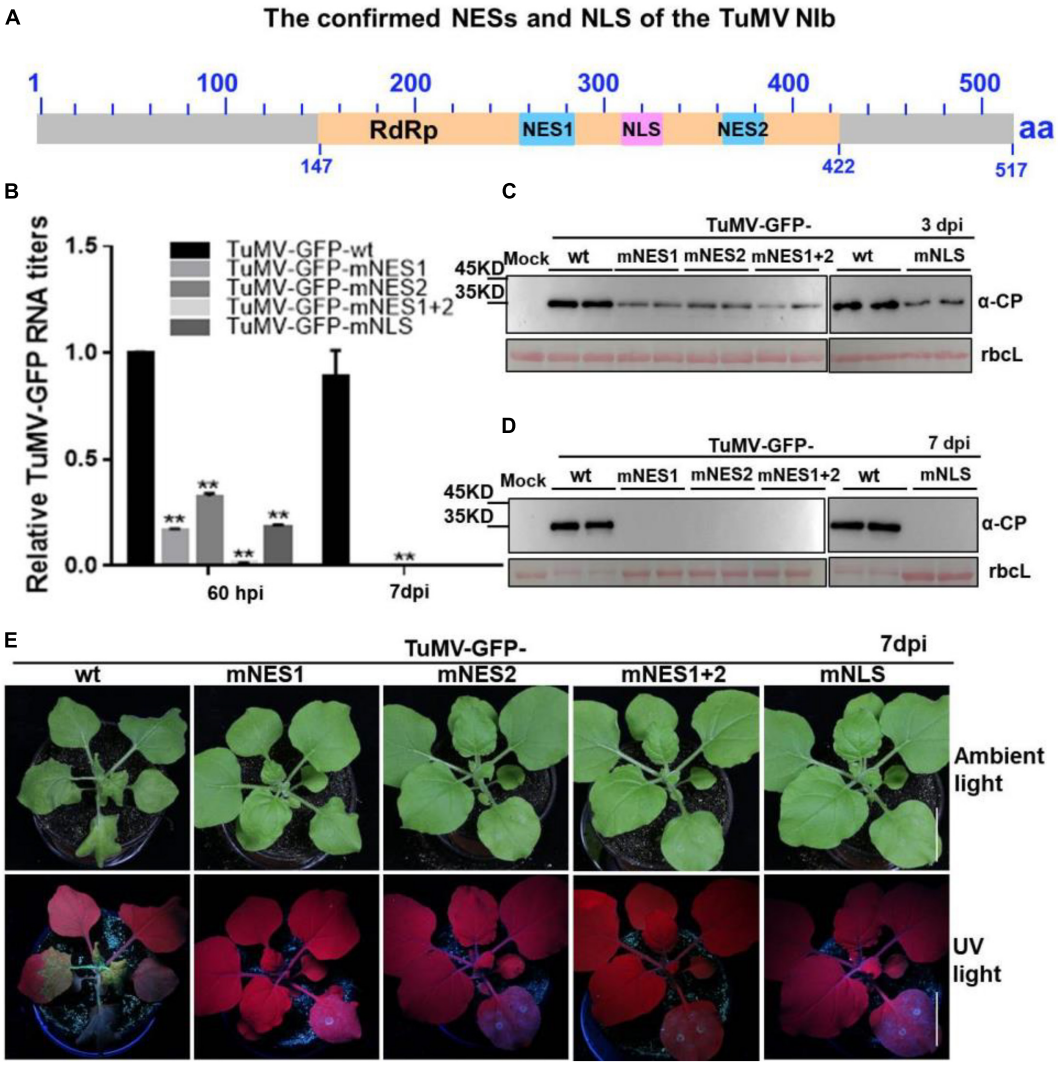

FIGURE 5 | The mutation of NESs and NLS of NIb impairs viral infection. **(A)** The confirmed NESs and NLS in this study were renamed and noted by solid blue boxes and solid pink box, respectively. RdRP, RNA-dependent RNA polymerase, was noted by yellow box. **(B–D)** The wild type (wt) TuMV-GFP infection clone, and the TuMV-GFP infection clone harboring the mutation of functional NES1, NES2, NES1 and NES2 (NES1/NES2), or NLS were infiltrated onto *N. benthamiana* leaves. At 60 hpi and 7 days post infiltration (dpi), total RNA and protein were extracted from the infiltrated leaves and systemic leaves for RT-qPCR analysis and western blot analysis **(B–D)**.Values represent means relative to the leaves infiltrated with TuMV plus Mock. Each average value was calculated by three representative replicates. The data were analyzed using Student's *t* test and double asterisks indicate $P < 0.01$. *NbActin* was used as an internal control. The large Rubisco subunit (rbcL) staining with Ponceau S showed the equal loading. **(E)** Viral symptoms and GFP fluorescence in plants inoculated with the indicated infectious clones were photographed under natural and UV light at 7 dpi.

the GDD sequence motif that is essential for RdRP activity and is a hallmark of viral RdRPs (De Farias et al., 2017; Shen et al., 2020). Of note, the TuMV NIb protein contains two functional NESs. Mutation of one of them did not affect the nuclear export of NIb, whereas mutation of both of them abolished the nuclear export capability of NIb (**Figure 2**). However, their individual mutation on the viral infections clone inhibited viral RNA accumulation and impaired viral systemic infection (**Figures 2–4**). These data demonstrate that the functional roles of the NES and NLS of NIb are not just limited to the NIb nucleocytoplasmic shuttling.

NbXPO1a contains four domains/fragments, namely (from the N-terminus), the IBN_N domain, the exportin 1-like protein (XPO1-L) domain, a fragment without any putative function and the CRM1_C domain (Zhang et al., 2021). Our previous study showed that the IBN_N and CRM1_C domains of XPO1 interact with TuMV NIb to facilitate viral infection. Here we further analyzed the interactions of NIb NESs and NLSs with XPO1 and its N-terminal and C-terminal domain. NIb NESs were found to bind to the CRM1 domain at the nuclear periphery. This finding was consistent with the fact that XPO1 mediates the nuclear export of target proteins that contain a leucine-rich NES (Fornerod et al., 1997; Fukuda et al., 1997; Ossareh-Nazari et al., 1997). Interestingly, we found that the NIb NLS bound to the IBN_N domain of

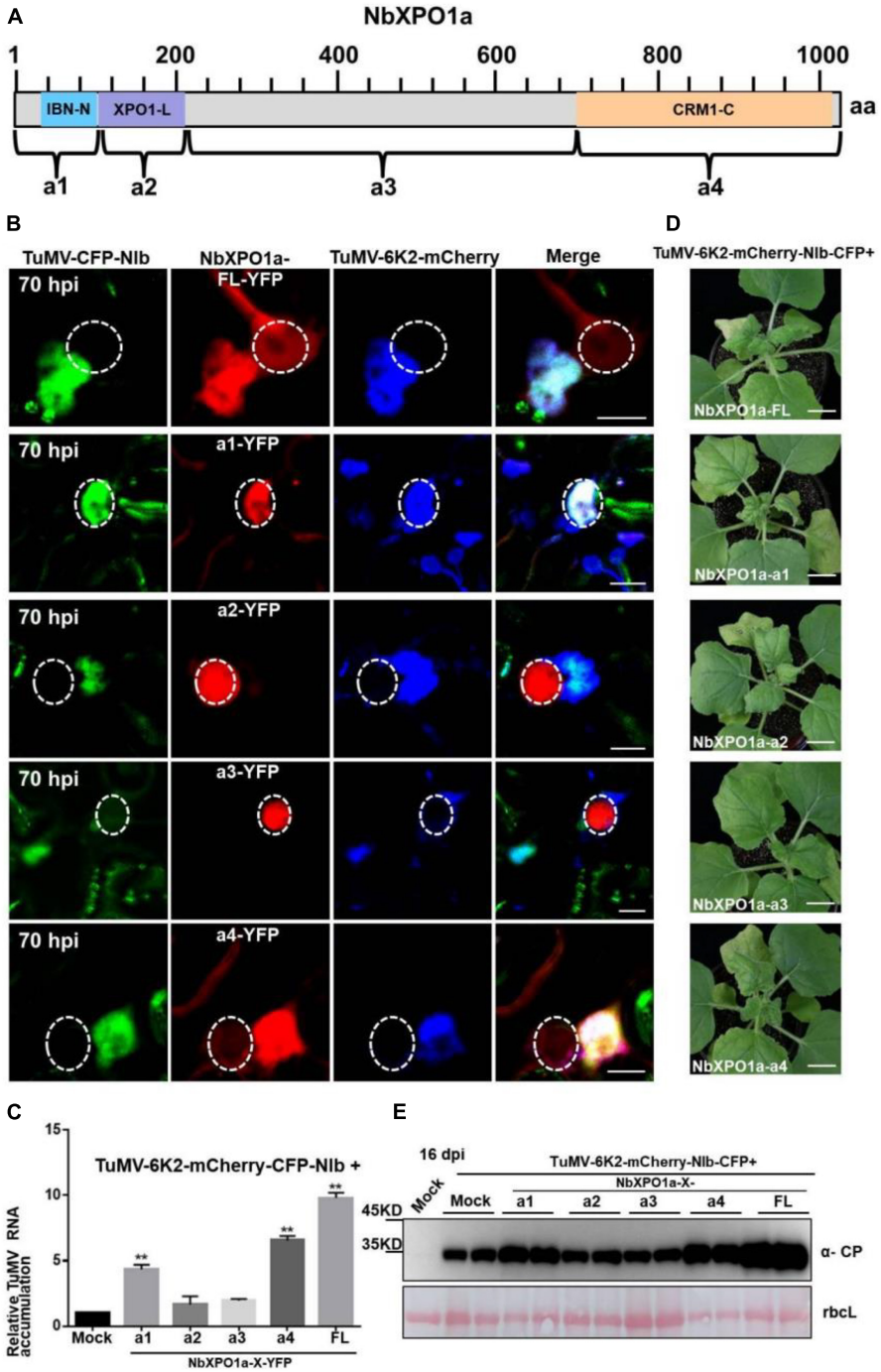

FIGURE 6 | Overexpression of the IBN_Nand CRM1_C domain of NbXPO1a facilitate viral accumulation and systemic infection. **(A)** Schematic representation of full-length NbXPO1a and four NbXPO1a fragments. **(B)** Transiently expressed YFP fusions with full-length NbXPO1a-YFP (FL), NbXPO1a-a1-YFP (a1), NbXPO1a-a2-YFP (a2), NbXPO1a-a3-YFP (a3), or NbXPO1a-a4-YFP (a4) in *N. benthamiana* leaf cells infected with TuMV-6K2-mCherry-CFP-Nlb at 70 hpi. Images represent single plain micrographs and bars = 10 μm. The region of nucleus is highlighted with a white circle. **(C)** RT-qPCR analyzed TuMV RNA levels. RNA was extracted from the infiltrated leaves as indicated in panel **(A)**. Values represent means relative to the leaves infiltrated with TuMV-6K2-mCherry-CFP-Nlb plus Mock. And each average value was calculated by three representative replicates. The data were analyzed using Student's *t* test and double asterisks indicate $P < 0.01$. *NbActin* was used as an internal control. **(D)** Viral symptoms of TuMV-6K2-mCherry-CFP-Nlb-infected *N. benthamiana* plants at 16 dpi. Transient overexpression of the full-length NbXPO1a and truncated NbXPO1a fragments in leaf cells infected with TuMV-6K2-mCherry-CFP-Nlb. Bars = 2 cm. **(E)** Western blot analysis of viral protein accumulation. Total protein was extracted from the systemic leaves indicated in panel **(C)**. Anti-TuMV CP antibodies were used, and the large Rubisco subunit (rbcL) staining with Ponceau S showed the equal loading. Mock: *N. benthamiana* plant was infiltrated with *Agrobacterium tumefaciens* culture carrying the empty vector.

XPO1 in the nucleus (**Figures 3**, **6**). Thus, the nuclear import of NIb is mediated likely via the interaction between the NIb NLS and the XPO1 IBN_N domain. Consistently, the mutated NIb NLS that failed to localize in the nucleus also lost the ability to interact with the XPO1a IBN_N domain (**Figures 3**, **4**). This result reveals that XPO1 has the nuclear import activity that is potentiated by the XPO1 IBN_N domain. Furthermore, over-expression of the IBN_N domain and CRM1_C domain of XPO1a co-localized with TuMV CFP-NIb in the nucleus and at the VRCs, respectively, and their expression increased viral RNA accumulation and systemic infection (**Figure 6**). These findings suggest that XPO1 could regulate NIb nuclear-cytosolic shuttling by its IBN domain-mediated nuclear import and its CRM1 domain-mediated nuclear export.

MATERIALS AND METHODS

Plant Materials and Growth Conditions

Nicotiana benthamiana were potted in sandy loam soil and placed in an insect-free growth chamber. The growth conditions consisted of 60% relative humidity and a day/night regime of 16 h in the light at 22°C followed by 8 h of darkness at 18°C. The transgenic RFP-H2B line was a gift of Dr. Michael M. Goodin (University of Kentucky, United States).

Information on Turnip Mosaic Virus and Its Infectious Clones

The NIb coding sequences of TuMV (nucleotides range: 7208–8758 nt; GenBank accession: NC002509) was used for the informatics and experimental analyses. TuMV-GFP infectious construct contains a GFP coding sequence that was inserted in between P1 and HC-Pro coding regions, TuMV-6K2-mCherry-CFP-NIb encodes 6K2-mCherry that was inserted in between P1 and HC-Pro coding regions and cyan fluorescent protein (CFP)-tagged NIb (Thivierge et al., 2008; Cotton et al., 2009; Cheng et al., 2017).

Plasmid Construction

Y2H constructs: AD or BD vector carrying TuMV NIb or its NLSs or NESs, NbXPO1a (Gene accession: MK935565) and its four fragments, and BiFC constructs: YN or YC carrying TuMV NIb or its NLSs or NESs, NbXPO1a and its four fragments have been described previously (Li et al., 2018; Zhang et al., 2021). Four putative NIb NESs, NLSs and their mutants were obtained by PCR using primers list in **Supplementary Table 1**. The full-length NIb derivatives harboring the NESb (NIb-mNESb), NESc (NIb-mNESc), or both the NESb and NESc (NIb-mNESb/c), or NLSc (NIb-mNLSc) mutations were engineered by overlapping PCR and specific primers (**Supplementary Table 1**). The resulting DNA fragments were purified and transferred into the entry vector pDONR221 (Invitrogen) by recombination using BP Clonase® (Invitrogen). Insertions in the resulting pDONR clones were verified by DNA sequencing and of the resulting intermediate pDONR221 cloned inserts were transferred into modified Gateway-compatible vectors including Y2H vectors, BiFC vectors and other transient expression vectors (Earley et al., 2006; Lu et al., 2010; Li et al., 2018).

For the generation of the mutated infectious clone TuMV carrying the mutation of NES1, NES2, NLS, or NES1 and NES2 (mNES1 + 2) of NIb (these NESs and NLS have been renamed based on their nuclear export and import activity), three round reactions of overlapping PCR were conducted using specific primers (**Supplementary Table 1**) and the fused PCR products were digested with restriction endonuclease *Avr*II. The digested fused PCR products were re-ligased into the pCambia2300-TuMV-GFP backbone vector in which the original fragment was removed by digestion of the same restriction enzymes. The recombinant plasmids were further confirmed by sequencing.

Agroinfiltration and Viral Inoculation

Wild type or RFP-H2B transgenic *N. benthamiana* plants at the 4 to 5 leaf stage were used for *Agrobacterium*-mediated transient expression of the recombinant binary constructs. The details of procedures as described (Li et al., 2017; Zhang et al., 2021). For TuMV infection analysis, *Agrobacterium* cultures carrying the wild type (wt) TuMV-GFP infection clone (OD_{600} = 0.5), and the TuMV-GFP infection clone harboring the mutation of NES1, NES2, NES1 and NES2 (NES1/NES2), or NLS (OD_{600} = 0.5, respectively) were infiltrated onto *N. benthamiana* leaves. Inoculated plants were photographed with a Canon 400D digital camera at various times.

RNA Extraction and RT-qPCR Analysis

Total RNA was extracted from *N. benthamiana* leaves with the RNeasy Plant Mini Kit and treated with DNase I as instructed by the manufacturer (Qiagen). Synthesis of cDNA and RT-qPCR were as described previously (Li et al., 2014). Primers used for RT-PCR are shown in **Supplementary Table 1**, and the specific primer pairs (**Supplementary Table 1**) used for RT-qPCR were designed by Primer Premier 5 software. RT-qPCR reactions were conducted and analyzed as described previously (Li et al., 2014).

Immunoblotting

TuMV-GFP infectious and its mutants that harbored the mutation of NES1, NES2, NLS, or NES1 and NES2 (mNES1 + 2) of NIb were infiltrated onto *N. benthamiana* leaves. The infiltrated leaves at 60 hpi and the newly emerged leaves at 7 dpi were collected for total protein extraction. Immunoblotting was performed with mouse monoclonal antibodies: anti-CP antibodies (1:10000). Immunoblotting of NESa-YFP, NESb-YFP, NESc-YFP, NESd-YFP, mNESb-YFP, mNESc-YFP, NLSa-YFP, NLSb-YFP, NLSc-YFP, NLSd-YFP, and mNLSc-YFP was performed with primary antibodies: anti-GFP polyclonal antibodies (1:5000; catalog number: 11814460001, Roche). Above reactions were followed by incubating with goat anti-mouse secondary antibodies obtained from Esaybio (1:5000, catalog number BE02) conjugated to horseradish peroxidase. Blotted membranes were washed thoroughly and chemiluminescence

was visualized as described by the manufacturer's protocol (ECL; GE Healthcare).

DATA AVAILABILITY STATEMENT

The original contributions presented in the study are included in the article/**Supplementary Material**, further inquiries can be directed to the corresponding authors.

AUTHOR CONTRIBUTIONS

FL designed the project. MZ, PG, LG, YL, ZC, and RQ conducted the experiments. FL, AW, and XZ wrote the manuscript. All authors analyzed the data and reviewed the manuscript.

FUNDING

This work was funded by the National Natural Science Foundation of China (31972244) to FL. The work in the Wang lab was supported Agriculture and Agri-Food Canada (AAFC) and the Natural Sciences and Engineering Research Council of Canada (NSERC).

ACKNOWLEDGMENTS

We thank Andrew O. Jackson for valuable suggestions and English editing of the manuscript. We thank Michael M. Goodin (University of Kentucky, United States) for seeds of the RFP-H2B transgenic line (Dutch and Whitfield, 2021; Verchot et al., 2021). We also thank Jianxiang Wu (Zhejiang University, China) for providing anti-TuMV CP antibodies, Yuhai Cui (AAFC) for the modified gateway vectors of pGADT7, pGBKT7, p35S-YN, and p35S-YC.

SUPPLEMENTARY MATERIAL

The Supplementary Material for this article can be found online at: https://www.frontiersin.org/articles/10.3389/fmicb.2021.780724/full#supplementary-material

REFERENCES

Anderson, G., Jang, C., Wang, R., and Goodin, M. (2018). Mapping the nuclear localization signal in the matrix protein of potato yellow dwarf virus. *J. Gen. Virol.* 99, 743–752. doi: 10.1099/jgv.0.001051

Bruenn, J. A. (2003). A structural and primary sequence comparison of the viral RNA-dependent RNA polymerases. *Nucleic Acids Res.* 31, 1821–1829. doi: 10.1093/nar/gkg277

Chang, C. H., Hsu, F. C., Lee, S. C., Lo, Y. S., Wang, J. D., Shaw, J., et al. (2016). The nucleolar fibrillarin protein is required for helper virus-independent long-distance trafficking of a subviral satellite RNA in plants. *Plant Cell* 28, 2586–2602. doi: 10.1105/tpc.16.00071

Cheng, X., Deng, P., Cui, H., and Wang, A. (2015). Visualizing double-stranded RNA distribution and dynamics in living cells by dsRNA binding-dependent fluorescence complementation. *Virology* 485, 439–451. doi: 10.1016/j.virol.2015.08.023

Cheng, X., Xiong, R., Li, Y., Li, F., Zhou, X., and Wang, A. (2017). Sumoylation of turnip mosaic virus RNA polymerase promotes viral infection by counteracting the host NPR1-mediated immune response. *Plant Cell* 29, 508–525. doi: 10.1105/tpc.16.00774

Cotton, S., Grangeon, R., Thivierge, K., Mathieu, I., Ide, C., Wei, T., et al. (2009). Turnip mosaic virus RNA replication complex vesicles are mobile, align with microfilaments, and are each derived from a single viral genome. *J. Virol.* 83, 10460–10471. doi: 10.1128/JVI.00819-09

De Farias, S. T., Dos Santos Junior, A. P., Rego, T. G., and Jose, M. V. (2017). Origin and evolution of RNA-dependent RNA polymerase. *Front. Genet.* 8:125. doi: 10.3389/fgene.2017.00125

Dong, X., Biswas, A., Suel, K. E., Martinez, R., Gu, H., and Chook, Y. M. (2009). Structural basis for leucine-rich nuclear export signal recognition by CRM1. *Nature* 458, 1136–1141. doi: 10.1038/nature07975

Dutch, R. E., and Whitfield, A. E. (2021). In memoriam: Michael M. Goodin (1967-2020). *Annu. Rev. Virol.* 8, viii–ix. doi: 10.1146/annurev-vi-08-121820-100011

Earley, K. W., Haag, J. R., Pontes, O., Opper, K., Juehne, T., Song, K., et al. (2006). Gateway-compatible vectors for plant functional genomics and proteomics. *Plant J.* 45, 616–629. doi: 10.1111/j.1365-313X.2005.02617.x

Eibauer, M., Pellanda, M., Turgay, Y., Dubrovsky, A., Wild, A., and Medalia, O. (2015). Structure and gating of the nuclear pore complex. *Nat. Commun.* 6:7532. doi: 10.1038/ncomms8532

Eulálio, A., Nunes-Correia, I., Carvalho, A. L., Faro, C., Ciovsky, V., Salas, J., et al. (2006). Nuclear export of African swine fever virus p37 protein occurs through two distinct pathways and is mediated by three independent signals. *J. Virol.* 80, 1393–1404. doi: 10.1128/JVI.80.3.1393-1404.2006

Ferrer-Orta, C., Ferrero, D., and Verdaguer, N. (2015). RNA-dependent RNA polymerases of picornaviruses: from the structure to regulatory mechanisms. *Viruses* 7, 4438–4460. doi: 10.3390/v7082829

Fornerod, M., Ohno, M., Yoshida, M., and Mattaj, I. W. (1997). CRM1 is an export receptor for leucine-rich nuclear export signals. *Cell* 90, 1051–1060. doi: 10.1016/s0092-8674(00)80371-2

Fukuda, M., Asano, S., Nakamura, T., Adachi, M., Yoshida, M., Yanagida, M., et al. (1997). CRM1 is responsible for intracellular transport mediated by the nuclear export signal. *Nature* 390, 308–311. doi: 10.1038/36894

Görlich, D., and Kutay, U. (1999). Transport between the cell nucleus and the cytoplasm. *Annu. Rev. Cell Dev. Biol.* 15, 607–660. doi: 10.1146/annurev.cellbio.15.1.607

Knockenhauer, K. E., and Thomas, U. S. (2016). The nuclear pore complex as a flexible and dynamic gate. *Cell* 164, 1162–1171. doi: 10.1016/j.cell.2016.01.034

Kosugi, S., Hasebe, M., Tomita, M., and Yanagawa, H. (2008). Nuclear export signal consensus sequences defined using a localization-based yeast selection system. *Traffic* 9, 2053–2062. doi: 10.1111/j.1600-0854.2008.00825.x

Kosugi, S., Hasebe, M., Tomita, M., and Yanagawa, H. (2009). Systematic identification of cell cycle-dependent yeast nucleocytoplasmic shuttling proteins by prediction of composite motifs. *Proc. Natl. Acad. Sci. U.S.A.* 106, 10171–10176. doi: 10.1073/pnas.0900604106

Kosugi, S., Yanagawa, H., Terauchi, R., and Tabata, S. (2014). NESmapper: accurate prediction of leucine-rich nuclear export signals using activity-based profiles. *PLoS Comput. Biol.* 10:e1003841. doi: 10.1371/journal.pcbi.1003841

Krichevsky, A., Kozlovsky, S. V., Gafni, Y., and Citovsky, V. (2006). Nuclear import and export of plant virus proteins and genomes. *Mol. Plant Pathol.* 7, 131–146. doi: 10.1111/j.1364-3703.2006.00321.x

Lange, A., Mills, R. E., Lange, C. J., Stewart, M., Devine, S. E., and Corbett, A. H. (2007). Classical nuclear localization signals: definition, function, and interaction with importin. *J. Biol. Chem.* 282, 5101–5105. doi: 10.1074/jbc.R600026200

Li, F., Huang, C., Li, Z., and Zhou, X. (2014). Suppression of RNA silencing by a plant DNA virus satellite requires a host calmodulin-like protein to repress RDR6 expression. *PLoS Pathog.* 10:e1003921. doi: 10.1371/journal.ppat.1003921

Li, F., Zhang, C., Li, Y., Wu, G., Hou, X., Zhou, X., et al. (2018). Beclin1 restricts RNA virus infection in plants through suppression and degradation of the viral polymerase. *Nat. Commun.* 9:1268. doi: 10.1038/s41467-018-03658-2

Li, F., Zhao, N., Li, Z., Xu, X., Wang, Y., Yang, X., et al. (2017). A calmodulin-like protein suppresses RNA silencing and promotes geminivirus infection by degrading SGS3 via the autophagy pathway in Nicotiana benthamiana. *PLoS Pathog.* 13:e1006213. doi: 10.1371/journal.ppat.1006213

Li, X. H., Valdez, P., Olvera, R. E., and Carrington, J. C. (1997). Functions of the tobacco etch virus RNA polymerase (NIb): subcellular transport and protein-protein interaction with VPg/proteinase (NIa). *J. Virol.* 71, 1598–1607. doi: 10.1128/JVI.71.2.1598-1607.1997

Lin, D. H., Stuwe, T., Schilbach, S., Rundlet, E. J., Perriches, T., Mobbs, G., et al. (2016). Architecture of the symmetric core of the nuclear pore. *Science* 352:aaf1015. doi: 10.1126/science.aaf1015

Lu, Q., Tang, X., Tian, G., Wang, F., Liu, K., Nguyen, V., et al. (2010). Arabidopsis homolog of the yeast TREX-2 mRNA export complex: components and anchoring nucleoporin. *Plant J.* 61, 259–270. doi: 10.1111/j.1365-313X.2009.04048.x

Martin, K., Kopperud, K., Chakrabarty, R., Banerjee, R., Brooks, R., and Goodin, M. M. (2009). Transient expression in *Nicotiana benthamiana* fluorescentmarker lines provides enhanced definition of protein localization, movement and interactions in planta. *Plant J.* 59, 150–162. doi: 10.1111/j.1365-313X.2009.03850

Meier, I. (2005). Nucleocytoplasmic trafficking in plant cells. *Int. Rev. Cytol.* 244, 95–135. doi: 10.1016/S0074-7696(05)44003-6

Merkle, T. (2011). Nucleo-cytoplasmic transport of proteins and RNA in plants. *Plant Cell Rep.* 30, 153–176. doi: 10.1007/s00299-010-0928-3

Nagy, P. D., and Pogany, J. (2011). The dependence of viral RNA replication on co-opted host factors. *Nat. Rev. Microbiol.* 10, 137–149. doi: 10.1111/tpj.14549

Nguyen Ba, A. N., Pogoutse, A., Provart, N., and Moses, A. M. (2009). NLStradamus: a simple Hidden Markov model for nuclear localization signal prediction. *BMC Bioinformatics* 10:202. doi: 10.1186/1471-2105-10-202

Nigg, E. A. (1997). Nucleocytoplasmic transport: signals, mechanisms and regulation. *Nature* 386, 779–787. doi: 10.1038/386779a0

Ohtsuka, J., Matsumoto, Y., Ohta, K., Fukumura, M., Tsurudome, M., Nosaka, T., et al. (2019). Nucleocytoplasmic shuttling of the human parainfluenza virus type 2 phosphoprotein. *Virology* 528, 54–63. doi: 10.1016/j.virol.2018.12.005

Ossareh-Nazari, B., Bachelerie, F., and Dargemont, C. (1997). Evidence for a role of CRM1 in signal-mediated nuclear protein export. *Science* 278, 141–144. doi: 10.1126/science.278.5335.141

Rajamäki, M. L., and Valkonen, J. P. (2009). Control of nuclear and nucleolar localization of nuclear inclusion protein a of picorna-like Potato virus A in Nicotiana species. *Plant Cell* 21, 2485–2502. doi: 10.1105/tpc.108.064147

Restrepo, M. A., Freed, D. D., and Carrington, J. C. (1990). Nuclear transport of plant potyviral proteins. *Plant Cell* 2, 987–998. doi: 10.1105/tpc.2.10.987

Revers, F., and García, J. A. (2015). Chapter three-molecular biology of potyviruses. *Adv. Virus Res.* 92, 101–199.

Sharma, P., and Ikegami, M. (2009). Characterization of signals that dictate nuclear/nucleolar and cytoplasmic shuttling of the capsid protein of Tomato leaf curl Java virus associated with DNA beta satellite. *Virus Res.* 144, 145–153. doi: 10.1016/j.viruses.2009.04.019

Shen, Q., Wang, Y. E., and Palazzo, A. F. (2021). Crosstalk between nucleocytoplasmic trafficking and the innate immune response to viral infection. *J. Biol. Chem.* 297:100856. doi: 10.1016/j.jbc.2021.100856

Shen, W., Shi, Y., Dai, Z., and Wang, A. (2020). The RNA-dependent RNA polymerase NIb of potyviruses plays multifunctional, contrasting roles during viral infection. *Viruses* 12:77. doi: 10.3390/v12010077

Sun, Q., Carrasco, Y. P., Hu, Y., Guo, X., Mirzaei, H., Macmillan, J., et al. (2013). Nuclear export inhibition through covalent conjugation and hydrolysis of Leptomycin B by CRM1. *Proc. Natl. Acad. Sci. U.S.A.* 110, 1303–1308. doi: 10.1073/pnas.1217203110

Tamura, K., and Hara-Nishimura, I. (2013). The molecular architecture of the plant nuclear pore complex. *J. Exp. Bot.* 64, 823–832.

Tamura, K., Fukao, Y., Iwamoto, M., Haraguchi, T., and Hara-Nishimura, I. (2010). Identification and characterization of nuclear pore complex components in *Arabidopsis thaliana*. *Plant Cell* 22, 4084–4097.

Thivierge, K., Cotton, S., Dufresne, P. J., Mathieu, I., Beauchemin, C., Ide, C., et al. (2008). Eukaryotic elongation factor 1A interacts with *Turnip mosaic virus* RNA-dependent RNA polymerase and VPg-Pro in virus-induced vesicles. *Virology 2008 Jul 20* 377, 216–225. doi: 10.1016/j.virol.2008.04.015

Ungricht, R., and Ulrike, K. (2017). Mechanisms and functions of nuclear envelope remodelling. *Nat. Rev. Mol. Cell Biol.* 18, 229–245. doi: 10.1038/nrm.2016.153

Verchot, J., Jackson, A. O., and Simon, A. E. (2021). In tribute to Michael Goodin. *Viruses* 13:78. doi: 10.3390/v13010078

Wagstaff, K. M., and Jans, D. A. (2009). Importins and beyond: non-conventional nuclear transport mechanisms. *Traffic* 10, 1188–1198. doi: 10.1111/j.1600-0854.2009.00937.x

Wang, A. (2015). Dissecting the molecular network of virus-plant interactions: the complex roles of host factors. *Annu. Rev. Phytopathol.* 53, 45–66. doi: 10.1146/annurev-phyto-080614-120001

Wang, R., and Brattain, M. G. (2007). The maximal size of protein to diffuse through the nuclear pore is larger than 60 kDa. *FEBS Lett.* 581, 3164–3170. doi: 10.1016/j.febslet.2007.05.082

Weidman, M. K., Sharma, R., Raychaudhuri, S., Kundu, P., Tsai, W., and Dasgupta, A. (2003). The interaction of cytoplasmic RNA viruses with the nucleus. *Virus Res.* 95, 75–85. doi: 10.1016/s0168-1702(03)00164-3

Weis, K. (2003). Regulating access to the genome: nucleocytoplasmic transport throughout the cell cycle. *Cell* 112, 441–451. doi: 10.1016/s0092-8674(03)00082-5

Xu, D., Farmer, A., and Chook, Y. M. (2010). Recognition of nuclear targeting signals by Karyopherin-β proteins. *Curr. Opin. Struct. Biol.* 20, 782–790. doi: 10.1016/j.sbi.2010.09.008

Xu, D., Marquis, K., Pei, J., Fu, S. C., Cağatay, T., Grishin, N. V., et al. (2015). LocNES: a computational tool for locating classical NESs in CRM1 cargo proteins. *Bioinformatics* 31, 1357–1365. doi: 10.1093/bioinformatics/btu826

Yang, X., Li, Y., and Wang, A. (2021). Research advances in potyviruses: from the laboratory bench to the field. *Annu. Rev. Phytopathol.* 59, 1–29. doi: 10.1146/annurev-phyto-020620-114550

Zhang, M., Gong, P., Ge, L., Chang, Z., Cheng, X., Zhou, X., et al. (2021). Nuclear exportin 1 facilitates turnip mosaic virus infection by exporting the sumoylated viral replicase and by repressing plant immunity. *New Phytol.* 232, 1382–1398. doi: 10.1111/nph.17657

Zhang, Y., Zhang, X., Niu, S., Han, C., Yu, J., and Li, D. (2011). Nuclear localization of beet black scorch virus capsid protein and its interaction with importin α. *Virus Res.* 155, 307–315. doi: 10.1016/j.virusres.2010.10.029

Conflict of Interest: The authors declare that the research was conducted in the absence of any commercial or financial relationships that could be construed as a potential conflict of interest.

Publisher's Note: All claims expressed in this article are solely those of the authors and do not necessarily represent those of their affiliated organizations, or those of the publisher, the editors and the reviewers. Any product that may be evaluated in this article, or claim that may be made by its manufacturer, is not guaranteed or endorsed by the publisher.

frontiers in Microbiology

ORIGINAL RESEARCH
published: 27 January 2022
doi: 10.3389/fmicb.2022.826677

Biocontrol Activity of Nonpathogenic Strains of *Fusarium oxysporum*: Colonization on the Root Surface to Overcome Nutritional Competition

Yuichiro Iida[1†], Aya Ogata[2], Hiroki Kanda[1,3], Oumi Nishi[1†], Hirotoshi Sushida[1†], Yumiko Higashi[1] and Takashi Tsuge[2†]*

[1] National Agriculture and Food Research Organization, Tsu, Japan, [2] Graduate School of Bioagricultural Sciences, Nagoya University, Nagoya, Japan, [3] Laboratory of Plant Protection and Biotechnology, Kinki University, Nara, Japan

Fusarium oxysporum is a soil-borne fungal pathogen that causes vascular wilts in a wide variety of crops. Certain nonpathogenic strains of *F. oxysporum* are known to protect crops against *F. oxysporum* pathogens. We assessed the biocontrol activities of nonpathogenic mutants of *F. oxysporum* ff. spp. *melonis* and *lycopersici* generated by disruption of the *FOW2* gene, which encodes a Zn(II)2Cys6-type transcriptional regulator essential for their pathogenicity. Pre-inoculation of melon or tomato roots with strain Δ*FOW2* conidia markedly reduced disease incidence caused by the parental wild-type strain in a concentration-dependent manner of conidial suspensions of Δ*FOW2* strains. The biocontrol effect caused by the Δ*FOW2* pre-inoculation lasted for at least 7 days. Pre-inoculation of melon roots with the wild-type or Δ*FOW2* strain of *F. oxysporum* f. sp. *lycopersici* and nonpathogenic *F. oxysporum* strain also led to biocontrol activity against *F. oxysporum* f. sp. *melonis*, indicating that the biocontrol activity of Δ*FOW2* strains is due to its nonpathogenic nature, not to the *FOW2* disfunction. Conidial germination and hyphal elongation of only the wild-type strain were inhibited on melon root surface pre-inoculated with conidia of strains nonpathogenic to melon plants. Expression of defense-related genes was not significantly induced in roots and aboveground parts of melon seedlings preinoculated with Δ*FOW2* conidia. Carbon source competition assay showed that nonpathogenic strains competed with the wild-type strain for a carbon source in soil. Strain Δ*FOW2* also competed with the oomycete pathogen *Pythium aphanidermatum* for carbon source and protected melon plants from *P. aphanidermatum*. Our results suggest that the biocontrol activity of the nonpathogenic *F. oxysporum* strains used in this study mainly depends on their extensive colonization of the root surface and outcompeting pathogens for nutrients.

Keywords: Fusarium wilt disease, biocontrol, nonpathogenic *Fusarium oxysporum*, *F. oxysporum* f. sp. *melonis*, *F. oxysporum* f. sp. *lycopersici*, pathogenicity mutant, nutrient competition, rhizosphere

OPEN ACCESS

Edited by:
Marco Scortichini, Council for Agricultural and Economics Research (CREA), Italy

Reviewed by:
Maria Aragona, Council for Agricultural and Economics Research (CREA), Italy
Rafael Jorge Leon-Morcillo, La Mayora Experimental Station, Spanish National Research Council (CSIC), Spain

****Correspondence:***
Yuichiro Iida
yuichiro.iida@setsunan.ac.jp

†Present address:
Yuichiro Iida, Laboratory of Plant Pathology, Faculty of Agriculture, Setsunan University, Hirakata, Japan
Oumi Nishi, Institute of Biological Control, Kyushu University, Fukuoka, Japan
Hirotoshi Sushida, National Agriculture and Food Research Organization, Tsukuba, Japan
Takashi Tsuge, College of Bioscience and Biotechnology, Chubu University, Kasugai, Japan

Specialty section:
This article was submitted to Microbe and Virus Interactions with Plants, a section of the journal Frontiers in Microbiology

Received: *01 December 2021*
Accepted: *04 January 2022*
Published: *27 January 2022*

INTRODUCTION

The soil-borne pathogen *Fusarium oxysporum* is a facultative fungus that causes economically important losses in a wide range of crops (Michielse and Rep, 2009; Edel-Hermann and Lecomte, 2019). Intraspecific variants of the fungus, called formae speciales (f. sp.), cause wilting symptoms (Fusarium wilt disease) on over 100 plant species. Hyphae of *F. oxysporum* penetrate the roots and invade the vascular system during the infection. Although the most practical control methods for this disease involve soil fumigation with chemicals and the use of resistant cultivars, the chemicals (e.g., trichloronitromethane and methyl bromide) have adverse effects on human and the environment, and new fungal races often emerge that can overcome resistant cultivars (Michielse and Rep, 2009). Some isolates cause Fusarium wilt disease on crops, but most strains are nonpathogenic soil saprophytes, and pretreatment of plants with some of these nonpathogenic strains often suppresses Fusarium wilt disease (Rouxel et al., 1979; Fravel et al., 2003; Alabouvette et al., 2009).

The idea of using nonpathogenic *F. oxysporum* to control Fusarium diseases came from studies of soils naturally suppressive to Fusarium wilts (Toussoun, 1975; Louvet et al., 1976). High populations of nonpathogenic *F. oxysporum* and *F. solani* in suppressive soils contribute to the suppressive effect (Rouxel et al., 1979), but nonpathogenic strains of *F. oxysporum* are much more effective than strains of other *Fusarium* species (Tamietti and Alabouvette, 1986). Interactions between pathogenic and nonpathogenic *F. oxysporum* strains in suppressive soils directly or indirectly contribute to disease control; therefore, nonpathogenic strains have been developed as biocontrol agents (Ogawa and Komada, 1984; Postma and Rattink, 1992; Alabouvette et al., 1993). Their main modes of action include competition for nutrients and trace elements in the rhizosphere and for infection sites on the root surface and induction of plant resistance (Ogawa and Komada, 1984; Postma and Luttikholt, 1996; Fuchs et al., 1997; Larkin and Fravel, 1998; Fravel et al., 2003; Alabouvette et al., 2009). These mechanisms vary in importance depending on the strain.

The endophytic strain Fo47, originally isolated from the suppressive soil, is one of the best-studied biocontrol agents (Alabouvette, 1986). Fo47 colonizes the root surface and the soil near root epidermal cells and competes for nutrients with pathogens (Larkin and Fravel, 1999; Olivain et al., 2003; Bolwerk et al., 2005). In addition, Fo47 induces plant defense responses but not via well-known defense pathways such as salicylic acid, jasmonic acid, ethylene, and pattern-triggered immunity (Constantin et al., 2019; de Lamo et al., 2020). Another well-studied nonpathogenic biocontrol strain of *F. oxysporum*, CS-20, triggers defense responses more strongly than Fo47, which correlates with CS-20 being the more potent biocontrol agent (Lemanceau et al., 1993; Larkin and Fravel, 1999; Bolwerk et al., 2005). Biocontrol strain MSA35 grows in association with a consortium of exogenous bacteria that inhibit mycelial growth and expression of pathogenicity genes in pathogenic *F. oxysporum*, and when "cured" of the bacteria, was identified as *F. oxysporum* f. sp. *lactucae* (Minerdi et al., 2008). MSA35 secretes volatile organic compounds into the soil, which reduce mycelial growth of pathogenic *F. oxysporum* strains (Minerdi et al., 2009). One of these volatiles, the sesquiterpene α-humulenone, represses the expression of pathogenicity genes in *F. oxysporum*. Thus, the biocontrol activity of nonpathogenic *F. oxysporum* strains is due to different mechanisms and sometimes to a combination of mechanisms. However, the molecular basis of the biocontrol potency of particularly effective strains is still far from being understood.

Many genes involved in pathogenicity of *F. oxysporum* have been identified (see review by Husaini et al., 2018). A mitogen-activated protein kinase (*FMK1*) (Di Pietro et al., 2001) and G protein subunits α (*FGA1*) and β (*FGB1*) (Jain et al., 2002, 2003) are required for normal germination of conidia of *F. oxysporum*. An F-box protein (*FRP1*) (Duyvesteijn et al., 2005) is indispensable for colonization on the root surface, and a putative β-1,3-glucanosyltransferase gene (*GAS1*) (Caracuel et al., 2005) appears to be essential for colony growth on solid substrates and for invasive growth in host tissue. A fungal-specific Zn(II)2Cys6-type transcriptional regulator Fow2 (Imazaki et al., 2007), is required for invasion of the root tissue and host colonization, but is dispensable for vegetative growth, conidiation, and the use of carbon sources. *FOW2* is widely conserved in formae speciales of *F. oxysporum* (Imazaki et al., 2007), whereas the genes regulated by Fow2 have not been identified. Knockout mutants of these pathogenicity genes have been reported to be nonpathogenic or have markedly reduced virulence (Di Pietro et al., 2001; Jain et al., 2002, 2003; Caracuel et al., 2005; Duyvesteijn et al., 2005; Imazaki et al., 2007). In this study, we investigated the biocontrol activity of these six mutants that have various defined characteristics at different stages of infection on the host roots. We compared the biocontrol activity of pathogenicity mutants, nonpathogenic *F. oxysporum*, and avirulent *F. oxysporum* f. sp. *lycopersici* as nonpathogenic strains against *F. oxysporum* f. sp. *melonis* after inoculation of melon plants. Hyphal growth of *F. oxysporum* strains on the root surface was observed with a confocal laser scanning microscope, and the ability of the strains to induce resistance was evaluated. The biocontrol effect of pathogenicity mutants of *F. oxysporum* was also verified against the soil-borne oomycete *Pythium aphanidermatum*, which causes damping-off and root rot diseases of cucurbitaceous plants.

MATERIALS AND METHODS

Fungal and Oomycete Strains

Fungal and oomycete strains used in this study are listed in **Table 1**. *F. oxysporum* f. sp. *melonis* strain Mel020120 and *F. oxysporum* f. sp. *lycopersici* strain CK3-1 were used as the pathogenic wild types (Namiki et al., 1994). Nonpathogenic *F. oxysporum* strain MFG6, a biocontrol agent against the strawberry pathogen *F. oxysporum* f. sp. *fragariae*, was kindly provided by Dr. Katsutoshi Kuroda (Mie Prefecture Agricultural Research Institute, Japan) (Kuroda et al., 2004). Knockout mutants and green fluorescent protein (GFP)-transformed strains were generated from these strains. For preparing conidia, strains were cultured in potato dextrose broth (PDB) (BD,

TABLE 1 | Fungal strains used in this study.

Strain	Description	References
Mel02010	*F. oxysporum* f. sp. *melonis*	Inoue et al., 2001
Mel02010-DsRed	DsRed-expressing Mel02010	
Mel02010-DsRed^{TR}	Thiophanate-methyl resistant Mel02010-DsRed	
MF2-1 and MF2-2	Δ*FOW2* Mel02010	Imazaki et al., 2007
MF2-1-GFP	GFP-expressing MF2-1	Imazaki et al., 2007
GA1 and GA2	Δ*FGA1* Mel02010	
GB1 and GB2	Δ*FGB1* Mel02010	
MK1 and MK2	Δ*FMK1* Mel02010	
RP1 and RP2	Δ*FRP1* Mel02010	
AS1 and AS2	Δ*GAS1* Mel02010	
CK3-1	*F. oxysporum* f. sp. *lycopersici*	Imazaki et al., 2007
CK3-1-GFP	GFP-expressing CK3-1	
LF2-1	Δ*FOW2* CK3-1	Imazaki et al., 2007
LF2-1-GFP	GFP-expressing LF2-1	
MFG6	Nonpathogenic *F. oxysporum* strain	Kuroda et al., 2004
MFG6-GFP	GFP-expressing MFG6	
WPy1	*Pythium aphanidermatum*	

Detroit, MI, United States) at 25°C for 3 to 4 days with shaking in the dark. The resulting conidia were collected by centrifugation, washed and resuspended in sterilized water.

The oomycete *P. aphanidermatum* stain WPy1, which causes damping-off and root rot of cucurbitaceous plants was used as a melon pathogen. Strain WPy1 isolated from watermelon was kindly provided by Dr. Masaharu Kubota (National Agriculture and Food Research Organization, Japan). For preparing oospores, the strain was statically grown in V8 broth [200 mL V8 vegetable juice (Campbell's, Camden, NJ, United States) and 3 g $CaCO_3$ per liter] at 25°C for 7 days in the dark. The resulting mycelial mats were washed with sterilized water and homogenized for 30 s in a blender (Waring, New Hartford, CT, United States). Oospores were collected by filtration through cheesecloth.

DNA was extracted from *F. oxysporum* using a NucleoMag Plant Kit (Macherey-Nagel, Düren, Germany).

Plants

Melon (*Cucumis melo* L.) cultivar Amus and tomato (*Solanum lycopersicum* L.) cultivar Ponderosa were used in inoculation tests. Seeds were sown in pots filled with fertilized granulated soil (Kumiai Nippi Engei Baido, Nihon Hiryo, Tokyo, Japan) and grown in a climate chamber at 25°C (approximately 60% relative humidity, 16 h light/8 h dark). Melon seedlings (3 weeks old) and tomato seedlings (2 weeks old) were used for inoculation tests.

Disruption of Pathogenicity Genes

Mutants of pathogenicity-related genes *FMK1*, *FGA1*, *FGB1*, *FRP1*, and *GAS1* were generated for *F. oxysporum* (**Supplementary Table 1**) using transformation-mediated gene disruption. The hygromycin B resistance gene (*hph*) cassette was amplified from pSH75 by PCR using primers PtrpC_f and TtrpC_r (**Supplementary Table 2**). The entire exon–intron regions of pathogenicity-related genes were amplified from total DNA of strain Mel02010 by PCR using respective primer sets (**Supplementary Table 2**) and cloned into the plasmid pGEM-T Easy (Promega, Fitchburg, WI, United States). These plasmids were linearized by inverse PCR using primer sets that contain a 5′ overhang sequence for overlapping with sequences at the ends of the *hph* cassette (**Supplementary Table 2**). The linearized plasmid and the *hph* cassette were combined in the In-Fusion HD EcoDry Cloning kit (Takara Bio, Shiga, Japan) and subsequently introduced into electrocompetent *Escherichia coli* DH5α (Takara Bio). Strain Mel02010 was transformed with the resulting disruption vectors (**Supplementary Table 3** and **Supplementary Figure 1**). Protoplasts were prepared and *F. oxysporum* was transformed as previously described (Inoue et al., 2001). Transformants were selected on regeneration media containing hygromycin B (Fujifilm-Wako Pure Chemical, Osaka, Japan) at 100 μg/mL. Disruption of the target genes in transformants were confirmed by PCR using respective primer sets (**Supplementary Table 2** and **Supplementary Figure 1**).

Inoculation Tests

Pathogenicity of *F. oxysporum* strains was tested by dipping roots of susceptible plants into conidial suspensions (5×10^5 conidia/mL) as previously described (Inoue et al., 2001).

To evaluate the biocontrol activity of *F. oxysporum* strains, roots of melon and tomato seedlings were dipped in conidial suspensions (1×10^6, 10^7 or 10^8 conidia/mL) of test strains for 15 s, then the seedlings were planted in pots of soil infested with conidia of the wild-type strains of *F. oxysporum* f. sp. *melonis* or f. sp. *lycopersici* (5×10^5 conidia/g soil). Melon seedlings pre-inoculated with test strains were also planted in the soil infested with oospores of *P. aphanidermatum* (5×10^5 oospores/g soil). Control seedlings were immersed in sterilized water and planted in infested and uninfested soils. Plants were incubated in a climate chamber at 25°C, and 16/8 h light/dark photoperiod. Disease symptoms were assessed 3 weeks after planting as follows: 0, no symptoms; 1, yellowing; 2, wilted; 3, dead.

To assess the durability of biocontrol effects after pre-inoculation of melon roots with strain Δ*FOW2* strain, pre-inoculated seedlings were grown in uninfested soil for 1, 3, or 7 days and then transplanted into soil infested with the wild-type strain (1×10^5 conidia/g soil). Disease symptoms were assessed 3 weeks after planting in the infested soil.

All inoculation tests were performed at least twice to ensure reproducibility, and representative result was shown.

Split-Root Inoculation

Root systems of melon seedlings were divided into two parts for the split-root inoculation as described previously (Larkin et al., 1996). One part was dipped in a conidial suspension of strain Δ*FOW2* (1×10^8 conidia/mL) and the other in sterilized water for 15 s, then the plants were planted in a pot of soil infested with the wild-type strain (1×10^5 conidia/g soil) or a pot of uninfested soil. Another part was planted in a separate pot filled with infested or uninfested soil. Plants were grown for 3 weeks, then disease symptoms were assessed as described above.

Quantitative Real-Time PCR

Melon genes that were analyzed by qPCR are listed in **Supplementary Table 4**.

Roots of melon seedlings were dipped in a conidial suspension of strain Δ*FOW2* (1×10^8 conidia/mL) for 15 s, and the seedlings were planted in soil infested with conidia of the wild-type strain (1×10^5 conidia/g soil) or in uninfested soil. Control seedlings were immersed in sterilized water and planted in infested or uninfested soil. Three melon seedlings in each treatment were removed from soil 1, 3, or 7 days after planting. Total RNA was extracted from roots and aboveground parts using RNeasy Plant Mini Kit (Qiagen, Hilden, Germany). The qPCR of melon genes was carried out with Mx3005P QPCR System (Agilent Technologies, Santa Clara, CA, United States) using One Step SYBR PrimeScript RT-PCR Kit II (Takara Bio). Target genes encode salicylic acid-, jasmonic acid-, and ethylene-responsive resistance genes: acidic chitinase (*PR-1a*) (Uknes et al., 1992; García-Gutiérrez et al., 2013), acidic thaumatin-like protein (*PR-5a*) (Uknes et al., 1992), acetylglucosaminyltransferase (*CGT*) (Bovie et al., 2004), acidic chitinase (*PR-8*) (Metraux et al., 1989), ethylene response factor 1 (*ERF1*) (Mizuno et al., 2006) and phenylalanine ammonia-lyase gene (*PAL1*) (Diallinas and Kanellis, 1994; **Supplementary Table 1**). PCR primers were designed to amplify cDNA fragments of 90–150 bp on the basis of melon-expressed sequence tags in the Cucurbit Genomics Database[1] (**Supplementary Table 4**). The efficiency of the primers was tested using a dilution series of genomic DNA from the melon plants. Raw data were analyzed using the $2^{-\Delta\Delta Ct}$ method (Livak and Schmittgen, 2001). The data were normalized to the transcript level of the actin gene, and the mRNA data of untreated melon seedlings was set to 1.0. Transcript levels of target genes in each RNA sample were measured for three independent inoculation experiments with two replicates and were analyzed for significant differences using Tukey–Kramer's multiple range test. All statistical analyses in this study were performed with R program version 4.0.3[2].

Construction of Green Fluorescent Protein- and Red Fluorescent Protein-Expression Vectors and Fungal Transformation

The GFP-expression vector pTEFEGFP, in which the *eGFP* gene was fused with the *Aureobasidium pullulans TEF* promoter and the *Aspergillus awamori gla* terminator (Vanden Wymelenberg et al., 1997), was used to make *F. oxysporum* strains constitutively expressing *GFP*. The red fluorescent protein (DsRed)-expression vector pTEFDsRed was constructed as follows. The pTEFEGFP DNA was linearized by inverse PCR using primers Ptef-RFP and Tgla-RFP (**Supplementary Table 2**). The DsRed gene was amplified from pDsRed-Express2 (Takara Bio) by PCR using primers RFP-F and RFP-R (**Supplementary Table 2**). These primers contain a 5′ overhang sequence for overlapping sequences at the ends of the linearized plasmid. PCR products were combined using the In-Fusion HD EcoDry Cloning kit (Takara Bio) and subsequently introduced into electrocompetent *Escherichia coli* DH5α (Takara Bio). PCR experiments were carried out using PrimeSTAR GXL DNA Polymerase (Takara Bio) or TaKaRa Ex Taq (Takara Bio) according to the manufacturer's instructions. The plasmids used in this study are listed in **Supplementary Table 3**.

The GFP-expressing vector pTEFEGFP and the DsRed-expressing vector pTEFDsRed were introduced into *F. oxysporum* strains by cotransformation with pII99, which carries the neomycin phosphotransferase gene (*nptII*) cassette (Namiki et al., 2001). Transformants carrying *nptII* cassette were selected on regeneration media containing G418 (geneticin) (Fujifilm-Wako Pure Chemical) at 200 μg/mL (Inoue et al., 2001). Hyphae of transformants were observed with a fluorescence microscope (IX73) (Olympus, Tokyo, Japan) using U-MNIB and U-MWIG filters (Olympus) to select GFP- and DsRed-expressing transformants, respectively. The selected transformants were confirmed to have hyphal growth, conidiation and pathogenicity on host plants typical of the parent strains.

Microscopic Observations

Melon roots were pre-inoculated with conidial suspension (1×10^8 conidia/mL) of the GFP-expressing strains by the root-dip method and planted in the soil infested with Mel02010-DsRed (1×10^5 conidia/g soil). Three plants were removed from the soil at 3 and 7 days after planting, and conidial germination and hyphal elongation on main root surface were observed using a confocal laser scanning microscope (CLSM) (LSM-700; Carl Zeiss, Oberkochen, Germany) (GFP: excitation 488 nm and emission 509 nm; DsRed: excitation 555 nm and emission 572 nm). At least six sections of the main roots of each seedling were observed, and germination rates of conidia and hyphal lengths were measured. Data were analyzed for significant differences using Tukey–Kramer's multiple range test.

For observing hyphae on the root surface using a scanning electron microscope, sections of the main roots were fixed twice in 2% (v/v) glutaraldehyde in 0.1 M sodium cacodylate buffer (pH 7.2) for 1 h and dehydrated using a graded ethanol series (20–100%), then immersed in 100% acetone. Samples were freeze-dried (JFD-300; JEOL, Tokyo, Japan), coated with a thin gold layer using a JEE-400 vacuum evaporator (JEOL) and observed using a JSM-5800 scanning electron microscope (JEOL).

Selection of Thiophanate-Methyl-Resistant Strains and Inoculation Test

A conidial suspension (1×10^6 cells/mL) of strain Mel02010-DsRed was irradiated for 1 to 5 min with UV light (GL15, 253.7 nm, 15W, Toshiba, Osaka, Japan) that was approximately 50 cm above the plate. The conidial suspension was plated on PDA containing 50 μg/mL thiophanate-methyl (Topsin-M; Nihon Nohyaku, Tokyo, Japan) and incubated at 25°C for 2 days. The growing colonies were subjected to single-conidial isolation three times on PDA supplemented with thiophanate-methyl, and the resistant strain Mel02010-DsRed^{TR} was selected. Strain

[1] http://www.icugi.org/

[2] www.r-project.org

Mel02010-DsRed^{TR} was confirmed to have normal mycelial growth, conidiation and pathogenicity to melon plants similar to the parent strain.

Melon roots were dipped in a conidial suspension (1×10^8 conidia/mL) of the GFP-expressing Δ*FOW2* strain MF2-1-GFP or in sterilized water, and the seedlings were planted in soil infested with Mel02010-DsRed^{TR} (1×10^5 conidia/g soil) or in uninfested soil. Soils mixed with or without thiophanate-methyl (50 μg/g soil) were used in each inoculation test. After inoculation for 24 h, seedlings were removed from three pots, and total DNA was extracted from roots using a NucleoMag Plant Kit (Macherey-Nagel). Fungal DNA was detected from root DNA by PCR amplification of the GFP gene of MF2-1-GFP and the DsRed gene of Mel02010-DsRed^{TR} using Takara Ex Taq (Takara) and specific primers for each gene (**Supplementary Table 2**). The elongation factor gene (*EF1α*) of melon was also amplified as a standard. The seedlings were grown for 3 weeks, and disease symptoms were assessed as described above.

Carbon Source Competition Assay

Carbon source competition in soil between nonpathogenic and wild-type strains was assayed using the buried membrane filter method of Larkin and Fravel (1999) with a slight modification. Fertilized granulated soil (Kumiai Nippi Engei Baido) was mixed with a glucose solution at final concentrations from 0 to 0.4 mg/g soil. One milliliter of 3×10^4 conidia/mL of the wild-type strain Mel02010 was deposited on a cellulose membrane filter (MF-Millipore, 0.45-μm pore, 47 mm diameter; Millipore, Billerica, MA, United States) by vacuum filtration. The membrane filters were buried in soil infested with nonpathogenic strains (1×10^5 conidia/g soil) and incubated in a moist chamber at 25°C for 3 days in the dark. The filters were removed from soil, rinsed with sterilized water and boiled in lactophenol-aniline blue solution (0.01% aniline blue in lactic acid/phenol/dH_2O/glycerol [1:1:1:1, v/v/v/v]). Length of hyphae elongated from conidia on the filters was measured using a light microscope (IX73, Olympus). At least 100 germinated conidia were observed in each sample, and the mean lengths were compared for significant differences among treatments using Student's *t*-test.

RESULTS

Biocontrol Activities of Pathogenicity Mutants Against the Wild-Type Strain

Imazaki et al. (2007) isolated Δ*FOW2* strains from strain Mel02010 of *F. oxysporum* f. sp. *melonis* and found that the mutants were not pathogenic to host plants. Here, we generated mutants of five other known pathogenicity genes from strain Mel02010: *FMK1* encoding protein kinase (Di Pietro et al., 2001), *FGA1* and *FGB1* encoding G protein subunit α and β, respectively (Jain et al., 2002; 2003), *FRP1* encoding an F-box protein (Duyvesteijn et al., 2005) and *GAS1* encoding a putative β-1,3-glucanosyltransferase (Caracuel et al., 2005; **Supplementary Table 1**). To generate mutants of these genes, we used homologous recombination to replace each gene with the plasmid, which contains the target gene fragment interrupted with the *hph* cassette (**Supplementary Figure 1**). Two independent mutants of each gene were assayed for pathogenicity on melon plants. Mutation of *FMK1* and *FRP1* in strain Mel02010 caused a drastic reduction in pathogenicity (**Supplementary Figure 2**). Although mutations of *FGA1*, *FGB1*, and *GAS1* reduced virulence, some of the inoculated plants still died or were severely wilted within 21 days post inoculation (dpi) (**Supplementary Figure 2**). The Δ*FOW2* strains were confirmed to lack pathogenicity on melon plants (Imazaki et al., 2007).

We tested for biocontrol activity of Δ*FMK1*, Δ*FRP1*, and Δ*FOW2* strains against the wild-type strain Mel02010. Melon seedlings were pre-inoculated with a conidial suspension (1×10^6, 10^7 or 10^8 conidia/mL) of each mutant by the root-dip method and grown in soil infested with Mel02010 (10^5 conidia/g soil). The nonpathogenic *F. oxysporum* strain MFG6, which was previously identified to have biocontrol activity against *F. oxysporum* pathogens, was also used for pre-inoculation. Roots of control seedlings were dipped in water and planted in infested soil, and within 15 dpi, plants had yellowing and wilting, and all plants died within 21 dpi (**Figure 1**). However, seedlings pre-inoculated with Δ*FOW2* strain MF2-1 or MFG6 were markedly reduced in disease severity, and some had no symptoms (**Figure 1**). The level of biocontrol activity was dependent on the concentration of conidia used for the pre-inoculations and was similar for MF2-1 and MFG6 (**Figure 1**). Such results were reproduced using another Δ*FOW2* strain MF2-2 (**Supplementary Figure 3B**). Symptom development on seedlings pre-inoculated with Δ*FMK1* strain MK1 was delayed, and severity was significantly reduced (**Figure 1**). Seedlings pre-inoculated with Δ*FRP1* strain RP1 had slightly lower disease severity (**Figure 1**). These results suggest that the weaker the virulence, the higher the biocontrol activity.

Biocontrol Activities of Δ*FOW2* Strains

FOW2 is conserved in *F. oxysporum* pathogens that infect different plants and is also essential for pathogenicity of *F. oxysporum* f. sp. *lycopersici* on tomato plants (Imazaki et al., 2007). We tested biocontrol activity of the Δ*FOW2* strain LF2-1 generated from *F. oxysporum* f. sp. *lycopersici*. Tomato seedlings were pre-inoculated with conidial suspensions (1×10^6, 10^7 or 10^8 conidia/mL) of LF2-1 and planted in soil infested with the wild-type strain CK3-1 (10^5 conidia/g soil). Mock seedlings in the infested soil died within 21 dpi (**Figure 2**). Pre-inoculation of tomato roots with a conidial suspension of LF2-1 apparently reduced disease severity in a concentration-dependent manner (**Figure 2**).

We also tested the biocontrol activity of *F. oxysporum* f. sp. *lycopersici* against *F. oxysporum* f. sp. *melonis* on melon plants. Melon seedlings pre-inoculated with wild-type or Δ*FOW2* strain of *F. oxysporum* f. sp. *lycopersici* had significantly reduced disease severity (**Figure 3**), indicating that all nonpathogenic strains used were active against *F. oxysporum* f. sp. *melonis*. These results suggest that the biocontrol activity of Δ*FOW2* strains would be due to their nonpathogenic nature, but not to the *FOW2* disfunction itself.

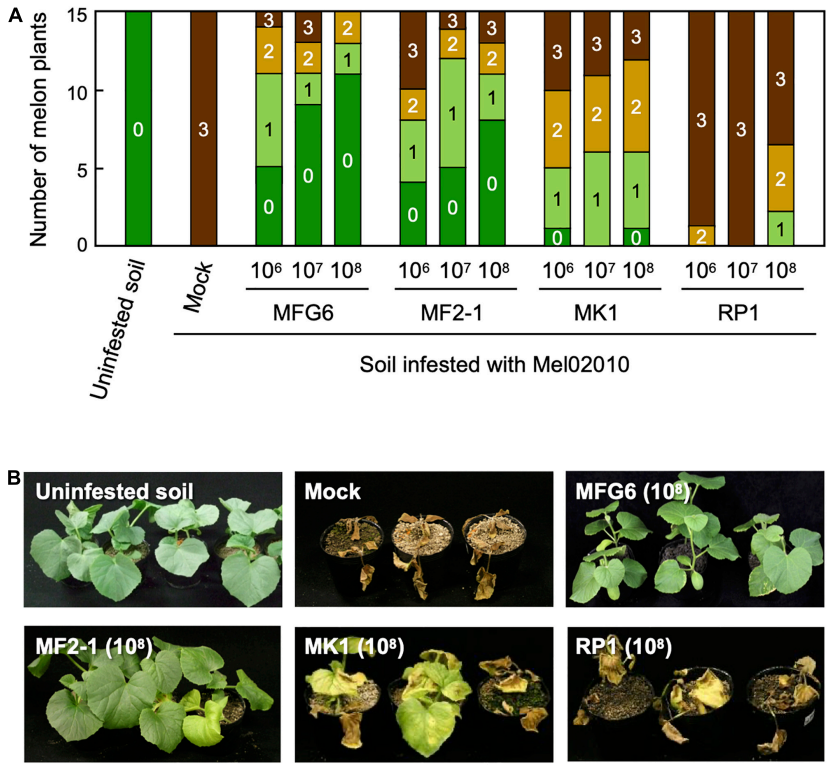

FIGURE 1 | Biocontrol activity of pathogenicity gene mutants of *Fusarium oxysporum* f. sp. *melonis* against the parental strain. Roots of melon seedlings were dipped in a conidial suspension (1×10^6, 10^7 or 10^8 conidia/mL) of Δ*FOW2* (MF2-1), Δ*FMK1* (MK1), and Δ*FRP1* (RP1) strains of *F. oxysporum* f. sp. *melonis* or nonpathogenic strain MFG6. The seedlings were planted in soil infested with the parental wild-type strain Mel02010 (1×10^5 conidia/g soil). Control seedlings were immersed in water and planted in uninfested or infested soil (Mock). **(A)** Symptoms were scored at 21 dpi as 0, no symptoms; 1, yellowing; 2, wilted; 3, dead. **(B)** Plants at 21 dpi.

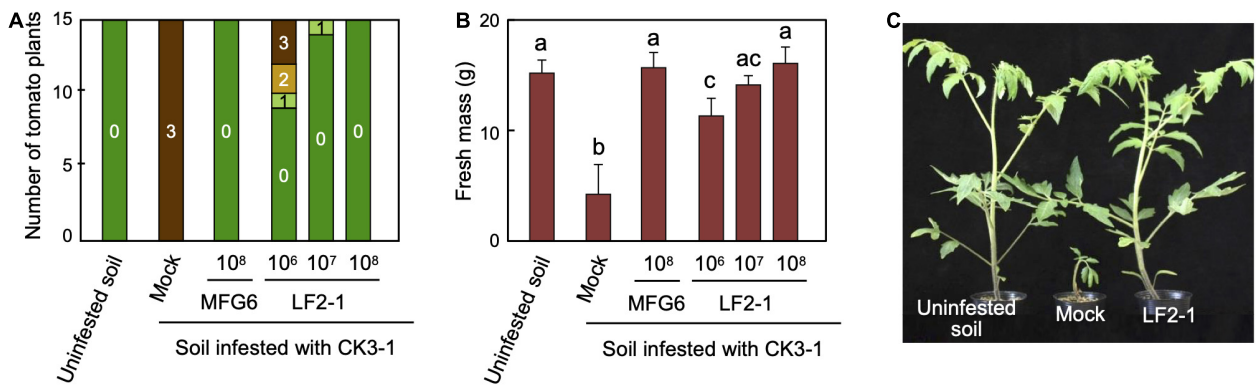

FIGURE 2 | Biocontrol activity of pathogenicity gene mutants of *Fusarium oxysporum* f. sp. *lycopersici* against the parental strain. Roots of tomato seedlings were dipped in conidial suspensions (1×10^6, 10^7 or 10^8 conidia/mL) of Δ*FOW2* strain LF2-1 of *F. oxysporum* f. sp. *lycopersici* or nonpathogenic strain MFG6. The seedlings were planted in soil infested with parental wild-type strain CK3-1 (1×10^5 conidia/g soil). Control seedlings were immersed in water and planted in uninfested or infested soil (Mock). **(A)** Symptoms were scored 21 dpi as 0, no symptoms; 1, yellowing; 2, wilted; 3, dead. **(B)** Fresh mass of aboveground parts of tomato seedlings ($n = 15$) at 21 dpi. Data represent averages and standard errors based on 15 seedlings. Columns with different letters indicate that means differed significantly at $P \leq 0.01$ in the Tukey–Kramer multiple range test. **(C)** Plants at 21 dpi.

We examined the durability of the biocontrol effect after melon roots were pre-inoculated with Δ*FOW2* strain MF2-1, planted in uninfested soil, then transplanted after 1, 3, and 7 days in soil infested with Mel02010 conidia. Mock seedlings without MF2-1 pre-inoculation developed severe symptoms within 21 dpi (**Figure 4**), whereas symptoms on MF2-1-pre-inoculated seedlings were less severe, and the transplanting timing did not conspicuously affect the biocontrol activity

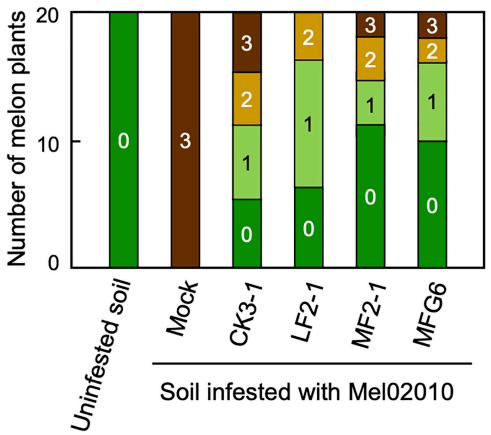

FIGURE 3 | Biocontrol activity of *Fusarium oxysporum* f. sp. *lycopersici* and its mutant Δ*FOW2* strain against *F. oxysporum* f. sp. *melonis*. Roots of melon seedlings were dipped in a conidial suspension (1×10^8 conidia/mL) of *F. oxysporum* f. sp. *lycopersici* strain CK3-1 or Δ*FOW2* strain LF2-1, and the seedlings were planted in soil infested with *F. oxysporum* f. sp. *melonis* strain Mel02010 (1×10^5 conidia/g soil). Control seedlings were immersed in water and planted in uninfested or infested soil (Mock). Symptoms were scored at 21 dpi as 0, no symptoms; 1, yellowing; 2, wilted; 3, dead. MF2-1, Δ*FOW2* strain of *F. oxysporum* f. sp. *melonis*; MFG6, nonpathogenic *F. oxysporum*.

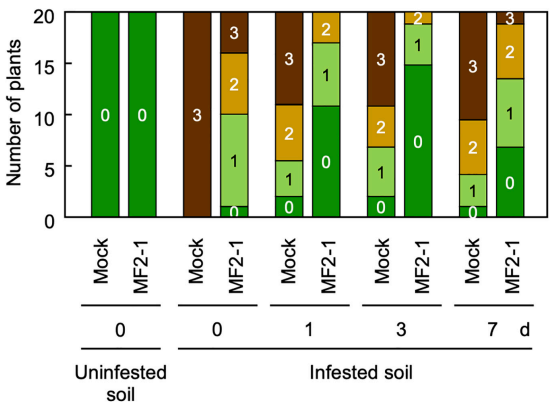

FIGURE 4 | Persistence of biocontrol effect after pre-inoculation of melon seedlings with Δ*FOW2* strain. Roots of melon seedlings were dipped in a conidial suspension (1×10^8 conidia/mL) of Δ*FOW2* strain MF2-1 or in water, and seedlings were planted in soil infested with wild-type strain Mel02010 (1×10^5 conidia/g soil) or in uninfested soil. After 1, 3, or 7 days, seedlings grown in uninfested soil were transplanted in Mel02010 infested soil. Symptoms were scored 3 weeks after planting in infested soil as 0, no symptoms; 1, yellowing; 2, wilted; 3, dead.

(**Figure 4**). These results indicated that the biocontrol effect lasted for at least 7 days.

Effect of Pre-inoculation of Melon Roots With Δ*FOW2* Strain on Expression of Defense-Related Genes

The transcription levels of salicylic acid-, jasmonic acid-, and ethylene-responsive resistance genes in roots and aboveground

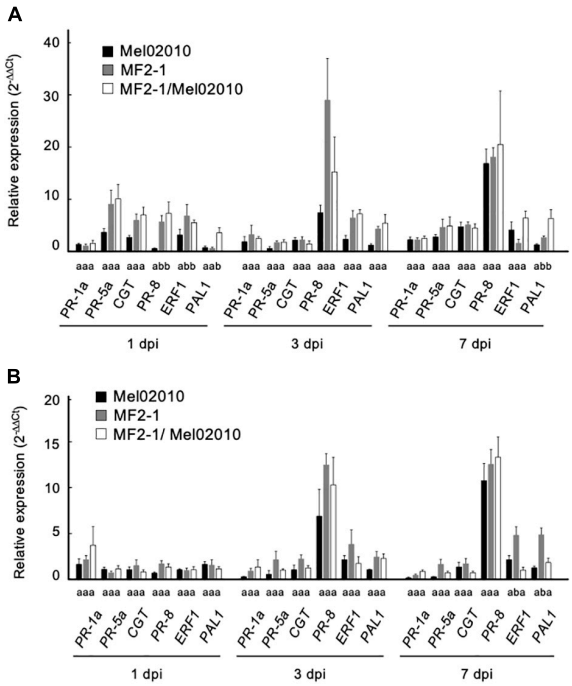

FIGURE 5 | Transcription levels of defense-related genes in melon seedlings inoculated with Δ*FOW2* strain. Roots of melon seedlings were dipped in a conidial suspension (1×10^8 conidia/mL) of Δ*FOW2* strain MF2-1, and seedlings were planted in soil uninfested (MF2-1) or infested with the wild-type strain Mel02010 (1×10^5 conidia/g soil) (MF2-1/Mel02010). Control seedlings were immersed in water and planted in Mel02010 infested soil (Mel02010) or uninfested soil. Seedlings were removed from soil 1, 3, or 7 dpi, and total RNA was extracted from roots **(A)** and aboveground parts **(B)** for quantitative real-time PCR analyses. Raw data were analyzed using the $2^{-\Delta\Delta Ct}$ method. Data were normalized against the actin gene, and those of uninoculated melon seedlings was set to 1.0. Error bars indicate the standard errors calculated from three independent inoculation experiments with two replicates. Columns with different letters indicate that means differed significantly at $P \leq 0.01$ in the Tukey–Kramer multiple range test.

part of inoculated plants were evaluated using qPCR and were compared among plants different in treatments: plants grown in Mel02010 infested soil without pre-inoculation, plants pre-inoculated with Δ*FOW2* strain MF2-1 and grown in uninfested soil; plants pre-inoculated with MF2-1 and grown in Mel02010 infested soil. Although all the target genes except *PR-1a* tended to be upregulated by MF2-1 pre-inoculation in roots and aboveground parts, statistically significant differences were detected at 1 and 7 dpi only for *PR-8*, *ERF1*, and *PAL1* in plants pre-inoculated with MF2-1 (**Figure 5**). These results suggest that the Δ*FOW2* strain did not markedly induce persistent expression of defense-related genes and that the biocontrol activity of the Δ*FOW2* strain was not due primarily to the induction of resistance, since these expression patterns were not consistent with the durability of the biocontrol effect lasting for 7 days.

To assess the systemic resistance induced by the pre-inoculation of melon seedlings with the Δ*FOW2* strain, we used a split-root inoculation method. Symptom development on the seedlings was similar to that on those without MF2-1, indicating

that systemic resistance was not induced by the inoculation of roots with the Δ*FOW2* strain (**Supplementary Figure 4**).

Colonization of Wild-Type Strain on Melon Roots Pre-inoculated With Δ*FOW2* Strain

We observed the effect of pre-inoculation of melon roots with the Δ*FOW2* strain on colonization of the wild-type strain on root surface. Melon seedlings were inoculated with the GFP-expressing Δ*FOW2* strain MF2-1-GFP and planted in the soil infested with the thiophanate-methyl-tolerant wild-type strain Mel02010-DsRed^{TR}. From total DNA of roots grown in thiophanate-methyl mixed soils, PCR amplified the DsRed gene fragments, but not the GFP gene fragments, confirming that MF2-1-GFP was not viable in the soil (**Supplementary Figure 5**). Although MF2-1-GFP had remarkable biocontrol activity against Mel02010-DsRed^{TR} in the absence of thiophanate-methyl in the soil, it lost its activity when thiophanate-methyl was present (**Supplementary Figure 5**), indicating that root colonization by the Δ*FOW2* strain was important for the biocontrol effect.

After roots of melon seedlings were dipped in a conidial suspension of MF2-1-GFP or in water, then planted in Mel02010-DsRed infested soil, CLSM showed that conidia of Mel02010-DsRed on the roots dipped in water had germinated and that hyphae had elongated by 3 dpi and, by 7 dpi, penetration hyphae were frequently observed in the epidermal cells (**Figure 6** and **Supplementary Figure 6**). On roots pre-inoculated with MF2-1-GFP, conidia of MF2-1-GFP had germinated and hyphae had elongated extensively on the root surface at 3 dpi (**Figure 6A**). In contrast, hyphae of Mel02010-DsRed were occasionally observed (**Figure 6A**). At 7 dpi, MF2-1-GFP had formed an extensive hyphal network that covered almost the entire root surface, and fluorescence from Mel02010-DsRed was not detected (**Figure 6B**). Conidial germination rates and hyphal lengths of Mel02010-DsRed and MF2-1-GFP on root surfaces at 3 and 7 dpi showed that germination and hyphal elongation of Mel02010-DsRed were inhibited when melon roots were pretreated with MF2-1-GFP.

Melon seedlings were pre-inoculated with conidial suspensions of strain CK3-1-GFP and its Δ*FOW2* strain LF2-1-GFP of *F. oxysporum* f. sp. *lycopersici* and nonpathogenic strain MFG6-GFP by the root-dip method and planted in the soil infested with Mel02010-DsRed. Conidia of pre-inoculated strains germinated, and hyphae had elongated extensively on the root surface similar to MF2-1-GFP, whereas conidial germination and hyphal elongation of Mel02010-DsRed on the root surface were significantly inhibited (**Figure 7**).

As seen with CLSM of MF2-1-GFP pre-inoculated roots, hyphae had not colonized epidermal cells by 7 dpi (**Supplementary Figure 6**), confirming that the Δ*FOW2* strain could not penetrate and colonize the epidermal cells; it only colonized the root surface. Strains CK3-1-GFP, LF2-1-GFP, and MFG6-GFP also colonized the melon root surface, but not in the epidermal cells (**Supplementary Figure 6**). These results strongly suggest that pre-colonization of the root surface by nonpathogenic strains inhibits conidial germination and hyphal development of the soil-borne, wild-type strain.

Carbon Source Competition Between Wild-Type and Δ*FOW2* Strain in the Rhizosphere

Conidial germination and hyphal elongation of the wild-type strain were markedly inhibited on the root surface pre-inoculated with the Δ*FOW2* strain (**Figure 6**). The Δ*FOW2* strain, however, did not inhibit conidial germination or hyphal elongation of the wild-type strain on any artificial media (data not shown). In the verification of carbon source competition using cellulose membrane filters with conidia of the wild-type strain Mel02010 set in soil mixed with glucose solution (0–0.4 mg/g soil) and conidia (1×10^5 conidia/g soil) of the Δ*FOW2* strain MF2-1 (**Supplementary Figure 7A**), after 3 days, mean hyphal length of Mel02010 had increased proportionally to glucose concentrations and was significantly reduced in the presence of MF2-1 conidia in the soil (**Figure 8A**). Hyphal elongation of Mel02010 was also inhibited in the presence of strain CK3-1 of *F. oxysporum* f. sp. *lycopersici*, its Δ*FOW2* strain LF2-1 or nonpathogenic MFG6 in the soils (**Supplementary Figure 7B**). Pre-inoculation of melon roots with these strains also inhibited conidial germination and hyphal elongation of Mel02010 on melon roots (**Figures 6**, **7**). These results suggest that these strains pre-colonized on the root surface have a competitive advantage over Mel02010 for carbon sources in the rhizosphere.

Biocontrol Activities of Δ*FOW2* Strain Against *Pythium aphanidermatum*

In the test of the biocontrol activity of the Δ*FOW2* strain MF2-1 against *P. aphanidermatum*, melon seedlings root-dipped in 1×10^8 conidia/mL of strain MF2-1 or nonpathogenic strain MFG6 and planted in soil infested with *P. aphanidermatum* strain WPy1 (10^5 oospores/g soil). Mock seedlings without pre-inoculation showed yellowing and damping-off by 14 dpi, and more than half of the seedlings had died by 21 dpi (**Figure 9A**). MF2-1-pre-inoculated plants in infested soil had chlorotic leaf edges, but symptoms were less severe, and pre-inoculation of seedlings with MFG6 also reduced severity (**Figure 9B**).

We also verified the carbon source competition between *P. aphanidermatum* and *F. oxysporum* strains in soil using oospores of strain WPy1 on cellulose membrane filters and set in the soil mixed with glucose solution (0–0.4 mg/g soil) and conidia (1×10^5 conidia/g soil) of MF2-1 or MFG6. After 3 days, hyphal growth of WPy1 was significantly inhibited in soils mixed with conidia of MF2-1 and MFG6 (**Figure 8B**). These results indicate that *F. oxysporum* strains also protect melon plants from infection with *P. aphanidermatum* probably due to their pre-colonization on the root surface.

DISCUSSION

In tests of three strains with a mutation in one of three pathogenicity genes that are conserved in *F. oxysporum* for

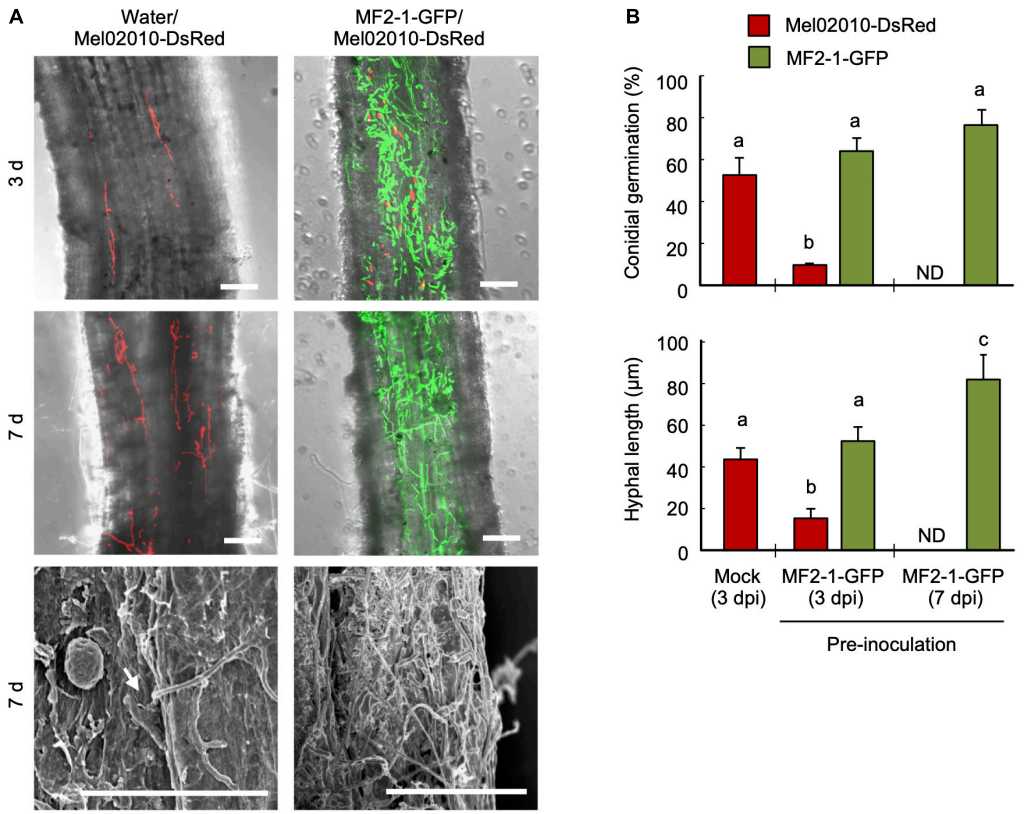

FIGURE 6 | Inhibition of conidial germination and hyphal growth of wild-type strain on root surface after pre-inoculation with Δ*FOW2* strain. Roots of melon seedlings were dipped in a conidial suspension (1×10^8 conidia/mL) of Δ*FOW2* strain MF2-1-GFP or in water, and seedlings were planted in soil infested with wild-type strain Mel02010-DsRed (1×10^5 conidia/g soil). Seedlings were removed from soil at 3 and 7 dpi. **(A)** The root surface was viewed with laser scanning confocal microscopy (LSCM; top and middle) or scanning electron microscopy (bottom). Bar = 50 μm. Arrow: possible penetration site. **(B)** Percentage of conidial germination and hyphal length of each strain on main roots at 3 and 7 dpi was determined using LSCM. Data represent means and standard errors of three replications. Columns with different letters indicate that means differed significantly at $P \leq 0.01$ in the Tukey–Kramer multiple range test. ND, not detected.

activity against a pathogenic strain of the fungus, pre-inoculation with the Δ*FOW2* strain yielded the best biocontrol against pathogenic strains of *F. oxysporum* ff. spp. *melonis* and *lycopersici*, and its activity was concentration dependent, like that of the biocontrol by nonpathogenic *F. oxysporum* strain MFG6. The same level of biocontrol was maintained against the wild-type strain for at least 7 days after pre-inoculation (**Figure 4**). Since the wild-type strain has already penetrated the root by 7 dpi when the biocontrol agent is not present (**Supplementary Figure 6**), we tested whether Δ*FOW2* strain had induced a plant defense response by 7 days. The qPCR analysis revealed only limited expression levels of some ethylene (*ERF1*) or jasmonic acid-responsive (*PAL1*) resistance genes in roots after pretreatment with strain Δ*FOW2* (**Figure 5A**), which did not correlate with the 7-day biocontrol effect of the Δ*FOW2* strain. None of the defense genes were expressed in the systemic aboveground parts of plants inoculated with the Δ*FOW2* strain and the wild-type strains (**Figure 5B**). Likewise, defense-related genes in tomato that were highly induced by a chitin synthase-deficient strain that was less virulent than the parental strain of *F. oxysporum* f. sp. *lycopersici* (Pareja-Jaime et al., 2010), were not distinctly altered in their expression in the roots or aboveground parts of tomato pre-inoculated with the Δ*FOW2* strain (data not shown). No biocontrol effect was observed in the systemically infected roots (**Supplementary Figure 4**). These results suggest that the high biocontrol activity of the Δ*FOW2* strain is not primarily due to the induction of plant resistance.

We then analyzed the effect of colonization by the Δ*FOW2* strain on the infection process of the wild-type strain, which is tolerant to the chemical fungicide thiophanate-methyl. The Δ*FOW2* strain was eradicated by thiophanate-methyl before its conidia germinated and hyphae grew, and the wild-type strain infected the host plants (**Supplementary Figure 5**), suggesting that preemptive colonization of Δ*FOW2* is essential for the biocontrol. Interestingly, conidial germination and hyphal elongation were inhibited only in the wild-type strain on the root pre-inoculated with the Δ*FOW2* strain, and the DsRed fluorescence of the wild-type strain had disappeared from the root surface by 3 dpi (**Figure 6**). Nevertheless, the pathogenic strain was still viable in the rhizosphere soil. In addition, the Δ*FOW2* strain colonizes the roots more rapidly than the wild-type strain does, even though their growth rates do not differ in culture (Imazaki et al., 2007). The Δ*FOW2* strain was not detected from inside the roots, meaning that it grows

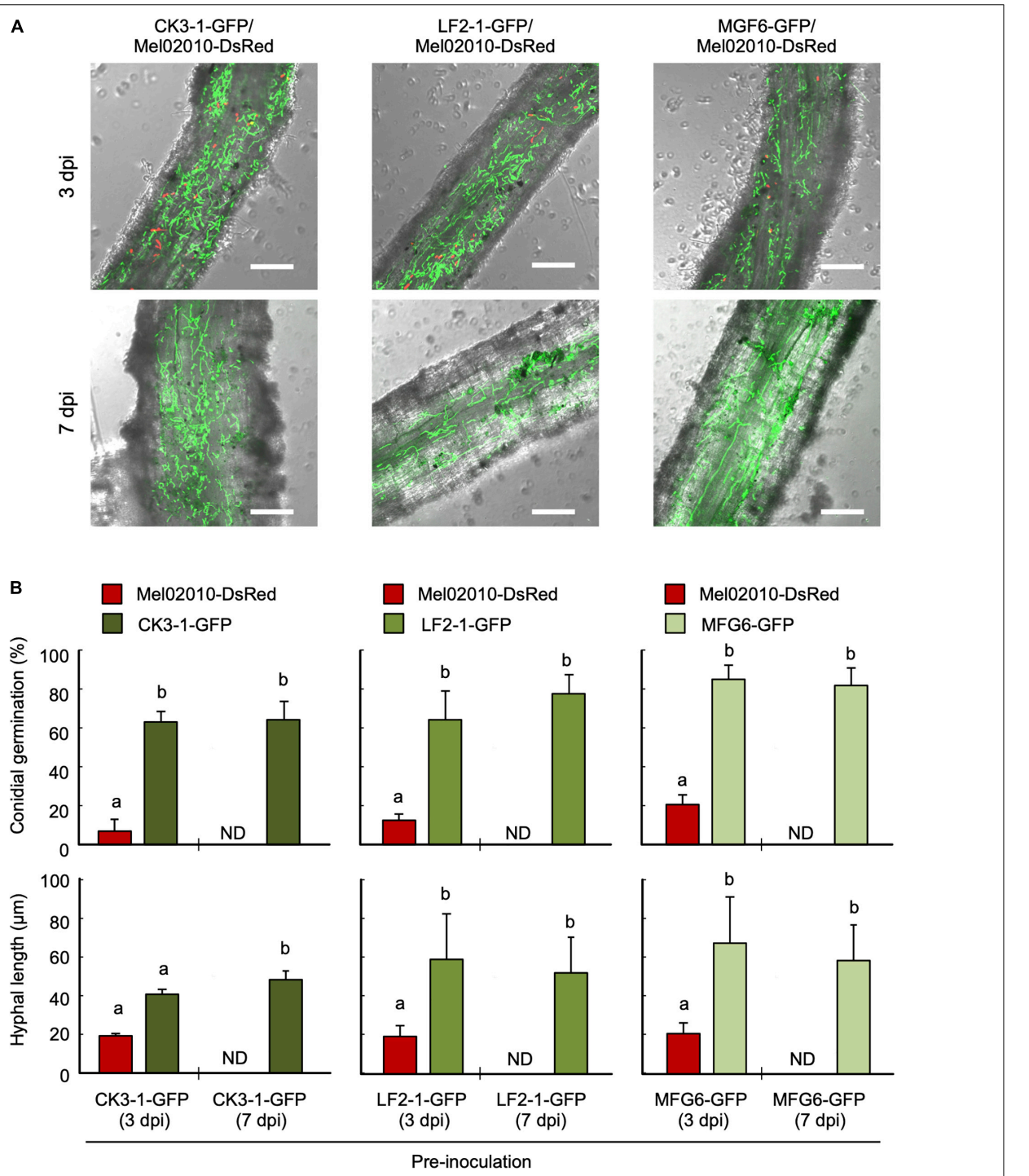

FIGURE 7 | Inhibition of conidial germination and hyphal growth of *F. oxysporum* f. sp. *melonis* on root surface by the pre-inoculation of *F. oxysporum* f. sp. *lycopersici* and its Δ*FOW2* strain. Roots of melon seedlings were dipped in a conidial suspension (1×10^8 conidia/mL) of *F. oxysporum* f. sp. *lycopersici* strains or in water, and seedlings were planted in soil infested with *F. oxysporum* f. sp. *melonis* strain (1×10^5 conidia/g soil). Seedlings were removed from soil at 3 and 7 dpi. **(A)** Root surface viewed with a laser scanning confocal microscopy (LSCM). Bar = 50 μm. **(B)** Percentage of conidial germination and hyphal length of each strain on main roots was determined 3 and 7 dpi using LSCM. Data represent means and standard errors of three replications. Columns with different letters indicate that means differed significantly at $P \leq 0.01$ in the Tukey–Kramer multiple range test. ND, not detected. Mel02010-DsRed, DsRed-expressing strain of *F. oxysporum* f. sp. *melonis*; CK3-1-GFP, GFP-expressing strain of *F. oxysporum* f. sp. *lycopersici*; LF2-1-GFP, *FOW2* mutant of CK3-1-GFP; MGF6-GFP, GFP-expressing nonpathogenic *F. oxysporum* strain.

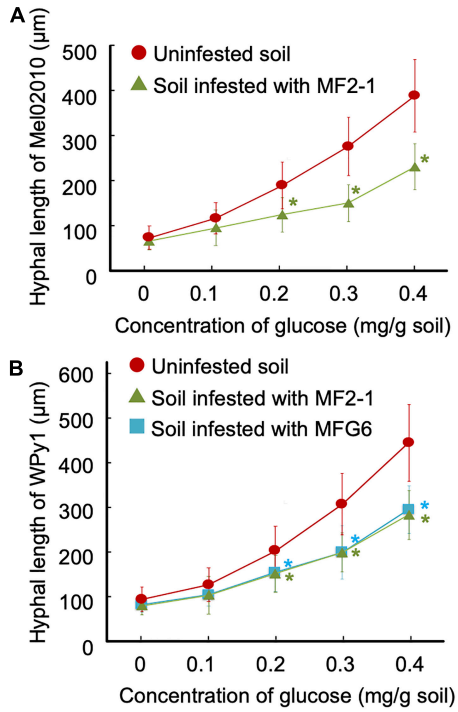

FIGURE 8 | Carbon source competition between pathogenic and nonpathogenic strains in soil. Cellulose membrane filters with conidia of strain Mel02010 of *Fusarium oxysporum* f. sp. *melonis* **(A)** and oospores of strain WPy1 of *Pythium aphanidermatum* **(B)** were set in soil mixed with glucose solution (0–0.4 mg/g soil) and a conidial suspension (1×10^5 conidia/g soil) of nonpathogenic strains. After 3 days, the filters were removed from the soil, and the length of hyphae of Mel02010 and WPy1 was measured. Data represent means and standard errors of three replicates. Asterisks indicate a significant difference in hyphal length from that in uninfested soil at each glucose concentration ($P < 0.001$; Student's *t*-test). MF2-1, *FOW2* mutant of Mel02010; MFG6, nonpathogenic *F. oxysporum*.

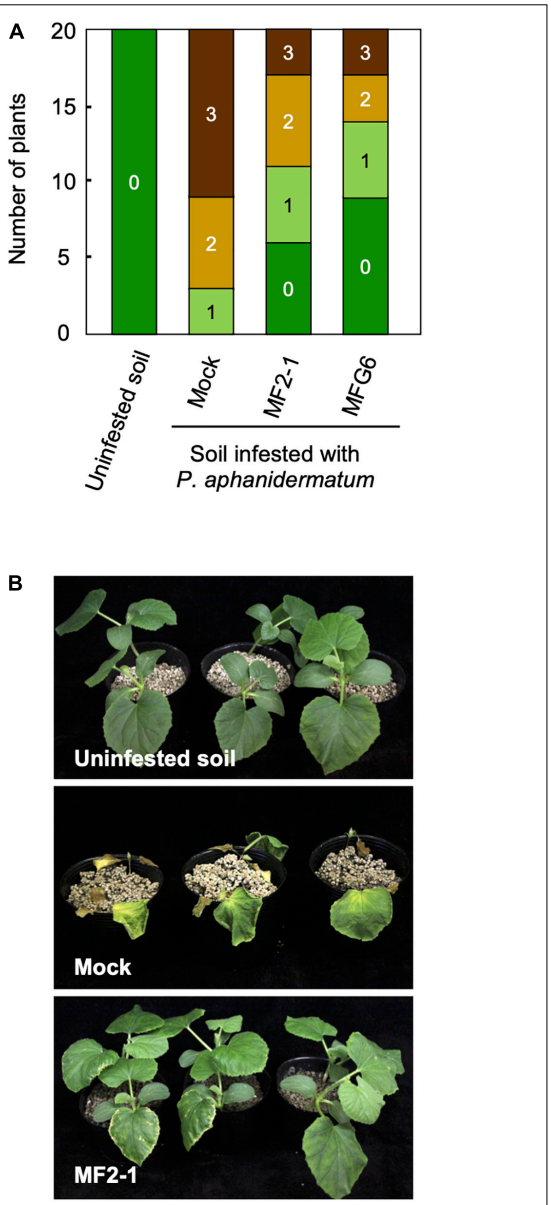

FIGURE 9 | Biocontrol activity of Δ*FOW2* strain of *Fusarium oxysporum* f. sp. *melonis* against *Pythium aphanidermatum*. Roots of melon seedlings were dipped in a conidial suspension (1×10^6, 10^7 or 10^8 conidia/mL) of Δ*FOW2* strain MF2-1 or nonpathogenic strain MFG6, and seedlings were planted in soil infested with *P. aphanidermatum* (1×10^5 oospores/g soil). Control seedlings were immersed in water and planted in uninfested or infested soil (Mock). **(A)** Symptoms were scored 21 dpi as 0, no symptoms; 1, yellowing; 2, wilted; 3, dead. **(B)** Plants at 21 dpi.

epiphytically on the root surface. This characteristic hyphal growth on melon roots was the same as that of *F. oxysporum* f. sp. *lycopersici* CK3-1 and nonpathogenic strain MFG6 when they were used for pre-inoculation (**Figure 7**). These results suggest that pre-inoculation with the Δ*FOW2* strain reduces the proliferation of wild-type strains on the plant surface, probably because the extensive hyphal network of the Δ*FOW2* strain covers the limited number of infection sites before the wild-type strain can reach them or a resistance mechanism is triggered that was not detected by any marker genes that we used.

In fact, it has been proposed that nonpathogenic biocontrol strains of *F. oxysporum* might induce a novel resistance pathway that differs from the well-studied plant hormone-mediated signaling pathways and microbe-associated molecular patterns (MAMPs)-triggered immunity: endophytic *F. oxysporum* strain Fo47 does not affect expression of salicylic acid, jasmonic acid, and ethylene responsive marker genes and is still able to control Fusarium wilt in tomato plants that are impaired in these plant hormones (Constantin et al., 2019). Nor is MAMPs-triggered immunity involved in Fo47-mediated resistance (de Lamo et al., 2020). However, this hypothesized pathway is unlikely to be involved in the biocontrol activity of the Δ*FOW2* strain. Since Δ*FOW2* strain is genetically identical to its parental strain *F. oxysporum* f. sp. *melonis*, the high selectivity of the biocontrol that appears only against pathogenic *F. oxysporum* cannot be explained by plant-mediated resistance alone. Similar to our findings in this study, the biocontrol activity of nonpathogenic *F. oxysporum* eliminates only pathogenic

F. oxysporum from the root surface and has no effect on the hyphal growth of nonpathogenic *F. oxysporum* (Olivain et al., 2003; Bolwerk et al., 2005). This high selectivity of biocontrol that appears commonly only against pathogenic *F. oxysporum* may be more strongly related to direct interaction with the nonpathogenic strains of *F. oxysporum*. For example, the sesquiterpene volatile α-humulenone emitted by nonpathogenic *F. oxysporum* strain stocktickerMSA35 represses the expression of pathogenicity genes in *F. oxysporum* (Minerdi et al., 2009). The endophyte *Serendipita indica* suppresses virulence of the barley root pathogen *Bipolaris sorokiniana* by affecting expression of genes involved in secondary metabolism and effectors (Sarkar et al., 2019). Trophic interactions might also explain the mechanisms of biocontrol by the Δ*FOW2* strain because the mutation in the *FOW2* gene does not affect the ability of the mutant to use any amino acids, nitrogen, or carbon sources (Imazaki et al., 2007).

In carbon source competition assays of nonpathogenic *F. oxysporum* strains that are well-known biocontrol agents, strain Fo47 competes for carbon source against pathogenic *F. oxysporum*, but strain CS-20, which mainly induces plant resistance, does not compete for glucose (Larkin and Fravel, 1999). Here, we found that not only the Δ*FOW2* strains (MF2-1 and LF2-1), but also the pathogenic strain of *F. oxysporum* f. sp. *lycopersici* competed with *F. oxysporum* f. sp. *melonis* for a carbon source in the soil. Thus, the mutation in the *FOW2* gene is not relevant to nutrient competition. Also, the Δ*FOW2* strain protected melon plants from the root rot by the oomycete *P. aphanidermatum* and competed for glucose in the soil. High population densities give nonpathogenic *F. oxysporum* strains an advantage in competition for the carbon sources against pathogens in the rhizosphere. The inoculum density of the endophytic strain Fo47 must be much higher than that of the pathogenic strain since it confers protection primarily through competition for nutrients and niches (Alabouvette et al., 1993; Lemanceau et al., 1993; Larkin and Fravel, 1999; Fravel et al., 2003; Bolwerk et al., 2005). In oligotrophic environments such as soil, nutrient competition between microorganisms is frequent, leading to soil fungistasis—the inhibition of conidial germination and/or hyphal growth—as observed in this study (Lockwood, 1977; de Boer et al., 2003).

Pre-inoculation with an avirulent strain of *F. oxysporum*, even a pathogenic strain belonging to another forma specialis, results in the mitigation of symptoms due to the mechanism called cross protection (Matta, 1989; Silvar et al., 2009). In the present study, *F. oxysporum* f. sp. *lycopersici* was highly effective against a virulent strain of *F. oxysporum* f. sp. *melonis* on melon and behaved similarly to the Δ*FOW2* strains on the root surface. The Δ*FOW2* strains of *F. oxysporum* f. sp. *lycopersici* had a protective effect similar to its parental strain on non-host melon in pre-inoculation tests (**Figure 2**), suggesting that the biocontrol effect of the Δ*FOW2* strains would not be due to the mutation of *FOW2* gene, but rather to cross protection based on its nonpathogenic nature. Likewise, a nonpathogenic mutant of the transcriptional regulator gene *SGE1*, which is required for penetration of the root cortex and expression of genes encoding effectors, and its parental strain *F. oxysporum* f. sp. *lycopersici* have a similar protective effect on the non-host flax plant against the flax pathogen *F. oxysporum* f. sp. *lini* (Michielse et al., 2009).

In summary, to elucidate the molecular basis for biocontrol by nonpathogenic *F. oxysporum* against the wilt disease caused by pathogenic *F. oxysporum*, we assessed the biocontrol activities of nonpathogenic mutants generated by disruption of pathogenicity genes. The Δ*FOW2* strain strains had concentration-dependent biocontrol activity against root-borne pathogens *F. oxysporum* and *P. aphanidermatum*. The Δ*FOW2* strains and the nonpathogenic strains such as MFG6 and *F. oxysporum* f. sp. *lycopersici* colonized the melon root surface and inhibited conidial germination and hyphal elongation of pathogenic *F. oxysporum*, probably by outcompeting for nutrients rather than by inducing resistance. Nonpathogenic strains, including Δ*FOW2* strains, never compete against themselves for nutrients, suggesting that nonpathogenic strains can distinguish themselves from pathogenic strains. Since nutrient competition occurs only against strains that are pathogenic to plants, nonpathogenic strains might recognize pathogenic strains via virulence factors such as effector proteins or secondary metabolites secreted from pathogenic strains.

DATA AVAILABILITY STATEMENT

The original contributions presented in the study are included in the article/**Supplementary Material**, further inquiries can be directed to the corresponding author.

AUTHOR CONTRIBUTIONS

YI and TT conceived and designed the experiments. YI, AO, HS, and YH carried out fungal transformation and inoculation tests. YI, HK, and YH performed qPCR analysis. YI and ON observed by laser scanning confocal microscopy and scanning electron microscopy. YI and TT analyzed all data, prepared tables, figures, and additional materials, and wrote the manuscript. All authors contributed to the article and approved the submitted version.

FUNDING

This work was supported by grants-in-aids from JSPS KAKENHI (19658017) (TT) and (17H05022 and 16H02536) (YI).

ACKNOWLEDGMENTS

We are grateful to D. Cullen and J. Andrews for providing pTEFEGFP and to K. Kuroda and M. Kubota for providing the strains MFG6 and WPy1, respectively.

SUPPLEMENTARY MATERIAL

The Supplementary Material for this article can be found online at: https://www.frontiersin.org/articles/10.3389/fmicb.2022.826677/full#supplementary-material

REFERENCES

Alabouvette, C. (1986). Fusarium-wilt suppressive soils from the chateaurenard region - review of a 10-year study. *Agronomie* 6, 273–284. doi: 10.1051/agro:19860307

Alabouvette, C., Lemanceau, P., and Steinberg, C. (1993). Recent advances in biological control of fusarium wilts. *Pestic. Sci.* 37, 365–373. doi: 10.1002/ps.2780370409

Alabouvette, C., Olivain, C., Migheli, Q., and Steinberg, C. (2009). Microbiological control of soil-borne phytopathogenic fungi with special emphasis on wilt-inducing *Fusarium oxysporum*. *New Phytol.* 184, 529–544. doi: 10.1111/j.1469-8137.2009.03014.x

Bolwerk, A., Lagopodi, A. L., Lugtenberg, B. J. J., and Bloemberg, G. V. (2005). Visualization of interactions between a pathogenic and a beneficial *Fusarium* strain during biocontrol of tomato foot and root rot. *Mol. Plant Microbe Interact.* 18, 710–721. doi: 10.1094/MPMI-18-0710

Bovie, C., Ongena, M., Thonart, P., and Dommes, J. (2004). Cloning and expression analysis of cDNAs corresponding to genes activated in cucumber showing systemic acquired resistance after BTH treatment. *BMC Plant Biol.* 4:15. doi: 10.1186/1471-2229-4-15

Caracuel, Z., Martínez-Rocha, A. L., Di Pietro, A., Madrid, M. P., and Roncero, M. I. G. (2005). Fusarium oxysporum gas1 encodes a putative β-1,3-glucanosyltransferase required for virulence on tomato plants. *Mol. Plant Microbe Interact.* 18, 1140–1147. doi: 10.1094/MPMI-18-1140

Constantin, M. E., de Lamo, F. J., Vlieger, B. V., Rep, M., and Takken, F. L. (2019). Endophyte-mediated resistance in tomato to *Fusarium oxysporum* is independent of ET, JA, and SA. *Front. Plant Sci.* 10:979. doi: 10.3389/fpls.2019.00979

de Boer, W., Verheggen, P., Klein Gunnewiek, P. J. A., Kowalchuk, G. A., and van Veen, J. A. (2003). Microbial community composition affects soil fungistasis. *Appl. Environ. Microbiol.* 69, 835–844. doi: 10.1128/AEM.69.2.835-844.2003

de Lamo, F. J., Šimkovicová, M., Fresno, D. H., de Groot, T., Tintor, N., Rep, M., et al. (2020). Pattern-triggered immunity restricts host colonization by endophytic fusaria, but does not affect endophyte-mediated resistance. *Mol. Plant Pathol.* 18, 1–12. doi: 10.1111/mpp.13018

Di Pietro, A. D., García-Maceira, F. I., Méglecz, E., and Roncero, I. G. (2001). A MAP kinase of the vascular wilt fungus *Fusarium oxysporum* is essential for root penetration and pathogenesis. *Mol. Microbiol.* 39, 1140–1152. doi: 10.1111/j.1365-2958.2001.02307.x

Diallinas, G., and Kanellis, A. K. (1994). A phenylalanine ammonia-lyase gene from melon fruit: cDNA cloning, sequence and expression in response to development and wounding. *Plant Mol. Biol.* 26, 473–479. doi: 10.1007/BF00039557

Duyvesteijn, R. G. E., Wijk, R. V., Boer, Y., Rep, M., Cornelissen, B. J. C., and Haring, M. A. (2005). Frp1 is a Fusarium oxysporum F-box protein required for pathogenicity on tomato. *Mol. Microbiol.* 57, 1051–1063. doi: 10.1111/j.1365-2958.2005.04751.x

Edel-Hermann, V., and Lecomte, C. (2019). Current status of Fusarium oxysporum formae speciales and races. *Phytopathology* 109, 512–530. doi: 10.1094/PHYTO-08-18-0320-RVW

Fravel, D., Olivain, C., and Alabouvette, C. (2003). Fusarium oxysporum and its biocontrol. *New Phytol.* 157, 493–502. doi: 10.1046/j.1469-8137.2003.00700.x

Fuchs, J.-G., Moënne-Loccoz, Y., and Défago, G. (1997). Nonpathogenic Fusarium oxysporum strain Fo47 induces resistance to *Fusarium* wilt in tomato. *Plant Dis.* 81, 492–496. doi: 10.1094/PDIS.1997.81.5.492

García-Gutiérrez, L., Zeriouh, H., Romero, D., Cubero, J., de Vicente, A., and Pérez-García, A. (2013). The antagonistic strain *Bacillus subtilis* UMAF6639 also confers protection to melon plants against cucurbit powdery mildew by activation of jasmonate- and salicylic acid-dependent defence responses. *Microb Biotechnol.* 6, 264–274. doi: 10.1111/1751-7915.12028

Husaini, A. M., Sakina, A., and Cambay, S. R. (2018). Host-pathogen interaction in fusarium oxysporum infections: where do we stand? *Mol. Plant Microbe Interact.* 31, 889–898.

Imazaki, I., Kurahashi, M., Iida, Y., and Tsuge, T. (2007). Fow2, a Zn(II)2Cys6-type transcription regulator, controls plant infection of the vascular wilt fungus *Fusarium oxysporum*. *Mol. Microbiol.* 63, 737–753. doi: 10.1111/j.1365-2958.2006.05554.x

Inoue, I., Ohara, T., Namiki, F., and Tsuge, T. (2001). Isolation of pathogenicity mutants of *Fusarium oxysporum* f. sp. melonis by insertional mutagenesis. *J. Gen. Plant Pathol.* 67, 191–199. doi: 10.1105/tpc.002576

Jain, S., Akiyama, K., Kan, T., Ohguchi, T., and Takata, R. (2003). The G protein β subunit FGB1 regulates development and pathogenicity in *Fusarium oxysporum*. *Curr. Genet.* 43, 79–86. doi: 10.1007/s00294-003-0372-9

Jain, S., Akiyama, K., Mae, K., Ohguchi, T., and Takata, R. (2002). Targeted disruption of a G protein α subunit gene results in reduced pathogenicity in *Fusarium oxysporum*. *Curr. Genet.* 41, 407–413. doi: 10.1007/s00294-002-0322-y

Kuroda, K., Suzuki, H., Tomikawa, A., Tanaka, K., Ito, T., and Yamamoto, T. (2004). Biological control of Fusarium wilt of strawberry with carbide of brewer's grains by previously infested with nonpathogenic Fusarium oxysporum. *Jpn. J. Phytopathol.* 70:246.

Larkin, R. P., and Fravel, D. R. (1998). Efficacy of various fungal and bacterial biocontrol organisms for control of *Fusarium* wilt of tomato. *Plant Dis.* 82, 1022–1028. doi: 10.1094/PDIS.1998.82.9.1022

Larkin, R. P., and Fravel, D. R. (1999). Mechanisms of action and dose-response relationships governing biological control of *Fusarium* wilt of tomato by nonpathogenic *Fusarium* spp. *Phytopathology* 89, 1152–1161. doi: 10.1094/PHYTO.1999.89.12.1152

Larkin, R. P., Hopkins, D. L., and Martin, F. N. (1996). Suppression of Fusarium wilt of watermelon by nonpathogenic *Fusarium oxysporum* and other microorganisms recovered from a disease-suppressive soil. *Phytopathology* 86, 812–819. doi: 10.1094/Phyto-86-812

Lemanceau, P., Bakker, P. A. H. M., De Kogel, W. J., Alabouvette, C., and Schippers, B. (1993). Antagonistic effect on nonpathogenic Fusarium oxysporum strain Fo47 and pseudobactin 358 upon pathogenic Fusarium oxysporum f. sp. dianthi. *Appl. Environ. Microb.* 59, 74–82. doi: 10.1128/aem.59.1.74-82.1993

Livak, K. J., and Schmittgen, T. D. (2001). Analysis of relative gene expression data using real-time quantitative PCR and the $2-\Delta\Delta$ CT method. *Methods* 25, 402–408.

Lockwood, J. L. (1977). Fungistasis in soils. *Biol. Rev.* 52, 1–43. doi: 10.1006/meth.2001.1262

Louvet, J., Rouxel, F., and Alabouvette, C. (1976). Recherches sur la résistance des sols aux maladies. I. Mise en évidence de la nature microbiologique de la résistance d'un sol au développement de la fusariose vasculaire du melon. *Ann. Phytopathology* 8, 425–436.

Matta, A. (1989). "Induced resistance to fusarium wilt diseases," in *Vascular Wilt Diseases of Plants – Basic Studies and Control*, eds E. C. Tjamos and C. H. Beckman (Berlin: Springer), 175–196. doi: 10.1007/978-3-642-73166-2_13

Metraux, J. P., Burkhart, W., Moyer, M., Dincher, S., Middlesteadt, W., Williams, S., et al. (1989). Isolation of a complementary DNA encoding a chitinase with structural homology to a bifunctional lysozyme/chitinase. *Proc. Natl. Acad. Sci. U.S.A.* 86, 896–900. doi: 10.1073/pnas.86.3.896

Michielse, C. B., and Rep, M. (2009). Pathogen profile update: *Fusarium oxysporum*. *Mol Plant Pathol* 10, 311–324. doi: 10.1111/j.1364-3703.2009.00538.x

Michielse, C. B., van Wijk, R., Reijnen, L., Manders, E. M., Boas, S., Olivain, C., et al. (2009). The nuclear protein Sge1 of *Fusarium oxysporum* is required for parasitic growth. *PLoS Pathog.* 5:e1000637. doi: 10.1371/journal.ppat.1000637

Minerdi, D., Bossi, S., Gullino, M. L., and Garibaldi, A. (2009). Volatile organic compounds: a potential direct long-distance mechanism for antagonistic action of *Fusarium oxysporum* strain MSA 35. *Environ. Microbiol.* 11, 844–854. doi: 10.1111/j.1462-2920.2008.01805.x

Minerdi, D., Moretti, M., Gilardi, G., Barberio, C., Gullino, M. L., and Garibaldi, A. (2008). Bacterial ectosymbionts and virulence silencing in a *Fusarium oxysporum* strain. *Environ. Microbiol.* 10, 1725–1741. doi: 10.1111/j.1462-2920.2008.01594.x

Mizuno, S., Hirasawa, Y., Sonoda, M., Nakagawa, H., and Sato, T. (2006). Isolation and characterization of three DREB/ERF-type transcription factors from melon (*Cucumis melo*). *Plant Sci.* 170, 1156–1163. doi: 10.1016/j.plantsci.2006.02.005

Namiki, F., Matsunaga, M., Okuda, M., Inoue, I., Nishi, K., Fujita, Y., et al. (2001). Mutation of an arginine biosynthesis gene causes reduced pathogenicity in *Fusarium oxysporum* f. sp. melonis. *Mol. Plant Microbe Interact.* 14, 580–584. doi: 10.1094/MPMI.2001.14.4.580

Namiki, F., Shiomi, T., Kayamura, T., and Tsuge, T. (1994). Characterization of the formae speciales of *Fusarium oxysporum* causing wilts of cucurbits by DNA fingerprinting with nuclear repetitive DNA sequences. *Appl. Environ. Microbiol.* 60, 2684–2691. doi: 10.1128/aem.60.8.2684-2691.1994

Ogawa, K., and Komada, H. (1984). Biological control of *Fusarium* wilt of sweet potato by non-pathogenic *Fusarium oxysporum*. *Ann. Phytopathol. Soc. Jpn.* 50, 1–9.

Olivain, C., Trouvelot, S., Binet, M. N., Cordier, C., Pugin, A., and Alabouvette, C. (2003). Colonization of flax roots and early physiological responses of flax cells inoculated with pathogenic and nonpathogenic strains of Fusarium oxysporum. *Appl. Environ. Microbiol.* 69, 5453–5462. doi: 10.1128/AEM.69.9.5453-5462.2003

Pareja-Jaime, Y., Martín-Urdíroz, M., González Roncero, M. I., González-Reyes, J. A., and Ruiz Roldán, M. D. C. (2010). Chitin synthase-deficient mutant of Fusarium oxysporum elicits tomato plant defense response and protects against wild-type infection. *Mol. Plant Pathol.* 11, 479–493. doi: 10.1111/j.1364-3703.2010.00624.x

Postma, J., and Luttikholt, A. J. G. (1996). Colonization of carnation stems by a nonpathogenic isolate of *Fusarium oxysporum* and its effect on *Fusarium oxysporum* f. sp. dianthi. *Can. J. Bot.* 74, 1841–1851. doi: 10.1139/b96-221

Postma, J., and Rattink, H. (1992). Biological control of *Fusarium* wilt of carnation with a nonpathogenic isolate of *Fusarium oxysporum*. *Can. J. Bot.* 70, 1199–1205. doi: 10.1139/b92-150

Rouxel, F., Alabouvette, C., and Louvet, J. (1979). Recherches sur la résistance des sols aux maladies. IV. Mise en évidence du rôle des *Fusarium* autochtones dans la résistance d'un sol à la fusariose vasculaire du melon. *Ann. Phytopathol.* 11, 199–207.

Sarkar, D., Rovenich, H., Jeena, G., Nizam, S., Tissier, A., and Balcke, G. U. (2019). The inconspicuous gatekeeper: endophytic *Serendipita vermifera* acts as extended plant protection barrier in the rhizosphere. *New Phytol.* 224, 886–901. doi: 10.1111/nph.15904

Silvar, C., Merino, F., and Díaz, J. (2009). Resistance in pepper plants induced by *Fusarium oxysporum* f. sp. lycopersici involves different defence-related genes. *Plant Biol.* 11, 68–74. doi: 10.1111/j.1438-8677.2008.00100.x

Tamietti, G., and Alabouvette, C. (1986). Résistance des sols aux maladies: XIII – rôle des *Fusarium oxysporum* non pathogènes dans les mécanismes de résistance d'un sol de Noirmoutier aux fusarioses vasculaires. *Agronomie* 6, 541–548.

Toussoun, T. A. (1975). "Fusarium-suppressive soils," in *Biology And Control Of Soil-Borne Plant Pathogen*, ed. G. W. Bruehl (St Paul, MN: American Phytopathological Society), 145–151.

Uknes, S., Mauch-Mani, B., Moyer, M., Potter, S., Williams, S., Dincher, S., et al. (1992). Acquired resistance in *Arabidopsis*. *Plant Cell* 4, 645–656. doi: 10.1105/tpc.4.6.645

Vanden Wymelenberg, A. J., Cullen, D., Spear, R. N., Schoenike, B., and Andrews, J. H. (1997). Expression of green fluorescent protein in *Aureobasidium pullulans* and quantification of the fungus on leaf surfaces. *BioTechniques* 23, 686–690. doi: 10.2144/97234st01

Conflict of Interest: The authors declare that the research was conducted in the absence of any commercial or financial relationships that could be construed as a potential conflict of interest.

Publisher's Note: All claims expressed in this article are solely those of the authors and do not necessarily represent those of their affiliated organizations, or those of the publisher, the editors and the reviewers. Any product that may be evaluated in this article, or claim that may be made by its manufacturer, is not guaranteed or endorsed by the publisher.

Citation: Iida Y, Ogata A, Kanda H, Nishi O, Sushida H, Higashi Y and Tsuge T (2022) Biocontrol Activity of Nonpathogenic Strains of Fusarium oxysporum: Colonization on the Root Surface to Overcome Nutritional Competition. Front. Microbiol. 13:826677. doi: 10.3389/fmicb.2022.826677

frontiers in Microbiology

ORIGINAL RESEARCH
published: 03 February 2022
doi: 10.3389/fmicb.2021.803789

Isolation, Characterization and Draft Genome Analysis of Bacteriophages Infecting *Acidovorax citrulli*

Katarina Gašić[1], Mina Obradović[2], Nemanja Kuzmanović[3], Nevena Zlatković[1], Milan Ivanović[4], Danijela Ristić[1] and Aleksa Obradović[4]**

[1] Institute for Plant Protection and Environment, Belgrade, Serbia, [2] Institute of Molecular Genetics and Genetic Engineering, University of Belgrade, Belgrade, Serbia, [3] Federal Research Centre for Cultivated Plants, Institute for Plant Protection in Horticulture and Forests, Julius Kühn-Institut, Braunschweig, Germany, [4] Faculty of Agriculture, University of Belgrade, Belgrade, Serbia

Bacterial fruit blotch and seedling blight, caused by *Acidovorax citrulli*, is one of the most destructive diseases of melon and watermelon in many countries. Pathogen-free seed and cultural practices are major pillars of the disease control. However, use of bacteriophages as natural biocontrol agents might also contribute to the disease management. Therefore, we isolated 12 bacteriophages specific to *A. citrulli*, from phyllosphere and rhizosphere of diseased watermelon plants. The phage strains were characterized based on their host range, plaque and virion morphology, thermal inactivation point, adsorption rate, one step growth curve, restriction fragment length polymorphism (RFLP), and genomic analysis. Transmission electron microscopy of three phage strains indicated that they belong to the order *Caudovirales*, family *Siphoviridae.* All phages lysed 30 out of 32 tested *A. citrulli* strains isolated in Serbia, and did not lyse other less related bacterial species. They produced clear plaques, 2 mm in diameter, on bacterial lawns of different *A. citrulli* strains after 24 h of incubation. The thermal inactivation point was 66 or 67°C. They were stable at pH 5–9, but were sensitive to chloroform and inactivated in either 5 or 10 min exposure to ultraviolet (UV) light. RFLP analysis using *Eco*RI, *Bsm*I and *Bam*HI enzymes did not show genetic differences among the tested phages. Adsorption rate and one step growth curve were determined for the *Acidovorax* phage ACF1. Draft genome sequence of the ACF1 phage was 59.377 bp in size, with guanine-cytosine (GC) content 64.5%, including 89 open reading frames. This phage shared a very high genomic identity with *Acidovorax* phage ACPWH, isolated in South Korea. Evaluation of systemic nature of ACF1 strain showed that it can be absorbed by roots and translocated to upper parts of watermelon plants where it survived up to 10 days.

Keywords: *Acidovorax citrulli*, bacteriophage, genome analysis, host specificity, phage therapy, biocontrol

OPEN ACCESS

Edited by:
Marco Scortichini, Council for Agricultural Research and Economics (CREA), Italy

Reviewed by:
Zoe Anne Dyson, University of London, United Kingdom
David J. Studholme, University of Exeter, United Kingdom

****Correspondence:***
Katarina Gašić
gasickatarina@yahoo.com
Aleksa Obradović
aleksao@agrif.bg.ac.rs

Specialty section:
This article was submitted to Microbe and Virus Interactions with Plants, a section of the journal Frontiers in Microbiology

Received: *28 October 2021*
Accepted: *06 December 2021*
Published: *03 February 2022*

Citation:
Gašić K, Obradović M, Kuzmanović N, Zlatković N, Ivanović M, Ristić D and Obradović A (2022) Isolation, Characterization and Draft Genome Analysis of Bacteriophages Infecting Acidovorax citrulli. Front. Microbiol. 12:803789. doi: 10.3389/fmicb.2021.803789

INTRODUCTION

Bacterial fruit blotch (BFB) of cucurbits is a disease caused by *Acidovorax citrulli*, a bacterium which can lead to serious yield and seed production losses in cucurbit crops. In several occasions, when conditions favored bacterial dissemination in the United States, watermelon crop damage reached 100% (Latin and Rane, 1990). Typical symptoms of BFB in watermelon, such as seedling water-soaked lesions and blotches on fruits, have been noticed since the mid-1960s

(Webb and Goth, 1965) but the pathogen responsible for the disease was first identified by Latin and Hopkins (1995). During the 1990s, BFB rapidly progressed toward other crops such as honeydew, pumpkin, and cucumber (Isakeit et al., 1997; Langston et al., 1999; Martin et al., 1999).

Acidovorax citrulli is a Gram-negative bacterium primarily disseminated by infected cucurbit seed (Rane and Latin, 1992). Usually, first symptoms appear on seedlings and young plants. The symptom development and spread of the infection are facilitated by the transplant growth conditions in nurseries. It has been shown that, under such conditions, a single seed containing 10 *A.citrulli* colony forming units (CFU) within a seed lot can lead to BFB transmission (Dutta et al., 2012a). The bacterium resides on the surface and underneath the seed coat, and if the seed infection originates from the blossom invasion, *A.citrulli* cells are deposited deep within the seed, which hinders their control (Dutta et al., 2012b).

Acidovorax citrulli has been detected in Serbia for the first time on watermelon plants in 2014 (Popović and Ivanović, 2014), causing significant economic loses. Although, it has been eradicated, sporadic occurrence of BFB was recorded in upcoming years, affecting watermelon production in main production regions in Serbia (Zlatković et al., 2015, 2017).

Different management strategies for BFB control have been attempted, including selection of the disease resistant or tolerant cultivars (Bahar et al., 2009), treatments with peroxyacetic acid (Hopkins et al., 2003) and chitosan solution (Li et al., 2013), as well as use of biological control approaches such as non-pathogenic *A. citrulli* strain (Johnson et al., 2011) or antagonistic rhizobacteria (Adhikari et al., 2017). Still, BFB is a considerable threat to watermelon and melon production worldwide (Burdman and Walcott, 2012).

Bacteriophages, viruses of bacteria, are considered promising biocontrol agents (Buttimer et al., 2017; Choudhary et al., 2022). Previous studies investigated their potential in use against different genera of phytopathogenic bacteria as previously reviewed (Jones et al., 2007; Buttimer et al., 2017; Stefani et al., 2021). Recently, Rahimi-Midani et al. (2018) reported for the first time isolation of phages infecting *A. citrulli.*

The aim of the present study was to isolate bacteriophages specific to *A. citrulli,* study their characteristics and evaluate possibilities of their use in biocontrol of BFB.

MATERIALS AND METHODS

Bacterial Strains and Culture Conditions

All bacterial strains used in this study (**Table 1**) were stored at −20 or −80°C in Nutrient Broth (NB) supplemented with 20 and 30% of glycerol, respectively. The strains were grown on Nutrient agar (NA) or King's medium B (KB) 24 h prior to use. Bacterial suspensions were prepared in sterile distilled water, and concentration was adjusted to 5×10^8 (OD_{600} = 0.3) and then diluted accordingly.

For phage detection and propagation, semisolid nutrient agar yeast extract medium (NYA; 0.8% NB, 0.6% agar, and 0.2% yeast extract) (Balogh et al., 2003) or NB was used. Phage concentration was determined by serial dilutions of phage suspension in sterile tap water or SM buffer (10 mM Tris–HCl, pH 7.5; 100 mM NaCl; 10 mM $MgSO_4$), followed by a plaque assay on NYA medium by using *A. citrulli* strain KBI 86 as a host, as previously described (Gašić et al., 2011, 2018).

Isolation, Purification and Propagation of Phages

Samples for phage isolation were collected from the watermelon field affected by *A. citrulli* during 2014. Watermelon plants and fruits showing symptoms of BFB as well as watermelon rhizosphere soil were used for phage isolation by enrichment method as follows: a flask containing 50 ml NB with 2.5 g $CaCO_3$ was inoculated with 5 ml suspension of *A. citrulli* strain KBI 86 in sterile distilled water (conc. 10^8 CFU/ml), followed by addition of 10 g of soil or 5 g of plant tissue; samples were incubated overnight on a horizontal rotary shaker (100 rpm) at 27°C; ten ml aliquots were centrifuged (10,000 *g*, 10 min), and resulting supernatant was filter sterilized to remove any remaining bacterial cells, and stored at 4°C.

The presence of specific phages in the suspension was tested by screening for lysis of the target bacterium *A. citrulli* strain KBI 86. Suspension of bacteria (100 μl, conc. 10^9 CFU/ml) was pipetted in the center of the empty Petri dish, followed by adding NYA medium (cooled to 48°C). Bacteria and medium were mixed by horizontal rotation of the plates. After medium solidified, 10 μl of tested suspensions was spotted on the surface of the medium and after 48 h of incubation appearance of plaques indicating lysis of the bacterial cells within the inoculated area were scored.

Phage purification was performed by three subsequent single plaque isolation steps as previously described (Gašić et al., 2011). Concentration of phage in suspension was determined by plating 100 μl of ten-fold dilution of purified phage suspension and 100 μl of suspension of *A. citrulli*, strain KBI 86 in NYA medium.

Phage propagation was performed by inoculation of actively growing culture of *A. citrulli* strain KBI 86 (conc. 10^8 CFU/ml) in NB, at the multiplicity of infection (MOI) of 0.1. After 24 h of incubation on the rotary shaker (150 rpm, 27°C), culture was filtered through a 0.22 μm membrane filter and stored either at 4°C, or for long term storage in NB containing 30% glycerol at −80°C (Gašić et al., 2011).

Host Range Analysis

The ability of *A. citrulli* specific phages to lyse bacterial strains isolated from watermelon samples collected from different regions in Serbia was investigated. Twelve phages were tested against 32 *A. citrulli* strains including *A. citrulli* type strain NCPPB 3679^T, as well as 22 strains of other phytopathogenic or saprophytic bacterial species. Phage suspensions (5 μl), prepared in sterile tap water, were spotted onto the surface of solidified NYA medium mixed with suspensions of selected bacterial strains. After 24 h of incubation at 27°C, plaque formation was observed. The test has been repeated three times.

TABLE 1 | The host range of studied bacteriophages.

Bacterial strain	Bacterial species	Host	Origin	Year of isolation	Acidovorax phages ACF1 –ACF12
KBI76	*Acidovorax citrulli*	*C. lanatus*	Ašanja, Serbia	2014	+
KBI77	*Acidovorax citrulli*	*C. lanatus*	Ašanja, Serbia	2014	–
KBI78	*Acidovorax citrulli*	*C. lanatus*	Ašanja, Serbia	2014	–
KBI79	*Acidovorax citrulli*	*C. lanatus*	Ašanja, Serbia	2014	+
KBI80	*Acidovorax citrulli*	*C. lanatus*	Ašanja, Serbia	2014	+
KBI81	*Acidovorax citrulli*	*C. lanatus*	Ašanja, Serbia	2014	+
KBI82	*Acidovorax citrulli*	*C. lanatus*	Ašanja, Serbia	2014	+
KBI83	*Acidovorax citrulli*	*C. lanatus*	Ašanja, Serbia	2014	+
KBI84	*Acidovorax citrulli*	*C. lanatus*	Ašanja, Serbia	2014	+
KBI85	*Acidovorax citrulli*	*C. lanatus*	Ašanja, Serbia	2014	+
KBI86	*Acidovorax citrulli*	*C. lanatus*	Ašanja, Serbia	2014	+
KFB340	*Acidovorax citrulli*	*C. lanatus*	Ašanja, Serbia	2014	+
KFB341	*Acidovorax citrulli*	*C. lanatus*	Ašanja, Serbia	2014	+
KFB342	*Acidovorax citrulli*	*C. lanatus*	Ašanja, Serbia	2014	+
KFB343	*Acidovorax citrulli*	*C. lanatus*	Ašanja, Serbia	2014	+
KFB344	*Acidovorax citrulli*	*C. lanatus*	Ašanja, Serbia	2014	+
KFB345	*Acidovorax citrulli*	*C. lanatus*	Ašanja, Serbia	2014	+
KFB346	*Acidovorax citrulli*	*C. lanatus*	Ašanja, Serbia	2014	+
KFB347	*Acidovorax citrulli*	*C. lanatus*	Ašanja, Serbia	2014	+
KFB348	*Acidovorax citrulli*	*C. lanatus*	Ašanja, Serbia	2014	+
KFB349	*Acidovorax citrulli*	*C. lanatus*	Ašanja, Serbia	2014	+
KFB350	*Acidovorax citrulli*	*C. lanatus*	Ašanja, Serbia	2014	+
KFB351	*Acidovorax citrulli*	*C. lanatus*	Čelarevo, Serbia	2014	+
KFB352	*Acidovorax citrulli*	*C. lanatus*	Čelarevo, Serbia	2014	+
KFB365	*Acidovorax citrulli*	*C. lanatus*	Rečka, Serbia	2015	+
KFB366	*Acidovorax citrulli*	*C. lanatus*	Rečka, Serbia	2015	+
KFB367	*Acidovorax citrulli*	*C. lanatus*	Rečka, Serbia	2015	+
KFB368	*Acidovorax citrulli*	*C. lanatus*	Rečka, Serbia	2015	+
KFB370	*Acidovorax citrulli*	*C. lanatus*	Šabac, Serbia	2016	+
KFB371	*Acidovorax citrulli*	*C. lanatus*	Šabac, Serbia	2016	+
KFB372	*Acidovorax citrulli*	*C. lanatus*	Šabac, Serbia	2016	+
NCPPB4156	*Ralstonia solanacearum*	*Solanum tuberosum*	Netherlands	1995	–
NCPPB 3679^T	*Acidovorax citrulli*	*Citrullus lanatus*	United States	unknown	–
NCPPB 2968	*X. euvesicatoria*	*Capsicum frutescens*	United States	1977	–
NCPPB 1423	*X. vesicatoria*	*Lycopersicon esculentum*	Hungary	1957	–
NCPPB 4321	*X. gardneri*	*Lycopersicon esculentum*	Serbia	1953	–
NCPPB 881	*X. perforans*	*Lycopersicon esculentum*	United States	1991	–
KBI32	*E. amylovora*	*Cydonia oblonga*	Serbia	2013	–
KFB68	*Pectobacterium carotovorum* ssp. *carotovorum*	*Brassica oleracea* var. *capitata*	Serbia	1999	–
KBI05	*Dickeya ssp.*	*Solanum tuberosum*	United Kingdom	unknown	–
KBI018	*Clavibacter michiganensis* ssp. *michiganensis*	*Lycopersicon esculentum*	Hungary	1957	–
KBI04	*C. m.* ssp. *sepedonicus*	*Solanum tuberosum*	Finland	1983	–
C58	*Agrobacterium tumefaciens*	*Prunus cerasus*	United States	1958	–
GSPB 1142	*Pseudomonas syringae* pv. *syringae*	*Phaseolus* sp.	Germany	1967	–
A1	*Pseudomonas graminis*	Apple phyllosphere	Serbia	2015	–
A2	*P. graminis*	Apple phyllosphere	Serbia	2015	–
A3	*P. graminis*	Apple phyllosphere	Serbia	2015	–
A4	*P. graminis*	Apple phyllosphere	Serbia	2015	–
B130	*Pseudomonas fluorescens*	Ji et al., 1996	–	–	–

+, clear plaque; – absence of plaque.

KBI – Collection of bacteria, Institute for Plant Protection and Environment, Belgrade; KFB – Collection of phytopathogenic bacteria, University of Belgrade, Faculty of Agriculture, Belgrade; NCPPB – The National Collection of Plant Pathogenic Bacteria, FERA, United Kingdom.

Transmission Electron Microscopy

Morphology of *Acidovorax* phages ACF1, ACF8, and ACF12 was observed by transmission electron microscopy (TEM) using the negative staining protocol with 1% uranyl acetate solution, as previously described (Balogh, 2006; Gašić et al., 2011). The phages were observed and photographed by TEM (JEOL JEM-1400 series) with an accelerating voltage of 120 kV. Phage dimensions were evaluated by measurement of head diameter and length of the tail, and calculated as an average value of five phage particles for each isolate.

Thermal Inactivation of Phages

Thermal point of inactivation was studied for three *Acidovorax* phages, ACF1, ACF8, and ACF12. In test tubes, 1 ml of each phage suspension (10^7 PFU/ml) in sterile tap water was exposed to temperatures ranging from 30 to 80°C, with intervals of 10°C, for 10 min in a water bath. The second repetition of the test was done in the temperature range from 61 to 70°C, with an interval of 1°C. After incubation, tubes with phage suspensions were transferred to 20°C water bath, in order to stop the extended effect of the temperature treatment. Viability of phages after different temperature treatments was assayed by the spot test on NYA medium with *A. citrulli* strain KBI 86. Plaque formation was observed after 20 h of incubation at 27°C. The temperature at which no viable phage particles capable of lysing bacterial cells were detected was defined as the thermal inactivation point.

The Effect of Ultraviolet Irradiation on Phage Viability *in vitro*

The effect of ultraviolet (UV) irradiation on three phage strains ACF1, ACF8, and ACF12 was studied. As a source of UV light, UV lamp integrated in the laminar flow hood was used (Philips TUV G30T8, UVC = 254 nm). Suspensions of phages were prepared in sterile tap water to the concentration of 10^5 PFU/ml and 10 ml was poured into each Petri dish. Suspensions were exposed to UV irradiation from the distance of 50 cm and for the duration of 5 and 10 min (Czajkowski et al., 2014). After the treatment, the titer of phages in the suspensions was assayed. In the second repetition of the experiment, the suspensions were exposed to the irradiation for either 2 or 5 min.

The Effect of Chloroform on Phage Vitality

Suspensions of phages ACF1, ACF8, and ACF12 (1 ml of 10^6 PFU/ml), were incubated on a shaker with or without the supplement of 20% chloroform for 1 h. Afterward, the phage titer in the suspensions was checked by plating decimal dilutions of the suspensions as described above. The experiment was repeated twice.

The Effect of pH on Phage Survival

For testing the effect of different pH values on phage survival, suspensions of three phage strains ACF1, ACF8, and ACF12 (10^4 PFU/ml) were prepared in SM buffer of different pH values (2, 5, 7, 9, and 11), and incubated for 24 h at room temperature, followed by the phage titer assay. The experiment was repeated twice.

Optimal Multiplicity of Infection

Optimal multiplicity of infection (MOI) of phage ACF1 was determined as previously described by Gašić et al. (2011), with slight modification. In order to eliminate bacterial cells, the phage suspensions were filtered by using 0.22 μm pore size filter (Sarstedt, syringe filter R-33 mm) instead of the chloroform treatment (10% v/v), after which the titer of multiplied phages was determined.

Adsorption Rate

Adsorption rate, i.e., a number of phage particles adsorbed to the host cell in particular time, was determined as described previously (Ellis and Delbrück, 1939; Gašić et al., 2011). Moreover, percentage of *Acidovorax* phage ACF1 particles adsorbed to the host *A. citrulli* KBI 86 was determined. The experiment was repeated three times.

One Step Growth Curve

In order to determine parameters of phage life cycle, a modification of the protocols of Ellis and Delbrück (1939) and Carlson (2005) was used, as described by Gašić et al. (2011). Briefly, *A. citrulli*, strain KBI 86 was grown in 40 ml NB at 27°C, with shaking until it reached the concentration 10^8 CFU/ml (OD_{600} = 0.3). One ml of the culture was transferred to a sterile microtube and 10 μl of ACF1 phage suspension (10^8 PFU/ml) was added. The mix was incubated for 20 min at 27°C, to allow the adsorption of phages to the bacterial cell surface, and afterward was diluted 10,000 times in NB. During further 110 min of incubation, starting from the moment of dilution, 100 μl of the suspension was collected every 10 min and phage titer was determined. Latent period, rise period and burst size was calculated as previously described (Gašić et al., 2011). The experiment was repeated three times.

Bacteriophage DNA Extraction

For genomic DNA extraction, 35 ml of phage suspension (conc. 10^9 PFU/ml) was centrifuged (28,000 *g*, 90 min, 4°C), and pellet containing phages was resuspended in 700 μl of SM buffer. In order to eliminate any bacterial nucleic acid, samples were treated with 10 μl/sample DNase I (1 U/μl) and 1 μl/sample RNase A (100 mg/ml) at 37°C for 60 min. DNA extraction was further performed as previously described by Lehman et al. (2009). DNA quality and quantity was assessed by NanoDrop (NanoPhotometer® N60), while DNA integrity was assessed by agarose (0.8% agarose) gel electrophoresis.

Restriction Fragment Length Polymorphism Analysis

DNA of three phages (ACF1, ACF8, and ACF12) was digested with *Bam*HI, *Eco*RI, and *Bsm*I restriction enzymes (Fermentas, Lithuania) as recommended by manufacturer. Digestion reaction contained 500 ng DNA, 1.5 μl buffer, 2 μl restriction enzyme and up to 15 μl nuclease-free water. The mixtures were incubated at

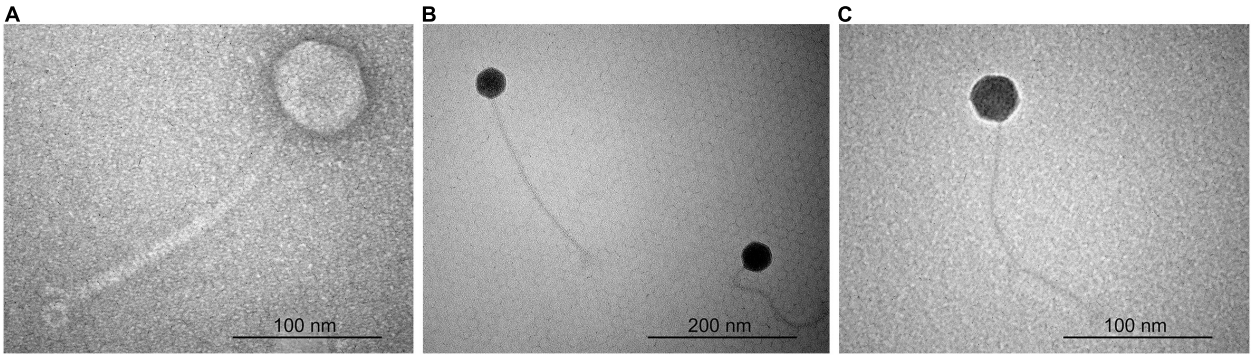

FIGURE 1 | Transmission electron micrograph of *Acidovorax* phage ACF1 **(A)**, ACF8 **(B)**, and ACF12 **(C)**.

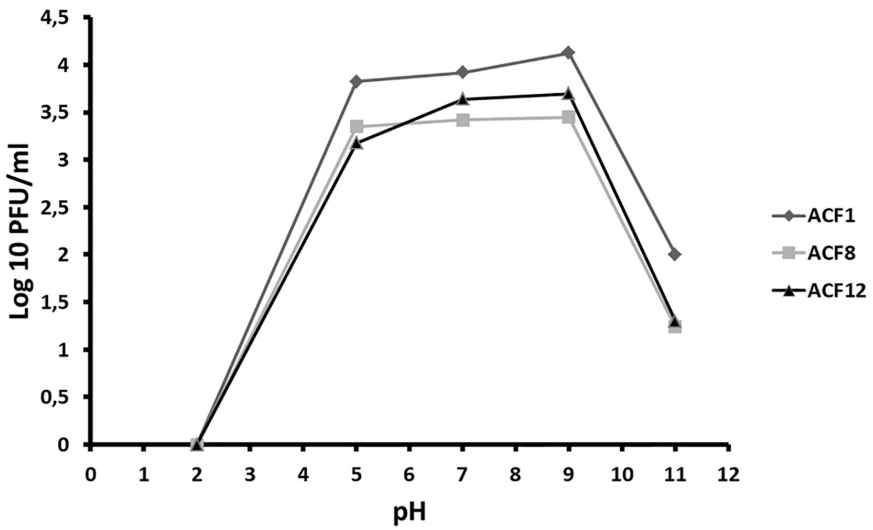

FIGURE 2 | The effect of pH on *Acidovorax* phage ACF1, ACF8, and ACF12 vitality.

37°C for 16 h. DNA fragments were separated by agarose (1%) gel electrophoresis in Tris-acetate-EDTA buffer, stained with Midori Green (MIDORI Green Advance, NIPPON Genetics EUROPE) 2% (v/v) and visualized by a digital imaging camera (Vilber Lourmat, France).

The *in silico* restriction fragment length polymorphism (RFLP) analysis was performed by pDRAW32 software (AcaClone Software)[1].

Phage Genome Sequencing and Bioinformatic Analysis

Genome of *Acidovorax* phage ACF1 was sequenced using the Illumina HiSeq 2500 system with paired-end reads at BaseClear, Leiden, Netherlands following the manufacturer's instructions. Initial quality assessment was based on data passing the Illumina Chastity filtering. Subsequently, reads containing PhiX control signal were removed using an in-house filtering protocol. In addition, reads containing (partial) adapters were clipped (up to minimum read length of 50 bp). The second quality assessment was based on the remaining reads using the FastQC quality control tool version 0.10.0. The quality of the FASTQ sequences was further enhanced by trimming off low-quality bases using the "Trim sequences" option of the CLC Genomics Workbench version 9.5.1 (Qiagen, Aarhus, Denmark). The *de novo* assembly was performed using the "*De novo* assembly" option of the same software. Misassemblies and nucleotide disagreement between the Illumina data and the contig sequences are corrected with Pilon version 1.20 (Walker et al., 2014). The accuracy of the assembly was checked by mapping reads back to contigs followed by visual inspection.

The assembled genome was annotated using RAST (Aziz et al., 2008; Overbeek et al., 2014; Brettin et al., 2015), Prokka (Seemann, 2014), and DFAST[2] (Tanizawa et al., 2018) tools. Functional bioinformatic annotation for predicted ORF

[1]http://www.acaclone.com

[2]https://dfast.ddbj.nig.ac.jp/

gene products was refined manually using BLASTP[3], Pfam[4] (Finn et al., 2010), and Virfam searches[5] (Lopes et al., 2014). The potential presence of virulence-associated genes and antibiotic resistance genes in the phage genome was analyzed by VirulenceFinder v. 2.0[6] and ResFinder ver. 4.1[7] (Kleinheinz et al., 2014). The presence of transfer RNA genes was assessed using ARAGORN[8] (Laslett and Canback, 2004) and tRNAscan-SE[9] (Lowe and Chan, 2016). The genome sequence was compared to other viruses using BLAST analysis (Altschul et al., 1990) and PASC web tool (Bao et al., 2014), while comparisons at the amino acid level were done using CoreGenes 3.5 (Zafar et al., 2002).

Phage genome comparison and its visualization was performed using Easyfig 2.2.5 (Sullivan et al., 2011). The genomic relatedness between phage genomes was performed by calculating average nucleotide identity (ANI) values. For this purpose, we used the JSpecies Web Service and employed blast algorithm (Richter et al., 2016). Phylogenetic analysis was carried out based on the amino acid sequences of the gene encoding DNA polymerase of the *Acidovorax* phage ACF1 and 24 members of *Siphoviridae* viruses found in the GenBank database, using a BLASTP *E*-value cutoff of 1e-03. The sequences were aligned using MAFFT v7 (Katoh and Standley, 2013). A maximum-likelihood phylogenetic tree was constructed using IQ-TREE v1.6.12 (Nguyen et al., 2015) with 1000 ultrafast bootstrap replications (Hoang et al., 2017) and LG + I + G4 substitution model suggested by ModelFinder (Kalyaanamoorthy et al., 2017).

Nucleotide Sequence Accession Number

The genome sequence of the *Acidovorax* phage ACF1 has been deposited at DDBJ/ENA/GenBank under the accession MZ547449 and BioProject PRJNA745195. The raw sequencing reads were deposited in the Sequence Read Archive (SRA) under the same BioProject PRJNA745195.

Phage Translocation in Watermelon Plants

The possibility of phages to be absorbed through the root system of plants and their further translocation through the plant vascular system has been studied based on experiments by Iriarte et al. (2012). The experiment was conducted three times. Commercial watermelon seeds cv. Crimson sweet (Hoya Seed) were planted and cultivated in a plant growth chamber, at 27°C day (16 h) and 15°C night (8 h) temperature. Two weeks after sprouting, the plants were drenched with 100 ml suspension of phage ACF1 at concentration 1.6×10^8 PFU/ml (first test) or 75 ml of phage suspension concentration 1.4×10^9 PFU/ml (second and third test). Total number of treated plants per assay was 21. Control group was treated with tap water in the same manner. Plants were sampled seven times: after 1, 2, 3, 5, 7, 10, and 14 days from the treatment. In each sampling, three treated and three control plants were dissected. The plants were carefully uprooted and divided into three sections: root, hypocotyl with cotyledons and foliage. Tissue of each section was homogenized by mortar and pestle in sterile distilled water (1 ml per 1 g of tissue) and filtered through a syringe filter (Sarstedt, R - 33 mm, pore size 0.22 μm). The filtrate of each section was tested for presence of phages and their titer was determined as previously described.

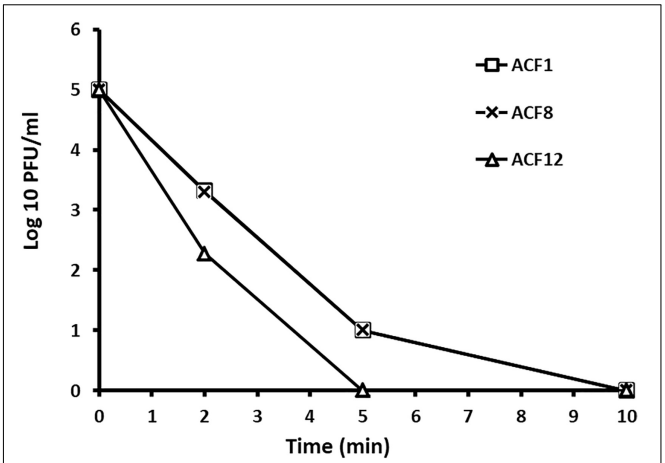

FIGURE 3 | The effect of UV light on *Acidovorax* phage ACF1, ACF8, and ACF12 vitality.

RESULTS

Phage Isolation

In September 2014, plant and soil samples were collected for phage isolation from a field of watermelon showing symptoms of BFB. After enrichment of potential phages in bacterial host culture, 12 samples yielded phages able to lyse *A. citrulli* strains. Nine phage samples originated from the watermelon rhizosphere soil (*Acidovorax* phage ACF1 – 9), while three phage strains (*Acidovorax* phage ACF10 – 12) were isolated from watermelon leaves showing symptoms of BFB. After purification, the phage strains' propagation resulted in titer ranging from 10^9 to 10^{10} PFU/ml, respectively. All phages formed plaques 1.5–2 mm in diameter surrounded by 0.5 mm halo, after 24 h incubation with host *A. citrulli* KBI 86. Three phage strains, ACF1, ACF8, and ACF12 were selected for further characterization.

Electron Microscopy

According to the particle morphology, i.e., presence of an icosahedral head and a long, flexible, non-contractile tail (**Figure 1**), observed by TEM, phages ACF1, ACF8, and ACF12 belong to the order *Caudovirales*, family *Siphoviridae*. Average head diameter of phage ACF1 was 64.4 nm, and length of tail was 220.9 nm. Phage ACF8 possesses head 45.8 nm in diameter and

[3]https://blast.ncbi.nlm.nih.gov/Blast.cgi?PAGE=Proteins
[4]http://pfam.xfam.org
[5]http://biodev.cea.fr/virfam/
[6]https://cge.cbs.dtu.dk/services/VirulenceFinder/
[7]https://cge.cbs.dtu.dk/services/ResFinder/
[8]http://130.235.46.10/ARAGORN/
[9]http://lowelab.ucsc.edu/tRNAscan-SE

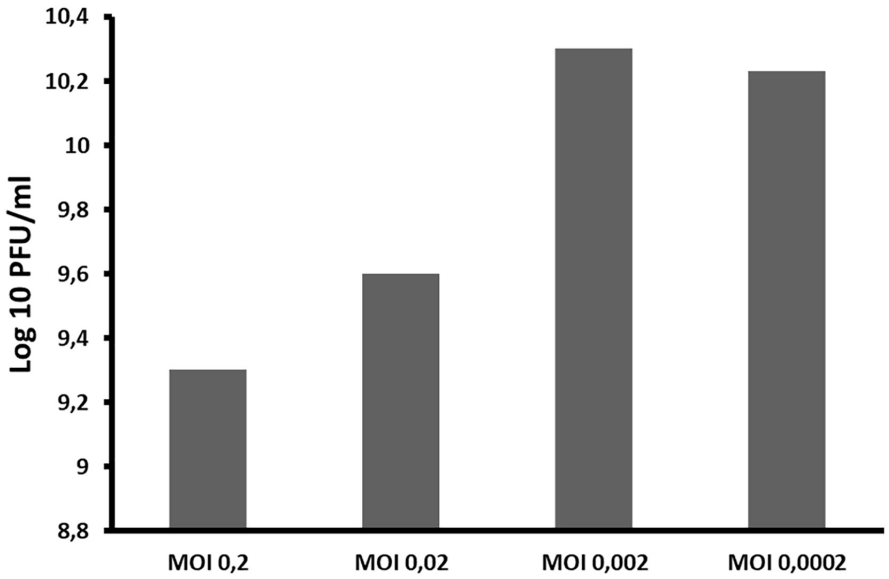

FIGURE 4 | The influence of different ratios of bacteriophages and bacteria in suspension (MOI) during phage ACF1 multiplication.

tail length 233.1 nm, while average dimensions of phage ACF12 were head 46.1 nm in diameter and tail 240.3 nm.

Host Range Analysis

All tested phages were species specific. They lysed 30 *A. citrulli* strains tested, and showed no activity to two *A. citrulli* strains isolated in Serbia nor to the type strain NCPPB 3679^T. However, the tested phage strains did not lyse any of the strains belonging to the different genera or less related bacterial species (**Table 1**).

The Effect of Temperature, Chloroform, pH and Ultraviolet Irradiation on Phage Survival *in vitro*

Acidovorax phage ACF8 was inactivated at 66°C, while the point of thermal inactivation for phages ACF1 and ACF12 was 67°C. The chloroform treatment negatively affected vitality of the phage strains ACF1, ACF8, and ACF12, while the strain ACF1 was the most sensitive. After 1 h incubation with 20% chloroform, titer of phages ACF8 and ACF12 decreased by 11%, while ACF1 phage titer decreased by 36.38%.

Tested phages were stable at range of pH 5–9 (**Figure 2**), but were inactivated after 5 min (ACF12) or 10 min (ACF1 and ACF8) exposure to UV (**Figure 3**).

Optimal Multiplicity of Infection, Adsorption Rate and One Step Growth Curve

The optimal MOI of ACF1 phage was determined to be 0.002 (**Figure 4**). The difference between the highest and the lowest phage titer produced by propagation at studied MOIs was 1 log unit.

Adsorption rate of phage ACF1 to *A. citrulli* (KBI 86) cells after 20 min of incubation was 90% (**Figure 5**). Within 1 min, 60.65% of phages were adsorbed and the rate increased proportionally to the incubation time.

With the one–step growth test, the replication cycle growth curve was determined. Based on the results, the latent period of *Acidovorax* phage ACF1 is 30 min and burst size (average number of released phage virions per infected bacterial cell) is 74 ± 5 plaque forming units per infected cell (**Figure 6**). The rise period, when the number of phages increases due to release from the lysed cells, lasted ca. 60 min. The replication cycle of ACF1 in total lasted 90 min.

Restriction Fragment Length Polymorphism Analysis of Phage DNA

Based on the RFLP analysis of phage's DNA, it was determined that all three strains (ACF1, ACF8, and ACF12) possess identical restriction profiles after digestion with *Eco*RI and *Bsm*I enzymes. However, no DNA digestion occurred using the *Bam*HI enzyme, indicating that the *A. citrulli* phage genomes do not possess specific restriction sites for this enzyme (**Supplementary Figure 1**). RFLP profiles indicated genetic relatedness of all three phages.

Phage ACF1 Genome Sequencing and Phylogenetic Analysis

Sequencing of *Acidovorax* phage ACF1 total DNA followed by genome assembly resulted in one long contig (∼60 kbp) and 152 short contigs (<1000 bp). Almost all the reads mapped to this long contig (99.9% of total bases) with high average coverage depth of 7194X. The average coverage depth of short contigs individually was relatively low (<20) and we therefore considered them as a contamination, which was also suggested by BLAST analysis. *In silico* RFLP analysis of the sequence corresponding to the large contig correlated to the patterns

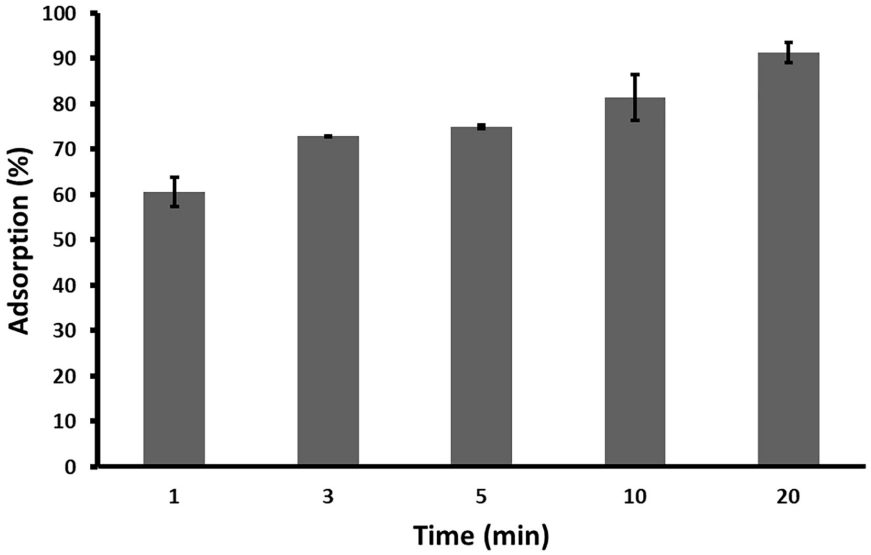

FIGURE 5 | Adsorption rate of *Acidovorax* phage ACF1 to bacterial cell surface. Means and standard errors from three independent experiments are shown.

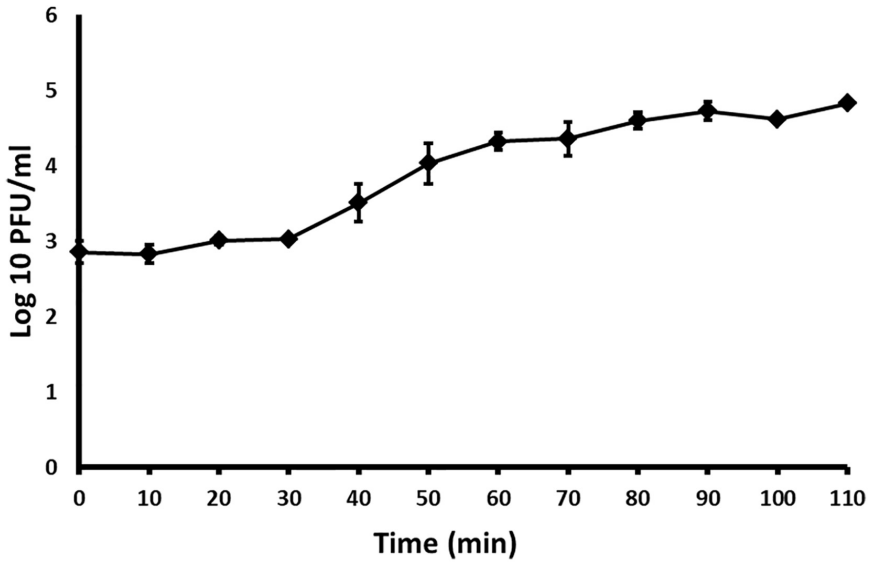

FIGURE 6 | One-step growth curve of *Acidovorax* phage ACF1 propagated in *A. citrulli* KBI 86. Means and standard errors from three independent experiments are shown.

obtained by digesting phage DNA (data not shown). Overall, we considered that large contig represents nearly complete (draft) genome of the phage ACF1.

The size of the draft genome of phage ACF1 was 59.377 bp with a guanine-cytosine (GC) content 64.5%. The final annotation submitted to GenBank was based on combination of results obtained by RAST and DFAST, including additional functional annotation on basis of BLASTP, Pfam, Virfam, ARAGORN, and tRNAscan-SE searches. Taken together, a total of 89 open reading frames (ORFs) and two tRNAs (Ser- tRNA anticodon GCT and Ala-tRNA anticodon CGC) were identified (**Figure 7**). Length of ORFs ranges from 117 to 4077 bp, encoding putative proteins of 38–1358 amino acids. Total of 92.3% of the genome consists of coding regions. Among all identified ORFs, 74 start with ATG as the start codon while 14 start with GTG and one with TTG codon. The orientation of genome annotation showed that 45 genes are on the plus strand, while 44 on the reverse strand. Out of 89 putative ORFs, 20 (22.5%) have an assigned function, while the rest of 73 ORFs (77.5%) were classified as hypothetical or phage proteins (**Supplementary Table 1** and **Figure 7**). Functional grouping of predicted ORFs revealed that nine ORFs encode phage

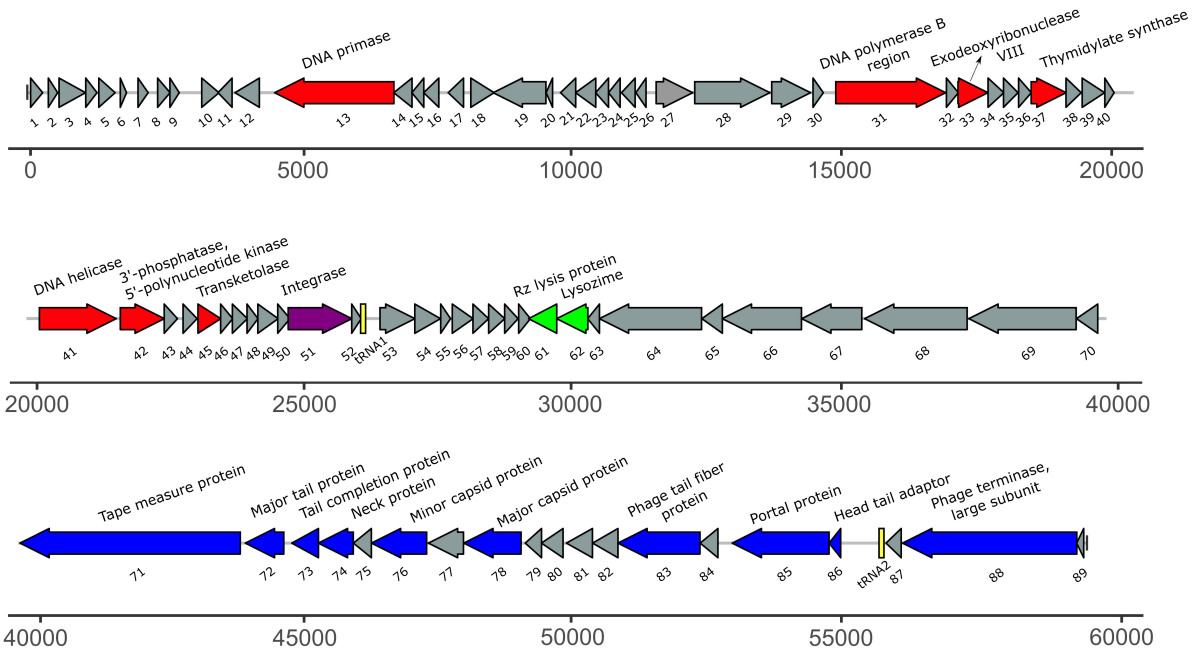

FIGURE 7 | The annotated draft genome of *Acidovorax* phage ACF1. The ORFs coding for proteins involved in DNA replication/modification/transcriptional regulations are marked in red; ORFs coding for structural proteins are marked in blue; ORFs coding for enzymes involved in host lysis are marked in green; ORF coding for recombination protein is marked in purple. ORFs coding for hypothetical and phage proteins are marked in gray while tRNAs are marked in yellow. Arrows indicate the direction of transcription and translation. Unit of the presented draft genome annotation is in bp.

structural proteins (tape measure protein, major tail protein, tail completion protein, neck protein, minor capsid protein, major capsid protein, tail fiber protein, portal protein, head-tail adaptor, and terminase large subunit), seven ORFs are involved in DNA replication/modification/transcriptional regulations (DNA primase, DNA polymerase B region, exodeoxyribonuclease VIII, thymidylate synthase, DNA helicase, 3′-phosphatase, 5′-polynucleotide kinase and transketolase), two ORFs coding the proteins involved in host lysis (Rz lysis protein, lysozyme), and one ORF coding for integrase protein was identified. The draft genome does not contain any genes encoding antibiotic resistance or toxins. Based on Virfam analysis of the sequences of head, neck and tail proteins, *Acidovorax* phage ACF1 was classified to belong to the family *Siphoviridae* of Type 1, Cluster 6 (**Supplementary Figure 2**), confirming previous observations by TEM.

The BLASTn search using draft genome sequence of *Acidovorax* phage ACF1 showed the best match (99.23% identity and 71% query coverage) with the *Acidovorax* phage ACPWH (Gene Bank Acc no. MH727593.1). The relatedness between *Acidovorax* phages ACF1 and ACPWH was further confirmed by the high ANI value obtained between their genomic sequences (>99%). Most of the genes were highly conserved between these two phages (**Figure 8**). A total of 64 predicted proteins of *Acidovorax* phage ACF1 shared homology with ACPWH, while 25 proteins were unique to ACF1 phage, as evaluated by CoreGenes. Moreover, the *Acidovorax* phage ACF1 was compared to characterized genera from *Siphoviridae*, *Podoviridae,* and *Myoviridae* family using the PASC tool comparison, showing highest nucleotide identity of 15.85% to unclassified *Ralstonia* phage RS138 and 13.78% to *Xylella* virus Salvo (Sanovirus) both belonging to the *Siphoviridae* family. Moreover, ACF1 phage showed some nucleotide identity with Rauchvirus *Bordetella* virus BPP1 (13.57%) and *Xanthomonas citri* phage CP2 (13.52%) from *Podoviridae* family.

Phylogenetic analysis of *Acidovorax* phage ACF1 based on DNA polymerase amino acid sequence revealed that ACF1 phage forms a clade with *Acidovorax* phage ACPWH that is distinct from the neighboring branch containing *Xanthomonas* phage FoX4 (**Figure 9**).

Translocation of Phages Through Watermelon Plants

Acidovorax phage ACF1 was detected in root, hypocotyl and leaf tissue 24 h after drenching the soil with phage suspension. The highest concentration of phages (6.03×10^4 PFU/g) was detected in the root system 3 days after treatment (**Figure 10**). Phages remained both in hypocotyl and root tissue for 10 days, but were not detectable in leaf tissue after 48 h.

DISCUSSION

Due to the extensive use of pesticides and ineffectiveness of conventional and chemical control of bacterial diseases, there is an increased interest in biologically based solutions (Buttimer et al., 2017). Bacteriophages are gaining more attention and

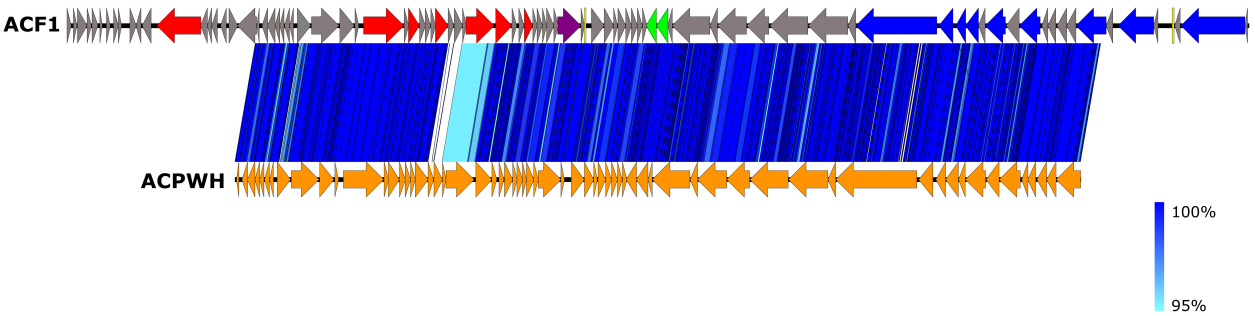

FIGURE 8 | Comparison of draft genome sequence of *Acidovorax* phage ACF1 and *Acidovorax* phage ACPWH using Easyfig. Arrows indicate ORFs and their orientation. ORFs are colored according to their functions (see **Figure 7**). The blue vertical blocks between the genome maps indicate the level of identity between sequences (see the legend on the right) according to tBLASTx.

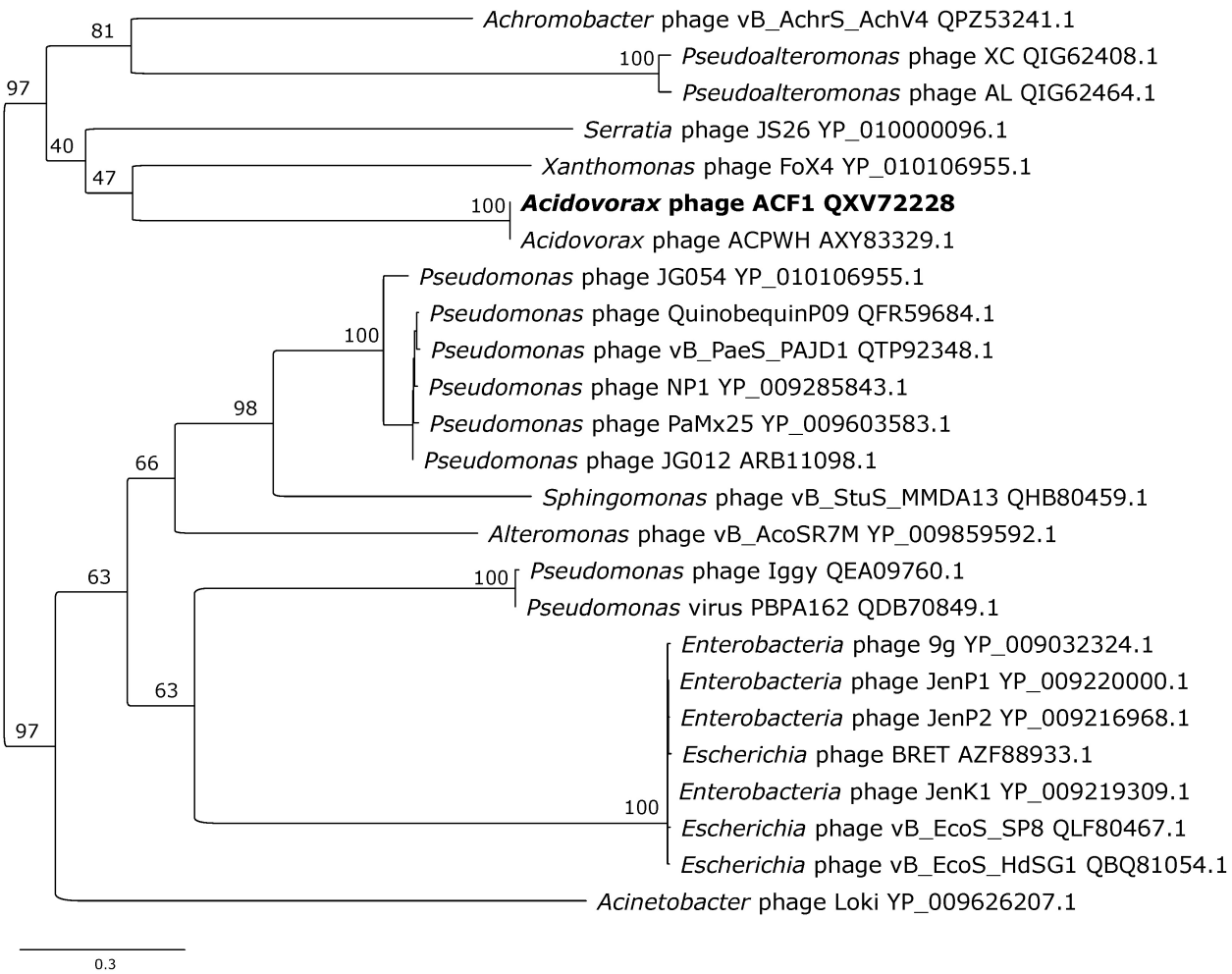

FIGURE 9 | Maximum likelihood tree based on the DNA polymerase of *Acidovorax* phage ACF1 (bold font) and homologous proteins from other phages of the *Siphoviridae* family. The numbers on the nodes indicate ultrafast bootstrap values. The tree was midpoint rooted. The scale bar represents the number of expected substitutions per site under the best-fitting LG + I + G4 model.

importance as potential biocontrol agents. Inadequate efficiency of available *A. citrulli* control methods requires innovative approaches. In this research, we studied several phage strains as potential biocontrol agents of *A. citrulli*. Particularly, we investigated their host range, survival in various conditions, replication cycle parameters and analyzed draft genome sequence

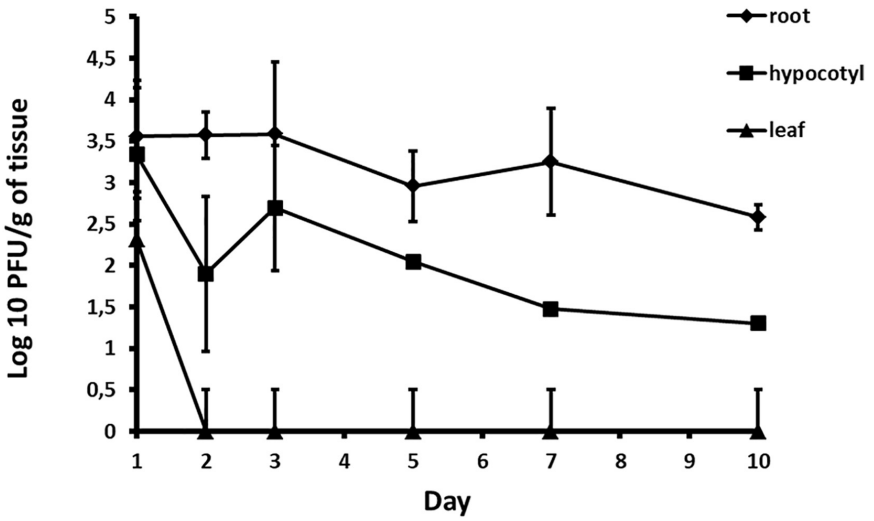

FIGURE 10 | Quantification of phage translocation through plant tissue. The results shown are mean values of three replications with standard deviations.

of one representative phage. The ACF1 phage uptake by watermelon root system and translocation in upper parts was investigated as well.

All phages formed clear plaques 1.5–2 mm in diameter with 0.5 mm halo zone. As reported previously, the halo is often correlated with the presence of exopolysaccharide depolymerases, resulting in depolymerization of the EPS, which increases the lawn transparency (van Charante et al., 2021). Additionally, the halo zones might also be due to diffusion of virus-encoded non-virion associated lytic enzymes such as endolysins, which degrade the cell wall of neighboring cells (Jurczak-Kurek et al., 2016).

As much as specificity of phages allows safe application as antimicrobials, without affecting other bacteria present in the environment, high specificity could be also one of the disadvantages for their application in biocontrol of plant pathogenic bacteria since they might be limited to infecting only particular strains of the target bacterial species (Jones et al., 2007). One way of expanding the phage treatment host range is using cocktails of different phage strains covering broader range of the host bacterium strains. The cocktail may contain phages targeting different receptor sites on the bacterial cell surface or affecting the biofilm formation. Phage cocktails also could reduce a chance of resistance development in pathogenic bacteria, considering low possibility of developing resistance simultaneously to multiple phages attacking the target bacterium (Choudhary et al., 2022). The fact that two *A. citrulli* strains were resistant to all 12 phage strains indicated a weak point in the phages' host range. Prior attempts for controlling the disease in a field, variation of the phage host range and possibility of expanding it must be studied in detail to avoid favoring of the resistant bacterial strains.

Results of one-step growth and adsorption studies, including draft genome analysis, support the use of *Acidovorax* phage ACF1 as biocontrol agent. ACF1 phage has a burst size of 74 ± 5 phage particles per infected cell and rapidly adsorbs to the host cells, with 90% of phages being attached after 20 min. Sensitivity of ACF1, ACF8, and ACF12 to chloroform and UV light could be an additional disadvantage that requires a solution, in regard of their application. Reduced viability of phages of *Dickeya solani, Erwinia amylovora,* and *Xanthomonas euvesicatoria* after treatment with UV light or chloroform has been already reported (Gašić et al., 2011; Czajkowski et al., 2014; Born et al., 2015). Chloroform is used in the process of phage isolation or multiplication in order to eliminate unlysed and phage resistant bacterial cells, especially if the volume of the phage suspension does not justify application of the filtering procedure (Clokie and Kropinski, 2009). Cost-effectiveness and feasibility of production and storage of phage preparations are some of the conditions that should be met. Sensitivity to UV illumination and low pH of ACF1, ACF8, and ACF12 is a shared trait with other bacteriophages of plant-associated bacteria. Jones et al. (2007) demonstrated that factors such as exposure to sunlight, high temperatures, extreme pHs and high ionic concentration inactivate phages and impose a practical problem for their application in agriculture.

Phage characterization by TEM revealed that isolated phages belong to the order *Caudovirales*, and the family *Siphoviridae* based on their head and tail morphology. Among all identified viruses, the *Caudovirales* or tailed phages are the most numerous. Ackermann and Prangishvili (2012) reported that 96.3% of the described phages belonged to the tailed phages, while only 230 (3.7%) are polyhedral, filamentous, or pleomorphic. Moreover, the family *Siphoviridae*, is the largest family with over 3600 descriptions, or 57.3% (Ackermann and Prangishvili, 2012). Size of studied phages corresponds to the size indicated for *Siphoviridae* (head 40–80 nm, tail 5–10 × 100–210 nm and genome size 21–134 kb) in the ICTV 9th report (King et al., 2011). So far, there are two described phages of *A. citrulli*, ACP17 belonging to the *Myoviridae* family (Rahimi-Midani et al., 2018), and phage ACPWH which belongs to the *Siphoviridae* family (Rahimi-Midani et al., 2020). Size of the phage ACF1 was similar

to the phage ACPWH (head is 55 ± 5 nm in width and 60 ± 5 nm in length, with a tail length of approximately 180 ± 5 nm) while the other two studied strains had smaller head and longer tail compared to the phage ACPWH.

Draft genome of *Acidovorax* phage ACF1 obtained in this study has a size of 59.377 bp, with 89 ORFs and two tRNA genes (**Figure 7** and **Supplementary Table 1**). ACF1 phage displayed a very high genomic identity with previously described *Acidovorax* phage ACPWH isolated in South Korea (Rahimi-Midani et al., 2018), as indicated by BLASTn and ANIb analyses. Nevertheless, the *Acidovorax* phage ACPWH, specific to *A. citrulli*, has a dsDNA genome of 42.499 bp which is smaller than the genome of ACF1, and encodes 64 ORFs, with no tRNA gene. The draft genome annotation showed that ACF1 has all basic structural and functional genes coding DNA replication proteins, host lysis proteins, and tail structure proteins. Moreover, gene with homology to known integrases was detected in the draft genome of ACF1. The presence of integrase in the phage genome suggests that the phages are able to integrate their genomes into the host genome and enter the lysogenic phase (Groth and Calos, 2004). Phage possessing lysogenic life cycle (temperate phages) are not considered suitable for therapeutic purposes due to their potential to transfer bacterial antibiotic resistance or virulence genes via transduction (Monteiro et al., 2019). However, recent advances in synthetic biology could enable engineering of temperate phages toward elimination of genes involved in a lysogenic life cycle or in bacterial virulence (Zhang et al., 2013; Pires et al., 2016; Kilcher et al., 2018). In this way temperate phage could become obligatory lytic and suitable for use in phage therapy (Monteiro et al., 2019). Lytic phages typically contain a DNA polymerase gene and other genes associated with DNA replication such as DNA primase and DNA helicase (Lohr et al., 2005). However, most of the lysogenic phage genomes of members of the *Siphoviridae* and *Myoviridae* do not possess these DNA replication genes (Lohr et al., 2005). The presence of an integrase gene, but also, DNA replication genes in the draft genome of phage ACF1, suggested that phage ACF1 might have some pseudolysogenic characteristics (Abedon, 2009; Cenens et al., 2013).

CoreGenes analysis showed that 64 protein-coding sequences shared homology with ACPWH phage, while 25 were unique to *Acidovorax* phage ACPWH. This is in accordance with the difference in size of two phages, since phage ACPWH possess 25 ORFs less then phage ACF1. Additionally, PASC analysis showed that ACF1 has common genes (13–15%) with *Ralstonia* phage RS138 and *Xylella* virus Salvo from *Siphoviridae* family, and *Bordetella* virus BPP1 and *Xanthomonas citri* phage CP2 (13.5%) from *Podoviridae*.

Since there is no universal gene present in all phages, some of the signature gene products could be used for study of virus diversity (Adriaenssens and Cowan, 2014). Phylogenetic analysis of *Acidovorax* phage ACF1 based on DNA polymerase amino acid sequence grouped together with phage ACPWH, near *Xanthomonas* phage XoF4.

Automated classification of tailed bacteriophages according to their neck organization by Virfam (Lopes et al., 2014), revealed that *Acidovorax* phage ACF1 belongs to *Siphoviridae* of Type 1, Cluster 6 (**Supplementary Figure 2**). Neck Type 1 phage genomes contain the following proteins: portal protein, Adaptor of type 1 (Ad1), Head-closure of type 1 (Hc1), Neck protein of type 1 (Ne1), and tail-completion of type 1 (Tc1). Cluster 6 is mostly composed of siphophages with small genome sizes that infect Proteobacteria and possess a different head-neck-tail gene order compared to that observed in the majority of siphoviruses. As it seen in **Figure 7**, gene coding for head-tail adaptor (Ad1) is positioned between the genes coding for the terminase and portal proteins, while in most Type 1 siphoviruses, Ad1 is usually located downstream from the major capsid protein gene.

Instead of treating the phyllosphere parts and expose phages to UV light, in this study we tested possibility of applying phage suspension by drenching the soil. It was determined that phage ACF1 can be absorbed from soil by the root system of watermelon plants and transported up to the leaves. The titer of phages was most stable in the root system and did not drop until 4 days after the phage treatment. Phages detected in the leaves were of a lower titer and endured shorter than in other parts of the plant. The highest titer of phages detected in the three trials was 6.03×10^4 PFU/g, which is 4.37 log units lower than the applied phage concentration (1.4×10^9 PFU/ml). This information and the variation of the detected titer values indicate the presence of obstacles in the absorption of phages. Previous research has shown that phages could be immobilized by biofilm formed in the substrate (Storey and Ashbolt, 2001), adsorbed to soil particles (Williams et al., 1987), as well as inactivated by low pH values of the substrate (Sykes et al., 1981). Also, the concentration of the phage suspension relative to the volume of rhizosphere to which it is applied significantly affects the detected concentration of phage, their persistency in plant tissue and efficacy of translocation. Iriarte et al. (2012) have shown that *Ralstonia solanacearum*, *Xanthomonas perforans,* and *X. euvesicatoria* phages were transported through the vascular elements of tomato plants up to the leaves. Furthermore, they showed that the translocation of phages can be affected by the type of phage, plant species, plant age, plant size and the type of substrate in which the plant was grown. Rahimi-Midani and Choi (2020) recently studied the transportation of *A. citrulli* phages throughout melon plants. They tracked the transport of phages through melon plant parts by PCR and fluorescent microscopy (Rahimi-Midani et al., 2020). The study demonstrated that phages applied to the soil can translocate through the melon plant vascular tissue up to leaves and decrease the disease severity to 27% and increase survival of the infected plants to 100%.

Our results indicated that considering lytic life cycle and some of the biological characteristics of investigated phage strains, they possess potential in control of watermelon fruit blotch pathogen. However, before going to the field, the risks such as host range, survival in an open environment, type and frequency of application, need to be addressed properly. Otherwise the application of these biocontrol agents may be compromised.

DATA AVAILABILITY STATEMENT

Data available at ncbi.nlm.nih.gov/nuccore/2071735446 BioProject PRJNA745195.

AUTHOR CONTRIBUTIONS

KG and AO conceived and designed the experiments. KG, MO, NK, NZ, MI, and DR performed the experiments. KG, NK, and MO analyzed the data. KG and MO wrote the manuscript. AO revised the manuscript. All authors read and approved the final manuscript.

FUNDING

KG, MO, NZ, MI, DR, and AO were supported by the Ministry of Education, Science and Technological Development, Serbia, Contract Nos. 451-03-9/2021-14/200010 (KG, NZ, and DR); 451-03-9/2021-14/200116 (MI and AO); 451-03-9/2021-14/200042 (MO). NK was funded by the Deutsche Forschungsgemeinschaft (DFG, German Research Foundation) – Projektnummer 429677233.

SUPPLEMENTARY MATERIAL

The Supplementary Material for this article can be found online at: https://www.frontiersin.org/articles/10.3389/fmicb.2021.803789/full#supplementary-material

Supplementary Figure 1 | Restriction DNA profiles of *Acidovorax* phage ACF1, ACF8, and ACF12 after digestion with enzymes *Eco*RI and *Bam*HI, M1 – Lambda DNA/*Eco*RI + *Hin*DIII Marker (Thermo Fisher, Lithuania), M2 – GeneRuler DNA Ladder Mix (Thermo Fisher, Lithuania).

Supplementary Figure 2 | Automated classification of *Acidovorax* phage ACF1 according to its neck organization by Virfam analysis (Lopes et al., 2014). The different branches of the tree were sorted into 10 Clusters, highlighted by different background colors and numbers.

Supplementary Table 1 | Putative open reading frames (ORFs) of *Acidovorax* phage ACF1, their predicted functions and detected conserved domains.

REFERENCES

Abedon, S. T. (2009). "Disambiguating bacteriophage pseudolysogeny: an historical analysis of pseudolysogeny, and the phage carrier state," in *Contemporary Trends in Bacteriophage Research*, ed. H. T. Adams (New York, NY: Nova Science Publishers).

Ackermann, H. W., and Prangishvili, D. (2012). Prokaryote viruses studied by electron microscopy. *Arch. Virol.* 157, 1843–1849. doi: 10.1007/s00705-012-1383-y

Adhikari, M., Yadav, D. R., Kim, S. W., Um, Y. H., Kim, H. S., Lee, S. C., et al. (2017). Biological control of bacterial fruit blotch of watermelon pathogen (*Acidovorax citrulli*) with rhizosphere associated bacteria. *Plant Pathol. J.* 33, 170–183. doi: 10.5423/PPJ.OA.09.2016.0187

Adriaenssens, E. M., and Cowan, D. A. (2014). Using signature genes as tools to assess environmental viral ecology and diversity. *Appl. Environ. Microbiol.* 80, 4470–4480. doi: 10.1128/AEM.00878-14

Altschul, S. F., Gish, W., Miller, W., Myers, E. W., and Lipman, D. J. (1990). Basic local alignment search tool. *J. Mol. Biol.* 215, 403–410. doi: 10.1016/S0022-2836(05)80360-2

Aziz, R. K., Bartels, D., Best, A. A., DeJongh, M., Disz, T., Edwards, R. A., et al. (2008). The RAST server: rapid annotations using subsystems technology. *BMC Genomics* 9:1–15. doi: 10.1186/1471-2164-9-75

Bahar, O., Kritzman, G., and Burdman, S. (2009). Bacterial fruit blotch of melon: screens for disease tolerance and role of seed transmission in pathogenicity. *Eur. J. Plant Pathol.* 123, 71–83. doi: 10.1007/s10658-008-9345-7

Balogh, B. (2006). *Characterization and Use of Bacteriophages Associated With Citrus Bacterial Pathogens for Disease Control*. Dissertation. Gainesville, FL: University of Florida.

Balogh, B., Jones, J. B., Momol, M. T., Olson, S. M., Obradović, A., King, B., et al. (2003). Improved efficacy of newly formulated bacteriophages for management of bacterial spot of tomato. *Plant Dis.* 87, 949–954. doi: 10.1094/PDIS.2003.87.8.949

Bao, Y., Chetvernin, V., and Tatusova, T. (2014). Improvements to pairwise sequence comparison (PASC): a genome-based web tool for virus classification. *Arch. Virol.* 159, 3293–3304. doi: 10.1007/s00705-014-2197-x

Born, Y., Bosshard, L., Duffy, B., Loessner, M. J., and Fieseler, L. (2015). Protection of *Erwinia amylovora* bacteriophage Y2 from UV-induced damage by natural compounds. *Bacteriophage* 5:e1074330. doi: 10.1080/21597081.2015.1074330

Brettin, T., Davis, J. J., Disz, T., Edwards, R. A., Gerdes, S., Olsen, G. J., et al. (2015). RASTtk: a modular and extensible implementation of the RAST algorithm for building custom annotation pipelines and annotating batches of genomes. *Sci Rep.* 5, 1–6. doi: 10.1038/srep08365

Burdman, S., and Walcott, R. O. N. (2012). *Acidovorax citrulli*: generating basic and applied knowledge to tackle a global threat to the cucurbit industry. *Mol. Plant Pathol.* 13, 805–815. doi: 10.1111/j.1364-3703.2012.00810.x

Buttimer, C., McAuliffe, O., Ross, R. P., Hill, C., O'Mahony, J., and Coffey, A. (2017). Bacteriophages and bacterial plant diseases. *Front. Microbiol.* 8:34. doi: 10.3389/fmicb.2017.00034

Carlson, K. (2005). "Working with bacteriophages: common techniques and methodological approaches," in *Bacteriophages: Biology and Applications*, eds E. Kutter and A. Sulakvelidze (Boca Raton, FL: CRC Press), 437–494.

Cenens, W., Makumi, A., Mebrhatu, M. T., Lavigne, R., and Aertsen, A. (2013). Phage–host interactions during pseudolysogeny. *Bacteriophage* 3:e25029. doi: 10.4161/bact.25029

Choudhary, M., Paret, M., Obradović, A., Gašić, K., and Jones, J. (2022). "Bacteriophages for plant disease control," in *Microbial Bioprotectants for Plant Disease Management*, eds J. Köhl and W. Ravensberg (Sawston: Burleigh Dodds Science Publishing), 473–506. doi: 10.19103/as.2021.0093.18

Clokie, M. R. J., and Kropinski, A. M. (2009). *Bacteriophages: Methods and Protocols. Volume 1: Isolation, Characterization, and Interactions*. Totowa, NJ: Humana Press.

Czajkowski, R., Ozymko, Z., and Lojkowska, E. (2014). Isolation and characterization of novel soilborne lytic bacteriophages infecting *Dickeya* spp. biovar 3 ('*D. solani*'). *Plant Pathol.* 63, 758–772.

Dutta, B., Avci, U., Hahn, M. G., and Walcott, R. R. (2012a). Location of *Acidovorax citrulli* in infested watermelon seeds is influenced by the pathway of bacterial invasion. *Phytopathology* 102, 461–468. doi: 10.1094/phyto-10-11-0286-r

Dutta, B., Scherm, H., Gitaitis, R. D., and Walcott, R. R. (2012b). *Acidovorax citrulli* seed inoculum load affects seedling transmission and spread of bacterial fruit blotch of watermelon under greenhouse conditions. *Plant Dis.* 96, 705–711. doi: 10.1094/PDIS-04-11-0292

Ellis, E. L., and Delbrück, M. (1939). The growth of bacteriophage. *J. Gen. Physiol.* 22, 365–384.

Finn, R. D., Mistry, J., Tate, J., Coggill, P., Heger, A., Pollington, J. E., et al. (2010). The Pfam protein families database. *Nucleic Acids Res.* 38(Suppl._1), D211–D222. doi: 10.1093/nar/gkp985

Gašić, K., Ivanović, M. M., Ignjatov, M., Ćalić, A., and Obradović, A. (2011). Isolation and characterization of *Xanthomonas euvesicatoria* bacteriophages. *J. Plant Pathol.* 2, 415–423.

Gašić, K., Kuzmanović, N., Ivanović, M., Prokić, A., Šević, M., and Obradović, A. (2018). Complete genome of the *Xanthomonas euvesicatoria* specific

bacteriophage K81, its survival and potential in control of pepper bacterial spot. *Front. Microbiol.* 9:2021. doi: 10.3389/fmicb.2018.02021

Groth, A. C., and Calos, M. P. (2004). Phage integrases: biology and applications. *J Mol Biol.* 335, 667–678. doi: 10.1016/j.jmb.2003.09.082

Hoang, D. T., Chernomor, O., von Haeseler, A., Minh, B. Q., and Vinh, L. S. (2017). UFBoot2: improving the ultrafast bootstrap approximation. *Mol. Biol. Evol.* 35, 518–522. doi: 10.1093/molbev/msx281

Hopkins, D. L., Thompson, C. M., Hilgren, J., and Lovic, B. (2003). Wet seed treatment with peroxyacetic acid for the control of bacterial fruit blotch and other seedborne diseases of watermelon. *Plant Dis.* 87, 1495–1499. doi: 10.1094/PDIS.2003.87.12.1495

Iriarte, F. B., Obradović, A., Wernsing, M. H., Jackson, L. E., Balogh, B., Hong, J. A., et al. (2012). Soil-based systemic delivery and phyllosphere in vivo propagation of bacteriophages: two possible strategies for improving bacteriophage persistence for plant disease control. *Bacteriophage* 2:e23530. doi: 10.4161/bact.23530

Isakeit, T., Black, M. C., Barnes, L. W., and Jones, J. B. (1997). First report of infection of honeydew with *Acidovorax avenae* subsp. *citrulli*. *Plant Dis.* 81:694. doi: 10.1094/PDIS.1997.81.6.694C

Ji, P., Kloepper, J. W., Wilson, M., and Campbell, H. L. (1996). Rhizobacterial-induced systemic resistance in tomato against bacterial speck. *Phytopathology* 86:S50.

Johnson, K. L., Minsavage, G. V., Le, T., Jones, J. B., and Walcott, R. R. (2011). Efficacy of a nonpathogenic *Acidovorax citrulli* strain as a biocontrol seed treatment for bacterial fruit blotch of cucurbits. *Plant Dis.* 95, 697–704. doi: 10.1094/PDIS-09-10-0660

Jones, J. B., Jackson, L. E., Balogh, B., Obradović, A., Iriarte, F. B., and Momol, M. T. (2007). Bacteriophages for plant disease control. *Annu. Rev. Phytopathol.* 45, 245–262.

Jurczak-Kurek, A., Gąsior, T., Nejman-Faleńczyk, B., Bloch, S., Dydecka, A., Topka, G., et al. (2016). Biodiversity of bacteriophages: morphological and biological properties of a large group of phages isolated from urban sewage. *Sci. Rep.* 6, 1–17. doi: 10.1038/srep34338

Kalyaanamoorthy, S., Minh, B. Q., Wong, T. K. F., Von Haeseler, A., and Jermiin, L. S. (2017). ModelFinder: fast model selection for accurate phylogenetic estimates. *Nat. Methods* 14, 587–589. doi: 10.1038/nmeth.4285

Katoh, K., and Standley, D. M. (2013). MAFFT multiple sequence alignment software version 7: improvements in performance and usability. *Mol. Biol. Evol.* 30, 772–780. doi: 10.1093/molbev/mst010

Kilcher, S., Studer, P., Muessner, C., Klumpp, J., and Loessner, M. J. (2018). Cross-genus rebooting of custom-made, synthetic bacteriophage genomes in L-form bacteria. *PNAS* 115, 567–572. doi: 10.1073/pnas.1714658115

King, A. M. Q., Lefkowitz, E., Adams, M. J., and Carstens, E. B. (2011). *Virus Taxonomy: Ninth Report of the International Committee on Taxonomy of Viruses*, Vol. 9. San Diego, CA: Elsevier Academic Press.

Kleinheinz, K. A., Joensen, K. G., and Larsen, M. V. (2014). Applying the ResFinder and VirulenceFinder web-services for easy identification of acquired antibiotic resistance and E. coli virulence genes in bacteriophage and prophage nucleotide sequences. *Bacteriophage.* 4:e27943. doi: 10.4161/bact.27943

Langston, D. B. Jr., Walcott, R. D., Gitaitis, R. D., and Sanders, F. H. Jr. (1999). First report of a fruit rot of pumpkin caused by *Acidivorax avenae* subsp. *citrulli* in Georgia. *Plant Dis.* 83, 199–199. doi: 10.1094/PDIS.1999.83.2.199B

Laslett, D., and Canback, B. (2004). ARAGORN, a program to detect tRNA genes and tmRNA genes in nucleotide sequences. *Nucleic Acids Res.* 32, 11–16. doi: 10.1093/nar/gkh152

Latin, R. X., and Hopkins, D. L. (1995). Bacterial fruit blotch or watermelon: the hypothetical exam question becomes reality. *Plant Dis.* 79, 761–765. doi: 10.1094/pd-79-0761

Latin, R. X., and Rane, K. K. (1990). Bacterial fruit blotch of watermelon in Indiana. *Plant Dis.* 74:331. doi: 10.1094/pd-74-0331b

Lehman, S. M., Kropinski, A. M., Castle, A. J., and Svircev, A. M. (2009). Complete genome of the broad-host-range *Erwinia amylovora* phage 0Ea21-4 and its relationship to *Salmonella* phage Felix O1. *Appl. Environ. Microbiol.* 75, 2139–2147. doi: 10.1128/AEM.02352-08

Li, B., Shi, Y., Shan, C., Zhou, Q., Ibrahim, M., Wang, Y., et al. (2013). Effect of chitosan solution on the inhibition of *Acidovorax citrulli* causing bacterial fruit blotch of watermelon. *J. Sci. Food Agric.* 93, 1010–1015. doi: 10.1002/jsfa.5812

Lohr, J. E., Chen, F., and Hill, R. T. (2005). Genomic analysis of bacteriophage PhiJL001: insights into its interaction with a sponge-associated alpha-proteobacterium. *Appl. Environ. Microbiol.* 71, 1598–1609. doi: 10.1128/AEM.71.3.1598-1609.2005

Lopes, A., Tavares, P., Petit, M. A., Guérois, R., and Zinn-Justin, S. (2014). Automated identification of tailed bacteriophages and classification according to their neck organization. *BMC Genomics* 15:1027. doi: 10.1186/1471-2164-15-1027

Lowe, T. M., and Chan, P. P. (2016). TRNAscan-SE on-line: integrating search and context for analysis of transfer RNA genes. *Nucleic Acids Res.* 44, W54–W57. doi: 10.1093/nar/gkw413

Martin, H. L., O'Brien, R. G., and Abbott, D. V. (1999). First report of *Acidovorax avenae* subsp. *citrulli* as a pathogen of cucumber. *Plant Dis.* 83:965.

Monteiro, R., Pires, D. P., Costa, A. R., and Azeredo, J. (2019). Phage therapy: going temperate? *Trends Microbiol.* 27, 368–378. doi: 10.1016/j.tim.2018.10.008

Nguyen, L.-T., Schmidt, H. A., Von Haeseler, A., and Minh, B. Q. (2015). IQ-TREE: a fast and effective stochastic algorithm for estimating maximum-likelihood phylogenies. *Mol. Biol. Evol.* 32, 268–274. doi: 10.1093/molbev/msu300

Overbeek, R., Olson, R., Pusch, G. D., Olsen, G. J., Davis, J. J., Disz, T., et al. (2014). The SEED and the Rapid Annotation of microbial genomes using Subsystems Technology (RAST). *Nucleic Acids Res.* 42, D206–D214. doi: 10.1093/nar/gkt1226

Pires, D. P., Cleto, S., Sillankorva, S., Azeredo, J., and Lu, T. K. (2016). Genetically Engineered Phages: a Review of Advances over the Last Decade. *Microbiol. Mol. Biol. Rev.* 80, 523–543. doi: 10.1128/MMBR.00069-15

Popović, T., and Ivanović, Ž (2014). Occurrence of *Acidovorax citrulli* causing bacterial fruit blotch of watermelon in Serbia. *Plant Dis.* 99:886. doi: 10.1094/pdis-12-14-1276-pdn

Rahimi-Midani, A., and Choi, T. J. (2020). Transport of phage in melon plants and inhibition of progression of bacterial fruit blotch. *Viruses* 12:477. doi: 10.3390/v12040477

Rahimi-Midani, A., Kim, J. O., Kim, J. H., Lim, J., Ryu, J. G., Kim, M. K., et al. (2020). Potential use of newly isolated bacteriophage as a biocontrol against *Acidovorax citrulli*. *Arch. Microbiol.* 202, 377–389. doi: 10.1007/s00203-019-01754-5

Rahimi-Midani, A., Lee, Y. S., Kang, S. W., Kim, M. K., and Choi, T. J. (2018). First isolation and molecular characterization of bacteriophages infecting *Acidovorax citrulli*, the causal agent of bacterial fruit blotch. *Plant Pathol. J.* 34, 59. doi: 10.5423/PPJ.NT.08.2017.0190

Rane, K. K., and Latin, R. X. (1992). Bacterial fruit blotch of watermelon: association of the pathogen with seed. *Plant Dis.* 76, 509–512. doi: 10.1094/pd-76-0509

Richter, M., Rosselló-Móra, R., Oliver Glöckner, F., and Peplies, J. (2016). JSpeciesWS: a web server for prokaryotic species circumscription based on pairwise genome comparison. *Bioinformatics* 32, 929–931. doi: 10.1093/bioinformatics/btv681

Seemann, T. (2014). Prokka: rapid prokaryotic genome annotation. *Bioinformatics* 30, 2068–2069. doi: 10.1093/bioinformatics/btu153

Stefani, E., Obradović, A., Gašić, K., Altin, I., Nagy, I. K., and Kovács, T. (2021). Bacteriophage-mediated control of phytopathogenic xanthomonads: a promising green solution for the future. *Microorganisms* 9:1056. doi: 10.3390/microorganisms9051056

Storey, M. V., and Ashbolt, N. J. (2001). Persistence of two model enteric viruses (B408 and MS-2 bacteriophages) in water distribution pipe biofilms. *Water Sci. Technol.* 43, 133–138. doi: 10.2166/wst.2001.0724

Sullivan, M. J., Petty, N. K., and Beatson, S. A. (2011). Easyfig: a genome comparison visualizer. *Bioinformatics* 27, 1009–1010. doi: 10.1093/bioinformatics/btr039

Sykes, I. K., Lanning, S., and Williams, S. T. (1981). The effect of pH on soil actinophage. *J. Gen. Microbiol.* 122, 271–280. doi: 10.1099/00221287-122-2-271

Tanizawa, Y., Fujisawa, T., and Nakamura, Y. (2018). DFAST: a flexible prokaryotic genome annotation pipeline for faster genome publication. *Bioinformatics* 34, 1037–1039. doi: 10.1093/bioinformatics/btx713

van Charante, F., Holtappels, D., Blasdel, B., and Burrowes, B. (2021). "Isolation of bacteriophages," in *Bacteriophages Biology, Technology, Therapy*, eds D. Harper,

S. Abedon, B. Burrowes, and M. McConville (Cham: Springer), 433–464. doi: 10.1007/978-3-319-41986-2_14

Walker, B. J., Abeel, T., Shea, T., Priest, M., Abouelliel, A., Sakthikumar, S., et al. (2014). Pilon: an integrated tool for comprehensive microbial variant detection and genome assembly improvement. *PLoS One* 9:e112963. doi: 10.1371/journal.pone.0112963

Webb, R. E., and Goth, R. W. (1965). A seedborne bacterium isolated from watermelon. *Plant Dis. Report.* 49, 818–821.

Williams, S. T., Mortimer, A. M., and Manchester, L. (1987). "Ecology of soil bacteriophages," in *Phage Ecology,* eds S. M. Goyal, C. P. Gerba, and G. Bitton (New York, NY: John Wiley and Sons), 157–179.

Zafar, N., Mazumder, R., and Seto, D. (2002). CoreGenes: a computational tool for identifying and cataloging "core" genes in a set of small genomes. *BMC Bioinf.* 3:12. doi: 10.1186/1471-2105-3-12

Zhang, H., Fouts, D. E., DePew, J., and Stevens, R. H. (2013). Genetic modifications to temperate *Enterococcus faecalis* phage Ef11 that abolish the establishment of lysogeny and sensitivity to repressor, and increase host range and productivity of lytic infection. *Microbiology* 159(Pt 6), 1023–1035. doi: 10.1099/mic.0.067116-0

Zlatković, N., Prokić, A., Gašić, K., Kuzmanović, N., Ivanović, M., Pavlović, Ž, et al. (2017). Identification and characterization of *Acidovorax citrulli* strains from Serbia, in abstracts of invited talks, oral and poster presentations given at the 15th Congress of the Mediterranean Phytopathological Union, June 20–23, 2017, in Córdoba, Spain. *Phytopathol. Mediterr.* 56:314. doi: 10.14601/Phytopathol_Mediterr-20879

Zlatković, N., Prokić, A., Kuzmanović, N., Gašić, K., Šević, M., Ivanović, M., et al. (2015). Bakteriozna mrljavost plodova lubenice u Srbiji. *Biljni Lekar* 43, 265–272.

Conflict of Interest: The authors declare that the research was conducted in the absence of any commercial or financial relationships that could be construed as a potential conflict of interest.

Publisher's Note: All claims expressed in this article are solely those of the authors and do not necessarily represent those of their affiliated organizations, or those of the publisher, the editors and the reviewers. Any product that may be evaluated in this article, or claim that may be made by its manufacturer, is not guaranteed or endorsed by the publisher.

frontiers in Microbiology

REVIEW
published: 07 March 2022
doi: 10.3389/fmicb.2022.833566

Microbe-Mediated Thermotolerance in Plants and Pertinent Mechanisms-A Meta-Analysis and Review

Khondoker M. G. Dastogeer[1], Mst. I. Zahan[2], Mohammad S. Rhaman[3], Mohammad S. A. Sarker[4] and Anindita Chakraborty[5]*

[1] Department of Plant Pathology, Bangladesh Agricultural University, Mymensingh, Bangladesh, [2] Scientific Officer (Breeding Division), Bangladesh Sugarcrop Research Institute, Pabna, Bangladesh, [3] Department of Seed Science and Technology, Bangladesh Agricultural University, Mymensingh, Bangladesh, [4] Basic and Applied Research on Jute Project, Bangladesh Jute Research Institute (BJRI), Dhaka, Bangladesh, [5] Department of Genetic Engineering and Biotechnology, Shahjalal University of Science and Technology, Sylhet, Bangladesh

Microbial symbionts can mediate plant stress responses by enhancing thermal tolerance, but less attention has been paid to measuring these effects across plant-microbe studies. We performed a meta-analysis of published studies as well as discussed with relevant literature to determine how the symbionts influence plant responses under non-stressed versus thermal-stressed conditions. As compared to non-inoculated plants, inoculated plants had significantly higher biomass and photosynthesis under heat stress conditions. A significantly decreased accumulation of malondialdehyde (MDA) and hydrogen peroxide (H_2O_2) indicated a lower oxidation level in the colonized plants, which was also correlated with the higher activity of catalase, peroxidase, glutathione reductase enzymes due to microbial colonization under heat stress. However, the activity of superoxide dismutase, ascorbate oxidase, ascorbate peroxidase, and proline were variable. Our meta-analysis revealed that microbial colonization influenced plant growth and physiology, but their effects were more noticeable when their host plants were exposed to high-temperature stress than when they grew under ambient temperature conditions. We discussed the mechanisms of microbial conferred plant thermotolerance, including at the molecular level based on the available literature. Further, we highlighted and proposed future directions toward exploring the effects of symbionts on the heat tolerances of plants for their implications in sustainable agricultural production.

Keywords: antioxidant, heat stress, meta-analysis, plant-microbe interaction, plant physiology, symbiosis

OPEN ACCESS

Edited by:
Marco Scortichini, Council for Agricultural and Economics Research (CREA), Italy

Reviewed by:
Laura Bertini, University of Tuscia, Italy
Vikas Srivastava, Central University of Jammu, India

****Correspondence:***
Khondoker M. G. Dastogeer
dastogeer.ppath@bau.edu.bd

Specialty section:
This article was submitted to Microbe and Virus Interactions with Plants, a section of the journal Frontiers in Microbiology

Received: *11 December 2021*
Accepted: *04 February 2022*
Published: *07 March 2022*

Citation:
Dastogeer KMG, Zahan MI, Rhaman MS, Sarker MSA and Chakraborty A (2022) Microbe-Mediated Thermotolerance in Plants and Pertinent Mechanisms-A Meta-Analysis and Review. Front. Microbiol. 13:833566. doi: 10.3389/fmicb.2022.833566

INTRODUCTION

Due to climate change, the constant rise of ambient temperature is one of the major global issues and has devastating impacts on crop growth and productivity, consequently, in food security. Results from various climate model simulations predict that the global average temperature could be between 1.1 to 5.4°C warmer in 2100 than it is today (IPCC, 2019). Heat stress causes a manifold adverse impact on the growth, development, physiological processes of plants (Wahid et al., 2007; Hasanuzzaman et al., 2013; Hassan et al., 2021; Jagadish et al., 2021). The

plant employs varying levels of adaptation, avoidance, acclimation, and tolerance mechanisms to cope with heat stress *via* physical, physiological, biochemical, and molecular strategies, including the use of ion transporters, proteins, osmolytes, antioxidants, and other factors involved in signaling and transcriptional regulation (Hasanuzzaman et al., 2013; Hassan et al., 2021; Jagadish et al., 2021; Zhao et al., 2021). Plant responses to abiotic stress have been studied widely for the last few years, and the role of microbes on plant stress responses has also been given attention in recent years. In particular, plant species commonly associated with microbial symbionts, known as plant microbiome, may influence responses of the host plant to environmental stimuli, including heat stress.

Microorganisms are ubiquitous, and all plants are colonized by various types of microbes which play important roles in plant ecology and physiology (Rodriguez et al., 2009; Turner et al., 2013; Compant et al., 2019; Dastogeer et al., 2020a). For example, AMF (arbuscular mycorrhizal fungi) present in the roots of 80% of terrestrial plants (Brachmann and Parniske, 2006) and microbial endophytes (both fungal and bacterial) are highly diverse and live asymptomatically in every plant studied so far. It is increasingly recognized that these microbes, as well as others including, e.g., epiphytes, viruses, ectomycorrhiza, N-fixers, etc., exert multiple effects on the plants particularly under adverse environmental conditions (Porras-Alfaro and Bayman, 2011; Hill et al., 2019; Dastogeer et al., 2020b; Kumar et al., 2020). These beneficial effects, which are strongly dependent on environmental conditions (Rodriguez et al., 2009; Hoeksema et al., 2010; Dastogeer, 2018), include priming against pests or herbivores, the acquisition of growth-limiting nutrients from the soil, tolerance to drought, salinity and thermal stress, etc. (Rodriguez et al., 2009; Goh et al., 2013; Hardoim et al., 2015; Azad and Kaminskyj, 2016; González-Teuber, 2016; Molina-Montenegro et al., 2016; Dastogeer and Wylie, 2017; Rho et al., 2018; Hill et al., 2019). Microbes produce a wide range of compounds to impact the responses of plants at the molecular level, triggering the biosynthesis of pigments, secondary metabolites, hormones, antioxidants, and alkaloids (Meena et al., 2017; Dastogeer et al., 2018; Basit et al., 2021; Naamala and Smith, 2021). Just as for other stresses, it is becoming increasingly evident that the heat stress responses of plants may be influenced by their interactions with microbes (Eerens et al., 1998; Ali et al., 2011; Khan A. L. et al., 2015; Ismail et al., 2020a; Li X. et al., 2021).

Despite the ubiquity and high diversity of microbial symbionts in plant tissues and the widespread effects and economic relevance of heat as a stress factor for plants, when compared with other abiotic factors such as drought, salinity, or nutrient limitation, the involvement of symbionts in plant host responses to heat stress have been received less attention (Meena et al., 2017; Kumar and Verma, 2018). The handful of studies available indicate that the magnitudes of the effect of microbes on plant heat stress tolerance and associated mechanisms such as accumulation of osmolytes, antioxidants, phytohormones, etc., vary among various studies (Meena et al., 2017; Kumar and Verma, 2018). We assume these differences could be associated with multiple factors such as level of stress, types of host and symbiont partners, environmental conditions, and their complex interactions. In order to gain insight into and harness the benefit of symbiont in agricultural management practice, it is imperative to elucidate the detailed mechanism of microbe-plant interaction under heat stress conditions (Harman and Uphoff, 2019). It is indeed tenuous and often erroneous to deduce the findings in general context from the individual investigation (Dastogeer, 2018). Therefore, to ascertain the central tendency and pinpoint the patterns of microbial influence on plants under stress and compare with them under control, it is paramount to integrate results across studies in order to determine if the factors can be known (Borenstein et al., 2009; Dastogeer, 2018). Here, we performed a meta-analysis to measure the overall strength and direction of effect (beneficial, harmful or neutral) of symbiosis on important plant characteristics associated with stress tolerance mechanisms. To the best of our knowledge, this aspect has not previously been discussed in a review of the published article, and thus present article fills a substantial gap in our understanding of interactions between plants and their symbiotic microbial partners.

A meta-analysis is a mathematical and statistical approach that pools the results of various investigations to estimate a mean effect size for treatment across a range of studies (Rosenberg et al., 2000). We can evaluate the findings of a study with respect to all other comparable studies to assess if the effect of a treatment is consistent across studies or if it differs substantially among studies and which factor might be accounted for the differences (Borenstein et al., 2009). The categorical variables or "moderators" are often included in meta-analyses to pinpoint which and how various features modulate the treatment effect of interest. This form of analysis has been, for example, used to determine the impact of microbial symbionts on plant response to salinity stress (Chandrasekaran et al., 2014, 2016; Rho et al., 2018), drought stress (Dastogeer, 2018; Rho et al., 2018), and cold stress (Acuna-Rodriguez et al., 2020). In the current study, we accumulated data from all studies to date and measured the effects of endophytes on 24 plant response parameters that encompass plant growth, photosynthesis, metabolites, and enzymatic activities that are subjected to change under thermal stress conditions. Our purpose was to answer the questions, broadly; what is the overall impact of microbial colonization on various plant growth and photosynthetic parameters of plants exposed to heat stress? Does the plant-symbiont relationship differ under heat-stressed conditions compared to unstressed conditions? What is the role of symbiosis in osmotic balance and antioxidant enzymes regulation in plants exposed to thermal stress? We supplemented our meta-analysis with a review of relevant literature for a deeper insight into this subject.

LITERATURE SEARCH AND STUDY SELECTION FOR META-ANALYSIS

The meta-data were collected by following the general guidelines of Field and Gillett (2010). We performed a literature search in Web of Science (Clarivate Analysis) and PubMed database through September 2020. Our search terms were: endophyte or AMF or mycorrhiza or bacteria or fungi AND either "heat

stress*" or "hot stress*" or "high temperature." The Boolean truncation ("*") was used so as to include the variations of the word such as fungi, fungus, and fungal. The search produced 4,562 unduplicated papers, and 90 peer-reviewed articles were considered likely to contain relevant information by reading the title and abstract. To finally select the papers for data extraction, we had preset criteria such as so that these studies can be included in our meta-analysis and extreme heterogeneity minimized (Cooper, 2015; Ahn and Kang, 2018; Cooper et al., 2019; Seidler et al., 2019):

(i) The article must describe the findings of original research, and as such, review papers, opinion articles, editorials, book chapters, and systematic reviews were discarded for inclusion into our meta-analysis.
(ii) The investigation had to use at least one microbial strain regardless of inoculation protocol or rate,
(iii) The inoculum was used singly, and we did not consider any mixed-inoculation for this meta-analysis,
(iv) Both microbe-inoculated and non-inoculated plants were grown under normal stressed and non-stressed conditions, and data provided,
(v) Any of the growth and other parameters, e.g., biomass, enzymes, hormones, etc., were measured
(vi) The papers must have provided sample size (i.e., replication), means, standard deviations/errors, and other relevant statistical data that could be converted to measure an effect size.

Based on the above criteria, most articles were excluded for meta-analysis, and only 39 peer-reviewed original research articles were retained for the final analysis (**Supplementary Table 1**). We accepted studies to differ in the levels of fertilizer applied, growth conditions (greenhouse, growth chamber, or field), duration of stress application, the magnitude of stress, and growth media into our meta-analysis. Papers spanned 23 years (1998–2021) and were in English. We apologize for not including the potential paper that contains data written in other languages or those that we might have unintentionally missed during our search or due to stipulated selection criteria.

DATA EXTRACTION AND META-ANALYSIS

When a publication provided results of more than one study system/group, those systems were taken as independent data points (Hedges et al., 1999). From these articles, we extracted information on host identity (plant species, genus, family), symbionts' identity (genus, species), plant biomass (shoot and root), length (shoot and root), relative water content, photosynthetic parameters, enzymes parameters, and other relevant data from the studies (**Supplementary Table 2**). The means, sample sizes (replications), standard deviation were recorded from each study. Standard deviation was calculated from standard errors (SE) using the equation: $SE = SD\ (n^{-1/2})$. Frequently the results were presented in a graph, and we used WebPlotDigitizer (Rohatgi, 2021) to digitize the values. If any paper reported multiple treatments or host/AMF combinations, these were included as an independent data unit in the analysis. However, it might increase the dependence of a particular study when considered them as an independent report (Gurevitch and Hedges, 1999). Nonetheless, this practice is assumed to increase the statistical power of meta-analysis (Lajeunesse and Forbes, 2003) and several biological meta-analyses papers also used the same (Holmgren et al., 2012; Veresoglou et al., 2012; Mayerhofer et al., 2013; McGrath and Lobell, 2013; Dastogeer, 2018).

Meta-analyses were conducted using the "metacont" function of the package "meta" (Balduzzi et al., 2019) implemented in R version 4.0.4 (R Core Team, 2021). Although the DerSimonian and Laird (DL) method is commonly used by default to estimate the between-study variance, it was suggested that for continuous data, the restricted maximum likelihood estimator (REML) are better alternatives to estimate the between-study variance (DerSimonian and Laird, 1986; Veroniki et al., 2016; Cooper et al., 2019). We used the Restricted maximum-likelihood estimator (REML) to make statistical inferences considering the effects as random. Standardized mean difference (SMD), which is defined as the ratio of the difference in mean performance between treatments to the pooled standard deviation, was calculated. This effect size measurement is done in meta-analyses that involve studies reporting continuous outcomes, similar to our study (Faraone, 2008). Generally, the SMD values of 0.3, 0.5, and 0.8 are considered as a small, medium, and large effect sizes, respectively (Cohen, 1988). Quantification of heterogeneity as well as testing the significance were estimated with Higgin's I^2 and Cochran's Q statistics. "I^2" is defined as the ratio of true heterogeneity to total heterogeneity across the effect sizes, whereas "Q" is the weighted deviations of the summary effect size that is due to true heterogeneity rather than sampling error (Higgins and Thompson, 2002; Higgins et al., 2003; Huedo-Medina et al., 2006). The I^2 values $< 25\%$, 25–75%, and $> 75\%$ are regarded as representing low, moderate, and high heterogeneity (Higgins et al., 2003) by convention. The coefficient of interval estimate of effect sizes was set to 95%, and the effect size (SMD) was considered significant when 95% CIs (confidence interval) did not cross zero. SMD of zero suggests that the two treatments (microbial inoculated or non-inoculated) have equivalent effects; SMDs greater than zero indicate the degree to which the microbial inoculated outperforms the non-inoculated samples and *vice-versa*.

Publication bias for each dataset of different parameters was tested by inspecting funnel plots and Egger regression test for funnel plot asymmetry (Begg and Mazumdar, 1994; Egger et al., 1997; Simonsohn et al., 2014). We found that for most of the parameters, there were no substantial publication biases in these datasets (**Supplementary Table 2**). For some parameters which showed some biases, then we took the effect sizes (SMD), CIs, and heterogeneity statistics after applying the trim-and-fill method to correct the biases (Duval and Tweedie, 2000). However, for the majority of the cases, the trim and fill did not substantially alter (decreased) the SMD values than the untrimmed SMD values (**Supplementary Table 2**). Therefore, we used the untrimmed SMD values (i.e., did not adjust for publication bias) for the sake of consistency for all the parameters for creating forest plots. After carefully observing the heterogeneity statistics as well as

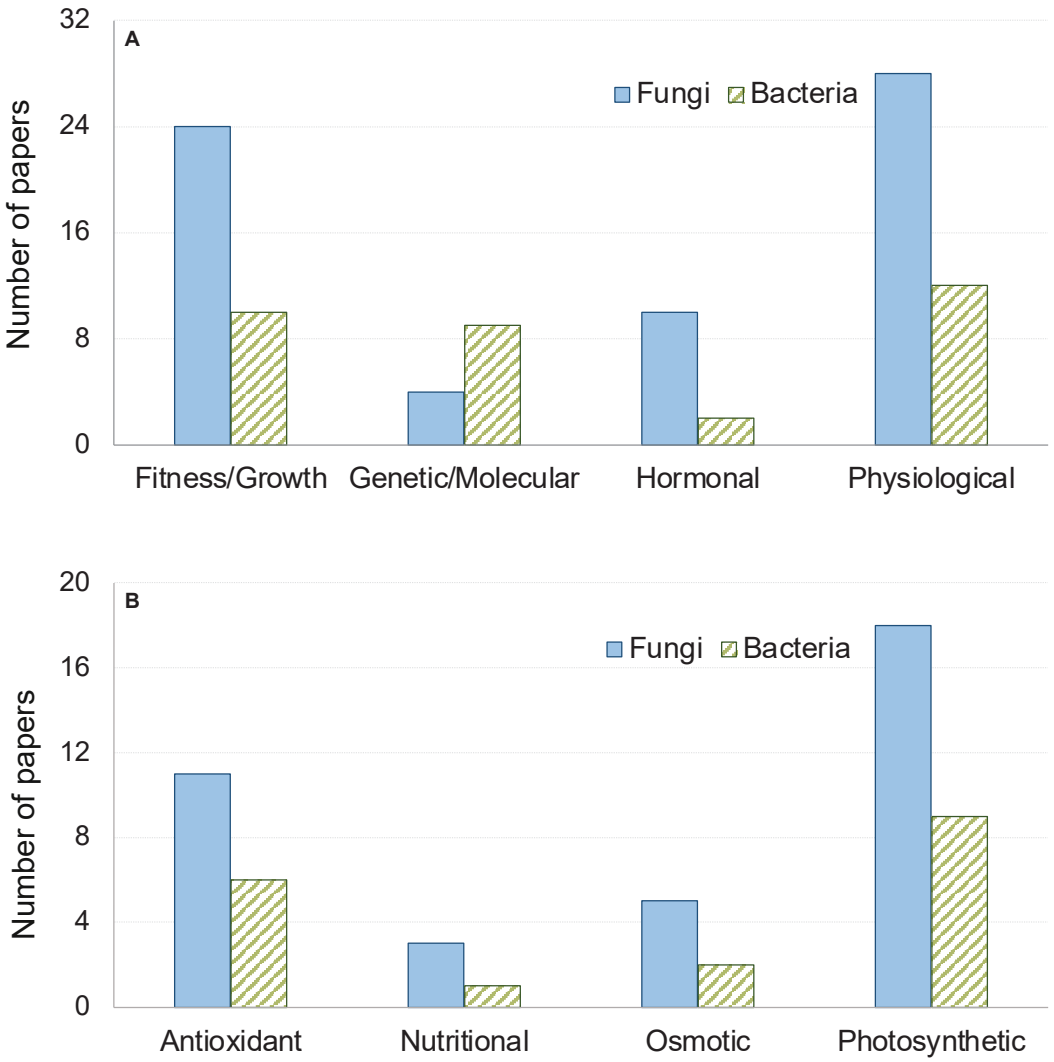

FIGURE 1 | Number of papers out of the total 42 papers reviewed here grouped by response variables. Broad categories of variable are shown in panel **(A)**, while physiological responses are shown in panel **(B)**.

significance level for SMDs, we performed subgroup analyses for root length parameters to determine the influence of the factors such as plant or endophyte identity, type, etc., because sufficient data were available. For a factor to be included in the analysis as a subgroup variable, it had to be reported from at least four studies.

META-ANALYTIC REVIEW AND DISCUSSION ON PLANT TOLERANCE TO THERMAL STRESS AS MEDIATED BY MICROBIAL COLONIZATION

The articles we reviewed presented findings of experiments involving various host-microbe systems. These investigations considered various parameters in evaluating the influences of microbial colonization in providing heat stress tolerances of plants such as plant biomass and response at the physiological, molecular, metabolic as well as the hormonal level (**Figure 1**). Effect of fungi was encountered more often, which accounted for 69% of the 42 articles used in our meta-analysis. In general, both fungal and bacterial symbionts were found to increase plant fitness under thermal stress by augmenting photosynthesis, improving antioxidant responses of plants, triggering earlier hormonal signaling, enhancing osmolyte and nutritional balance (**Table 1**). In the next section, we outlined the influence of microbial symbionts on plant thermal stress tolerance as obtained from our meta-analysis and discussed in light of available literature.

Microbial Symbionts on Plant Growth and Relative Water Content Under Thermal Stress

The microbial symbiosis significantly stimulated plant shoot dry biomass as well as increased shoot length both under normal and

TABLE 1 | The 39 investigations that were included in the review here reporting the effects of microbial symbionts on plant responses to thermal stresses.

References	Host species	Symbiont	Key findings
Abd El-Daim et al. (2014)	Wheat (*T. aestivum*)	*Bacillus amyloliquefaciens; Azospirillum brasilense* (Bacteria)	Bacterial treatment with *Bacillus amyloliquefaciens* UCMB5113 or *Azospirillum brasilense* NO40 improved heat stress tolerance of wheat seedlings which were associated with reduced generation of reactive oxygen species and transcript levels of several stress related genes.
Abd El-Daim et al. (2018)	Wheat (*Triticum aestivum*)	*B. amyloliquefaciens* (Bacteria)	Wheat seeds treated with *B. amyloliquefaciens* enhanced heat tolerance by molecular modifications in wheat leaf transcript patterns.
Abd El-Daim et al. (2019)	Wheat (*T. aestivum*)	*B. velezensis* (Bacteria)	*B. velezensis* 5113 inoculations resulted in a significant metabolic modulation and regulation of metabolic pathways of amino acids and enhanced expression of several proteins related to heat tolerance.
Ali et al. (2009)	*Sorghum (Sorghum bicolor)*	*Pseudomonas sp.* (Bacteria)	*Pseudomonas* sp. strain AKM-P6 enhanced tolerance of sorghum seedlings to elevated temperatures by enhancing bio-physiological changes such as higher biomass, proline, sugar, amino acids content in the plant.
Ali et al. (2011)	Wheat (*Triticum spp*.)	*P. putida* (Bacteria)	Inoculation with *P. putida* strain AKMP7 significantly increased the root and shoot length, dry biomass, tiller, spikelet and grain formation of wheat and enhanced biochemical parameters such as chlorophyll, total sugars, proline, starch, amino acids and protein content of wheat under heat stress.
Ali et al. (2018)	Cucumber (*Cucumis sativus*)	Theromophilic endophytic fungus	A thermophilic endophytic (CpE) fungus (92% sequence homology with *Thermomyces sp*.) mediated heat stress tolerance in cucumber plants by maintaining maximum quantum efficiency of photosystem II, photosynthesis rate, water use efficiency and increased root length.
Ali et al. (2019)	*Cullen plicata*	*Thermomyces lanuginosus* (Endophytic fungus)	*T. lanuginosus* had a beneficial effect on its host for resisting heat under heat stress condition. AM fungus enhanced the *C. plicata* plant heat stress tolerance by changing secondary metabolite accumulations and antioxidant activities and improving the growth and development of its host.
Bruno et al. (2020)	*Sorghum (S. bicolor)*	*B. cereus, Providencia rettgeri, Myroides odoratimimus* (Bacteria)	Inoculation of sorghum with chromium reducing-thermotolerant plant growth promoting bacteria (CRT-PGPB) increased plant growth, antioxidant enzyme activities and decreased proline and malondialdehyde contents in plants under heat stress and enhanced heat tolerance
Bunn et al. (2009)	*Agrostis scabra, Dichanthelium lanuginosum, Mimulus guttatus*	Arbuscular mycorrhizal fungi	Biomass of the facultative thermal plants *Agrostis scabra* and *Mimulus guttatus* decreased under high temperature and AMF inoculation did not have any effect on the plant traits. On the other hand, mycorrhizal inoculation increased the biomass and total root length of the obligate thermal plant *Dichanthelium lanuginosum* under high temperatures. Again, the source of the AMF inoculum (nonthermal-AMF and thermal-AMF), had no effect on colonization level, host plant biomass, or flowering for any host species in either temperature treatment, suggesting that AMF from thermal soils are not specifically adapted to higher temperatures.
Cabral et al. (2016)	Wheat (*T. aestivum)*	Arbuscular mycorrhizal fungi	AMF increased grain number in wheat plants, alter nutrient allocation and tiller number composition in the plants under heat-stress.
Duc et al. (2018)	Tomato (*Solanum lycopersicum*)	*Septoglomus deserticola and Septoglomus constrictum* (Arbuscular mycorrhizal fungi)	Inoculation with AMF reduced oxidative stress by decreasing lipid peroxidation and hydrogen peroxide levels and enhancing antioxidant enzyme activities.
Eerens et al. (1998)	Ryegrass (*Lolium perenne*)	*Neotyphodium lolii* (Endophytic fungus)	The endophyte affects the morphology and physiology of the ryegrass plant. The interaction between endophyte and temperature was significant for ergovaline concentration and wilt score.
Hennessy et al. (2016)	Perennial ryegrass (*L. perenne* L.); Italian ryegrass (*L. multiflorum* Lam.)	*Epichloë festucae* (Endophytic fungus)	The endophyte strain AR37 (*Epichloë festucae* var. lolii) provided ryegrass with resistance against *Porina larvae*, a major pasture pest in cooler areas of New Zealand by producing high concentrations of epoxy-janthitrem alkaloids at high temperature. In contrast, AR37-infected ryegrass grown at low temperature produced low concentration of epoxy-janthitrem resulting in a small anti-feedant effect against pasture pest only in perennial ryegrass.
Hubbard et al. (2012)	Durum wheat (*T. turgidum)*	Endophytic Ascomycetous mitosporic fungi	Fungal endophytes increased wheat seed germination percentage, improved the hydrothermal time (HTT) and energy of germination (EG) value and enhanced resistance to wheat exposed to heat *in vitro* as measured by fresh weight of seedlings

(Continued)

TABLE 1 | (Continued)

References	Host species	Symbiont	Key findings
Hubbard et al. (2014)	Durum wheat (*T. turgidum*)	Endophytic Ascomycetous mitosporic fungi	Endophytes enhanced wheat tolerance against heat stress in parental plants and second-generation seeds which was measured by quantifying efficiency of photosystem II, average seed weight (ASW), total seed weight (TSW), water-use efficiency (WUE), time to 50% germination and percentage germination of second-generation seeds produced under heat stress.
Ismail et al. (2018)	Sunflower (*H. annuus*); Soybean (*G. max*)	*A. japonicus* (Endophytic fungus)	*A. japonicus* EuR-26 endophytic fungus isolated from the wild plant *Euphorbia indica* L. have heat stress relief potential. *A. Japonicus* can modulate the growth of host plants under heat stress and can be used in arid and semiarid regions of the world as a thermal stress alleviator.
Ismail et al. (2019)	Sunflower (*H. annuus*) and Soybean (*G. max*	*A. flavus* (Endophytic fungus)	Harms due to heat stress on soybean and sunflower appeased by inoculating endophytic fungi *A. flavus* isolated from *Euphorbia indica*. In fact, the endophytic fungi influenced to regulate the concentration of ABA, proline, phenols, flavonoids, catalase and ascorbic acid oxidase to withstand soybean and sunflower plants against heat stress.
Ismail et al. (2020a)	Sunflower (*Helianthus annuus*); Soybean (*Glycine max*)	*A. niger* (Endophytic fungus)	Endophytic fungi *A. niger* isolated from *Sonchus asper* protected soybean and sunflower from excessive thermal stress by increasing plant height, biomass and chlorophyll content. In fact, *A. niger* alter plant physiology in such a way that, concentration of AAO, CAT, GR, SOD, POD, proline and phenolics were augmented while lipid peroxidation, ROS ad ABA reduced under thermal stress at 40°C.
Ismail et al. (2020b)	Sunflower (*H. annuus*); Soybean (*G. max*)	*A. violaceofuscus* (Endophytic fungus)	Endophytic fungi *A. violaceofuscus* isolated from the fern *Dryopteris flix* L. protected sunflower and soybean against thermal stress through secreting secondary metabolites. Such secretion increased the total chlorophyll content, plant height by decreasing the concentration of reactive oxygen species, abscisic acid, catalase, ascorbic acid oxidase, proline.
Ismail et al. (2020c)	Sunflower (*H. annuus*); Soybean (*G. max*)	*Rhizopus oryzae* (Endophytic fungus)	Thermal stress to soybean and sunflower caused by climatic change can be mitigated to a great extent by using *R. oryzae*, an endophytic fungus isolated from roots and leaves of *Adiantum capillus-veneris* L. The plant growth promoting fungus, *R. oryzae,* improved heat stress tolerance of plants through inducing high concentration of phenolics, flavonoids, salicylic acid (SA) and indole 3-acetic acid (IAA), ascorbic acid oxidase (AAO), catalase (CAT), proline, sugars, proteins and lipids.
Issa et al. (2018)	Tomato (*S. lycopersicum*)	*Paraburkholderia phytofirmans* (Bacteria)	Bacterial inoculation with *P. phytofirmans* strain PsJN improved tomato plant growth by enhancing chlorophyll content and gas exchange parameters and increased the accumulations of sugars, total amino acids, proline, and malate.
Khan et al. (2012a)	*C. sativus*	*Paecilomyces formosus* LHL10 (Endophytic fungus)	The association with endophytic fungus, *P. formosus* LHL10 significantly improved growth parameters of cucumber plants such as higher leaf area, chlorophyll contents, shoot fresh and dry weights compared to control even under stress conditions. *P. formosus* helped the plant to cope with the adverse effects of temperature stress, especially low-temperature stress.
Khan et al. (2012b)	*C. sativus*	*Exophiala sp. LHL08* (Endophytic fungus)	*Exophiala* sp. inoculated plants had significantly higher plant growth characteristics (shoot length, plant biomass, chlorophyll quality, and leaf area) than heat stress control. Exophiala sp.'s interaction with cucumber host plants can modulate heat stress by influencing plant physiological and biochemical traits under heat stress.
Khan et al. (2013)	Pepper (*Capsicum annuum)*	*Penicillium resedanum* (Endophytic fungus)	The endophytic fungus *P. resedanum* LK6 significantly increased the shoot length, shoot fresh and dry wrights of *C. annuum* L. plant with or without the exposure to heat stress as compared to non-infected plants. The leaf damage and wilting process were significantly lower in endophyte-treated plants than control under heat stress. Proline and ammonium accumulation and flavonoids synthesis were significantly induced in the endophyte-inoculated plants.
Khan A. L. et al. (2015)	Pepper (*C. annuum*)	*P. resedanum* (Endophytic fungus)	*P. resedanum* LK6 treatment significantly improved shoot length and shoot dry weight of capsicum plants compared with the controls under heat stresses. Endophyte helps the host to response against stresses by reprogramming the physiological responses of host plant.

(Continued)

TABLE 1 | (Continued)

References	Host species	Symbiont	Key findings
Khan et al. (2020a)	Tomato (*S. lycopersicum*)	*B. cereus* (Bacteria)	Simultaneous use of plant growth-promoting endophytic bacteria *B. cerus* and humic acid (HA) can counteract the negative effects of heat stress. Co-application of *B. cereus* SA1 and humic acid (HA) on tomato seedlings can protect against heat stress by balancing required biochemicals like ABA, SA, APX, GSH, SOD, Fe, P, K. As a result, SA1 and HA can be used as a commercial biofertilizer.
Khan et al. (2020b)	Soybean (*G. max*)	*B. cereus* (Bacteria)	Negative impact of heat stress on growth and yield of soybean due to global climatic change can be mitigate by using thermo tolerant *B. cereus* bacteria. In fact, *B. cereus* can be used as a bio fertilizer as it can promotes biologically active metabolites like GA, IAA and organic acids besides maintaining optimum balance of ABA, SA, protein ad antioxidant concentration.
Li X. et al. (2021)	Ryegrass (*L. perenne*)	*A. aculeatus* (Endophytic fungus)	Inoculation with fungus improved heat tolerance by enhancing the photosynthetic apparatus, decreased the antioxidant enzyme activities, and mitigated membrane lipid peroxidation.
Martin and Stutz (2004)	Pepper (*C. annuum*)	*Glomus intraradices, Glomus sp. (AZ 112)* (AM fungi)	At moderate temperatures, phosphorus uptake by all AM colonized pepper plants was enhanced relative to non-AM plants but there was no corresponding enhancement of growth. In contrast, at high temperature, pepper growth was increased as a result of inoculation of the *G. intraradices* isolate and the Glomus isolate mixture as compared to non-AM controls, despite relatively less phosphorus transfer to the plant by the fungi.
Mathur and Jajoo (2020)	Maize (*Zea mays*)	*Glomus sp.*	AMF exerted their beneficial effects by altering PSII heterogeneity under high temperature. Presence of AMF was able to protect maize plants by regulating electron transport through PSII and thus regulating reducing side heterogeneity of PSII under high temperature stress.
Maya and Matsubara (2013)	*Cyclamen persicum*	*G. fasciculatum (AM fungus)*	Symbiotic association of *G. fasciculatum,* an arbuscular mycorrhizal (AM) fungus, and *Cyclamen persicum* mitigated heat stress damage by enhancing antioxidant concentration like superoxide dismutase, ascorbate peroxidase, ascorbic acid, and polyphenol. Moreover, compare to control mycorrhizal symbiosis provokes higher plant biomass in the host plants.
Mukhtar et al. (2020)	Tomato (*S. lycopersicum*)	*B. cereus* (Bacteria)	Bacterial inoculation promoted shoot, root length, leaf surface area, fresh and dry weight and enhanced extracellular polymeric substances (EPS) production and reduced the adverse effects of heat on tomato growth.
Sangamesh et al. (2018)	Rice (*Oryza sativa*)	*Chaetomium sp.* (Fungus)	Inoculation with *Chaetomium* sp. increased root and shoot growth as well as survival percentage under heat stress.
Sarkar et al. (2018)	Wheat (*T. aestivum*)	*B. safensis and Ochrobactrum pseudogrignonense* (Bacteria)	PGPR enhanced thermotolerance by reduction of ROS production, membrane damage, maintenance of chloroplast structure and enhanced chlorophyll content, increased expression of an array of redox enzymes and accumulation of osmolytes.
Shekhawat et al. (2020)	*Arabidopsis thaliana*	*Enterobacter sp.* (Endophytic bacterium)	*Enterobacter* sp. SA187 increased significant heat stress tolerance in *A. thaliana*. *Enterobacter* sp. SA187 enhanced the expression of heat-responsive and heat memory-related genes upon heat stress, therefore helping plants to survive better to heat stress.
Tian et al. (2015)	*Festuca rubra*	*Epichloë festucae* (Endophytic fungus)	*E. festucae* infection did not affect the physiological responses of the plants on improving heat stress tolerance in strong creeping red fescue.
Waqas et al. (2015)	Rice (*O. sativa*)	*P. formosus* (Endophytic fungus)	The phytohormones and other secondary metabolites formed by the endophytic fungus *P. formosus* LWL1 in the Dongjin Japanese rice cultivar played a potential role in heat-stress mitigation. These fungal endophytes may be useful for the sustainable production of crops under high ambient temperature levels as they showed positive result.
Yeasmin et al. (2019)	*Asparagus officinalis*	*G. intraradices (AM fungus)*	Arbuscular mycorrhizal fungi (AMF) *G. intraradices* ameliorated damage of asparagus crop caused by heat stress. AMF-inoculated asparagus plants compare to control performed better regarding growth, nutrient uptake, heat stress responses. Besides, increased antioxidative activities of SOD and ascorbate peroxidase in inoculated plants lessen leaf browning.

(Continued)

TABLE 1 | (Continued)

References	Host species	Symbiont	Key findings
Zhu et al. (2011)	Maize (*Z. mays*)	*G. etunicatum (AM fungus)*	Compared to control, maize plants inoculated by AM fungus *G. etunicatum* showed better performance regarding photosynthesis, stomatal conductance, and transpiration in leaves. Furthermore, AM fungus may protect maize plants against high temperature stress by improving water use efficiency.

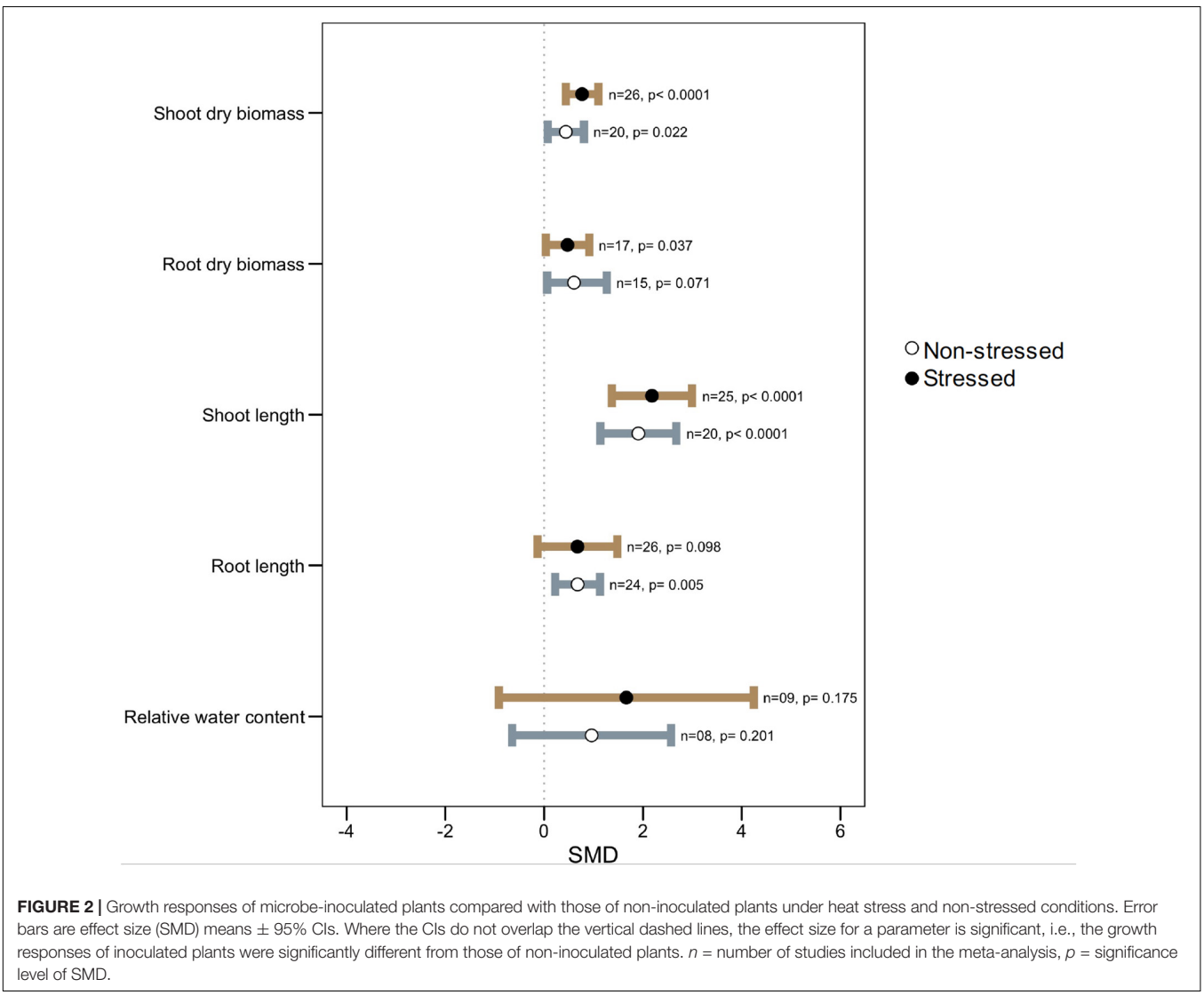

FIGURE 2 | Growth responses of microbe-inoculated plants compared with those of non-inoculated plants under heat stress and non-stressed conditions. Error bars are effect size (SMD) means ± 95% CIs. Where the CIs do not overlap the vertical dashed lines, the effect size for a parameter is significant, i.e., the growth responses of inoculated plants were significantly different from those of non-inoculated plants. *n* = number of studies included in the meta-analysis, *p* = significance level of SMD.

high-temperature stress (**Figure 2**). Although root dry biomass was found to be significantly augmented (SMD: 0.4728, *p:* 0.037) by microbial colonization under heat stress, its effect on the length of the root was variable and less prominent (SMD: 0.6739, *p:* 0.098) even though under non-stressed conditions microbial colonization resulted in longer roots in host plants (**Figure 2**).

Leaf relative water content (RWC) did not show any significant changes due to microbial colonization either under stress or non-stressed conditions. However, the wider CI values propose that the influence on plant RWC varies by some factors (**Figure 2**).

Since there was significant heterogeneity in microbial impact on plant root length, we attempted to identify the potential moderators by categorical analysis. We noticed that microbes had a substantial impact on root length regardless of whether the host belonged to the legume with non-legume or whether the symbiont belonged to fungi or bacteria under thermal stress (**Figures 3A,D**). However, under normal conditions, bacterial symbiont had significantly increased root length, but fungi did not demonstrate this effect. The roots of dicotyledonous plants increased significantly in the presence of microbial symbionts regardless of stress impact, but those of monocotyledons did

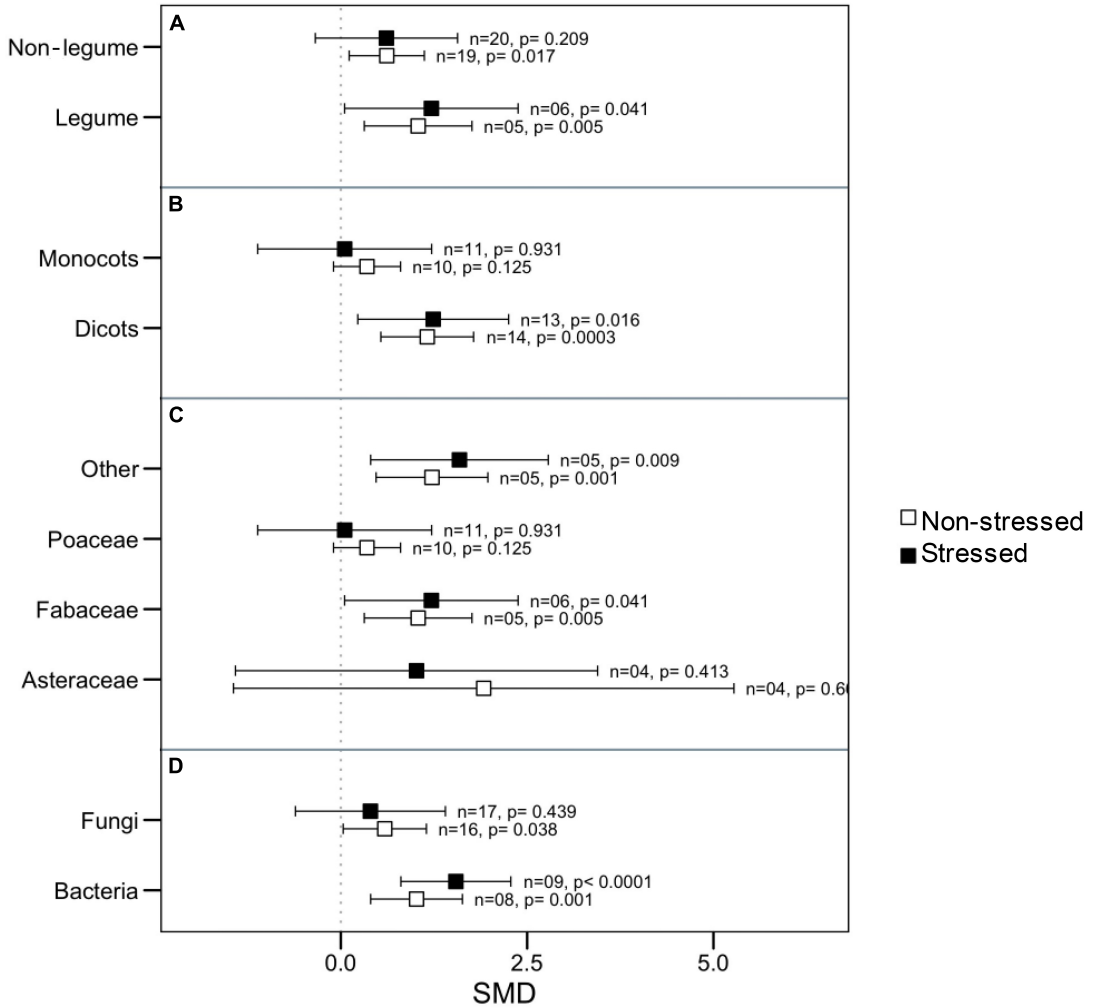

FIGURE 3 | Effects of microbial inoculation on plant root length under normal and high temperature stress conditions for various categorical variables such as **(A)** Plant nodulation, **(B)** Plant clade, **(C)** Plant Family, and **(D)** microbes' types (fungi or bacteria). Error bars are the effect size means ± 95% CIs. Where the CIs do not overlap the vertical dashed lines, the effect size for a parameter is significant, i.e., the growth responses of AMF plants were significantly different from those of non-AMF plants. *n* = number of studies included in the meta-analysis, *p* = significance level of SMD.

not show this response (**Figure 3B**). When considering the plant family as a moderator, Poaceae and Asteraceae had an overall neutral influence in root length, but Fabaceae and those belong the other family had significantly positive responses to microbial colonization under both stressed and normal temperature (**Figure 3C**).

Microbial Symbiosis on Plant Photosynthesis Under Thermal Stress

All photosynthetic parameters considered, however, tended to be influenced more under stress than under non-stress conditions, as evident from their larger effect sizes (**Figure 4**). Microbial colonization significantly increased net photosynthesis, maximum photochemical efficiency (Fv/Fm), and photosynthetic pigments such as chlorophyll, carotenoids, flavonoids, and phenolics in plants under high-temperature stress as compared to non-colonized plants. However, under normal temperature, these effects were not as strong as under stressed conditions (**Figure 4**). For example, symbiotic plants had 25% (1.37, p = 0.0002) and 51% (2.80, p = 0.004) higher total chlorophyll and net photosynthesis, respectively, over non-symbiotic plants under stress but these were only 11% (0.94, p = 0.004) and 16% (1.79, p = 0.035) higher under ambient conditions (**Figure 4**). There was no significant effect on stomatal conductance in general, but the wider CI-values, as well as heterogeneity statistics, showed that it varies due to different plant-microbe systems.

Improvement in the photosynthetic ability of symbiotic plants is correlated clearly with the increased plant biomass of inoculated plants. Thermal stress exerts a negative impact on photosynthetic machinery and gas exchange in plants causing altered physiological and biochemical processes. Similar to heat stress, early reaction to water deficit could result in

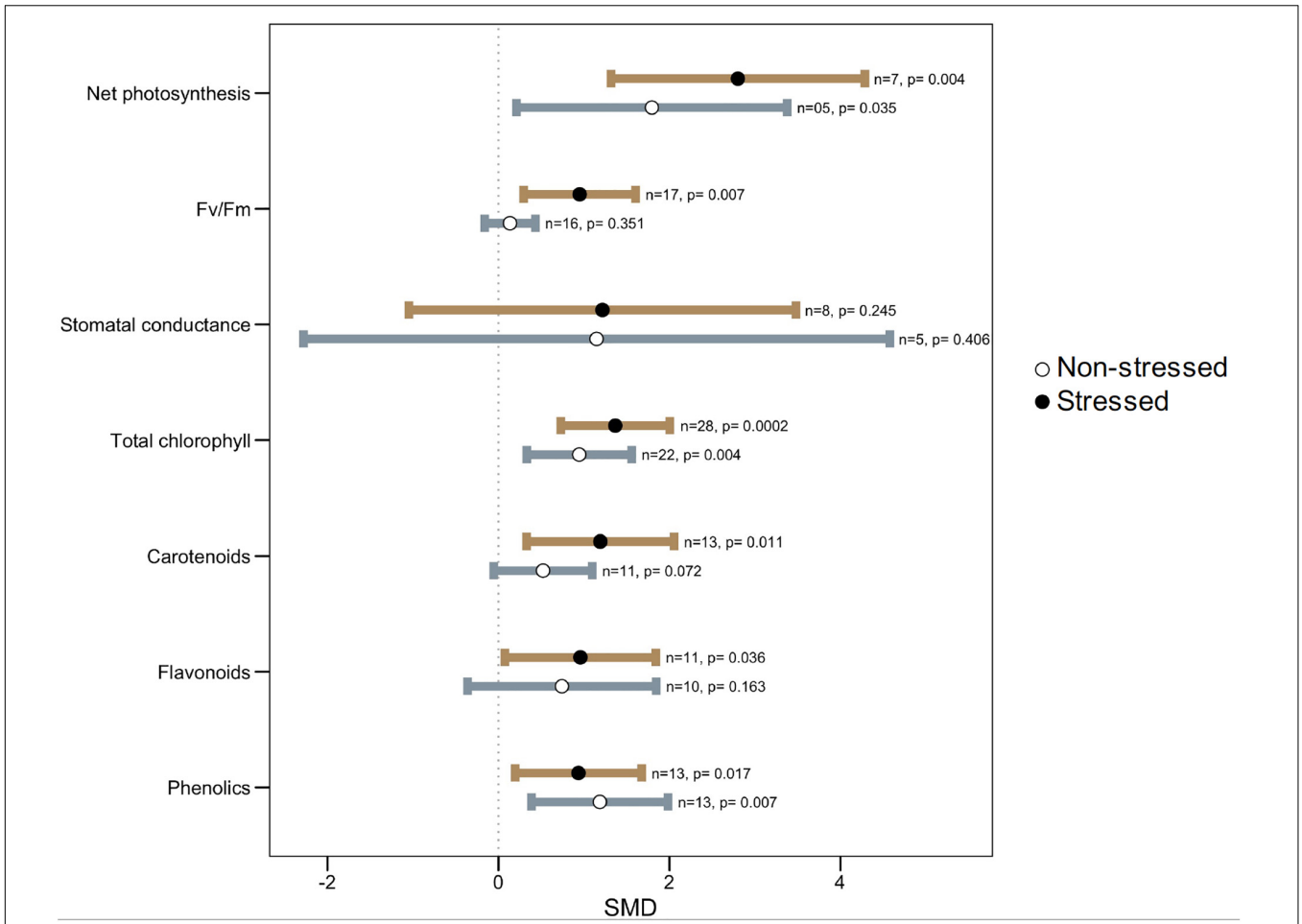

FIGURE 4 | Effect of microbe inoculation on photosynthetic parameters compared with those of non-inoculated plants under heat stress and non-stressed conditions. Error bars are effect size (SMD) means ± 95% CIs. Where the CIs do not overlap the vertical dashed lines, the effect size for a parameter is significant, i.e., the growth responses of inoculated plants were significantly different from those of non-inoculated plants. *n* = number of studies included in the meta-analysis, *p* = significance level of SMD.

accelerated stomatal closure and reduced water loss (Malinowski and Belesky, 2000) in microbial colonized plants. Also, an augmented chlorophyll pigment in symbiotic plants under stress reflects their better photosynthesis which corelates with their stress tolerance (Harman, 2000; Harman et al., 2004; Bae et al., 2009). Carotenoids and flavonoids are efficient quenchers of ROS, such as peroxide radicals and singlet oxygen molecules, and thus abate oxidative damage (Wahid et al., 2007; Agati et al., 2012). Increased carotenoids content in microbe-treated plants compared to untreated under heat stress provides evidence of involvement of this antioxidant in the microbe mediated ROS scavenging pathway for increasing plant heat stress tolerance (**Figure 4**). It has been shown that carotenoids of the xanthophyll family and some other terpenoids bring about a decreased fluidity (thermostability) of the lipid membrane, resulting in reduced susceptibility to lipid peroxidation under high temperatures (Havaux, 1998; Velikova et al., 2004; Sharkey, 2005). It is also worthwhile mentioning that in a recent paper it was demonstrated that plants grown under warmer conditions are able to better control oxidative stress and lipid peroxidation thanks to the activation of higher antioxidant defenses (Bertini et al., 2021). Phenolics, flavonoids, anthocyanins, lignins, etc., are important secondary metabolites in plants and are involved in stress tolerance in the plant (Chalker-Scott, 2002; Wahid, 2007; Wahid et al., 2007). We noted that microbial colonization significantly increased phenolics and flavonoids in plants under heat stress (**Figure 4**). Increased accumulation of phenolics under heat stress was shown to be associated with higher phenyl ammonia-lyase (PAL) and lower peroxidase and polyphenol lyase activities (Rivero et al., 2001).

Microbial Symbiosis on Osmolytes and Hormones Accumulation Under Thermal Stress

One of the important mechanisms plants employ to withstand various stresses, including extreme temperatures stress, is the accumulation of certain organic compounds known as

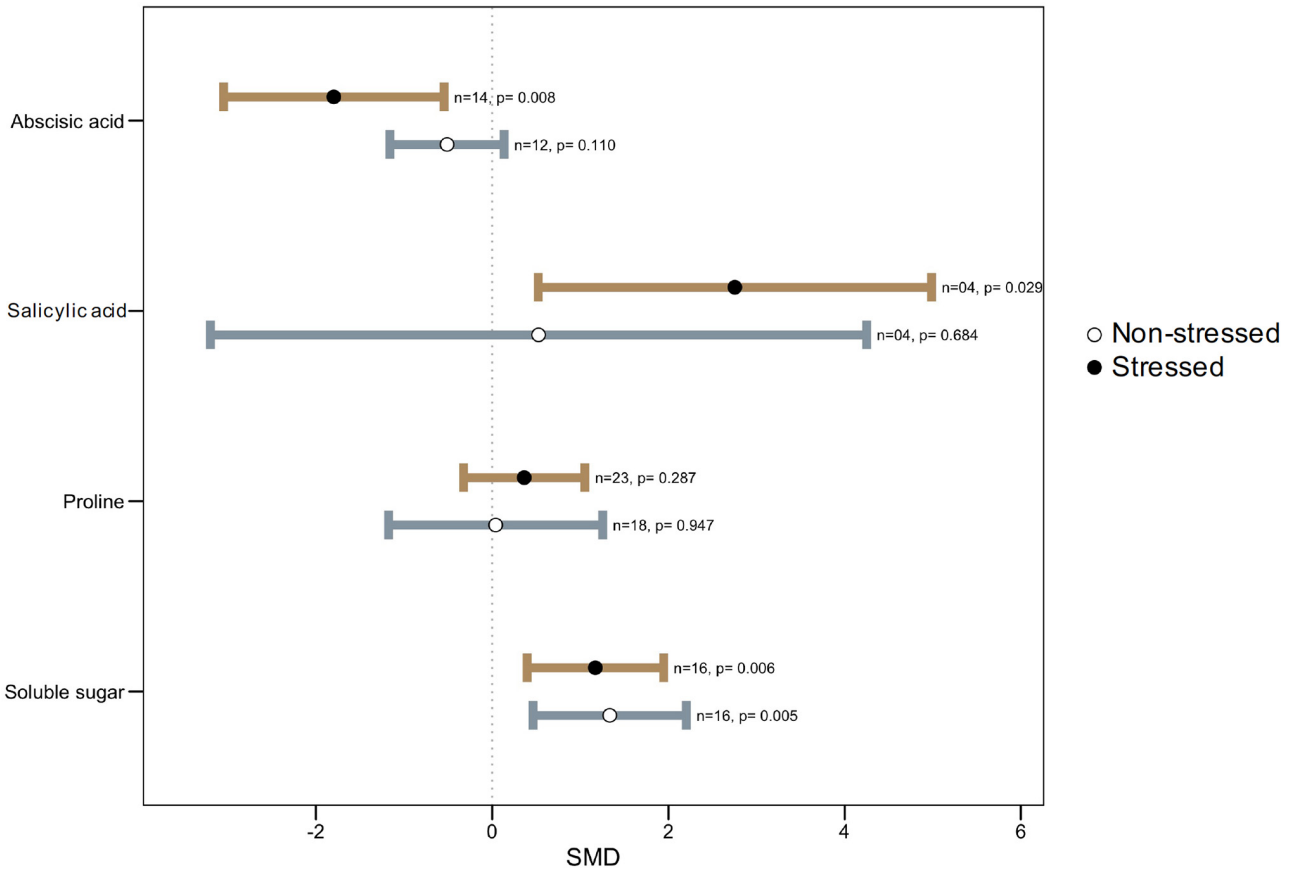

FIGURE 5 | Effect of microbe inoculation on osmplytes and hormones compared with those of non-inoculated plants under heat stress and non-stressed conditions. Error bars are effect size (SMD) means ± 95% CIs. Where the CIs do not overlap the vertical dashed lines, the effect size for a parameter is significant, i.e., the growth responses of inoculated plants were significantly different from those of non-inoculated plants. *n* = number of studies included in the meta-analysis, *p* = significance level of SMD.

compatible osmolytes (Hare et al., 1998; Sakamoto and Murata, 2002). Depending on the plant species and stress type and severity, various compounds such as sugars, sugar alcohols, proline, glycinebetaine (GB), and tertiary sulfonium compounds are accumulated (Sairam and Tyagi, 2004). In plants, GB plays a vital role as an osmolyte under various stresses, such as drought, salinity, or high temperature (Giri, 2011). Different plants showed varying capacity to synthesize GB under stress (Ashraf and Foolad, 2007; Wahid et al., 2007). However, we did not come across any study that investigated the involvement of GB in microbial-mediated plant heat stress tolerance; there is room for future researchers to find out the role of this compound.

Similar to GB, proline also accumulates in plants under stresses and take part in plant abiotic stress tolerances. Proline accumulation helps in osmotic adjustment and plays a protective role as a ROS scavenger under thermal stress (Szabados and Savouré, 2010; Kaur and Asthir, 2015). However, it is still controversial if its presence is an adaptive response that provides greater stress tolerance or if its increase is a symptom of stress injury (Ashraf and Foolad, 2007). Apparently, no significant difference in proline accumulation in colonized plants versus non-colonized plants (**Figure 5**) suggests that the effect of proline is not independent but relies on many factors, one among them being phytohormones (Iqbal et al., 2019). Similar findings were reported on proline accumulation and its association in microbe-mediated plant drought tolerance (Dastogeer, 2018). It was hypothesized that relatively higher levels of proline in microbial colonized plants indicate a reduced extent of damage in a stressed plant (Dastogeer and Wylie, 2017; Dastogeer et al., 2018). Proline functions as low-molecular weight chaperones in plants and helps avoid the stress effect (Gupta et al., 2013). Because of its zwitter ion nature, proline accumulates to high-concentration in cell cytoplasm during stress. Yet, over-accumulation of proline could show toxicity to plant cells (Rizhsky et al., 2004). Genotypic variations for varying levels of proline due to stress have been known in earlier studies with sunflower (Amutha et al., 2007; Harsh et al., 2016). Therefore, the status of proline level is not a reliable indicator of stress tolerance of plants (Silvente et al., 2012).

Similarly, the accumulation of soluble sugars under heat stress has been reported in sugarcane, which entails great implications for heat tolerance (Wahid and Close, 2007). Under

high temperatures, fruit set in tomato plants failed due to the disruption of sugar metabolism and proline transport during the narrow window of male reproductive development (Sato et al., 2006). Among other osmolytes, 4-aminobutyric acid (GABA), a non-protein amino acid, is widely distributed throughout the biological world to act as a compatible solute. Several studies showed that various environmental stresses increase GABA accumulation through metabolic or mechanical disruptions, thus leading to cytosolic acidification. Rapid accumulation of GABA in stressed tissues may provide a critical link in the chain of events stemming from perception of environmental stresses to timely physiological responses (Kinnersley and Turano, 2000).

Phytohormones, like abscisic acid (ABA), salicylic acid (SA), and jasmonic acid (JA), serve as signaling compounds during stress (Shinozaki and Yamaguchi-Shinozaki, 2007). ABA, an isoprenoid phytohormone, is involved in the regulation of many physiological processes in plants, including stomatal opening and closing, protein storage, and adaptation to stress. In nature, where heat and drought stress usually coincide, induction of ABA is an important element of thermotolerance, pointing to its role in biochemical pathways essential for survival under heat stress (Maestri et al., 2002; Sah et al., 2016). Several studies highlighted that induction of various heat shock proteins (HSPs) (e.g., HSP70) by ABA may be one mechanism whereby it confers thermotolerance (Pareek et al., 1998). Interestingly, however, in our meta-analysis, ABA level was found significantly lower in colonized plants as compared to the non-colonized plants (**Figure 5**). Some microbes produce biologically active gibberellins (GAs), which might be associated with plant growth promotion through reducing stress hormones like ABA (Zhang et al., 2014; Verma et al., 2016; Bashar et al., 2019). Under stressful conditions, the plant regulates stress hormones like ABA through active chemical signals, which induce extreme sensitivity to stomatal conductance (de Ollas and Dodd, 2016; Verma et al., 2016).

The salicyclic acid (SA) is an important signaling component in response to systemic acquired resistance (SAR) and the hypersensitive response (HR) (Kawano et al., 1998) and modulates plant growth, development, flowering, stomatal response, ethylene synthesis, and respiration (Waqas et al., 2012; Khan M. I. R. et al., 2015; Wani et al., 2017). Various studies highlighted the roles of SA in improving plant tolerance to heat stress (Larkindale and Knight, 2002; Wang L.-J. et al., 2010; Khan M. I. R. et al., 2015). The SA stabilizes the trimers of heat shock transcription factors and helps them bind heat shock elements to the promoter of heat shock-related genes. SA-induced thermotolerance involves Ca^{2+} homeostasis and antioxidant systems (Wang and Li, 2006). Our meta-analysis showed that microbial inoculation greatly enhanced SA levels in plants under heat stress conditions (**Figure 5**).

The Jasmonic acid (JA) has roles in the biosynthesis of defensive secondary metabolites and proteins (Balbi and Devoto, 2008) as well as it is involved in many physiological processes such as resistance to insects and pathogen, pollen development, senescence, and root growth (Lorenzo et al., 2004). Khan et al. (2012b) and Waqas et al. (2015) reported a substantially low induction of this hormone in microbial colonized plants under stress suggesting its involvement in heat tolerance. The JA level was increased in *Exophiala* sp.-inoculated plants under growth conditions significantly reduced as compared to non-inoculated plants (Waqas et al., 2015). Further studies are needed to observe if reduction of JA is common in all microbe-mediated thermotolerance and what are the underlying mechanisms involved.

Another hormone, ethylene is involved in almost all growth and developmental processes in plants, including stress tolerance (Iqbal et al., 2017). Variable responses in ethylene production (i.e., increase or decrease) in plants have been reported under heat stress conditions (Antunes and Sfakiotakis, 2000; Arshad and Frankenberger, 2002; Larkindale and Huang, 2005). We did not come across any study that looked into ethylene production for microbial colonized versus non-colonized plants under normal or stress conditions, and this is an area of future research.

The hormones gibberellins and cytokinins show contrasting roles on plant heat tolerance to ABA (Liu and Hou, 2018; Li N. et al., 2021). However, there are insufficient studies on the effect of gibberellins and cytokinins on microbial conferred heat tolerance for inclusion into our meta-analysis. In a study, an endophyte *Penicillium resedanum* LK6 produces gibberellins and improves growth, and provides resilience to environmental stresses (Khan A. L. et al., 2015). Further investigation is necessary for revealing the involvement of gibberellins and cytokinins in this regard.

Microbial Symbiosis on Activity of Antioxidant Enzymes Under Thermal Stress

Reactive oxygen species (ROS) are produced in the plant as by-products of aerobic metabolism and exist in several forms such as hydroxyl radicals ($^{\bullet}OH$) and superoxide anions (O_2^-), hydrogen peroxide (H_2O_2), or singlet oxygen ($^1O_2$) (Blokhina et al., 2003; Apel and Hirt, 2004; Mittler et al., 2004). The ROS functions as signaling molecules, at low levels, they are necessary for basic biological processes of the plant, but higher levels are detrimental and may cause DNA damage and incorrect timing of programmed cell death (PCD) directly (Tsukagoshi et al., 2010; Zafra et al., 2010; Xie et al., 2014). The plant has an efficient well-coordinated, and rapidly responsive antioxidant system, including both non-enzymatic and enzymatic processes to mitigate the effect of overproduction of ROS. However, the equilibrium between synthesis and removal of ROS may be perplexed under various biotic and abiotic stresses (Quan et al., 2008; Huang et al., 2019). For example, at higher temperatures, there is an increased production of ROS causing a disparity between ROS production and the ability of the scavenging process to detoxify and remove the reactive intermediates (Saidi et al., 2011; Hemantaranjan et al., 2014). The association of microbial symbiosis has been described for higher tolerance to different environmental stresses (Hernandez et al., 2000; Larkindale and Knight, 2002; Halliwell, 2006). Thus, the involvement of the microbiome in mitigating oxidative stress in the plant has recently attracted research interest.

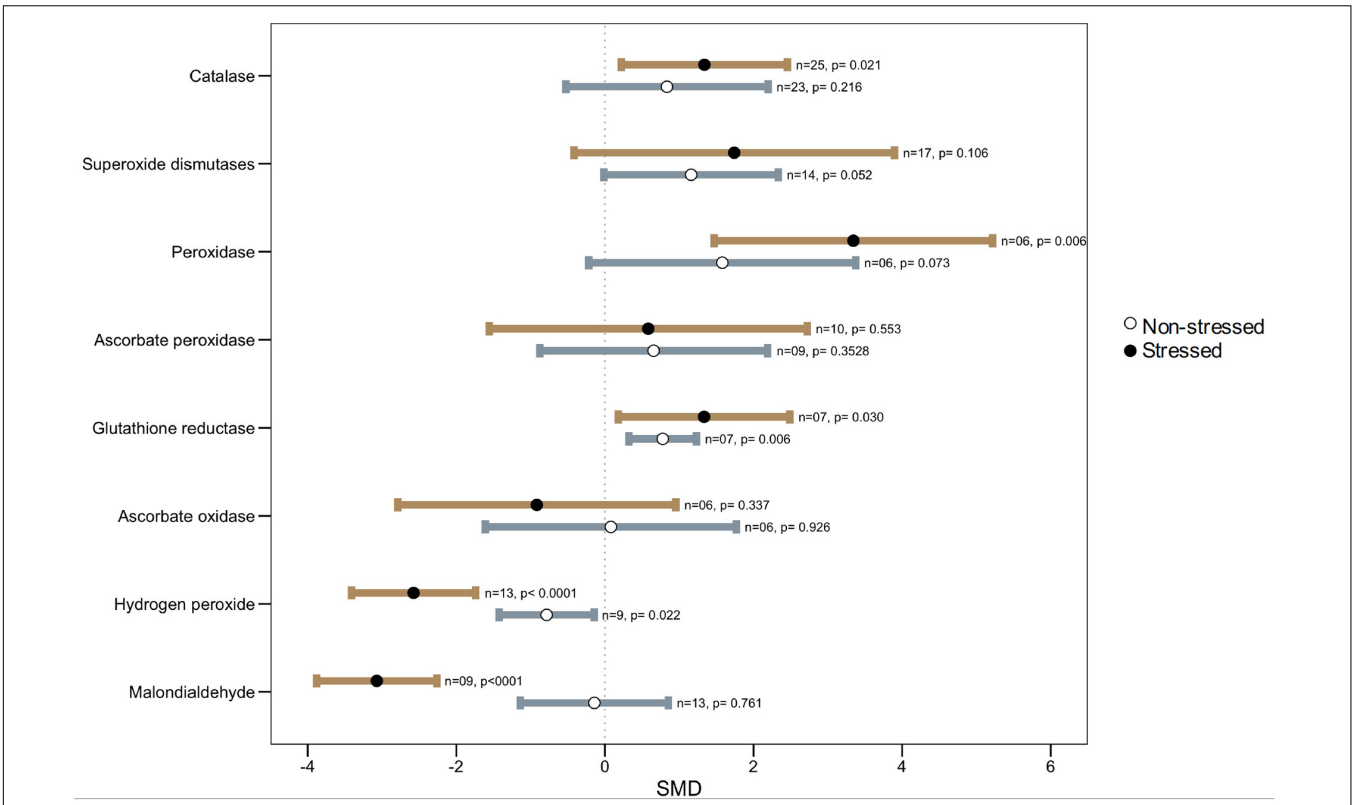

FIGURE 6 | Effects of microbial inoculation on plant ROS production and antioxidant enzymatic activity under non-stressed, and heat stress. Error bars are means ± 95% CIs. Where the CIs do not overlap the vertical dashed lines, the effect size for a parameter is significant. *n* = number of studies included in the meta-analysis, *p* = significance level of SMD.

Ascorbate-Glutathione Cycle

It has been shown in several studies that microbial-mediated plant heat stress tolerance is associated with heightened antioxidant defense in inoculated plants. The contributions of the ascorbate-glutathione (AsA-GSH) cycle on plant tolerance under various abiotic stresses have been reported in many plant species (Anjum et al., 2010; Bartoli et al., 2017; Kuźniak et al., 2017). The four enzymes that steer the cycle are ascorbate peroxidase (APX), dehydroascorbate reductase (DHAR), mono-dehydroascorbate reductase (MDHAR), and glutathione reductase (GR) (Quan et al., 2008; Noctor et al., 2014; Mohi-Ud-Din et al., 2021). In our analysis, we found that there were no overall changes in APX activity in colonized plants under heat stress (**Figure 6**). However, the wider CI values indicated that the APX accumulation is variable depending on host-microbe types or other factors. For example, it was reported that treatment with bacteria (*Bacillus amyloliquefaciens* or *Azospirillum brasilense*) decreased the activity of this enzyme as well as significantly lower expression of the APX1 gene was observed in heat exposed wheat seedlings (Abd El-Daim et al., 2014). A strikingly different finding was reported in several other studies where microbial treatment increased the level of APX accumulation over non-treated plants under high heat conditions (Maya and Matsubara, 2013; Yeasmin et al., 2019; Khan et al., 2020b). The other two enzymes: DHAR and MDHAR, could not be included in our meta-analysis because of the insufficient number of reports, but both of them were found to increase significantly in plants under elevated temperature, and microbial colonization results in lower accumulation as compared to non-colonized plants (Abd El-Daim et al., 2014, 2019). In general, a significantly higher accumulation of GR in the microbial colonized plants over non-colonized plants was observed through our meta-analysis (**Figure 6**). The GR plays a crucial role in controlling the levels of reduced glutathione in the plant (Huang et al., 2019). Glutathione modulates ROS levels in cells through both auxin/PLETHORA (PLT) dependent and independent pathways, thereby participating in and maintaining ROS homeostasis in the plant (Yu et al., 2013).

Antioxidant Enzymes

Apart from the AsA-GSH cycle, SOD (superoxide dismutase), CAT (catalase), POD (peroxidase), glutathione peroxidases (GPX), and glutathione-*S*-transferases (GST) are important antioxidant enzymes in plants taking part in ROS homeostasis under stress. In the plant cells, SOD provides primary protection against $O_2^{\bullet -}$, which is then converted to H_2O_2 for subsequent metabolism to H_2O by CAT and peroxidases (POD, APX, and GPX), thus protecting the cell damage (Mittler et al., 2004; Gill and Tuteja, 2010; Wang G. et al., 2010; Mohi-Ud-Din et al., 2021). The current meta-analysis showed no

apparent disparity in SOD measurement in colonized over non-colonized plants, but the higher CI values indicated that SOD accumulation varied significantly among studies. For example, in a study, Li X. et al. (2021) did not notice any changes in SOD accumulation in *Aspergillus aculeatus* inoculated *Lolium perenne,* although this fungus improved the heat tolerance of this plant. Similar results have been reported for *Septoglomus deserticola* and *Septoglomus constrictum* (AM fungi) mediated heat stress tolerance in the tomato plant with no apparent changes in SOD activity (Duc et al., 2018). In contrast, a few studies reported a significant increase in SOD in microbial colonized plants under high-temperature stress (Maya and Matsubara, 2013; Yeasmin et al., 2019; Bruno et al., 2020; Khan et al., 2020a). Regarding CAT and POD, they showed consistently higher accumulation (CAT, $p = 0.021$; POD, $p = 0.006$) in colonized plants as compared to non-colonized controls under heat stress across various studies (**Figure 6**).

Also, a significantly decreased level of hydrogen peroxide (H_2O_2) and Malondialdehyde (MDA) ($p < 0.001$) in microbial-treated plants adds further support to a lower level of heat stress injury due to the increased induction of the antioxidant defense systems compared to the non-treated plants (**Figure 6**). The MDA is the principal and extensively studied product of polyunsaturated fatty acid (PUFAs) peroxidation. The MDA levels are used as a measure of membrane lipid peroxidation and oxidative stress and the impact it has on membrane fluidity, leakiness, and damage of membrane proteins, enzymes, and ion channels (Garg and Manchanda, 2009; de Dios Alché, 2019).

MICROBIAL SYMBIOSIS ON PLANT THERMOTOLERANCE: MOLECULAR ASPECTS

There is a huge lack of understanding of the mechanisms of microbe-mediated plant heat stress tolerance at the molecular level. The heat shock protein (HSPs) act as "molecular chaperones," and their upregulation is well known to increase thermotolerance in plants. The expression of heat stress-dependent regulatory proteins such as heat shock transcription factors (HSFs) and heat shock proteins (HSPs) have been described. The HSPs are crucial in regulating and restoring protein structures and maintaining the condition of plants under heat stress (Queitsch et al., 2000; Nakamoto and Vigh, 2007; Xu et al., 2012; Wang et al., 2014). Several studies reported an increased level of expression of HSPs in the microbial colonized plant compared to non-colonized plants under heat stress (Abd El-Daim et al., 2019; Bruno et al., 2020; Li X. et al., 2021). To reveal the mechanisms through which Enterobacter sp. SA187 mediates plant thermotolerance in *Arabidopsis* Shekhawat et al. (2020) carried out RNA-seq and targeted transcriptomic analyses. They described that the bacteria-mediated heat tolerance is associated with the gene networks for heat protection of plants similar to that of the heat priming (pre-exposure of plants to heat that enables plants to be better prepared to response to heat stress). For example, heat tolerance is associated with the upregulation of genes related to the auxin and gibberellin hormones and the down-regulation of the genes related to jasmonic and abscisic acid. It was also found to be related to hyper-induction of heat-responsive and heat memory genes, which is proven in heat primed plants (Lämke et al., 2016; Ling et al., 2018; Liu et al., 2018). The bacteria inoculated plants resulted in higher expression of several heat-responsive genes such as HSFA2, HSP101, HSP70, HSP70B, GA3OX1, HSP90.1, and ATERDJ3A as well as heat memory genes; APX2 (ascorbate peroxidase 2), HSP18.2, H3K4me3 (epigenetic modification to the DNA packaging protein Histone H3) (Lämke et al., 2016; Sedaghatmehr et al., 2016). In a study, increased expression of heat shock protein gene HSP17.8 and Dehydration-responsive gene DREB1 and decreased expression of POD47 and FeSOD have been reported for fungal (*Aspergillus aculeatus*) conferred heat stress tolerance in *Lolium perenne* grass (Li X. et al., 2021). Khan et al. (2020b) reported that GmLAX3 and GmAKT2, the key genes involved in the regulation of the ABA-dependent pathway, were downregulated initially but upregulated after 5 and 10 days in the inoculated soybean plant under thermal stress. The expression of these genes may be linked with plant stress response by modulating auxin and ABA signaling, decreasing ROS production and enhancing K^+ gradients, which are critical in plant tissues under various stresses (Zhou et al., 2014; Chai et al., 2016). The *B. velezensis* inoculation induced an increased abiotic stress tolerance, and the pattern of metabolic modulation and abundance of several proteins were found to be similar in wheat challenged with different abiotic stress factors such as heat, cold, and drought (Abd El-Daim et al., 2019).

Taken together, high-temperature influences plant growth by affecting photosynthesis, osmotic balance, enzymatic activities, and metabolic activities. Microbial symbionts consistently help plants reduce the impact of thermal stress by manipulating physiological processes (**Figure 7**). Microbe-induced plant heat stress tolerance has broad ecological and agricultural implications. In some regions, increased stress tolerance can result in higher crop yield under higher temperature environments. Continued interest in the microbiome and their functional roles in uncovering the underlying mechanisms of plant-microbe interaction appears well-justified.

FUTURE DIRECTION AND CONCLUSION

Despite the evidence of global warming and the importance of heat stress on plant ecology and productivity (Wahid et al., 2007; Teixeira et al., 2013; Jagadish et al., 2021) and the increasing evidence of microbial functions of plant stress tolerance (**Table 1** and **Figure 1**), the current review here identified a significant lack in our knowledge on microbial conferred plant performance and productivity under high-temperature conditions. Apparently, the most crucial of these is the lack of experiments that demonstrate how do microbes actually influence plant responses in the natural environment. Most of the investigations reviewed here were carried out under controlled environmental conditions and on cultivated host species. Therefore, experiments focusing on the impacts of symbionts on wild and crop plants exposed to heat stresses in the natural environment are required. In a recent

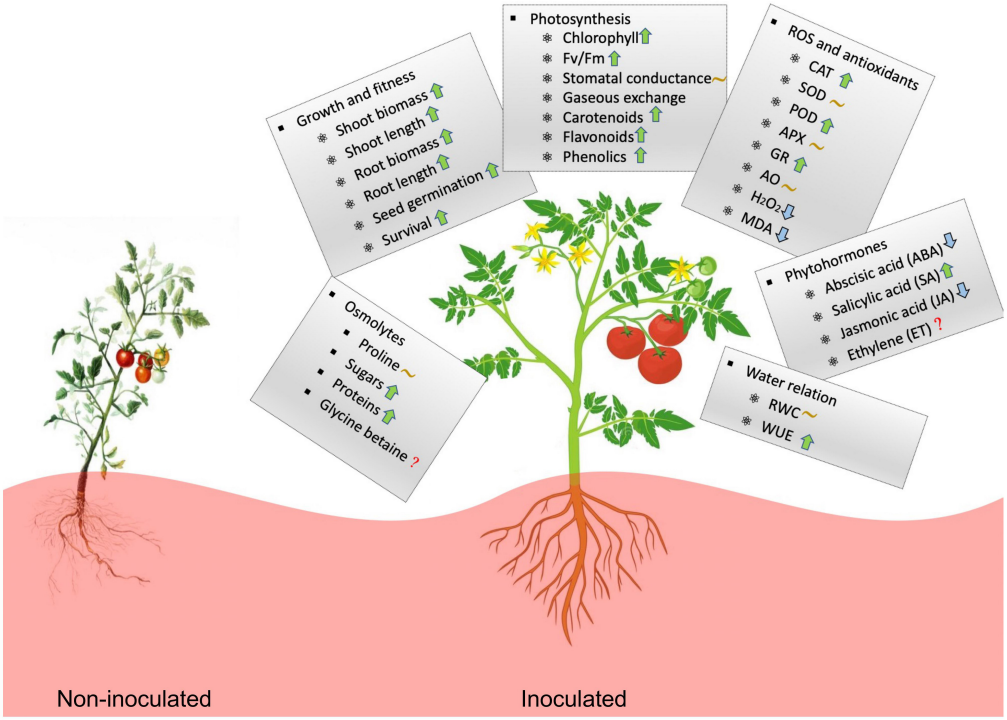

FIGURE 7 | Illustration of the effects of microbial inoculation on plant physiological activity and stress tolerance under high temperature. The upward arrow (↑) indicates increase of the value for microbial-treated plants compared to non-treated plants whereas, downward arrow (↓) indicates decease, wavy line (∼) indicates the effect is variable and the question mark (?) unavailable information.

paper, Ballesteros et al. (2020) analyzed metatranscriptomic data from the Antarctic plant *Colobanthus quitensis*, highlighting that the plant-associated fungal community provides beneficial effects, such as increased plant growth, tolerance to abiotic stress, and higher leaf carbon gain, when plants are grown under a simulated global warming scenario. The reports from these investigations should include mean values of response variables, measures of variance, and replication and preferably provide the actual dataset as the **Supplementary Data** so that these data can be used in future meta-analyses. Although it was shown that increasing temperatures due to climate change might negatively impact the outcomes of symbioses (Kiers et al., 2010), the current meta-analyses indicated that microbial symbionts have more positive effects on plant performance under heat stress than under normal conditions. It is not clear why microbial inoculation exerts its effects in more stressed conditions than under normal temperatures conditions, but putatively, this is associated with plant stress acclimation at the molecular or cellular levels. Tolerance of non-colonized plants to heat stress is well studied, and the reports suggested that the mechanisms are associated with enhanced expression of a variety of heat shock proteins, other related proteins, production of ROS, and induction of mitogen-activated protein kinase (MAPK) and calcium-dependent protein kinase (CDPK) cascades, and, most importantly, chaperone signaling and transcriptional activation (Wahid et al., 2007). As previously shown for abiotic stresses such as freezing and drought and assumed for microbial conferred cold adaptation (Knight and Knight, 2001; Acuna-Rodriguez et al., 2020), some kind of cross-talk between the proteins common to signaling pathways are present for responses to heat and microbial colonization leading to enhanced plant metabolism. The involvement of microbial elicitors at the plant cell surface resulting in increases in cytosolic $Ca2^{+}$ concentrations could be another possibility (Sanders et al., 1999; Acuna-Rodriguez et al., 2020). However, more research is needed to establish whether these or similar mechanisms might explain the beneficial effects of microbial symbionts on plants at higher temperatures. As discussed by Acuna-Rodriguez et al. (2020), less attention has been paid toward understanding the differences in the optimum growth temperatures of microbial symbionts and their plant hosts. For instance, in the *Epichloe* symbiosis, the seemingly decreased plant performance at low temperatures in the natural conditions could be that the minimum temperatures requirement of the endophytes being higher than those of their hosts (Casler and Van Santen, 2008; Wäli et al., 2008). Extensive surveys to identify novel microbial symbionts capable of improving plant performance under stress are advocated. Isolation of naturally occurring plant and soil microbiomes and screening them for potential symbiotic benefits is a continuous process. Developing a rapid but robust screening method is important so that a large collection of microbes can be tested for their effects, and the results should be supported by field experiments in order to translate the research into the field.

A few surveys focused on endophytes collected from hot environments, and some of the endophytes tested were found to grow at high temperatures (Zhou et al., 2015; Dastogeer et al., 2019). Studies on other components of the plant microbiome such as algae, protists, and viruses revealed that they are also present in the tissues or in the rhizosphere of many plant species and provide some fitness benefits (Roossinck, 2015; Gao et al., 2019; Dastogeer et al., 2020a; Dumack and Bonkowski, 2021; Lee and Ryu, 2021). For example, rhizosphere protists altered the metabolites of the maize plant, particularly, polyols. This alteration is presumably to be associated with reduction of the impact of stress caused due to grazing (Kuppardt et al., 2018). A plant virus, yellowtail flower mild mottle virus (YTMMV, genus Tobamovirus), enhanced drought stress tolerance in *Nicotiana benthamiana* plants by modulating its metabolic compounds (Dastogeer et al., 2018). However, the effect of many of the microbiome components has received less attention. We also suggest studies that consider microbial symbionts on plant heat tolerance should take into account the involvement of secondary metabolites because many microbes utilize these compounds in the interaction with plants and with environments (Zaynab et al., 2018; Ullah et al., 2020). Another important area of research, but has so far been neglected, is to study the multi-partite interaction of microbes and their impact on stress tolerance, such as thermal tolerance. It was found that a fungus can increase the heat tolerance of a plant only in the presence of a virus within it, whereas neither virus nor the plant separately could confer this benefit. Therefore, a three-way symbiosis is required for thermal tolerance. In nature, plants do not remain in isolation but in continuous interaction with a wide variety of microbes (Marquez et al., 2007). In addition to microbe-plant interaction, microbe-microbe and microbe-environment interaction should be taken into account to understand the stable functions of a particular microbe in its potential application in agricultural settings, which is a dynamic environment and subject to continuous changes (Dastogeer et al., 2020a).

AUTHOR CONTRIBUTIONS

KD developed the concept, performed the database search, partially collected the data, analyzed and interpreted the results, and wrote the draft. MZ, MR, and MS extracted the data, produced the graphs, discussed the results, and revised the manuscript. AC produced the table and discussed the results. All authors approved the final version of the manuscript.

SUPPLEMENTARY MATERIAL

The Supplementary Material for this article can be found online at: https://www.frontiersin.org/articles/10.3389/fmicb.2022.833566/full#supplementary-material

REFERENCES

Abd El-Daim, I. A., Bejai, S., Fridborg, I., and Meijer, J. (2018). Identifying potential molecular factors involved in *Bacillus amyloliquefaciens* 5113 mediated abiotic stress tolerance in wheat. *Plant Biol.* 20, 271–279. doi: 10.1111/plb.12680

Abd El-Daim, I. A., Bejai, S., and Meijer, J. (2014). Improved heat stress tolerance of wheat seedlings by bacterial seed treatment. *Plant Soil* 379, 337–350. doi: 10.1007/s11104-014-2063-3

Abd El-Daim, I. A., Bejai, S., and Meijer, J. (2019). *Bacillus velezensis* 5113 induced metabolic and molecular reprogramming during abiotic stress tolerance in wheat. *Sci. Rep.* 9, 1–18. doi: 10.1038/s41598-019-52567-x

Acuna-Rodriguez, I. S., Newsham, K. K., Gundel, P. E., Torres-Diaz, C., and Molina-Montenegro, M. A. (2020). Functional roles of microbial symbionts in plant cold tolerance. *Ecol. Lett.* 23, 1034–1048. doi: 10.1111/ele.13502

Agati, G., Azzarello, E., Pollastri, S., and Tattini, M. (2012). Flavonoids as antioxidants in plants: location and functional significance. *Plant Sci.* 196, 67–76. doi: 10.1016/j.plantsci.2012.07.014

Ahn, E., and Kang, H. (2018). Introduction to systematic review and meta-analysis. *Korean J. Anesthesiol.* 71:103.

Ali, A. H., Abdelrahman, M., Radwan, U., El-Zayat, S., and El-Sayed, M. A. (2018). Effect of Thermomyces fungal endophyte isolated from extreme hot desert-adapted plant on heat stress tolerance of cucumber. *Appl. Soil Ecol.* 124, 155–162. doi: 10.1016/j.apsoil.2017.11.004

Ali, A. H., Radwan, U., El-Zayat, S., and El-Sayed, M. A. (2019). The role of the endophytic fungus, *Thermomyces lanuginosus*, on mitigation of heat stress to its host desert plant *Cullen plicata*. *Biol. Futura* 70, 1–7. doi: 10.1556/019.70.2019.01

Ali, S. Z., Sandhya, V., Grover, M., Kishore, N., Rao, L. V., and Venkateswarlu, B. (2009). *Pseudomonas* sp. strain AKM-P6 enhances tolerance of sorghum seedlings to elevated temperatures. *Biol. Fertil. Soils* 46, 45–55. doi: 10.1007/s00374-009-0404-9

Ali, S. Z., Sandhya, V., Grover, M., Linga, V. R., and Bandi, V. (2011). Effect of inoculation with a thermotolerant plant growth promoting *Pseudomonas putida* strain AKMP7 on growth of wheat (*Triticum* spp.) under heat stress. *J. Plant Interact.* 6, 239–246. doi: 10.1080/17429145.2010.545147

Amutha, R., Muthulaksmi, S., Baby Rani, W., Indira, K., and Mareeswari, P. (2007). Studies on biochemical basis of heat tolerance in sunflower (*Helianthus annus* L.). *Res. J. Agric. Biol. Sci.* 3, 234–238.

Anjum, N. A., Umar, S., and Chan, M.-T. (2010). *Ascorbate-Glutathione Pathway and Stress Tolerance in Plants*. Berlin: Springer Science & Business Media.

Antunes, M., and Sfakiotakis, E. (2000). Effect of high temperature stress on ethylene biosynthesis, respiration and ripening of 'Hayward'kiwifruit. *Postharvest Biol. Technol.* 20, 251–259. doi: 10.1016/s0925-5214(00)00136-8

Apel, K., and Hirt, H. (2004). Reactive oxygen species: metabolism, oxidative stress, and signal transduction. *Annu. Rev. Plant Biol.* 55, 373–399. doi: 10.1146/annurev.arplant.55.031903.141701

Arshad, M., and Frankenberger, W. T. Jr. (2002). *Ethylene: Agricultural Resources and Applications*. Berlin: Springer science & Business media.

Ashraf, M., and Foolad, M. R. (2007). Roles of glycine betaine and proline in improving plant abiotic stress resistance. *Environ. Exp. Bot.* 59, 206–216.

Azad, K., and Kaminskyj, S. (2016). A fungal endophyte strategy for mitigating the effect of salt and drought stress on plant growth. *Symbiosis* 68, 73–78. doi: 10.1371/journal.pone.0014823

Bae, H., Sicher, R. C., Kim, M. S., Kim, S. H., Strem, M. D., Melnick, R. L., et al. (2009). The beneficial endophyte *Trichoderma hamatum* isolate DIS 219b promotes growth and delays the onset of the drought response in *Theobroma cacao*. *J. Exp. Bot.* 60, 3279–3295. doi: 10.1093/jxb/erp165

Balbi, V., and Devoto, A. (2008). Jasmonate signalling network in *Arabidopsis thaliana*: crucial regulatory nodes and new physiological scenarios. *New Phytol.* 177, 301–318. doi: 10.1111/j.1469-8137.2007.02292.x

Balduzzi, S., Rücker, G., and Schwarzer, G. (2019). How to perform a meta-analysis with R: a practical tutorial. *Evidence Based Ment. Health* 22, 153–160. doi: 10.1136/ebmental-2019-300117

Ballesteros, G. I., Torres-Diaz, C., Bravo, L. A., Balboa, K., Caruso, C., Bertini, L., et al. (2020). In silico analysis of metatranscriptomic data from the Antarctic vascular plant *Colobanthus quitensis*: responses to a global warming scenario

through changes in fungal gene expression levels. *Fung. Ecol.* 43:100873. doi: 10.1016/j.funeco.2019.100873

Bartoli, C. G., Buet, A., Grozeff, G. G., Galatro, A., and Simontacchi, M. (2017). "Ascorbate-glutathione cycle and abiotic stress tolerance in plants," in *Ascorbic Acid in Plant Growth, Development and Stress Tolerance*, eds M. A. Hossain, S. Munné-Bosch, D. J. Burritt, P. Diaz-Vivancos, M. Fujita, and A. Lorence (Berlin: Springer), 177–200. doi: 10.1007/978-3-319-74057-7_7

Bashar, K. K., Tareq, M., Amin, M., Honi, U., Tahjib-Ul-Arif, M., Sadat, M., et al. (2019). Phytohormone-mediated stomatal response, escape and quiescence strategies in plants under flooding stress. *Agronomy* 9:43.

Basit, A., Shah, S. T., Ullah, I., Ullah, I., and Mohamed, H. I. (2021). "Microbial bioactive compounds produced by endophytes (bacteria and fungi) and their uses in plant health," in *Plant Growth-Promoting Microbes for Sustainable Biotic and Abiotic Stress Management*, eds H. I. Mohamed, H. E. D. Saad El-Beltagi, and K. A. Abd-Elsalam (Berlin: Springer), 285–318.

Begg, C., and Mazumdar, M. (1994). Operating characteristics of a rank correlation test for publication bias. *Biometrics* 50, 1088–1101. doi: 10.2307/2533446

Bertini, L., Cozzolino, F., Proietti, S., Falconieri, G. S., Iacobucci, I., Salvia, R., et al. (2021). What antarctic plants can tell us about climate changes: temperature as a driver for metabolic reprogramming. *Biomolecules* 11:1094. doi: 10.3390/biom11081094

Blokhina, O., Virolainen, E., and Fagerstedt, K. V. (2003). Antioxidants, oxidative damage and oxygen deprivation stress: a review. *Ann. Bot.* 91, 179–194. doi: 10.1093/aob/mcf118

Borenstein, M., Hedges, L. V., Higgins, J. P. T., and Rothstein, H. R. (2009). *Introduction to Meta-Analysis*. Chichester: Wiley.

Brachmann, A., and Parniske, M. (2006). The most widespread symbiosis on earth. *PLoS Biol.* 4:e239. doi: 10.1371/journal.pbio.0040239

Bruno, L. B., Karthik, C., Ma, Y., Kadirvelu, K., Freitas, H., and Rajkumar, M. (2020). Amelioration of chromium and heat stresses in Sorghum bicolor by Cr6+ reducing-thermotolerant plant growth promoting bacteria. *Chemosphere* 244:125521. doi: 10.1016/j.chemosphere.2019.125521

Bunn, R., Lekberg, Y., and Zabinski, C. (2009). Arbuscular mycorrhizal fungi ameliorate temperature stress in thermophilic plants. *Ecology* 90, 1378–1388. doi: 10.1890/07-2080.1

Cabral, C., Ravnskov, S., Tringovska, I., and Wollenweber, B. (2016). Arbuscular mycorrhizal fungi modify nutrient allocation and composition in wheat (*Triticum aestivum* L.) subjected to heat-stress. *Plant Soil* 408, 385–399. doi: 10.1007/s11104-016-2942-x

Casler, M. D., and Van Santen, E. (2008). Fungal endophyte removal does not reduce cold tolerance of tall fescue. *Crop Sci.* 48, 2033–2039. doi: 10.2135/cropsci2007.11.0615

Chai, C., Wang, Y., Valliyodan, B., and Nguyen, H. T. (2016). Comprehensive analysis of the soybean (*Glycine max*) GmLAX auxin transporter gene family. *Front. Plant Sci.* 7:282. doi: 10.3389/fpls.2016.00282

Chalker-Scott, L. (2002). Do anthocyanins function as osmoregulators in leaf tissues? *Adv. Bot. Res.* 37, 103–127. doi: 10.1007/s00709-015-0771-z

Chandrasekaran, M., Boughattas, S., Hu, S., Oh, S.-H., and Sa, T. (2014). A meta-analysis of arbuscular mycorrhizal effects on plants grown under salt stress. *Mycorrhiza* 24, 611–625. doi: 10.1007/s00572-014-0582-7

Chandrasekaran, M., Kim, K., Krishnamoorthy, R., Walitang, D., Sundaram, S., Joe, M. M., et al. (2016). Mycorrhizal symbiotic efficiency on C3 and C4 plants under salinity stress–a meta-analysis. *Front. Microbiol.* 7:1246. doi: 10.3389/fmicb.2016.01246

Cohen, J. (1988). *Statistical Power Analysis for the Behavioral Sciences*. Hillsdale, NJ: L. Erlbaum Associates.

Compant, S., Samad, A., Faist, H., and Sessitsch, A. (2019). A review on the plant microbiome: ecology, functions, and emerging trends in microbial application. *J. Adv. Res.* 19, 29–37. doi: 10.1016/j.jare.2019.03.004

Cooper, H. (2015). *Research Synthesis and Meta-Analysis: A Step-By-Step Approach*. Thousand Oaks, CA: Sage publications.

Cooper, H., Hedges, L. V., and Valentine, J. C. (2019). *The Handbook of Research Synthesis and Meta-Analysis*. New York, NY: Russell Sage Foundation.

Dastogeer, K. M. (2018). Influence of fungal endophytes on plant physiology is more pronounced under stress than well-watered conditions: a meta-analysis. *Planta* 248, 1403–1416. doi: 10.1007/s00425-018-2982-y

Dastogeer, K. M., Tumpa, F. H., Sultana, A., Akter, M. A., and Chakraborty, A. (2020a). Plant microbiome–an account of the factors that shape community composition and diversity. *Curr. Plant Biol.* 23:100161. doi: 10.1016/j.cpb.2020.100161

Dastogeer, K. M., Zahan, M. I., Tahjib-Ul-Arif, M., Akter, M. A., and Okazaki, S. (2020b). Plant salinity tolerance conferred by arbuscular mycorrhizal fungi and associated mechanisms: a meta-analysis. *Front. Plant Sci.* 11:588550. doi: 10.3389/fpls.2020.588550

Dastogeer, K. M. G., Li, H., Sivasithamparam, K., Jones, M. G. K., and Wylie, S. J. (2018). Fungal endophytes and a virus confer drought tolerance to *Nicotiana benthamiana* plants through modulating osmolytes, antioxidant enzymes and expression of host drought responsive genes. *Environ. Exp. Bot.* 149, 95–108. doi: 10.1016/j.envexpbot.2018.02.009

Dastogeer, K. M. G., Li, H., Sivasithamparam, K., and Wylie, S. J. (2019). In vitro salt and thermal tolerance of fungal endophytes of *Nicotiana* spp. growing in arid regions of north-western Australia. *Arch. Phytopathol. Plant Protect.* 52, 602–616. doi: 10.1080/03235408.2018.1503762

Dastogeer, K. M. G., and Wylie, S. J. (2017). "Plant–fungi association: role of fungal endophytes in improving plant tolerance to water stress," in *Plant-Microbe Interactions in Agro-Ecological Perspectives*, eds D. P. Singh, H. B. Singh, and R. Prabha (Cham: Springer Nature Singapore Pte Ltd.).

de Dios Alché, J. (2019). A concise appraisal of lipid oxidation and lipoxidation in higher plants. *Redox Biol.* 23:101136. doi: 10.1016/j.redox.2019.101136

de Ollas, C., and Dodd, I. C. (2016). Physiological impacts of ABA–JA interactions under water-limitation. *Plant Mol. Biol.* 91, 641–650. doi: 10.1007/s11103-016-0503-6

DerSimonian, R., and Laird, N. (1986). Meta-analysis in clinical trials. *Control. Clin. Trials* 7, 177–188.

Duc, N. H., Csintalan, Z., and Posta, K. (2018). Arbuscular mycorrhizal fungi mitigate negative effects of combined drought and heat stress on tomato plants. *Plant Physiol. Biochem.* 132, 297–307. doi: 10.1016/j.plaphy.2018.09.011

Dumack, K., and Bonkowski, M. (2021). "Protists in the plant microbiome: an untapped field of research," in *The Plant Microbiome*, eds L. C. Carvalhais and P. G. Dennis (Cham: Springer), 77–84. doi: 10.1007/978-1-0716-1040-4_8

Duval, S., and Tweedie, R. (2000). Trim and fill: a simple funnel-plot–based method of testing and adjusting for publication bias in meta-analysis. *Biometrics* 56, 455–463. doi: 10.1111/j.0006-341x.2000.00455.x

Eerens, J. P. J., Lucas, R. J., Easton, S., and White, J. G. H. (1998). Influence of the endophyte (*Neotyphodium lolii*) on morphology, physiology, and alkaloid synthesis of perennial ryegrass during high temperature and water stress. *N. Zeal. J. Agric. Res.* 41, 219–226. doi: 10.1080/00288233.1998.9513305

Egger, M., Smith, G. D., Schneider, M., and Minder, C. (1997). Bias in meta-analysis detected by a simple, graphical test. Increase in studies of publication bias coincided with increasing use of meta-analysis. *Br. Med. J.* 316, 629–634.

Faraone, S. V. (2008). Interpreting estimates of treatment effects: implications for managed care. *Pharm. Ther.* 33:700.

Field, A. P., and Gillett, R. (2010). How to do a meta-analysis. *Br. J. Math. Stat. Psychol.* 63, 665–694.

Gao, Z., Karlsson, I., Geisen, S., Kowalchuk, G., and Jousset, A. (2019). Protists: puppet masters of the rhizosphere microbiome. *Trends Plant Sci.* 24, 165–176. doi: 10.1016/j.tplants.2018.10.011

Garg, N., and Manchanda, G. (2009). ROS generation in plants: boon or bane? *Plant Biosyst.* 143, 81–96.

Gill, S. S., and Tuteja, N. (2010). Reactive oxygen species and antioxidant machinery in abiotic stress tolerance in crop plants. *Plant Physiol. Biochem.* 48, 909–930. doi: 10.1016/j.plaphy.2010.08.016

Giri, J. (2011). Glycinebetaine and abiotic stress tolerance in plants. *Plant Signal. Behav.* 6, 1746–1751.

Goh, C.-H., Vallejos, D. F. V., Nicotra, A. B., and Mathesius, U. (2013). The impact of beneficial plant-associated microbes on plant phenotypic plasticity. *J. Chem. Ecol.* 39, 826–839. doi: 10.1007/s10886-013-0326-8

González-Teuber, M. (2016). The defensive role of foliar endophytic fungi for a South American tree. *AoB Plants* 8:lw050. doi: 10.1093/aobpla/plw050

Gupta, N., Agarwal, S., Agarwal, V., Nathawat, N., Gupta, S., and Singh, G. (2013). Effect of short-term heat stress on growth, physiology and antioxidative defence system in wheat seedlings. *Acta Physiol. Plant.* 35, 1837–1842.

Gurevitch, J., and Hedges, L. (1999). Statistical issues in ecological metaanalyses. *Ecology* 80, 1142–1149. doi: 10.1890/0012-9658(1999)080[1142:siiema]2.0.co;2

Halliwell, B. (2006). Reactive species and antioxidants. Redox biology is a fundamental theme of aerobic life. *Plant Physiol.* 141, 312–322. doi: 10.1104/pp.106.077073

Hardoim, P. R., Van Overbeek, L. S., Berg, G., Pirttilä, A. M., Compant, S., Campisano, A., et al. (2015). The hidden world within plants: ecological and evolutionary considerations for defining functioning of microbial endophytes. *Microbiol. Mol. Biol. Rev.* 79, 293–320. doi: 10.1128/MMBR.00050-14

Hare, P. D., Cress, W. A., and Van Staden, J. (1998). Dissecting the roles of osmolyte accumulation during stress. *Plant Cell Environ.* 21, 535–553. doi: 10.1046/j.1365-3040.1998.00309.x

Harman, G. E. (2000). Myths and dogmas of biocontrol. Changes in perceptions derived from research on *Trichoderma harzianum* T-22. *Plant Dis.* 84, 377–393. doi: 10.1094/PDIS.2000.84.4.377

Harman, G. E., Howell, C. R., Viterbo, A., Chet, I., and Lorito, M. (2004). Trichoderma species – opportunistic, avirulent plant symbionts. *Nat. Rev. Microbiol.* 2, 43–56. doi: 10.1038/nrmicro797

Harman, G. E., and Uphoff, N. (2019). Symbiotic root-endophytic soil microbes improve crop productivity and provide environmental benefits. *Scientifica* 2019:9106395. doi: 10.1155/2019/9106395

Harsh, A., Sharma, Y., Joshi, U., Rampuria, S., Singh, G., Kumar, S., et al. (2016). Effect of short-term heat stress on total sugars, proline and some antioxidant enzymes in moth bean (*Vigna aconitifolia*). *Ann. Agric. Sci.* 61, 57–64. doi: 10.1016/j.aoas.2016.02.001

Hasanuzzaman, M., Nahar, K., Alam, M., Roychowdhury, R., and Fujita, M. (2013). Physiological, biochemical, and molecular mechanisms of heat stress tolerance in plants. *Int. J. Mol. Sci.* 14, 9643–9684. doi: 10.3390/ijms14059643

Hassan, M. U., Chattha, M. U., Khan, I., Chattha, M. B., Barbanti, L., Aamer, M., et al. (2021). Heat stress in cultivated plants: nature, impact, mechanisms, and mitigation strategies—A review. *Plant Biosyst. Int. J. Deal. Aspects Plant Biol.* 155, 211–234. doi: 10.1080/11263504.2020.1727987

Havaux, M. (1998). Carotenoids as membrane stabilizers in chloroplasts. *Trends Plant Sci.* 3, 147–151. doi: 10.1016/s1360-1385(98)01200-x

Hedges, L. V., Gurevitch, J., and Curtis, P. S. (1999). The meta-analysis of response ratios in experimental ecology. *Ecology* 80, 1150–1156.

Hemantaranjan, A., Bhanu, A. N., Singh, M., Yadav, D., Patel, P., Singh, R., et al. (2014). Heat stress responses and thermotolerance. *Adv. Plants Agric. Res.* 1, 1–10.

Hennessy, L. M., Popay, A. J., Finch, S. C., Clearwater, M. J., and Cave, V. M. (2016). Temperature and plant genotype alter alkaloid concentrations in ryegrass infected with an Epichloë endophyte and this affects an insect herbivore. *Front. Plant Sci.* 7:1097. doi: 10.3389/fpls.2016.01097

Hernandez, J. A., Jiménez, A., Mullineaux, P., and Sevilia, F. (2000). Tolerance of pea (*Pisum sativum* L.) to long-term salt stress is associated with induction of antioxidant defences. *Plant Cell Environ.* 23, 853–862.

Higgins, J. P., Thompson, S. G., Deeks, J. J., and Altman, D. G. (2003). Measuring inconsistency in meta-analyses. *Br. Med. J.* 327, 557–560. doi: 10.1136/bmj.327.7414.557

Higgins, J. P. T., and Thompson, S. G. (2002). Quantifying heterogeneity in a meta-analysis. *Stat. Med.* 21, 1539–1558. doi: 10.1002/sim.1186

Hill, P. W., Broughton, R., Bougoure, J., Havelange, W., Newsham, K. K., Grant, H., et al. (2019). Angiosperm symbioses with non-mycorrhizal fungal partners enhance N acquisition from ancient organic matter in a warming maritime Antarctic. *Ecol. Lett.* 22, 2111–2119. doi: 10.1111/ele.13399

Hoeksema, J. D., Chaudhary, V. B., Gehring, C. A., Johnson, N. C., Karst, J., Koide, R. T., et al. (2010). A meta-analysis of context-dependency in plant response to inoculation with mycorrhizal fungi. *Ecol. Lett.* 13, 394–407. doi: 10.1111/j.1461-0248.2009.01430.x

Holmgren, M., Gómez-Aparicio, L., Quero, J. L., and Valladares, F. (2012). Non-linear effects of drought under shade-reconciling physiological and ecological models in plant communities. *Oecologia* 169, 293–305. doi: 10.1007/s00442-011-2196-5

Huang, H., Ullah, F., Zhou, D.-X., Yi, M., and Zhao, Y. (2019). Mechanisms of ROS regulation of plant development and stress responses. *Front. Plant Sci.* 10:800. doi: 10.3389/fpls.2019.00800

Hubbard, M., Germida, J., and Vujanovic, V. (2012). Fungal endophytes improve wheat seed germination under heat and drought stress. *Bot. Botanique* 90, 137–149. doi: 10.1139/B11-091

Hubbard, M., Germida, J. J., and Vujanovic, V. (2014). Fungal endophytes enhance wheat heat and drought tolerance in terms of grain yield and second-generation seed viability. *J. Appl. Microbiol.* 116, 109–122. doi: 10.1111/jam.12311

Huedo-Medina, T. B., Sánchez-Meca, J., Marín-Martínez, F., and Botella, J. (2006). Assessing heterogeneity in meta-analysis: Q statistic or I2 index? *Psychol. Methods* 11, 193–206. doi: 10.1037/1082-989X.11.2.193

IPCC (2019). *An IPCC Special Report on the Impacts of Global Warming of 1.5° C above Pre-Industrial Levels and Related Global Greenhouse Gas Emission Pathways*. Geneva: IPCC.

Iqbal, N., Fatma, M., Khan, N. A., and Umar, S. (2019). "Regulatory role of proline in heat stress tolerance: modulation by salicylic acid," in *Plant Signaling Molecules*, eds M. I. Khan, P. Sudhakar Reddy, A. Ferrante, and N. A. Khan (Amsterdam: Elsevier), 437–448.

Iqbal, N., Khan, N. A., Ferrante, A., Trivellini, A., Francini, A., and Khan, M. (2017). Ethylene role in plant growth, development and senescence: interaction with other phytohormones. *Front. Plant Sci.* 8:475. doi: 10.3389/fpls.2017.00475

Ismail, I., Hamayun, M., Hussain, A., Afzal Khan, S., Iqbal, A., and Lee, I.-J. (2019). *Aspergillus flavus* promoted the growth of soybean and sunflower seedlings at elevated temperature. *BioMed Res. Int.* 2019:1295457. doi: 10.1155/2019/1295457

Ismail, I., Hamayun, M., Hussain, A., Iqbal, A., Khan, S. A., and Lee, I. J. (2018). Endophytic fungus aspergillus japonicus mediates host plant growth under normal and heat stress conditions. *Biomed Res. Int.* 2018:7696831. doi: 10.1155/2018/7696831

Ismail, I., Hamayun, M., Hussain, A., Iqbal, A., Khan, S. A., and Lee, I.-J. (2020a). *Aspergillus niger* boosted heat stress tolerance in sunflower and soybean via regulating their metabolic and antioxidant system. *J. Plant Interact.* 15, 223–232.

Ismail, I., Hamayun, M., Hussain, A., Khan, S. A., Iqbal, A., and Lee, I. J. (2020b). An endophytic fungus *Aspergillus violaceofuscus* can be used as heat stress adaptive tool for *Glycine max* L. and *Helianthus annuus* L. *J. Appl. Bot. Food Qual.* 93, 112–125. doi: 10.5073/Jabfq.2020.093.014

Ismail, I., Hussain, A., Mehmood, A., Qadir, M., Husna, H., Iqbal, A., et al. (2020c). Thermal stress alleviating potential of endophytic fungus rhizopus oryzae inoculated to sunflower (*Helianthus annuus* L.) and Soybean (*Glycine max* L.). *Pak. J. Bot.* 52, 1857–1865. doi: 10.30848/Pjb2020-5(10)

Issa, A., Esmaeel, Q., Sanchez, L., Courteaux, B., Guise, J.-F., Gibon, Y., et al. (2018). Impacts of *Paraburkholderia phytofirmans* strain PsJN on tomato (*Lycopersicon esculentum* L.) under high temperature. *Front. Plant Sci.* 9:1397. doi: 10.3389/fpls.2018.01397

Jagadish, S. K., Way, D. A., and Sharkey, T. D. (2021). Plant heat stress: concepts directing future research. *Plant Cell Environ.* 44, 1992–2005. doi: 10.1111/pce.14050

Kaur, G., and Asthir, B. (2015). Proline: a key player in plant abiotic stress tolerance. *Biol. Plant.* 59, 609–619.

Kawano, T., Sahashi, N., Takahashi, K., Uozumi, N., and Muto, S. (1998). Salicylic acid induces extracellular superoxide generation followed by an increase in cytosolic calcium ion in tobacco suspension culture: the earliest events in salicylic acid signal transduction. *Plant Cell Physiol.* 39, 721–730.

Khan, A. L., Hamayun, M., Radhakrishnan, R., Waqas, M., Kang, S.-M., Kim, Y.-H., et al. (2012a). Mutualistic association of *Paecilomyces formosus* LHL10 offers thermotolerance to *Cucumis sativus*. *Antonie van Leeuwenhoek* 101, 267–279. doi: 10.1007/s10482-011-9630-x

Khan, A. L., Hamayun, M., Waqas, M., Kang, S. M., Kim, Y. H., Kim, D. H., et al. (2012b). Exophiala sp.LHL08 association gives heat stress tolerance by avoiding oxidative damage to cucumber plants. *Biol. Fertil. Soils* 48, 519–529. doi: 10.1007/s00374-011-0649-y

Khan, A. L., Kang, S. M., Dhakal, K. H., Hussain, J., Adnan, M., Kim, J. G., et al. (2013). Flavonoids and amino acid regulation in Capsicum annuum L. by endophytic fungi under different heat stress regimes. *Sci. Hortic.* 155, 1–7. doi: 10.1016/j.scienta.2013.02.028

Khan, A. L., Waqas, M., and Lee, I.-J. (2015). Resilience of *Penicillium resedanum* LK6 and exogenous gibberellin in improving *Capsicum annuum* growth under abiotic stresses. *J. Plant Res.* 128, 259–268. doi: 10.1007/s10265-014-0688-1

Khan, M. A., Asaf, S., Khan, A. L., Jan, R., Kang, S.-M., Kim, K.-M., et al. (2020a). Extending thermotolerance to tomato seedlings by inoculation with SA1 isolate of *Bacillus cereus* and comparison with exogenous humic acid application. *PLoS One* 15:e0232228. doi: 10.1371/journal.pone.0232228

Khan, M. A., Asaf, S., Khan, A. L., Jan, R., Kang, S. M., Kim, K. M., et al. (2020b). Thermotolerance effect of plant growth-promoting *Bacillus cereus* SA1 on soybean during heat stress. *BMC Microbiol.* 20:175. doi: 10.1186/s12866-020-01822-7

Khan, M. I. R., Fatma, M., Per, T. S., Anjum, N. A., and Khan, N. A. (2015). Salicylic acid-induced abiotic stress tolerance and underlying mechanisms in plants. *Front. Plant Sci.* 6:462. doi: 10.3389/fpls.2015.00462

Kiers, E. T., Palmer, T. M., Ives, A. R., Bruno, J. F., and Bronstein, J. L. (2010). Mutualisms in a changing world: an evolutionary perspective. *Ecol. Lett.* 13, 1459–1474. doi: 10.1111/j.1461-0248.2010.01538.x

Kinnersley, A. M., and Turano, F. J. (2000). Gamma aminobutyric acid (GABA) and plant responses to stress. *Crit. Rev. Plant Sci.* 19, 479–509.

Knight, H., and Knight, M. R. (2001). Abiotic stress signalling pathways: specificity and cross-talk. *Trends Plant Sci.* 6, 262–267. doi: 10.1016/s1360-1385(01)01946-x

Kumar, A., Singh, S., Gaurav, A. K., Srivastava, S., and Verma, J. P. (2020). Plant growth-promoting bacteria: biological tools for the mitigation of salinity stress in plants. *Front. Microbiol.* 11:1216. doi: 10.3389/fmicb.2020.01216

Kumar, A., and Verma, J. P. (2018). Does plant—microbe interaction confer stress tolerance in plants: a review? *Microbiol. Res.* 207, 41–52. doi: 10.1016/j.micres.2017.11.004

Kuppardt, A., Fester, T., Härtig, C., and Chatzinotas, A. (2018). Rhizosphere protists change metabolite profiles in *Zea mays*. *Front. Microbiol.* 9:857. doi: 10.3389/fmicb.2018.00857

Kuźniak, E., Kopczewski, T., and Chojak-Koźniewska, J. (2017). "Ascorbate-glutathione cycle and biotic stress tolerance in plants," in *Ascorbic Acid in Plant Growth, Development and Stress Tolerance*, eds M. A. Hossain, S. Munné-Bosch, D. J. Burritt, P. Diaz-Vivancos, M. Fujita, and A. L. Springer (Berlin: Springer), 201–231.

Lajeunesse, M. J., and Forbes, M. R. (2003). Variable reporting and quantitative reviews: acomparison of three meta-analytical techniques. *Ecol. Lett.* 6, 448–454. doi: 10.1046/j.1461-0248.2003.00448.x

Lämke, J., Brzezinka, K., Altmann, S., and Bäurle, I. (2016). A hit-and-run heat shock factor governs sustained histone methylation and transcriptional stress memory. *EMBO J.* 35, 162–175. doi: 10.15252/embj.201592593

Larkindale, J., and Huang, B. (2005). Effects of abscisic acid, salicylic acid, ethylene and hydrogen peroxide in thermotolerance and recovery for creeping bentgrass. *Plant Growth Regul.* 47, 17–28.

Larkindale, J., and Knight, M. R. (2002). Protection against heat stress-induced oxidative damage in *Arabidopsis* involves calcium, abscisic acid, ethylene, and salicylic acid. *Plant Physiol.* 128, 682–695. doi: 10.1104/pp.010320

Lee, S.-M., and Ryu, C.-M. (2021). Algae as new kids in the beneficial plant microbiome. *Front. Plant Sci.* 12:91. doi: 10.3389/fpls.2021.599742

Li, N., Euring, D., Cha, J. Y., Lin, Z., Lu, M., Huang, L.-J., et al. (2021). Plant hormone-mediated regulation of heat tolerance in response to global climate change. *Front. Plant Sci.* 11:627969. doi: 10.3389/fpls.2020.627969

Li, X., Zhao, C., Zhang, T., Wang, G., Amombo, E., Xie, Y., et al. (2021). Exogenous *Aspergillus aculeatus* enhances drought and heat tolerance of perennial ryegrass. *Front. Microbiol.* 12:593722. doi: 10.3389/fmicb.2021.593722

Ling, Y., Serrano, N., Gao, G., Atia, M., Mokhtar, M., Woo, Y. H., et al. (2018). Thermopriming triggers splicing memory in *Arabidopsis*. *J. Exp. Bot.* 69, 2659–2675. doi: 10.1093/jxb/ery062

Liu, H. C., Lämke, J., Lin, S. Y., Hung, M. J., Liu, K. M., Charng, Y. Y., et al. (2018). Distinct heat shock factors and chromatin modifications mediate the organ-autonomous transcriptional memory of heat stress. *Plant J.* 95, 401–413. doi: 10.1111/tpj.13958

Liu, X., and Hou, X. (2018). Antagonistic regulation of ABA and GA in metabolism and signaling pathways. *Front. Plant Sci.* 9:251. doi: 10.3389/fpls.2018.00251

Lorenzo, O., Chico, J. M., Saénchez-Serrano, J. J., and Solano, R. (2004). JASMONATE-INSENSITIVE1 encodes a MYC transcription factor essential to discriminate between different jasmonate-regulated defense responses in *Arabidopsis*. *Plant Cell* 16, 1938–1950. doi: 10.1105/tpc.022319

Maestri, E., Klueva, N., Perrotta, C., Gulli, M., Nguyen, H. T., and Marmiroli, N. (2002). Molecular genetics of heat tolerance and heat shock proteins in cereals. *Plant Mol. Biol.* 48, 667–681. doi: 10.1023/a:1014826730024

Malinowski, D. P., and Belesky, D. P. (2000). Adaptation of endophyte-infected cool-season grasses to environmental stresses: mechanisms of drought and mineral stress tolerance. *Crop Sci.* 40, 923–940. doi: 10.2135/cropsci2000.404923x

Marquez, L. M., Redman, R. S., Rodriguez, R. J., and Roossinck, M. J. (2007). A virus in a fungus in a plant: three-way symbiosis required for thermal tolerance. *Science* 315, 513–515. doi: 10.1126/science.1136237

Martin, C. A., and Stutz, J. C. (2004). Interactive effects of temperature and arbuscular mycorrhizal fungi on growth, P uptake and root respiration of *Capsicum annuum* L. *Mycorrhiza* 14, 241–244. doi: 10.1007/s00572-003-0261-6

Mathur, S., and Jajoo, A. (2020). Arbuscular mycorrhizal fungi protects maize plants from high temperature stress by regulating photosystem II heterogeneity. *Ind. Crops Product.* 143:111934. doi: 10.1016/j.indcrop.2019.111934

Maya, M. A., and Matsubara, Y. (2013). Influence of arbuscular mycorrhiza on the growth and antioxidative activity in cyclamen under heat stress. *Mycorrhiza* 23, 381–390. doi: 10.1007/s00572-013-0477-z

Mayerhofer, M. S., Kernaghan, G., and Harper, K. A. (2013). The effects of fungal root endophytes on plant growth. *Mycorrhiza* 23, 199–128.

McGrath, J. M., and Lobell, D. B. (2013). Reduction of transpiration and altered nutrient allocation contribute to nutrient decline of crops grown in elevated CO2 concentrations. *Plant Cell Environ.* 36, 697–705. doi: 10.1111/pce.12007

Meena, K. K., Sorty, A. M., Bitla, U. M., Choudhary, K., Gupta, P., Pareek, A., et al. (2017). Abiotic stress responses and microbe-mediated mitigation in plants: the omics strategies. *Front. Plant Sci.* 8:172. doi: 10.3389/fpls.2017.00172

Mittler, R., Vanderauwera, S., Gollery, M., and Van Breusegem, F. (2004). Reactive oxygen gene network of plants. *Trends Plant Sci.* 9, 490–498. doi: 10.1016/j.tplants.2004.08.009

Mohi-Ud-Din, M., Siddiqui, M., Rohman, M., Jagadish, S., Ahmed, J. U., Hassan, M. M., et al. (2021). Physiological and biochemical dissection reveals a trade-off between antioxidant capacity and heat tolerance in bread wheat (*Triticum aestivum* L.). *Antioxidants* 10:351. doi: 10.3390/antiox10030351

Molina-Montenegro, M. A., Oses, R., Torres-Díaz, C., Atala, C., Zurita-Silva, A., and Ruiz-Lara, S. (2016). Root-endophytes improve the ecophysiological performance and production of an agricultural species under drought condition. *AoB Plants* 8:lw062. doi: 10.1093/aobpla/plw062

Mukhtar, T., Rehman, S. U., Smith, D., Sultan, T., Seleiman, M. F., Alsadon, A. A., et al. (2020). Mitigation of heat stress in *Solanum lycopersicum* L. by ACC-deaminase and exopolysaccharide producing *Bacillus cereus*: effects on biochemical profiling. *Sustainability* 12:2159. doi: 10.3390/su12062159

Naamala, J., and Smith, D. L. (2021). Microbial derived compounds, a step toward enhancing microbial inoculants technology for sustainable agriculture. *Front. Microbiol.* 12:634807. doi: 10.3389/fmicb.2021.634807

Nakamoto, H., and Vigh, L. (2007). The small heat shock proteins and their clients. *Cell. Mol. Life Sci.* 64, 294–306. doi: 10.1007/s00018-006-6321-2

Noctor, G., Mhamdi, A., and Foyer, C. H. (2014). The roles of reactive oxygen metabolism in drought: not so cut and dried. *Plant Physiol.* 164, 1636–1648. doi: 10.1104/pp.113.233478

Pareek, A., Singla, S. L., and Grover, A. (1998). Proteins alterations associated with salinity, desiccation, high and low temperature stresses and abscisic acid application in seedlings of Pusa 169, a high-yielding rice (*Oryza sativa* L.) cultivar. *Curr. Sci.* 75, 1023–1035.

Porras-Alfaro, A., and Bayman, P. (2011). Hidden fungi, emergent properties: endophytes and microbiomes. *Annu. Rev. Phytopathol.* 49, 291–315. doi: 10.1146/annurev-phyto-080508-081831

Quan, L. J., Zhang, B., Shi, W. W., and Li, H. Y. (2008). Hydrogen peroxide in plants: a versatile molecule of the reactive oxygen species network. *J. Integr. Plant Biol.* 50, 2–18. doi: 10.1111/j.1744-7909.2007.00599.x

Queitsch, C., Hong, S.-W., Vierling, E., and Lindquist, S. (2000). Heat shock protein 101 plays a crucial role in thermotolerance in *Arabidopsis*. *Plant Cell* 12, 479–492. doi: 10.1105/tpc.12.4.479

R Core Team (2021). *R: A Language and Environment for Statistical Computing*. Vienna: R Foundation for Statistical Computing.

Rho, H., Hsieh, M., Kandel, S. L., Cantillo, J., Doty, S. L., and Kim, S.-H. (2018). Do endophytes promote growth of host plants under stress? A meta-analysis on plant stress mitigation by endophytes. *Microb. Ecol.* 75, 407–418. doi: 10.1007/s00248-017-1054-3

Rivero, R. M., Ruiz, J. M., Garcıa, P. C., Lopez-Lefebre, L. R., Sánchez, E., and Romero, L. (2001). Resistance to cold and heat stress: accumulation of phenolic compounds in tomato and watermelon plants. *Plant Sci.* 160, 315–321. doi: 10.1016/s0168-9452(00)00395-2

Rizhsky, L., Liang, H., Shuman, J., Shulaev, V., Davletova, S., and Mittler, R. (2004). When defense pathways collide. The response of *Arabidopsis* to a combination of drought and heat stress. *Plant Physiol.* 134, 1683–1696. doi: 10.1104/pp.103.033431

Rodriguez, R., White, J. Jr., Arnold, A., and Redman, A. R. A. (2009). Fungal endophytes: diversity and functional roles. *New Phytol.* 182, 314–330. doi: 10.1111/j.1469-8137.2009.02773.x

Rohatgi, A. (2021). *Webplotdigitizer: Version 4.5*.

Roossinck, M. J. (2015). A new look at plant viruses and their potential beneficial roles in crops. *Mol. Plant Pathol.* 16:331. doi: 10.1111/mpp.12241

Rosenberg, M. S., Adams, D. C., and Gurevitch, J. (2000). *Metawin: Statistical Software for Meta-Analysis. Version 2*. Sunderland, MA: Sinauer Associates.

Sah, S. K., Reddy, K. R., and Li, J. (2016). Abscisic acid and abiotic stress tolerance in crop plants. *Front. Plant Sci.* 7:571. doi: 10.3389/fpls.2016.00571

Saidi, Y., Finka, A., and Goloubinoff, P. (2011). Heat perception and signalling in plants: a tortuous path to thermotolerance. *New Phytol.* 190, 556–565. doi: 10.1111/j.1469-8137.2010.03571.x

Sairam, R., and Tyagi, A. (2004). Physiology and molecular biology of salinity stress tolerance in plants. *Curr. Sci.* 86, 407–421.

Sakamoto, A., and Murata, N. (2002). The role of glycine betaine in the protection of plants from stress: clues from transgenic plants. *Plant Cell Environ.* 25, 163–171. doi: 10.1046/j.0016-8025.2001.00790.x

Sanders, D., Brownlee, C., and Harper, J. F. (1999). Communicating with calcium. *Plant Cell* 11, 691–706. doi: 10.2307/3870893

Sangamesh, M., Jambagi, S., Vasanthakumari, M., Shetty, N. J., Kolte, H., Ravikanth, G., et al. (2018). Thermotolerance of fungal endophytes isolated from plants adapted to the Thar Desert, India. *Symbiosis* 75, 135–147. doi: 10.1007/s13199-017-0527-y

Sarkar, J., Chakraborty, B., and Chakraborty, U. (2018). Plant growth promoting rhizobacteria protect wheat plants against temperature stress through antioxidant signalling and reducing chloroplast and membrane injury. *J. Plant Growth Regul.* 37, 1396–1412. doi: 10.1007/s00344-018-9789-8

Sato, S., Kamiyama, M., Iwata, T., Makita, N., Furukawa, H., and Ikeda, H. (2006). Moderate increase of mean daily temperature adversely affects fruit set of *Lycopersicon esculentum* by disrupting specific physiological processes in male reproductive development. *Ann. Bot.* 97, 731–738. doi: 10.1093/aob/mcl037

Sedaghatmehr, M., Mueller-Roeber, B., and Balazadeh, S. (2016). The plastid metalloprotease FtsH6 and small heat shock protein HSP21 jointly regulate thermomemory in *Arabidopsis*. *Nat. Commun.* 7, 1–14. doi: 10.1038/ncomms12439

Seidler, A. L., Hunter, K. E., Cheyne, S., Ghersi, D., Berlin, J. A., and Askie, L. (2019). A guide to prospective meta-analysis. *BMJ* 367:l5342. doi: 10.1136/bmj.l5342

Sharkey, T. D. (2005). Effects of moderate heat stress on photosynthesis: importance of thylakoid reactions, rubisco deactivation, reactive oxygen species, and thermotolerance provided by isoprene. *Plant Cell Environ.* 28, 269–277. doi: 10.1111/j.1365-3040.2005.01324.x

Shekhawat, K., Sheikh, A., Mariappan, K., Jalal, R., and Hirt, H. (2020). *Enterobacter* sp. SA187 mediates plant thermotolerance by chromatin modification of heat stress genes. *bioRxiv* [Preprint]. doi: 10.1101/2020.01.16.908756

Shinozaki, K., and Yamaguchi-Shinozaki, K. (2007). Gene networks involved in drought stress response and tolerance. *J. Exp. Bot.* 58, 221–227. doi: 10.1093/jxb/erl164

Silvente, S., Sobolev, A. P., and Lara, M. (2012). Metabolite adjustments in drought tolerant and sensitive soybean genotypes in response to water stress. *PLoS One* 7:e38554. doi: 10.1371/journal.pone.0038554

Simonsohn, U., Nelson, L. D., and Simmons, J. P. (2014). P-curve: a key to the file-drawer. *J. Exp. Psychol. Gen.* 143:534. doi: 10.1037/a0033242

Szabados, L., and Savouré, A. (2010). Proline: a multifunctional amino acid. *Trends Plant Sci.* 15, 89–97. doi: 10.1016/j.tplants.2009.11.009

Teixeira, E. I., Fischer, G., Van Velthuizen, H., Walter, C., and Ewert, F. (2013). Global hot-spots of heat stress on agricultural crops due to climate change. *Agric. For. Meteorol.* 170, 206–215. doi: 10.1016/j.agrformet.2011.09.002

Tian, Z. P., Huang, B. R., and Belanger, F. C. (2015). Effects of epichloe festucae fungal endophyte infection on drought and heat stress responses of strong creeping red fescue. *J. Am. Soc. Hortic. Sci.* 140, 257–264. doi: 10.21273/Jashs.140.3.257

Tsukagoshi, H., Busch, W., and Benfey, P. N. (2010). Transcriptional regulation of ROS controls transition from proliferation to differentiation in the root. *Cell* 143, 606–616. doi: 10.1016/j.cell.2010.10.020

Turner, T. R., James, E. K., and Poole, P. S. (2013). The plant microbiome. *Genome Biol.* 14, 1–10. doi: 10.3390/microorganisms9010188

Ullah, A., Bano, A., and Janjua, H. T. (2020). "Microbial secondary metabolites and defense of plant stress," in *Microbial Services in Restoration Ecology*, eds J. Shankar Singh and S. R. Vimal (Amsterdam: Elsevier), 37–46. doi: 10.1016/b978-0-12-819978-7.00003-8

Velikova, V., Edreva, A., and Loreto, F. (2004). Endogenous isoprene protects *Phragmites australis* leaves against singlet oxygen. *Physiol. Plant.* 122, 219–225. doi: 10.1111/j.0031-9317.2004.00392.x

Veresoglou, S. D., Menexes, G., and Rillig, M. C. (2012). Do arbuscular mycorrhizal fungi affect the allometric partition of host plant biomass to shoots and roots? A meta-analysis of studies from1990 to 2010. *Mycorrhiza* 22, 227–235. doi: 10.1007/s00572-011-0398-7

Verma, V., Ravindran, P., and Kumar, P. P. (2016). Plant hormone-mediated regulation of stress responses. *BMC Plant Biol.* 16:86. doi: 10.1186/s12870-016-0771-y

Veroniki, A. A., Jackson, D., Viechtbauer, W., Bender, R., Bowden, J., Knapp, G., et al. (2016). Methods to estimate the between-study variance and its uncertainty in meta-analysis. *Res. Synthesis Methods* 7, 55–79. doi: 10.1002/jrsm.1164

Wahid, A. (2007). Physiological implications of metabolite biosynthesis for net assimilation and heat-stress tolerance of sugarcane (*Saccharum officinarum*) sprouts. *J. Plant Res.* 120, 219–228. doi: 10.1007/s10265-006-0040-5

Wahid, A., and Close, T. (2007). Expression of dehydrins under heat stress and their relationship with water relations of sugarcane leaves. *Biol. Plant.* 51, 104–109. doi: 10.1007/s10535-007-0021-0

Wahid, A., Gelani, S., Ashraf, M., and Foolad, M. R. (2007). Heat tolerance in plants: an overview. *Environ. Exp. Bot.* 61, 199–223. doi: 10.1016/j.envexpbot.2007.05.011

Wäli, P., Helander, M., Nissinen, O., Lehtonen, P., and Saikkonen, K. (2008). Endophyte infection, nutrient status of the soil and duration of snow cover influence the performance of meadow fescue in sub-artic conditions. *Grass Forage Sci.* 63, 324–330. doi: 10.1111/j.1365-2494.2008.00639.x

Wang, G., Zhang, X., Li, F., Luo, Y., and Wang, W. (2010). Overaccumulation of glycine betaine enhances tolerance to drought and heat stress in wheat leaves in the protection of photosynthesis. *Photosynthetica* 48, 117–126.

Wang, K., Zhang, X., Goatley, M., and Ervin, E. (2014). Heat shock proteins in relation to heat stress tolerance of creeping bentgrass at different N levels. *PLoS One* 9:e102914. doi: 10.1371/journal.pone.0102914

Wang, L.-J., Fan, L., Loescher, W., Duan, W., Liu, G.-J., Cheng, J.-S., et al. (2010). Salicylic acid alleviates decreases in photosynthesis under heat stress and accelerates recovery in grapevine leaves. *BMC Plant Biol.* 10:34. doi: 10.1186/1471-2229-10-34

Wang, L.-J., and Li, S.-H. (2006). Salicylic acid-induced heat or cold tolerance in relation to Ca2+ homeostasis and antioxidant systems in young grape plants. *Plant Sci.* 170, 685–694.

Wani, A. B., Chadar, H., Wani, A. H., Singh, S., and Upadhyay, N. (2017). Salicylic acid to decrease plant stress. *Environ. Chem. Lett.* 15, 101–123.

Waqas, M., Khan, A. L., Kamran, M., Hamayun, M., Kang, S.-M., Kim, Y.-H., et al. (2012). Endophytic fungi produce gibberellins and indoleacetic acid and promotes host-plant growth during stress. *Molecules* 17, 10754–10773. doi: 10.3390/molecules170910754

Waqas, M., Khan, A. L., Shahzad, R., Ullah, I., Khan, A. R., and Lee, I. J. (2015). Mutualistic fungal endophytes produce phytohormones and organic acids that promote japonica rice plant growth under prolonged heat stress. *J. Zhejiang Univ. Sci. B* 16, 1011–1018. doi: 10.1631/jzus.B1500081

Xie, H.-T., Wan, Z.-Y., Li, S., and Zhang, Y. (2014). Spatiotemporal production of reactive oxygen species by NADPH oxidase is critical for tapetal programmed cell death and pollen development in *Arabidopsis*. *Plant Cell* 26, 2007–2023. doi: 10.1105/tpc.114.125427

Xu, Z.-S., Li, Z.-Y., Chen, Y., Chen, M., Li, L.-C., and Ma, Y.-Z. (2012). Heat shock protein 90 in plants: molecular mechanisms and roles in stress responses. *Int. J. Mol. Sci.* 13, 15706–15723. doi: 10.3390/ijms131215706

Yeasmin, R., Bonser, S. P., Motoki, S., and Nishihara, E. (2019). Arbuscular mycorrhiza influences growth and nutrient uptake of *Asparagus* (*Asparagus officinalis* L.) under heat stress. *Hortscience* 54, 846–850. doi: 10.21273/Hortsci13587-18

Yu, X., Pasternak, T., Eiblmeier, M., Ditengou, F., Kochersperger, P., Sun, J., et al. (2013). Plastid-localized glutathione reductase2–regulated glutathione redox status is essential for *Arabidopsis* root apical meristem maintenance. *Plant Cell* 25, 4451–4468. doi: 10.1105/tpc.113.117028

Zafra, A., Rodríguez-García, M. I., and de Dios Alché, J. (2010). Cellular localization of ROS and NO in olive reproductive tissues during flower development. *BMC Plant Biol.* 10:36. doi: 10.1186/1471-2229-10-36

Zaynab, M., Fatima, M., Abbas, S., Sharif, Y., Umair, M., Zafar, M. H., et al. (2018). Role of secondary metabolites in plant defense against pathogens. *Microb. Pathog.* 124, 198–202. doi: 10.1016/j.micpath.2018.08.034

Zhang, H. J., Zhang, N., Yang, R. C., Wang, L., Sun, Q. Q., Li, D. B., et al. (2014). Melatonin promotes seed germination under high salinity by regulating antioxidant systems, ABA and GA 4 interaction in cucumber (*Cucumis sativus* L.). *J. Pineal Res.* 57, 269–279. doi: 10.1111/jpi.12167

Zhao, J., Lu, Z., Wang, L., and Jin, B. (2021). Plant responses to heat stress: physiology, transcription, noncoding RNAs, and epigenetics. *Int. J. Mol. Sci.* 22:117. doi: 10.3390/ijms22010117

Zhou, L., He, H., Liu, R., Han, Q., Shou, H., and Liu, B. (2014). Overexpression of GmAKT2 potassium channel enhances resistance to soybean mosaic virus. *BMC Plant Biol.* 14:154. doi: 10.1186/1471-2229-14-154

Zhou, W.-N., White, J. F., Soares, M. A., Torres, M. S., Zhou, Z.-P., and Li, H.-Y. (2015). Diversity of fungi associated with plants growing in geothermal ecosystems and evaluation of their capacities to enhance thermotolerance of host plants. *J. Plant Interact.* 10, 305–314.

Zhu, X. C., Song, F. B., Liu, S. Q., and Liu, T. D. (2011). Effects of arbuscular mycorrhizal fungus on photosynthesis and water status of maize under high temperature stress. *Plant Soil* 346, 189–199. doi: 10.1007/s11104-011-0809-8

Conflict of Interest: The authors declare that the research was conducted in the absence of any commercial or financial relationships that could be construed as a potential conflict of interest.

Publisher's Note: All claims expressed in this article are solely those of the authors and do not necessarily represent those of their affiliated organizations, or those of the publisher, the editors and the reviewers. Any product that may be evaluated in this article, or claim that may be made by its manufacturer, is not guaranteed or endorsed by the publisher.

frontiers | Frontiers in Microbiology

ORIGINAL RESEARCH
published: 08 April 2022
doi: 10.3389/fmicb.2022.857160

Comparative Metabolomic Profiling of Compatible and Incompatible Interactions Between Potato and *Phytophthora infestans*

Jingyu Zhu[1†], Xue Tang[1†], Yining Sun[1], Yan Li[1], Yajie Wang[1], Yusong Jiang[3], Huanhuan Shao[1], Bin Yong[1], Honghao Li[2] and Xiang Tao[1]**

[1] College of Life Sciences, Sichuan Normal University, Chengdu, China, [2] Key Laboratory of Integrated Pest Management on Crops in Southwest, Institute of Plant Protection, Ministry of Agriculture, Sichuan Academy of Agricultural Sciences, Chengdu, China, [3] Research Institute for Special Plants, Chongqing University of Arts and Sciences, Chongqing, China

OPEN ACCESS

Edited by:
Marco Scortichini,
Council for Agricultural Research and Economics (CREA), Italy

Reviewed by:
Msizi Innocent Mhlongo,
University of Johannesburg, South Africa
Hyong Woo Choi,
Andong National University, South Korea

***Correspondence:**
Honghao Li
leehh071@126.com
Xiang Tao
taoxiang@sicnu.edu.cn

[†] These authors have contributed equally to this work

Specialty section:
This article was submitted to Microbe and Virus Interactions with Plants, a section of the journal Frontiers in Microbiology

Received: 18 January 2022
Accepted: 07 March 2022
Published: 08 April 2022

Citation:
Zhu J, Tang X, Sun Y, Li Y, Wang Y, Jiang Y, Shao H, Yong B, Li H and Tao X (2022) Comparative Metabolomic Profiling of Compatible and Incompatible Interactions Between Potato and Phytophthora infestans. Front. Microbiol. 13:857160. doi: 10.3389/fmicb.2022.857160

Late blight is one of the main biological stresses limiting the potato yield; however, the biochemical mechanisms underlying the infection process of *Phytophthora infestans* remain unrevealed. In this study, the late blight-resistant potato cultivar Ziyun No.1 (R) and the susceptible cultivar Favorita (S) were inoculated with *P. infestans*. Untargeted metabolomics was used to study the changes of metabolites in the compatible and incompatible interactions of the two cultivars and the pathogen at 0, 48, and 96 h postinoculation (hpi). A total of 819 metabolites were identified, and the metabolic differences mainly emerged after 48 hpi. There were 198 and 115 differentially expressed metabolites (DEMs) in the compatible and incompatible interactions. These included 147 and 100 upregulated metabolites during the compatible and incompatible interactions, respectively. Among them, 73 metabolites were identified as the *P. infestans*-responsive DEMs. Furthermore, the comparisons between the two cultivars identified 57 resistance-related metabolites. Resistant potato cultivar had higher levels of salicylic acid and several upstream phenylpropanoid biosynthesis metabolites, triterpenoids, and hydroxycinnamic acids and their derivatives, such as sakuranetin, ferulic acid, ganoderic acid Mi, lucidenic acid D2, and caffeoylmalic acid. These metabolites play crucial roles in cell wall thickening and have antibacterial and antifungal activities. This study reports the time-course metabolomic responses of potatoes to *P. infestans*. The findings reveal the responses involved in the compatible and incompatible interactions of potatoes and *P. infestans*.

Keywords: metabolomics, *Phytophthora infestans*, potato cultivars, compatible, incompatible

INTRODUCTION

Potato (*Solanum tuberosum*) ranks among the top four most important food crops worldwide and is the third most-produced crop after rice and wheat. China has been the biggest potato producer since the 17th century (Conghua, 2012). Potato late blight, caused by a hemibiotrophic oomycetes *Phytophthora infestans*, is the most devastating disease of potato (Rodenburg et al., 2019). *P. infestans* has a broad host range within the *Solanaceae* family, including potato, tomato, and tobacco (Lu et al., 2021). Zoospores are the main dispersal forms of *P. infestans*, which were released

from sporangia. Once zoospores reach the host surface, they germinate to produce germ tubes (Boevink et al., 2020). The germ tubes grow on the host surface, forming the appressorium-like swellings or penetrating the anticlinal walls using cell wall-degrading enzymes on locating a suitable host entry site (Kubicek et al., 2014; Boevink et al., 2020; Sabbadin et al., 2021). During biotrophic growth, haustoria are formed in cells contacted by the hyphae and then delivers Arg-X-Leu-Arg (RXLR) effectors into host cells to subvert plant immune responses and promote colonization (Boevink et al., 2020), which is a phenomenon that has contributed to the evolution of a more complex immune system in potatoes (Collinge and Boller, 2001; King et al., 2014; Zheng et al., 2014; Boevink et al., 2016; Yang et al., 2016). However, the prolonged "zigzag" evolution (Jones and Dangl, 2006) of the RXLR effectors, resulting in 563 RXLR effector genes in *P. infestans* (Haas et al., 2009), has enabled the pathogen to successfully infect the host plants (Birch et al., 2008; Raffaele et al., 2010). The disease led to the Irish famine in the mid-19th century, leaving one million people dead and forcing three million individuals to emigrate from Ireland (Ndala et al., 2019). Under favorable environmental conditions, *P. infestans* can destroy potato fields in less than a week (Fry, 2008), resulting in an annual economic loss of up to $6.7 billion, corresponding to about 15% of the total potato production (Tadesse et al., 2021). Applying chemical fungicides and breeding-resistant cultivars is the most effective method for preventing and controlling potato late blight. However, the fungicides and host-driven selective pressure cause the pathogen effector genes to mutate rapidly, allowing *P. infestans* to escape the host's defense and fungicide's killing effects (Yang et al., 2017). Besides, the excessive use of chemical fungicides can adversely affect human and environmental health (Peerzada et al., 2020).

Metabolomics is a cost-effective technology that allows for the qualitative and quantitative characterization of thousands of metabolites and has been widely used in the last 20 years in the fields of Biology, Agriculture, and Medicine in the last two decades (Arbona et al., 2013; Gao and Xu, 2014). The technology has also revealed that the response processes of plants to pathogens involve various metabolites (Shulaev et al., 2008; Cajka et al., 2014). Furthermore, the metabolomic responses of cereal crops to their important diseases have been well characterized. It has been found that the tolerance is due to the accumulation of resistance-related (RR) metabolites, including hydroxycinnamic acid amides (HCAAs), flavonoids, phenylpropanoids, fatty acids, terpenoid, and alkaloids (Chamarthi et al., 2013; Gunnaiah and Kushalappa, 2014; Azizi et al., 2019; Madhavan et al., 2019). These metabolic compounds can act both as physical barriers to biotic stresses and antagonists of invasive pathogens (Bellincampi et al., 2014). Host plants thicken their cell walls by producing large amounts of HCAAs, such as feruloyltyramine and feruloylputrescine, to prevent the spread of disease (Pushpa et al., 2014; Yogendra et al., 2014). Other chemical groups, such as benzylisoquinoline, flavonoid glycosides, and fatty acids, also play crucial roles in cell wall thickening (Morimoto et al., 2003; Franke et al., 2012; Gunnaiah et al., 2012), thus forming a physical barrier against *P. infestans* infection (Yogendra et al., 2015). Over the past two decades, significant efforts have also been undertaken to determine the metabolomic responses of potatoes to the pathogen. Abu-Nada et al. (2007) identified 42 significantly increased and reduced pathogenesis-related metabolites in potato leaves. Furthermore, it was demonstrated that phenylpropanoids, flavonoid, and alkaloid chemical groups were highly induced in resistant potato genotypes (AC04 and AC09) compared to the susceptible ones (Criolla Colombia) (Yogendra et al., 2015). In a study by Pushpa et al. (2014), HCAAs of the shunt phenylpropanoid pathway were highly induced following the pathogen inoculation of the F06037-resistant potato cultivars. Thus, remarkable progress in understanding potato metabolomic responses to potato late blight pathogen has been achieved; however, the time course of these metabolomic responses is still poorly understood.

This study used the non-targeted metabolomic techniques to characterize the time-course metabolomic responses of two potato cultivars (late blight-resistant cultivar Ziyun No.1 and susceptible cultivar Favorita) infected with *P. infestans*. This study gives a preliminary yet substantial insight into the possible molecular mechanisms of potatoes against potato late blight.

MATERIALS AND METHODS

Plant Materials and Growth Conditions

Virus-free seedlings of two potato cultivars [late blight-resistant cultivar Ziyun No.1 (R) and susceptible cultivar Favorita (S)] were cultured on 1 × MS medium for 28 days under a 16-h/8-h day/night photoperiod until the seedlings grew to 5–7 cm. Growth conditions included a light intensity of 2,000 lux, day/night temperature of 25°C/22°C, and relative humidity of 70%. Thereafter, the seedlings were transplanted into plastic pots (with a diameter of 7 cm and a height of 7.5 cm) containing TS1 fine matrix (Klasmann-Deilmann, Germany) and placed in a light incubator under the similar growth conditions described above.

Pathogen Infection and Sample Collection

The *P. infestans* (SCPZ16-3-1) used in this study was isolated from infected potato leaves without any genetic modification and stored them on the Rye agar medium until use. A 1 cm^2 fungus block was cut from the Rye agar medium and transferred under a sterilized potato chip and then cultured at 18°C in dark for 5 days. Later, the mycelia were collected into 5 ml of sterile water, homogenized, and filtered using a single-layer gauze to sporangia suspension. The suspension was then incubated at 7°C for 2–4 h to stimulate the release of zoospores whose concentration was adjusted to 5×10^4 zoospores per ml. After the virus-free seedlings grew to about 10 cm high, 60 plantlets with healthy growth vigor were selected and sprayed with zoospore suspension (50 ml). The plantlets were then placed in sealed boxes with moist tissue to maintain humidity and incubated in the dark for 12 h to reduce ultraviolet (UV) degradation of the inoculum. Subsequently, they were moved to a 16-h/8-h day/night photoperiod chamber with a light intensity of 2,000 lux, day/night temperature of 25°C/22°C, and relative humidity of 100%. All equipment, materials, and facilities used in this study

(including the cubicle greenhouse, pots, and steam-sterilized nutrient soil) were sterilized by UV irradiation or autoclaving before and after the experiment.

Leaf samples were collected at 0 h before inoculation (0 hbi) and at 48 and 96 h postinoculation (hpi) from both the cultivars, Ziyun No.1 (R) and Favorita (S), corresponding to six sample groups (R1, R2, and R3 for Ziyun No.1, and S1, S2, and S3 for Favorita). Each sample group consisted of six biological replicates, and each replicate contained at least ten leaves from three plants. The leaf samples were immediately snap-frozen in liquid nitrogen and then submitted to Shanghai Majorbio Biopharm Technology Co., Ltd., for the liquid chromatography-mass spectrometry (LC-MS) non-targeted metabolomic analysis.

Metabolite Extraction and Analysis

We weighed 50 mg of leaves for each sample replicate into a 2-ml microcentrifuge tubes containing a grinding bead (with a diameter of 6 mm) and added 400 μl of methanol: water (4:1, v/v) solution. In the solution, 2-chloro-L-phenylalanine (0.02 mg/ml) was added in advance to serve as an internal standard (IS). The mixture was treated with a high-throughput tissue crusher Wonbio-96c (Shanghai Wanbo Biotechnology Co., Ltd.) at a frequency of 50 Hz at −10°C for 6 min, followed by ultrasonication at a frequency of 40 kHz at 5°C for 30 min. The samples were subsequently incubated at −20°C for 30 min to precipitate proteins and centrifuged at a speed of 13,000 × *g* at 4°C for 15 min. The supernatant was then carefully transferred to sample vials for the subsequent analysis. Thereafter, 20 μl of the supernatant was collected from each sample and pooled together to serve as the quality control sample (QC). All metabolic extracts were then analyzed using LC coupled to hybrid mass spectrometers [LC-MS, ExionLC AD System, AB SCIEX; Ultra High-Performance Liquid Chromatography (UHPLC)-Triple TOF, AB SCIEX-Triple TOF 5600+].

The chromatographic separation of the metabolites was performed on a UHPLC-Triple TOF system equipped with an ACQUITY UPLC HSS T3 column (100 mm × 2.1 mm i.d., 1.8 μm) (Waters, Milford, CT, United States). Mobile phase A consists of 0.1% formic acid, 5% acetonitrile, and 95% water, whereas mobile phase B consists of 0.1% formic acid, 47.5% acetonitrile, 47.5% isopropanol, and 5% water. Additionally, the solvent gradient was set according to the following ratio ranges of solvent A and B for system equilibration from 0 to 16 min: (1) maintained at 100% (A): 0% (B) from 0 to 0.5 min, (2) 100% (A): 0% (B) to 75% (A): 25% (B) from 0.5 to 2.5 min, (3) 75% (A): 25% (B) to 0% (A): 100% (B) from 2.5 to 9 min, (4) maintained at 0% (A): 100% (B) from 9 to 13 min, (5) 0% (A): 100% (B) to 100% (A): 0% (B) from 13 to 13.1 min, and (6) maintained at 100% (A): 0% (B) from 13.1 to 16 min. The sample injection volume and the flow rate were 10 μl and 0.4 ml/min, respectively, and the column temperature was maintained at 40°C. All analytic experiments were performed at 4°C, and the mass spectrometric data were collected using a UHPLC-Triple TOF equipped with an electrospray ionization (ESI) source, operated in both positive and negative ionization mode. The mass spectrophotometer optimal conditions were set as follows: scan type, 50–1,000 *m/z*; ion source gas1, 50 psi; ion source gas2, 50 psi; curtain gas, 30 psi; source temperature, 550°C; IonSpray Voltage Floating (+), 5,000 V; IonSpray Voltage Floating (−), −4,000 V; interface heater, on; declustering potential, 80 V; collision energy, 40 ± 20 eV; cycle time, 510 ms.

Liquid Chromatography-Mass Spectrometry Data Processing and Annotation

The raw data, without any pretreatment, were imported into the Progenesis QI 2.3 (Non-linear Dynamics, Waters, United States) for peak detection and alignment using default parameters. The data matrix of the preprocessed results consisted of the retention time (RT), mass-to-charge ratio (m/z) values, and peak intensity. At least 80% of the metabolic features detected in any set of samples were retained. After filtering, the minimum metabolite values were imputed for specific samples with the metabolite levels below the lower quantitation limit, and each metabolic feature was normalized by summation. The IS was used for data quality control, and the metabolic features with the relative standard deviation (RSD) of QC > 30% were discarded. Following normalization and imputation processes, statistical analysis was performed on the log-transformed data to identify the significant differences in the metabolite levels between the comparable groups. Thereafter, the mass spectra of these metabolic features were identified using the accurate mass, MS/MS fragments spectra, and isotope ratio difference by searching through reliable biochemical databases, such as the Human Metabolome Database (HMDB)[1] and METLIN database[2]. For metabolites having MS/MS confirmation, only those with MS/MS fragments score above 30 were considered as confidently identified. The mass tolerance between the measured m/z values and the exact mass of the components of interest was ±10 ppm.

Data Statistical Analysis

A multivariate statistical analysis was performed on the free online platform of Majorbio Cloud Platform[3]. Partial Least Squares-Discriminant Analysis (PLS-DA) was used to determine the global metabolic changes between the comparable groups after the metabolite variables were subjected to Pareto Scaling, with a confidence level of 0.95. Variable importance in projection (VIP) was also calculated using the Orthogonal Projections to Latent Structures-Discriminant Analysis (OPLS-DA) model. Furthermore, *p*-values were estimated using the one-way paired *t*-test. A total of 5,945 and 5,644 peaks were selected for the electrospray ionized (ESI +) and non-electrospray ionized (ESI-) metabolites, respectively. Metabolites with the threshold of $|\log_2 \text{fold change (FC)}| > 1$, $p < 0.05$, and VIP value > 1 were considered differential and mapped to the KEGG pathway database through metabolic enrichment pathway analysis (KEGG[4]). These metabolites were then classified according to the KEGG annotation.

[1]http://www.hmdb.ca/

[2]https://metlin.scripps.edu/

[3]https://cloud.majorbio.com

[4]http://www.genome.jp/kegg/

RESULTS

Phenotypic Responses to *P. infestans*

Both the late blight-resistant potato cultivar Ziyun No.1 (R) and the susceptible cultivar Favorita (S) were inoculated with *P. infestans* isolate SCPZ16-3-1. At 48 hpi, small late blight lesions can be observed on the leaf surface of Favorita (**Figure 1A**) but are almost invisible for Ziyun No.1 (**Figure 1B**). The Favorita cultivar had its leaf margins curled, and more than 50% of leaf area was covered in late blight lesions, while Ziyun No.1 exhibited a few tiny hypersensitive response (HR) spots distributed on its leaf surface at 96 hpi. The two potato cultivars exhibited different disease-resistant phenotypes.

Global Metabolomic Responses to *P. infestans*

Leaf samples of Ziyun No.1 and Favorita were collected at 0 hbi and at 48 and 96 hpi to investigate the metabolomic responses during the interaction between the virus-free potato seedlings and *P. infestans*. The PLS-DA analyses of the six sample sets, including S1, S2, and S3 for Favorita and R1, R2, and R3 for Ziyun No. 1, showed that the sample groups clustered together during the incompatible interaction but dispersed relatively during the compatible interaction. The metabolites obtained from R and S samples differed, and the S3 samples showed relatively large distances to the others (**Figure 2A** and **Supplementary Figure 1**), consistent with the phenotypic responses. Pearson's correlation coefficient analysis showed that the biological replicates in each sample set exhibited strong correlations. Six replicates of the S1, S2, and S3 groups clustered into one group separately, unlike the R1, R2, and R3 groups. A relative similarity was observed among the R1, R2, and R3 samples, but S3 differed from S1 and S2, which exhibited relatively high correlations. Moreover, most of the Pearson's correlation coefficients between S3 and the other samples were lower than 0.5 (**Figure 2B** and **Supplementary Figure 1**). A total of 819 (364 from positive and 455 from negative models) metabolites corresponding to 5,945 and 5,644 peaks were identified from the six sample groups (**Supplementary Table 1**). These 819 metabolites were mainly distributed in the metabolism of lipids (30 metabolites), amino acid (30 metabolites), carbohydrate (25 metabolites), and in the ABC transporters (13 metabolites), purine metabolism (9 metabolites), Cyl-tRNA biosynthesis (8 metabolites), and phenylalanine metabolism (7 metabolites) pathways.

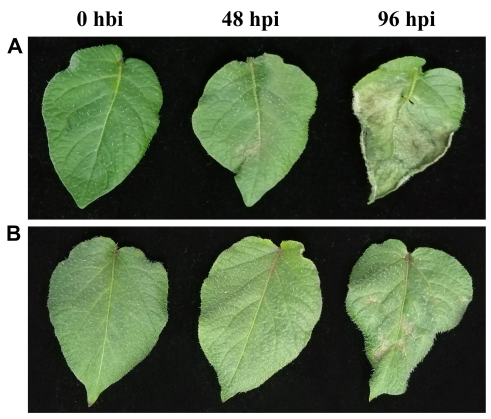

FIGURE 1 | Phenotypic changes of potato leaves at different time points of *Phytophthora infestans* infection. Virus-free seedlings of Favorita **(A)** and Ziyun No.1 **(B)** inoculated with *P. infestans* isolate SCPZ16-3-1 at 0 h before infection (hbi), 48 h postinoculation (hpi), and 96 hpi.

Time-Course Analyses of the Differentially Expressed Metabolites in Different Potato Cultivars

Differentially expressed metabolites (DEMs) were identified using the threshold of $|\log_2 FC| > 1$, $p < 0.05$, and VIP value > 1. A total of 198 DEMs, including 175, 155, and 26 DEMs, were identified from comparing S3vsS1, S3vsS2, and S2vsS1 of the susceptible cultivar Favorita, respectively (**Figure 3A** and **Supplementary Table 2A**). Moreover, 134 DEMs were shared by S3vsS1 and S3vsS2, whereas only seven DEMs (arginyl-phenylalanine, myricanene B 5-[arabinosyl-(1- > 6)-glucoside], 20-hydroxylipoxin A4, goshonoside F7, lubiprostone, sterol, and mahaleboside) were common across the three comparisons (S3vsS1, S3vsS2, and S2vsS1). The seven DEMs were annotated as sterol, mahaleboside, arginyl-phenylalanine, myricanene B 5-[arabinosyl-(1- > 6)-glucoside], 20-hydroxylipoxin A4, goshonoside F7, and lubiprostone. Among them, five DEMs were upregulated during the compatible interactions, while the other two (arginyl-phenylalanine and 20-hydroxylipoxin A4) were downregulated in the first 48 h but later upregulated after 48 h. Only two DEMs (prostaglandin F1a and *O*-phosphotyrosine) were identified between 0 and 48 hpi, while 13 were identified between 48 and 96 hpi. Metab_3648 was annotated as cascarillin, a diterpenoid, and had abundances of 1.400, 0.919, and 2.717 in S1, S2, and S3, respectively. Conversely, metab_4842 (tricosane) was annotated as an antimicrobial compound, with abundances of 1.250, 0.811, and 2.314 in S1, S2, and S3, respectively. Among the 198 DEMs, 147 were upregulated due to the infection with *P. infestans*, while only 40 were downregulated (**Figure 3D**).

Contrarily, 115 DEMs, including 100, 59, and 39 DEMs, were identified from the comparing R3vsR1, R3vsR2, and R2vsR1 of the resistant cultivar Ziyun No.1, respectively (**Figure 3B** and **Supplementary Table 2B**). The R3vsR1 and R3vsR2 shared 50 DEMs, whereas only six DEMs (zedoarondiol, lacto-*N*-triaose, 5′-carboxy-gamma-chromanol, 1-(Malonylamino)cyclopropanecarboxylic acid (MACC), 1,8-diazacyclotetradecane-2,9-dione, and *trans*-isoeugenol-*O*-glucuronide) were common across the three comparisons (R3vsR1, R3vsR2, and R2vsR1). Metab_14352 was annotated as zedoarondiol ($C_{15}H_{24}O_3$), a sesquiterpene lactone, and exhibited average abundances of 0.004, 0.306, and 1.476 in R1, R2, and R3, respectively. Additionally, metab_14855 was denoted lacto-N-triaose ($C_{20}H_{35}NO_{16}$) and had downregulated abundances of 1.447, 0.714, and 0.141 at 0, 48, and 96 hpi, respectively. Metab_15479 was annotated as MACC ($C_7H_9NO_5$), an ethylene biosynthesis compound (Hoffman et al., 1982). The compound

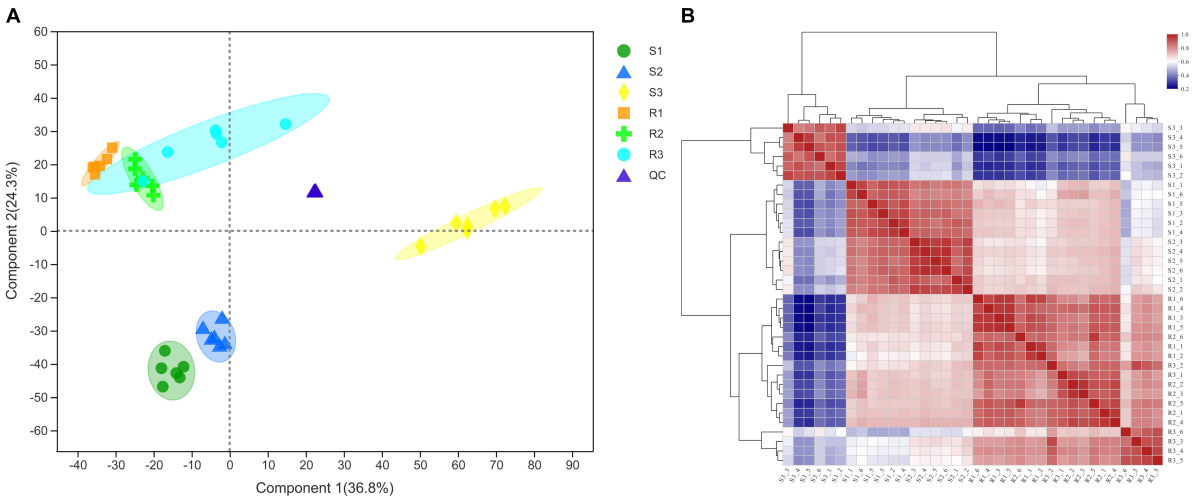

FIGURE 2 | Correlation analyses of the different samples collected from the compatible and incompatible interactions. **(A)** Sample correlation Partial Least Squares-Discriminant Analysis (PLS-DA) diagram. **(B)** Sample correlation heatmap. R1, R2, and R3 represent the samples collected at 0, 48, and 96 hpi, respectively, in incompatible interactions. S1, S2, and S3 denote the samples collected at 0, 48, and 96, respectively, in the compatible interactions. QC, quality control sample.

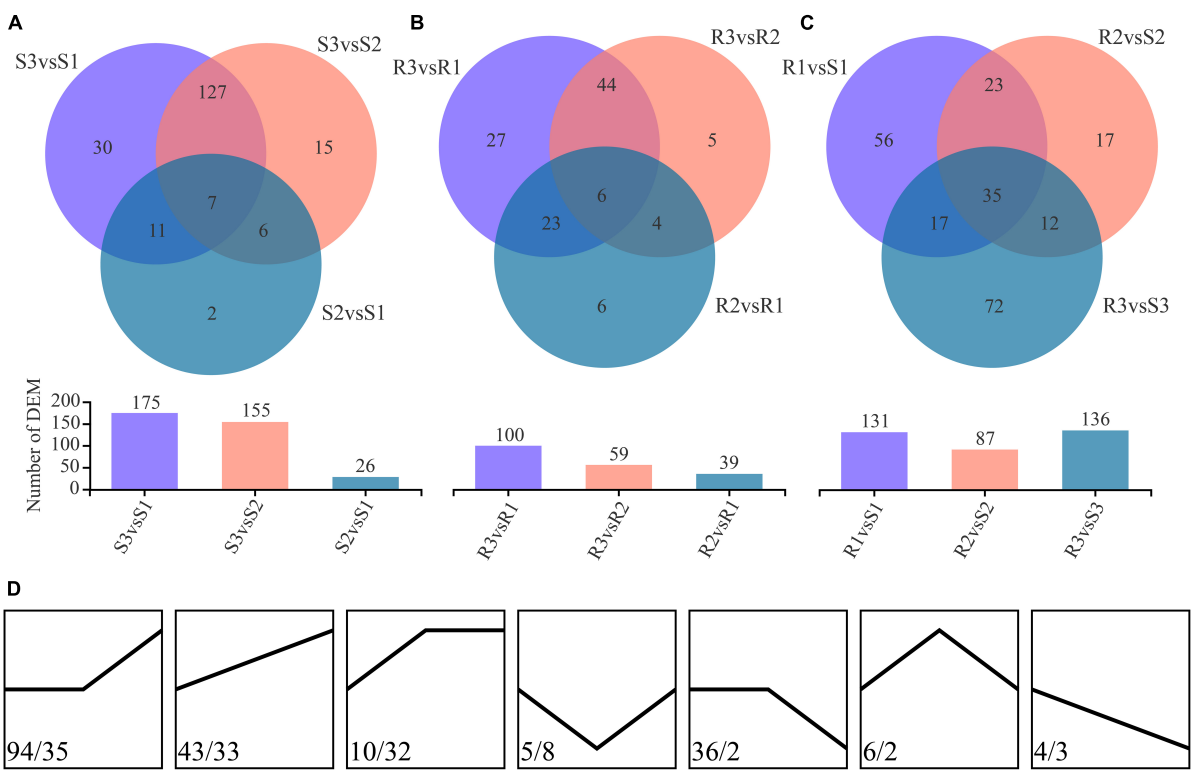

FIGURE 3 | Differentially expressed metabolites (DEMs) identified during the infection process. **(A)** DEMs identified during the compatible interactions. **(B)** DEMs identified during the incompatible interactions. **(C)** DEMs identified between the compatible and incompatible interactions. **(D)** Change trend of the DEMs in the compatible (the values before the slash) and the incompatible (the values after the slash) interactions.

was upregulated from 0.074 to 0.381 and 1.214 at 48 and 96 hpi, respectively. Meanwhile, metab_8811 was *trans*-isoeugenol-*O*-glucuronide and was upregulated from 0.023 to 0.530 and 1.908. Among the 115 DEMs, 100 were upregulated due to the infection with *P. infestans*, but only five were downregulated at 96 hpi (**Figure 3D**).

We identified 73 metabolites as DEMs in compatible and incompatible interactions, while 125 and 42 DEMs

were specially identified in compatible and incompatible interactions, respectively (**Supplementary Tables 2A,B**). Among them, only one metabolite (metab_14855, lacto-*N*-triaose) was downregulated in both the compatible and incompatible interactions, while 59 DEMs were consistently upregulated in the two interaction patterns. Metab_12647 (PE(15:0/22:2(13Z,16Z))) was the only DEM that showed contradicting change trends in the two interaction patterns with the abundances of 0.769, 0.755, 2.450, 1.462, 0.957, and 0.545 in S1, S2, S3, R1, R2, and R3, respectively. Besides, 38 metabolites were upregulated in R samples but had no obvious changes in S samples.

Expression Differences Between the Two Potato Cultivars

The pairwise comparison analysis of compatible and incompatible interactions identified 131, 87, and 136 DEMs in the comparisons between S1 and R1, S2 and R2, and S3 and R3, respectively (**Figure 3C** and **Supplementary Table 2C**). Among the 131 DEMs, 62 showed higher abundance in the resistant potato cultivar, Ziyun No.1, of which metab_14383 was annotated as precarthamin, a compound possessing antibacterial and antifungal activities (Salem et al., 2014). Its abundance was much higher in Ziyun No.1 (2.241) than in Favorita (0.883) but decreased in both cultivars due to *P. infestans* infection. Salicylic acid (SA, metab_3112), an important phytohormone, also displayed the same expression pattern as precarthamin before the inoculation; however, its abundance was significantly upregulated in Favorita (from 0.163 to 0.397 and 1.896). Several other important metabolites, including lucidenic acid D2, lucuminic acid, ferulic acid (FA), folic acid, somniferine, gliadorphin, 18-hydroxycortisol, *O*-phosphotyrosine, and mahaleboside, also showed higher abundances in Ziyun No.1 (**Figure 4**).

Among the 364 DEMs identified between the three comparisons (R1 and S1, R2 and S2, and R3 and S3), 35 DEMs were shared across the three comparisons, and only 15 were upregulated in the resistant cultivar (**Table 1**). To identify more potato late blight RR metabolites, we divided the 364 metabolites with altered abundances at 96 hpi into 10 subclusters (1–10) (irrespective of the *p*-value and VIP value). Subclusters 2, 5, 8, and 9 represented the 140 metabolites, which were upregulated in R3 compared to S3 (**Figure 5**). We also found that 132 and 140 metabolites were upregulated at 0 and 48 hpi, respectively (**Supplementary Figures 2**, **3**), while 57 were consistently upregulated at 0, 48, and 96 hpi in the incompatible interactions (**Table 1**).

Phenylpropanoid Metabolism-Associated Metabolites

Phenylpropanoid metabolites have a well-documented association with oxidative stress and pathogen resistance (Duthie and Crozier, 2000). A total of 57 phenylpropanoid-related metabolites were identified (**Figure 6A** and **Supplementary Table 3A**); however, only six (3,5,6-trihydroxy-1-methyl-4,5-diphenylpiperidin-2-one, tetramethylquercetin 3-rutinoside, sakuranetin, *N-trans*-feruloyloctopamine, spinacetin 3-[p-coumaroyl-(- > 2)-glucosyl-(1- > 6)-[apiosyl-(1- > 2)]-glucoside], and cyanidin 3-(6″-(E)-*p*-coumarylsambubioside) 5-glucoside) had significant changes on the infection of the resistant cultivar Ziyun No.1 with *P. infestans*. Four out of the six metabolites were upregulated, while the remaining two (spinacetin 3-[*p*-coumaroyl-(- > 2)-glucosyl-(1- > 6)-[apiosyl-(1- > 2)] -glucoside] and cyanidin 3-(6″-(E)-*p*-coumarylsambubioside) 5-glucoside) were downregulated. The 20 phenylpropanoid-related metabolites identified from the susceptible cultivar Favorita infected with *P.*

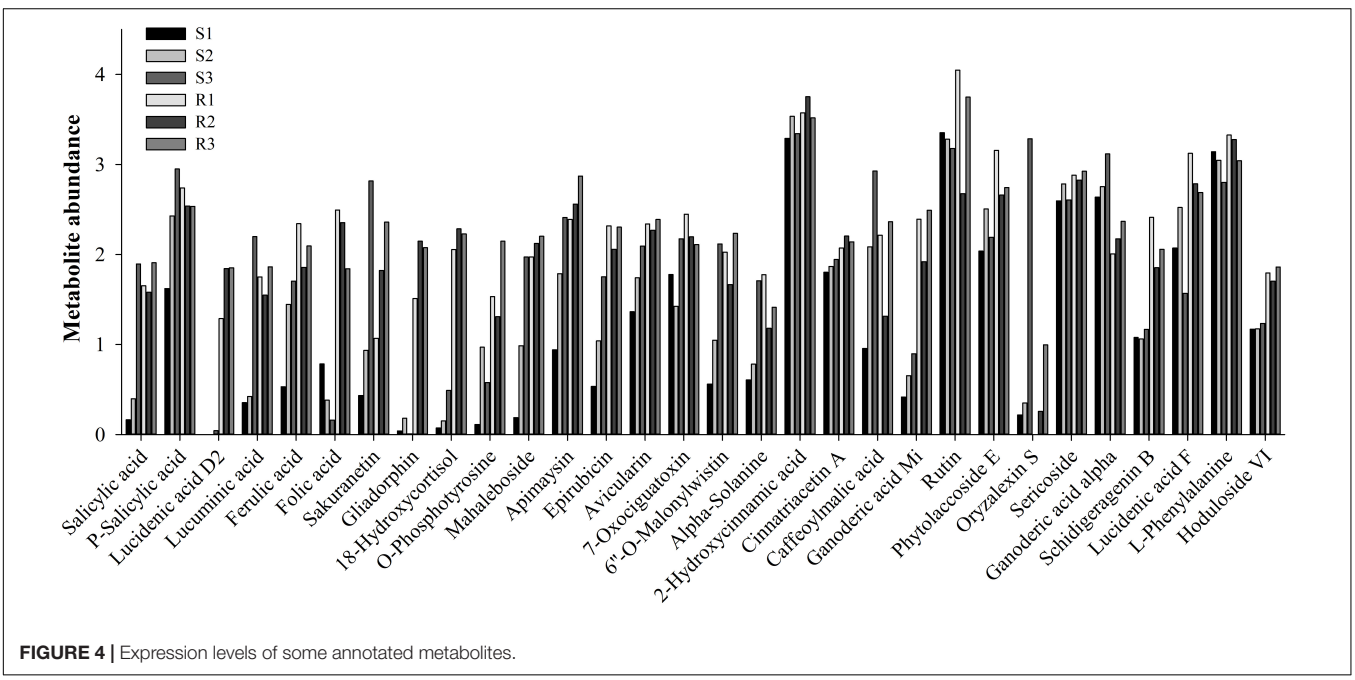

FIGURE 4 | Expression levels of some annotated metabolites.

TABLE 1 | Late blight resistance-related (RR) metabolites identified in resistant potato cultivar.

Metab ID	Metabolite	Class	S1	S2	S3	R1	R2	R3
metab_8880	Beta1-tomatidine	Steroids and steroid derivatives	1.813	2.147	1.275	3.120	2.675	2.734
metab_10888	Alpha-solamarine	Steroids and steroid derivatives	1.152	1.015	1.031	3.200	1.954	2.049
metab_11205	Coroloside	Steroids and steroid derivatives	0.932	0.887	1.113	1.778	2.298	2.379
metab_13219	18-hydroxycortisol	Steroids and steroid derivatives	0.073	0.152	0.490	2.055	2.286	2.229
metab_14158	Tetrahydroaldosterone-3-glucuronide	Steroids and steroid derivatives	2.448	2.253	1.645	3.249	3.410	3.262
metab_13870	Yuccoside C	Steroids and steroid derivatives	0.520	0.511	0.524	2.744	1.940	2.027
metab_2817	Coprocholic acid	Steroids and steroid derivatives	1.925	1.444	1.636	2.789	2.348	2.515
metab_6384	Polypodoside C	Steroids and steroid derivatives	0.449	0.545	0.635	2.032	1.464	1.733
metab_10764	Halobetasol propionate	Steroids and steroid derivatives	0.780	1.358	1.506	2.387	2.357	2.289
metab_1467	Chinenoside VI	Steroids and steroid derivatives	1.137	1.121	1.229	2.483	2.019	2.018
metab_6929	Ponasteroside A	Steroids and steroid derivatives	2.196	2.391	1.844	3.687	3.394	3.459
metab_3718	Fistuloside B	Steroids and steroid derivatives	0.733	0.706	1.246	2.459	2.145	2.141
metab_6336	Neogitogenin 3-[glucosyl-(1- > 2)-glucosyl-(1- > 4)-galactoside]	Steroids and steroid derivatives	3.115	3.391	3.487	4.415	4.058	4.209
metab_8968	Alliosterol 1-(4′′-galactosylrhamnoside) 16-galactoside	Steroids and steroid derivatives	2.620	2.480	0.887	3.692	3.109	3.182
metab_6682	25-hydroxyvitamin D3-26,23-lactol	Steroids and steroid derivatives	0.804	0.788	0.907	2.660	2.271	2.387
metab_14064	12-hydroxy-13-*O*-D-glucuronoside-octadec-9Z-enoate	Saccharolipids	1.347	1.529	1.487	2.276	2.799	2.582
metab_10366	Alkaloid RC	Rheadine alkaloids	1.700	1.708	1.414	2.928	3.125	2.970
metab_6468	Zanthodioline	Quinolines and derivatives	1.340	1.175	1.280	1.941	1.686	2.130
metab_11087	Riboflavine 2′,3′,4′,5′-tetrabutanoate	Pteridines and derivatives	0.263	0.415	0.923	1.811	1.995	1.828
metab_15462	Monotropein	Prenol lipids	0.861	1.877	0.777	2.563	2.518	2.364
metab_11767	Lucidenic acid D2	Prenol lipids	0.004	0.004	0.042	1.287	1.845	1.852
metab_6925	Schidigeragenin B	Prenol lipids	1.077	1.061	1.168	2.413	1.854	2.058
metab_14681	Assamsaponin F	Prenol lipids	2.469	2.593	2.236	4.019	3.704	3.725
metab_8277	(1R*,2R*,4R*,8S*)-*p*-menthane-1,2,8,9-tetrol 9-glucoside	Prenol lipids	2.903	2.981	2.662	3.503	3.706	3.454
metab_11510	Goshonoside F1	Prenol lipids	1.263	1.224	1.322	1.950	2.147	2.216
metab_5461	Ganoderic acid Mi	Prenol lipids	0.416	0.653	0.898	2.392	1.921	2.491
metab_3043	5-*O*-a-L-arabinofuranosyl-L-arabinose	Organooxygen compounds	1.190	1.395	1.898	1.897	1.861	2.480
metab_10398	4-(4-chlorophenyl)-1-[4-(4-fluorophenyl)-4-oxobutyl]-pyridinium (HPP+)	Organooxygen compounds	1.358	1.661	0.891	2.527	2.329	2.282
metab_7239	Galactose-beta-1,4-xylose	Organooxygen compounds	1.450	1.560	1.311	2.192	2.161	2.134
metab_1020	3,4,5-trihydroxy-6-(2-hydroxy-6-methoxyphenoxy)oxane-2-carboxylic acid	Organooxygen compounds	0.886	1.215	0.766	2.401	1.959	2.107
metab_15233	Caffeic acid 4-*O*-glucuronide	Organooxygen compounds	1.948	2.152	1.778	3.388	2.793	2.826

(Continued)

TABLE 1 | (Continued)

Metab ID	Metabolite	Class	S1	S2	S3	R1	R2	R3
metab_10661	3,4,5-trihydroxy-6-{[3-(3-hydroxyphenyl)propanoyl]oxy}oxane-2-carboxylic acid	Organooxygen compounds	1.496	1.884	2.446	3.278	2.807	3.221
metab_3695	6-({[3,4-dihydroxy-4-(hydroxymethyl)oxolan-2-yl]oxy}methyl)oxane-2,3,4,5-tetrol	Organooxygen compounds	1.063	1.080	0.716	2.327	2.586	2.019
metab_10121	*N*-desmethyl-*o*-*O*-sulfate rosiglitazone	Organic sulfuric acids and derivatives	1.168	1.446	0.704	1.887	2.016	1.928
metab_10831	Somniferine	Morphinans	0.016	0.099	0.783	0.938	1.737	1.811
metab_14383	Precarthamin	Flavonoids	0.883	0.617	0.321	2.241	1.728	1.533
metab_10533	*Cis*-3-hexenyl b-primeveroside	Fatty acyls	1.483	1.328	2.196	2.850	2.975	2.861
metab_7463	1,2-anhydridoniveusin	Fatty acyls	2.032	2.039	2.266	2.809	2.787	2.866
metab_14094	Ascladiol	Dihydrofurans	0.274	0.268	0.514	1.925	1.130	1.863
metab_8298	5′-((Z)-feruloyl) 3-(2′-methylarabinosylxylose)	Cinnamic acids and derivatives	2.536	2.923	2.758	4.121	3.427	3.721
metab_11122	Ac-Ser-Asp-Lys-Pro-OH	Carboxylic acids and derivatives	2.428	2.225	2.177	2.982	3.154	2.944
metab_14191	Endomorphin-1	Carboxylic acids and derivatives	1.159	1.100	1.509	2.570	2.625	2.317
metab_14210	Gliadorphin	Carboxylic acids and derivatives	0.040	0.181	0.009	1.511	2.148	2.076
metab_14282	Rigin	Carboxylic acids and derivatives	1.906	1.566	0.814	2.790	2.849	2.613
metab_14635	Canavaninosuccinate	Carboxylic acids and derivatives	1.223	0.882	1.403	2.098	2.524	2.363
metab_15201	Folic acid	Carboxylic acids and derivatives	0.784	0.382	0.160	2.494	2.354	1.843
metab_8130	L-*cis*-3-Amino-2-pyrrolidinecarboxylic acid	Carboxylic acids and derivatives	0.410	0.252	0.286	2.290	2.333	2.210
metab_14816	L-hypoglycin A	Carboxylic acids and derivatives	0.405	0.507	0.618	1.823	1.517	1.695
metab_10278	D-vacciniin	Benzene and substituted derivatives	1.805	2.105	1.985	2.733	2.820	2.785
metab_15419	Meta-*O*-dealkylated flecainide lactam	Benzene and substituted derivatives	0.994	1.569	1.077	2.745	2.335	2.565
metab_15390	Methyl 6-*O*-galloyl-beta-D-glucopyranoside	Benzene and substituted derivatives	1.064	1.459	1.252	2.485	2.033	2.538
metab_10554	2-hydroxy-desipramine glucuronide	Benzazepines	2.018	1.860	1.934	2.676	2.801	2.653
metab_1609	Nuatigenin	–	2.531	2.149	2.153	4.472	4.243	4.297
metab_3052	2-formyloxymethylclavam	–	0.839	1.178	0.835	1.699	1.921	1.761
metab_7055	Homostypolhydroperoxide	–	1.087	1.265	0.686	2.219	1.807	1.902
metab_15545	UDP-D-galactose	–	1.823	2.074	1.352	3.187	3.233	2.943
metab_6502	(20R,22R)-20,22-dihydroxycholesterol	–	0.823	0.924	0.141	2.568	2.245	2.307

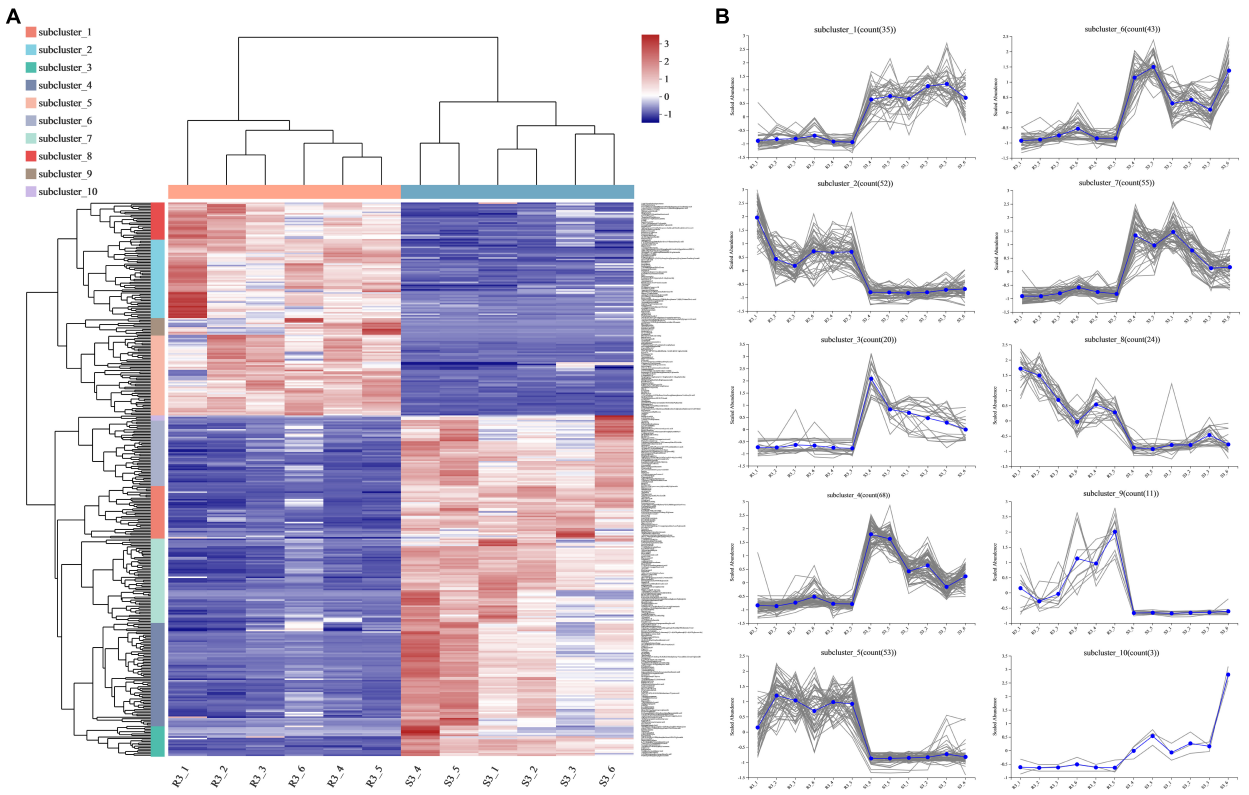

FIGURE 5 | Metabolites expression patterns between the compatible and incompatible interaction at 96 hpi. **(A)** Metabolites with altered abundances [irrespective of the *p*-value and variable importance in projection (VIP) value] at 96 hpi were divided into ten subclusters according to the expression patterns; each column represents a sample, each row represents a metabolite, and the color indicates the relative abundance of metabolites. **(B)** Number of metabolites for each subcluster.

infestans were considered as DEMs. Among them, 15 were significantly upregulated in Favorita, while four (metab_7888, metab_8835, metab_3327, and metab_10519) were significantly upregulated in Ziyun No.1. Metab_7888 and metab_8835 were annotated as tetramethylquercetin 3-rutinoside and *N-trans*-feruloyloctopamine, respectively. Moreover, metab_3327 was denoted as sakuranetin, and its abundance in Favorita increased from 0.433 to 0.935 and 2.817 at 48 and 96 hpi, respectively. The abundance of sakuranetin was much higher in Ziyun No.1 (1.067) than in Favorita (0.433) before infection. FA (metab_7058) was upregulated from 0.531 to 1.444 and 1.705 in the compatible interactions at 48 and 96 hpi, respectively. For the incompatible interactions, FA had abundances of 2.343, 1.857, and 2.095 at 0, 48, and 96 hpi, respectively. The abundance of FA was much higher in Ziyun No.1 than in Favorita at 0 hbi. Several other phenylpropanoid-related metabolites also showed the same expression patterns as FA. These included mahaleboside (metab_7979), apimaysin (metab_10825), epirubicin (metab_10359), avicularin (metab_7392), 7-oxociguatoxin (metab_10922), (3,4,5,6-tetrahydroxyoxan-2-yl) methyl 3-(4-hydroxy-3-methoxyphenyl) prop-2-enoate (metab_8289), 6′′-*O*-malonylwistin (metab_3480), and alpha-solanine (metab_11026) (**Figure 6A** and **Supplementary Table 3**).

Among these phenylpropanoid metabolites, 10 were annotated as hydroxycinnamic acids and derivatives. No significant changes were observed for the metabolites during the infection processes, except *N-trans*-feruloyloctopamine (metab_8835). However, six hydroxycinnamic acids and derivatives [2-hydroxycinnamic acid, (3,4,5,6-tetrahydroxyoxan-2-yl) methyl 3-(4-hydroxy-3-methoxyphenyl) prop-2-enoate, 5′-((Z)-Feruloyl) 3-(2′-methylarabinosylxylose), cinnatriacetin A, caffeoylmalic acid, and 1-*O*-*p*-coumaroyl-beta-D-glucose] were relatively higher in the resistant cultivar than in the susceptible cultivar before infection (**Figure 6A** and **Supplementary Table 3**).

Terpenoid Metabolites

Terpenoids are among the most abundant classes of plant secondary metabolites. A total of 69 metabolites were identified as terpenoids, including 6 monoterpenoids, 9 diterpenoids, 38 sesquiterpenoids, 15 triterpenoids, and 1 tetraterpenoid (**Figure 6B** and **Supplementary Table 3B**). Most diterpenoids (five metabolites) and sesquiterpenoids showed lower abundances in the resistant cultivar Ziyun No.1 than in the susceptible cultivar Favorita; however, most triterpenoids (10 metabolites) were higher in Ziyun No.1, before and after infection. Most monoterpenoids, diterpenoids, and sesquiterpenoids were upregulated, whereas the triterpenoids showed an opposite trend in the host plants inoculated with *P. infestans*. The abundances of metab_5461 (Ganoderic acid Mi)

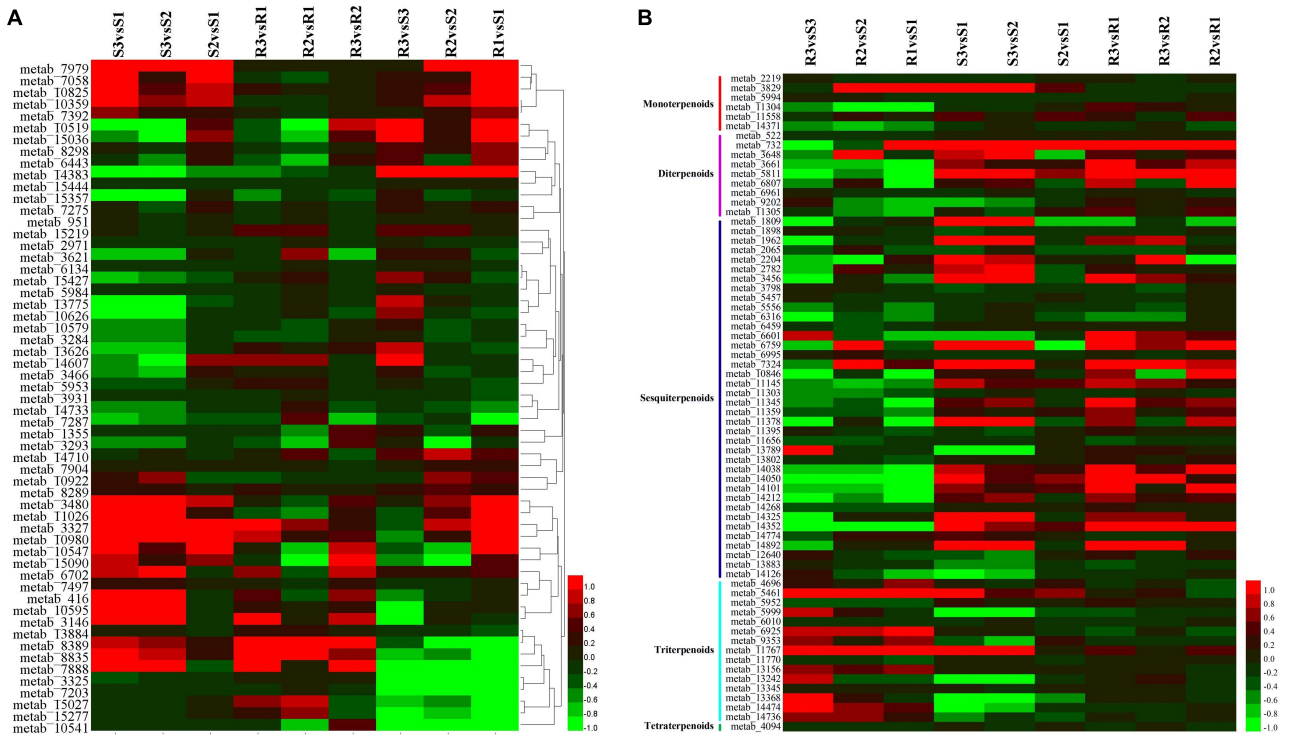

FIGURE 6 | Expression patterns of **(A)** phenylpropanoids biosynthesis- and **(B)** terpenoids-related metabolites. Each row represents a metabolite, while each column represents metabolite comparisons. For example, the S3vsS1 column means the $\log_2$ (S3/S1). The heatmap was developed *via* Heml toolkit using $\log_2$ fold change ($\log_2$FC) values (Deng et al., 2014).

were 0.416, 0.653, 0.898, 2.392, 1.921, and 2.491 in S1, S2, S3, R1, R2, and R3, respectively. Conversely, metab_5811, annotated as oryzalexin S, had abundances of 0.218, 0.349, 3.286, 0.003, 0.258, and 0.997 in S1, S2, S3, R1, R2, and R3, respectively. Lucidenic acid D2 (metab_11767) was upregulated from 0.004, 0.004, and 0.042 in susceptible cultivar Favorita but downregulated to 1.287, 1.845, and 1.852 in Ziyun No.1 at 0, 48, and 96 hpi, respectively (**Figure 4** and **Supplementary Table 3**).

DISCUSSION

Time-Course Metabolomic Profiling Identified Pathogen Resistance-Related Metabolites

A previous study identified 42 significantly increased and decreased pathogenesis-related metabolites by analyzing 95 metabolites; however, it was hard to determine the real metabolomic responses (Abu-Nada et al., 2007), which is hard to reflect the real metabolomic responses. Pushpa et al. (2014) and Yogendra et al. (2015) employed non-targeted metabolic profiling to identify RR metabolites and obtained 4,100 and 4,204 metabolite peaks that were analyzed, respectively. However, the samples used in these studies were only collected at 72 hpi, thus limiting the time-course determination of metabolomic mechanisms involved. To overcome this limitation, we performed the non-targeted metabolic profiling of two potato cultivars in response to *P. infestans* at different time points. A total of 11,589 metabolite peaks and 819 metabolites were identified from the two cultivars. Among them, 73 were identified as DEMs both in the compatible and incompatible interactions and were considered as responsive metabolites of the late blight pathogen because most of them were upregulated during the infection process. Additionally, 57 metabolites were identified as RR metabolites after comparing the two cultivars, which is more than those identified in the previous studies (Abu-Nada et al., 2007; Pushpa et al., 2014; Yogendra et al., 2015). Therefore, these findings will enrich the knowledge on the interaction mechanisms between *P. infestans* and potatoes.

Salicylic Acid Plays a Crucial Role in Late Blight Resistance

Phytohormones are small endogenous, low-molecular-weight molecules, which cross talk to form a complex regulatory network for plant disease and pest resistance (Robert-Seilaniantz et al., 2010; Yang et al., 2015). SA is a beta hydroxy acid with hormonal function synthesized from the amino acid phenylalanine or chorismate in plants and was first reported to serve as an inducer of plant disease resistance by White (1979). Thus, it has been recently demonstrated that SA accumulation is essential for stimulating multiple components of plant disease resistance (Delaney et al., 1994;

Zhang and Li, 2019). It was found that SA (metab_3112) was much higher (1.653) in the resistant cultivar Ziyun No.1 than in the susceptible cultivar (0.163) before infection. Moreover, SA levels remained high in Ziyun No.1, which should be one of the most important reasons that Ziyun No.1 possesses high late blight resistance. SA was induced rapidly as a pathogenic response in the susceptible cultivar. P-SA (metab_14399), an isomer of SA, was also induced in the susceptible cultivar. However, its levels remained high in the resistant cultivar, which may be one of the main reasons for its resistance. Furthermore, SA is one of the most widely studied stress-signaling molecules in plants and has been reported to regulate the production of terpenoids, alkaloids, flavonoids, and phytoalexins (Ali et al., 2006; Tounekti et al., 2013; Wang et al., 2015). The different SA levels observed between the two cultivars may be associated with late blight resistance occurring through the downstream late blight responses.

The phenylpropanoid biosynthesis pathway is the main pathway of flavonoids and lignins biosynthesis. Phenylalanine is converted to *trans*-cinnamic acid by phenylalanine ammonia lyase (PAL, EC: 4.3.1.24), forming phenolic acids such as *trans*-cinnamic acid, *p*-coumaric acid, erucic acid, and FA through the action of cinnamate-4-hydroxylase (C4H, EC: 1.14.14.91). *P*-coumaric acid is then transformed by 4-coumarate-CoA ligase (4CL, EC: 6.2.1.12) into *p*-coumaroyl CoA, a universal substrate for the downstream flavonoids and lignins biosynthesis (Hahlbrock and Grisebach, 1979; Dong and Lin, 2021). It was found that the upstream intermediates of the phenylpropanoid biosynthesis pathway, including phenylalanine (metab_15444), 2-hydroxycinnamic acid (metab_951), FA (metab_7058), and sakuranetin (metab_3327), were higher in the resistant cultivar than in the sensitive cultivar before *P. infestans* infection. These may have subsequently induced the biosynthesis of the downstream flavonoids and lignins, which was confirmed by the abundances of several downstream metabolites [including acacetin 7-[apiosyl(1- > 6)-glucoside] (metab_6702) and rutin (metab_1355)]. Therefore, the abundance of these upstream intermediates may confer resistance to *P. infestans* since phenylpropanoids mediate plant responses to biotic and abiotic stimuli (Shirley, 1996; Bodini et al., 2009; Vogt, 2010; Brunetti et al., 2013; Liu et al., 2018). For example, it has been demonstrated that FA can protect plant cells against hydrolytic enzymes (Graf, 1992) and fungal infections (Putman et al., 1989).

It has been shown that HCAAs were increased in the phenylpropanoid pathway of the resistant potato cultivar following infection with *P. infestans* (Yogendra et al., 2014). This subsequently increased cell wall thickness and inhibited pathogen colonization in potatoes (Yogendra et al., 2014). No significant changes were observed in this study for most of the identified hydroxycinnamic acid-related compounds, except for *N-trans*-feruloyloctopamine. However, the relatively higher abundance of the six hydroxycinnamic acids and derivatives (2-hydroxycinnamic acid, (3,4,5,6-tetrahydroxyoxan-2-yl) methyl 3-(4-hydroxy-3-methoxyphenyl) prop-2-enoate, 5′-((Z)-feruloyl) 3-(2′-methylarabino sylxylose), cinnatriacetin A, caffeoylmalic acid, and 1-*O*-*p*-coumaroyl-beta-D-glucose) in the resistant cultivar, before infection, may indicate that the two cultivars have different cell wall characteristics.

Secondary metabolites are organic compounds that are not directly involved in the normal growth, development, or reproduction of an organism but are often involved in plant protection against biotic and abiotic stresses (Fraenkel, 1959; Pagare et al., 2015). Terpenoids are the most abundant class of plant secondary metabolites, and previous studies have shown that SA can increase triterpenoid content (Ye et al., 2018; Jiang et al., 2022). Therefore, higher SA abundance in the resistant potato cultivar Ziyun No.1 increased the levels of several triterpenoids, including phytolaccoside E, ganoderic acid Mi, schidigeragenin B, lucidenic acid F, lucidenic acid D2, hoduloside VI, sericoside, ganoderic acid alpha, and 3alpha,15alpha-Diacetoxy-(22R)-hydroxylanosta-7,9(11),24-trien-26-oic acid (**Figure 4** and **Supplementary Table 3**). SA and P-SA increased rapidly in the susceptible cultivar Favorita as a response to *P. infestans* infection but maintained at a relatively high abundance or slightly upregulated in the resistant cultivar Ziyun No.1. Consequently, various diterpenoids and sesquiterpene were accumulated during the compatible interaction; however, most diterpenoids (7 of 9 diterpenoids) and sesquiterpenes (27 of 38 sesquiterpenoids) were higher in the sensitive cultivar than in the resistant cultivar at 96 hpi. This may be explained by the regulation of the newly synthesized SA during the infection process in Favorita. Since most terpenoids have antibacterial and fungicidal activities (Graham and Stephen, 1994), we speculate that the terpenes may have played important roles in the resistance of Ziyun No.1.

CONCLUSION

A total of 819 metabolites were identified and quantified. Resistant and sensitive potato cultivars had different metabolomic responses against *P. infestans*, and the metabolic differences were mainly observed after 48 hpi. Additionally, *P. infestans*-responsive and RR metabolites were also identified. SA, triterpenoids, hydroxycinnamic acids, and phenylpropanoid biosynthesis-related metabolites may promote potato late blight resistance. Our results provide a reference for understanding the molecular mechanisms of potato late blight resistance.

DATA AVAILABILITY STATEMENT

The datasets presented in this study can be found in online repositories. The names of the repository/repositories and accession number(s) can be found below: https://www.ebi.ac.uk/metabolights/, MTBLS4365.

AUTHOR CONTRIBUTIONS

XiT and HL conceived the study, carried out the data analysis, drafted, and revised the manuscript. JZ and XuT carried out the experimental analysis, drafted, and revised the manuscript. YS, YL, and YW carried out the data analysis. YJ, HS, and BY

revised the manuscript. All authors contributed to the article and approved the submitted version.

FUNDING

This study was supported by the Sichuan Science and Technology Program (2022YFQ0032 and 2021YFYZ0021), the Key Research and Development Program of Chengdu (No. 2019-YF05-02019-SN), and the Open Project Program of Panxi Crops Research and Utilization Key Laboratory of Sichuan Province (No. SZKF2107).

SUPPLEMENTARY MATERIAL

The Supplementary Material for this article can be found online at: https://www.frontiersin.org/articles/10.3389/fmicb.2022.857160/full#supplementary-material

Supplementary Figure 1 | Correlation analyses of different samples collected from compatible and incompatible interactions. Correlation analyses were performed based on the metabolites identified under the positive ion model. **(A)** Sample correlation PLS-DA diagram. **(B)** Sample correlation heatmap.

Supplementary Figure 2 | Metabolites expression patterns between the compatible and incompatible interaction at 0 hbi. Metabolites with altered abundances (irrespective of the *p*-value and VIP value) at 0 hbi were divided into ten subclusters according to the expression patterns **(A)**. A number of metabolites for each subcluster were counted **(B)**. Each column represents a sample, each row represents a metabolite, and the color indicates the relative abundance of metabolites.

Supplementary Figure 3 | Metabolites expression patterns between the compatible and incompatible interaction at 48 hpi. Metabolites with altered abundances (irrespective of the *p*-value and VIP value) at 48 hpi were divided into ten subclusters according to the expression patterns **(A)**. A number of metabolites for each subcluster were counted **(B)**. Each column represents a sample, each row represents a metabolite, and the color indicates the relative abundance of metabolites.

REFERENCES

Abu-Nada, Y., Kushalappa, A. C., Marshall, W. D., Al-Mughrabi, K., and Murphy, A. (2007). Temporal dynamics of pathogenesis-related metabolites and their plausible pathways of induction in potato leaves following inoculation with *Phytophthora infestans*. *Eur. J. Plant Pathol.* 118, 375–391. doi: 10.1007/s10658-007-9150-8

Ali, M. B., Yu, K. W., Hahn, E. J., and Paek, K. Y. (2006). Methyl jasmonate and salicylic acid elicitation induces ginsenosides accumulation, enzymatic and non-enzymatic antioxidant in suspension culture *Panax ginseng* roots in bioreactors. *Plant Cell Rep.* 25, 613–620. doi: 10.1007/s00299-005-0065-6

Arbona, V., Manzi, M., Ollas, C., and Gomez-Cadenas, A. (2013). Metabolomics as a tool to investigate abiotic stress tolerance in plants. *Int. J. Mol. Sci.* 14, 4885–4911. doi: 10.3390/ijms14034885

Azizi, P., Osman, M., Hanafi, M., Sahebi, M., Rafii, M., and Taheri, S. (2019). Adaptation of the metabolomics profile of rice after *Pyricularia oryzae* infection. *Plant Physiol. Biochem.* 144, 466–479. doi: 10.1016/j.plaphy.2019.10.014

Bellincampi, D., Cervone, F., and Lionetti, V. (2014). Plant cell wall dynamics and wall-related susceptibility in plant-pathogen interactions. *Front. Plant Sci.* 5:228. doi: 10.3389/fpls.2014.00228

Birch, P. R. J., Boevink, P. C., Gilroy, E. M., Hein, I., Pritchard, L., and Whisson, S. C. (2008). Oomycete RXLR effectors: delivery, functional redundancy and durable disease resistance. *Curr. Opin. Plant Biol.* 11, 373–379. doi: 10.1016/j.pbi.2008.04.005

Bodini, S. F., Manfredini, S., Epp, M., Valentini, S., and Santori, F. (2009). Quorum sensing inhibition activity of garlic extract and p-coumaric acid. *Lett. Appl. Microbiol.* 49, 551–555. doi: 10.1111/j.1472-765X.2009.02704.x

Boevink, P. C., Birch, P. R. J., Turnbull, D., and Whisson, S. C. (2020). Devastating intimacy: the cell biology of plant-phytophthora interactions. *New Phytol.* 228, 445–458. doi: 10.1111/nph.16650

Boevink, P. C., Wang, X., Mclellan, H., He, Q., Naqvi, S., Armstrong, M. R., et al. (2016). A *Phytophthora infestans* RXLR effector targets plant PP1c isoforms that promote late blight disease. *Nat. Commun.* 7:10311. doi: 10.1038/ncomms10311

Brunetti, C., Di Ferdinando, M., Fini, A., Pollastri, S., and Tattini, M. (2013). Flavonoids as antioxidants and developmental regulators: relative significance in plants and humans. *Int. J. Mol. Sci.* 14, 3540–3555. doi: 10.3390/ijms14023540

Cajka, T., Vaclavikova, M., Dzuman, Z., Vaclavik, L., Ovesna, J., and Hajslova, J. (2014). Rapid LC-MS-based metabolomics method to study the *Fusarium* infection of barley. *J. Sep. Sci.* 37, 912–919. doi: 10.1002/jssc.201301292

Chamarthi, S. K., Kumar, K., Gunnaiah, R., Kushalappa, A. C., Dion, Y., and Choo, T. M. (2013). Identification of fusarium head blight resistance related metabolites specific to doubled-haploid lines in barley. *Eur. J. Plant Pathol.* 138, 67–78. doi: 10.1007/s10658-013-0302-8

Collinge, M., and Boller, T. (2001). Differential induction of two potato genes, Stprx2 and StNAC, in response to infection by *Phytophthora infestans* and to wounding. *Plant Mol. Biol.* 46, 521–529. doi: 10.1023/a:1010639225091

Conghua, X. (2012). Potato industry: status and development. *J. Huazhong Agric. Univ.* 97, 1–4.

Delaney, T. P., Uknes, S., Vernooij, B., Friedrich, L., Weymann, K., Negrotto, D., et al. (1994). A central role of salicylic acid in plant disease resistance. *Science* 266, 1247–1250. doi: 10.1126/science.266.5188.1247

Deng, W., Wang, Y., Liu, Z., Cheng, H., and Xue, Y. (2014). HemI: a toolkit for illustrating heatmaps. *PLoS One* 9:e111988. doi: 10.1371/journal.pone.0111988

Dong, N. Q., and Lin, H. X. (2021). Contribution of phenylpropanoid metabolism to plant development and plant-environment interactions. *J. Integr. Plant Biol.* 63, 180–209. doi: 10.1111/jipb.13054

Duthie, G., and Crozier, A. (2000). Plant-derived phenolic antioxidants. *Curr. Opin. Clin. Nutr. Metab. Care* 3, 447–451. doi: 10.1097/00075197-200011000-00006

Fraenkel, G. S. (1959). The raison d'Être of secondary plant substances. *Science* 129, 1466–1470. doi: 10.1126/science.129.3361.1466

Franke, R. B., Dombrink, I., and Schreiber, L. (2012). Suberin goes genomics: use of a short living plant to investigate a long lasting polymer. *Front. Plant Sci.* 3:4. doi: 10.3389/fpls.2012.00004

Fry, W. (2008). Phytophthora infestans: the plant (and R gene) destroyer. *Mol. Plant Pathol.* 9, 385–402. doi: 10.1111/j.1364-3703.2007.00465.x

Gao, P., and Xu, G. (2014). Mass-spectrometry-based microbial metabolomics: recent developments and applications. *Anal. Bioanal. Chem.* 407, 669–680. doi: 10.1007/s00216-014-8127-7

Graf, E. (1992). Antioxidant potential of ferulic acid. *Free Radic. Biol. Med.* 13, 435–448. doi: 10.1016/0891-5849(92)90184-I

Graham, W., and Stephen, C. F. (1994). Phenolic components of the plant cell wall. *Int. Rev. Cytol.* 151, 229–267. doi: 10.1016/S0074-7696(08)62634-0

Gunnaiah, R., and Kushalappa, A. C. (2014). Metabolomics deciphers the host resistance mechanisms in wheat cultivar Sumai-3, against trichothecene producing and non-producing isolates of *Fusarium graminearum*. *Plant Physiol. Biochem.* 83, 40–50. doi: 10.1016/j.plaphy.2014.07.002

Gunnaiah, R., Kushalappa, A. C., Duggavathi, R., Fox, S., and Somers, D. J. (2012). Integrated metabolo-proteomic approach to decipher the mechanisms by which wheat QTL (Fhb1) contributes to resistance against *Fusarium graminearum*. *PLoS One* 7:e40695. doi: 10.1371/journal.pone.0040695

Haas, B. J., Kamoun, S., Zody, M. C., Jiang, R. H. Y., Handsaker, R. E., Cano, L. M., et al. (2009). Genome sequence and analysis of the Irish potato famine pathogen *Phytophthora infestans*. *Nature* 461, 393–398. doi: 10.1038/nature08358

Hahlbrock, K., and Grisebach, H. (1979). Enzymic controls in the biosynthesis of lignin and flavonoids. *Annu. Rev. Plant Biol.* 30, 105–130. doi: 10.1146/annurev.pp.30.060179.000541

Hoffman, N. E., Yang, S. F., and McKeon, T. (1982). Identification of 1-(malonylamino)cyclopropane-1-carboxylic acid as a major conjugate of 1-aminocyclopropane-1-carboxylic acid, an ethylene precursor in higher plants. *Biochem. Biophys. Res. Commun.* 104, 765–770. doi: 10.1016/0006-291X(82)90703-3

Jiang, B., Liu, R., Fang, X., Tong, C., Chen, H., and Gao, H. (2022). Effects of salicylic acid treatment on fruit quality and wax composition of blueberry (*Vaccinium virgatum* Ait). *Food Chem.* 368:130757. doi: 10.1016/j.foodchem.2021.130757

Jones, J. D., and Dangl, J. L. (2006). The plant immune system. *Nature* 444, 323–329. doi: 10.1038/nature05286

King, S. R. F., Mclellan, H., Boevink, P. C., Armstrong, M. R., Bukharova, T., Sukarta, O., et al. (2014). *Phytophthora infestans* RXLR effector PexRD2 interacts with host MAPKKK epsilon to suppress plant immune signaling. *Plant Cell* 26, 1345–1359. doi: 10.1105/tpc.113.120055

Kubicek, C. P., Starr, T. L., and Glass, N. L. (2014). Plant cell wall-degrading enzymes and their secretion in plant-pathogenic fungi. *Annu. Rev. Phytopathol.* 52, 427–451. doi: 10.1146/annurev-phyto-102313-045831

Liu, Q., Luo, L., and Zheng, L. (2018). Lignins: biosynthesis and biological functions in plants. *Int. J. Mol. Sci.* 19:335. doi: 10.3390/ijms19020335

Lu, J., Liu, T., Zhang, X., Li, J., Wang, X., Liang, X., et al. (2021). Comparison of the distinct, host-specific response of three Solanaceae hosts induced by *Phytophthora infestans*. *Int. J. Mol. Sci.* 22:11000. doi: 10.3390/ijms222011000

Madhavan, S., Paranidharan, V., Erban, A., Al-Sadi, A. M., Kopka, J., and Velazhahan, R. (2019). The metabolic response of suspension-cultured cells from blast-resistant and -susceptible rice (*Oryza sativa* L.) genotypes to a *Pyricularia oryzae* elicitor. *Indian Phytopathol.* 72, 195–202. doi: 10.1007/s42360-019-00131-y

Morimoto, S., Suemori, K., Taura, F., and Shoyama, Y. (2003). New dimeric morphine from opium poppy (*Papaver somuniferum*) and its physiological function. *J. Nat. Prod.* 66, 987–989. doi: 10.1021/np020583l

Ndala, R. I., Mbega, E. R., and Ndakidemi, P. A. (2019). Different plant extracts against *Phytophthora infestans* (Mont.) de Bary in tomato in vitro. *Am. J. Plant Sci.* 10, 698–708. doi: 10.4236/ajps.2019.104050

Pagare, S., Bhatia, M., Tripathi, N., and Bansal, Y. K. (2015). Secondary metabolites of plants and their role: overview. *Curr. Trends Biotechnol. Pharm.* 9, 293–304.

Peerzada, S. H., Bhat, K. A., and Viswanath, H. S. (2020). Studies on management of late blight (*Phytophthora infestans* (Mont) de Bary) of potato using organic soil amendments. *Int. J. Curr. Microbiol. Appl. Sci.* 9, 2093–2099. doi: 10.20546/ijcmas.2020.902.237

Pushpa, D., Yogendra, K. N., Gunnaiah, R., Kushalappa, A. C., and Murphy, A. (2014). Identification of late blight resistance-related metabolites and genes in potato through nontargeted metabolomics. *Plant Mol. Biol. Rep.* 32, 584–595. doi: 10.1007/s11105-013-0665-1

Putman, L. J., Laks, P. E., and Pruner, M. S. (1989). Chemical constituents of black locust bark and their biocidal activity. *Holzforschung Int. J. Biol. Chem. Phys. Technol. Wood* 43, 219–224. doi: 10.1515/hfsg.1989.43.4.219

Raffaele, S., Win, J., Cano, L. M., and Kamoun, S. (2010). Analyses of genome architecture and gene expression reveal novel candidate virulence factors in the secretome of *Phytophthora infestans*. *BMC Genomics* 11:637. doi: 10.1186/1471-2164-11-637

Robert-Seilaniantz, A., Grant, M., and Jones, J. (2010). Hormone crosstalk in plant disease and defense: more than just jasmonate-salicylate antagonism. *Annu. Rev. Phytopathol.* 49, 317–343. doi: 10.1146/annurev-phyto-073009-114447

Rodenburg, S. Y. A., Seidl, M. F., Judelson, H. S., Vu, A. L., Govers, F., de Ridder, D., et al. (2019). Metabolic model of the *Phytophthora infestans*-tomato interaction reveals metabolic switches during host colonization. *mBio* 10, e00454-19. doi: 10.1128/mBio.00454-19

Sabbadin, F., Urresti, S., Henrissat, B., Avrova, A. O., Welsh, L. R. J., Lindley, P. J., et al. (2021). Secreted pectin monooxygenases drive plant infection by pathogenic oomycetes. *Science* 373, 774–779. doi: 10.1126/science.abj1342

Salem, N., Msaada, K., Elkahoui, S., Mangano, G., Azaeiz, S., Ben Slimen, I., et al. (2014). Evaluation of antibacterial, antifungal, and antioxidant activities of safflower natural dyes during flowering. *Biomed. Res. Int.* 2014:762397. doi: 10.1155/2014/762397

Shirley, B. W. (1996). Flavonoid biosynthesis: 'new' functions for an 'old' pathway. *Trends Plant Sci.* 1, 377–382. doi: 10.1016/S1360-1385(96)80312-8

Shulaev, V., Cortes, D., Miller, G., and Mittler, R. (2008). Metabolomics for plant stress response. *Physiol. Plant.* 132, 199–208. doi: 10.1111/j.1399-3054.2007.01025.x

Tadesse, Y., Gebeyehu, D., and Kesho, A.s (2021). Plant pathology & microbiology recent advances in potato late blight disease management strategies. *J. Plant Pathol. Microbiol.* 12:559.

Tounekti, T., Hernández, I., and Munné-Bosch, S. (2013). "Salicylic acid biosynthesis and role in modulating terpenoid and flavonoid metabolism in plant responses to abiotic stress," in *Salicylic Acid: Plant Growth and Development*, eds S. Hayat, A. Ahmad, and M. N. Alyemeni (Dordrecht: Springer Netherlands), 141–162. doi: 10.1007/978-94-007-6428-6_8

Vogt, T. (2010). Phenylpropanoid biosynthesis. *Mol. Plant* 3, 2–20. doi: 10.1093/mp/ssp106

Wang, X. M., Yang, B., Ren, C. G., Wang, H. W., Wang, J. Y., and Dai, C. C. (2015). Involvement of abscisic acid and salicylic acid in signal cascade regulating bacterial endophyte-induced volatile oil biosynthesis in plantlets of *Atractylodes lancea*. *Physiol. Plant.* 153, 30–42. doi: 10.1111/ppl.12236

White, R. F. (1979). Acetylsalicylic acid (aspirin) induces resistance to tobacco mosaic virus in tobacco. *Virology* 99, 410–412. doi: 10.1016/0042-6822(79)90019-9

Yang, B., Wang, Q., Jing, M., Guo, B., Wu, J., Wang, H., et al. (2017). Distinct regions of the *Phytophthora* essential effector Avh238 determine its function in cell death activation and plant immunity suppression. *New Phytol.* 214, 361–375. doi: 10.1111/nph.14430

Yang, L. N., Mclellan, H., Naqvi, S., He, Q., Boevink, P. C., Armstrong, M., et al. (2016). Potato NPH3/RPT2-like protein StNRL1, targeted by a *Phytophthora infestans* RXLR effector, is a susceptibility factor. *Plant Physiol.* 171, 645–657. doi: 10.1104/pp.16.00178

Yang, Y. X., Ahammed, G. J., Wu, C., Fan, S. Y., and Zhou, Y. H. (2015). Crosstalk among jasmonate, salicylate and ethylene signaling pathways in plant disease and immune responses. *Curr. Protein Peptide Sci.* 16, 450–461. doi: 10.2174/1389203716666150330141638

Ye, L., Liu, S., Xie, F., Zhao, L., and Wu, X. (2018). Enhanced production of polysaccharides and triterpenoids in *Ganoderma lucidum* fruit bodies on induction with signal transduction during the fruiting stage. *PLoS One* 13:e0196287. doi: 10.1371/journal.pone.0196287

Yogendra, K. N., Kushalappa, A. C., Sarmiento, F., Rodriguez, E., and Mosquera, T. (2015). Metabolomics deciphers quantitative resistance mechanisms in diploid potato clones against late blight. *Funct. Plant Biol.* 42, 284–298. doi: 10.1071/Fp14177

Yogendra, K. N., Pushpa, D., Mosa, K. A., Kushalappa, A. C., Murphy, A., and Mosquera, T. (2014). Quantitative resistance in potato leaves to late blight associated with induced hydroxycinnamic acid amides. *Funct. Integr. Genomics* 14, 285–298. doi: 10.1007/s10142-013-0358-8

Zhang, Y., and Li, X. (2019). Salicylic acid: biosynthesis, perception, and contributions to plant immunity. *Curr. Opin. Plant Biol.* 50, 29–36. doi: 10.1016/j.pbi.2019.02.004

Zheng, X. Z., Mclellan, H., Fraiture, M., Liu, X. Y., Boevink, P. C., Gilroy, E. M., et al. (2014). Functionally redundant RXLR effectors from *Phytophthora infestans* act at different steps to suppress early flg22-triggered immunity. *PLoS Pathog.* 10:e1004057. doi: 10.1371/journal.ppat.1004057

Conflict of Interest: The authors declare that the research was conducted in the absence of any commercial or financial relationships that could be construed as a potential conflict of interest.

Publisher's Note: All claims expressed in this article are solely those of the authors and do not necessarily represent those of their affiliated organizations, or those of the publisher, the editors and the reviewers. Any product that may be evaluated in this article, or claim that may be made by its manufacturer, is not guaranteed or endorsed by the publisher.

frontiers | Frontiers in Microbiology

ORIGINAL RESEARCH
published: 25 April 2022
doi: 10.3389/fmicb.2022.840893

In vivo Antiphytoviral Activity of Essential Oils and Hydrosols From *Origanum vulgare*, *Thymus vulgaris,* and *Rosmarinus officinalis* to Control Zucchini Yellow Mosaic Virus and Tomato Leaf Curl New Delhi Virus in *Cucurbita pepo* L.

Anna Taglienti[1], Livia Donati[1], Luca Ferretti[1], Laura Tomassoli[1], Filippo Sapienza[2], Manuela Sabatino[2], Gaia Di Massimo[2], Simona Fiorentino[3], Valerio Vecchiarelli[3], Paolo Nota[1] and Rino Ragno[2]*

[1] Research Centre for Plant Protection and Certification, Council for Agricultural Research and Economics, Rome, Italy, [2] Department of Drug Chemistry and Technology, University "La Sapienza," Rome, Italy, [3] Centro Appenninico del Terminillo "Carlo Jucci," Perugia University, Rieti, Italy

OPEN ACCESS

Edited by:
Elvira Fiallo-Olivé, La Mayora Experimental Station (CSIC), Spain

Reviewed by:
Hayssam M. Ali, King Saud University, Saudi Arabia
Islam Hamim, Bangladesh Agricultural University, Bangladesh

***Correspondence:**
Anna Taglienti
anna.taglienti@crea.gov.it

Specialty section:
This article was submitted to Microbe and Virus Interactions with Plants, a section of the journal Frontiers in Microbiology

Received: *21 December 2021*
Accepted: *15 March 2022*
Published: *25 April 2022*

Citation:
Taglienti A, Donati L, Ferretti L, Tomassoli L, Sapienza F, Sabatino M, Di Massimo G, Fiorentino S, Vecchiarelli V, Nota P and Ragno R (2022) In vivo Antiphytoviral Activity of Essential Oils and Hydrosols From Origanum vulgare, Thymus vulgaris, and Rosmarinus officinalis to Control Zucchini Yellow Mosaic Virus and Tomato Leaf Curl New Delhi Virus in Cucurbita pepo L. Front. Microbiol. 13:840893. doi: 10.3389/fmicb.2022.840893

In the last decades, the interest in biological activity of natural compounds has been growing. In plant protection, essential oils have been reported to exhibit antiviral, antimycotic, and antiparasitic activities, and are regarded as promising for the formulation of safe antimicrobial agents. Attention has also been focused on hydrosols, the by-products of hydro-distillation of essential oils. Their production is easy, fast, and cheap, and they seem to arise less concern for human health than essential oils. Plant viruses represent a major concern for agricultural crops since no treatment compound is available for virus control. This work was aimed at evaluating the antiphytoviral effectiveness of treatments with three essential oils and corresponding hydrosols extracted from *Origanum vulgare*, *Thymus vulgaris,* and *Rosmarinus officinalis* on *Cucurbita pepo* plants infected by zucchini yellow mosaic virus or tomato leaf curl New Delhi virus. Treatments were applied either concurrently or after virus inoculation to ascertain an inhibition or curative activity, respectively. Symptoms were observed and samplings were performed weekly. Virus titer and expression levels of phenylalanine ammonia lyase gene (PAL) were measured on treated and untreated infected plants by real-time PCR. PAL gene plays an important role in plant defense response as it is involved in tolerance/resistance to phytopathogens. Results indicated that treatments were effective against tomato leaf curl New Delhi virus whether applied simultaneously with the inoculation or after. A major inhibition was observed with *O. vulgare* essential oil and hydrosol, resulting in 10^{-4}-fold decrease of virus titer 3 weeks after treatment. Curative activity gave maximum results with all three essential oils and *T. vulgaris* and *R.*

officinalis hydrosols, recording from 10^{-2}-fold decrease to virus not detected 4 weeks after treatment. An induction of PAL gene expression was recorded at 12 d.p.i. and then was restored to the levels of untreated control. This allows to hypothesize an early plant defense response to virus infection, possibly boosted by treatments. Plant extracts' composition was characterized by gas chromatography-mass spectrometry. Phenols were largely main components of *O. vulgare* and *T. vulgaris* extracts (carvacrol and thymol, respectively), while extracts from *R. officinalis* were based on monoterpene hydrocarbons (essential oil) and oxygenated monoterpenes (hydrosol).

Keywords: essential oil, hydrosol, plant virus, antiphytoviral, defense response

INTRODUCTION

Essential oils (EOs) are complex mixtures of low molecular weight and volatile compounds that are formed and stored in aromatic plant families (e.g., *Apiaceae*, *Asteraceae*, *Lamiaceae*, *Myrataceae*) particularly rich in these secondary metabolites (Baser and Buchbauer, 2015). They are usually obtained by steam or hydro-distillation (Speranza and Corbo, 2010; Garzoli et al., 2015; Božović et al., 2017), with the components belonging to a wide variety of chemical classes: aliphatic and aromatic compounds, hydrocarbons, alcohols, aldehydes, ketones, esters, phenols, and acids. Many of these substances are reported to display antimicrobial, antiviral, antimycotic, antiparasitic, and insecticidal properties both against mammalian and plant pathogens (Bakkali et al., 2008; Civitelli et al., 2014; Garzoli et al., 2018; Sabatino et al., 2020). In literature, the separated condensed water, saturated of water-soluble essential oil components, produced during the distillation process of EOs is reported under various terms, including hydrosol (HS), hydrolate, hydroflorate, and aromatic water (Rajeswara Rao, 2013). Herein, this extract is referred to as HS. Regardless of the used name, their composition is known to be represented by a small quantity of EO (i.e., < 1 g/L) and by polar, oxygenated, and hydrophilic oil components forming hydrogen bonds with water (Labadie et al., 2016).

Virus infection in plants is a major concern for agricultural crops, causing considerable economical losses worldwide (Lecoq and Katis, 2014). Since no curative treatment consisting of application of compounds of natural or synthetic origin is available for virus control in plants, such as for bacteria and fungi (Rubio et al., 2020), most of defense strategies lie on prevention (e.g., use of sanitarily certified propagation material, control of insect vectors) (Fereres and Raccah, 2015; Golino et al., 2017). Other control measures require the use of resistant varieties developed by breeding (Paris and Brown, 2005; Martín-Hernández and Picó, 2020). Engineered mild virus strains for accomplishing cross-protection or transgenic plants represent promising approaches which, to date, are limited to a few plant/virus species (You et al., 2005; Jia et al., 2017; Hamim et al., 2018). Their employment is further restrained because applied research and use of transgenic plants are forbidden in many countries. When no other measure is feasible, *in vitro* virus elimination is accomplished with different techniques (thermotherapy, meristem culture, cryotherapy, micro-grafting) which are all very expensive, time-consuming, and do not suite all plant/virus pathosystems (Naik and Buckseth, 2018).

Various substances of natural and synthetic origin have been used for plant virus infection control, and in some studies, the antiphytoviral activity of EOs has been reported (Zhao et al., 2017; Raveau et al., 2020). Such treatments aim at moderating symptom expression and limiting the yield losses due to infection by reducing the viral titer or inactivating some viral functional genes. Further, the application of treatments based on natural products is also gaining interest in view of the envisaged restrictions to the synthetic chemicals' overuse that has been proved to cause environmental and human health issues. Such limitations (e.g., Regulation 1107/2009/EC, 2011) drive the demand for alternative control methods and integrated pest management systems (Lamichhane et al., 2016). Therefore, many studies have focused on the use of natural products for virus control in plants. Trials involving tobacco mosaic virus (TMV) were based on the count of local lesions. Bishop (1995) and Lu (2013) both worked on a *Nicotiana glutinosa* experimental host, reporting an inhibition of local symptoms development upon treatments with EOs from *Melaleuca alternifolia*, ginger, lemon, tea tree, tangerine peel, artemisia, and lemongrass. Dunkić et al. (2010) used *Satureja montana* EO as a treatment for *Chenopodium quinoa* and *Chenopodium amaranticolor* hosts infected with TMV and cucumber mosaic virus (CMV). Further experiments involving *C. quinoa*-CMV pathosystem (Bezić et al., 2011; Vuko et al., 2019) reported the ability of EOs from *Micromeria croatia* and *Teucrium* species to reduce the local lesion number. The effectiveness of *Nigella sativa* seed extract against zucchini yellow mosaic virus (ZYMV) in *C. pepo* was investigated both *in vitro* and *in vivo* (Abdel-Shafi, 2013). Local lesion number and physiological parameters (leaves number, shoot length, etc.) were measured for assessing antiphytoviral activity. The detailed mechanism of such activity is yet to be fully explored. It has been hypothesized that EO components could either directly inactivate viral particles or induce resistance/tolerance response in the host (Othman and Shoman, 2004). HSs have often been considered a waste by-product of EO distillation, but recently they have gained a growing interest due to their reported antimicrobial activity both *in vitro* and *in situ* (Sağdıç, 2003; Tornuk et al., 2011; Ozturk et al., 2016). Furthermore, their use has been endorsed for their low production cost. In the field of plant protection,

antiphytoviral activity of HSs from various plant species against TMV has been reported (Nazlić et al., 2021; Vuko et al., 2021a,b).

Based on these findings, we hypothesized that EOs and HSs could have a potential antiphytoviral activity *in vivo*. In particular, in this study, we aimed at verifying whether EOs and HSs from *Origanum vulgare* (OV), *Thymus vulgaris* (TV), and *Rosmarinum officinalis* (RO) could be effective for the control of ZYMV and tomato leaf curl New Delhi virus (ToLCNDV) in *Cucurbita pepo* L. plants *in vivo*. ZYMV, a member of the genus *Potyvirus*, family *Potyviridae*, is a ssRNA (+) virus efficiently transmitted by aphids in a non-persistent manner. It affects all members of the *Cucurbitaceae* family, including pumpkin, squash, vegetable marrow, zucchini, melon, watermelon, cucumber, and gherkin (Gal-On, 2007). It induces symptoms such as severe leaf mosaic and yellowing. The fruits are stunted, twisted and deformed by raised protuberances, which makes them unmarketable. In cultivated crops, plants cease marketable production within 1–2 weeks post infection. Hence, serious economic losses, reducing yield up to 90%, can occur, particularly in zucchini and marrow crops (Walkey et al., 1992). ToLCNDV is a bipartite begomovirus (family *Geminiviridae*) that was identified for the first time in 1995 in Asia (Padidam et al., 1995), from where it recently spread into the Mediterranean basin (Navas-Castillo et al., 2011; Juárez et al., 2014; Luigi et al., 2016; Bertin et al., 2018), becoming a serious threat to a number of economically important crops and is therefore responsible for severe production losses. ToLCNDV genome is constituted of two circular ssDNA components, named DNA-A and DNA-B. In zucchini plants, it causes a wide and severe symptomatology, including leaf curling, swelling of veins and yellow mosaic on leaves, stems with shortened internodes, and fruits showing skin roughness and reduced size (Panno et al., 2016). The virus is transmitted by the whitefly *Bemisia tabaci* (Gennadius) in a persistent manner.

The EOs and HSs antiphytoviral activity, foreseen in our hypothesis, was assessed by comparing the relative virus titer in systemically infected treated and untreated plants in order to ascertain if, and to what extent, treatments were able to decrease virus titer in a systemically infected leaf tissue of *C. pepo*. Several studies have established that plants were able to set up a defense response upon virus infection by using a wide range of regulation mechanisms (Soosaar et al., 2005). The phenylpropanoid pathway plays a role in such defense strategies by regulating the synthesis of phenolic compounds. Phenylalanine ammonia lyase (PAL) is the entry enzyme of this metabolic pathway, and the related gene is known to be involved in plant response to biotic stress through transcriptional regulation (Kim and Hwang, 2014; Abdelkhalek et al., 2018). Under the hypothesis of effectiveness of EOs and HSs treatments in plant virus control, PAL expression level was also quantified in treated and untreated infected plants in order to investigate the possible mechanism of action. Finally, symptom expression was also observed for evaluating disease incidence. To the best of our knowledge, this is the first report in which the EOs and HSs antiphytoviral activity is investigated *in vivo* on a vegetal species of agricultural interest and by means of quantification of viral titer and PAL expression levels by real-time (RT-)PCR.

MATERIALS AND METHODS

Essential Oils and Hydrosols Production

Plants of OV, TV, and RO, which are used to produce EOs and HSs, were cultivated and harvested in Latium, central Italy at the agricultural experimental field Centro Appenninico del Terminillo "Carlo Jucci" in Rieti. EOs and HSs were produced by steam-distillation for 1 h using a Clevenger-type apparatus according to the procedures described in the *European Pharmacopeia*. Fresh leaves (2 kg) of aerial parts from each plant species were used for distillation. HSs were separated by decantation, and the EOs were treated twice with diethyl ether (Sigma-Aldrich, Italy) to eliminate the water through a separation funnel. EO/diethyl ether layer were dried with anhydrous sodium sulfate (Sigma-Aldrich, Italy) and the solvent was evaporated. EOs yields were 3.48, 0.26, and 0.43% for OV, TV, and RO, respectively. EOs were stored at −20°C and HSs at 4°C, both in the dark in glass vials.

Gas Chromatography/Mass Spectrometry Analysis

Gas chromatography/mass spectrometry (GC-MS) analyses of EOs and HSs were performed using a Thermo Scientific gas chromatograph Focus GC, equipped with a fused silica capillary TG-SQC (30 m × 0.25 mm, film thickness 0.25 μm Thermo Fisher Scientific, United States) and a mass spectrometer 700 ITQ MS as detector. n-Hexane (97.0% grade) and all standard references (standard analytical grade) were supplied by Sigma Aldrich (Milan, Italy) with the exception of piperitenone oxide, which was in-house purified from *Mentha suaveolens* EO as previously described (Civitelli et al., 2014). Prior to injection, EOs were diluted 1:1,000 V/V with n-hexane, while HSs were previously liquid-liquid extracted in n-hexane 1:1 V/V and then diluted 1:100 V/V with n-hexane shortly before analysis. The organic fraction was separated, dried with anhydrous sodium sulfate, and the solvent was evaporated. GC-MS was performed according to the chromatographic and mass conditions described in Daferera et al. (2000), modified as follows: splitless mode injection, oven temperature program, 6 min of 60°C isothermal, then 3°C/min gradient up to 132°C, 10°C/min–180°C, and finally 15°C/min–240°C and held for 5 min. Injection volume was adjusted to 2 μl, while helium (99.9%) was the carrier gas at a constant flow rate of 1 ml/min. For GC-MS detection, detector temperature was set to 250°C, MS spectra were monitored between 50 and 450 amu (full scan mode), and the ionization mode used was an electronic impact at 70 eV. Compound identification was carried out to compare the relative retention times and mass spectra of the molecules with commercial libraries (NIST, 2017). When available, identification was confirmed by co-injection with a standard reference compound. Moreover, relative quantitation of these compounds was also accomplished by evaluating the relative percentage for each peak [peak area/total ion chromatogram (TIC) area] (**Table 1**).

TABLE 1 | Phytochemical composition (%) of essential oils (EOs) and hydrosols (HSs) used in this study, by GC-MS.

Component	Rt (min)	OV EO	OV HS	TV EO	TV HS	RO EO	RO HS	Identification
Monoterpene hydrocarbons		*2.42*	*5.81*	*12.64*	*10.62*	*56.29*	*2.15*	
α-pinene	7.78	tr	–	0.22	–	32.55	1.94	MS
Camphene	8.40	–	–	tr	–	9.35	0.21	Co-GC
β-pinene	9.64	–	–	tr	–	2.06	–	Co-GC
Myrcene	10.40	–	–	0.18	–	2.31	–	Co-GC
Limonene	12.12	–	–	–	–	3.57	–	Co-GC
α-thujene	7.52	tr	–	tr	–	tr	–	MS
α-terpinolene	15.10	–	–	Tr	0.32	–	–	MS
α-terpinene	11.55	tr	–	0.23	–	0.55	–	Co-GC
γ-terpinene	13.64	–	5.04	0.60	–	0.84	–	Co-GC
p-cymene	11.93	2.27	0.77	11.78	10.30	5.03	–	Co-GC
Oxygenated monoterpenes		*5.45*	–	*6.05*	*27.35*	*26.49*	*95.55*	
Linalool	15.71	–	–	1.82	6.61	1.07	2.10	Co-GC
Camphor	17.69	0.71	–	0.40	1.90	6.67	20.89	Co-GC
Borneol	17.78	0.68	–	0.94	8.74	5.55	15.10	Co-GC
Terpinen-4-ol	19.36	0.92	–	2.06	6.47	0.42	1.62	Co-GC
Bornyl acetate	24.45	–	–	0.17	–	4.97	0.58	Co-GC
1,8-cineole	12.23	1.03	–	0.42	2.45	7.26	20.14	Co-GC
(Z)-p-menth-2-en-1-ol	16.66	–	–	tr	–	–	–	MS
α-terpineol	20.02	–	–	0.21	0.86	0.55	1.86	MS
p-cymen-8-ol	19.80	–	–	–	0.33	–	–	MS
Cis-sabinene hydrate	14.02	0.27	–	–	–	–	–	MS
Trans-sabinene hydrate	15.52	0.23	–	–	–	–	–	MS
Piperitenone oxide	28.01	1.62	–	–	–	–	–	MS
Verbenone	20.86	–	–	–	–	2.72	33.26	Co-GC
Sesquiterpene hydrocarbons		*0.53*	*1.06*	*2.35*	–	*5.24*	–	
β-caryophyllene	30.23	0.53	1.06	1.74	–	4.86	–	Co-GC
Allo-aromadendrene	32.70	–	–	Tr	–	tr	–	MS
Germacrene D	33.02	–	–	0.35	–	0.12	–	MS
β-copaene	32.10	–	–	0.17	–	tr	–	MS
α-cubebene	28.40	–	–	–	–	0.13	–	
Oxygenated sesquiterpenes		–	–	–	–	*tr*	–	
Caryophyllene oxide	34.90	–	–	–	–	tr	–	MS
Phenolic compounds		*90.62*	*93.13*	*75.95*	*61.04*	*1.83*	–	
Thymol	24.93	1.41	1.54	68.02	57.35	1.56	–	Co-GC
Carvacrol	25.34	88.64	91.59	5.71	3.69	tr	–	Co-GC
Thymol methyl ether	22.14	–	–	1.38	–	–	–	MS
Methyl carvacrol	22.56	0.57	–	0.83	–	0.16	–	MS
Hydrocarbons		*0.27*	–	*0.87*	–	–	–	
Cadina-1,3,5-triene	33.23	0.27	–	0.87	–	–	–	MS
Alcohols		–	–	*0.11*	*0.63*	–	–	
1-octen-2-ol	9.89	–	–	0.11	0.63	–	–	MS
Total identified		99.29	100.00	98.56	99.63	92.55	97.70	

MS, identification by NIST (2017) spectral database; Co-GC, identification confirmed with reference compound; tr, traces (<0.1%). Values in bold represent the quantitation for the relevant class of compounds.

Plant Material

Plant Host

Seeds of *Cucurbita pepo* "Tullio" were sown in 12 cm plastic pots containing soil "Completo" (Vigorplant, Italy) and maintained in a greenhouse (23°C, 16 h light photoperiod) with watering as required. The obtained plants were grown in an insect-proof greenhouse under the same conditions. Experimental plants were selected 3 weeks after sowing, when they had two fully expanded cotyledons. Care was taken to ensure that the experimental plants were as uniform in size as possible.

Virus Inoculum

ZYMV and ToLCNDV isolates from the Research Centre for Plant Protection and Certification (CREA-DC) collection were propagated in the plant host *C. pepo* "Tullio" under the greenhouse conditions above described. Systemically infected

young leaves were ground with chilled 0.1 M pH 7.4 phosphate buffer (1:5 w/V) in an extraction bag (Bioreba, Switzerland) to prepare virus *inocula* for the following experiments.

Experimental Trials

Treatments Applied at the Same Time With Inoculation of Zucchini Yellow Mosaic Virus or Tomato Leaf Curl New Delhi Virus

The ZYMV or ToLCNDV *inoculum* was mixed with EO or HS solution in 0.1 M pH 7.4 phosphate buffer (final concentrations: 1:10 V/V virus *inoculum*; 300 μg/ml EO or 1:2 V/V hydrosol, see **Table 2**) and incubated for 1 h on ice. Then, the mixtures were used to mechanically inoculate host plants. For ZYMV trial, host plants were inoculated at the developmental stage of fully expanded cotyledons, and the 20 μl of mixtures ZYMV + treatment described above were applied to each cotyledon. For the ToLCNDV trial, plants were inoculated when they had cotyledons and the first true leaf fully expanded, and 80 μl were applied to each cotyledon and leaf. Three biological replicates were used per treatment, and controls were represented by (i) treatment with ribavirin (final concentrations: 1:10 V/V virus inoculum; 300 μg/ml ribavirin); (ii) infected no-treatment (final concentration: 10:10 V/V virus inoculum); and (iii) healthy (mock-inoculated with phosphate buffer). When the first new leaf was expanded 5 days post infection (d.p.i.), i.e., first true leaf for ZYMV trial, second true leaf for ToLCNDV trial, plants were sampled by removing a disk from the abovementioned leaf. Biological replicates (three plants per treatment) were pooled and downstream analyzed as a single sample. Each sample was thus submitted to quantification of virus titer and expression level of PAL gene by real-time (RT-)PCR as described below. The above described and following experimental procedures are depicted as a flow diagram in **Supplementary Figure 1**.

Treatments Applied at the Same Time With Inoculation of Tomato Leaf Curl New Delhi Virus (Time Course)

Based on the results obtained for samples collected at 5 d.p.i. (see section "Treatments Applied at the Same Time With Inoculation of ZYMV or ToLCNDV"), the above trial on ToLCNDV was repeated, extending the period of observation, and after the first collection time point at 5 d.p.i., three more samplings were performed on a weekly basis. Each sampling involved a new leaf (i.e., third, fourth, and fifth leaf corresponding to sampling times 12, 19, and 26 d.p.i.), and as above, biological replicates were pooled and downstream analyzed as a single sample.

TABLE 2 | Summary of treatments applied in experimental trials.

Entry	Product	Plant species	Concentration
1	EO	*Origanum vulgare*	300 μg/ml
2	HS	*Origanum vulgare*	1:2 V/V
3	EO	*Thymus vulgaris*	300 μg/ml
4	HS	*Thymus vulgaris*	1:2 V/V
5	EO	*Rosmarinus officinalis*	300 μg/ml
6	HS	*Rosmarinus officinalis*	1:2 V/V
7	Ribavirin	N/A	300 μg/ml

Positive (i.e., infected no-treatment plants) and negative (i.e., mock-inoculated plants) controls were also included in each trial.

Treatments Applied After Inoculation of Tomato Leaf Curl New Delhi Virus (Time Course)

Based on the results obtained from the above-described trials, in which the treatments were applied concurrently with virus inoculation, further experiments were run only on ToLCNDV to evaluate the effect of the tested plant extracts post *inoculum*. In the literature, such activity is often addressed to as "curative" since the treated plants have already started the infection process. In this regard, host plants were inoculated in the same conditions described in section "Treatments Applied at the Same Time With Inoculation of ZYMV or ToLCNDV" (final concentration: 1:10 V/V virus *inoculum*), but no treatment was mixed with the *inoculum*. After 5 h, treatments were applied by smearing the leaf surface with the EO or HS solution described in section "Treatments Applied at the Same Time With Inoculation of ZYMV or ToLCNDV" (final concentration: 300 μg/ml EO or 1:2 V/V HS). Three biological replicates were used per treatment and controls were represented by (i) treatment with ribavirin (final concentration: 300 μg/ml); (ii) infected no-treatment (final concentration: 10:10 V/V virus inoculum); and (iii) healthy (mock-inoculated with phosphate buffer). When the first new leaf, i.e., the second true leaf, was expanded (5 d.p.i.), plants were sampled as above described. Biological replicates were pooled and downstream analyzed as a single sample. Additional samplings were performed as described in section "Treatments Applied at the Same Time With Inoculation of ToLCNDV (Time Course)."

Nucleic Acid Extraction and Real-Time (RT-)PCR

Total RNA of samples collected from the ZYMV trial was extracted using RNeasy Plant Mini Kit (Qiagen, Milan, Italy). Total nucleic acid (TNA) of samples collected from the ToLCNDV trials (in treatments together with or after inoculation) was extracted using DNeasy "Mericon" Food Kit (Qiagen, Milan, Italy). Both kits were used according to the manufacturer's instructions. Extracts were checked for purity and concentration by NanoDrop™ spectrophotometer (Thermo Fisher Scientific, Milan, Italy).

Total RNA samples (ZYMV trial) were treated with 2 U DNase I (Life Technologies, Milan, Italy) per 1 μg RNA, at room temperature for 15 min. Then, 1 μl of 50 mM EDTA was added, and the mix was incubated at 65°C for 10 min in a CFX96 Touch PCR System (Bio-Rad, Milan, Italy) to inactivate DNase and stop the reaction.

Total nucleic acid samples (ToLCNDV trial) were reverse transcribed to cDNA in order to convert plant transcriptome into DNA substrate suitable for real-time PCR. The reaction was carried out in a final volume of 19 μl using 5X first-strand buffer (Invitrogen), 5 μM random hexamers (Promega, San Diego, CA, United States), 10 μM dNTPs, 100 U M-MLV (Promega, San Diego, CA, United States), and 2 μl TNA. The reaction was incubated for 45 min at 42°C, 3 min at 94°C in a CFX96 Touch PCR System (Bio-Rad, Milan, Italy) before 1 μl

RNase cocktail mix (Life Technologies, Milan, Italy) was added to remove residual unreacted RNA.

The relative quantification of ZYMV was carried out on total RNA, treated as described above with TaqMan® real-time RT-PCR assay using the species-specific primers and probe designed on the coat protein (CP) gene by Manglli et al. (2019). The reaction had a final volume of 20 µl, containing 2X TaqMan® RT-PCR Master Mix and 40X TaqMan® RT Enzyme Mix (TaqMan® RNA-to-C_T™ 1-Step Kit, Life Technologies, Milan, Italy), 300 nM of each primer, 50 nM probe, and 1 µl DNase-treated RNA.

The relative quantification of ToLCNDV was carried out with TaqMan® real-time PCR assay using the species-specific primers and probe designed on the A genome of ToLCNDV by Simón et al. (2018). The reaction had a final volume of 10 µl containing 2X TaqMan® RT-PCR Master Mix, 100 nM of each primer and probe, and 1 µl of RNase-treated cDNA.

The relative expression of PAL was quantified with SYBR Green® real-time RT-PCR assay using primers designed by Zhang et al. (2021). The reaction had a final volume of 10 µl containing 2X SsoAdvanced Universal SYBR Green Supermix (Bio-Rad, Milan, Italy), 150 nM of each primer, and 1 µl of template.

All real-time (RT-)PCR assays were performed on a CFX96 Touch RT-PCR System (Bio-Rad, Milan, Italy). The threshold was automatically set by the instrument.

The virus relative titer and PAL expression level were determined using the method of ΔΔCt (Livak and Schmittgen, 2001). The elongation factor EF-1α gene of *C. pepo* was used as housekeeping for both assays using previously published primers and probe (Obrero et al., 2011). All samples represented a pool of the three biological replicates (i.e., plants in the same pot) and were assayed in two technical replicates. Relative virus titer and PAL expression level, defined as $2^{-\Delta\Delta Ct}$ were calculated by CFX Maestro Software v. 2.2 (Bio-Rad, Milan, Italy) and the results were expressed as mean ± standard error (SE).

RESULTS

Plant extracts (EOs and HSs) from OV, TV, and RO were characterized by GC-MS in order to assess their specific composition, which is known to strongly depend on environmental and plant characteristics.

Under greenhouse conditions, the antiviral activities of these plant extracts were evaluated on *C. pepo* plants experimentally inoculated with either ZYMV or ToLCNDV. Using real-time PCR, both the relative virus titer and the relative expression of PAL were measured on treated plants with respect to control plants (i.e., infected no-treatment). Symptoms were also recorded on the inoculated test plants in order to observe possible phenotypical modification and symptom intensity and variability induced by treatments. Preliminarily, symptoms on control plants were evaluated and resulted as expected. In all experiments, the inoculated no-treatment control plants displayed symptoms of the relevant infection. Healthy

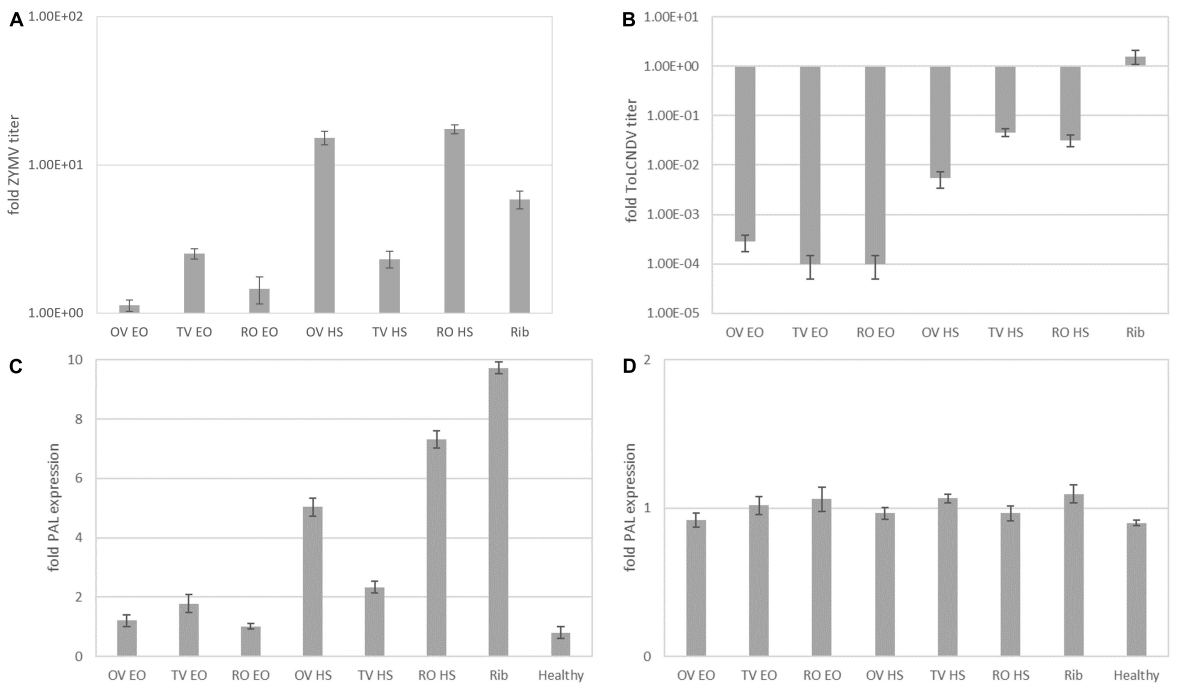

FIGURE 1 | Fold change of zucchini yellow mosaic virus coat protein (ZYMV-CP) **(A)**, tomato leaf curl New Delhi virus (ToLCNDV)-A **(B)**, and relative expression of phenylalanine ammonia lyase (PAL) in ZYMV-infected treated **(C)** and ToLCNDV-infected treated **(D)** at 5 d.p.i. with respect to infected no-treatment control. OV EO, *O. vulgare* essential oil; TV EO, *T. vulgaris* essential oil; RO EO, *R. officinalis* essential oil; OV HS, *O. vulgare* hydrosol; TV HS, *T. vulgaris* hydrosol; RO HS, *R. officinalis* hydrosol; Rib, ribavirin; Healthy, mock-inoculated plants. Columns represent mean value from 2 technical replicates on 3 pooled biological replicates, and bars indicate standard error (± SE).

no-treatment control plants coherently showed no symptoms at any time. They did not display any signal in real-time PCR assays for virus presence and were not included in relevant figures (**Figures 1A,B**, **2**).

Gas Chromatography/Mass Spectrometry Analysis

The compounds identified in EOs and HSs by GC-MS are listed in **Table 1**. Thirty-four compounds belonging to 7 chemical classes and 22 compounds belonging to 5 classes were identified in EOs and HSs, respectively. In all cases, identified compounds totally accounted for 92.55–100% of EO or HS. Phenolic compounds, mostly thymol and carvacrol, were main constituents of EOs and HSs from OV and TV, while RO EO and HS were largely composed of monoterpene hydrocarbons and oxygenated monoterpenes, respectively.

In OV EO, carvacrol accounted for 88.64% composition, followed by minor amounts of p-cymene (2.27%), thymol (1.41%), and piperitenone oxide (1.62%). As expected, due to the polarity of its phenolic moiety, a large amount of carvacrol (91.95%) was also found in the respective HS. Thymol was also present in HS and EO in similar amounts. Thymol was the main constituent of TV EO (68.02%), but in this case, p-cymene and carvacrol were also found in fairly high proportions (11.78 and 5.71%, respectively). As in the case of OV extracts, the main component of TV HS was the same of the corresponding EO (57.35%) and compounds bearing oxygenated polar groups as oxygenated monoterpenes and phenolic compounds were found in similar or higher proportions (borneol 8.74%, linalool 6.61%, terpinen-4-ol 6.47%, carvacrol 3.69%). The highest number of identified compounds (26) characterized RO EO. Its composition was described in terms of a main constituent α-pinene, accounting for 32.55% composition, followed by 7 compounds at medium concentrations ranging from 4.86 to 9.35% that belong to monoterpene hydrocarbons, oxygenated monoterpenes, and sesquiterpene hydrocarbon classes, and 13 minor components (0.12–3.57%). In the corresponding HS, oxygenated monoterpenes were main components (verbenone 33.26%, camphor 20.92%, 1,8 cineole 20.72%, borneol 15,12%).

Virus Quantification and Symptoms Expression

The relative virus titer was determined by the ΔΔCt method based on the Ct values obtained by real-time PCR amplifications and considering the EF-1α gene as the housekeeping gene and the infected no-treatment group as the control.

Treatments Applied at the Same Time With Inoculation of Zucchini Yellow Mosaic Virus or Tomato Leaf Curl New Delhi Virus

Figure 1 reports the fold change of relative virus titer (i.e., $2^{-\Delta\Delta Ct}$) for the experimental trial vs. ZYMV and ToLCNDV described in section "Treatments Applied at the Same Time With Inoculation of ZYMV or ToLCNDV." The ZYMV relative virus titer (**Figure 1A**) increased with respect to the infected no-treatment control in all treatments. Hence, in treated plants, a stimulation of virus replication rather than inhibition was observed. This effect was particularly prominent in OV and RO HS treatments. Also, the ribavirin-treated positive control gave an increase of relative virus titer. The observation of symptoms also confirmed a noticeable virus infection on all treated plants, with severe malformation of new and systemically infected leaves (**Figure 3**).

Results on ToLCNDV are reported in **Figure 1B**. The decrease of relative ToLCNDV titer with respect to infected no-treatment control was recorded in all treatments, with fold changes ranging from 10^{-3} to 10^{-4} for EOs and from 10^{-2} to 10^{-1} for HSs.

In both trials, ribavirin did not show to work as a proper positive treatment control, giving rise to an increase of relative ZYMV titer and being quite ineffective on the relative ToLCNDV titer, with respect to infected no-treatment controls.

The visual inspection of the test plants recorded severe symptoms (mosaic, malformation, blistering, stunting on leaves) on ZYMV-infected plants, independently of the treatment type. Conversely, only mild yellow mosaic was observed on treated plants inoculated with ToLCNDV, whereas severe symptoms (i.e., leaf curling, vein swelling, plant stunting) were only observed in the infected no-treatment control (**Figure 3**).

Based on these results, further experiments were performed on ToLCNDV, which proved to be more affected by EOs and HSs treatments than ZYMV, both in virus titer decrease and symptom development.

Treatments Applied at the Same Time With Inoculation of Tomato Leaf Curl New Delhi Virus (Time Course)

The evolution of ToLCNDV relative titer in leaves of treated *C. pepo* plants over time was investigated by means of an extended trial involving repeated weekly samplings until 26 d.p.i. as described in section "Treatments Applied at the Same Time With Inoculation of ToLCNDV (Time Course)." **Figure 2A** shows the fold change values obtained for relative ToLCNDV titer at different sampling times for all treatments. In the first sampling (i.e., 5 d.p.i.), the results were quite similar to the previous experiment on ToLCNDV (section "Treatments Applied at the Same Time With Inoculation of ZYMV or ToLCNDV"). At 12 d.p.i., the relative titer increased with respect to the first sampling in nearly all treatments (RO HS remaining about the same), but it remained lower than the infected no-treatment control, with fold changes ranging from 10^{-2} to 10^{-1}. At 19 d.p.i., treatments with either OV EO or OV HS were still very effective in reducing virus titer (i.e., 10^{-4}–10^{-3}-fold change). Virus titer in other treatments (i.e., TV and RO EOs and HSs) was comparable to that measured at 12 d.p.i. In the final sampling, i.e., 26 d.p.i., an increasing of virus titer ranging from 10^{1} to 10^{2} -fold was recorded in all treatments with respect to no-treatment infected control. EOs generally recorded increases of lower extent than HSs. Ribavirin treatment confirmed not to be a suitable positive control since an increase of virus titer was observed at all sampling times. The evolution of symptoms expression during time is shown in **Figure 4**, upper panels, in which at both 19 and 26 d.p.i., EO treated plants were displaying less symptoms with respect to HS plants, and more similar to healthy control.

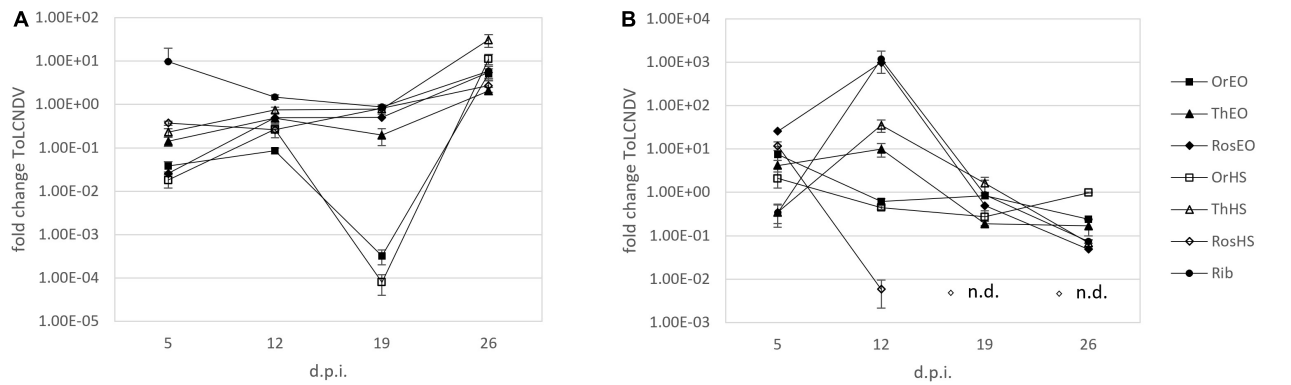

FIGURE 2 | Fold change of ToLCNDV-A in plants treated together with inoculation **(A)** and treated after inoculation **(B)** of ToLCNDV on leaves harvested at 5, 12, 19, and 26 d.p.i. OV EO, *O. vulgare* essential oil; TV EO, *T. vulgaris* essential oil; RO EO, *R. officinalis* essential oil; OV HS, *O. vulgare* hydrosol; TV HS, *T. vulgaris* hydrosol; RO HS, *R. officinalis* hydrosol; Rib ribavirin. Columns represent mean value from 2 technical replicates on 3 pooled biological replicates and bars indicate standard error (± SE).

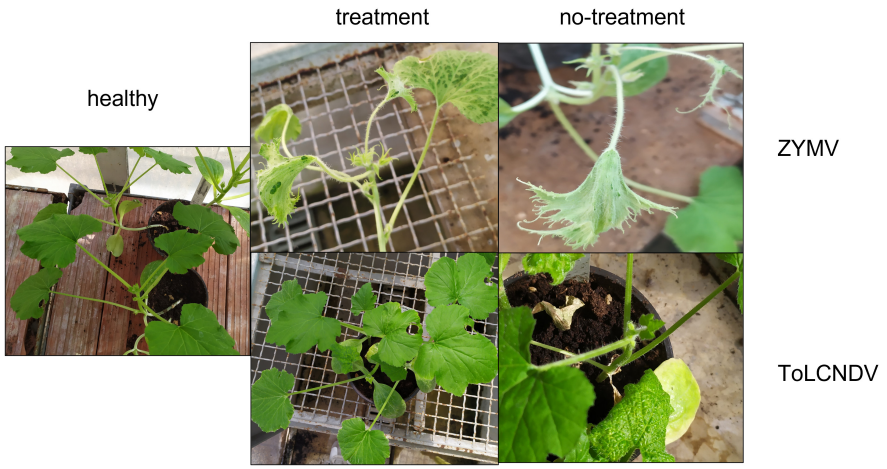

FIGURE 3 | Visual inspection of plants treated together with inoculation of ZYMV or ToLCNDV: one example treatment and the relevant no-treatment is shown for each virus.

Treatments Applied After Inoculation of Tomato Leaf Curl New Delhi Virus (Time Course)

The experimental trial described in section "Treatments Applied After Inoculation of ToLCNDV (Time Course)" was designed to evaluate the effectiveness of treatments when applied after virus inoculation (i.e., curative effect). In this case, at 5 d.p.i., ToLCNDV titer was higher in all treatments with respect to no-treatment infected control, except for TV HS. Here, we observed a viral titer reduced to one-third of the control (**Figure 2B**). In the sampling at 12 d.p.i., three treatments (i.e., OV EO and HS, and RO HS) showed a decrease of ToLCNDV titer compared to the control. Particularly, results were ca. 10^{-1}-fold decrease for OV EO and HS and ca. 10^{-3}-fold decrease for RO HS. At 19 d.p.i. in all treatments except TV HS, a decrease of virus titer was observed. In RO HS, as in the previous sampling, the decrease was most remarkable, with the virus target not detected at all in the samples. In the final sampling at 26 d.p.i., all treatments showed a virus titer lower than the control: fold changes ranged from 10^{-1} for OV EO and HS and TV EO to 10^{-2} for RO EO and TV HS. The most prominent effect was again observed in RO HS treatment, in which the virus was not detected. Pictures of the plants of these experiments at 19 and 26 d.p.i are shown in **Figure 4**, lower panels, in which HS plants appeared less diseased than EO plants, with the latter displaying leaf mosaic and curling. This observation is in agreement with the results of virus titer quantification. Specifically, HS plants shown in the pictures were those treated with RO HS, appearing completely free from disease symptoms and identical to healthy control, both at 19 and 26 d.p.i. In the same plants, ToLCNDV was not detected by real-time PCR at the same d.p.i.

Phenylalanine Ammonia Lyase Gene Expression

The relative PAL expression was determined by the $\Delta\Delta$Ct method based on the Ct values obtained by real-time

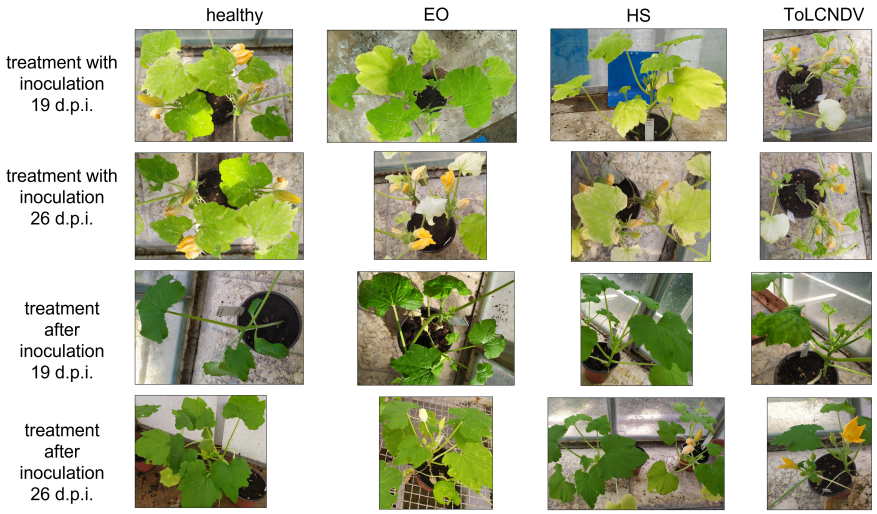

FIGURE 4 | Visual inspection of plants treated together with inoculation (upper panels) and after inoculation (lower panels) at 19 and 26 d.p.i.; the relevant healthy and infected no-treatment control is shown for each entry.

PCR amplifications and considering the EF-1α gene as the housekeeping gene and the infected no-treatment group as the control. In this work, PAL represents the first gene analyzed to investigate the antiviral mode of action performed by EOs or HSs in plant defense response.

Treatments Applied at the Same Time With Inoculation of Zucchini Yellow Mosaic Virus or Tomato Leaf Curl New Delhi Virus

Phenylalanine ammonia lyase gene relative expression levels were measured at 5 d.p.i. on treated plants compared to the infected no-treatment control for the two experimental trials on ZYMV and ToLCNDV described in section "Treatments Applied at the Same Time With Inoculation of ZYMV or ToLCNDV." The transcription levels of PAL were significantly upregulated in treated leaves infected with ZYMV (**Figure 1C**). In HS treatments, the relative expression levels increased by 5.0, 2.3, and 7.3-fold compared to the control for OV, TV, and RO, respectively. Such performance of HS treatment was of the same order of magnitude of ribavirin treatment (9.7-fold increased PAL expression level).

In ToLCNDV-infected plants (**Figure 1D**) no significant increase in PAL expression levels associated to any treatment was recorded. In order to better investigate and confirm or discard this trend, a time course experiment was run with a higher number of samplings as described in section "Treatments Applied at the Same Time With Inoculation of ToLCNDV (Time Course)".

Treatments Applied at the Same Time With Inoculation of Tomato Leaf Curl New Delhi Virus (Time Course)

The evolution of PAL expression over time in all treatments when applied at the same time of inoculation is shown in **Figure 5A**. An increased level of PAL transcript was recorded in treatments with TV and RO EOs at 12 d.p.i. (i.e., 1.3 and 1.2-fold higher than infected no-treatment control, respectively, and similar to ribavirin treatment). In samples collected at later times, no significant difference was evidenced between treatments and control.

Treatments Applied After Inoculation of Tomato Leaf Curl New Delhi Virus (Time Course)

Phenylalanine ammonia lyase gene expression levels were also studied during the time when treatments were applied 5 h after inoculation (curative effect, **Figure 5B**). In the first sampling, at 5 days d.p.i., PAL transcript showed the greatest increase observed in our experiments, with all treatments except TV HS reaching the order of magnitude of 10-fold increase with respect to control. This trend was weaker in the following observations: treatments showing signs of upregulation (i.e., TV HS at 12, 19, and 26 d.p.i, RO HS at 19 and 26 d.p.i, RO EO at 26 d.p.i.) had relative expression levels of ca. 1.2. Other treatments did not record any change in the expression of PAL with respect to infected no-treatment control.

DISCUSSION

The use of natural products from plant sources for the treatment of plant viruses is a topic of growing interest and application. Previous studies demonstrated that EOs and HSs are effective in reducing the number of local lesions due to virus infection in experimental hosts for a number of plant/virus pathosystems (Bishop, 1995; Dunkić et al., 2010; Bezić et al., 2011; Lu, 2013; Vuko et al., 2019, 2021a,b; Nazlić et al., 2021). Furthermore, gene expression studies were performed in order to identify genes and metabolic pathways involved in this action (Vuko et al., 2019). In this study, we aimed at broadening the state-of-the-art knowledge by testing two typologies of natural products (i.e., EOs

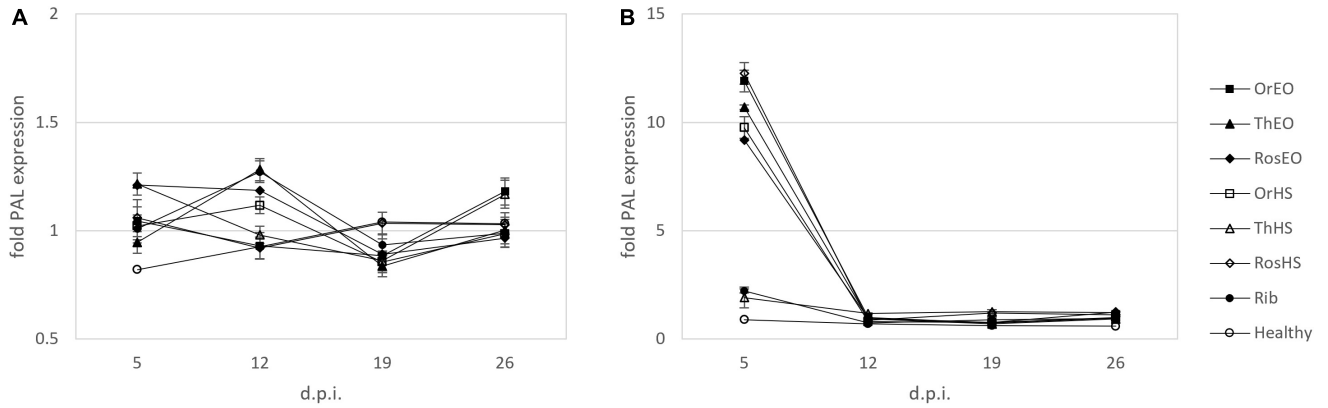

FIGURE 5 | Relative expression of PAL in plants treated together with inoculation **(A)** and treated after inoculation of ToLCNDV **(B)** on leaves harvested at 5, 12, 19, and 26 d.p.i. OV EO, *O. vulgare* essential oil; TV EO, *T. vulgaris* essential oil; RO EO, *R. officinalis* essential oil; OV HS, *O. vulgare* hydrosol; TV HS, *T. vulgaris* hydrosol; RO HS, *R. officinalis* hydrosol; Rib, ribavirin; Healthy, mock-inoculated plants. Columns represent mean value from 2 technical replicates on 3 pooled biological replicates and bars indicate standard error (± SE).

and HSs) *in vivo* on *C. pepo* plants infected by two viruses. The choice of the plant species sources of extracts to be tested was based on preliminary results from a screening of 60 EOs from different officinal plant species, indicating that OV, TV, and RO EOs can significantly decrease (Student's *t*-test) the number of local lesions in *Chenopodium amaranticolor* infected by ZYMV (data not shown, manuscript in preparation). The respective HSs from the same plant species were also included in experiments in view of the recent literature supporting biological activity of HSs as antimicrobials and antivirals (D'Amato et al., 2018; Vuko et al., 2021a,b). *C. pepo* was chosen as the host plant, being an important agricultural crop and not a model experimental host but sharing the features of easy management in greenhouse raising, artificial inoculations, and setting up of experimental trials involving biological replicates. The target viruses (i.e., ZYMV and ToLCNDV) were selected considering the great impact they have on *C. pepo* crops, causing diseases responsible for significant economic losses. Moreover, the two viruses are considerably different in some features which could be relevant for the liability of treatments, i.e., symptomatology, taxonomy, geographical distribution, genome structure and organization, and transmission mode. Resistant varieties are currently used for the control of ZYMV in *C. pepo*, but resistance breaking (RB) viral strains are becoming more and more frequent. For ToLCNDV, being an emerging pathogen, no direct control measure is yet available. Hence, for both viruses, alternative control strategies are needed. In this study, we hypothesized that the above mentioned EOs and HSs exert an antiphytoviral activity against ZYMV and ToLCNDV in *C. pepo*. We aim at demonstrating the effectiveness of such treatments in terms of virus titer and symptoms development. Further, we explore a possible mechanism of action by the quantification of PAL expression levels. These findings provide quantitative data on the effectiveness of EOs and HSs in virus control, improving the knowledge on this important topic. Our data could represent a basis for future scientific research on the mechanism of action of such treatments, and the formulation of a possible remedy which is needed in *C. pepo* cropping.

The qualitative and quantitative EO compositions reported in this work are overall in fair agreement with literature data, considering the intrinsic variability of these extracts due to a number of factors influencing the biosynthesis and metabolism of EOs components. Exogenous factors (i.e., temperature, photoperiod, soil, agronomic conditions, harvesting season, distillation methodology, plant chemotype, and cultivar) and endogenous features (i.e., part, tissue, age of the plant) are all aspects reported to strongly affect EOs composition (Barra, 2009). In OV EO, we identified carvacrol as main compound, with minor amounts of p-cymene and thymol as confirmed by previous works (Béjaoui et al., 2013; Soltani et al., 2021). The prevalence of thymol in TV EO used in our experiments identified it as belonging to the thymol chemotype (Thompson et al., 2003). RO EO was characterized by a broader composition whose main components (i.e., α-pinene, camphene, 1,8 cineole) were all reported in the literature as identified in various geographical origin RO extracts (Verma et al., 2020). HSs are still poorly studied with respect to EOs. Hence, limited data can be found in the literature regarding their main components. The composition of some HSs closely resembles that of their related EOs. Nevertheless, in some cases, HSs were reported to be completely different in quantitative and qualitative terms (Inouye et al., 2008). A general trend has risen from the analysis of several HSs compared with the associated EOs, indicating oxygenated compounds (i.e., aldehydes, alcohols, phenols, ketones, esters, and phenol methyl ethers) to often be main components (Inouye et al., 2008), while monoterpene and sesquiterpene hydrocarbons, though present in high concentrations in EOs, were quite absent in most HSs (Bellahsene et al., 2015). In agreement with this outline and with previous literature (Khan et al., 2018), carvacrol was the main compound of OV HS in our study, accounting for more than 90% of total composition. In agreement with literature data, thymol was the main component of TV HS

(D'Amato et al., 2018) and in the corresponding EO. RO HS in our experiments was characterized by a broader composition, as was also established for its related EO. Particularly, none of the components exceeded 33% of the total. Four oxygenated monoterpenes (verbenone, camphor, 1,8 cineole, and borneol), which were constituents of EO, were found in rather high proportions in HS.

Experiments in which the treatment was simultaneously applied with virus inoculation indicated an effective antiphytoviral activity vs. ToLCNDV, especially for treatments with EOs. This can probably be attributed to phenolic main compounds in OV and TV EOs, and thymol and carvacrol, having been reported as antiphytovirals (Dunkić et al., 2010). Due to the more complex composition of RO EO, speculations on the components most likely playing such biological activity are not possible. Hence, further investigation is needed. Conversely, no significant virus titer decrease was observed in ZYMV infected plants. In addition, treatments with OV and RO HSs resulted in more than 10-fold increased ZYMV titer. Further, whereas the visual inspection of symptoms provided evidence of an actual inhibition of ToLCNDV, an increase of disease severity in ZYMV infected treated plants was recorded. On the contrary, inhibition effect on ZYMV was observed in preliminary experiments on *C. amaranticolor* as described above. We hypothesize that such huge difference in activity by the same treatments against different plant or virus species could be related to the mechanism of action and nature of either the host or the virus. The poor results on ZYMV were, however, in agreement with previous literature. Particularly, that a number of EOs, including RO EO, did not display any activity against TMV *in vitro* at concentration of the same order of magnitude of our study (Lu, 2013).

For the different effectiveness against ZYMV infection on the two plant hosts, it has to be emphasized that local infection was evaluated in *C. amaranticolor,* while in experiments on *C. pepo*, systemic infection on new leaves was assayed. Hence, in the case of ZYMV, treatments could be effective locally but not systemically. In this context, the increased PAL expression levels recorded in ZYMV-infected treated plants was probably not meaningful. PAL may not be involved in effective defense response to ZYMV infection in our experimental conditions. To date, the increase of PAL expression levels as a response to virus control strategies has only been reported in case of resistance/tolerance mechanisms (Kavil et al., 2021).

A notable difference in activity was also recorded on the same host, against the two viruses, and both assayed in systemic infection. ToLCNDV and ZYMV have been classified apart in the largest subdivision of plant viruses, which was based on the chemical structure of their genomes: ToLCNDV is a ssDNA virus, while ZYMV has an RNA genome. This aspect could represent a possible reason for the different activity of extracts. Due to the unlike intrinsic nature of the genetic material, their life cycles are often very distinct from each other. For example, in the infection process, DNA viruses require a transcription step, and must be translocated to the nucleus for such stage, whereas both types need a translation step (Gergerich and Dolja, 2006). The reported and well-known activity of EOs and HSs against pathogens with DNA genome, such as bacteria and fungi (Bakkali et al., 2008; D'Amato et al., 2018), was found in agreement with the hypothesized target pest genome chemical structure role in the control of pathogenesis exerted by plant extracts. This could make DNA viruses generally more susceptible than RNA viruses to such treatments.

The positive control included in the trial (**Table 2**) was represented by treatment with ribavirin, a broad-spectrum antiviral guanosine analog (Sidwell et al., 1972). Nucleoside analogs, bearing a modified nitrogenous base, exert antiviral activity by converting into nucleotide metabolites, causing mutations in viral RNA and thus increasing the frequency of defective viral RNA. Ribavirin is reported to have inhibitory activity on plant viruses (Cassells, 1983; Lerch, 1987) and is currently used as a chemotherapy agent for *in vitro* virus elimination on many plant species (Panattoni et al., 2013; Wang et al., 2018). It had been included as a synthetic benchmark for evaluating antiphytoviral activity. Due to the unavailability of actual compounds active against plant viruses in agronomic practices, any comparison with a well characterized remedy was prevented to set up. Despite this, in our experiments, it is notable that ribavirin control did not work as expected.

The extended trial of ToLCNDV-infected treated plants was set up based on the promising data arising from the first experiment involving one single sampling at 5 d.p.i. In fact, further analyses covered a period until 26 d.p.i. and let us gain more information on the evolution of infection. In particular, when treatments were applied with inoculation, the virus titer was still lower in treated than untreated plants at 19 d.p.i. and only started to exceed the control values at 26 d.p.i. At that time, it was also noticeable that EO treatments generally caused a milder increase of virus titer with respect to HSs. We can therefore conclude that, in these experimental conditions, EOs' activity was generally slightly longer-lasting than HSs'. This could be due to the differences in amounts of active compounds and/or in chemical nature (i.e., EOs hydrophobic, HSs hydrophilic) of the two types of extract. Hence, this could result in diverse viability of treatments on plant tissues.

Virus infection evolution and plant response were also investigated in treatments applied after inoculation. The effects of treatments were generally delayed but longer lasting compared to treatments simultaneously applied with virus *inoculum*. An effective decrease of virus titer was observed only after the second sampling time, regardless of treatments. Particular attention should be paid to the remarkable effect of RO HS. Particularly, in plants treated with such extract, the virus was not detected by real-time PCR at 19 and 26 d.p.i. Additionally, tested plants did not show any symptom. The results of such time-course observations suggested that the treatments' effect on symptoms was probably longer lasting than previous studies reported. In literature, the observation was limited to one single time point, to the few hours immediately after treatment, or within a maximum period of 7 days (Helal, 2019; Vuko et al., 2021b).

Besides the assessment of virus titer, the quantification of PAL expression levels was also accomplished in order to verify whether this gene is involved in the plant defense response stimulated by treatments. PAL is the entry enzyme of the phenylpropanoid pathway, and phenylpropanoid compounds are

well known as key elements in plant defense against many microbial pathogens (La Camera et al., 2004). Hence, PAL is one of the most extensively studied enzymes in the field of plant response to biotic and abiotic stress. It has also been reported to be upregulated in case of virus infection (Gutha et al., 2010; Abdelkhalek et al., 2020) and in the set-up of resistance development (Kim and Hwang, 2014; Abdelkhalek et al., 2018) in various plant/pathogen systems.

When treatments were simultaneously applied with virus *inoculum*, this quantification showed that TV extracts were effective in increasing accumulation of PAL transcripts, especially at 12 d.p.i. TV EO has recently been reported to trigger such effect. For this elicitor activity, it has been proposed for sustainable plant protection against pathogens (Bill et al., 2017). Our results showed an early response of PAL to biotic stress that is limited to 5–12 d.p.i. In this context, earlier sampling times (i.e., < 5 d.p.i.) were envisaged in order to explore the trend of PAL transcripts in the very first few hours/days after treatment. This strategy was actually limited by the requirement to systemically sample infected new leaves. Hence, a period of delay between treatment and first sampling, which was necessary for the development of the first new, not locally inoculated/treated leaf, appeared to be unavoidable.

In the assessment of curative activity, we recorded the highest response in terms of PAL transcripts in all treatments except TV HS. The effect was limited to 5 d.p.i., while following observation points led to transcript levels similar to the control. In view of the above, we speculated that at least one part of the defense response mechanism triggered by EOs and HSs against ToLCNDV involved a modulation of expression of PAL gene.

CONCLUSION

Carvacrol and thymol were the main constituents of EO and HS extracted from OV and TV, while RO extracts displayed a more complex chemical composition, mostly monoterpene hydrocarbons in EO and oxygenated monoterpenes in HS. Antiphytoviral assays showed a decrease of ToLCNDV titer, while no or adverse effects of treatments were recorded against ZYMV. The application of treatments after inoculation, rather than simultaneously, led to a longer-lasting effect on the virus titer. In such conditions, the level of PAL transcripts also recorded a more prominent increase than in the co-inoculation of virus and treatment, although limited to the first sampling time. In our experiments, the best performance combination of treatment, mode of application, and virus was displayed by RO HS applied after ToLCNDV inoculation. In such conditions, the virus was not detected on systemically infected leaves by real-time PCR at 19 and 26 d.p.i.

Overall, our results support the feasibility of using OV, TV, and RO EOs and HSs as potential treatments for ToLCNDV-infected *C. pepo* plants under greenhouse conditions. Further investigation is needed to evaluate the applicability of such treatments for practical use in greenhouse and in the field.

DATA AVAILABILITY STATEMENT

The raw data supporting the conclusions of this article will be made available by the authors, without undue reservation.

AUTHOR CONTRIBUTIONS

AT and LT: conceptualization. AT, LT, and RR: methodology. AT, LD, and PN: formal analysis and data curation. AT, LD, FS, MS, GD, SF, VV, and RR: investigation. AT: writing—original draft preparation and visualization. AT, LD, LF, LT, MS, FS, and RR: writing—review and editing. AT and RR: supervision. All authors have read and agreed to the published version of the manuscript.

ACKNOWLEDGMENTS

We gratefully acknowledge Dr. Francesco Faggioli for helpful discussion and revision of this work.

SUPPLEMENTARY MATERIAL

The Supplementary Material for this article can be found online at: https://www.frontiersin.org/articles/10.3389/fmicb.2022.840893/full#supplementary-material

Supplementary Figure 1 | Flow diagram of the experimental procedures described in section "Treatments Applied at the Same Time With Inoculation of ZYMV or ToLCNDV"—"Treatments Applied at the Same Time With Inoculation of ToLCNDV (Time Course)" (flow **A**), and in section "Treatments Applied After Inoculation of ToLCNDV (Time Course)" (flow **B**).

REFERENCES

Abdelkhalek, A., Al-Askar, A. A., and Hafez, E. (2020). Differential induction and suppression of the potato innate immune system in response to *Alfalfa mosaic* virus infection. *Physiol. Mol. Plant Pathol.* 110:101485. doi: 10.1016/j.pmpp.2020.101485

Abdelkhalek, A., Dessoki, E. S., and Hafez, E. (2018). Polyphenolic genes expression pattern and their role in viral resistance in tomato plant infected with Tobacco mosaic virus. *Biosci. Res.* 15, 3349–3356.

Abdel-Shafi, S. (2013). Preliminary studies on antibacterial and antiviral activities of five medicinal plants. *J. Plant Pathol. Microbiol.* 04:7. doi: 10.4172/2157-7471.1000190

Bakkali, F., Averbeck, S., Averbeck, D., and Idaomar, M. (2008). Biological effects of essential oils – A review. *Food Chem. Toxicol.* 46, 446–475. doi: 10.1016/j.fct.2007.09.106

Barra, A. (2009). Factors affecting chemical variability of essential oils: a review of recent developments. *Nat. Prod. Commun.* 4, 1147–1154.

Baser, K. H. C., and Buchbauer, G. (eds) (2015). *Handbook of Essential Oils*. Boca Raton, FL: CRC Press. doi: 10.1201/b19393

Béjaoui, A., Chaabane, H., Jemli, M., Boulila, A., and Boussaid, M. (2013). Essential Oil composition and antibacterial activity of *Origanum vulgare* subsp. *glandulosum* Desf. at different phenological stages. *J. Med. Food* 16, 1115–1120. doi: 10.1089/jmf.2013.0079

Bellahsene, C., Bendahou, M., Khadir, A., Zenati, F., Benbelaid, F., Aissaoui, N., et al. (2015). Antimicrobial activity and chemical composition of essential oil and hydrosol extract of *Nepeta nepetella* subsp. *amethystina* (Poir.) Briq. from Algeria. *J. Appl. Pharm. Sci.* 5, 021–025. doi: 10.7324/JAPS.2015.50904

Bertin, S., Luigi, M., Parrella, G., Giorgini, M., Davino, S., and Tomassoli, L. (2018). Survey of the distribution of *Bemisia tabaci* (Hemiptera: Aleyrodidae) in Lazio region (Central Italy): a threat for the northward expansion of Tomato leaf curl New Delhi virus (Begomovirus: Geminiviridae) infection. *Phytoparasitica* 46, 171–182. doi: 10.1007/s12600-018-0649-7

Bezić, N., Vuko, E., Dunkić, V., Ruščić, M., Blažević, I., and Burčul, F. (2011). Antiphytoviral activity of sesquiterpene-rich essential oils from four croatian *Teucrium* species. *Molecules* 16, 8119–8129. doi: 10.3390/molecules16098119

Bill, M., Korsten, L., Remize, F., Glowacz, M., and Sivakumar, D. (2017). Effect of thyme oil vapours exposure on phenylalanine ammonia-lyase (PAL) and lipoxygenase (LOX) genes expression, and control of anthracnose in 'Hass' and 'Ryan' avocado fruit. *Sci. Hortic.* 224, 232–237. doi: 10.1016/j.scienta.2017.06.026

Bishop, C. D. (1995). Antiviral activity of the essential oil of *Melaleuca alternifolia* (Maiden amp; Betche) cheel (Tea Tree) against *Tobacco mosaic virus*. *J. Essent. Oil Res.* 7, 641–644. doi: 10.1080/10412905.1995.9700519

Božović, M., Navarra, A., Garzoli, S., Pepi, F., and Ragno, R. (2017). Esential oils extraction: a 24-hour steam distillation systematic methodology. *Nat. Prod. Res.* 31, 2387–2396. doi: 10.1080/14786419.2017.1309534

Cassells, A. C. (1983). Chemical control of virus diseases of plants. *Prog. Med. Chem.* 20, 119–155. doi: 10.1016/S0079-6468(08)70218-2

Civitelli, L., Panella, S., Marcocci, M. E., de Petris, A., Garzoli, S., Pepi, F., et al. (2014). *In vitro* inhibition of herpes simplex virus type 1 replication by *Mentha suaveolens* essential oil and its main component piperitenone oxide. *Phytomedicine* 21, 857–865. doi: 10.1016/j.phymed.2014.01.013

D'Amato, S., Serio, A., López, C. C., and Paparella, A. (2018). Hydrosols: biological activity and potential as antimicrobials for food applications. *Food Control* 86, 126–137. doi: 10.1016/j.foodcont.2017.10.030

Daferera, D. J., Ziogas, B. N., and Polissiou, M. G. (2000). GC-MS analysis of essential oils from some Greek aromatic plants and their fungitoxicity on *Penicillium digitatum*. *J. Agric. Food Chem.* 48, 2576–2581. doi: 10.1021/jf990835x

Dunkić, V., Bezić, N., Vuko, E., and Cukrov, D. (2010). Antiphytoviral activity of *Satureja montana* L. ssp. *variegata* (Host) P. W. Ball essential oil and phenol compounds on CMV and TMV. *Molecules* 15, 6713–6721. doi: 10.3390/molecules15106713

Fereres, A., and Raccah, B. (2015). *Plant Virus Transmission by Insects*. Chichester: John Wiley & Sons.

Gal-On, A. (2007). Zucchini yellow mosaic virus: insect transmission and pathogenicity?the tails of two proteins. *Mol. Plant Pathol.* 8, 139–150. doi: 10.1111/j.1364-3703.2007.00381.x

Garzoli, S., Božović, M., Baldisserotto, A., Sabatino, M., Cesa, S., Pepi, F., et al. (2018). Essential oil extraction, chemical analysis and anti- *Candida* activity of *Foeniculum vulgare* Miller – new approaches. *Nat. Prod. Res.* 32, 1254–1259. doi: 10.1080/14786419.2017.1340291

Garzoli, S., Pirolli, A., Vavala, E., di Sotto, A., Sartorelli, G., Božović, M., et al. (2015). Multidisciplinary approach to determine the optimal time and period for extracting the essential oil from *Mentha suaveolens* Ehrh. *Molecules* 20, 9640–9655. doi: 10.3390/molecules20069640

Gergerich, R. C., and Dolja, V. V. (2006). Introduction to plant viruses, the invisible Foe. *Plant Health Instr.* doi: 10.1094/PHI-I-2006-0414-01

Golino, D. A., Fuchs, M., Rwahnih, M. A., Farrar, K., Schmidt, A., and Martelli, G. P. (2017). "Regulatory aspects of grape viruses and virus diseases: certification, quarantine, and harmonization," in *Grapevine Viruses: Molecular Biology, Diagnostics and Management*, eds B. Meng, G. P. Martelli, D. A. Golino, and M. Fuchs (Cham: Springer), 581–598. doi: 10.1007/978-3-319-57706-7_28

Gutha, L. R., Casassa, L. F., Harbertson, J. F., and Naidu, R. A. (2010). Modulation of flavonoid biosynthetic pathway genes and anthocyanins due to virus infection in grapevine (*Vitis vinifera* L.) leaves. *BMC Plant Biol.* 10:187. doi: 10.1186/1471-2229-10-187

Hamim, I., Borth, W. B., Marquez, J., Green, J. C., Melzer, M. J., and Hu, J. S. (2018). Transgene-mediated resistance to *Papaya ringspot* virus: challenges and solutions. *Phytoparasitica* 46, 1–18. doi: 10.1007/s12600-017-0636-4

Helal, I. M. (2019). Use of biocides for controlling viral diseases that attack common bean and cucumber plants. *Folia Hortic.* 31, 159–170. doi: 10.2478/fhort-2019-0011

Inouye, S., Takahashi, M., and Abe, S. (2008). A comparative study on the composition of fourty four hydrosols and their essential oils. *Int. J. Essent. Oil Therap.s* 2, 89–104.

Jia, R., Zhao, H., Huang, J., Kong, H., Zhang, Y., Guo, J., et al. (2017). Use of RNAi technology to develop a PRSV-resistant transgenic papaya. *Sci. Rep.* 7:12636. doi: 10.1038/s41598-017-13049-0

Juárez, M., Tovar, R., Fiallo-Olivé, E., Aranda, M. A., Gosálvez, B., Castillo, P., et al. (2014). First detection of *Tomato leaf curl New Delhi virus* infecting zucchini in spain. *Plant Dis.* 98, 857–857. doi: 10.1094/PDIS-10-13-1050-PDN

Kavil, S., Otti, G., Bouvaine, S., Armitage, A., and Maruthi, M. N. (2021). PAL1 gene of the phenylpropanoid pathway increases resistance to the Cassava brown streak virus in cassava. *Virol. J.* 18:184. doi: 10.1186/s12985-021-01649-2

Khan, M., Khan, S. T., Khan, N. A., Mahmood, A., Al-Kedhairy, A. A., and Alkhathlan, H. Z. (2018). The composition of the essential oil and aqueous distillate of *Origanum vulgare* L. growing in Saudi Arabia and evaluation of their antibacterial activity. *Arab. J. Chem.* 11, 1189–1200. doi: 10.1016/j.arabjc.2018.02.008

Kim, D. S., and Hwang, B. K. (2014). An important role of the pepper phenylalanine ammonia-lyase gene (PAL1) in salicylic acid-dependent signalling of the defence response to microbial pathogens. *J. Exp. Bot.* 65, 2295–2306. doi: 10.1093/jxb/eru109

La Camera, S., Gouzerh, G., Dhondt, S., Hoffmann, L., Fritig, B., Legrand, M., et al. (2004). Metabolic reprogramming in plant innate immunity: the contributions of phenylpropanoid and oxylipin pathways. *Immunol. Rev.* 198, 267–284. doi: 10.1111/j.0105-2896.2004.0129.x

Labadie, C., Cerutti, C., and Carlin, F. (2016). Fate and control of pathogenic and spoilage micro-organisms in orange blossom (*Citrus aurantium*) and rose flower (*Rosa centifolia*) hydrosols. *J. Appl. Microbiol.* 121, 1568–1579. doi: 10.1111/jam.13293

Lamichhane, J. R., Dachbrodt-Saaydeh, S., Kudsk, P., and Messéan, A. (2016). Toward a reduced reliance on conventional pesticides in European agriculture. *Plant Dis.* 100, 10–24. doi: 10.1094/PDIS-05-15-0574-FE

Lecoq, H., and Katis, N. (2014). Control of cucurbit viruses. *Adv. Virus Res.* 90, 255–296. doi: 10.1016/B978-0-12-801246-8.00005-6

Lerch, B. (1987). On the inhibition of plant virus multiplication by ribavirin. *Antiviral Res.* 7, 257–270. doi: 10.1016/0166-3542(87)90010-6

Livak, K. J., and Schmittgen, T. D. (2001). Analysis of relative gene expression data using real-time quantitative PCR and the 2–ΔΔCT method. *Methods* 25, 402–408. doi: 10.1006/meth.2001.1262

Lu, M. (2013). *In vitro* and *in vivo* anti-*Tobacco mosaic virus* activities of essential oils and individual compounds. *J. Microbiol. Biotechnol.* 23, 771–778. doi: 10.4014/jmb.1210.10078

Luigi, M., Manglli, A., Valdes, M., Sitzia, M., Davino, S., and Tomassoli, L. (2016). Occurrence of *Tomato leaf curl New Delhi virus* infecting Zucchini in Sardinia (Italy). *J. Plant Pathol.* 98, 677–697.

Manglli, A., Bertin, S., and Tomassoli, L. (2019). Preliminary analysis of ZYMV and WMV interaction in mixed infection by ΔΔCt Rt-qPCR. *Int. Adv. Plant Virol.* 2019:95.

Martín-Hernández, A. M., and Picó, B. (2020). Natural resistances to viruses in cucurbits. *Agronomy* 11:23. doi: 10.3390/agronomy11010023

Naik, P. S., and Buckseth, T. (2018). "Recent advances in virus elimination and tissue culture for quality potato seed production," in *Biotechnologies of Crop Improvement*, Vol. Volume 1, eds S. Gosal and S. H. Wani (Cham: Springer International Publishing), 131–158. doi: 10.1007/978-3-319-78283-6_4

Navas-Castillo, J., Fiallo-Olivé, E., and Sánchez-Campos, S. (2011). Emerging virus diseases transmitted by whiteflies. *Annu. Rev. Phytopathol.* 49, 219–248. doi: 10.1146/annurev-phyto-072910-095235

Nazlić, M., Fredotović, Ž, Vuko, E., Fabijanić, L., Kremer, D., Stabentheiner, E., et al. (2021). Wild Species *Veronica officinalis* L. and *Veronica saturejoides* Vis. ssp. saturejoides—biological potential of Free Volatiles. *Horticulturae* 7:295. doi: 10.3390/horticulturae7090295

NIST (2017). *NIST/EPA/NIH EI-MS Library*. Gaithersburg, MD: NIST.

Obrero, Á, Die, J. V., Román, B., Gómez, P., Nadal, S., and González-Verdejo, C. I. (2011). Selection of reference genes for gene expression studies in Zucchini

(*Cucurbita pepo*) using qPCR. *J Agric. Food Chem.* 59, 5402–5411. doi: 10.1021/jf200689r

Othman, B. A., and Shoman, S. A. (2004). Antiphytoviral activity of the *Plectranthus tenuiflorus* on some important viruses. *Int. J. Agric. Biol.* 6, 844–849.

Ozturk, I., Tornuk, F., Caliskan-Aydogan, O., Durak, M. Z., and Sagdic, O. (2016). Decontamination of iceberg lettuce by some plant hydrosols. *LWT* 74, 48–54. doi: 10.1016/j.lwt.2016.06.067

Padidam, M., Beachy, R. N., and Fauquet, C. M. (1995). Tomato leaf curl geminivirus from India has a bipartite genome and coat protein is not essential for infectivity. *J. Gen. Virol.* 76, 25–35. doi: 10.1099/0022-1317-76-1-25

Panattoni, A., Luvisi, A., and Triolo, E. (2013). Review. Elimination of viruses in plants: twenty years of progress. *Span. J. Agric. Res.* 11:173. doi: 10.5424/sjar/2013111-3201

Panno, S., Iacono, G., Davino, M., Marchione, S., Zappardo, V., Bella, P., et al. (2016). First report of *Tomato leaf curl New Delhi virus* affecting zucchini squash in an important horticultural area of southern Italy. *New Dis. Rep.* 33:6. doi: 10.5197/j.2044-0588.2016.033.006

Paris, H. S., and Brown, R. N. (2005). The genes of pumpkin and squash. *HortScience* 40, 1620–1630. doi: 10.21273/HORTSCI.40.6.1620

Rajeswara Rao, B. R. (2013). Hydrosols and water-soluble essential oils: medicinal and biological properties. *Recent Progr. Med. Plants Essent. Oils I* 36, 119–140.

Raveau, R., Fontaine, J., and Lounès-Hadj Sahraoui, A. (2020). Essential oils as potential alternative biocontrol products against plant pathogens and weeds: a review. *Foods* 9:365. doi: 10.3390/foods9030365

Rubio, L., Galipienso, L., and Ferriol, I. (2020). Detection of plant viruses and disease management: relevance of genetic diversity and evolution. *Front. Plant Sci.* 11:1092. doi: 10.3389/fpls.2020.01092

Sabatino, M., Fabiani, M., Božović, M., Garzoli, S., Antonini, L., Marcocci, M. E., et al. (2020). Experimental data based machine learning classification models with predictive ability to select *in vitro* active antiviral and non-toxic essential oils. *Molecules* 25:2452. doi: 10.3390/molecules25102452

Sağdıç, O. (2003). Sensitivity of four pathogenic bacteria to Turkish thyme and oregano hydrosols. *LWT Food Sci. Technol.* 36, 467–473. doi: 10.1016/S0023-6438(03)00037-9

Sidwell, R. W., Huffman, J. H., Khare, L. G. P., Allen, B., Witkowski, R. J. T., and Robins, K. (1972). Broad-spectrum antiviral activity of virazole: 1-β-D-Ribofuranosyl-1,2,4-triazole-3-carboxamide. *Science* 177, 705–706. doi: 10.1126/science.177.4050.705

Simón, A., Ruiz, L., Velasco, L., and Janssen, D. (2018). Absolute quantification of *Tomato leaf curl New Delhi virus* Spain strain, ToLCNDV-ES: virus accumulation in a host-specific manner. *Plant Dis.* 102, 165–171. doi: 10.1094/PDIS-06-17-0840-RE

Soltani, S., Shakeri, A., Iranshahi, M., and Boozarib, M. (2021). A review of the phytochemistry and antimicrobial properties of *Origanum vulgare* L. and subspecies. *Iran J. Pharm. Res.* 20, 268–285. doi: 10.22037/ijpr.2020.113874.14539

Soosaar, J. L. M., Burch-Smith, T. M., and Dinesh-Kumar, S. P. (2005). Mechanisms of plant resistance to viruses. *Nat. Rev. Microbiol.* 3, 789–798. doi: 10.1038/nrmicro1239

Speranza, B., and Corbo, M. R. (2010). *Application Of Alternative Food-Preservation Technologies To Enhance Food Safety And Stability*, eds A. Bevilacqua, M. Rosaria, and M. Sinigaglia (Sharjah: Bentham Science Publishers). doi: 10.2174/9781608050963110010 1

Thompson, J. D., Chalchat, J.-C., Michet, A., Linhart, Y. B., and Ehlers, B. (2003). Qualitative and quantitative variation in monoterpene co-occurrence and composition in the essential oil of *Thymus vulgaris* chemotypes. *J. Chem. Ecol.* 29, 859–880. doi: 10.1023/A:1022927615442

Tornuk, F., Cankurt, H., Ozturk, I., Sagdic, O., Bayram, O., and Yetim, H. (2011). Efficacy of various plant hydrosols as natural food sanitizers in reducing *Escherichia coli* O157:H7 and *Salmonella typhimurium* on fresh cut carrots and apples. *Int. J. Food Microbiol.* 148, 30–35. doi: 10.1016/j.ijfoodmicro.2011.04.022

Verma, R. S., Padalia, R. C., Chauhan, A., Upadhyay, R. K., and Singh, V. R. (2020). Productivity and essential oil composition of rosemary (*Rosmarinus officinalis* L.) harvested at different growth stages under the subtropical region of north India. *J. Essent. Oil Res.* 32, 144–149. doi: 10.1080/10412905.2019.1684391

Vuko, E., Dunkić, V., Maravić, A., Ruščić, M., Nazlić, M., Radan, M., et al. (2021a). Not only a weed plant—biological activities of essential oil and hydrosol of *Dittrichia viscosa* (L.) Greuter. *Plants* 10:1837. doi: 10.3390/plants10091837

Vuko, E., Dunkić, V., Ruščić, M., Nazlić, M., Mandić, N., Soldo, B., et al. (2021b). Chemical composition and new biological activities of essential oil and hydrosol of *Hypericum perforatum* L. ssp. *veronense* (Schrank) H. Lindb. *Plants* 10:1014. doi: 10.3390/plants10051014

Vuko, E., Rusak, G., Dunkić, V., Kremer, D., Kosalec, I., Rađa, B., et al. (2019). Inhibition of satellite RNA associated cucumber mosaic virus infection by essential oil of *Micromeria croatica* (Pers.) Schott. *Molecules* 24:1342. doi: 10.3390/molecules24071342

Walkey, D. G. A., Lecoq, H., Collier, R., and Dobson, S. (1992). Studies on the control of zucchini yellow mosaic virus in courgettes by mild strain protection. *Plant Pathol.* 41, 762–771. doi: 10.1111/j.1365-3059.1992.tb02560.x

Wang, M.-R., Cui, Z.-H., Li, J.-W., Hao, X.-Y., Zhao, L., and Wang, Q.-C. (2018). *In vitro* thermotherapy-based methods for plant virus eradication. *Plant Methods* 14:87. doi: 10.1186/s13007-018-0355-y

You, B.-J., Chiang, C.-H., Chen, L.-F., Su, W.-C., and Yeh, S.-D. (2005). Engineered mild strains of *Papaya ringspot* virus for broader cross protection in *Cucurbits*. *Phytopathology®* 95, 533–540. doi: 10.1094/PHYTO-95-0533

Zhang, S., Liu, J., Xu, B., and Zhou, J. (2021). Differential responses of *Cucurbita pepo* to *Podosphaera xanthii* reveal the mechanism of powdery mildew disease resistance in pumpkin. *Front. Plant Sci.* 12:633221. doi: 10.3389/fpls.2021.633221

Zhao, L., Feng, C., Wu, K., Chen, W., Chen, Y., Hao, X., et al. (2017). Advances and prospects in biogenic substances against plant virus: a review. *Pestic. Biochem. Physiol.* 135, 15–26. doi: 10.1016/j.pestbp.2016.07.003

Conflict of Interest: The authors declare that the research was conducted in the absence of any commercial or financial relationships that could be construed as a potential conflict of interest.

Publisher's Note: All claims expressed in this article are solely those of the authors and do not necessarily represent those of their affiliated organizations, or those of the publisher, the editors and the reviewers. Any product that may be evaluated in this article, or claim that may be made by its manufacturer, is not guaranteed or endorsed by the publisher.

frontiers | Frontiers in Microbiology

ORIGINAL RESEARCH
published: 29 April 2022
doi: 10.3389/fmicb.2022.889878

Retrieving the *in vivo* Scopoletin Fluorescence Excitation Band Allows the Non-invasive Investigation of the Plant–Pathogen Early Events in Tobacco Leaves

Giovanni Agati[1,2], Cecilia Brunetti[3], Lorenza Tuccio[1,2], Ilaria Degano[4] and Stefania Tegli[2,5]*

[1] Istituto di Fisica Applicata "Nello Carrara" (IFAC), Consiglio Nazionale delle Ricerche, Sesto Fiorentino, Italy, [2] Consortium INSTM-Italian Interuniversity Consortium for Science and Technology of Materials, Firenze, Italy, [3] Istituto per la Protezione Sostenibile delle Piante (IPSP), Consiglio Nazionale delle Ricerche, Sesto Fiorentino, Italy, [4] Dipartimento di Chimica e Chimica Industriale, Università di Pisa, Pisa, Italy, [5] Department of Agriculture, Food, Environment and Forestry (DAGRI), University of Florence, Sesto Fiorentino, Italy

OPEN ACCESS

Edited by:
Marco Scortichini, Council for Agricultural Research and Economics (CREA), Italy

Reviewed by:
Yasuhiro Ishiga, University of Tsukuba, Japan
Karin E. Groten, Max Planck Institute for Chemical Ecology, Germany
Monica De Caroli, University of Salento, Italy

***Correspondence:**
Giovanni Agati
g.agati@ifac.cnr.it

Specialty section:
This article was submitted to Microbe and Virus Interactions with Plants, a section of the journal Frontiers in Microbiology

Received: *04 March 2022*
Accepted: *25 March 2022*
Published: *29 April 2022*

Citation:
Agati G, Brunetti C, Tuccio L, Degano I and Tegli S (2022) Retrieving the in vivo Scopoletin Fluorescence Excitation Band Allows the Non-invasive Investigation of the Plant–Pathogen Early Events in Tobacco Leaves. Front. Microbiol. 13:889878. doi: 10.3389/fmicb.2022.889878

In this study, we developed and applied a new spectroscopic fluorescence method for the *in vivo* detection of the early events in the interaction between tobacco (*Nicotiana tabacum* L.) plants and pathogenic bacteria. The leaf disks were infiltrated with a bacterial suspension in sterile physiological solution (SPS), or with SPS alone as control. The virulent *Pseudomonas syringae* pv. *tabaci* strain ATCC 11528, its non-pathogenic Δ*hrpA* mutant, and the avirulent *P. syringae* pv. *tomato* strain DC3000 were used. At different post-infiltration time–points, the *in vivo* fluorescence spectra on leaf disks were acquired by a fiber bundle-spectrofluorimeter. The excitation spectra of the leaf blue emission at 460 nm, which is mainly due to the accumulation of coumarins following a bacterial infiltration, were processed by using a two-bands Gaussian fitting that enabled us to isolate the scopoletin (SCT) contribution. The pH-dependent fluorescence of SCT and scopolin (SCL), as determined by *in vitro* data and their intracellular localization, as determined by confocal microscopy, suggested the use of the longer wavelength excitation band at 385 nm of 460 nm emission (F_{385_460}) to follow the metabolic evolution of SCT during the plant–bacteria interaction. It was found to be directly correlated (R^2 = 0.84) to the leaf SCT content, but not to that of SCL, determined by HPLC analysis. The technique applied to the time-course monitoring of the bacteria–plant interaction clearly showed that the amount and the timing of SCT accumulation, estimated by F_{385_460}, was correlated with the resistance to the pathogen. As expected, this host defense response was delayed after *P. syringae* pv. *tabaci* ATCC 11528 infiltration, in comparison to *P. syringae* pv. *tomato* DC3000. Furthermore, no significant increase of F_{385_460} (SCT) was observed when using the non-pathogenic Δ*hrpA* mutant of *P. syringae* pv. *tabaci* ATCC 11528, which lacks a functional Type Three Secretion System (TTSS). Our study showed the reliability of the developed fluorimetric method

for a rapid and non-invasive monitoring of bacteria-induced first events related to the metabolite-based defense response in tobacco leaves. This technique could allow a fast selection of pathogen-resistant cultivars, as well as the on-site early diagnosis of tobacco plant diseases by using suitable fluorescence sensors.

Keywords: fluorescence spectroscopy, non-destructive detection, scopolin, scopoletin, *Nicotiana tabacum*, *Pseudomonas syringae*, hypersensitive response, type III secretion system

INTRODUCTION

During the interaction with their potential host plants, the pathogenic microorganisms are exposed to a wide array of antimicrobial compounds. Phytoalexins are among the most important plant secondary metabolites, playing a key role in the host immune response. These low molecular weight compounds are newly produced and locally accumulate in the plant tissues following the application of biotic or abiotic stresses (Ahmed and Kovinich, 2021). Despite their common and conserved biological activity, phytoalexins belong to several chemical families, which can be sometimes specifically associated to different botanical families.

The phytoalexin scopoletin (6-methoxy-7-hydroxycoumarin) (SCT) is synthesized through the phenylpropanoid pathway by many plant species. The SCT and other coumarins are beneficial for plants because of their antimicrobial and antioxidant properties (Stringlis et al., 2019), as well as for their role in iron uptake (Robe et al., 2020). In addition, coumarins are rather valuable for humans because of their multiple pharmacological properties (Stefanachi et al., 2018).

Together with capsidiol, SCT represents the major phytoalexin in tobacco (*Nicotiana tabacum* L.), and its accumulation in the leaf tissues has been correlated with *N. tabacum* resistance toward several phytopathogens (Ahuja et al., 2012). Actually, unless a stress is applied, SCT is not generally present in the plant tissues in its free state, because for the most part it accumulates in the vacuoles as its 7-β-D-glucoside form, named scopolin (SCL) (Hino et al., 1982).

Similar to most coumarins, SCT and SCL are strongly fluorescent under UVA excitation, as already reported in the 1960s (Crosby and Berthold, 1962; Dieterman et al., 1964), and thus their presence in plant tissues can be detected by fluorescence spectroscopy. An *in vivo* bright blue autofluorescence under UV excitation was first observed in tobacco leaf tissues treated with a hypersensitive reaction-inducing elicitor, and it was related to the SCT accumulation into plant tissues upon elicitor exposure (Dorey et al., 1997).

A correlation between the presence of SCL and SCT and the UV-excited blue fluorescence was then confirmed in tobacco leaves infected with the tobacco mosaic virus (TMV) (Chong et al., 2002; Costet et al., 2002).

In addition, SCT was linked to the blue autofluorescence detected 4 days after the infection by *B. cinerea* of the tobacco resistant Petit Havana cultivar (El Oirdi et al., 2010).

The resistance of *N. attenuata* to *A. alternata* was also associated with a strong blue autofluorescence, depending on a functional feruloyl-CoA 6′-hydroxylase 1, that is the essential enzyme in the SCT biosynthesis. Accordingly, the accumulation of SCT and SCL, the fluorescence intensity, and the resistance to *A. alternata* infection were higher in young leaves than in fully expanded leaves (Sun et al., 2014).

Overall, these evidences suggest that the non-destructive optical sensing of *in planta* fluorescence could be employed for the quantitative monitoring of the very early defense events related to the attack by a virulent or avirulent pathogen. So far, the multispectral fluorescence and thermal imaging have been successfully proved to detect the first steps of the interaction occurring between plants and their viral, bacterial and even fungal pathogens (Chaerle et al., 2007; Barón et al., 2016; Hupp et al., 2019). A similar non-destructive approach may represent an efficient and cost-effective strategy for monitoring the plant health status in the field. Time-course analyses on the very same plant would also be possible, avoiding most of the variability inherent to the biological samples. Moreover, its application on a laboratory scale would be a valid alternative to the current methods used for the quantitative evaluation of coumarins in leaf exudates (El Modafar et al., 1995; Churngchow and Rattarasarn, 2001) or leaf extracts (Sun et al., 2014). However, the fluorescence-based techniques used up to now are based on a single excitation wavelength and the related blue emission band detection, usually calibrated against SCT, and they cannot distinguish between the contribution to fluorescence of the coumarins present in the tobacco plants.

The present work aimed to characterize the *in vivo* fluorescence signals of *N. tabacum* bacteria-infected leaves by spectroscopic methods. Here, for the first time, the *in vivo* blue fluorescence contributions given by SCL and SCT, were discriminated by the elaboration of the fluorescence excitation spectra from tobacco leaves infiltrated with virulent, avirulent and even non-pathogenic *Pseudomonas syringae* strains. This allowed the validation of the spectroscopic approach as a new and efficient non-destructive technique for diagnostic monitoring of the very early events of the plant–pathogen interaction.

MATERIALS AND METHODS

Plants and Bacteria Used

The tobacco plants (*N. tabacum* var. ITB 6178) (Bergerac Seed & Breeding Soc., Bergerac, France) were grown into pots containing a compost–soil substrate, under controlled conditions (16 h day/8 h night, at temperature 22°C/18°C, and 70% relative humidity). Fully expanded leaves from 10 to 14 weeks old plants were used for the experiments.

P. syringae pv. *tomato* DC3000, *P. syringae* pv. *tabaci* ATCC 11528 and its Δ*hrpA* mutant, constructed according to Cerboneschi et al. (2016) (Tegli, unpublished data), were routinely grown at 26°C in liquid or agarised King's B medium (KB) (King et al., 1954), and long-term stored in 40% (v/v) aqueous glycerol solution at −80°C.

Leaf Disks Bacterial Infiltration

Overnight liquid bacterial cultures (20 ml KB) were incubated at 26°C, under continuous orbital shaking (100 rpm). Then, the bacterial cultures were centrifuged at 8.000*g* for 10 min, and the pellet washed twice in sterile physiological solution (SPS) (0.85% NaCl in distilled water), and resuspended up in SPS to a final OD_{600} = 0.5 (approximately 0.5 × 10^8 CFU ml^{-1}).

Leaf disks were obtained from the youngest fully expanded leaves of adult plants, by using a cork borer (11-mm diameter). From each freshly detached leaf, 35 disks were obtained and placed into Petri dishes containing SPS until used for bacterial infiltration. For each bacterial treatment, a sample of 10 disks randomly selected was used, and three replicates were made for each inoculation trial. Each leaf disk sample was then placed in a 50-ml sterile centrifuge tube containing a 20-ml bacterial suspension, and then infiltrated under vacuum, according to Johansson with minor modifications (Johansson et al., 2015). As a negative control, SPS was used for infiltration. For each treatment, infiltrated leaf disks were separately processed. After the vacuum infiltration step, the leaf disks were rinsed 3 times with sterile distilled water, then transferred on sterile filter paper to dry the excess of water, before to be incubated into sterile empty Petri dishes (90-mm diameter) in moist sterile conditions at 28°C in the dark.

In situ and *in vitro* Fluorescence Spectroscopy

Scopolin (PhytoLab GmbH & Co. KG, Vestenbergsgreuth, Germany), SCT, and chlorogenic acid (CGA) (both from Sigma–Aldrich, Milano, Italy) were dissolved in ethanol (0.3–0.6 mg ml^{-1}) and then diluted with a phosphate buffer solution at different pH values (2.6, 5.4, 6.7, 7.2, 7.6, and 8.5), to achieve final concentrations ranging between 30 and 70 μM. The actual pH of solutions was measured with a HI 2211 pH meter (Hanna Instruments, Woonsocket, RI, United States). All chemicals and solvents used were of HPLC grade.

The UV-absorbance spectra were recorded by a Jasco V-560 spectrophotometer (Jasco, Tokyo, Japan). The fluorescence spectra were recorded by a Cary Eclipse spectrofluorimeter (Agilent Technologies, Cernusco sul Naviglio, Milano, Italy) in a 10 × 10-mm quartz cuvette, after diluting the sample solutions to get an absorbance of about 0.1 at the excitation wavelength. Setting of acquisition parameters, gain and slit width, were adjusted for each sample to avoid signal saturation.

To compare the *in vitro* fluorescence efficiency of compounds, the same acquisition parameters (exc/em slits = 2.5/2.5 nm, PMT voltage = 850 V) were used and fluorescence intensities were divided by the absorbed fraction (1 - $10^{-A\lambda exc}$) at the excitation wavelength.

The *in vivo* fluorescence spectra on leaf disks were acquired at different times of incubation by the above described spectrofluorimeter equipped with a bifurcate fiber bundle on a spot of 6-mm diameter, with a PMT voltage of 850 V, slit widths of exc/em monochromators of 5/10 nm and 10/5 nm for the excitation and emission acquisition, respectively. The scan rate was 600 nm min^{-1} and the averaging time was 0.2 s.

The excitation spectra were corrected for the wavelength dependency of the detector system.

Confocal Laser Scanning Microscopy

Leaf disks (11-mm diameter) were mounted in water on microscope slides and observed by using a Leica TCS SP8 confocal upright microscope (Leica Microsystems CMS, Mannheim, Germany) equipped with a 63× objective (HC PL APO CS2 63 × /1.40 OIL).

The laser excitation at 405 nm was set at 40% of maximal intensity and used to acquire blue fluorescence of coumarins over the 430–498-nm emission spectral band, with gain at 850. The chlorophyll fluorescence was acquired under 638-nm excitation at 35% of maximal intensity over the 695–765-nm emission spectral band, with gain at 632. The image spatial calibration was between 0.057 and 0.241 μm $pixels^{-1}$.

Extraction and Analysis of Phenolic Compounds

Leaf disks (30 mg/sample) were ground with liquid nitrogen and extracted 3 times with 0.5 ml of 75% MeOH/H_2O adjusted to pH 2.5 with formic acid. The supernatant was defatted with 1 ml of *n*-hexane and then centrifuged before 20 μl of the extract was injected into the Jasco HPLC system. It consisted of a Jasco PU-4180 RHPLC pump, a MD-4010 PDA detector followed in series by a FP-4025 fluorescence detector, an AS-4050 autosampler injection valve and LC-Net II/ADC interface [Jasco Europe S.R.L., Cremella (LC), Italy].

The LC separation was performed on a reverse phase column (Kinetex Phenomenex C18, 150 × 4.6 mm, 5 μm) maintained at 25°C (Jasco CO-4060 column oven) and using mobile phase A (water 0.1% formic acid) and mobile phase B (CH_3CN 0.1% formic acid) in a gradient program with a flow of 0.6 ml min^{-1}: 0-2 min 100% A, 2-22 min 100-80% A, 22-24 min 80% A, 24-34 min 80-10% A, 34-44 min 10-0% A, 44-50 min 100% B. Then SCT, SCL, and CGA were identified by comparison of their retention times and UV spectral characteristics with those of authentic standards and quantified using five-point calibration curves of authentic standards. Chlorogenic acid was quantified by absorbance at 330 nm, whereas SCT and SCL were quantified using fluorescence chromatograms with excitation wavelength at 340 nm and emission responses at 460 nm, with the PMT gain value set at 100.

A further HPLC-ESI-MS/MS analysis was used to investigate the leaf extract composition and the possible assignment of the minor fluorescent compounds with retention times longer than 30 min.

For the HPLC-MS analysis the system consisted of an HPLC 1200 Infinity, coupled with a quadrupole-time of flight mass

spectrometer Infinity Q-ToF 6530 detector through a Jet Stream ESI interface (Agilent Technologies). The ESI conditions were as listed as follows: Drying and sheath gas N_2, purity > 98%, temperature 350°C, flow 10 L/min and temperature 375°C, flow 11 L/min, respectively; capillary voltage 4.5 kV; nebulizer gas pressure 35 psi. The fragmentor, nozzle, skimmer, and octapole RF voltages were set at 175, 1000, 65, and 750 V, respectively. The high-resolution MS and MS/MS acquisition range was set from 100 to 1000 m/z in in positive mode, with acquisition rate 1.04 spectra/s. For the MS/MS experiments, 30 V were used (collision gas N_2).

The eluents used for the HPLC–ESI–Q–ToF analyses were LC–MS grade (Sigma–Aldrich, United States) water (eluent A) and acetonitrile (eluent B), both added with 0.1% v/v formic acid (98% purity, J.T. Baker, United States).

The chromatographic separation was performed at 30°C on an analytical reversed-phase column Poroshell 120 EC-C18 (3.0 × 75-mm, 2.7 μm) with a Zorbax pre-column (4.6 × 12.5 mm, 5 μm), both Agilent Technologies. The flow rate was 0.4 ml/min and the program was 0–2.6 min 5% B, 2.6–15.6 min 5–50% B, 15.6–20.8 min 50–70% B, 20.8–27 min 70–100% B, then held for 7 min. The re-equilibration took 10 min. The injection volume was 20 μl.

Data Analysis

Statistical analysis and curve fitting were carried out with the SigmaPlot for Windows Version 14.0 software (Systat Software, Inc., San Jose, CA). Mean values of data underwent t-test or one-way analysis of variance (ANOVA) repeated measures and were compared by the all pairwise multiple comparison Holm–Sidak test; $p < 0.05$ values were considered statistically significant.

The fitting of the excitation fluorescence spectra of SCL and SCT standard compounds at pH 5.4 was performed by using a single-Gaussian curve with a 3-parameter function:

$$f = ae^{-\left[\frac{1}{2}\cdot\left(\frac{x-x_0}{b}\right)^2\right]} \quad (1)$$

where, a is the amplitude of the curve band, x_0 is the central wavelength, and b is the standard deviation of a normal data distribution, which is related to the full width at half maximum (FWHM) of the band by $b \approx 2.355/\mathrm{FWHM}$. In the fitting, these three parameters were set to be free, without any constraint.

For the SCT coumarin at pH 8.5, the linear combination of two-Gaussian curves with a user-defined function:

$$f = ae^{-\left[\frac{1}{2}\cdot\left(\frac{x-x_0}{b}\right)^2\right]} + ce^{-\left[\frac{1}{2}\cdot\left(\frac{x-x_1}{d}\right)^2\right]} \quad (2)$$

was applied. So that three additional parameters c, x_1, and d, corresponding to the amplitude, central wavelength, and standard deviation of the second Gaussian curve were added. In the fitting, the central wavelength and bandwidth of one curve, x_0 and b, respectively, were set close to those found for SCT at pH 5.4, while the other four parameters were set to be free.

The *in vivo* fluorescence excitation spectra measured on leaf disks were fitted with the two-Gaussian curve (Eq. 2).

The coefficient of determination, R^2, was used to estimate the fitting quality.

RESULTS

The early responses of the tobacco leaves during the interaction with several *P. syringae* strains was evaluated by measuring *in situ* the excitation and emission fluorescence spectra of leaf disks. In **Figure 1**, the spectra acquired on samples at different times (h) post-infiltration (hpi) with *P. syringae* pv. *tomato* DC3000 are reported.

The leaf fluorescence emission and excitation spectra were both observed to significantly increase with post-infiltration time. Interestingly, while the shape of the emission spectra, peaked at 460 nm, did not change with time, the main band of the excitation spectra shifted from around 335 nm to 360 nm, receiving a larger contribution at longer wavelengths.

Confocal Microscopy

Knowing the distribution of fluorophores inside the leaf tissues is fundamental for the analysis of the *in situ* fluorescence spectra. Therefore, we performed confocal microscopy analyses of leaf disks infiltrated by *P. syringae* pv. *tomato* DC3000 or SPS as shown in **Figure 2**. The intracellular localization of blue autofluorescence, under excitation at 405 nm, appeared rather heterogenous between vacuole and cytoplasm depending on the treatment and the time post-inoculation. Some samples presented strictly vacuolar localization of blue fluorescence (**Figures 2B,E,F**). Others clearly showed the presence of intense cytoplasmatic blue fluorescence, besides vacuolar fluorescence, as "lenticels" shape structures confined near to plasma membrane (**Figures 2A,C,D**). In the bacterial infiltrated samples, a much higher fluorescence than that of the SPS-infiltrated samples was observed in the epidermal cells (**Figure 2G** vs. **Figure 2H**). The control SPS-infiltrated leaf disks showed fluorescence only in the vacuole, even long time (i.e., 51 hpi) after the treatment (**Figures 2E,F**).

The leaf fluorescence assignment to specific compounds during the interaction with pathogens can be better addressed on the basis of the *N. tabacum* leaf phytochemical composition and the *in vitro* absorption and fluorescence properties of the major constituents.

Main Phenolic Compounds in Untreated and Infiltrated Leaves

The polyphenolic composition of tobacco leaves was determined by the HPLC analysis of leaf disk extracts collected before and after the bacterial infiltration. In **Figure 3**, chromatograms representative of the leaf samples at 18 hpi are reported. The principal phenolic compounds were CGA, SCL, and SCT. Some other minor peaks appeared at retention times higher than 30 min. These compounds could not be definitely identified because of their low contributions to the HPLC absorbance signals that impaired the acquisition of proper DAD spectra. Their detection by tandem mass spectrometry did not provide conclusive results. We estimated, however, that in the fluorescence chromatograms the sum of the unidentified peaks relative to those of SCL plus SCT was less than 10% on average. Therefore, we consider them not relevant.

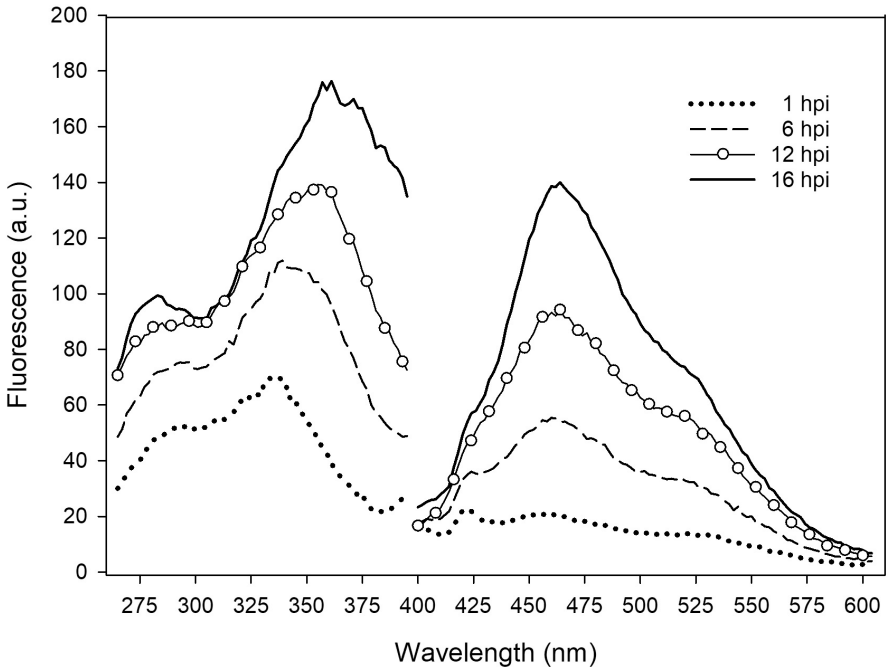

FIGURE 1 | *In situ* emission and excitation fluorescence spectra of tobacco leaf disk infiltrated with *P. syringae* pv. *tomato* DC3000 recorded on the adaxial side at different hpi. The emission spectra were acquired under excitation at 370 nm. The excitation spectra were acquired with emission at 460 nm. Each spectrum is the average of 6 measurements; a.u., arbitrary units.

The HPLC–MS/MS analysis confirmed the presence of CGA, SCL and SCT according to their fragmentation pattern as reported in **Supplementary Table 1**.

By plotting the concentrations of the two coumarins against each other, we found that they were related by an exponential decay function (**Figure 4**) indicating that the maximal level of SCT corresponded to the minimum level of SCL.

Figure 4 also shows the content of the coumarins as function of the infiltration treatment. When leaf disks were only infiltrated with SPS, the highest levels of SCL and the lowest levels of SCT were found, likely due to the stress induced by cutting. Conversely, the largest and the lowest amounts of SCT and SCL, respectively, were observed after infiltration with *P. syringae* pv. *tomato* DC3000, which is avirulent on tobacco. At last, intermediate values of both these two coumarins were obtained after leaf infiltration with *P. syringae* pv. *tabaci* ATCC 11528, the virulent bacterium for tobacco.

In vitro Fluorescence of Standard Compounds

To identify the principal contributors to the tobacco leaf fluorescence under pathogen infiltration, we analyzed the fluorescence properties of the main phenolic compounds found by the HPLC analysis.

Since coumarin fluorescence is strongly pH-dependent (Fink and Koehler, 1970; Pina et al., 2019; Pham et al., 2020), we investigated the fluorescence properties of SCT and SCL, and also CGA, in buffer solutions of different acidity. The excitation and emission spectra of SCT, SCL, and CGA in phosphate buffer at various pH values are reported in **Figure 5**. Moving the pH from 5.4 to 8.5, the excitation spectrum of SCT showed a decrease of the peak around 340 nm and a relative increase of the band at 385 nm (**Figure 5A**). The same pH-dependence was observed for the SCT absorption spectra (see **Supplementary Figure 1**).

The emission band peaked at 460 nm and remained unchanged with increasing pH (**Figure 5D**).

Scopolin was characterized by a fluorescence excitation spectrum with a main peak at around 340 nm and a second band at 290 nm (**Figure 5B**). This spectrum matched closely the absorption spectrum and was not affected by pH change.

The emission band of SCL peaked at 420 nm and was independent of the buffer pH (**Figure 5E**).

The fluorescence spectra of CGA as function of pH behaved similarly to those of SCT (**Figures 5C,F**). The intensity of the CGA fluorescence, however, was largely weaker than that of the coumarins. Note that even if in **Figure 5**, the CGA fluorescence intensity values were similar to those of SCT, the photomultiplier gain and the monochromator slits set in the spectrofluorimeter to measure the CGA signals were much higher than those used to detect the coumarin fluorescence. Nevertheless, the presence of an apparent excitation band at 398 nm corresponding to the Raman scatter band of water at 460 nm in the excitation spectrum of CGA (**Figure 5C**), not visible in the spectra of SCT and SCL (**Figures 5A,B**), confirms the weakness of the CGA fluorescence with respect to that of coumarins.

The comparison of the fluorescence signals among the three major phenolic compounds present in the tobacco leaves was

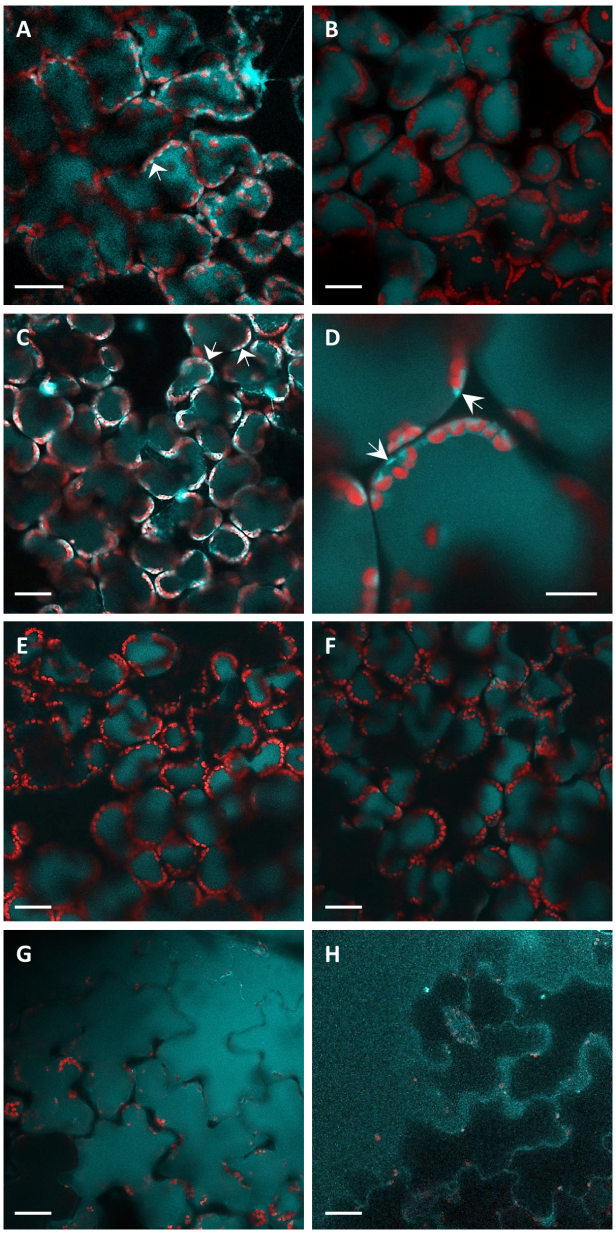

FIGURE 2 | The CLSM fluorescence imaging of leaf disks observed from the adaxial side. Light-blue fluorescence, acquired under excitation at 405 nm and detection at 430–498 nm, represents localization of coumarins. Red fluorescence coming from the chlorophyll of the chloroplasts was acquired under excitation at 638 nm and detection at 695–765 nm. Images were acquired at 9 **(A)**, 22 **(B)**, 28 **(C,G)**, 31 **(E,H)**, 48 **(D)**, and 51 **(F)** hpi. **(A–D,G)** Report images of *P. syringae* pv. *tomato* DC3000 infiltrated leaf disks. **(E,F,H)** Report the images of SPS-infiltrated leaf disks (controls). The bar in **(D)** represents 10 μm, all the other panel bars represent 30 μm. The arrows indicate the cytoplasmatic localization of blue fluorescence.

further achieved by measuring the relative fluorescence quantum yields. The fluorescence quantum yield of SCT in buffer at pH 5.4 resulted to be about 740 and 3.2 folds higher than that of CGA and SCL, respectively. Scopolin is in turn about 230 folds more fluorescent than CGA. Still, the anionic form of SCT was at least 1.5 times more fluorescent than its neutral form, in accordance with data from the literature (Masilamani and Sivaram, 1981; Pina et al., 2019).

Gaussian Fitting of Spectra

Since the excitation spectra of SCL and SCT partially overlapped, especially at lower pH values, we performed a Gaussian curve spectral fitting to separate their contribution to the *in vivo* fluorescence.

We considered the spectral range above 300 nm, neglecting the shorter waveband of the excitation spectra (see **Figure 5**) since *in vivo*, the contribution of UVB-excitation wavelengths to the blue fluorescence of leaf cells is expected to be minimal due to the large absorption in this region by the cuticle, waxes, and trichomes of the outer layers of the leaf.

Excitation fluorescence spectra of SCL and SCT standard compounds at pH 5.4 can be fitted by a single-Gaussian curve (**Figures 6A,B**). The excitation spectrum of SCT at pH 8.5 was fitted by the sum of two-Gaussian functions (**Figure 6C**) to take into account the residual contribution from the neutral molecular species of the acid-base equilibrium present in solution (Pina et al., 2019). The FWHM of all the Gaussian curves was around 52 nm, while the peak wavelength was 338, 342, and 385 nm for SCL at pH 5.4, SCT at pH 5.4, and SCT at pH 8.5, respectively. The coefficient of determination, R^2, of the fitting varied between 0.994 and 0.996.

Based on this, we were able to perform the spectral fitting of *in vivo* leaf fluorescence excitation spectra by two-Gaussian curves centered at around 360 and 385 nm.

Before leaf disk punching and infiltration, the excitation spectra were recorded *in planta*, on the very same leaves, then detached and used for the processing. These spectra were subtracted from those measured on the leaf disks at different times after infiltration to take scattering effects due to the leaf structures into account.

An example of the spectral fitting is reported in **Figure 7** for the excitation fluorescence spectrum recorded on a leaf disk at 16 hpi with *P. syringae* pv. t*omato* DC3000.

Correlation Between Fluorescence Signals and the Leaf Coumarin Content

The two-Gaussian fitting of excitation spectra (for emission at 460 nm) was applied to the data measured on the different leaf disk samples that were then processed for the HPLC analysis of phenolic compounds. The samples selected were those infiltrated with *P. syringae* pv. *tomato* DC3000, *P. syringae* pv. *tabaci* ATCC11528, or SPS, both at 18 and 24 hpi, derived from three different leaves of three different tobacco plants.

By comparing the concentration values of the different compounds obtained by the HPLC analysis with the intensity of the two fluorescence bands derived by the Gaussian fitting of the spectra, a good correlation was found between SCT and the band at 385 nm (F_{385_460}). The direct relationship could be fitted by an exponential function [$F_{385\_460} = 13.81 + 436.9 \times (1 - e^{-0.05C})$, with C = SCT concentration] with $R^2 = 0.84$ (**Figure 8**).

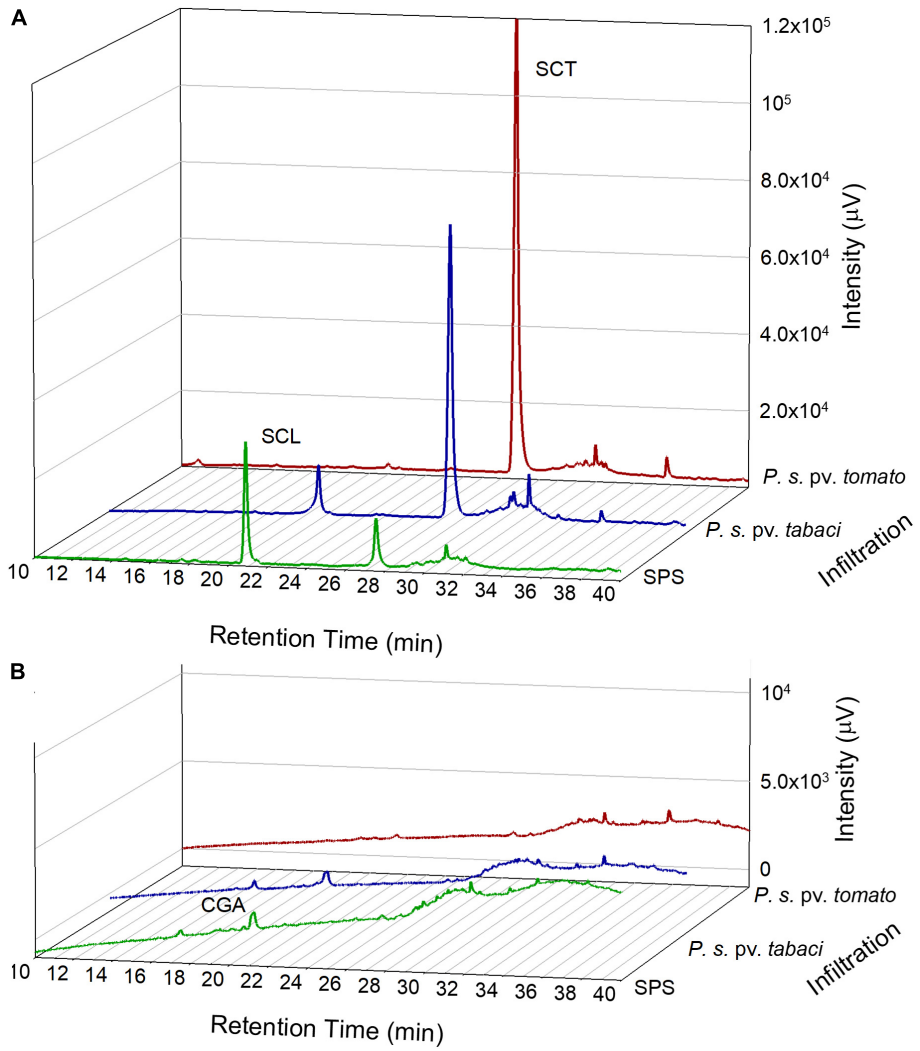

FIGURE 3 | Representative chromatograms from the HPLC analysis of tobacco leaf disk extracts acquired by a fluorescence detector, excitation at 340 nm and emission at 460 nm **(A)** and by a diode array detector at 330 nm **(B)**. Leaf samples were analyzed at 18 hpi with SPS, *P. syringae* pv. *tabaci* ATCC 11528 or *P. syringae* pv. *tomato* DC3000.

Both SCL and CGA did not show any direct correlation to either the 360 nm or the 385 nm fluorescence excitation bands (see **Supplementary Figure 2**).

Time-Course Monitoring of the Bacteria–Plant Interaction

We applied the deconvolution of the excitation spectra by two-Gaussian fitting to the spectra measured on leaf disks under different bacterial treatments at increasing post-infiltration time. In **Figure 9A**, the average excitation fluorescence spectra, for emission at 460 nm, of leaf disks infiltrated with *P. syringae* pv. *tomato* DC3000, *P. syringae* pv. *tabaci* and SPS at 24 hpi are shown.

Figure 9B displays the time-course of the F_{385_460} fluorescence excitation band, determined by the previously described fitting spectral analysis, representing the evolution of SCT, and normalized to that of control samples.

Additionally, we compared the F_{385_460} fluorescence excitation band induced by the previous treatments with that generated by the Δ*hrpA* mutant of *P. syringae* pv. *tabaci* ATCC11528 (**Figure 9C**).

The *P. syringae* pv. *tomato* DC3000 treatment induced a faster and much higher increase of the fluorescence intensity with respect to that caused by *P. syringae* pv. *tabaci* ATCC11528 infiltration. A plateau is reached even as early as 7 hpi (**Figure 9C**), and a decreasing trend was observed after 24 hpi (**Figure 9B**). Then F_{385_460} relative to SPS in leaf disks infiltrated with *P. syringae* pv. *tabaci* ATCC11528 increased linearly from 7 to 9 hpi up to 24 hpi and then remained stable. Under the infiltration with its Δ*hrpA* mutant, F_{385_460} oscillated with time remaining close to that of the SPS control (**Figure 9C**). At 17 and

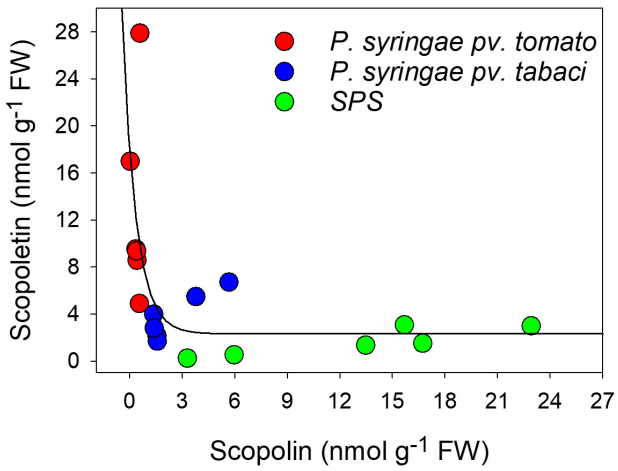

FIGURE 4 | Relationship between SCT and SCL concentrations and the infiltration treatments, evaluated by chromatographic methods. The solid line represents a curve fitting by an exponential decay function.

24 hpi, it was significantly lower than the fluorescence induced by the *P. syringae* pv. *tabaci* ATCC11528 wild type strain.

DISCUSSION

The *in situ* tobacco leaf fluorescence spectroscopy during the first hours of the plant–bacteria interaction showed clearly that the excitation spectra changed shape with time (**Figure 1**).

The possible contributors to the observed leaf blue fluorescence were identified to be SCL and SCT, as resulted by the HPLC analysis of leaf disk extracts collected before and after the bacterial infiltration, as well as by the *in vitro* fluorescence properties of these compounds.

The levels of SCL and SCT in untreated tobacco leaves were low, ranging 70–154 ng g^{-1} FW and 15–38 ng g^{-1} FW, respectively. The concentration of CGA ranged 330–600 $\mu g\ g^{-1}$ FW. This was consistent with the CGA levels previously found in *N. tabacum* leaves (Baker et al., 2017), considering also its high variability due to the growing conditions, leaf age and position on the plant.

After bacterial infiltration, the concentration of both SCL and SCT significantly increased up to 0.56 and 5.36 $\mu g\ g^{-1}$ FW, respectively, while that of CGA markedly decreased. In SPS-infiltrated leaves, SCL reached the maximal concentration of 8.13 $\mu g\ g^{-1}$ FW, while SCT was utmost 0.59 $\mu g\ g^{-1}$ FW. A high variability between plants in the coumarin accumulation was, however, observed as function of the type of bacteria, the time after bacterial infiltration and the mock infiltration with SPS.

Fluorescence Properties of Tobacco Phenolic Compounds

The SCT excitation spectra showed the typical changes with pH observed for the acid–base equilibrium of mono-hydroxycoumarins (Simkovitch et al., 2016). Increasing the pH from 5.4 to 8.5, the neutral form of SCT, with excitation band at around 340 nm, decreased while a relative increase of the anion band at longer wavelengths, at 385 nm, appeared (**Figure 5A**). The excitation spectrum of SCT at pH 8.5 can then be considered as due to the pure anionic molecular species, in accordance with the literature (Pina et al., 2019; Pham et al., 2020).

The emission band peaking at 460 nm remained unchanged with increasing pH (**Figure 5D**) because, in the considered pH range, the intensity of the neutral form near 430 nm is much weaker than that of the anion. In fact, SCT is defined as a photoacid, which means that its excited neutral form can easily lose a proton and fluoresce as the anion. Accordingly, the ground-state pKa of SCT of 7.4 is reduced to about 1 in the excited-state (Pina et al., 2019; Pham et al., 2020). This process can occur through the intermolecular excited-state proton-transfer (ESPT) to water.

Scopolin was characterized by the fluorescence excitation and emission spectra independent of pH (**Figures 5B,E**) due to the glucoside-substitution of the hydroxy group in position 7 that does not allow any deprotonation of the molecule.

The pH-dependence of the CGA fluorescence spectra (**Figures 5C,F**) was similar to that of SCT. This indicates that CGA can be considered a photoacid and undergoes to ESPT as observed in other phenolic compounds (Kaneko et al., 2009).

The *in vitro* fluorescence analysis, both considering spectral shape and relative quantum yields of compounds, suggested SCL and SCT as the main contributors to the leaf blue fluorescence observed under bacterial infiltration. Yet, the excitation spectrum for emission at 460 nm seems to be the most useful tool to discriminate the two coumarins during the plant–pathogen interaction, based on its specific responsiveness to pH changes. These results further support the hypothesis that the leaf blue fluorescence of bacterial inoculated samples receive contributions from the vacuolar SCL and the extra-vacuolar SCT, as evidenced by confocal microscopy (**Figure 2**) and discussed in the following section.

Leaf Tissue Localization and Diffusion of Coumarins

The confocal microscopy analysis of leaf disks infiltrated by *P. syringae* pv. *tomato* or SPS showed the localization of blue autofluorescence in the vacuole and cytoplasm of palisade cells, as well as in the adaxial epidermal cells, depending on treatment and time after infiltration. Therefore, the fluorophores at all these leaf tissue compartments can contribute to the in situ measured leaf fluorescence.

Microimages of vacuolar blue fluorescence, excited at 364 nm, similar to those we found were observed and assigned to SCL in the epidermal and mesophyll cells of leaves from *Arabidopsis thaliana* plants grown for 4 weeks at 20°C and then kept for 1 week at 10°C (Döll et al., 2018).

It is widely recognized that the toxic SCT is converted by glucosyltransferases to the glycosylated form SCL (Ibrahim and Boulay, 1980), which is transported to the vacuoles for storage. In response to the defense activation induced by a pathogen or elicitor, SCL can be excreted into the cytosol

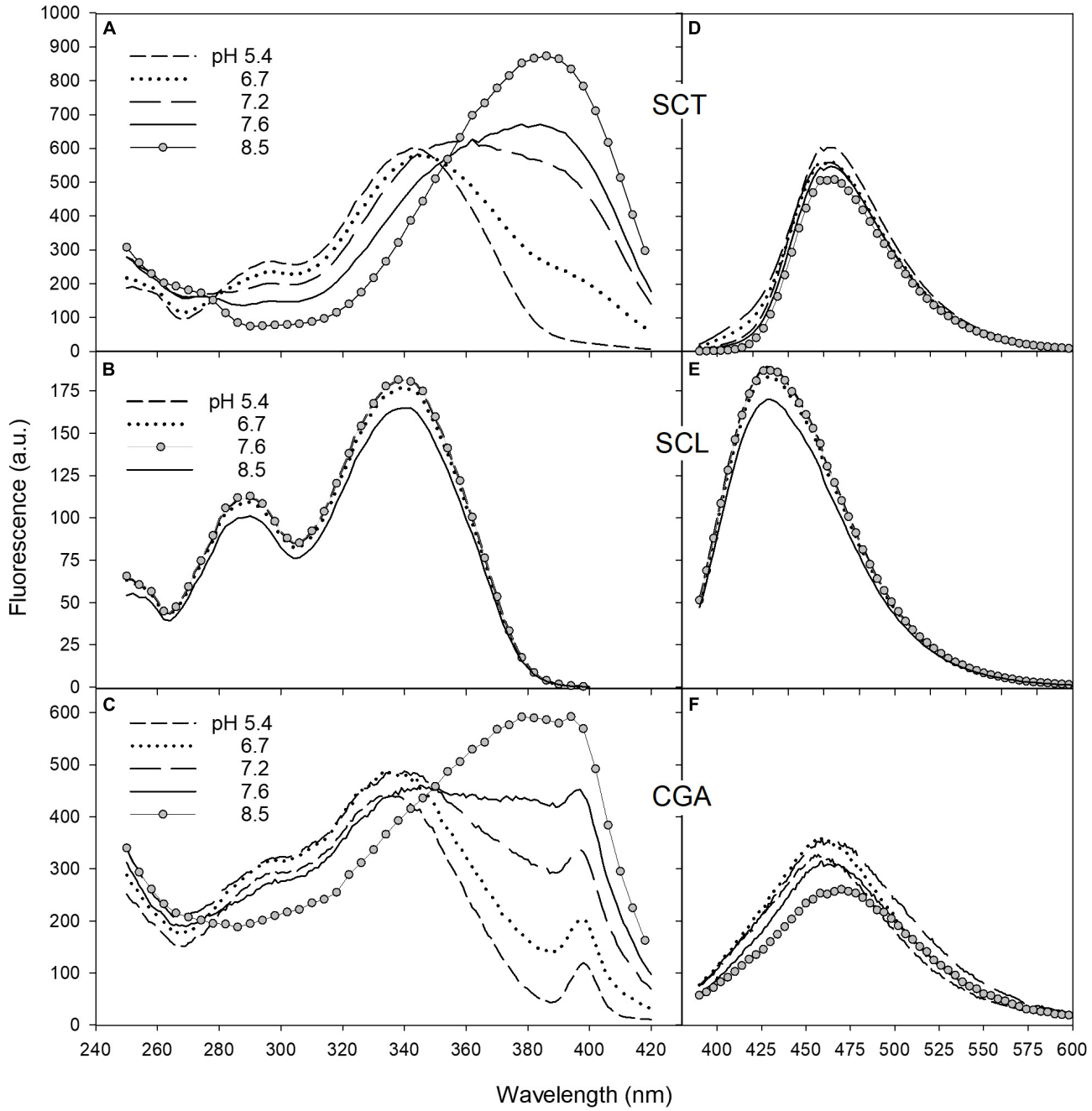

FIGURE 5 | The fluorescence excitation and emission spectra of SCT **(A,D)**, SCL **(B,E)**, and CGA **(C,F)** in phosphate buffer at different pH. Excitation spectra were recorded with emission wavebands set at 460 nm for SCT and CGA and at 420 nm for SCL. The peak observed in C at 398 nm corresponds to the excitation wavelength of the Raman scatter band of water at 460 nm. For emission spectra, excitation wavelengths were set at 330, 340, and 350 nm for CGA, SCL, and SCT, respectively. The acquisition parameters for SCT and SCL were ex/em slit width of 2.5/5 nm for excitation, 5/2.5 nm for emission, PMT voltage = 600 V; for CGA, they were ex/em slit width of 5/10 nm for excitation, 10/5 nm for emission, PMT voltage = 900 V.

and apoplast and converted back to SCT by β-glucosidases (Stringlis et al., 2019). In this way, SCT can exert its antimicrobial activity and scavenge H_2O_2 in the infected tissues (Chong et al., 1999).

On the other hand, SCL possesses lower antioxidant activity than SCT (Al-Rifai, 2018) because of the glucosylation of the reactive hydroxyl group at position 7. Also, SCL showed less-effective inhibitory capacity than its aglycone toward various fungal and bacterial pathogens (Ahl Goy et al., 1993; Beyer et al., 2019). Therefore, it is expected that the tobacco plant response to biotic oxidative stresses will favor the accumulation of SCT rather than SCL.

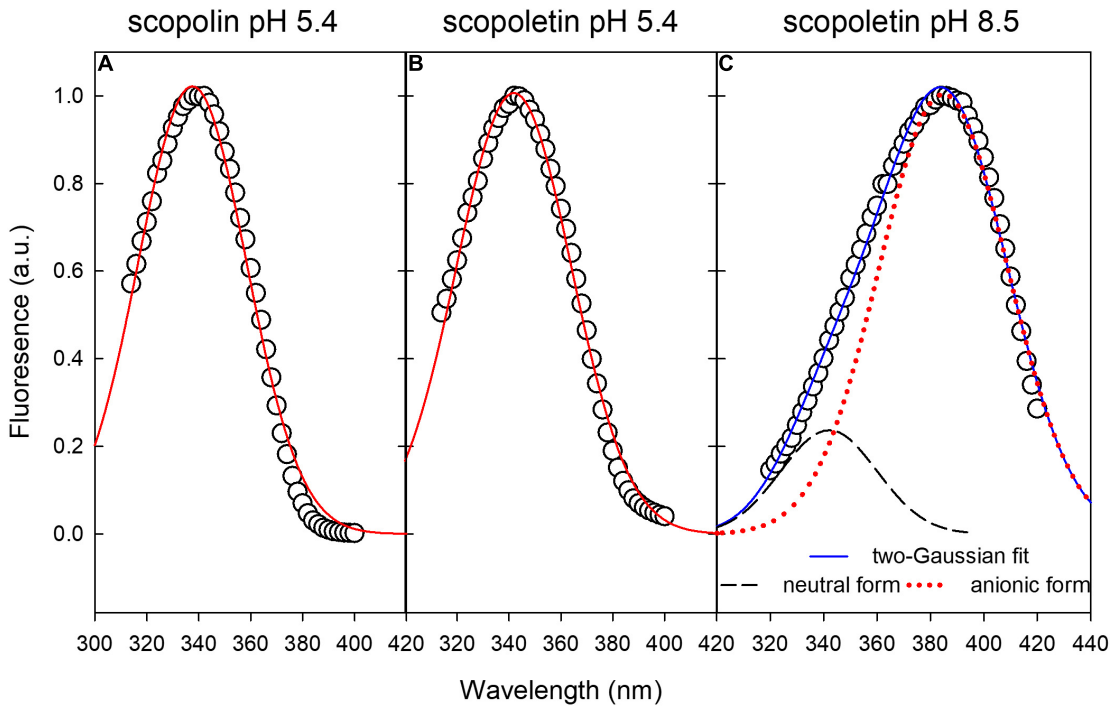

FIGURE 6 | Gaussian fitting of excitation fluorescence spectra of standard compounds in buffer solution. **(A,B)** Single-Gaussian curve fitting of SCL and SCT at pH 5.4, respectively. **(C)** Two-Gaussian curve fitting to take into account the residual component from the neutral form of SCT.

In *Hevea brasiliensis*, leaves inoculated with *Phytophthora palmivora* excreted a single coumarin compound, identified as SCT, in the droplets recovered from the inoculated site (Churngchow and Rattarasarn, 2001).

Taguchi et al. (2000) proved the uptake of SCT added to the culture medium of tobacco cells treated with the synthetic auxin 2,4-dichlorophenoxyacetic acid. Scopoletin was mostly completely glucosylated to SCL in the cytoplasm, and transferred to the vacuole. Only a 2% fraction of SCT with respect to SCL was determined in the cell vacuoles.

The process of conversion from SCL to SCT and their different compartmentalization in response to biotic stresses to scavenge reactive oxygen species (Chong et al., 1999; Stringlis et al., 2019)

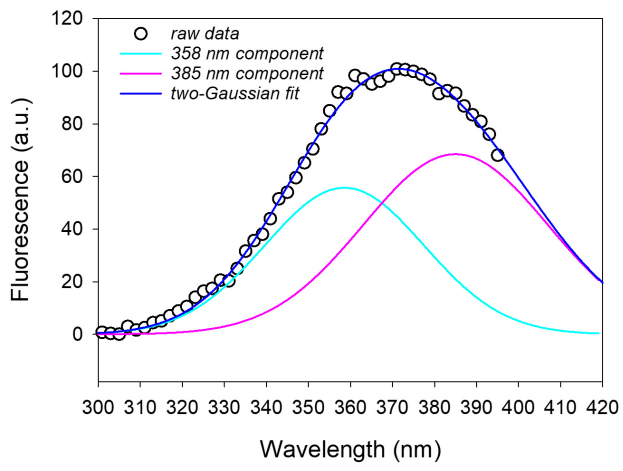

FIGURE 7 | Two-Gaussian curves fitting of the fluorescence excitation spectrum (emission at 460 nm) measured on a leaf disk after 16 h from infiltration with *P. syringae* pv. *tomato* DC3000. The on plant average excitation spectrum was removed from the leaf disk spectrum before fitting. R^2 = 0.997.

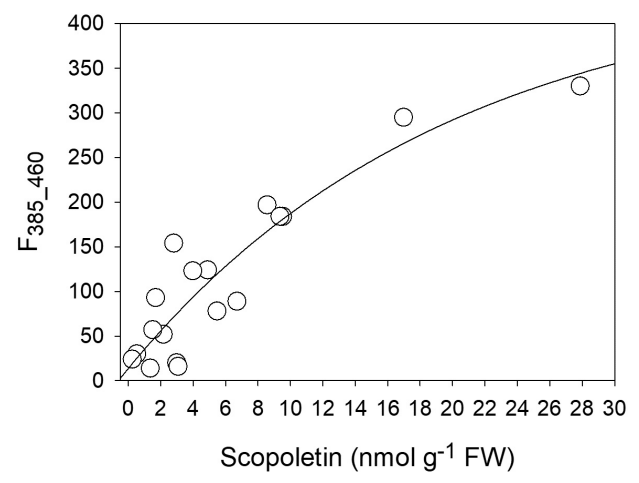

FIGURE 8 | The correlation between the intensity of the 385 nm fluorescence excitation band (F_{385_460}) and the SCT concentration as evaluated by chromatographic methods.

is also supported by the exponential decay relationship we found between SCT and SCL concentrations (**Figure 4**), indicating that the maximal level of SCT corresponded to the minimum level of SCL.

Based on these results, we hypothesize that the intense blue autofluorescence observed in the cytoplasm of our samples was due to the presence of SCT produced after excretion of SCL from the vacuole following the infiltration with *P. syringae* pv. *tomato*. The vacuolar fluorescence instead was mainly due to SCL. This is consistent with the *in vitro* fluorescence properties of coumarins (**Figure 5**) considering that while the vacuolar pH in higher plant cells is typically between 5.0 and 6.0, higher pH values up to 7.5 could be measured in the cytoplasm (Kurkdjian and Guern, 1989; Martinière et al., 2013).

The increase of fluorescence in the epidermal cells after bacterial infiltration can be explained by the transportation of defense compounds from the synthesis site through symplasmic domains toward the leaf edges (Jørgensen et al., 2015). Accordingly, both SCL and SCT (and also ayapin) were found on the surface of fungi-infected sunflower leaves (Prats et al., 2007). The resistance to rust infection induced in sunflower by acibenzolar-S-methyl was correlated to an increased synthesis of coumarins and their excretion to the leaf surface, especially in the case of SCT (Prats et al., 2002). Other hydroxylated coumarins, such as esculin and esculetin, were found in the vacuole of subsidiary cells of stomata and guard cells of the epidermis and the mesophyll protoplasts in *Arabidopsis thaliana* (Rottmann et al., 2018) and in the vacuole of epidermal and palisade cells of *Fraxinus ornus* leaves (Tattini et al., 2014).

The dynamics of compound diffusion among cell compartments during the plant–bacteria interaction (Baker et al., 2018) or in tobacco leaf tissues treated by HR-inducing elicitors (Dorey et al., 1997) can explain the heterogenous response in term of the tobacco leaf phenolic composition during the bacterial and mock treatments (the range of concentrations found at 18 and 24 hpi was 0.26–99.67, 0.15–81.88, and 0.24–27.87 nmol g^{-1} FW for CGA, SCL, and SCT, respectively).

The Scopoletin F_{385_460} Fluorescence as Marker of the Plant–Bacteria Interaction

The two-Gaussian fitting deconvolution of fluorescence excitation spectra was able to discriminate the contribution of SCT from that of SCL to total leaf fluorescence. This was proved by the good direct correlation found between the F_{385_460} signal and the concentration of SCT determined destructively (**Figure 8**). On the other hand, the other main phenolic fluorophores present, SCL and CGA, did not show any direct correlation with F_{385_460} (**Supplementary Figure 2**). We could then use the developed methodology to monitor *in vivo* the evolution of SCT during a 42-h period of the plant–pathogen interaction (**Figures 9B,C**). A large difference in the leaf blue autofluorescence intensity and spectral shape between the various trials was found. This was likely due to differences in leaf and plant age, as well as in the general plant physiological state. In fact, the production of SCT was proved to increase in tobacco resistant cultivars after infection with

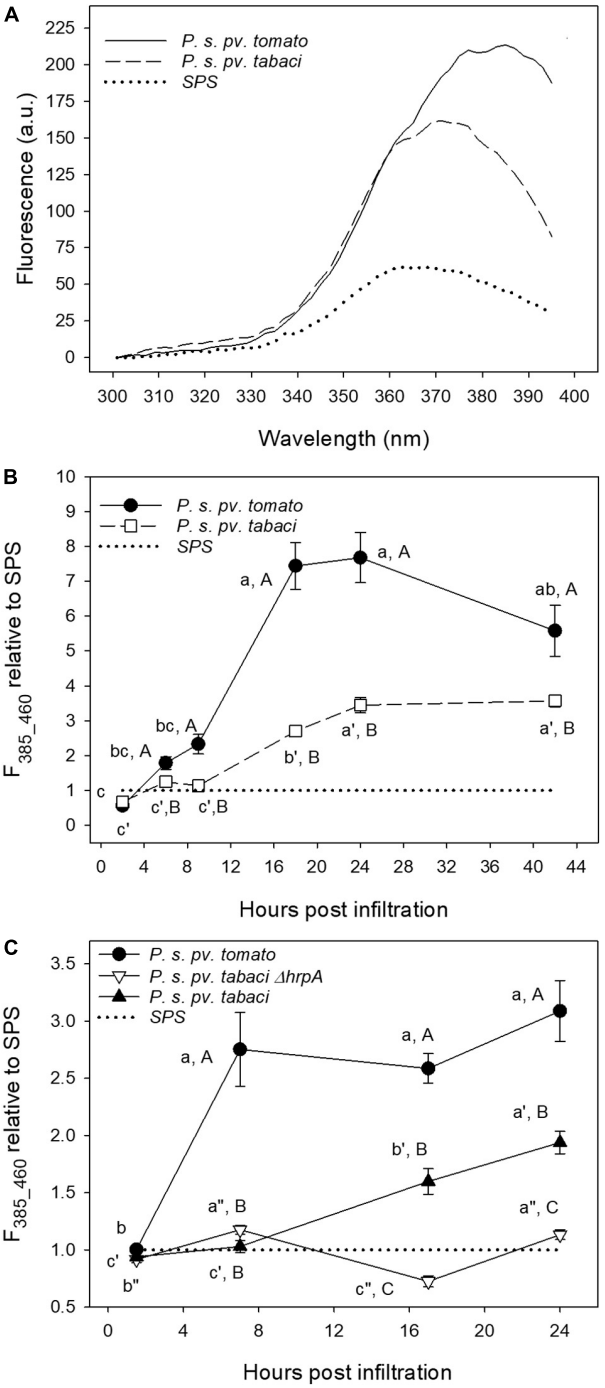

FIGURE 9 | The fluorescence excitation spectra of tobacco leaf disks measured at 24 hpi **(A)**, and time evolution of the 385 nm fluorescence excitation band (emission at 460 nm, F_{385_460}) **(B,C)**. The leaf disks were separately infiltrated with *P. syringae* pv. *tabaci* ATCC11528, its Δ*hrpA* mutant, *P. syringae* pv. *tomato*, and with SPS as negative control. Each point is the mean (±SE) of leaf disks (n = 24–45) from three different leaves of three different plants. The average excitation spectrum *in planta* on attached leaves was subtracted from the leaf disks spectra. In **(B,C)**, the values marked by a different lower case letter and primed or double-primed letter for the same treatment, and by an upper case letter for each time are significantly different ($p < 0.05$) according to the Holm–Sidak test.

P. syringae pv *tabaci* depending on an increase in cytokinins concentration (Großkinsky et al., 2011). Since the content of cytokinins is markedly dependent on the leaf position on the plant, decreasing from the uppermost leaves to the bottom (Veselov et al., 1999), it is expected to find rather quantitative different responses to the pathogen infiltration as a function of the leaf and plant age.

The common aspects observed among the trials concerned two main differences related to the resistance response of tobacco to avirulent bacterial Gram negative plant pathogens. The shape of the excitation spectrum at 24 hpi peaked at around 380–390 nm only on samples infiltrated with *P. syringae* pv. *tomato* DC3000. Moreover, a clear and faster accumulation of extra-vacuolar SCT was detectable under *P. syringae* pv. *tomato* DC3000 than under *P. syringae* pv. *tabaci* infiltration.

Overall, our results clearly show that the amount and the timing of SCT accumulation, estimated by F_{385_460}, is linked to the level of tobacco resistance to the tested pathogens.

The rapid rise of the SCT concentration following *P. syringae* pv. *tomato* DC3000 infiltration is consistent with early studies on the accumulation of SCT in attached tobacco leaves treated with an elicitor of the hypersensitive reaction (Dorey et al., 1997). They reported an increase of this coumarin in the tissue surrounding the infiltration zone already 6 h after the treatment, reaching a maximum after 24 h. In the elicitor-treated zone, SCT slightly increased because of its high sensitivity to oxidation. The delayed increase of the F_{385_460} fluorescence in tobacco leaf disks infiltrated with *P. syringae* pv. *tabaci* ATCC11528 with respect to *P. syringae* pv. *tomato* DC3000 (**Figures 9B,C**) is a typical feature of the defense responses triggered into a plant host against a virulent pathogen, allowing the infection to progress. The plant barriers against an avirulent pathogen, such as *P. syringae* pv. *tomato* DC3000 with tobacco, are rapidly activated and their effects are evident from the first few hours of post-infiltration. It is worth to mention that a functional TTSS is essential to trigger accumulation of coumarins in tobacco tissues by a Gram negative plant pathogenic bacterium. No significant increase of F_{385_460} (i.e., SCT) was ever observed in tobacco leaf disks infiltrated with the non-pathogenic Δ*hrpA* mutant of *P. syringae* pv. *tabaci* ATCC11528. This effect is in accordance with the additional role of the HrpA protein. Besides to be the major component of the TTSS pilus, HrpA has been demonstrated to positively affect TTSS gene expression in phytopathogenic bacteria belonging to the *P. syringae* complex, by acting upstream to the expression cascade of TTSS genes, that is on the hrpRS operon (Wei et al., 2000; Tang et al., 2006; Ortiz-Martín et al., 2010; Tegli et al., 2011). Therefore, these overall data are further confirming both sensitivity and reliability of the fluorimetric method developed in this study.

CONCLUSION

We developed a new fluorescence spectroscopic method able to selectively control *in vivo* the evolution of the SCT phytoalexin following a bacterial infiltration of tobacco leaves. It is based on the elaboration of the fluorescence excitation spectra recorded at different times during the elicitation process. The key point of the method relies on the dependence of the SCT fluorescence excitation spectrum on pH. This allowed the detection of an excitation fluorescence band around 385 nm specific of SCT located in the cytoplasmatic cell compartment and free of the SCL contribution.

The Gaussian curve deconvolution analysis of leaf blue autofluorescence excitation spectra permitted, for the first time, separating the contribution to leaf fluorescence of SCL from that of SCT. It represents a fundamental improvement in the development of non-destructive methods for the early diagnosis of tobacco plant diseases and in the discrimination of the plant response to specific pathogens and likely to other stresses.

The outcome of the present study can be exploited to define a screening technique for the early diagnosis of plant diseases, even in the field by using suitable portable fluorescence sensors. It could also find application for an early and rapid selection of tobacco cultivars resistant against virulent pathogens.

DATA AVAILABILITY STATEMENT

The raw data supporting the conclusions of this article will be made available by the authors, without undue reservation.

AUTHOR CONTRIBUTIONS

GA and ST: conceptualization, funding acquisition, and project administration. GA: data curation, formal analysis, software, and writing the original draft. CB, ID, and ST: investigation, validation, and reviewing and editing the content. LT: investigation. All authors contributed to the article and approved the submitted version.

FUNDING

This research was partially funded by the Regione Toscana under the Programma Operativo Regionale FSE 2014-2020 and by the Società Azienda Fattoria Autonoma Tabacchi, Città di Castello (PG)—Italy.

ACKNOWLEDGMENTS

We are grateful to the Fattoria Autonoma Tabacchi for providing the tobacco seedling used in the experimentation, and to Enrica Bargiacchi and Sergio Miele, INSTM Firenze, Italy for useful discussions.

SUPPLEMENTARY MATERIAL

The Supplementary Material for this article can be found online at: https://www.frontiersin.org/articles/10.3389/fmicb.2022.889878/full#supplementary-material

REFERENCES

Ahl Goy, P., Signer, H., Reist, R., Aichholz, R., Blum, W., Schmidt, E., et al. (1993). Accumulation of scopoletin is associated with the high disease resistance of the hybrid *Nicotiana glutinosa* x *Nicotiana* debneyi. *Planta* 191, 200–206. doi: 10.1007/BF00199750

Ahmed, S., and Kovinich, N. (2021). Regulation of phytoalexin biosynthesis for agriculture and human health. *Phytochem. Rev.* 20, 483–505. doi: 10.1007/s11101-020-09691-8

Ahuja, I., Kissen, R., and Bones, A. M. (2012). Phytoalexins in defense against pathogens. *Trends Plant Sci.* 17, 73–90. doi: 10.1016/j.tplants.2011.11.002

Al-Rifai, A. (2018). Identification and evaluation of in-vitro antioxidant phenolic compounds from the Calendula tripterocarpa Rupr. *S. Afr. J. Bot.* 116, 238–244. doi: 10.1016/j.sajb.2018.04.007

Baker, C. J., Mock, N. M., and Aver'yanov, A. A. (2017). A simplified technique to detect variations of leaf chlorogenic acid levels between and within plants caused by maturation or biological stress. *Physiol. Mol. Plant Pathol.* 98, 97–103. doi: 10.1016/j.pmpp.2017.04.003

Baker, C. J., Mock, N. M., and Aver'yanov, A. A. (2018). The dynamics of apoplast phenolics across the apoplast/symplast barrier in tobacco leaves following bacterial inoculation. *Physiol. Mol. Plant Pathol.* 103, 114–121. doi: 10.1016/j.pmpp.2018.05.007

Barón, M., Pineda, M., and Pérez-Bueno, M. L. (2016). Picturing pathogen infection in plants. *Z. Naturforsch. C J. Biosci.* 71, 355–368. doi: 10.1515/znc-2016-0134

Beyer, S. F., Beesley, A., Rohmann, P. F. W., Schultheiss, H., Conrath, U., and Langenbach, C. J. G. (2019). The *Arabidopsis* non-host defence-associated coumarin scopoletin protects soybean from Asian soybean rust. *Plant J.* 99, 397–413. doi: 10.1111/tpj.14426

Cerboneschi, M., Decorosi, F., Biancalani, C., Ortenzi, M. V., Macconi, S., Giovannetti, L., et al. (2016). Indole-3-acetic acid in plant–pathogen interactions: a key molecule for in planta bacterial virulence and fitness. *Res. Microbiol.* 167, 774–787. doi: 10.1016/j.resmic.2016.09.002

Chaerle, L., Lenk, S., Hagenbeek, D., Buschmann, C., and Van Der Straeten, D. (2007). Multicolor fluorescence imaging for early detection of the hypersensitive reaction to tobacco mosaic virus. *J. Plant Physiol.* 164, 253–262. doi: 10.1016/j.jplph.2006.01.011

Chong, J., Baltz, R., Fritig, B., and Saindrenan, P. (1999). An early salicylic acid-, pathogen- and elicitor-inducible tobacco glucosyltransferase: role in compartmentalization of phenolics and H2O2 metabolism. *FEBS Lett.* 458, 204–208. doi: 10.1016/S0014-5793(99)01154-0

Chong, J., Baltz, R., Schmitt, C., Beffa, R., Fritig, B., and Saindrenan, P. (2002). Downregulation of a pathogen-responsive tobacco UDP-Glc:phenylpropanoid glucosyltransferase reduces scopoletin glucoside accumulation, enhances oxidative stress, and weakens virus resistance. *Plant Cell* 14, 1093–1107. doi: 10.1105/tpc.010436

Churngchow, N., and Rattarasarn, M. (2001). Biosynthesis of scopoletin in *Hevea brasiliensis* leaves inoculated with *Phytophthora palmivora*. *J. Plant Physiol.* 158, 875–882. doi: 10.1078/0176-1617-00230

Costet, L., Fritig, B., and Kauffmann, S. (2002). Scopoletin expression in elicitor-treated and *Tobacco mosaic virus*-infected tobacco plants. *Physiol. Plant.* 115, 228–235. doi: 10.1034/j.1399-3054.2002.1150208.x

Crosby, D. G., and Berthold, R. V. (1962). Fluorescence spectra of some symple coumarins. *Anal. Biochem.* 357, 349–357. doi: 10.1016/0003-2697(62)90136-7

Dieterman, L. J., Rohrbaugh, L. M., Lin, C., and Wender, S. H. (1964). Accumulation of ayapin and scopolin in sunflower plants treated with 2,4-dichlorophenoxyscetic acid. *Arch. Biochem. Biophys.* 106, 275–279. doi: 10.1016/0003-9861(64)90188-2

Döll, S., Kuhlmann, M., Rutten, T., Mette, M. F., Scharfenberg, S., Petridis, A., et al. (2018). Accumulation of the coumarin scopolin under abiotic stress conditions is mediated by the *Arabidopsis thaliana* THO/TREX complex. *Plant. J.* 93, 431–444. doi: 10.1111/tpj.13797

Dorey, S., Baillieul, F., Pierrel, M. A., Saindrenan, P., Fritig, B., and Kauffmann, S. (1997). Spatial and temporal induction of cell death, defense genes, and accumulation of salicylic acid in tobacco leaves reacting hypersensitively to a fungal glycoprotein elicitor. *Mol. Plant-Microbe Interact.* 10, 646–655. doi: 10.1094/MPMI.1997.10.5.646

El Modafar, C., Clérivet, A., Vigouroux, A., and Macheix, J. J. (1995). Accumulation of phytoalexins in leaves of plane tree (*Platanus* spp.) expressing susceptibility or resistance to *Ceratocystis fimbriata* f. sp. platani. *Eur. J. Plant Pathol.* 101, 503–509. doi: 10.1007/BF01874474

El Oirdi, M., Trapani, A., and Bouarab, K. (2010). The nature of tobacco resistance against *Botrytis cinerea* depends on the infection structures of the pathogen. *Environ. Microbiol.* 12, 239–253. doi: 10.1111/j.1462-2920.2009.02063.x

Fink, D. W., and Koehler, W. R. (1970). pH effects on fluorescence of umbelliferone. *Anal. Chem.* 42, 990–993. doi: 10.1021/ac60291a034

Großkinsky, D. K., Naseem, M., Abdelmohsen, U. R., Plickert, N., Engelke, T., Griebel, T., et al. (2011). Cytokinins mediate resistance against *Pseudomonas syringae* in tobacco through increased antimicrobial phytoalexin synthesis independent of salicylic acid signaling. *Plant Physiol.* 157, 815–830. doi: 10.1104/pp.111.182931

Hino, F., Okazaki, M., and Miura, Y. (1982). Effect of 2,4-dichlorophenoxyacetic acid on glucosylation of scopoletin to scopolin in tobacco tissue culture. *Plant Physiol.* 69, 810–813. doi: 10.1104/pp.69.4.810

Hupp, S., Rosenkranz, M., Bonfig, K., Pandey, C., and Roitsch, T. (2019). Noninvasive phenotyping of plant–pathogen interaction: consecutive in situ imaging of fluorescing *Pseudomonas* syringae, plant phenolic fluorescence, and chlorophyll fluorescence in *Arabidopsis* leaves. *Front. Plant Sci.* 10:1239. doi: 10.3389/fpls.2019.01239

Ibrahim, R. K., and Boulay, B. (1980). Purification and some properties of UDP-glucose: o-dihydroxycoumarins 7-O-glucosyltransferase from tobacco cell cultures. *Plant Sci. Lett.* 18, 177–184. doi: 10.1016/0304-4211(80)90048-6

Johansson, O. N., Nilsson, A. K., Gustavsson, M. B., Backhaus, T., Andersson, M. X., and Ellerström, M. (2015). A quick and robust method for quantification of the hypersensitive response in plants. *PeerJ.* 3:e1469. doi: 10.7717/peerj.1469

Jørgensen, M. E., Nour-Eldin, H. H., and Halkier, B. A. (2015). Transport of defense compounds from source to sink: lessons learned from glucosinolates. *Trends Plant Sci.* 20, 508–514. doi: 10.1016/j.tplants.2015.04.006

Kaneko, S., Yotoriyama, S., Koda, H., and Tobita, S. (2009). Excited-state proton transfer to solvent from phenol and cyanophenols in water. *J. Phys. Chem. A* 113, 3021–3028. doi: 10.1021/jp8086489

King, E. O., Ward, M. K., and Raney, D. E. (1954). Two simple media for the demonstration of pyocyanin and fluorescin. *J. Lab. Clin. Med.* 44, 301–307.

Kurkdjian, A., and Guern, J. (1989). Intracellular pH: measurement and importance in cell activity. *Annu. Rev. Plant Physiol. Plant Mol. Biol.* 40, 271–303. doi: 10.1146/annurev.pp.40.060189.001415

Martinière, A., Bassil, E., Jublanc, E., Alcon, C., Reguera, M., Sentenac, H., et al. (2013). In vivo intracellular pH measurements in tobacco and *Arabidopsis* reveal an unexpected pH gradient in the endomembrane system. *Plant Cell.* 25, 4028–4043. doi: 10.1105/tpc.113.116897

Masilamani, V., and Sivaram, B. M. (1981). Spectral and laser gain characteristics of solvated species of scopoletin. *J. Lumin.* 22, 211–220. doi: 10.1016/0022-2313(81)90010-7

Ortiz-Martín, I., Thwaites, R., Macho, A. P., Mansfield, J. W., and Beuzón, C. R. (2010). Positive regulation of the Hrp type III secretion system in *Pseudomonas* syringae pv. phaseolicola. *Mol. Plant Microbe Interact* 23, 665–681. doi: 10.1094/mpmi-23-5-0665

Pham, H. T., Yoo, J., VandenBerg, M., and Muyskens, M. A. (2020). Fluorescence of scopoletin including its photoacidity and large Stokes shift Fluorescence of scopoletin including its photoacidity and large Stokes shift. *J. Fluoresc.* 30, 71–80. doi: 10.1007/s10895-019-02471-4

Pina, J., Castro, C. S., Delgado-pinar, E., and Melo, J. S. S. D. (2019). Characterization of 4-methylesculetin and of its mono- and di-methoxylated derivatives in water and organic solvents in its ground, singlet and triplet excited states. *J. Mol. Liq.* 278, 616–626. doi: 10.1016/j.molliq.2019.01.083

Prats, E., Llamas, M. J., Jorrin, J., and Rubiales, D. (2007). Constitutive coumarin accumulation on sunflower leaf surface prevents rust germ tube growth and appressorium differentiation. *Crop Sci.* 47, 1119–1124. doi: 10.2135/cropsci2006.07.0482

Prats, E., Rubiales, D., and Jorrín, J. (2002). Acibenzolar-S-methyl-induced resistance to sunflower rust (*Puccinia helianthi*) is associated with an enhancement of coumarins on foliar surface. *Physiol. Mol. Plant Pathol.* 60, 155–162. doi: 10.1006/pmpp.2002.0385

Robe, K., Gao, F., Lefebvre-legendre, L., Sylvestre-gonon, E., Hem, S., Rouhier, N., et al. (2020). Coumarin accumulation and trafficking in *Arabidopsis thaliana*: a

complex and dynamic process. *New Phytol.* 229, 2062–2079. doi: 10.1111/nph.17090

Rottmann, T. M., Fritz, C., Lauter, A., Schneider, S., Fischer, C., Danzberger, N., et al. (2018). Protoplast-esculin assay as a new method to assay plant sucrose transporters: characterization of AtSUC6 and AtSUC7 sucrose uptake activity in *Arabidopsis* Col-0 ecotype. *Front. Plant Sci.* 9:430. doi: 10.3389/fpls.2018.00430

Simkovitch, R., Pinto da Silva, L., Esteves da Silva, J. C., and Huppert, D. (2016). Comparison of the photoprotolytic processes of three 7-hydroxycoumarins. *J. Phys. Chem. B* 120, 10297–10310. doi: 10.1021/acs.jpcb.6b01383

Stefanachi, A., Leonetti, F., Pisani, L., Catto, M., and Carotti, A. (2018). Coumarin: a natural, privileged and versatile scaffold for bioactive compounds. *Molecules* 23:250. doi: 10.3390/molecules23020250

Stringlis, I. A., De Jonge, R., and Pieterse, C. M. J. (2019). The age of coumarins in plant-microbe interactions. *Plant Cell Physiol.* 60, 1405–1419. doi: 10.1093/pcp/pcz076

Sun, H., Wang, L., Zhang, B., Ma, J., Hettenhausen, C., Cao, G., et al. (2014). Scopoletin is a phytoalexin against alternaria alternata in wild tobacco dependent on jasmonate signalling. *J. Exp. Bot.* 65, 4305–4315. doi: 10.1093/jxb/eru203

Taguchi, G., Fujikawa, S., Yazawa, T., Kodaira, R., Hayashida, N., Shimosaka, M., et al. (2000). Scopoletin uptake from culture medium and accumulation in the vacuoles after conversion to scopolin in 2,4-D-treated tobacco cells. *Plant Sci.* 151, 153–161. doi: 10.1016/S0168-9452(99)00212-5

Tang, X., Xiao, Y., and Zhou, J. M. (2006). Regulation of the type III Secretion system in phytopathogenic bacteria. *Mol. Plant Microbe Interact* 19, 1159–1166. doi: 10.1094/MPMI-19-1159

Tattini, M., Di Ferdinando, M., Brunetti, C., Goti, A., Pollastri, S., Bellasio, C., et al. (2014). Esculetin and esculin (esculetin 6-O-glucoside) occur as inclusions and are differentially distributed in the vacuole of palisade cells in *Fraxinus ornus* leaves: a fluorescence microscopy analysis. *J. Photochem. Photobiol. B Biol.* 140, 28–35. doi: 10.1016/j.jphotobiol.2014.06.012

Tegli, S., Gori, A., Cerboneschi, M., Cipriani, M. G., and Sisto, A. (2011). Type three secretion system in *Pseudomonas savastanoi* pathovars: does timing matter? *Genes* 2, 957–979. doi: 10.3390/genes2040957

Veselov, S. Y., Valcke, R., Van Onckelen, H., and Kudoyarova, G. R. (1999). Cytokinin content and location in the leaves of the wild-type and transgenic tobacco plants. *Russ. J. Plant Physiol.* 46, 26–31. doi: 10.1093/jxb/erl235

Wei, W., Plovanich-Jones, A., Deng, W. L., Jin, Q. L., Collmer, A., Huang, H. C., et al. (2000). The gene coding for the Hrp pilus structural protein is required for type III secretion of Hrp and Avr proteins in *Pseudomonas syringae* pv. tomato. *Proc. Natl. Acad. Sci. U.S.A.* 97, 2247–2252. doi: 10.1073/pnas.040570097

Conflict of Interest: The authors declare that the research was conducted in the absence of any commercial or financial relationships that could be construed as a potential conflict of interest.

Publisher's Note: All claims expressed in this article are solely those of the authors and do not necessarily represent those of their affiliated organizations, or those of the publisher, the editors and the reviewers. Any product that may be evaluated in this article, or claim that may be made by its manufacturer, is not guaranteed or endorsed by the publisher.

frontiers | Frontiers in Microbiology

ORIGINAL RESEARCH
published: 29 April 2022
doi: 10.3389/fmicb.2022.837056

Comparative Transcriptome Analysis of Fungal Pathogen *Bipolaris maydis* to Understand Pathogenicity Behavior on Resistant and Susceptible Non-CMS Maize Genotypes

Shweta Meshram[1], Robin Gogoi[1], Bishnu Maya Bashyal[1], Aundy Kumar[1], Pranab Kumar Mandal[2] and Firoz Hossain[3]*

[1] Division of Plant Pathology, Indian Council of Agricultural Research (ICAR)-Indian Agricultural Research Institute, New Delhi, India, [2] Indian Council of Agricultural Research (ICAR)-National Institute for Plant Biotechnology, New Delhi, India, [3] Division of Genetics, Indian Council of Agricultural Research (ICAR)-Indian Agricultural Research Institute, New Delhi, India

OPEN ACCESS

Edited by:
Marco Scortichini, Council for Agricultural and Economics Research (CREA), Italy

Reviewed by:
Rui Shi, North Carolina State University, United States
Jialing Bao, Southwest University, China

***Correspondence:**
Robin Gogoi
r.gogoiiari@gmail.com

Specialty section:
This article was submitted to Microbe and Virus Interactions with Plants, a section of the journal Frontiers in Microbiology

Received: *16 December 2021*
Accepted: *02 March 2022*
Published: *29 April 2022*

Citation:
Meshram S, Gogoi R, Bashyal BM, Kumar A, Mandal PK and Hossain F (2022) Comparative Transcriptome Analysis of Fungal Pathogen Bipolaris maydis to Understand Pathogenicity Behavior on Resistant and Susceptible Non-CMS Maize Genotypes. Front. Microbiol. 13:837056. doi: 10.3389/fmicb.2022.837056

Bipolaris maydis is pathogen of maize which causes maydis leaf blight disease. In India major losses occur due to the *B. maydis* race "O" pathogen, whereas in other parts of the world, major losses are due to the race "T" pathogen. In the present study, we conducted an *in planta* transcriptomics study of the *B. maydis* race "O" pathogen after infection on non-CMS maize resistant and susceptible genotypes by mRNA sequencing to understand the molecular basis of pathogenicity for better management of the pathogen. Approximately 23.4 GB of mRNA-seq data of *B. maydis* were obtained from both resistant and susceptible maize backgrounds for fungus. Differentially expressed genes (DEGs) analysis of *B. maydis* in two different genetic backgrounds suggested that the majority of highly DEGs were associated with mitochondrial, cell wall and chitin synthesis, sugar metabolism, peroxidase activity, mitogen-activated protein kinase (MAPK) activity, and shikimate dehydrogenase. KEGG analysis showed that the biosynthetic pathways for secondary metabolism, antibiotics, and carbon metabolism of fungus were highly enriched, respectively, in susceptible backgrounds during infection. Previous studies in other host pathogen systems suggest that these genes play a vital role in causing disease in their host plants. Our study is probably the first transcriptome study of the *B. maydis* race "O" pathogen and provides in-depth insight of pathogenicity on the host.

Keywords: *Bipolaris maydis* race "O", non-CMS maize, RNA-seq, host–pathogen interaction, differentially expressed genes (DEGs), effectors

INTRODUCTION

Bipolaris maydis (*Cochliobolus heterostrophus*) is a necrotrophic ascomycete belonging to the order Pleosporales, which causes maydis leaf blight (MLB) or southern corn leaf blight. In India, yield losses occur due to the *B. maydis* race "O" pathogen in maize, unlike the rest of the world where major losses are due to the race "T" pathogen. Maize (*Zea mays* L.) is the third most widely grown

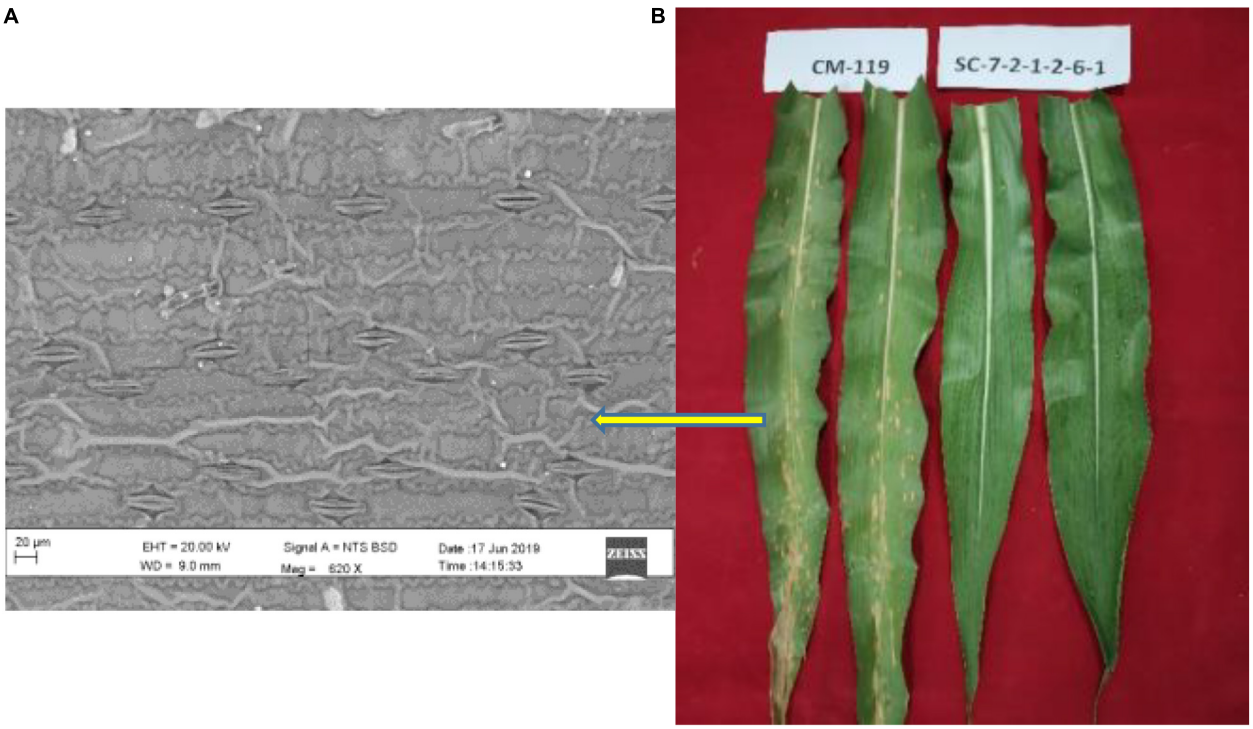

FIGURE 1 | (A) Scanning electron micrograph showing abundant fungal hyphae in susceptible (CM 119) line after infection with *Bipolaris maydis*. **(B)** Symptoms of maydis leaf blight on susceptible CM 119 (score 4) and resistant SC-7 (score 1) and both genotypes under field conditions.

TABLE 1 | Summary of the Illumina sequence reads obtained from *Zea mays* plants inoculated with *B. maydis* pathogen grown on sorghum seeds.

Sample*	Total clean reads	Data (GB)	Q30%	Paired total	Paired aligned uniquely	Unpaired total	Unpaired aligned uniquely	Overall alignment rate
RI	34527322	5.24	89.8	17263661	17215458	34430916	56440	0.45
RIR	29461518	4.46	90.54	14730759	14687660	29375320	59682	0.5
SI	42163024	6.3	91.11	21081512	20621885	41243770	68621	2.35
SIR	50012112	7.5	90.23	25006056	23866276	47732552	171279	4.91

**RI, resistant inoculated; RIR, resistant inoculated replicate; SI, susceptible inoculated; SIR, susceptible inoculated replicate.*

cereal crop after rice and wheat in India (Hussain, 2011). Losses in India due to MLB disease may extend up to 70% (Kumar et al., 2016). Infected maize typically causes tan and elliptical to rectangular lesions (White, 1999) on the leaves and under the surface of foliage which later coalesce and result in an extensive blight appearance. Among the 65 major foliar diseases of maize, MLB is an important disease of maize (Rahul and Singh, 2002). MLB is reported from almost all maize growing regions in the world but more severe in areas where environmental conditions are hot and humid. Three races (C, O, and T) of *B. maydis* have been identified in maize crop so far. Race "O" is more prevalent than "T" in India, whereas worldwide, race "T" is a major concern; race "C" is reported only in China (Mubeen et al., 2017).

Bipolaris maydis race "O" is predominant in tropical and sub-tropical areas. It infects a broad range of maize genotypes including CMS and non-CMS maize lines. Studies reported that inoculated susceptible lines with race "O" showed a 50% yield loss (Fisher et al., 1976; Gregory et al., 1978). Typical symptoms of race "O" are small lesions which eventually become diamond-shaped and rectangular as they mature and are restricted to leaf veins (Ali et al., 2011). Race "T" attacks CMS maize which promotes Texas male-sterile cytoplasm (cms-T), this race historically caused an epidemic in the United States in 1970 and 1971. Typical symptoms of race "T" develop on leaves, husks, and ears, and produce small lesions on maize (Ullstrup, 1972). Races "O" and "T" can be identified best with a host differential test, *viz*., a pathogenicity test of cms-T plants, and also by physiological/morphological characteristics on culture media (Leonard, 1977; Warren et al., 1977).

Combatting losses caused by MLB resistance varieties is the best solution. Maize crop is resistant to race "T" with normal cytoplasm therefore management of race "T" can be achieved with elimination of cms-T from cultivars of high agronomic importance (Hyre, 1970; Ullstrup, 1972). In India, a broad range of maize genotypes serve as the major host of race

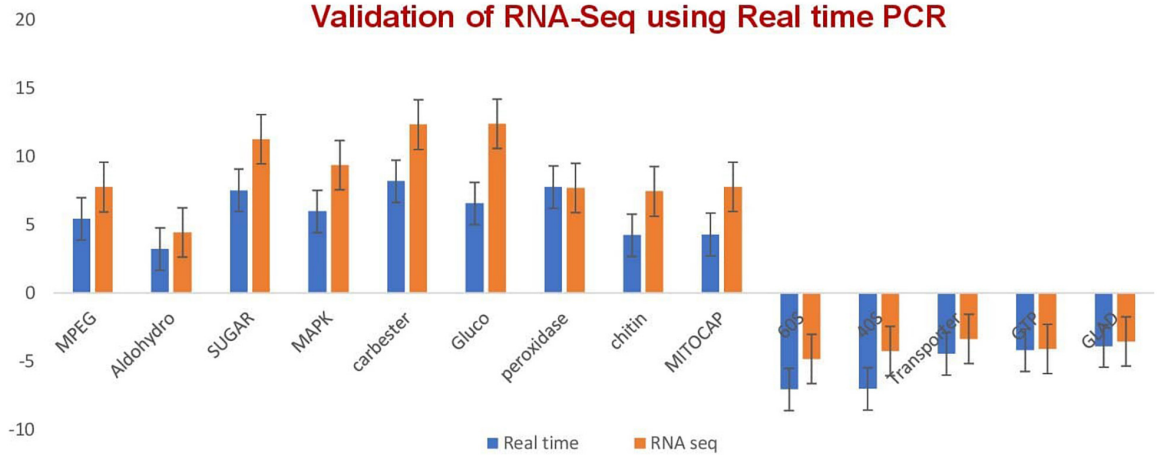

FIGURE 2 | qRT-PCR validation of the relative expression data of genes obtained in RNA-seq analysis. Expression levels of selected transcripts are shown in dark blue (qRT-PCR) and orange (RNA-seq). The fungal actin gene was used for transcript normalization of the signal intensity which is shown on the *y* axis. The *x* axis shows comparisons of the results of the two analyses. Error bars show standard deviations for triplicate assays.

TABLE 2 | Top 20 highly upregulated genes of *B. maydis* differentially expressed in inoculated resistant and susceptible plants.

Gene ID	Log fold	Annotation	Protein ID
COCHEDRAFT_1021363	12.60451532	Domain of unknown function (DUF3328)	EMD91267
COCHEDRAFT_1093124	10.37257746	EthD domain	EMD94050
COCHEDRAFT_1202737	12.82138123	Cerato-platanin	EMD92796
COCHEDRAFT_1101487	12.45535783	Domain of unknown function (DUF3328)	EMD91266
COCHEDRAFT_1140189	12.39934756	Glucanosyl transferase	EMD90599
COCHEDRAFT_1140839	12.33128367	Carboxylesterase family	EMD89062
COCHEDRAFT_16026	7.231602644	1941118.1	EMD92794
COCHEDRAFT_1185072	12.98058241	Tannase and feruloyl esterase	EMD86863
COCHEDRAFT_1147694	13.19280605	13684.SNOT_06000	EMD85980
COCHEDRAFT_1198613	7.756361319	MAPEG family	EMD85630
COCHEDRAFT_1028180	6.882906745	Cutinase	EMD94256
COCHEDRAFT_1134453	14.34810723	EXS family	EMD92204
COCHEDRAFT_1193999	14.27393273	Cytochrome P450	EMD92530
COCHEDRAFT_1222232	15.00590358	GMC oxidoreductase	EMD94987
COCHEDRAFT_1166191	6.417942179	Alcohol dehydrogenase GroES-like domain	EMD95758
COCHEDRAFT_1019411	6.282567882	Inherit from ascNOG: conserved hypothetical protein	EMD95841
COCHEDRAFT_1219056	4.855362398	Bi functional enzyme with both catalase and broad spectrum peroxidase activity (by similarity)	EMD85713
COCHEDRAFT_1113526	6.25668138	D-Isomer specific 2-hydroxyacid dehydrogenase, catalytic domain	EMD87549
COCHEDRAFT_1224654	6.163316228	Aldehyde dehydrogenase family	EMD91526
COCHEDRAFT_1130430	5.564541045	Flavodoxin-like fold	EMD94134

"O," which causes huge loss. So far, we only know that the rhm recessive gene of *C. heterostrophus* confers resistance to race "O" (Zaitlin et al., 1993). Various screening techniques, *viz*., detached leaf techniques (Lakshmi and Sharma, 1987), tissue culture (Kuehnle and Earle, 1988), and seedling assays (Tajimi et al., 1985) have been investigated for disease resistance. Conventional breeding or recurrent selection is also an effective method to improve resistance against MLB (Shieh and Lu, 1993). On the pathogen side, very few studies have been conducted to understand the race "O" pathogen. In the present study, whole transcriptome analysis was done by mRNA sequencing of the *B. maydis* race "O" pathogen after infection of resistant and susceptible non-CMS maize inbred lines to understand the molecular basis of pathogenicity leading to better management of the pathogen. The race "O" pathogen used in this study was re-confirmed by Venkatesh et al. (2021). So far transcriptome analysis of fungal pathogen *B. sorokiniana* on infected wheat (Ye et al., 2019) and *B. sorghicola* on sorghum (Mizuno et al., 2012; Yazawa et al., 2013) has been completed. Here we present probably the first *in planta* transcriptome study of the *B. maydis* race "O" pathogen on non-CMS maize lines. RNA-seq and fold change were calculated by comparing *B. maydis* infection on susceptible inoculated (SI) versus resistant inoculated (RI) lines.

TABLE 3 | Top 20 highly downregulated genes of *B. maydis* differentially expressed in inoculated resistant and susceptible plants.

Gene ID	Log fold	Annotation	Protein ID
COCHEDRAFT_1195	−3.861184569	40s ribosomal protein	EMD89020
COCHEDRAFT_1177804	−4.236671634	40S ribosomal protein S3	EMD89815
COCHEDRAFT_1021505	−4.212183943	60S ribosomal protein	EMD91574
COCHEDRAFT_1225360	−3.861184569	L 21 protein	EMD89740
COCHEDRAFT_1157448	−4.430696422	40S ribosomal protein S3	EMD90435
COCHEDRAFT_1173335	−4.540817315	40S ribosomal protein S1	EMD91948
COCHEDRAFT_1214489	−4.814349769	60s ribosomal protein l11	EMD91114
COCHEDRAFT_1225361	−5.094309904	40S ribosomal protein S9	EMD89741
COCHEDRAFT_1127623	−3.48264224	40S ribosomal protein S8	EMD96126
COCHEDRAFT_1224611	−3.530642646	Ribosomal protein	EMD91465
COCHEDRAFT_1145202	−3.550348853	Glyceraldehyde-3-phosphate dehydrogenase	EMD87494
COCHEDRAFT_1019764	−3.442593019	Ribosomal protein S13/S18	EMD94767
COCHEDRAFT_1164310	−3.783863683	Ribosomal protein L11, N-terminal domain	EMD97422
COCHEDRAFT_1139445	−4.098487448	Promotes the GTP-dependent binding of aminoacyl-tRNA to the A-site of ribosomes during protein biosynthesis (by similarity)	EMD90278
ENSRNAG049949382	−3.809190151	–	
ENSRNAG049949379	−5.40016	–	
ENSRNAG049949459	−4.76472	–	
COCHEDRAFT_1122518	−5.724881452	H3	EMD84642
COCHEDRAFT_1103804	−5.871461339	3027035.1	EMD91248

MATERIALS AND METHODS

Plant Material and Fungal Inoculation

Two extreme genotypes of maize inbred lines differing in their susceptibility to *B. maydis* were used in this study. Line SC-7-2-1-2-6-1 (SC-7) which is registered (INGR 07025) as a highly resistant non-CMS line and CM 119 which is established as a standard susceptible marker against *B. maydis*. The experiment was conducted under greenhouse conditions. The *B. maydis* New Delhi isolate was maintained in pure culture and later mass-multiplied on soaked sorghum seeds. After 30 days, old plants were inoculated with pathogen *B. maydis* according to the method described by Payak and Sharma (1983). Inoculated samples were collected for RNA-seq at 48 h post inoculation (disease phase, Liu et al., 2015). Symptoms started appearing and fungal signs were noticed more clearly on susceptible line CM 119 (**Figure 1**).

RNA Extraction, Library Preparation, and Sequencing

Total RNA was extracted from infected CM 119 and SC-7 at 48 h post inoculation and their non-inoculated controls with an RNAeasy plant mini kit (Qiagen) following the manufacturer's instructions. Total RNA of each sample was quantified and qualified by an Agilent 2100 Bioanalyzer (Agilent Technologies, Palo Alto, CA, United States), NanoDrop (Thermo Fisher Scientific Inc.), and 1% agarose gel. One microgram of total RNA with an RIN value above 7 was used for the following library preparation. Next-generation sequencing library preparations were carried out as instructed in the manufacturer's protocol (NEBNext® Ultra™ RNA Library Prep Kit for Illumina®).

Quality Control and Read Mapping to the Reference Genome

Quality checks for the raw fastq files were conducted through a pipeline consisting of FastQC. The minimum quality score was 30 (Qphred). HISAT2 software was selected according to the characteristics of the reference genome. The reference genome used for this study was Bipolaris_maydis_c5_gca_000338975.CocheC5_3.dna.toplevel.fa. Raw read counts mapped to each gene from the HiSat2-generated alignments were obtained using the feature counts command (Liao et al., 2014) of the subread package (Liao et al., 2013).

Differential Gene Expression Analysis

For differentially expressed gene (DEG) identification, DESEq2 V1.21.17 with a replicated package was run with parametric fit Padj < 0.05. A false discovery rate (FDR) of 0.05 and a fold change of >0 were set as thresholds for DEG calling, as previously described (Bagnaresi et al., 2012; Li and Lan, 2015) and *P*-value >0.05 was set. The list of all DEGs is provided (**Supplementary Table 1**) to allow any further DEG sub-setting based on different FDRs or fold changes.

GO Enrichment and KEGG Analyses

GO enrichment analyses were conducted with topGO, an R-bioconductor package for enrichment analysis version 2.28.0., and a *P*-value of 0.001 was used with classic Fisher ordering, ranks= topgoFisher. The Bioconductor package ClusterProfiler version 3.10.0 was used to generate relevant KEGG pathway pictures incorporating color-coded expression values (Padj < 0.05). A pie chart for GO enrichment is provided along with enriched genes (**Supplementary Tables 2–4**).

TABLE 4 | Important upregulated genes for pathogen fitness and pathogenesis.

Gene and gene ID	Log fold change	Description	References
Mitochondrial genes			
Mitochondrial carrier protein COCHEDRAFT_1139719	7.7685614	Transport of ions, nucleotide, amino acid, and cofactors across membrane	Bertrand, 2000; Arcila et al., 2021
Mitochondrial 18 kDa protein COCHEDRAFT_1024553	8.172178	Mitochondrial fission, morphology, and development of mitochondria, mutation leads to apoptosis	
AMP-binding enzyme COCHEDRAFT_1105220	10.68332	Mitochondrial biogenesis	
ATP-dependent serine protease COCHEDRAFT_1207993	8.95483288	Participates in the regulation of mitochondrial gene expression and in the maintenance of the integrity of the mitochondrial genome	
YmL38 YmL34 7.407734745	7.407734745	Mitochondrial 54S ribosomal protein	
Mitochondrial protein synthesis	7.976810257	Promotes mitochondrial ribosomes in a GTP-dependent manner	
Fungal cell wall and chitin synthesis genes			
Chitin synthase III catalytic subunit COCHEDRAFT_1197445	7.451803741	Responsible for the synthesis of the majority of the chitin found in the cell wall periphery	Banks et al., 2005; Langner and Göhre, 2016; Pusztahelyi, 2018; Garcia-Rubio et al., 2020
Chitin synthase. COCHEDRAFT_1192892	10.12960501	Chitin synthases (CHSs) are key enzymes in the biosynthesis of chitin, an important structural component of fungal cell walls	
Chitin synthesis regulation, resistance to Congo red COCHEDRAFT_1152857	3.273618	Regulates chitin deposition in the fungal cell wall	
Sugar metabolism			
Sugar transporter COCHEDRAFT_1186319	11.2559271	Sugar transporters (STs) that are essential for taking up the mono- and short oligosaccharides, resulting from extracellular enzymatic digestion of lignocellulose, into the fungal cell	Vankuyk et al., 2004; Lv et al., 2020; Monfared et al., 2020
Glucanases COCHEDRAFT_1118047	7.355847304	Plays a role in cell expansion during growth, in cell–cell fusion during mating, and in spore release during sporulation. This enzyme may be involved in beta-glucan degradation	
Genes related to toxin (polyketide cyclases)			
Polyketide cyclases family COCHEDRAFT_1167946	7.332835	T-toxin is a family of linear polyketides 37–45 carbons in length, of which the major component is 41 carbons	Gaffoor et al., 2005; Schindler and Nowrousian, 2014
Acetoacetate decarboxylase COCHEDRAFT_1103773	8.894696	Catalyzes the conversion of acetoacetate to acetone and carbon dioxide	
LAM1 COCHEDRAFT_1167244	8.228607	3-Hydroxyacyl-CoA dehydrogenase, NAD-binding domain	
Other important genes associated with secondary metabolites and signaling			
Peroxidase COCHEDRAFT_1125365	7.721354	Peroxidases are a group of oxidoreductases which mediate electron transfer from hydrogen peroxide (H_2O_2) and organic peroxide to various electron acceptors	Mir et al., 2015
Reactive mitochondrial oxygen species modulator COCHEDRAFT_1022035	8.233186	Required in fungal differentiation processes that are necessary for virulence	Hansberg et al., 2012; Mir et al., 2015; Martínez-Soto and Ruiz-Herrera, 2017
Mitogen-activated protein kinase COCHEDRAFT_1207640	9.375412764	Involved in fungal development, sexual reproduction, pathogenicity and/or virulence in many filamentous plant pathogenic fungi	
Catalase COCHEDRAFT_1179052	8.872981819	Catalyzes the reaction of cyanate with bicarbonate to produce ammonia and carbon dioxide	
Shikimate dehydrogenase substrate binding domain COCHEDRAFT_1228346	9.422273	Catalytic domain at N terminus binds to the substrate, 3-dehydroshikimate	
Signal-recognition-particle (SRP) COCHEDRAFT_1187286	8.077532	Signal-recognition-particle assembly has a crucial role in targeting secretory proteins to the rough endoplasmic reticulum membrane	

TABLE 5 | List of candidate effector genes identified in *B. maydis*.

Gene ID	Annotation	CDS	Effector prediction	Description based on UniProt/InterPro and similarity
COCHEDRAFT_1093124	EthD domain Ethyl tert-butyl ether degradation	103	0.916	Contributes to conidial pigmentation that provides protection from UV radiation, heat and cold stress
COCHEDRAFT_1202737	Hypothetical protein	138	0.918	Protein occurs in the cell wall of the fungus and is involved in the host-plane interaction and induces both cell necrosis and phytoalexin synthesis which is one of the first plant defense-related events
COCHEDRAFT_1134423	Hypothetical protein	130	0.999	Component of the endoplasmic reticulum-associated degradation (ERAD) pathway
COCHEDRAFT_1155213	Hypothetical protein	162	0.997	Integral component of cell membrane
COCHEDRAFT_1193149	Conserved hypothetical protein	165	0.691	Integral component of cell membrane
COCHEDRAFT_1020438	Conserved hypothetical protein	86	0.539	NADH dehydrogenase (ubiquinone) 1 alpha subcomplex subunit 1
COCHEDRAFT_1094426	Conserved hypothetical protein	211	0.888	Thioredoxin-like fold domain-containing protein
COCHEDRAFT_1168141	Hypothetical protein	169	0.965	Uncharacterized protein
COCHEDRAFT_1149474	Proteasome subunit	205	0.767	Cleavage of peptide bonds with very broad specificity, endopeptidase
COCHEDRAFT_1199047	ATP synthase E chain	90	0.71	Mitochondrial membrane ATP synthase
COCHEDRAFT_1024634	Cytidine and deoxycytidylate deaminase zinc-binding region	185	0.948	Scavenges exogenous and endogenous cytidine and 2′-deoxycytidine for UMP synthesis
COCHEDRAFT_1188666	Antibiotic biosynthesis monooxygenase	108	0.992	ABM domain-containing protein
COCHEDRAFT_1148964	Hypothetical protein	72	0.966	Membrane-associated and mitochondrion-associated cellular component
COCHEDRAFT_1207896	Synaptobrevin	200	0.976	Vesicle-mediated transport
COCHEDRAFT_1088730	Dienelactone hydrolase family	250	0.555	DLH domain, hydrolase activity
COCHEDRAFT_1019519	Redoxin	167	0.856	Thiol-specific peroxidase that catalyzes the reduction of hydrogen peroxide and organic hydroperoxides to water and alcohols, respectively. Plays a role in cell protection against oxidative stress by detoxifying peroxides
COCHEDRAFT_1221715	Protein of unknown function (DUF1687)	150	0.98	Putative mitochondrial redox protein which could be involved in the reduction of small toxic molecules
COCHEDRAFT_1221723	Ubiquitin-conjugating enzyme	149	0.779	Glycyl thioester intermediate, ATP binding, transferase activity
COCHEDRAFT_1019537	Mitochondrial ribosomal protein L51/S25/CI-B8 domain	93	0.986	Electron transport, respiratory chain
COCHEDRAFT_1166992	ATP synthase delta (OSCP) subunit	231	0.978	ATP synthase subunit 5, mitochondrial, proton-transporting ATP synthase activity
COCHEDRAFT_1191234	Cytochrome *c* domain-containing protein	108	0.999	Electron carrier protein. The oxidized form of the cytochrome *c* heme group can accept an electron from the heme group of the cytochrome c1 subunit of cytochrome reductase. Cytochrome *c* then transfers this electron to the cytochrome oxidase complex, the final protein carrier in the mitochondrial electron-transport chain (by similarity)
COCHEDRAFT_1127633	Stress-response A/B barrel domain-containing protein	110	0.931	Stress-response A/B barrel domain-containing protein

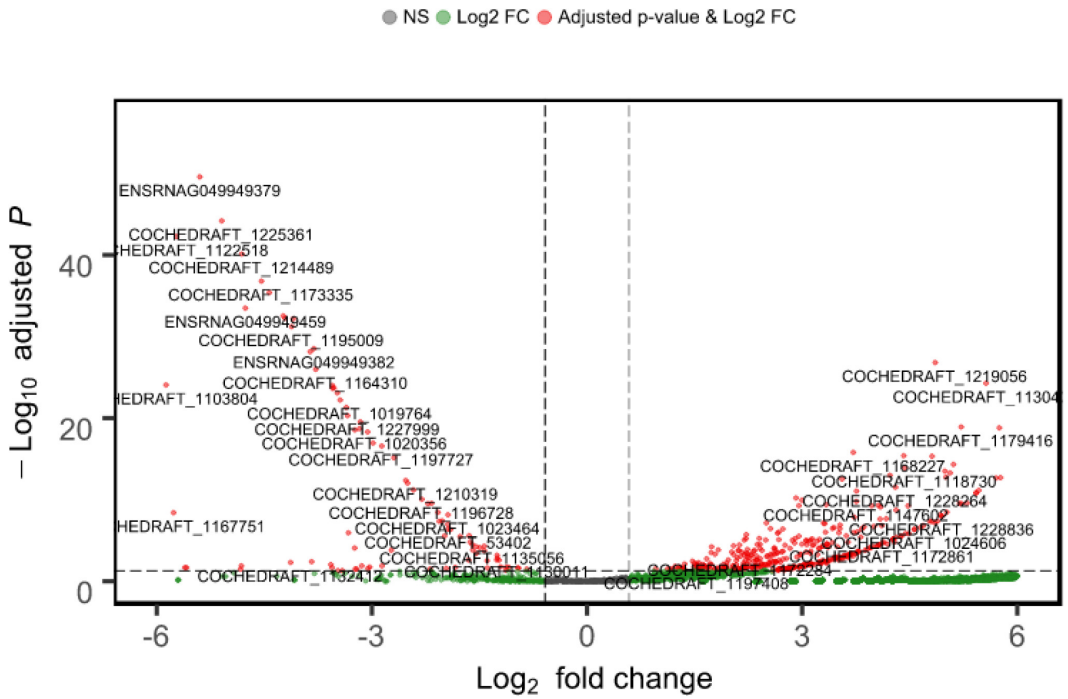

FIGURE 3 | Mean expression versus log fold change plots (MA-plots). Transcriptional changes of *B. maydis* are presented in SC-7 and CM 119 48 h post inoculation. Normalized *P*-values are plotted versus Log2 fold changes. Genes with an FDR < 0.05 are plotted.

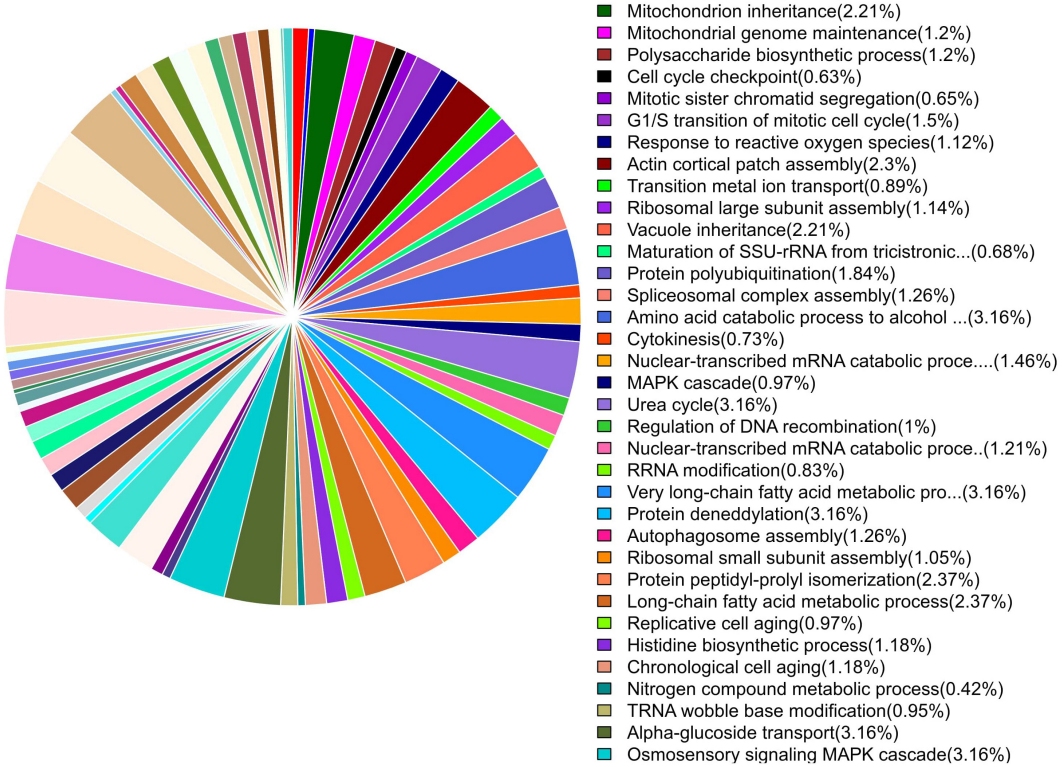

FIGURE 4 | Pie chart of enriched GO terms of *B. maydis* for biological functions differentially expressed in inoculated resistant and susceptible plants.

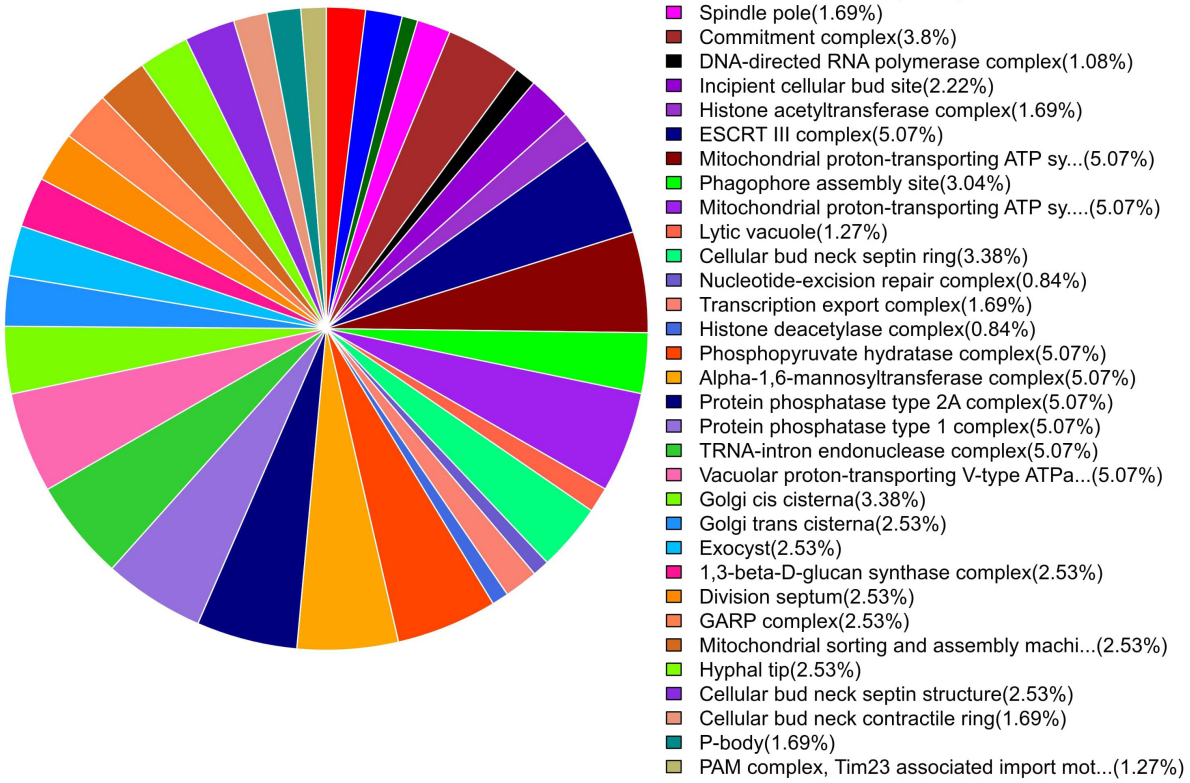

FIGURE 5 | Pie chart of enriched GO terms of *B. maydis* for cellular functions differentially expressed in inoculated resistant and susceptible plants.

qRT-PCR for Expression of Selected Genes

The validation of the RNA-seq technique was performed by quantitative RT-PCR through monitoring the expression levels of seven selected transcripts (**Figure 2** and **Supplementary Table 5**) after designing primers for selected genes (**Supplementary Table 6**). A melt curve is also provided in **Supplementary Figure 1**.

Statistical Analysis

qRT-PCR data were analyzed by analysis of variance (ANOVA) using the Statistical Package for Social Science (SPSS, IBM, Chicago, IL, United States) version 16.0. The statistical significance was judged at $P < 0.05$.

RESULTS

Disease Development

There were no observable phenotypic differences between the susceptible and resistant maize inbred lines without pathogen inoculation at all-time points. We observed prominent symptoms on susceptible line CM 119. Non-inoculated controls never showed necrotic lesions. Lesions were visible from 72 h after inoculation. In the resistant line, lesions were small and fewer in numbers. There was a noticeable symptom difference between the susceptible and resistant maize inbred lines at 96 h after inoculation (**Figure 1**).

Sequencing and Mapping

From the sequencing of *in planta* libraries, approximately 31,994,420 resistant and 46,087,568 susceptible lines reads were generated (**Table 1**). The genome was mapped with reference genome Bipolaris_maydis_c5_gca_000338975.CocheC5_3.dna.toplevel.fa., and mapping statistics are provided in **Supplementary Figure 2**.

Differential Gene Expression Analysis

Approximately 23.4 GB of mRNA-seq data of *B. maydis* were obtained from both resistant and susceptible maize backgrounds. DEG analysis was conducted to detect *B. maydis* transcriptome changes during the pathogenesis of maize. Out of 10,363 mapped genes, 3313 genes were upregulated and only 100 genes were downregulated, and 6949 genes were commonly expressed in *B. maydis* SI plants compared to RI plants. A list of genes and their expression is provided in **Supplementary Table 1**. Log FCs and *P*-value are shown in **Figure 3**.

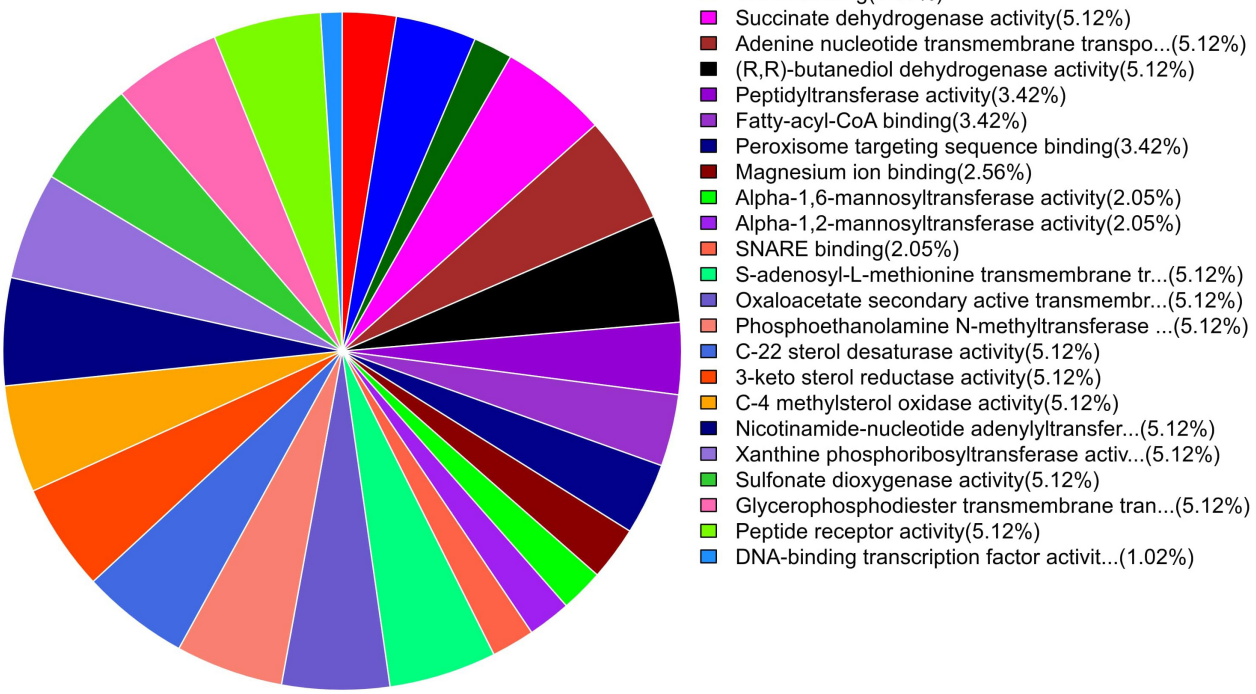

FIGURE 6 | Pie chart of enriched GO terms of *B. maydis* for molecular functions differentially expressed in inoculated resistant and susceptible plants.

TABLE 6 | Top 10 important enriched GO terms of *B. maydis* for biological functions differentially expressed in inoculated resistant and susceptible plants.

Gene ID	Annotation	Enriched genes	Function
1	GO:0000003	Reproduction	188
2	GO:0002181	Cytoplasmic translation	67
3	GO:0007275	Multicellular organism development	41
4	GO:0000054	Ribosomal subunit export from nucleus	21
5	GO:0000096	Sulfur amino acid metabolic process	21
6	GO:0000122	Negative regulation of transcription	22
7	GO:0000272	Polysaccharide catabolic process	21
8	GO:0000375	RNA splicing *via* transesterification	33
9	GO:0008150	Biological process	730
10	GO:0000001	Mitochondrion inheritance	14

TABLE 7 | Top 10 important enriched GO terms of *B. maydis* for cellular functions differentially expressed in inoculated resistant and susceptible plants.

Gene ID	Annotation	Enriched genes	Number
1	GO:0005575	Cellular component	555
2	GO:0000139	Golgi membrane	72
3	GO:0000322	Storage vacuole	58
4	GO:0000502	Proteasome complex	25
5	GO:0000313	Organellar ribosome	22
6	GO:0000151	Ubiquitin ligase complex	12
7	GO:0000228	Nuclear chromosome	15
8	GO:0000922	Spindle pole	10
9	GO:0000243	Commitment complex	6
10	GO:0000428	DNA-directed RNA polymerase complex	10

TABLE 8 | Top 10 important enriched GO terms of *B. maydis* for molecular functions differentially expressed in inoculated resistant and susceptible plants.

Gene ID	Annotation	Enriched genes	Number
1	GO:0003674	Molecular function	626
2	GO:0000166	Nucleotide binding	97
3	GO:0000030	Mannosyl transferase activity	10
4	GO:0001671	ATPase activator activity	3
5	GO:0000049	tRNA binding	4
6	GO:0000104	Succinate dehydrogenase activity	2
7	GO:0000295	Adenine nucleotide transmembrane transport	2
8	GO:0000721	(R,R)-butanediol dehydrogenase activity	2
9	GO:0000048	Peptidyltransferase activity	2
10	GO:0000062	Fatty-acyl-CoA binding	2

Transcriptome analysis of the top 40 DEGs suggested 20 upregulated and 20 downregulated genes, the detailed description of genes along with their fold change and function is provided in **Tables 2**, **3**. Further, these DEGs were studied for genes related to pathogenesis and pathogen fitness which revealed important aspects, as shown in **Table 4** and **Supplementary Table 1**. On the other hand, the data were also analyzed *in silico* to find out putative effectors using the Effector database and 22 effectors were predicted (**Table 5**).

GO Categories and Enrichment Analysis

GO enrichment suggested that most of the genes under DEGs were associated with pathogen fitness and reproduction. The results are presented in **Figures 4–6** and described in **Tables 6–8**, with additional information available in **Supplementary Tables 2–4**.

DISCUSSION

Enrichment analysis and the expression patterns of the highly upregulated genes indicated that successful pathogenicity of *B. maydis* depends on pathogen fitness genes such as mitochondrial genes, cell wall synthesis, toxin-related effector molecules, and on other hand, cell wall degradation of the host, detoxification, and host defense evasion (**Figures 7–9**). Understanding the pathogen's molecular pathways during the infection process using transcriptome analysis can contribute significantly to identifying new targets for SSR control, novel genes, and pathogenicity-related pathways (Ribeiro et al., 2020; Poretti et al., 2021).

Mitochondrial Genes

Mitochondria have diverse functions to perform in fungal cells. Mitochondria play a major role in fungal metabolism

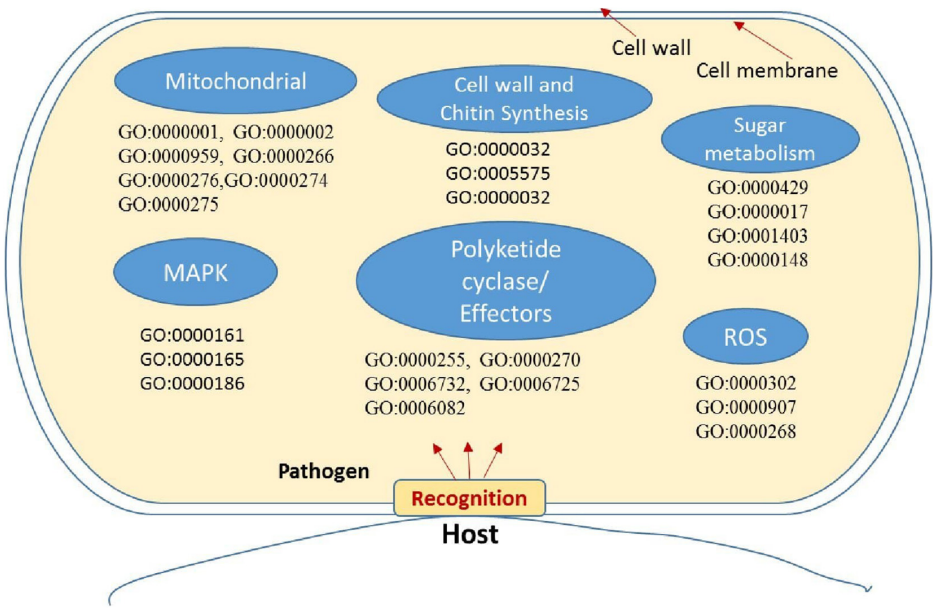

FIGURE 7 | Putative representation of possible activation of genes and GO enriched terms in fungal pathogen *Bipolaris maydis* in susceptible maize (CM 119) compared to resistant maize (SC-7) during early stages of infection. GO term and associated gene IDs are provided in **Supplementary Table 7**.

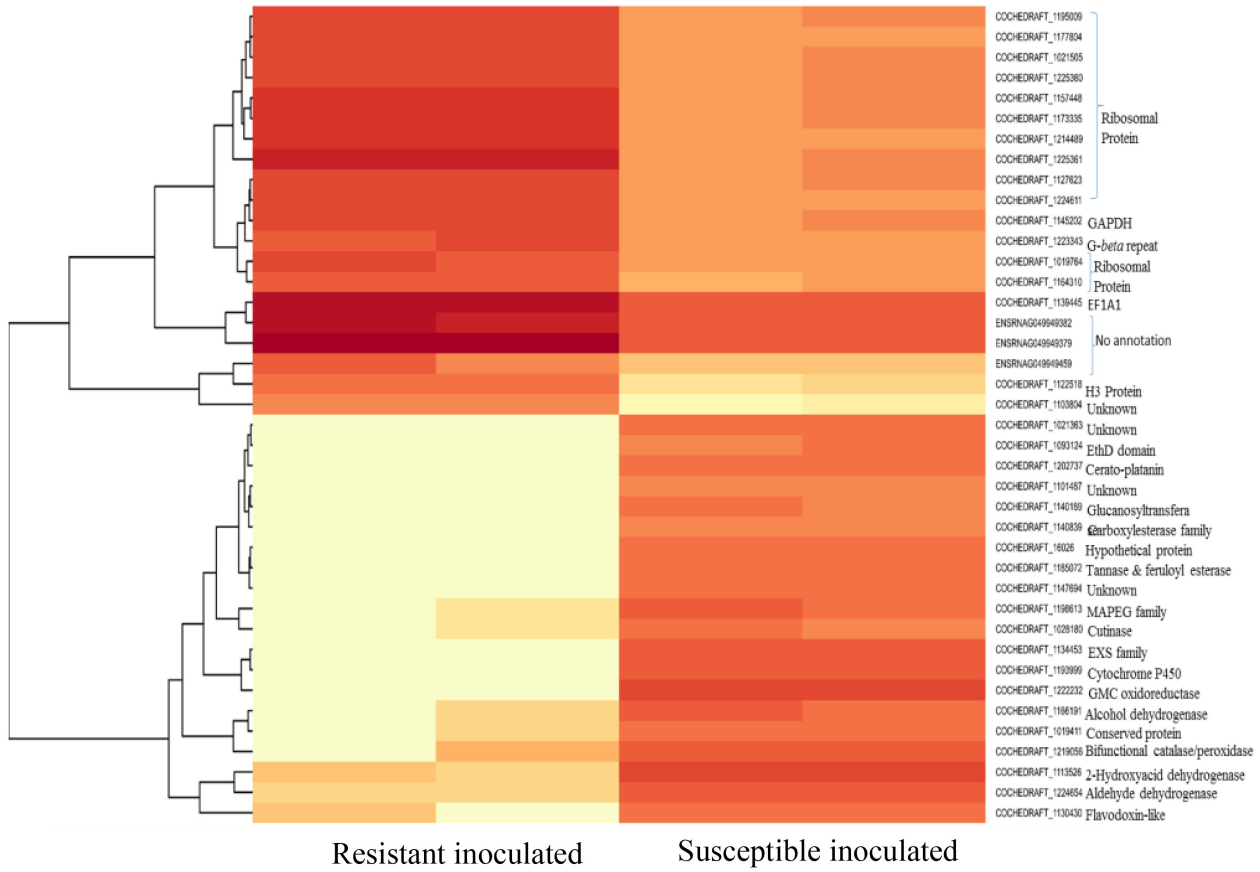

FIGURE 8 | Heat map of top 40 differentially expressed genes of *B. maydis* in resistant and susceptible maize genotypes 48 h post inoculation.

and fungicide resistance (Arcila et al., 2021). In the present study, genes associated with mitochondrial functions for *B. maydis* race "O" were upregulated in the susceptible line (CM 119), which suggests that CM 119 supports the growth of *B. maydis*, and on the other hand, SC-7 restricts the cellular activity of fungus (**Figure 8**). Previously studies suggested that fungal mitochondria play a significant role in determining fungal fitness and virulence (Calderone et al., 2015; Medina et al., 2020). A recent study suggests that endoplasmic reticulum (ER) and mitochondrial interactions along with the ER-mitochondria organizing network (ERMIONE) play important roles in adaptive responses in fungi, particularly in response to cell surface-related mechanisms that facilitate fungal invasion, growth, and stress responsive behaviors that support fungal pathogenicity (Koch et al., 2017). An investigation on *C. parasitica* study suggested the role of mitochondria in hypo virulence (Bertrand, 2000). Another study on the mitochondria genome of phytopathogens *Synchytrium endobioticum* and *Phlebia radiate* showed that alteration in the mitochondrial genome majorly affects the ability of fungi to adapt to changing environments (Medina et al., 2020). Overall, fungal mitochondria play a crucial role in determining pathogenicity of the host, and in susceptible backgrounds of the host, these genes are more expressed whereas resistant genotypes have a tendency to suppress the mitochondrial genes and ultimately the pathogen becomes less virulent, which we found in the present study.

Fungal Cell Wall and Chitin Synthesis Genes

The cell wall is an important component of fungal cells which mediates fungal cell interactions with its external environment and hyphal development (Castro et al., 2022). Chitin is the main component for cell wall synthesis. The cell wall protects the cell content, provides rigidity, and determines the cellular structure. It also protects the cell from various stresses including osmotic changes which are significant for healthy fungal cells. It also carries some proteins that play a role in recognition, adhesion, and receptor activity. There are several studies which establish the role of the fungal cell wall in pathogen fitness and its association with pathogenesis (Banks et al., 2005; Langner and Göhre, 2016; Pusztahelyi, 2018; Garcia-Rubio et al., 2020). It has also been investigated whether the fungal cell wall plays a crucial role in spore development (Backes et al., 2020) and in antifungal resistance activity (Díaz-Jiménez et al., 2012). In the present study, the high expression of cell wall-associated genes reconfirmed the fact that the fungal cell wall plays an

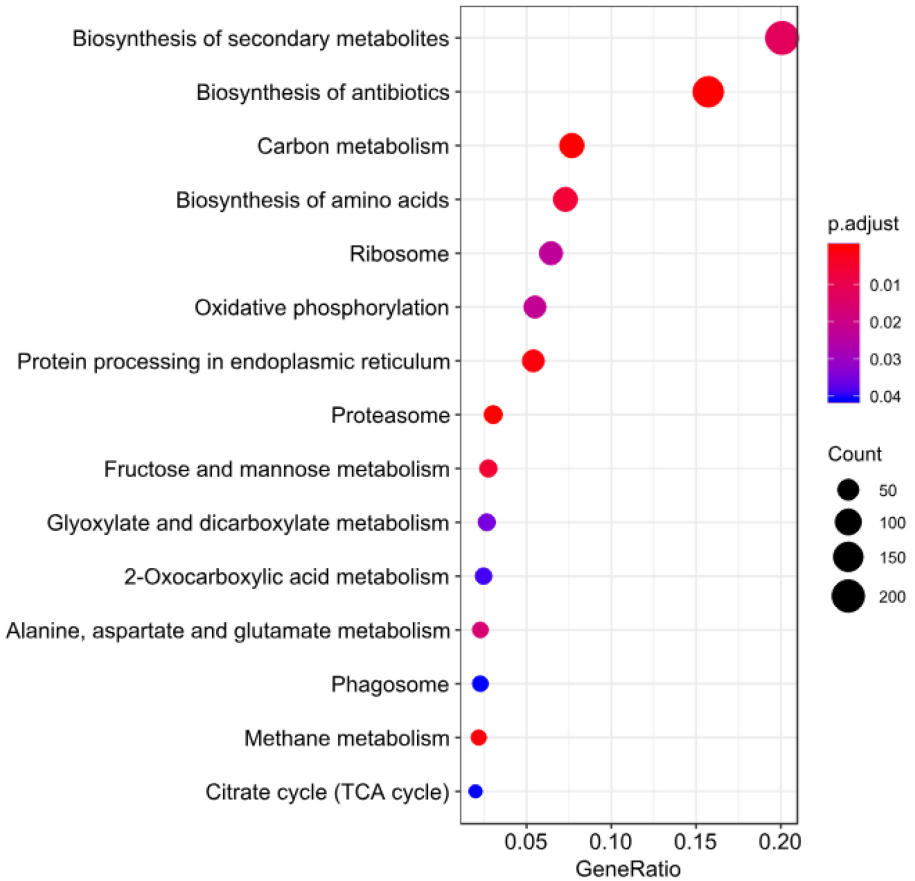

FIGURE 9 | KEGG enrichment analysis for DEGs of *B. maydis* in maize susceptible and resistant genotypes at 96 h post inoculation.

essential role in disease development in susceptible hosts and also showed that the resistant genotype had the capacity to hinder the expression of fungal cell wall genes during the interaction (**Figure 7**).

Sugar Metabolism

Sugar transporter genes of filamentous fungi are associated with multiple physiological and biochemical processes, such as the response to various stresses (Vankuyk et al., 2004; Lv et al., 2020; Monfared et al., 2020). They were also found to be linked with many salt tolerance and sophisticated transcriptional processes. In the present transcriptome profile of *B. maydis*, genes of sugar metabolism (**Figure 9**) such as sugar transporter and glucanases were upregulated which suggests that these genes play an essential role in pathogen proliferation under susceptible backgrounds of the host.

Gene-Related Polyketides

Polyketides (PKs) play a role in mycelial growth and development of asexual and sexual structures of fungi (Gaffoor et al., 2005; Schindler and Nowrousian, 2014) including shikimate dehydrogenase (Kinghorn, 2000). A study on *B. maydis* race "T" demonstrated the association of a toxin-related locus with polyketide biosynthesis and high virulence on T-cytoplasm maize (Rose et al., 2002), similarly in the present study, high expression of PKs was investigated which suggests there could be a possible association of toxin "O" with PKs.

Other Important Genes Associated With Secondary Metabolites and Signaling

Recent studies proposed peroxidases, catalases, and reactive oxygen species (ROS) as components of the antioxidant defense system in fungal pathogens and were also associated with conidial production (Zhang et al., 2020). A study on fungal pathogen *Magnaporthe oryzae* suggested significant and positive correlations among sensitivity to H_2O_2, peroxidase activity, and fungal pathogenicity (Garre et al., 1998; Hansberg et al., 2012; Mir et al., 2015; Chittem et al., 2020). On the other hand, mitogen-activated protein kinase (MAPK) signaling pathways play an important role in cell cycle control, mating, morphogenesis, response to different stresses, resistance to UV radiation, temperature changes, cell wall assembly and integrity, degradation of cellular organelles, virulence, cell–cell signaling, fungus-plant interaction, and response to damage-associated molecular patterns (DAMPs) (Martínez-Soto and Ruiz-Herrera, 2017). Upregulation of these genes in the *B. myadis* race "O"

pathogen indicated the interconnected nature in determining the fungal infection strategy in susceptible hosts (**Figure 7**).

Candidate Effector Genes Identified in *Bipolaris maydis*

At least 22 transcripts showing homology to genes previously reported to be involved in fungal infection were predicted as effector proteins (**Table 5** and **Figure 9**) in the Effector database using the CSIRO tool EffectorP2 (a machine learning method for fungal effector prediction in secretomes) (Sperschneider et al., 2018). The majority of them showed a probability above 60–90%. This fact can provide evidence for the pathogenicity behavior of *B. myadis* race "O" on susceptible lines.

CONCLUSION

Based on the observation of present and previous studies in other host pathogen systems, we suggest that the above cited genes play a vital role in causing disease in their host plants. The DEG study of pathogen genes can provide evidence for its sensitive targets, virulence toward hosts, and resistance against chemicals. This is probably the first transcriptome study of the *B. maydis* pathogen during infection in a non-CMS maize genotype, differing in their susceptibility to the pathogen. The findings from this study emphasize the role of mitochondrial-associated genes and pathways. In addition, cell wall synthesis, genes related to synthesis of polyketides, toxins, and putative candidate effector genes were found to be the key compounds underlying the pathogenesis of the *B. maydis* race "O" pathogen.

DATA AVAILABILITY STATEMENT

The datasets presented in this study can be found in online repositories. The names of the repository/repositories and accession number(s) can be found below: NCBI BioProject – PRJNA689117.

AUTHOR CONTRIBUTIONS

SM, RG, BB, PM, FH, and AK were involved in the conceptualization of the project, study design, critical inputs, and finalization of the manuscript. PM, AK, and BB were involved in wet lab experiments. BB and PM were involved in bio-informatics analyses and data compilation. SM, RG, BB, and PM drafted the manuscript. All authors have read and approved the final manuscript.

FUNDING

SM was thankful to Centres for Advanced Agricultural Science and Technology – National Agricultural Higher Education Project (CAAST-NAHEP) for providing financial support and the Division of Plant Pathology, ICAR-IARI, New Delhi.

SUPPLEMENTARY MATERIAL

The Supplementary Material for this article can be found online at: https://www.frontiersin.org/articles/10.3389/fmicb.2022.837056/full#supplementary-material

REFERENCES

Ali, F., Rahman, H., Durrishahwar, N. F., Munir, M., and Ullah, H. (2011). Genetic analysis of maturity and morphological traits under maydis leaf blight (MLB) epiphytotics in maize (Zea mays L.). *J. Agric. Biol. Sci.* 6, 13–11.

Arcila, J. E., Arango, R. E., Torres, J. M., and Arias, T. (2021). Comparative genomics in plant fungal pathogens (Mycosphaerellaceae): variation in mitochondrial composition due to at least five independent intron invasions. *Life* 11:215.

Backes, A., Hausman, J. F., Renaut, J., Ait Barka, E., Jacquard, C., and Guerriero, G. (2020). Expression analysis of cell wall-related genes in the plant pathogenic fungus drechslera teres. *Genes* 11:300. doi: 10.3390/genes11030300

Bagnaresi, P., Biselli, C., Orrù, L., Urso, S., Crispino, L., Abbruscato, P., et al. (2012). Comparative transcriptome profiling of the early response to *Magnaporthe oryzae* in durable resistant vs susceptible rice (*Oryza sativa* L.) genotypes. *PloS One* 7:e51609. doi: 10.1371/journal.pone.0051609

Banks, I. R., Specht, C. A., Donlin, M. J., Gerik, K. J., Levitz, S. M., and Lodge, J. K. (2005). A chitin synthase and its regulator protein are critical for chitosan production and growth of the fungal pathogen Cryptococcus neoformans. *Eukaryot. Cell* 4, 1902–1912. doi: 10.1128/EC.4.11.1902-1912.2005

Bertrand, H. (2000). Role of mitochondrial DNA in the senescence and hypovirulence of fungi and potential for plant disease control. *Annu. Rev. Phytopathol.* 38, 397–422. doi: 10.1146/annurev.phyto.38.1.397

Calderone, R., Li, D., and Traven, A. (2015). System-level impact of mitochondria on fungal virulence: to metabolism and beyond. *FEMS Yeast. Res.* 15:fov027. doi: 10.1093/femsyr/fov027

Castro, I. S. L., Freitas-Lopes, R. D. L., Ferreira, S. D. S., Maciel, T. E. F., Florez, J. C., Zambolim, E. M., et al. (2022). Transcriptome Analysis Uncovers the Gene Expression Profile of Hemileia vastatrix (Race XXXIII) during the Interactions with Resistant and Susceptible Coffee. *Agronomy* 12:444.

Chittem, K., Yajima, W. R., Goswami, R. S., del Río, and Mendoza, L. E. (2020). Transcriptome analysis of the plant pathogen *Sclerotinia sclerotiorum* interaction with resistant and susceptible canola (*Brassica napus*) lines. *PLoS One* 15:e0229844. doi: 10.1371/journal.pone.0229844

Díaz-Jiménez, D. F., Pérez-García, L. A., Martínez-Álvarez, J. A., and Mora-Montes, H. M. (2012). Role of the fungal cell wall in pathogenesis and antifungal resistance. *Curr. Fungal Infect.* Rep. 6, 275–282.

Fisher, D. E., Hooker, A. L., Lim, S. M., and Smith, D. R. (1976). Leaf infection and yield loss caused by four *Helminthosporium* leaf diseases of corn. *Phytopath* 66, 942–944.

Gaffoor, I., Brown, D. W., Plattner, R., Proctor, R. H., Qi, W., and Trail, F. (2005). Functional analysis of the polyketide synthase genes in the filamentous fungus *Gibberella zeae* (anamorph *Fusarium graminearum*). *Eukaryot. Cell* 4, 1926–1933. doi: 10.1128/EC.4.11.1926-1933.2005

Garcia-Rubio, R., de Oliveira, H. C., Rivera, J., and Trevijano-Contador, N. (2020). The fungal cell wall: *Candida, Cryptococcus*, and *Aspergillus* species. *Front. Microbiol.* 10:2993. doi: 10.3389/fmicb.2019.02993

Garre, V., Tenberge, K. B., and Eising, R. (1998). Secretion of a fungal extracellular catalase by *Claviceps purpurea* during infection of rye: putative role in pathogenicity and suppression of host defense. *Phytopath* 88, 744–753. doi: 10.1094/PHYTO.1998.88.8.744

Gregory, L. V., Ayers, J. E., and Nelson, R. R. (1978). Predicting yield losses in corn from southern corn leaf blight. *Phytopath* 68, 517–521.

Hansberg, W., Salas-Lizana, R., and Domínguez, L. (2012). Fungal catalases: function, phylogenetic origin and structure. *Arch. Biochem. Biophys.* 525, 170–180. doi: 10.1016/j.abb.2012.05.014

Hussain, N. (2011). Screening of maize varieties for grain yield at Dera Ismail Khan. *J. Anim. Plant Sci.* 21, 626–628.

Hyre, R. A. (1970). Epidemiology of southern corn leaf blight exploratory experiments. *Plant Dis. Rep.* 54, 1131–1133.

Kinghorn, A. D. (2000). *Volume 1. Polyketides and Other Secondary Metabolites Including Fatty Acids and Their Derivatives Edited by Ushio Sankawa*. Japan: Toyama Medical and Pharmaceutical University.

Koch, B., Tucey, T. M., Lo, T. L., Novakovic, S., Boag, P., and Traven, A. (2017). The mitochondrial GTPase Gem1 contributes to the cell wall stress response and invasive growth of *Candida albicans*. *Front. Microbiol.* 8:2555. doi: 10.3389/fmicb.2017.02555

Kuehnle, A. R., and Earle, E. D. (1988). Evaluation of tissue culture-derived methomyl resistant cms-T lines. *Maize Genet. Coop. Newslett.* 62:68.

Kumar, R., Mina, U., Gogoi, R., Bhatia, A., and Harit, R. C. (2016). Effect of elevated temperature and carbon dioxide levels on maydis leaf blight disease tolerance attributes in maize. *Agric. Ecosyst. Enviro.* 231, 98–104.

Lakshmi, P., and Sharma, R. C. (1987). Evaluation of maize germplasm to *Helminthosporium maydis* using detached leaf technique. *Ann. Agric. Res.* 8, 34–40.

Langner, T., and Göhre, V. (2016). Fungal chitinases: function, regulation, and potential roles in plant/pathogen interactions. *Curr. Genet.* 62, 243–254. doi: 10.1007/s00294-015-0530-x

Leonard, K. J. (1977). Races of Bipolaris maydis in the South eastern US from 1974-1976. *Plant Dis. Rep.* 61, 914–915.

Li, W., and Lan, P. (2015). Re-analysis of RNA-seq transcriptome data reveals new aspects of gene activity in *Arabidopsis* root hairs. *Front. Plant Sci.* 6:421. doi: 10.3389/fpls.2015.00421

Liao, Y., Smyth, G. K., and Shi, W. (2013). The Subread aligner: fast, accurate and scalable read mapping by seed-and-vote. *Nucleic Acids Res.* 41, e108–e108. doi: 10.1093/nar/gkt214

Liao, Y., Smyth, G. K., and Shi, W. (2014). featureCounts: an efficient general purpose program for assigning sequence reads to genomic features. *Bioinformatics* 30, 923–930. doi: 10.1093/bioinformatics/btt656

Liu, M., Gao, J., Yin, F., Gong, G., Qin, C., Ye, K., et al. (2015). Transcriptome analysis of maize leaf systemic symptom infected by *Bipolaris zeicola*. *Plos One* 10:e0119858. doi: 10.1371/journal.pone.0119858

Lv, G., Jiang, C., Liang, T., Tu, Y., Cheng, X., Zeng, B., et al. (2020). Identification and Expression Analysis of Sugar Transporter Gene Family in *Aspergillus oryzae*. *Int. J. Genomics* 2020:7146701. doi: 10.1155/2020/7146701

Martínez-Soto, D., and Ruiz-Herrera, J. (2017). Functional analysis of the MAPK pathways in fungi. *Rev. Iberoam. Micol.* 34, 192–202. doi: 10.1016/j.riam.2017.02.006

Medina, R., Franco, M. E. E., Bartel, L. C., Alcántara, V. M., Saparrat, M. C. N., and Balatti, P. A. (2020). Fungal Mitogenomes: Relevant Features to Planning Plant Disease Management. *Front. Microbiol.* 11:978. doi: 10.3389/fmicb.2020.00978

Mir, A. A., Park, S. Y., Sadat, M. A., Kim, S., Choi, J., Jeon, J., et al. (2015). Systematic characterization of the peroxidase gene family provides new insights into fungal pathogenicity in *Magnaporthe oryzae*. *Sci. Rep.* 5, 1–14. doi: 10.1038/srep11831

Mizuno, H., Kawahigashi, H., Kawahara, Y., Kanamori, H., Ogata, J., Minami, H., et al. (2012). Global transcriptome analysis reveals distinct expression among duplicated genes during sorghum-*Bipolaris sorghicola* interaction. *BMC Plant Biol.* 12:1–15. doi: 10.1186/1471-2229-12-121

Monfared, H. H., Chew, J. K., Azizi, P., Xue, G. P., Ee, S. F., Kadkhodaei, S., et al. (2020). Overexpression of a rice monosaccharide transporter gene (OsMST6) confers enhanced tolerance to drought and salinity stress in *Arabidopsis thaliana*. *Plant Mol. Biol. Rep.* 38, 151–164.

Mubeen, S., Rafique, M., Munis, M. F. H., and Chaudhary, H. J. (2017). Study of southern corn leaf blight (SCLB) on maize genotypes and its effect on yield. *J. Saudi Soc. Agric. Sci.* 16, 210–217.

Payak, M. M., and Sharma, R. C. (1983). *Disease Rating Scales in Maize in India. In Techniques of Scoring for Resistance to Disease of Maize in India. All India Co-ordinated Maize Improvement project*. New Delhi: IARI, 1–4.

Poretti, M., Sotiropoulos, A. G., Graf, J., Jung, E., Bourras, S., Krattinger, S. G., et al. (2021). Comparative transcriptome analysis of wheat lines in the field reveals multiple essential biochemical pathways suppressed by obligate pathogens. *Front. Plant Sci.* 17:70462. doi: 10.3389/fpls.2021.720462

Pusztahelyi, T. (2018). Chitin and chitin-related compounds in plant–fungal interactions. *Mycology* 9, 189–201. doi: 10.1080/21501203.2018.1473299

Rahul, K., and Singh, I. S. (2002). Inheritance of resistance to banded leaf and sheath blight (*Rhizoctonia solam* f. sp. *Sasakii*) of maize. *Proc. 8th Asian Reg. Maize Works. Bangkok, Thailand* 5, 356–365.

Ribeiro, T. H. C., Fernandes-Brum, C. N., de Souza, C. R., Dias, F. A. N., Almeida-Junior, O. D., Regina, M. D. A., et al. (2020). Transcriptome analyses suggest that changes in fungal endophyte lifestyle could be involved in grapevine bud necrosis. *Sci. Rep.* 10, 1–13. doi: 10.1038/s41598-020-66500-0

Rose, M. S., Yun, S. H., Asvarak, T., Lu, S. W., Yoder, O. C., and Turgeon, B. G. (2002). A decarboxylase encoded at the Cochliobolus heterostrophus translocation-associated Tox1B locus is required for polyketide (T-toxin) biosynthesis and high virulence on T-cytoplasm maize. *Mol. Plant Microbe Interact.* 15, 883–893. doi: 10.1094/MPMI.2002.15.9.883

Schindler, D., and Nowrousian, M. (2014). The polyketide synthase gene pks4 is essential for sexual development and regulates fruiting body morphology in *Sordaria macrospora*. *Fung. Genet. Biol.* 68, 48–59. doi: 10.1016/j.fgb.2014.04.008

Shieh, G. J., and Lu, H. S. (1993). Diallel analysis of mature plant resistance to *Helminthosporium maydis* in maize. *J. Agric. Res. China* 42, 12–18.

Sperschneider, J., Dodds, P. N., Gardiner, D. M., Singh, K. B., and Taylor, J. M. (2018). Improved prediction of fungal effector proteins from secretomes with EffectorP 2.0. *Mol. Plant Pathol.* 19, 2094–2110. doi: 10.1111/mpp.12682

Tajimi, A., Ando, N., and Teranaka, M. (1985). Seedling test for resistance to southern leaf blight in corn under greenhouse conditions. III Virulence of six isolates of *Bipolaris maydis* collected at six localities in southwest Japan. *Bull. Natl. Grassl. Res. Inst.* 31, 68–72.

Ullstrup, A. J. (1972). The impacts of the southern corn leaf blight epidemics of 1970-1971. *Annu. Rev. Phytopathol.* 10, 37–50.

Vankuyk, P. A., Diderich, J. A., MacCABE, A. P., Hererro, O., Ruijter, G. J., and Visser, J. (2004). *Aspergillus niger* mstA encodes a high-affinity sugar/H+ symporter which is regulated in response to extracellular pH. *Biochem. J.* 379, 375–383. doi: 10.1042/BJ20030624

Venkatesh, I., Gogoi, R., Hossain, F., Kumar, A., Aggarwal, R., and Mandal, P. K. (2021). Confirmation of physiological race of Bipolaris maydis causing maydis leaf blight of maize in India. *Ind. J. Agri. Sci.* 91, 613–618.

Warren, H. L., Jones, A., and Huber, D. M. (1977). Morphological and physiological differences between *Bipolaris maydis* races O and T. *Mycologia* 69, 773–782.

White, D. G. (1999)*Compendium of Corn Diseases, third ed*. St. Paul, MN, USA: American Phytopathological Society.

Yazawa, T., Kawahigashi, H., Matsumoto, T., and Mizuno, H. (2013). Simultaneous transcriptome analysis of Sorghum and *Bipolaris sorghicola* by using RNA-seq in combination with de novo transcriptome assembly. *PloS One* 8:e62460. doi: 10.1371/journal.pone.0062460

Ye, W., Liu, T., Zhang, W., Li, S., Zhu, M., Li, H., et al. (2019). Disclosure of the Molecular Mechanism of Wheat Leaf Spot Disease Caused by *Bipolaris sorokiniana* through Comparative Transcriptome and Metabolomics Analysis. *Int. J. Mol. Sci.* 20:6090. doi: 10.3390/ijms20236090

Zaitlin, D., DeMars, S., and Ma, Y. (1993). Linkage of rhm, a recessive gene for resistance to southern corn leaf blight, to RFLP marker loci in maize (*Zea mays*) seedlings. *Genome* 36, 555–564. doi: 10.1139/g93-076

Zhang, M. Z., Sun, C. H., Liu, Y., Feng, H. Q., Chang, H. W., Cao, S. N., et al. (2020). Transcriptome analysis and functional validation reveal a novel gene, BcCGF1, that enhances fungal virulence by promoting infection-related development and host penetration. *Mol. Plant Path.* 21, 834–853. doi: 10.1111/mpp.12934

Conflict of Interest: The authors declare that the research was conducted in the absence of any commercial or financial relationships that could be construed as a potential conflict of interest.

Publisher's Note: All claims expressed in this article are solely those of the authors and do not necessarily represent those of their affiliated organizations, or those of the publisher, the editors and the reviewers. Any product that may be evaluated in this article, or claim that may be made by its manufacturer, is not guaranteed or endorsed by the publisher.

frontiers | Frontiers in Microbiology

ORIGINAL RESEARCH
published: 03 May 2022
doi: 10.3389/fmicb.2022.864619

Bacteria Community Inhabiting *Heterobasidion* Fruiting Body and Associated Wood of Different Decay Classes

Wenzi Ren[1], *Reijo Penttilä*[2], *Risto Kasanen*[1] *and Fred O. Asiegbu*[1]*

[1] *Department of Forest Sciences, University of Helsinki, Helsinki, Finland,* [2] *Natural Resources Institute of Finland (Luke), Helsinki, Finland*

OPEN ACCESS

Edited by:
Marco Scortichini, Council for Agricultural and Economics Research (CREA), Italy

Reviewed by:
Ari Mikko Hietala, Norwegian Institute of Bioeconomy Research (NIBIO), Norway
Tālis Gaitnieks, Latvian State Forest Research Institute Silava (LSFRI), Latvia

***Correspondence:**
Fred O. Asiegbu
fred.asiegbu@helsinki.fi

Specialty section:
This article was submitted to Microbe and Virus Interactions with Plants, a section of the journal Frontiers in Microbiology

Received: *28 January 2022*
Accepted: *04 April 2022*
Published: *03 May 2022*

Citation:
Ren W, Penttilä R, Kasanen R and Asiegbu FO (2022) Bacteria Community Inhabiting Heterobasidion Fruiting Body and Associated Wood of Different Decay Classes. Front. Microbiol. 13:864619. doi: 10.3389/fmicb.2022.864619

The microbiome of *Heterobasidion*-induced wood decay of living trees has been previously studied; however, less is known about the bacteria biota of its perennial fruiting body and the adhering wood tissue. In this study, we investigated the bacteria biota of the *Heterobasidion* fruiting body and its adhering deadwood. Out of 7,462 operational taxonomic units (OTUs), about 5,918 OTUs were obtained from the fruiting body and 5,469 OTUs were obtained from the associated dead wood. Interestingly, an average of 52.6% of bacteria biota in the fruiting body was shared with the associated dead wood. The overall and unique OTUs had trends of decreasing from decay classes 1 to 3 but increasing in decay class 4. The fruiting body had the highest overall and unique OTUs number in the fourth decay class, whereas wood had the highest OTU in decay class 1. *Sphingomonas* spp. was significantly higher in the fruiting body, and phylum Firmicutes was more dominant in wood tissue. The FAPROTAX functional structure analysis revealed nutrition, energy, degradation, and plant-pathogen-related functions of the communities. Our results also showed that bacteria communities in both substrates experienced a process of a new community reconstruction through the various decay stages. The process was not synchronic in the two substrates, but the community structures and functions were well-differentiated in the final decay class. The bacteria community was highly dynamic; the microbiota activeness, community stability, and functions changed with the decay process. The third decay class was an important turning point for community restructuring. Host properties, environmental factors, and microbial interactions jointly influenced the final community structure. Bacteria community in the fruiting body attached to the living standing tree was suppressed compared with those associated with dead wood. Bacteria appear to spread from wood tissue of the standing living tree to the fruiting body, but after the tree is killed, bacteria moved from fruiting body to wood. It is most likely that some of the resident endophytic bacteria within the fruiting body are either parasitic, depending on it for their nutrition, or are mutualistic symbionts.

Keywords: wood decay process, bacteria community, *Heterobasidion*, fruiting body, network analysis

INTRODUCTION

The genus *Heterobasidion* within the phylum Basidiomycota contains 13 species with saprotrophic and necrotrophic lifestyles. The species complex, *H. annosum s.l.,* has a necrotrophic lifestyle and contains five species, namely, *H. abietinum*, *H. annosum sensu stricto* (s.s.), *H. irregulare*, *H. parviporum,* and *H. occidentale* (Ioos et al., 2019). Among these, *H. annosum* and *H. parviporum* are the most severe root rot disease causal agents, posing a major threat to conifer forests of the northern hemisphere (Asiegbu et al., 2005). The primary infection of *Heterobasidion* is mediated by basidiospores dispersal and germination on wounds or exposed stump surfaces. The secondary infection continuously spreads the disease to the adjacent healthy tree by root-to-root contact (Korhonen and Stenlid, 1998; Zaluma et al., 2019). The current control methods include silvicultural, chemical, and biological control approaches (Mesanza et al., 2016). Chemical and biological control methods are the most efficient (Pellicciaro et al., 2021). However, the application of chemical treatment such as urea is restricted in Europe due to its potential negative impacts on the environment (EU Reg. 2020/1160). In contrast, the persistent use of the biocontrol product (e.g., Rotstop), which is based on a single natural isolate of *Phlebiopsis gigantea,* might increase the ecological risks of pathogen tolerance (GŽibovska, 2016). Exploring other alternative efficient control approaches is therefore required.

Fruiting body is a highly nutritious multicellular structure containing spores of fungi and other microbes (Maurice et al., 2021). Its morphology, sporulation period, and longevity vary in different species (Moore et al., 2008). *Heterobasidion* species tend to be active when the temperature is above 5°C, and the spore deposition rate for each square meter can be over 1,000 basidiospores per hour (Gonthier et al., 2005; Müller et al., 2014). The spreading distance could reach 1,000 m (Möykkynen et al., 1997). It has been observed that spruce logs left on peat soil form the most abundant fruiting body (Gaitnieks et al., 2021), cull lumbar piece was also found to be significant to the fruiting body formation (Müller et al., 2007). The fruiting body provides habitat or food resources for diverse organisms, including bacteria and fungi (Elliott et al., 2019; Legzdina et al., 2021; Maurice et al., 2021). The interactions between *Heterobasidion* and associated organisms influence the development of each other and will produce a dynamic counterbalance (Deveau et al., 2018). The fruiting body associated with wood often has biochemical mechanism to defend itself against external injuries, however, with the progression of the decay process, biochemical compounds fade away, and the physical structure of fruiting body changes (Venkatesh and Keller, 2019; Legzdina et al., 2021; Maurice et al., 2021). These physical-chemical property variations influence the microbial interactions inside the fruiting body (Gohar et al., 2020). Thus, the microbiome composition of fruiting body might be of relevance for *Heterobasidion* primary infection. Despite the potential importance of fruiting body microbiome in the ecological interactions (Gohar et al., 2020; Maurice et al., 2021), almost no information is available on *Heterobasidion* fruiting body.

In contrast, deadwood is a major substrate for most wood-inhabiting fungi, and the associated fungal fruiting bodies play an important ecological role in the ecosystem. Deadwood is important for nutrient cycling, carbon sequestration, soil property, and biodiversity (Brunner and Kimmins, 2003; Litton et al., 2007; Rondeux and Sanchez, 2010; Błońska et al., 2017). Both quality and quantity of deadwood have impact on its ecological roles (Müller and Bütler, 2010). Deadwood might be also an incubator for forest diseases, since pathogens with dual lifestyles are known to survive over decades on deadwood by aid of their saprotrophic feeding (Cleary et al., 2013). *Heterobasidion* has been reported to remain in deadwood and retain infectious activity for over 62 years after clear cutting. Also, the *Heterobasidion* fruiting body can develop on 25 to 45-year-old rotted spruce wood (Piri, 1996; Gaitnieks et al., 2021). Deadwood volume, property, and mechanisms for its decay are all vital parameters for forest management (Müller and Bütler, 2010). A number of recent studies have reported on *Heterobasidion*'s decay impact on trees, the tree resistance against *Heterobasidion*, the microbiome associated with the pathosystem but not much on the fruiting body microbiome (Puentes Rodriguez et al., 2013; Keilhofer et al., 2018; Probst et al., 2018; Ren et al., 2019; Pellicciaro et al., 2021).

The bacteria-fungi or fruiting body interactions (BFIs) could be beneficial, neutral, or detrimental to each other (Wargo and Hogan, 2006). The symbionts could be obligate or facultative. The obligate symbiotic bacteria are usually beneficial to its fungal host, as they are highly dependent, while the facultative bacteria have more diverse influences. Endosymbiont usually has a positive effect, while the ectosymbiont's effects on hosts are diverse (Bastías et al., 2020).

Bacillus subtilis, a soil-dwelling bacterium, can form a biofilm to attach on the fungus surface (Kjeldgaard et al., 2019). Bacterium *Pseudomonas fluorescens* was recorded to stimulate both colonization and growth of the fungus *Laccaria bicolor* (Deveau et al., 2007). In a mutual interaction, bacteria consume metabolites from the fungus and contribute amino acids in return (Lackner et al., 2011) or benefit of carbon and nitrogen exchange (Sharmin et al., 2018). The symbiont could also help the fungus (Guo et al., 2017) or bacteria (Ruiz-Lozano and Bonfante, 2000) to establish or facilitate invasion to other fungi (Spraker et al., 2016) or plant tissues (Ruiz-Lozano and Bonfante, 2000). At the other extreme, the BFIs could also suppress each other. Strain GB 4-2 from the genus *Streptomyces* was reported to suppress *Heterobasidion* infection through promoting plant resistance (Lehr et al., 2008). However, some bacteria genera have an opportunistic influence on fungal pathogenicity (e.g., *Pseudomonas* spp.) (GŽibovska, 2016; Lipps and Samac, 2021; Pellicciaro et al., 2021).

Bacteria-fungi or fruiting body interactions can also increase host's tolerance to stress and promote nutrient uptake as well as plant growth (Steffan et al., 2020; Asiegbu and Kovalchuk, 2021).

The structure of microbial community in this pathosystem might result as a consequence of tripartite (bacteria-fruiting body-plant) overall interactions. Understanding the structure of the community is therefore the crucial foundation to unravel the functional mechanism of the interacting partners. Other

than their direct and indirect effect on each other, many other factors also contribute to the microbial structure formation. Soil properties (Pent et al., 2017), host genetics (Maurice et al., 2021), host physical and chemical properties (Maurice et al., 2021), and microclimate (Fravolini et al., 2016) have been reported to have profound influence on the microbial structure. Besides, being different from dead wood, the appearance of fruiting body may already indicate a specific environment background. For example, moisture and temperature were recorded to have a significant impact on the fungus sporulation (Moore et al., 2008). The microbes inhabiting the fruiting body could have a smaller range compared with those in dead wood. The aims of this study were to unravel (1) the bacteria biota of fruiting body and associated dead wood of different decay classes, (2) their possible nature and functional characteristics, and (3) using the network model to unravel their potential interactions among each other, as well as possible impact on *Heterobasidion* pathogenesis.

MATERIALS AND METHODS

Sampling

In each sampling spot, *Heterobasidion* fruiting body and the associated wood were collected; the dead wood was classified to decay classes 1 to 4 based on how deep the knife was able to penetrate the wood (Mäkinen et al., 2006). Samples were collected from a total of 38 spots. Notably, 12 of the fruiting bodies were from wood classified as decay class 1, i.e., recently dead wood; eight from decay class 2, weakly decayed; five from decay class 3, medium decayed; and 13 from decay class 4, highly decayed (decay classes represented as D1F–D4F for fruiting body and D1W–D4W for wood). All samples were collected from six Norway spruce dominated boreal forest sites in Uusimaa region, located in Viikki (Helsinki) and Myrskylä, two sites from Lapinjärvi, and two sites from Sipoo. Forest types under different management purposes were also considered in the sampling. Viikki forest site is mainly used for recreational purpose; sites from Sipoo and one site from Lapinjärvi are nature conservation areas, with or without minor human interference; and the other sites from Lapinjärvi and Myrskylä forest are managed sites.

The fruiting body and associated dead wood samples were collected from stumps, logs, and standing tree wood. Wood tissue immediately below and attached to the basidiocarp was collected, with the aid of a sharp knife and an ax if necessary. The stand age of sampling sites ranged from 0 to 109 years, the canopy cover ranged from 0% to over 71%. The elevation of sites ranged from 7.42 to 102.67 m above the sea level. The diameter of selected wood ranged from 9 to 40 cm for managed forest and from 15 to 40 cm for unmanaged forest. Stand age and canopy cover of each spot were obtained from National Land Survey of Finland (**Supplementary Table 1**; https://kartta.paikkatietoikkuna.fi/). Samples were stored in a cooling box before storage in −20°C. Sample collections were conducted in June 2020.

A combination of visual morphological identification and ITS-based analysis was used to confirm that the collected fruiting bodies were *Heterobasidion* spp., and that the associated deadwood was infected by it.

DNA Extraction, Amplification of 16S rDNA Region, and Sequencing

All samples were prewashed over running water followed by immersion in 70% ethanol (EtOH) for 1 min and 1% commercial bleach for 5 min and rinsed several times with sterile distilled water in order to remove surface adhering microbes. Samples were dried with paper towel and air-dried before homogenization (Moreno et al., 2014). To avoid bias, subsamples from the fruiting body were collected from four directions as well as the middle part, whereas the entire wood sample was fully homogenized. Samples were extracted following a standard cetyltrimethylammonium bromide (CTAB) method (Chang et al., 1993) with modifications (Terhonen et al., 2011). The concentration and purity of DNA were measured using the NanoDrop ND-1000 spectrophotometer (Thermo Fisher Scientific, USA). PCR amplification of the bacterial 16S rDNA V3–V4 region and sequencing were performed at Novogene (Cambridge Science Park, UK). The PCR products were purified and sequenced with the Illumina NovaSeq platform. The amplification primers were 341F 5′-CCTAYGGGRBGCASCAG-3′ and 806R 5′-GGACTACNNGGGTATCTAAT-3′. Approximately 250 nucleotides per sequencing reads were produced. Raw sequences obtained in this study are available from the Sequence Read Archive (SRA) of National Center for Biotechnology Information (NCBI) under project number PRJNA800074.

Data Processing

The raw 16S rRNA sequences were preprocessed at Novogene, UK. The paired-end reads were merged using FLASH Version 1.2.7 (Magoč and Salzberg, 2011); the pair-end reads were spliced when reads overlapped with the same fragment. The sequence data were filtered by Qiime pipeline (Caporaso et al., 2010) to get high-quality sequences. Chimera was detected by comparing to Gold database with the UCHIME algorithm (Haas et al., 2011) and removed using the UPARSE software (Edgar, 2013). The preprocessed data were analyzed and grouped into operational taxonomic units (OTUs) using UPARSE. Sequences with ≥97% similarity were assigned to the same OTUs (Wang et al., 2007). Representative sequence for each OTU was screened for further annotation. OTUs were assigned to taxonomic groups using the Mothur software by performing sequence against the SSUrRNA database of SILVA Database (Quast et al., 2013) (taxonomic rank threshold: 0.8–1). Normalization was conducted using a standard of sequence number corresponding to the sample with the least sequences. The subsequent analysis was performed based on this normalized data. Chao1 (Chao, 1984), Shannon diversity index (H) (Shannon and Weaver, 1949), and Shannon evenness index (SEI) (Heip, 1974) were chosen to represent community species richness, diversity, and evenness. One-way ANOVA tests were conducted to identify the differences in community richness, diversity, evenness, and abundance of taxonomic groups. Principal coordinates analysis (PCoA) was used to visualize the bacterial community structure with weighted unifrac distance matrix using relative abundance of OTUs calculated by the QIIME software (Version 1.7.0). PCoA

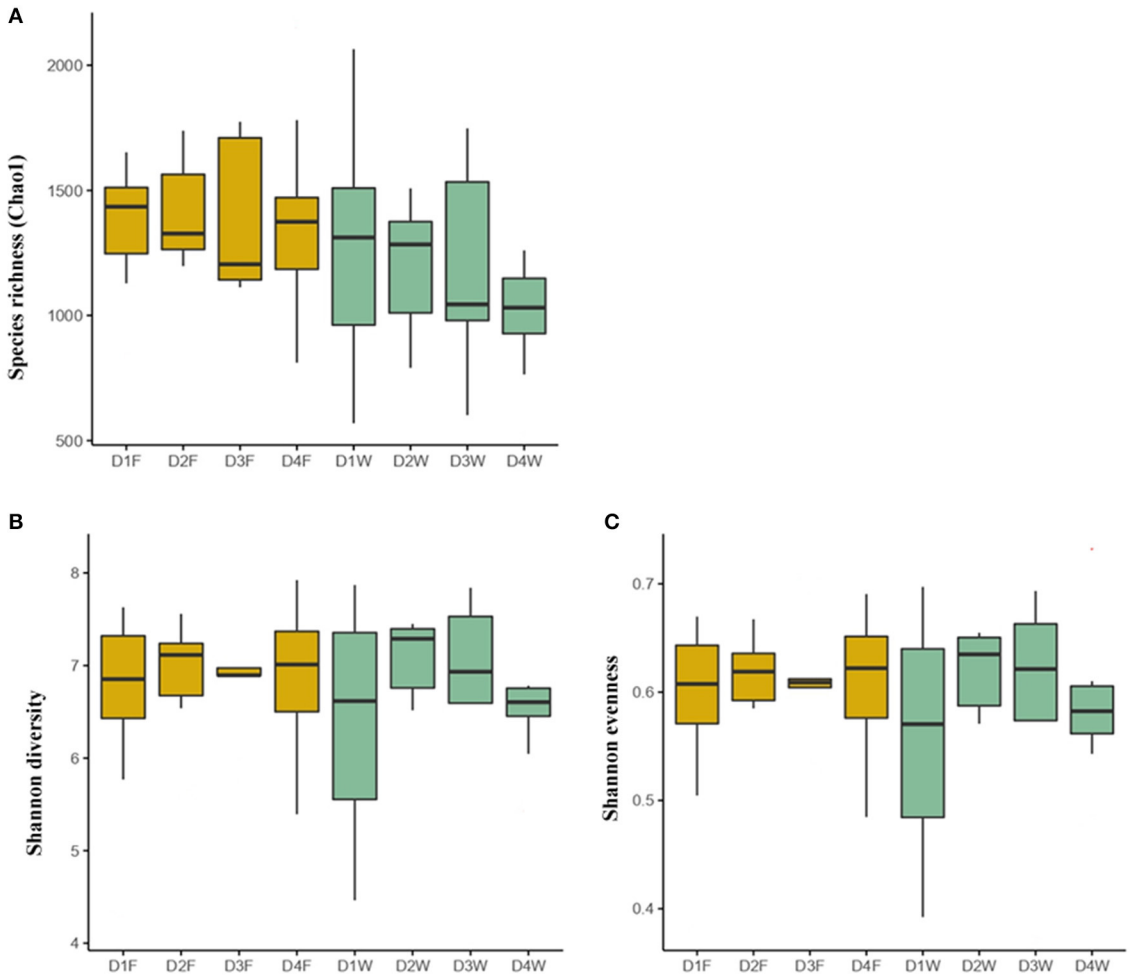

FIGURE 1 | The bacterial community indices in the fruiting body and wood of different decay classes. **(A)** Species richness, **(B)** Shannon diversity, and **(C)** Shannon evenness. The outliers were removed. D1F and D1W refer to the fruiting body and wood from the first decay class; D2F and D2W refer to the fruiting body and wood from the second decay class; D3F and D3W refer to the fruiting body and wood from the third decay class; D4F and D4W refer to the fruiting body and wood from the fourth decay class.

was performed by vegan package and ggplot2 package in the R software (Version 2.15.3). Functional annotation of prokaryotic taxa (FAPROTAX) database was used to identify bacterial function *via* the annotation of 16S sequence classification (Louca et al., 2016; Sansupa et al., 2021). Linear discriminant analysis (LDA) effect size (LEfSe) and one-way ANOVA tests were used to identify bacterial taxonomic and functional groups difference between different decay class samples (Segata et al., 2011). We implemented microbiome ecological network (de Vries et al., 2018) by calculating the spearman correlation of OTUs abundance among different groups through psych package in R and visualized the result by Gephi (Version 0.9.2).

RESULTS

Information on the NovaSeq PE250 Sequencing

There were 6,198,431 high-quality sequences in total after denoising and quality filtering. After filtering out unclassified sequences, singletons, and sequences assigned to plant and animal specific sequences, a core set of 5,921,960 sequences was obtained. Due to the technical problem of PCR amplification and sequencing, eight samples with low read numbers were excluded; the remaining 68 samples were used for further analysis. Details on the deleted samples are stated in **Supplementary Table 1**. The remaining samples had sequence numbers ranging from 49,011 to 114,758 with the average number as 87,088 ± 12,577 (mean ± standard deviation). A random normalization was conducted based on the smallest sample size of 49,011 sequences among all samples and was used in the further analysis. All samples had over 99% of average Good's coverage. The rarefaction curves in **Supplementary Figure 1** showed the sequencing depth.

Bacterial Community Diversity of Fruiting Body and Wood in the Four Decay Classes

The bacterial species richness (Chao1), diversity (Shannon diversity), and evenness (Shannon even) did not differ neither among the fruiting body and dead wood in the four decay classes

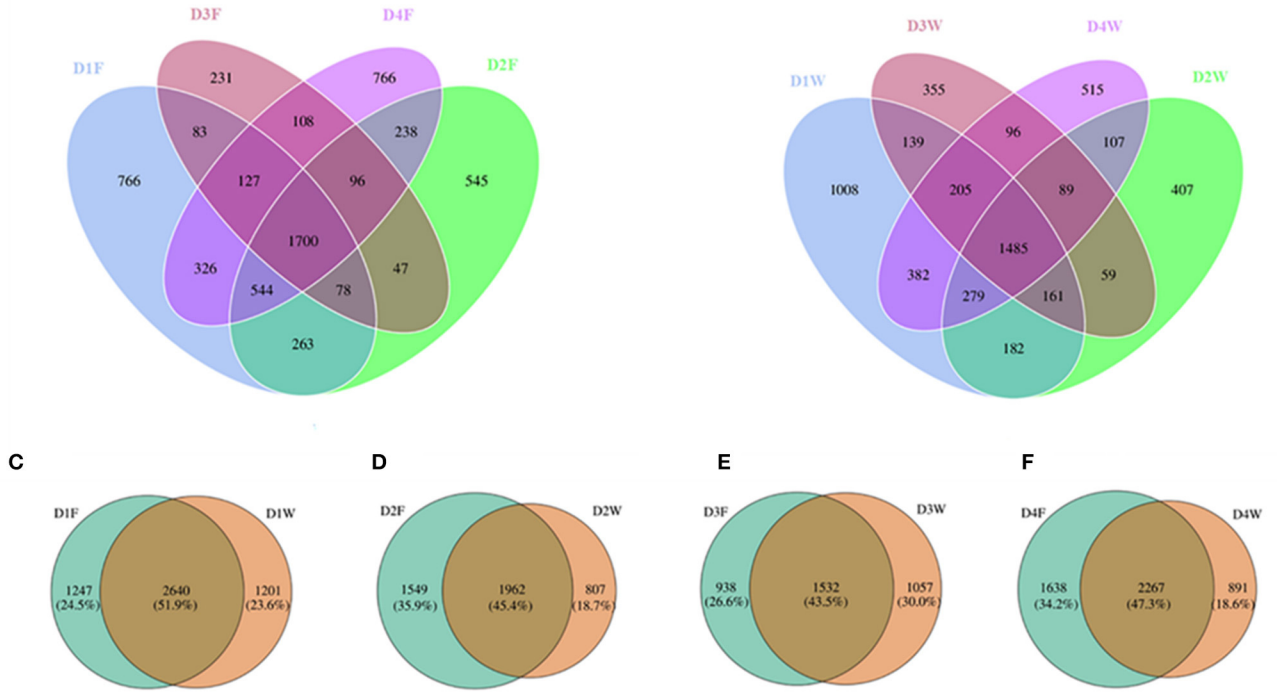

FIGURE 2 | Venn diagram showing the unique and shared operational taxonomic units (OTUs) among different decay classes from **(A)** fruiting body, **(B)** dead wood, between fruiting body and dead wood from decay classes 1 **(C)**, 2 **(D)**, 3 **(E)**, and 4 **(F)**.

nor between fruiting body and wood under the same decay class ($P > 0.05$; **Figure 1**).

Bacterial Community Structure on OTU Level

Across all samples, a total of 7,462 OTUs were obtained, where 5,918 OTUs were obtained from fruiting body and 5,469 OTUs were obtained from wood, 52.6% of all OTUs was shared between the two substrates. The Venn diagram revealed that the overall, common, and unique OTUs from both substrates had a varying trend of high abundance in decay class 1 with decreases in decay classes 2 and 3, and high again in decay class 4 (**Figures 2A,B**).

When comparing OTU numbers between wood and fruiting body in the same decay class, decay class 1 showed the highest proportion of OTUs that were common to both fruiting body and wood, and decay class 3 showed the lowest (**Figures 2C,E**). Wood had the maximum overall and unique OTUs in D1W and minimum in D3W and D2W (**Figures 2C–E**). The fruiting body had the maximum overall and unique OTUs in D4F and minimum in D3F (**Figures 2E,F**). In the last decay class, the fruiting body had 391 more OTUs compared with those in the initial decay stages, while wood had 310 less.

Principal coordinates analysis based on OTUs data explained 39.4% of the variation, the clusters were distinct between fruiting body and dead wood in all decay class except decay class 1 (**Figure 3**). The subsequent PERMANOVA confirmed the significant differences of all classes ($P < 0.05$). However, the differences were not significant among decay classes in the same substrate (**Supplementary Figures 2**, **3**; $P > 0.05$).

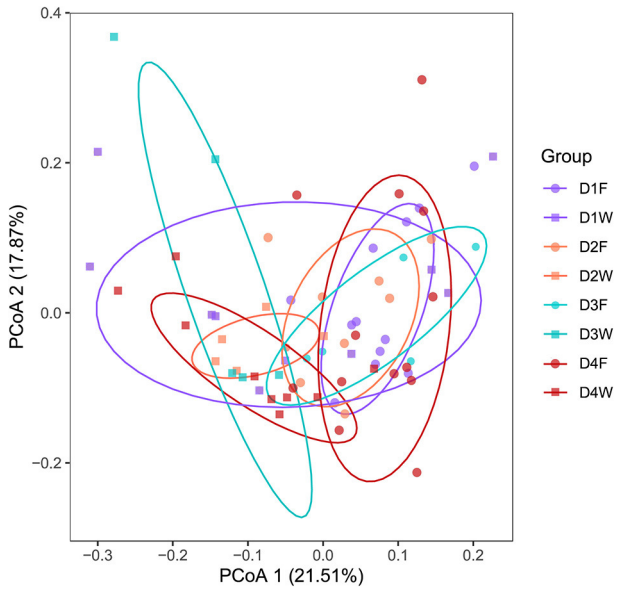

FIGURE 3 | Principal-coordinate analysis (PCoA) showing the bacterial community structures of fruiting body and wood from four decay classes.

TABLE 1A | The most abundant operational taxonomic units (OTUs) in top 50 showing significant different patterns between fruiting body (F) and wood (W) in each decay class.

Decay class	OTUs	Taxonomy	*P*	Abundance pattern
1	OTU00047	*Labrys sp.*	0.0089	F > W
2	-	-	-	-
3	OTU00021	*Edaphobacter sp.*	0.0036	F > W
	OTU00007	*Sphingomonas sp.*	0.0007	F > W
	OTU02337	*Mycobacterium sp.*	0.0203	F > W
	OTU00061	*Pseudomonas viridiflava*	0.0361	F > W
4	OTU00058	*Inquilinus sp.*	0.0008	F > W
	OTU00026	*Roseiarcus sp.*	0.0011	F < W
	OTU00006	Rhizobiaceae	0.0069	F > W
	OTU00057	*Acidibacter sp.*	0.0477	F < W

TABLE 1B | The most abundant OTUs in top 50 showing significant different patterns among four decay classes (D) from fruiting body (F) and wood (W).

Substrate	Abundance pattern	*P*	OTUs	Taxonomy
Fruiting body	D3F > D1F	0.0202		
	D3F > D4F	0.0014	OTU00007	*Sphingomonas sp.*
	D3F > D2F	0.0134		
	D3F > D1F	0.0146	OTU00061	*Pseudomonas viridiflava*
	D3F > D4F	0.0195		
	D3F > D2F	0.0089	OTU00021	*Edaphobacter sp.*
	D3F > D4F	0.0360	OTU02337	*Mycobacterium sp.*
Wood	D2W > D4W	0.0361	OTU02338	*Sphingomonas sp.*
	D2W > D4W	0.0330	OTU00008	Microbacteriaceae
	D3W > D1W	0.0131	OTU00013	*Acidibacter sp.*
	D3W > D4W	0.0497		
	D3W > D1W	0.0475	OTU00033	*Staphylococcus sp.*
	D4W > D2W	0.0066	OTU00026	*Roseiarcus sp.*
	D4W > D1W	0.0016		
	D4W > D1W	0.0429	OTU00015	*Acidiphilium sp.*

In the top 50 most abundant OTUs, several OTUs contributed to the significant differences between fruiting body and dead wood in decay classes 1, 3, and 4. In classes 1 and 3, the significant patterns were higher bacteria abundance in fruiting body than dead wood. In decay class 4, both substrates had two significant abundant OTUs (**Table 1A**).

Considering the same substrate, only the third decay class had significantly higher abundant OTUs than the other decay classes in the fruiting body, while in dead wood, all decay classes except class 1 had significant abundant OTUs (**Table 1B**).

Bacterial Community Structure on Taxonomic Level

Sequences were classified to 34 phyla, Proteobacteria was the most dominant of all groups, followed by Actinobacteria, Acidobacteria, Bacteroidetes, and Firmicutes, where they accounted for over 93.7% of the total sequences. The changing patterns of relative abundance in both substrates were the same in phyla Actinobacteria, Acidobacteria, and Cyanobacteria, while phyla Firmicutes and Bacteroidetes had the opposite trend (**Figure 4A**).

In the fruiting body, *Burkholderia*, *Sphingomonas*, and *Pseudommonas* were the most abundant identified genera. The genus *Luteibacter* had stable abundance associated with all decay classes of the fruiting body. In wood tissue, each genus had quite balanced proportions in the first decay stage, but the proportion of most genera reduced with prolonged decay (**Figure 4B**).

The Genus *Staphylococcus* had the highest relative abundance in D3W and was significantly higher than D1F, D4F, and D1W among all the group comparisons (**Figure 4B**; $P < 0.05$). The genus *Sphingomonas* was significantly higher in D3F than D1W–D4W (**Figure 4B**; $P < 0.05$).

Linear discriminant analysis effect size revealed that decay classes 2, 3, and 4 had significant higher taxonomic groups in the fruiting body and wood. In the fruiting body, decay class 4 had more abundant taxonomies, but wood had more in decay class 2 (LDA > 2.0, $P < 0.05$; **Figures 5A,B**). Similar differences also existed between both substrates in all classes (LDA > 4.0, $P < 0.05$; **Figures 5C–F**).

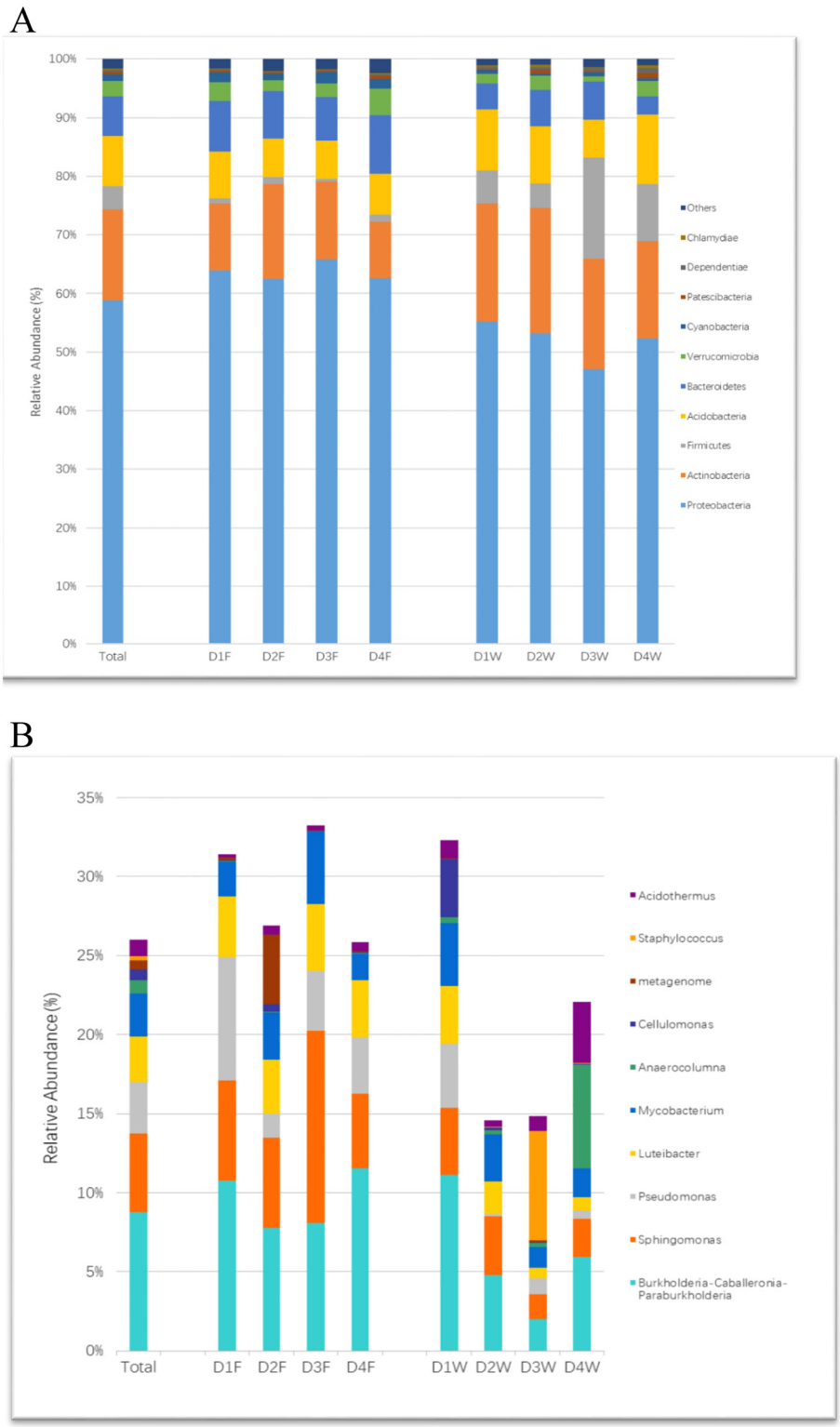

FIGURE 4 | The relative abundance of bacterial community at different taxonomic levels in study groups. **(A)** Phylum and **(B)** genus.

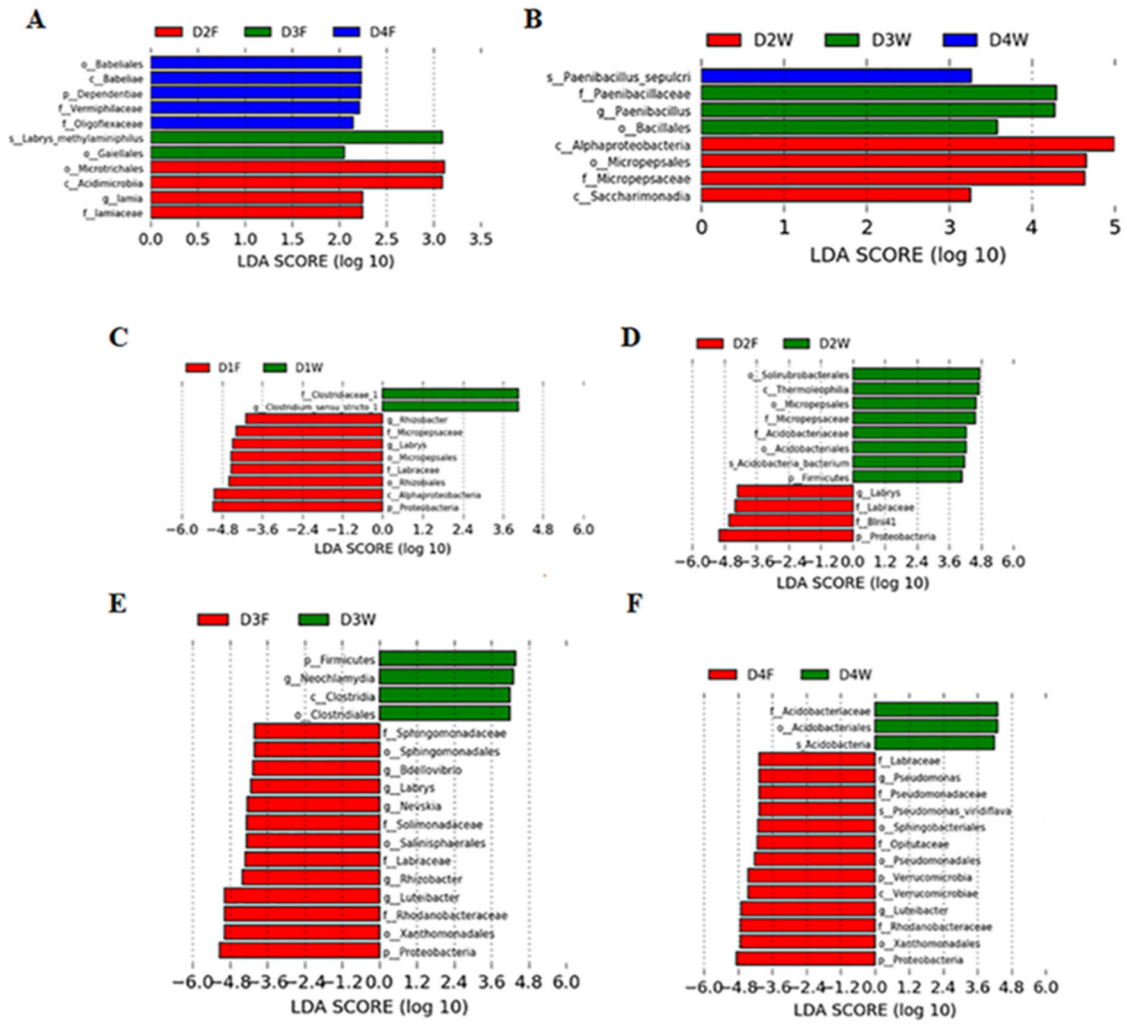

FIGURE 5 | Linear discriminant analysis (LDA) effect size (LEfSe) showing bacterial phyla, class, order, family, genus, and species, which were significantly different in **(A)** fruiting body, **(B)** wood under different decay classes, and between fruiting body and wood in the same decay class, **(C)** class 1, **(D)** class 2, **(E)** class 3, and **(F)** class 4. p, phylum; c, class; o, order; f, family; g, genus; s, species.

Potential Bacterial Functional Structure Analysis

The top 252 OTUs, which cover 80.0% of all sequences, were assigned to 16 functional groups in FAPROTAX analysis. In total, 251 records (37.9%) were assigned to at least one group (Li et al., 2021). Chemoheterotrophy (42.2%) and aerobic chemoheterotrophy (41.4%) were the most abundant functions and were involved in carbon cycle, followed by nitrogen fixation (7.3%) and ureolysis (2.2%), which were involved in N cycle, together with fermentation (1.4%), cellulolysis (1.1%), non-photosynthetic Cyanobacteria (1.0%), plant pathogen related (0.8%), and hydrocarbon degradation (0.2%). The detailed information is found in **Supplementary Table 2**.

There was no functional group differences among bacteria biota observed among the decay classes in wood samples, however, in the fruiting body, phototrophy showed a pattern of D4F < D2F ($P < 0.05$); plant pathogen-related function was higher in D3F compared with that in D1F and D4F ($P < 0.05$).

Comparing between wood and fruiting body in the same decay class, classes 1, 3, and 4 had significant abundant functional groups (LDA > 3.0, $P < 0.05$; **Figure 6**), and they changed with progress of decay. The fruiting body had more diverse abundant functional groups, while dead wood only had fermentation group in the third and fourth classes (**Figure 6**).

Predicted Bacterial Interaction Analysis

The complex microbial network was unraveled by the nature of its topology characteristics (Blondel et al., 2008; Paranyushkin, 2012a). The most important topology parameters of connectivity, modularity, and Po/Ne ratio of the communities' network were selected and used to explain its activeness (Hartman et al., 2018),

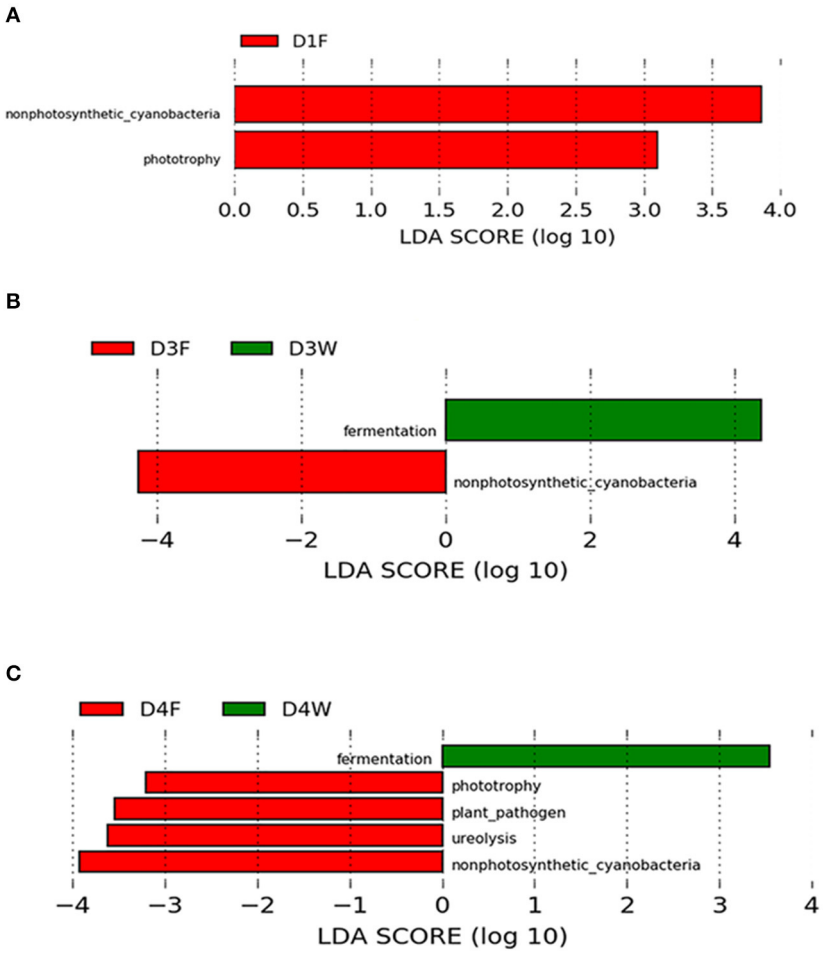

FIGURE 6 | LEfSe (LDA > 3.0, $P < 0.05$) showing the predicted functional groups significantly abundant in decay classes 1 **(A)**, 3 **(B)**, and 4 **(C)**.

function-related modularization (Newman, 2006), and stability (de Vries et al., 2018). The top 252 OTUs with $\rho > 0.7$, $P < 0.001$ of Spearman correlation values were used for the network analysis (**Supplementary Tables 3, 4**). Overall, OTU numbers that satisfied the threshold ranged from 164 to 207 in the fruiting body and 155 to 200 in the dead wood (**Supplementary Table 3**).

The connectivity in both substrates had the changing pattern of increasing before the third decay stage and decreasing at the fourth stage. The third decay class had the peak connectivity in both substrates, the lowest point was observed in D1F and D4W (**Table 2**; **Figure 7**). Connectivity in wood was higher than in the fruiting body in all the decay classes, which means that bacteria hosted by the decayed wood were more actively interacting with each other (Hartman et al., 2018). The modularity had a pattern of decrease-increase-decrease in the fruiting body, where D3F reached the peak and D4F was the lowest. In wood, the modularity had the opposite pattern, where D2W had the highest value, and D4W was the lowest (**Table 2**). The value of modularity indicated the modularization of community, which could be related to their function (Newman, 2006) and stability (Paranyushkin, 2012b).

The positive and negative connecting ratio (Po/Ne) used to represent connection stability (de Vries et al., 2018) had the opposite changing pattern to their modularity in both substrates. D3F and D2W had the minimum value, and D1F and D1W reached the peak (**Table 2**; **Figure 7**). Our result indicated that the communities in the fruiting body were more stable compared with wood as their Po/Ne values had smaller changing range (**Table 2**). Moreover, the thicker linking edges in the middle decay classes in both substrates also showed stronger connections (**Figure 7**). We selected nodes with top 1% connectivity in each group as the keystone OTUs (Hartman et al., 2018). We found that phylum Proteobacteria existed in all networks except D2F and was the only phylum that existed at the end of the decay process (**Table 2**). Among all selected OTUs, 11 of them were in top 50 abundant group; only OTU6319 reoccurred in D1F and D3F; OTU209 appeared in D3F and D3W; and all the rest were unique (**Table 2**).

TABLE 2 | Detailed network properties of study groups.

Group	OTUs	Connections	Connectivity	Po/Ne	Modularity	keystone		
						No.	Phylum	OTU ID
D1F	164	219	2.67	6.87	0.81	2	Proteobacteria	6319
							Bacteroidetes	3156
D2F	165	283	3.43	5.29	0.75	1	Acidobacteria	254
D3F	207	619	5.98	2.89	0.88	18	Proteobacteria	26, 1, 13, 71, 251, 1121, 2914, 209, 67, 182, 220, 84, 6319, 5730, 811
							Cyanobacteria	7105
							Acidobacteria	36
							Verrucomicrobia	6984
D4F	146	245	3.36	5.45	0.74	1	Proteobacteria	57
D1W	189	333	3.52	22.81	0.79	1	Proteobacteria	54
D2W	159	303	3.81	1.97	0.89	6	Proteobacteria	2338, 7324, 31
							Actinobacteria	3094, 3544
							Acidobacteria	6429
D3W	200	833	8.33	15.03	0.88	19	Proteobacteria	5754, 6, 47, 431, 72, 209, 4967, 6196, 65, 375, 180, 5160
							Actinobacteria	6433, 124
							Acidobacteria	21, 36, 3738
							Cyanobacteria	18
							Verrucomicrobia	554
D4W	155	261	3.37	9.87	0.71	1	Proteobacteria	6517

OTUs: Number of network nodes.
Connections: Number of network edges.
Connectivity: Mean number of connections per node.
Keystone OTUs: Selected based on the top 1% of node degree values of each network. Po/Ne: The positive and negative connecting ratio.

DISCUSSION

The Bacterial Communities of Fruiting Body and Associated Wood of Different Decay Classes

The alpha diversity and beta diversity of bacterial community did not show any significant differences neither in wood tissue nor in fruiting body. However, community structures, activeness, stabilities, and functions kept changing. At the end of the fourth decay process, new bacterial communities replaced the old ones previously constructed in living standing tree. Changes from host chemical-physical properties (Pent et al., 2020), interactions between hosts (Steffan et al., 2020) and microbiome (Bastías et al., 2020) might be the key parameters contributing to the bacterial community restructuring. This could be partly because the environmental factors such as soil property, moisture, and temperature were quite similar in the fruiting body as well as its adhering wood tissue.

At the first decay stage, bacterial biota in the fruiting body were more abundant, unique, active, and functional, however, the opposite trend was observed in the wood tissue. We assumed that in standing living tree, bacterial community of the fruiting body associated to it may have been suppressed, compared with dead wood tissue. However, the effect and trend weakened with progress of decay. It is very probable that the active defense system and associated chemical compounds in living trees (Asiegbu et al., 2005; Arnerup et al., 2010) may have contributed to the migration of the bacteria to the fruiting body. It is also likely that in decay class 1, bacteria were able to metabolize easily degradable sugars and carbohydrates, as well as utilizing the opportunity to source for nutrients directly from woody tissues (Clausen, 1996). Ray cell, which provides this kind of nutrients, was considered to be partly decomposed during this stage. Additionally, the increasing permeability of cellulosic substrates provides more chance for lateral bacterial groups to invade (Greaves, 1971). At the second decay class, a considerable number of bacteria groups dead from the first decay class serves as an important nitrogen resource, which lack in wood tissue. With further progress of the decay, more nitrogen and carbon resources become available (Greaves, 1971; King and White, 1976). Based on these, increasing number of nitrogen fixing bacteria start to be active with a better niche and able to have access to more resources (Johnston et al., 2016). In contrast to the living wood, plant endophytes and mycorrhiza helper bacteria (Lehr et al., 2007; Terhonen et al., 2016; Lipps and Samac, 2021) have been reported to support diverse microbial communities in that niche.

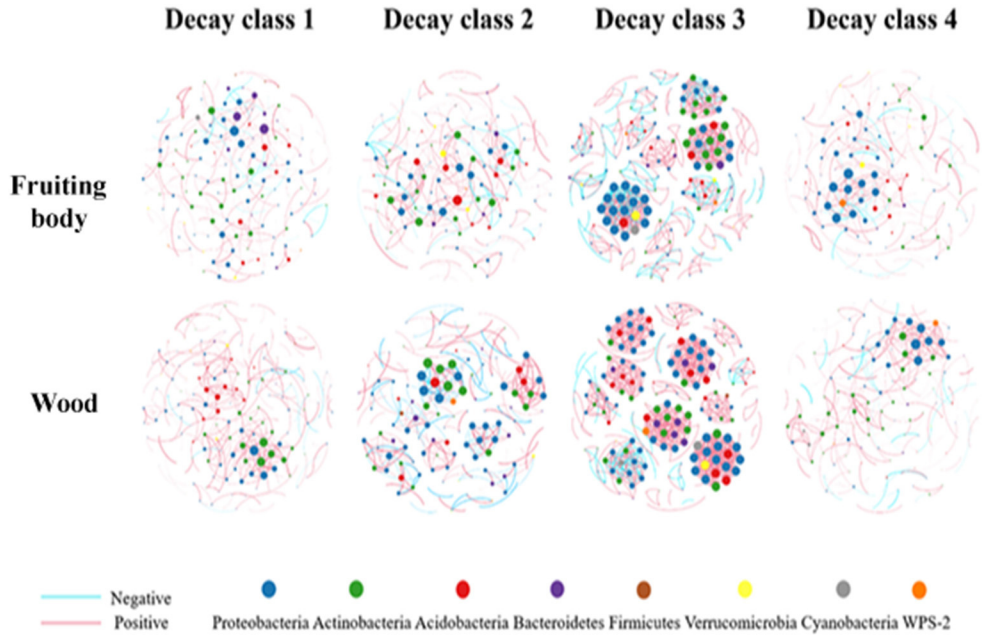

FIGURE 7 | Co-occurrence networks of top 252 OTUs showing the significant correlations in fruiting body and wood over decay. Nodes represent individual OTUs; edges represent significant Spearman correlations ($\rho > 0.7$, $P < 0.001$). The size of node represents its link degree, the larger node has more connections with other nodes. The thickness of edge represents the correlation level. The red and blue edges show the positive and negative connections between nodes separately.

The third decay class was an important turning point for the whole decay process where diversity indicators, OTUs structures, the network topological parameters reached the extreme points, and functional groups started to be differentiated between the two study materials. According to previous studies (Mäkinen et al., 2006), the wood density and stem mass start to have a sharp decrease for conifer tissues at this stage. The physical status of deadwood directly changes the accessible oxygen for wood inhabiting microbiome. The aerobic bacteria have better chance to thrive, while the anaerobic bacteria are much more at a disadvantage in the community. It is therefore possible that at this decay class, the community might reach the limitation range due to constraints of nutrition (Hacquard et al., 2015), host property (Swedjemark et al., 1998; Gohar et al., 2020), and environmental factors (Probst et al., 2018).

We observed a dramatic change in stability indicator (Po/Ne) between D2W and D3W. Besides the accumulated nutritional factors, external perturbations rather than the gradual microenvironmental changes could also be the possible reason. The previous study showed that though a higher modularity indicated a higher network stability when facing external perturbations, the network would be susceptible when targeted attack happens on community's key stone OTUs (Paranyushkin, 2012b) or by uncertain perturbations (Kitano, 2004). The obvious keystone OTUs change between D2W and D3W, and the activated Cyanobacteria and Verrucomicrobia in D3W support this concept.

In the last decay stage, as the nutrition from the old resources diminishes, a new successional group of bacteria community was observed. The new bacterial structures and functional groups were well shaped in both substrates. However, the increased instability (Po/Ne) may indicate a new community restructuring phase, as the decomposed wood turns into the soil organic layer, and soil properties take the dominant role to influence the microbial community (Fierer et al., 2007; Johnston et al., 2016; Uroz et al., 2016; Dong et al., 2021).

We also found several soil- or plant-dwelling bacteria on *Heterobasidion* fruiting body, *Bacillus* spp. (Kjeldgaard et al., 2019), for example. As discussed in previous studies, the fruiting body microbiome was also mobile as mobility is a significant microbial feature (Mitchell and Kogure, 2006; Son et al., 2015). It is most probable that bacteria might be moving from living wood tissue to the fruiting body attached or associated with it. This is reflected in the increased number of bacteria OTUs in the fruiting body. However, when the tree is dead, the active bacteria in the fruiting body start to invade dead wood with extended duration or progress of decay process. It is also possible that the low numbers of OTUs in living wood are due to the less nutritious properties of wood (Maurice et al., 2021). The higher community activity and decreasing OTUs abundance in wood might also imply that the community members were more stable in wood, making it difficult for new species to join the community. The predominant bacteria in wood might be highly selected because of a tougher niche due to various plant secondary metabolites (Garzoli et al., 2021).

In this study, the environmental factors had no significant impact on the decay classes (Pent et al., 2017).

The Ecological Functions of Bacteria Biota in Fruiting Body and Dead Wood

The FAPROTEX analysis confirmed nutrition, energy, degradation, and plant pathogen-related functions of the bacterial community. Several dominant taxonomic groups or those that showed significant changes were also of interest, as their functions are closely related to the community structure (Fierer et al., 2007).

Burkholderia spp. was the most abundant phylum in both substrates and was active in all decay classes (**Figure 4**; **Supplementary Table 3**). The abundance decreased with decay process in wood, though it was more consistent in the fruiting body. This result is similar to a previous observation on bacteria biota of the decayed wood (Probst et al., 2018). The genus' typical characteristic of being a fungal symbiont with associated fungal host protecting capability might explain its consistence in the fruiting body (Partida-Martinez and Hertweck, 2005; Marupakula et al., 2016; Sharmin et al., 2018). Furthermore, its general functions as nitrogen fixing (Sun et al., 2014), cellulose, and aromatic degrading (Kielak et al., 2016) made it lose competitive advantage in wood.

Firmicutes was much more abundant in wood tissue than in fruiting body across all decay classes and was significantly abundant in D3W. This result was similar to previous studies, where Firmicutes takes less proportion in mycorrhizosphere but is abundant in soil and wood tissue (Vik et al., 2013; Timonen et al., 2017). This might be because bacteria from this phylum have strong resilient capability in anaerobic condition (Hartmann et al., 2014). Studies from Shen et al. (2015) showed that enrichment of Firmicutes (*Bacillus*) suppresses Fusarium wilt disease. Studies by Trivedi et al. (2017) and Xiong et al. (2017) also indicate that Firmicutes is more abundant in disease-suppressed soil. Interestingly, this phylum acted non-remarkably in all decay stages and were mostly interacting within the phylum (**Supplementary Figure 4**). It is very probable that its powerful pathogen-suppressing capability contributed to its high stability and abundance.

Cyanobacteria and Verrucomicrobia only appeared in the third decay class in both substrates and only co-existed within the same module (**Figure 7**). Environmental factors were shown to be the primary driver for cyanobacterial community structuring (Rigonato et al., 2012). The decayed wood tissue might be the trigger driving the community restructuring as well as the secondary metabolites produced by Cyanobateria could suppress the pathogenic activity (Suurnäkki, 2015). Verrucomicrobia was proved to be an important phylum for plant health (Buée et al., 2009; Da Rocha et al., 2013), nutrient availability is the key factor for verrucomicrobial assemblage (Da Rocha et al., 2013; Uroz et al., 2013). Cyanobacteria provided nutrition by fixing nitrogen and carbon (Rigonato et al., 2012), which was also crucial for the activeness of both groups.

Pseudomonas spp. was abundant in both substrates in the first decay class; however, it decreased dramatically with progress of wood decay (**Figure 4**; **Supplementary Tables 3**, **4**). Its ecological function might be different in the two substrates and in the different decay classes. In woody tissue, it could be endobacteria in a living tree (GŽibovska, 2016). The tree might also have supported its existence, but the beneficial interaction stopped when the tree was killed. Consequently, the genus had difficulty to survive on dead wood tissue (Pellicciaro et al., 2021). In the fruiting body, *Pseudomonas* decreased in relative abundance at the start of decay, which later increased considerably. Some species in this genus are also known to be opportunistic pathogens (Lipps and Samac, 2021). It is likely that *Pseudomonas viridiflava*, identified in this study, could be a pathogen, endophyte, or saprotroph (Lipps and Samac, 2021). The species might live as an endophyte when tree was alive but shifted to pathogenic behavior triggered by bacterial competition (Lipps and Samac, 2021). With no suppression from tree resistance, resulting in its increased abundance (**Supplementary Table 3**).

The Network Analysis Advantages in Microbial Community Study

Microbiome analysis of *Heterobasidion* associated organisms has been widely conducted on the group level (e.g., fungi, bacteria, or virus) and specific species level; however, not much has been explored at the network level. Network metrics in this study indicated more detailed ecological (Bascompte, 2010; Thébault and Fontaine, 2010) and evolutionary (Olesen et al., 2007) information. The changing characteristics of the community were evident in this study. To our knowledge, this is the first study on the network analysis of bacteria from *Heterobasidion* fruiting body and its associated decaying wood. Our study also revealed a more complete changing trend of important bacteria throughout the various decay stages. However, the participation of fungi in both substrates merits to be investigated as it might provide further useful insight on the community structure, functions, and interaction with bacteria as well as the complete microbiome picture.

CONCLUSION

The bacterial communities inhabiting the fruiting body and wood were found to be highly dynamic through the entire wood decay process. Physical-chemical properties of fruiting body and wood, properties of bacteria species, and the interactions among fruiting body-wood-bacteria might probably have had influence in the community assembly. The third decay class was an important shifting point for both study materials as reflected by network metrics and functional groups' differentiation. The bacterial community assembled in the course of the decay process in both fruiting body and wood tend to start a new round of successional

changes reflecting the transition from living tree to dead wood and *vice versa*.

DATA AVAILABILITY STATEMENT

The datasets presented in this study can be found in online repositories. The names of the repository/repositories and accession number(s) can be found in the article/**Supplementary Material**.

AUTHOR CONTRIBUTIONS

FA and WR designed the study. RP, RK, and WR collected samples in the field. WR performed the experiments, analyzed the data, and wrote the manuscript. FA conceived the study and contributed in drafting the manuscript. All authors edited and approved the manuscript.

FUNDING

This study was supported by Ministry of Agriculture and Forestry (Grant number 4400T-2002). This study was also supported by the Chinese Scholarship Council Doctoral Stipendium.

ACKNOWLEDGMENTS

We would like to acknowledge National Land Survey of Finland for kindly providing us with the stand details.

SUPPLEMENTARY MATERIAL

The Supplementary Material for this article can be found online at: https://www.frontiersin.org/articles/10.3389/fmicb.2022.864619/full#supplementary-material

Supplementary Figure 1 | Rarefaction curve of study groups showing the sequence depth.

Supplementary Figure 2 | PCoA analysis of bacterial communities in four decay stages in fruiting body.

Supplementary Figure 3 | PCoA analysis of bacterial communities in four decay stages in wood tissue.

Supplementary Figure 4 | Co-occurrence networks of Firmicutes from top 252 OTUs in fruiting body and wood over decay.

Supplementary Table 1 | The basic information of each sampling point.

Supplementary Table 2 | The relative abundance of functional groups.

Supplementary Table 3 | The basic information of OTUs Node in the networks.

Supplementary Table 4 | The basic information of co-occurrence edge in networks.

REFERENCES

Arnerup, J., Swedjemark, G., Elfstrand, M., Karlsson, B., and Stenlid, J. (2010). Variation in growth of Heterobasidion parviporum in a full-sib family of Picea abies. *Scand. J. Forest Res.* 25, 106–110. doi: 10.1080/02827581003730799

Asiegbu, F. O., Adomas, A., and Stenlid, J. (2005). Conifer root and butt rot caused by *Heterobasidion annosum* (Fr.) Bref. s.l. *Mol. Plant Pathol.* 6, 395–409. doi: 10.1111/j.1364-3703.2005.00295.x

Asiegbu, F. O., and Kovalchuk, A. (2021). *Forest Microbiology: Volume 1: Tree Microbiome: Phyllosphere, Endosphere, and Rhizosphere*. London: Elsevier Publishers.

Bascompte, J. (2010). Structure and dynamics of ecological networks. *Science.* 329, 765–766. doi: 10.1126/science.1194255

Bastías, D. A., Johnson, L. J., and Card, S. D. (2020). Symbiotic bacteria of plant-associated fungi: friends or foes? *Curr. Opin. Plant Biol.* 56, 1–8. doi: 10.1016/j.pbi.2019.10.010

Blondel, V. D., Guillaume, J. L., Lambiotte, R., and Lefebvre, E. (2008). Fast unfolding of communities in large networks. *J. Stat. Mech. Theory Exp.* 2008, 1–12. doi: 10.1088/1742-5468/2008/10/P10008

Błońska, E., Kacprzyk, M., and Spólnik, A. (2017). Effect of deadwood of different tree species in various stages of decomposition on biochemical soil properties and carbon storage. *Ecol. Res.* 32, 193–203. doi: 10.1007/s11284-016-1430-3

Brunner, A., and Kimmins, J. P. (2003). Nitrogen fixation in coarse woody debris of Thuja plicata and Tsuga heterophylla forests on northern Vancouver Island. *Can. J. For. Res.* 33, 1670–1682. doi: 10.1139/x03-085

Buée, M., de Boer, W., Martin, F., van Overbeek, L., and Jurkevitch, E. (2009). The rhizosphere zoo: an overview of plant-associated communities of microorganisms, including phages, bacteria, archaea, and fungi, and of some of their structuring factors. *Plant Soil* 321, 189–212. doi: 10.1007/s11104-009-9991-3

Caporaso, J. G., Kuczynski, J., Stombaugh, J., Bittinger, K., Bushman, F. D., Costello, E. K., et al. (2010). QIIME allows analysis of high-throughput community sequencing data. *Nat. Methods* 7, 335–336. doi: 10.1038/nmeth.f.303

Chang, S., Puryear, J., and Cairney, J. (1993). A simple and efficient method for isolating RNA from pine trees. *Plant Mol. Biol. Rep.* 11, 113–116. doi: 10.1007/BF02670468

Chao, A. (1984). Nonparametric estimation of the number of classes in a population. *Scand. J. Statis.* 11, 265–270.

Clausen, C. A. (1996). Bacterial associations with decaying wood: a review. *Int. Biodeterior. Biodegrad.* 37, 101–107. doi: 10.1016/0964-8305(95)00109-3

Cleary, M. R., Arhipova, N., Morrison, D. J., Thomsen, I. M., Sturrock, R. N., Vasaitis, R., et al. (2013). Stump removal to control root disease in Canada and Scandinavia: a synthesis of results from long-term trials. *For. Ecol. Manage.* 290, 5–14. doi: 10.1016/j.foreco.2012.05.040

Da Rocha, U. N., Plugge, C. M., George, I., Van Elsas, J. D., and Van Overbeek, L. S. (2013). The rhizosphere selects for particular groups of Acidobacteria and Verrucomicrobia. *PLoS ONE* 8, e82443. doi: 10.1371/journal.pone.0082443

de Vries, F. T., Griffiths, R. I., Bailey, M., Craig, H., Girlanda, M., Gweon, H. S., et al. (2018). Soil bacterial networks are less stable under drought than fungal networks. *Nat. Commun.* 9, 3033. doi: 10.1038/s41467-018-05516-7

Deveau, A., Bonito, G., Uehling, J., Paoletti, M., Becker, M., Bindschedler, S., et al. (2018). Bacterial-fungal interactions: ecology, mechanisms and challenges. *FEMS Microbiol. Rev.* 42, 31–48. doi: 10.1093/femsre/fuy008

Deveau, A., Palin, B., Delaruelle, C., Peter, M., Kohler, A., Pierrat, J. C., et al. (2007). The mycorrhiza helper Pseudomonas fluorescens BBc6R8 has a specific priming effect on the growth, morphology and gene expression of the ectomycorrhizal fungus Laccaria bicolor S238N. *New Phytol.* 175, 743–755. doi: 10.1111/j.1469-8137.2007.02148.x

Dong, M., Kowalchuk, G. A., Liu, H., Xiong, W., Deng, X., Zhang, N., et al. (2021). Microbial community assembly in soil aggregates: a dynamic interplay of stochastic and deterministic processes. *Appl. Soil Ecol.* 163, 103911. doi: 10.1016/j.apsoil.2021.103911

Edgar, R. C. (2013). UPARSE: highly accurate OTU sequences from microbial amplicon reads. *Nat. Methods.* 10, 996–998. doi: 10.1038/nmeth.2604

Elliott, T. F., Jusino, M. A., Trappe, J. M., Lepp, H., Ballard, G. A., Bruhl, J. J., et al. (2019). *A Global Review of the Ecological Significance of Symbiotic Associations Between Birds and Fungi*. Heidelberg: Springer Netherlands. doi: 10.1007/s13225-019-00436-3

Fierer, N., Bradford, M. A., and Jackson, R. B. (2007). Toward an ecological classification of soil bacteria. *Ecology* 88, 1354–1364. doi: 10.1890/05-1839

Fravolini, G., Egli, M., Derungs, C., Cherubini, P., Ascher-Jenull, J., Gómez-Brandón, M., et al. (2016). Soil attributes and microclimate are important drivers of initial deadwood decay in sub-alpine Norway spruce forests. *Sci. Total Environ.* 569–570, 1064–1076. doi: 10.1016/j.scitotenv.2016.06.167

Gaitnieks, T., Bruna, L., Zaluma, A., Burnevica, N., Klavina, D., Legzdina, L., et al. (2021). Development of *Heterobasidion* spp. fruit bodies on decayed Piecea abies. *For. Ecol. Manage.* 12, 1–12. doi: 10.1016/j.foreco.2020.118835

Garzoli, S., Masci, V. L., Caradonna, V., Tiezzi, A., Giacomello, P., and Ovidi, E. (2021). Liquid and vapor phase of four conifer-derived essential oils: comparison of chemical compositions and antimicrobial and antioxidant properties. *Pharmaceuticals* 14, 1–15. doi: 10.3390/ph14020134

Gohar, D., Pent, M., Poldmaa, K., Bahram, M., Aittaleb, M., Gao, G., et al. (2020). Bacterial community dynamics across developmental stages of fungal fruiting bodies. *Cell. Signal.* 96, 1–8. doi: 10.1093/femsec/fiaa175

Gonthier, P., Garbelotto, M. M., and Nicolotti, G. (2005). Seasonal patterns of spore deposition of Heterobasidion species in four forests of the western Alps. *Phytopathology* 95, 759–767. doi: 10.1094/PHYTO-95-0759

Greaves, H. (1971). The bacterial factor in wood decay. *Wood Sci. Technol.* 5, 6–16. doi: 10.1007/BF00363116

Guo, H., Glaeser, S. P., Alabid, I., Imani, J., Haghighi, H., Kämpfer, P., et al. (2017). The abundance of endofungal bacterium Rhizobium radiobacter (syn. *Agrobacterium tumefaciens*) increases in its fungal host *Piriformospora indica* during the tripartite sebacinalean symbiosis with higher plants. *Front. Microbiol.* 8, 629. doi: 10.3389/fmicb.2017.00629

GŽibovska, Z. (2016). *Evaluation of Phlebiopsis gigantea and Pseudomonas spp. for biocontrol of Heterobasidion spp. in Norway spruce* (Master thesis). Swedish University of Agricultural Sciences, Uppsala, Sweden.

Haas, B. J., Gevers, D., Earl, A. M., Feldgarden, M., Ward, D. V, Giannoukos, G., et al. (2011). Genome Research. Available online at: genome.cshlp.org (accessed April 12, 2022).

Hacquard, S., Garrido-Oter, R., González, A., Spaepen, S., Ackermann, G., Lebeis, S., et al. (2015). Microbiota and host nutrition across plant and animal kingdoms. *Cell Host Microbe* 17, 603–616. doi: 10.1016/j.chom.2015.04.009

Hartman, K., van der Heijden, M. G. A., Wittwer, R. A., Banerjee, S., Walser, J. C., and Schlaeppi, K. (2018). Cropping practices manipulate abundance patterns of root and soil microbiome members paving the way to smart farming. *Microbiome* 6, 1–15. doi: 10.1186/s40168-017-0389-9

Hartmann, M., Niklaus, P. A., Zimmermann, S., Schmutz, S., Kremer, J., Abarenkov, K., et al. (2014). Resistance and resilience of the forest soil microbiome to logging-associated compaction. *ISME J.* 8, 226–244. doi: 10.1038/ismej.2013.141

Heip, C. (1974). A new index measuring evenness. *J. Mar. Biol. Assoc. UK.* 54, 555–557.

Ioos, R., Chrétien, P., Perrault, J., Jeandel, C., Dutech, C., Gonthier, P., et al. (2019). Multiplex real-time PCR assays for the detection and identification of *Heterobasidion* species attacking conifers in Europe. *Plant Pathol.* 68, 1493–1507. doi: 10.1111/ppa.13071

Johnston, S. R., Boddy, L., and Weightman, A. J. (2016). Bacteria in decomposing wood and their interactions with wood-decay fungi. *FEMS Microbiol. Ecol.* 92, fiw179. doi: 10.1093/femsec/fiw179

Keilhofer, N., Nachtigall, J., Kulik, A., Ecke, M., Hampp, R., Süssmuth, R. D., et al. (2018). Streptomyces AcH 505 triggers production of a salicylic acid analogue in the fungal pathogen Heterobasidion abietinum that enhances infection of Norway spruce seedlings. *Antonie van Leeuwenhoek, Int. J. Gen. Mol. Microbiol.* 111, 691–704. doi: 10.1007/s10482-018-1017-9

Kielak, A. M., Scheublin, T. R., Mendes, L. W., van Veen, J. A., and Kuramae, E. E. (2016). Bacterial community succession in pine-wood decomposition. *Front. Microbiol.* 7, 231. doi: 10.3389/fmicb.2016.00231

King, B., and White, J. (1976). Translocation of nitrogen to wood by fungi. *Znt. Biodet. Bull.* 15, 29–35.

Kitano, H. (2004). Biological robustness. *Nat. Rev. Genet.* 5, 826–837. doi: 10.1038/nrg1471

Kjeldgaard, B., Listian, S. A., Ramaswamhi, V., Richter, A., Kiesewalter, H. T., and Kovács, Á. T. (2019). Fungal hyphae colonization by *Bacillus subtilis* relies on biofilm matrix components. *Biofilm* 1, 100007. doi: 10.1016/j.bioflm.2019.100007

Korhonen, K., and Stenlid, J. (1998). *Biology of Heterobasidion annosum*. Wallingford: CAB Int. 43–70.

Lackner, G., Moebius, N., Partida-Martinez, L. P., Boland, S., and Hertweck, C. (2011). Evolution of an endofungal Lifestyle: deductions from the *Burkholderia rhizoxinica* genome. *BMC Genomics* 12, 210. doi: 10.1186/1471-2164-12-210

Legzdina, L., Spungis, V., Burnevica, N., Gaitnieks, T., and Menkis, A. (2021). Invertebrates in fruitbodies of *Heterobasidion* spp., infected picea abies logs and adjacent soil. *Forests* 12, 1–12. doi: 10.3390/f12081100

Lehr, N. A., Schrey, S. D., Bauer, R., Hampp, R., and Tarkka, M. T. (2007). Suppression of plant defence response by a mycorrhiza helper bacterium. *New Phytol.* 174, 892–903. doi: 10.1111/j.1469-8137.2007.02021.x

Lehr, N. A., Schrey, S. D., Hampp, R., and Tarkka, M. T. (2008). Root inoculation with a forest soil streptomycete leads to locally and systemically increased resistance against phytopathogens in Norway spruce. *New Phytol.* 177, 965–976. doi: 10.1111/j.1469-8137.2007.02322.x

Li, H., La, S., Zhang, X., Gao, L., and Tian, Y. (2021). Salt-induced recruitment of specific root-associated bacterial consortium capable of enhancing plant adaptability to salt stress. *ISME J.* 15, 2865–2882. doi: 10.1038/s41396-021-00974-2

Lipps, S. M., and Samac, D. A. (2021). Pseudomonas viridiflava: an internal outsider of the *Pseudomonas syringae* species complex. *Mol. Plant Pathol.* 23, 3–15. doi: 10.1111/mpp.13133

Litton, C. M., Raich, J. W., and Ryan, M. G. (2007). Carbon allocation in forest ecosystems. *Glob. Chang. Biol.* 13, 2089–2109. doi: 10.1111/j.1365-2486.2007.01420.x

Louca, S., Parfrey, L. W., and Doebeli, M. (2016). Decoupling function and taxonomy in the global ocean microbiome. *Science* 353, 1272–1277. doi: 10.1126/science.aaf4507

Magoč, T., and Salzberg, S. L. (2011). FLASH: fast length adjustment of short reads to improve genome assemblies. *Bioinformatics* 27, 2957–2963. doi: 10.1093/bioinformatics/btr507

Mäkinen, H., Hynynen, J., Siitonen, J., and Sievänen, R. (2006). Predicting the decomposition of scots pine, norway spruce, and birch stems in Finland. *Ecol. Appl.* 16, 1865–1879. doi: 10.1890/1051-0761(2006)0161865:PTDOSP2.0.CO;2

Marupakula, S., Mahmood, S., and Finlay, R. D. (2016). Analysis of single root tip microbiomes suggests that distinctive bacterial communities are selected by *Pinus sylvestris* roots colonized by different ectomycorrhizal fungi. *Environ. Microbiol.* 18, 1470–1483. doi: 10.1111/1462-2920.13102

Maurice, S., Arnault, G., Nordén, J., Botnen, S. S., Miettinen, O., and Kauserud, H. (2021). Fungal sporocarps house diverse and host-specific communities of fungicolous fungi. *ISME J.* 15, 1445–1457. doi: 10.1038/s41396-020-00862-1

Mesanza, N., Iturritxa, E., and Patten, C. L. (2016). Native rhizobacteria as biocontrol agents of *Heterobasidion annosum* s.s. and *Armillaria mellea* infection of Pinus radiata. *Biol. Control* 101, 8–16. doi: 10.1016/j.biocontrol.2016.06.003

Mitchell, J. G., and Kogure, K. (2006). Bacterial motility: links to the environment and a driving force for microbial physics. *FEMS Microbiol. Ecol.* 55, 3–16. doi: 10.1111/j.1574-6941.2005.00003.x

Moore, D., Gange, A. C., Gange, E. G., and Boddy, L. (2008). Chapter 5 Fruit bodies: their production and development in relation to environment. *Br. Mycol. Soc. Symp. Ser.* 28, 79–103. doi: 10.1016/S0275-0287(08)80007-0

Moreno, D., Gil, M., and Piccoli, P. (2014). Bacteria isolated from roots and rhizosphere of Vitis vinifera retard water losses, induce abscisic acid accumulation and synthesis of defense-related terpenes in *in vitro*. *Physiol. Plant* 151, 359–374. doi: 10.1111/ppl.12117

Möykkynen, T., Von Weissenberg, K., and Pappinen, A. (1997). Estimation of dispersal gradients of S- and P-type basidiospores of *Heterobasidion annosum*. *Eur. J. For. Pathol.* 27, 291–300. doi: 10.1111/j.1439-0329.1997.tb01083.x

Müller, J., and Bütler, R. (2010). A review of habitat thresholds for dead wood: a baseline for management recommendations in European forests. *Eur. J. For. Res.* 129, 981–992. doi: 10.1007/s10342-010-0400-5

Müller, M. M., Heinonen, J., and Korhonen, K. (2007). Occurrence of *Heterobasidion basidiocarps* on cull pieces of Norway spruce left on cutting areas and in mature spruce stands. *For. Pathol.* 37, 374–386. doi: 10.1111/j.1439-0329.2007.00516.x

Müller, M. M., Sievänen, R., Beuker, E., Meesenburg, H., Kuuskeri, J., Hamberg, L., et al. (2014). Predicting the activity of *Heterobasidion parviporum* on Norway

spruce in warming climate from its respiration rate at different temperatures. *For. Pathol.* 44, 325–336. doi: 10.1111/efp.12104

Newman, M. E. J. (2006). Modularity and community structure in networks. *Proc. Natl. Acad. Sci. U. S. A.* 103, 8577–8582. doi: 10.1073/pnas.0601602103

Olesen, J. M., Bascompte, J., Dupont, Y. L., and Jordano, P. (2007). The modularity of pollination networks. *Proc. Natl. Acad. Sci. U. S. A.* 104, 19891–19896. doi: 10.1073/pnas.0706375104

Paranyushkin, D. (2012a). Informational Epidemics and Synchronized Viral Contagion in Social Networks. *Nodus Labs*. Available online at: https://noduslabs.com/

Paranyushkin, D. (2012b). Metastability of Cognition in the Body-Mind-Environment Network ! *Nodus Labs*. 1–35.

Partida-Martinez, L. P., and Hertweck, C. (2005). Pathogenic fungus harbours endosymbiotic bacteria for toxin production. *Nature* 437, 884–888. doi: 10.1038/nature03997

Pellicciaro, M., Lione, G., Giordano, L., and Gonthier, P. (2021). Biocontrol potential of Pseudomonas protegens against *Heterobasidion* species attacking conifers in Europe. *Biol. Control* 157, 104583. doi: 10.1016/j.biocontrol.2021.104583

Pent, M., Bahram, M., and Põldmaa, K. (2020). Fruitbody chemistry underlies the structure of endofungal bacterial communities across fungal guilds and phylogenetic groups. *ISME J.* 14, 2131–2141. doi: 10.1038/s41396-020-0674-7

Pent, M., Põldmaa, K., and Bahram, M. (2017). Bacterial communities in boreal forest mushrooms are shaped both by soil parameters and host identity. *Front. Microbiol.* 8, 836. doi: 10.3389/fmicb.2017.00836

Piri, T. (1996). The spreading of the S type of *Heterobasidion annosum* from Norway spruce stumps to the subsequent tree stand. *Eur. J. For. Pathol.* 26, 193–204. doi: 10.1111/j.1439-0329.1996.tb00839.x

Probst, M., Gómez-Brandón, M., Bardelli, T., Egli, M., Insam, H., and Ascher-Jenull, J. (2018). Bacterial communities of decaying Norway spruce follow distinct slope exposure and time-dependent trajectories. *Environ. Microbiol.* 20, 3657–3670. doi: 10.1111/1462-2920.14359

Puentes Rodriguez, Y., Morales, L., Willför, S., Pulkkinen, P., Peltola, H., and Pappinen, A. (2013). Wood decay caused by *Heterobasidion parviporum* in juvenile wood specimens from normal- and narrow-crowned Norway spruce. *Scand. J. For. Res.* 28, 331–339. doi: 10.1080/02827581.2012.746387

Quast, C., Pruesse, E., Yilmaz, P., Gerken, J., Schweer, T., Yarza, P., et al. (2013). The SILVA ribosomal RNA gene database project: Improved data processing and web-based tools. *Nucleic Acids Res.* 41, 590–596. doi: 10.1093/nar/gks1219

Ren, F., Kovalchuk, A., Mukrimin, M., Liu, M., Zeng, Z., Ghimire, R. P., et al. (2019). Tissue microbiome of Norway spruce affected by *Heterobasidion*-induced wood decay. *Microb. Ecol.* 77, 640–650. doi: 10.1007/s00248-018-1240-y

Rigonato, J., Alvarenga, D. O., Andreote, F. D., Dias, A. C. F., Melo, I. S., Kent, A., et al. (2012). Cyanobacterial diversity in the phyllosphere of a mangrove forest. *FEMS Microbiol. Ecol.* 80, 312–322. doi: 10.1111/j.1574-6941.2012.01299.x

Rondeux, J., and Sanchez, C. (2010). Review of indicators and field methods for monitoring biodiversity within national forest inventories. Core variable: Deadwood. *Environ. Monit. Assess.* 164, 617–630. doi: 10.1007/s10661-009-0917-6

Ruiz-Lozano, J. M., and Bonfante, P. (2000). A Burkholderia strain living inside the arbuscular mycorrhizal fungus Gigaspora margarita possesses the vacB gene, which is involved in host cell colonization by bacteria. *Microb. Ecol.* 39, 137–144. doi: 10.1007/s002480000008

Sansupa, C., Wahdan, S. F. M., Hossen, S., Disayathanoowat, T., Wubet, T., and Purahong, W. (2021). Can we use functional annotation of prokaryotic taxa (Faprotax) to assign the ecological functions of soil bacteria? *Appl. Sci.* 11, 1–17. doi: 10.3390/app11020688

Segata, N., Izard, J., Waldron, L., Gevers, D., Miropolsky, L., Garrett, W. S., et al. (2011). Metagenomic biomarker discovery and explanation. *Genome Biol.* 12, 1–18. doi: 10.1186/gb-2011-12-6-r60

Shannon, C., and Weaver, W. (1949). *The Mathematical Theory of Communication*. Urbana, IL: University of Illinois Press. doi: 10.1145/584091.584093

Sharmin, D., Guo, Y., Nishizawa, T., Ohshima, S., Sato, Y., Takashima, Y., et al. (2018). Comparative genomic insights into endofungal lifestyles of two bacterial endosymbionts, mycoavidus cysteinexigens and burkholderia rhizoxinica. *Microbes Environ.* 33, 66–76. doi: 10.1264/jsme2.ME17138

Shen, Z., Ruan, Y., Wang, B., Zhong, S., Su, L., Li, R., et al. (2015). Effect of biofertilizer for suppressing Fusarium wilt disease of banana as well as enhancing microbial and chemical properties of soil under greenhouse trial. *Appl. Soil Ecol.* 93, 111–119. doi: 10.1016/j.apsoil.2015.04.013

Son, K., Brumley, D. R., and Stocker, R. (2015). Live from under the lens: exploring microbial motility with dynamic imaging and microfluidics. *Nat. Rev. Microbiol.* 13, 761–775. doi: 10.1038/nrmicro3567

Spraker, J. E., Sanchez, L. M., Lowe, T. M., Dorrestein, P. C., and Keller, N. P. (2016). Ralstonia solanacearum lipopeptide induces chlamydospore development in fungi and facilitates bacterial entry into fungal tissues. *ISME J.* 10, 2317–2330. doi: 10.1038/ismej.2016.32

Steffan, B. N., Venkatesh, N., and Keller, N. P. (2020). Let's get physical: bacterial-fungal interactions and their consequences in agriculture and health. *J. Fungi* 6, 1–18. doi: 10.3390/jof6040243

Sun, H., Terhonen, E., Kasanen, R., and Asiegbu, F. O. (2014). Diversity and community structure of primary wood-inhabiting bacteria in Boreal forest. *Geomicrobiol. J.* 31, 315–324. doi: 10.1080/01490451.2013.827763

Suurnäkki, S. (2015). *Anatoxin-a and Odorous Metabolites in Cyanobacteria: Molecular Detection of the Producers* (Doctoral thesis). University of Helsinki, Finland. Available online at: https://helda.helsinki.fi/handle/10138/156512

Swedjemark, G., Stenlid, J., and Karlsson, B. (1998). Genetic variation among clones of Picea abies in resistance to growth of *Heterobasidion annosum*. *Silvae Genet.* 46, 369–374.

Terhonen, E., Marco, T., Sun, H., Jalkanen, R., Kasanen, R., Vuorinen, M., et al. (2011). The effect of latitude, season and needle-age on the mycota of scots pine. *Silva Fenn.* 45, 301–317. doi: 10.14214/sf.104

Terhonen, E., Sipari, N., and Asiegbu, F. O. (2016). Inhibition of phytopathogens by fungal root endophytes of Norway spruce. *Biol. Control* 99, 53–63. doi: 10.1016/j.biocontrol.2016.04.006

Thébault, E., and Fontaine, C. (2010). Stability of ecological communities and the architecture of mutualistic and trophic networks. *Science.* 329, 853–856. doi: 10.1126/science.1188321

Timonen, S., Sinkko, H., Sun, H., Sietiö, O. M., Rinta-Kanto, J. M., Kiheri, H., et al. (2017). Ericoid roots and mycospheres govern plant-specific bacterial communities in Boreal forest humus. *Microb. Ecol.* 73, 939–953. doi: 10.1007/s00248-016-0922-6

Trivedi, P., Delgado-Baquerizo, M., Trivedi, C., Hamonts, K., Anderson, I. C., and Singh, B. K. (2017). Keystone microbial taxa regulate the invasion of a fungal pathogen in agro-ecosystems. *Soil Biol. Biochem.* 111, 10–14. doi: 10.1016/j.soilbio.2017.03.013

Uroz, S., Ioannidis, P., Lengelle, J., Cébron, A., Morin, E., Buée, M., et al. (2013). Functional assays and metagenomic analyses reveals differences between the microbial communities inhabiting the soil horizons of a norway spruce plantation. *PLoS ONE* 8, e55929. doi: 10.1371/journal.pone.0055929

Uroz, S., Oger, P., Tisserand, E., CéBron, A., Turpault, M. P., Bueé, M., et al. (2016). Specific impacts of beech and Norway spruce on the structure and diversity of the rhizosphere and soil microbial communities. *Sci. Rep.* 6, 1–11. doi: 10.1038/srep27756

Venkatesh, N., and Keller, N. P. (2019). Mycotoxins in conversation with bacteria and fungi. *Front. Microbiol.* 10, 1–10. doi: 10.3389/fmicb.2019.00403

Vik, U., Logares, R., Blaalid, R., Halvorsen, R., Carlsen, T., Bakke, I., et al. (2013). Different bacterial communities in ectomycorrhizae and surrounding soil. *Sci. Rep.* 3, 3471. doi: 10.1038/srep03471

Wang, Q., Garrity, G. M., Tiedje, J. M., and Cole, J. R. (2007). Naïve Bayesian classifier for rapid assignment of rRNA sequences into the new bacterial taxonomy. *Appl. Environ. Microbiol.* 73, 5261–5267. doi: 10.1128/AEM.00062-07

Wargo, M. J., and Hogan, D. A. (2006). Fungal-bacterial interactions: a mixed bag of mingling microbes. *Curr. Opin. Microbiol.* 9, 359–364. doi: 10.1016/j.mib.2006.06.001

Xiong, W., Li, R., Ren, Y., Liu, C., Zhao, Q., Wu, H., et al. (2017). Distinct roles for soil fungal and bacterial communities associated with the suppression of vanilla Fusarium wilt disease. *Soil Biol. Biochem.* 107, 198–207. doi: 10.1016/j.soilbio.2017.01.010

Zaluma, A., MuiŽnieks, I., Gaitnieks, T., Burneviča, N., Jansons, Ā., Jansons, J., et al. (2019). Infection and spread of root rot caused by *Heterobasidion* spp. in

Pinus contorta plantations in Northern Europe: three case studies. *Can. J. For. Res.* 49, 969–977. doi: 10.1139/cjfr-2018-0507

Conflict of Interest: The authors declare that the research was conducted in the absence of any commercial or financial relationships that could be construed as a potential conflict of interest.

Publisher's Note: All claims expressed in this article are solely those of the authors and do not necessarily represent those of their affiliated organizations, or those of the publisher, the editors and the reviewers. Any product that may be evaluated in this article, or claim that may be made by its manufacturer, is not guaranteed or endorsed by the publisher.

frontiers | Frontiers in Microbiology

ORIGINAL RESEARCH
published: 09 May 2022
doi: 10.3389/fmicb.2022.862075

Effects of Biochar on the Growth and Development of Tomato Seedlings and on the Response of Tomato Plants to the Infection of Systemic Viral Agents

Marta Luigi[1], *Ariana Manglli*[1], *Immacolata Dragone*[1], *Maria Grazia Antonelli*[2], *Mario Contarini*[2], *Stefano Speranza*[2], *Sabrina Bertin*[1], *Antonio Tiberini*[1], *Andrea Gentili*[1], *Leonardo Varvaro*[2], *Laura Tomassoli*[1] *and Francesco Faggioli*[1]*

[1] *Council for Agricultural Research and Economics-Research Centre for Plant Protection and Certification (CREA-DC), Rome, Italy,* [2] *Department of Agriculture and Forest Sciences, University of Tuscia, Viterbo, Italy*

OPEN ACCESS

Edited by:
Elvira Fiallo-Olivé, Spanish National Research Council (CSIC), Spain

Reviewed by:
Dilfuza Jabborova, Academy of Sciences Republic of Uzbekistan (UzAS), Uzbekistan
Claudio Altomare, National Research Council (CNR), Italy

***Correspondence:**
Francesco Faggioli
francesco.faggioli@crea.gov.it

Specialty section:
This article was submitted to Microbe and Virus Interactions with Plants, a section of the journal Frontiers in Microbiology

Received: *25 January 2022*
Accepted: *25 March 2022*
Published: *09 May 2022*

Citation:
Luigi M, Manglli A, Dragone I, Antonelli MG, Contarini M, Speranza S, Bertin S, Tiberini A, Gentili A, Varvaro L, Tomassoli L and Faggioli F (2022) Effects of Biochar on the Growth and Development of Tomato Seedlings and on the Response of Tomato Plants to the Infection of Systemic Viral Agents. Front. Microbiol. 13:862075. doi: 10.3389/fmicb.2022.862075

Biochar is a rich carbon product obtained by pyrolysis of biomass under a limited supply of oxygen. It is composed mainly of aromatic molecules, but its agronomic value is hard to evaluate and difficult to predict due to its great variable characteristics depending on the type of starting biomass and the conditions of pyrolysis. Anyway, it could be used as soil amendment because it increases the soil fertility of acidic soils, increases the agricultural productivity, and seems to provide protection against some foliar and soilborne diseases. In this study, the effects of biochar, obtained from olive pruning, have been evaluated on tomato seedlings growth and on their response to systemic agents' infection alone or added with beneficial microorganisms (*Bacillus* spp. and *Trichoderma* spp.). First, experimental data showed that biochar seems to promote the development of the tomato seedlings, especially at concentrations ranging from 1 to 20% (w/w with peat) without showing any antimicrobial effects on the beneficial soil bacteria at the tomato rhizosphere level and even improving their growth. Thus, those concentrations were used in growing tomato plants experimentally infected with tomato spotted wilt virus (TSWV) and potato spindle tuber viroid (PSTVd). The biochar effect was estimated by evaluating three parameters, namely, symptom expression, number of infected plants, and pathogen quantification, using RT-qPCR technique and $-\Delta\Delta$Ct analysis. Biochar at 10–15% and when added with *Trichoderma* spp. showed that it reduces the replication of PSTVd and the expression of symptoms even if it was not able to block the start of infection. The results obtained on TSWV-infected plants suggested that biochar could contribute to reducing both infection rate and virus replication. For systemic viral agents, such as PSTVd and TSWV, there are no curative control methods, and therefore, the use of prevention means, as can be assumed the use biochar, for example, in the nursery specialized in horticultural crops, can be of great help. These results can be an encouraging starting point to introduce complex biochar formulates among the sustainable managing strategies of plant systemic diseases.

Keywords: potato spindle tuber viroid, tomato spotted wilt virus, biochar, tomato, systemic infection

INTRODUCTION

Nowadays, biomass conversion represents a new approach to obtain renewable energy in several fields, such as urban waste recycling, biofuel production, and industrial processes. The agricultural productions also benefit from biomass-derived amendments for sustaining the soil fertility. Biochar is a solid and carbonaceous amendment obtained from various materials by pyrolysis, a heating process under a limited supply of oxygen (Laird et al., 2009), and it has been described as an "anthropogenically produced black carbon (BC) material" (Lorenz and Lal, 2018). In the twenty-first century, the use of biochar has seen a renewed interest because of its longevity in the soil, estimated between hundreds and thousands of years or more, and its role as a carbon removal from the atmosphere, sequestering CO_2, with beneficial effects in mitigating the climate changes (Frenkel et al., 2017). Biochar is composed mainly of aromatic molecules with base cations that form bridges between the organic particles of the soil. These structures improve the soil pH (Yamato et al., 2006), as well as the retention of both the soil water and nutrients (Bronick and Lal, 2005; Chan et al., 2007, 2008; Rajkovich et al., 2012). In this way, biochar promotes the transformation and turnover of nutritional elements (Pietikäinen et al., 2000) and contributes to expand beneficial microbial population like rhizobacteria and fungi (Graber et al., 2010) and neutralize phytotoxic molecules (Wardle et al., 1998). The biochar effects on the soil biomass composition often result in enhanced plant fitness and productivity, as already observed for several crops such as wheat, maize, cucumber, bean, tomato, strawberry, and sweet pepper (Graber et al., 2010; Harel et al., 2012; Cornelissen et al., 2013; Jaiswal et al., 2014, 2015; De Tender et al., 2016). In a few cases, no effects, or even unwanted effects, were described (Jeffery et al., 2011; Kammann et al., 2015; Haider et al., 2016; Shackley et al., 2016), showing that the agronomic value of biochar can be variable. This is mainly due to the fact that both structure and biological activity of biochar can be affected by several factors, including the type of starting biomass and the conditions of pyrolysis (temperature and time of heat action), as well as climatic and soil chemistry conditions (Elad et al., 2011; Juriga and Šimanský, 2018).

Among the contributions to plant growth, biochar is known to potentiate the plant response to biotic stresses. Its use against airborne and soilborne fungal pathogens already showed positive effects that are attributable to interactions with soil microbes and plants rather than to the direct release of fungitoxic compounds (Bonanomi et al., 2015). Concerning the direct effects on plants, it has been suggested that biochar can induce both systemic-acquired resistant and inducing systemic resistant (Harel et al., 2012), even if the mechanisms have not been well-understood yet and the results observed so far seem to be dose dependent. In contrast, there is more robust empirical evidence that biochar can promote the development and activity of plant growth-promoting microorganisms (PGPMs), such as rhizobacteria, mycorrhizal, and other endophytic fungi. These microorganisms effectively exploit biochar porous structure to find refuge from predators, such as mites, collembolan, protozoans, and nematodes, whereas the biochar-derived organic carbon contributes to sustain their saprophytic growth (Bonanomi et al., 2018). The PGPMs in turn play a crucial role in protection against pathogens by means of competition for nutrients and space, direct parasitism, and antagonism through the production of secondary metabolites (Bonanomi et al., 2018). For example, the fungi *Trichoderma* spp. are known to be efficient competitors for space and nutrients and to rapidly colonize plant roots. Their beneficial effects on root system architecture, as well as their secondary metabolites released in the rhizosphere, promote plant growth and elicit plant responses against several pathogens (Vicente et al., 2022). Similarly, the bacteria *Bacillus* spp. can trigger plant defenses and improve plant fitness and nutrition through the production of bioactive secondary metabolites and phytohormones (Poveda and González-Andrés, 2021; Dimki et al., 2022). The presence of biochar has been shown to enhance these beneficial effects in a wide range of host plants, including horticultural crops, cereals, soybean, and woody plants, and has therefore promoted the use of this amendment as a carrier of PGPMs (Ribera et al., 2017; Ahmad et al., 2020; Sani et al., 2020; Haider et al., 2021).

The use of biochar, alone or together with PGPMs in the soil, has repeatedly proved to be effective against fungal pathogens, whereas little information is available about the possible protection from viral diseases. In this study, the effects of biochar obtained from olive pruning (certified by EUROFINS) have been evaluated on tomato plants infected by potato spindle tuber viroid (PSTVd) and tomato spotted wilt virus (TSWV), two regulated non-quarantine pests in Europe (Commission Implementing regulation EU 2019/2072; Annex IV) and included in the European and Mediterranean Plant Protection Organization (EPPO, 2022) list A2 (https://www.eppo.int/ACTIVITIES/plant_quarantine/A2_list). PSTVd, the type species of the genus *Pospiviroid* in the family Pospiviroidae (Di Serio et al., 2014), is a very damaging pathogen of a high number of Solanaceae species. Different degrees of symptom severity can be observed in tomato, ranging from leaf chlorosis and growth reduction to the loss of flower and fruit production (Owens and Verhoeven, 2017). TSWV is the type species of the genus *Orthotospovirus* (family Tospoviridae); it is responsible for severe damages to tomato cultivations, causing plant stunting and yield reduction, and blemishing the fruit with necrotic or chlorotic ringspots that make it unmarketable (Stevens et al., 1991). The impact of biochar on the virus-/viroid-infected tomato plants was assessed for a possible application in sustainable programs of disease prevention and protection. In this frame, the effects of biochar on the tomato seedling growth, as well as on the virus/viroid titer and symptom expression in infected plants, were evaluated. Besides the effects of biochar itself, the potential role as a carrier of PGPM was also investigated (using *Trichoderma* spp. and *Bacillus* spp.-based products).

MATERIALS AND METHODS

Preliminary Evaluation of Biochar Activity

The amendment used in this study was obtained from the transformation of olive tree pruning chopped directly in the field, transformed into pellets and subsequently into biochar

(by S.E.A. Company, University of Tuscia, Viterbo, Italy; Zambon et al., 2016). The physical and chemical characteristics were evaluated according to the European Biochar Certificate guidelines (EBC, 2012–2022) at the EUROFINS laboratory (Niederlassung Freiberg, Germany). The EBC analysis of the physiochemical characteristics confirmed that the biochar used in this study completely complied with the European legislation in the matter of soil improvers, thereby authorizing its use as a soil amendment (Zambon et al., 2016). All the ratios between biochar and peat reported in this study were calculated considering the dry weight of both substrates. The composition of the peat was organic component 57.4%, mineral component 42.6, pH 3.4.

Biochar as a Promoter of Plant Growth

Different concentrations of biochar (1, 2, 5, 10, 20, 30, 40, and 50% in ratio to peat) were evaluated in a "split-pot" bioassay in triplicate. The different concentrations were chosen to highlight the potential positive effects at low concentrations of biochar, as well as possible phytotoxic effects at high levels of biochar (>10%). Tomato seedlings were planted into small pots, each split in a first half filled up with peat only and in a second half filled up with a substrate composed of peat and biochar at different concentrations. After 30 days, the dry weight of the tomato roots was analyzed.

Biochar as a Promoter of Rhizobacteria in Soil

Rhizobacteria were isolated from the rhizosphere of tomato plants that were grown both in peat and the substrates containing 1, 2, 5, and 10% of biochar. Specifically, 10 g of soil was suspended in 90 ml of saline solution (0.85% NaCl), shaken for 30 min, and the soil suspensions were then 10-fold diluted and plated onto King B medium [10 g glycerol, 1.5 g K_2HPO_4, 1.5 g $MgSO_4.7H_2O$, 20 g Proteose peptone No. 3 (Difco), 15 g technical agar (1.5% w/v) per liter] and trypticase soy agar medium (casein peptone 15 g, soy peptone 5 g, sodium chloride 5 g, agar 15 per liter) in Petri dishes that were incubated at 28°C (Alves Silva et al., 2003).

Biochar as a Carrier of Plant Growth Promoters (PGP)

Two commercial products of PGPMs were used in this study, namely, Remedier (Gowan, Ravenna, Italy) containing *Trichoderma gamsii* strain icc 080 and *Trichoderma asperellum* strain icc 012 (3×10^7 CFU/g) and Sublic Linea Activator (Microspore, Campobasso, Italy) containing *Bacillus licheniformis* and *Bacillus subtilis* (10^9 CFU/g). The growth of *Trichoderma* spp. was evaluated on potato starch dextrose agar (potato starch 4 g, dextrose 20 g, agar 15 g per liter) plates added with different concentrations of biochar (1, 2, 5, and 10%) with diameter < 1 mm. Specifically, five different isolates of the two *Trichoderma* species (icc 080 and icc 012 obtained from Remedier product) were plated, and the mycelial growth was evaluated at 24, 48, and 72 h. The growth of *Bacillus* spp. was evaluated using both *B. subtilis* and *B. licheniformis*. Specifically, colonies of *B. subtilis* (2.3×10^5 CFU/ml) and *B. licheniformis* (7×10^5 CFU/ ml) were grown (120 rpm, 26°C ± 1°C) in liquid broth added with biochar (1, 2, 5, and 10%) with <1 mm of diameter, and then reisolated and counted after 48 h. The survival of *Bacillus* spp. and *Trichoderma* spp. on biochar was also estimated after 90 days from the preparation. Biochar was stirred for 2 h in aqueous suspension with either "Sublic" or "Remedier," the substrate was then dried and kept at room temperature. Reisolations were performed at 10, 20, 60, and 90 days after the treatment.

TABLE 1 | Composition of the six basic substrates used in the experiments.

	Peat	Biochar	*Bacillus* spp.	*Trichoderma* spp.
A0	+	−	−	−
A	+	+	−	−
B1	+	+	+	−
B2	+	+	−	+
C1	+	−	+	−
C2	+	−	−	+

Substrates A, B1, and B2 were prepared with five different biochar concentrations (1, 2, 5, 10, and 15%).

Experimental Design

In a two-year research, the effects of biochar and PGPMs at different concentrations were evaluated on PSTVd- and TSWV-infected tomato seedlings in three independent experiments per pathogen.

Tomato seedlings (cultivar Roma) were grown in peat for 30–40 days following an organic cultivation. Then, the seedlings were transplanted in six substrates, including the control (A0) containing only peat (**Table 1**). Substrate A was prepared by combining peat and biochar at 1, 2, 5, 10, and 15%. Substrates B1 and B2 were the same as substrate A with the addition of *Bacillus* spp. and *Trichoderma* spp., respectively, at different concentrations that depended on the adsorption of those microorganisms on the biochar. Specifically, the initial concentration of *Trichoderma* spp. was 2×10^4 CFU/g and of *Bacillus* spp. of 3.5×10^6 CFU/g. In substrates C1 and C2, *Bacillus* spp. and *Trichoderma* spp. were added to the peat without biochar at the same concentration of the B1 and B2 media, respectively.

Mechanical inoculations of the virus/viroid were performed on transplanted seedlings at four/five true leaf stage. An isolate of PSTVd (isolate Sj1—GenBank Accession No. HQ452413, belonging to the pathogen collection of the CREA-DC) and an isolate of TSWV (VE-TSWV-not breaking resistance-RB), provided by the Institute for Sustainable Plant Protection—National Research Council, Italy, were chosen as the source of inoculum. Sap for inoculum was prepared by grinding infected material in sterilized phosphate buffer (0.1 M, pH 7.2) at the concentration of 1:20 W/V. In addition, 40 µl of the solution was used to inoculate the two last expanded apical leaves (20 µl each) previously covered by abrasive powder (celite). The infectious status of all the inoculated plants was tested at 30 days post inoculation (dpi) when the first symptoms appeared.

All experimental trials were conducted in a greenhouse at 20–24°C with a 12–14-h photoperiod.

Evaluation of Biochar Activity on Systemic Pathogens

In the first experiment (trial 1), plants were grown onto all the typologies of substrates (A, B1, B2, C1, and C2) supplied with biochar at 1, 2, and 5%. Each treatment was carried out on 3 and 6 seedlings inoculated with PSTVd and TSWV, respectively. The second experiment (trial 2) followed the same scheme as trial 1, but nine PSTVd and nine TSWV inoculated seedlings were used per treatment and the biochar concentration was increased up to 10 and 15%. In both trials 1 and 2, the PSTVd and TSWV titer was measured at 30th dpi. A third experiment (trial 3) was carried out using only the combination of biochar/PGPMs concentrations selected for the best effects observed against the viroid/virus in the previous experiments. In this trial, the seedlings were allowed to grow to an adult stage, and 12 inoculated plants per treatment/per pathogen were evaluated only for growth and symptoms expression at 90th dpi.

For each experiment and substrate typology, three healthy (non-inoculated) plants were used as control in order to distinguish the viroid/virus symptoms from possible alterations due to the different combinations/concentrations of biochar or other environmental factors.

Symptom Visual Examination

Starting from 1 week after the inoculation, the plants of the first and second experiments were periodically inspected by visual examination for systemic symptoms development and plant growth rate until 30th dpi when leaf samples were collected for virus/viroid titer quantification. In the third experiment, the plants were maintained until 90th dpi for the symptom examination only. Specifically, three classes of severity were defined for the symptoms induced by each pathogen at 90 dpi. For PSTVd, the classes were no symptoms; mild symptoms corresponding to leaf mosaic and curling; and severe symptoms corresponding to necrosis of leaves, shortened internodes, apical bunching, and stunted growth. For TSWV, the classes were no symptoms; mild/middle symptoms corresponding to chlorotic and/or necrotic spots on leaves with normal growth of the plants; and severe symptoms corresponding to necrotic spots, leaf distortion, apical necrosis, and stunted growth of the plants.

Pathogen Detection and Relative Quantification

Three leaf samples corresponding to the basal, medium, and apical positions were collected at the 30th dpi from each plant in trials 1 and 2. Total RNA (TRNA) was extracted from 0.1 g of powdered leaves (obtained using liquid nitrogen) using Spectrum Plant Total RNA kit (Sigma, Deisenhofer, Germany) and TRNA tissues and cells kit (Danagen, Spain) for PSTVd and TSWV, respectively.

The detection of PSTVd was performed by the end-point RT-PCR according to Faggioli et al., (2013), and the quantification was performed by RT-qPCR according to Boonham et al. (2004). The detection of TSWV was achieved using a DAS-ELISA Kit (Loewe Biochemica GmbH, Germany), and the quantification was performed by RT-qPCR using the primers and probes reported in **Table 2**. The relative quantification of both pathogens was carried out using the cytochrome oxidase gene (Weller et al., 2000) as endogenous control.

TABLE 2 | Sequence of primers and probe used for TSWV quantification.

Name	Sequence (5′-3′)	Position
TSWV333F	AAGCTACCTCCCAGCATTATGG	2,352–2,373
TSWV415R	TCTCACCCTTTGATTCAAGCCTAT	2,411–2,434
TSWV356T	6-FAM-AAGCCTCACAGACTTTGCATCATCAA GAGG-BHQ1	2,375–2,404

Position is referred from the sequence LC549181 of the NCBI database.

All RT-qPCR tests were performed including 2 μl of total RNA to the following 18 μl reaction mixture, namely, 1X TaqMan® RT-PCR Mix and 1X TaqMan® RT Enzyme Mix (TaqMan® RNA-to-CT™ 1 Step Kit from Thermo Fisher Scientific, MA, USA), 0.8 μM primer forward; 0.8 μM primer reverse; 0.2 or 0.4 μM, for PSTVd and TSWV, respectively, of the probe labeled in FAM/BH1 (BioFab Research, Italy). The same mixture was used for the endogenous control amplification; also, this probe was labeled FAM/BH1 (BioFab Research, Italy). All amplifications were performed in an Abi7500Fast thermocycler (Life Technologies, CA, USA) using the cycling conditions 10 min at 50°C for reverse transcription followed by 5 min at 95°C; amplification was performed for 40 cycles with denaturation for 10 s at 95°C and annealing combined with extension for 30 s at 60°C.

Data Analysis

The comparison of the concentrations of the pathogens obtained from the plants grown on different media was done using the $-\Delta\Delta$Ct method, subtracting the cycle thresholds (Cts) of treated samples (A, B1, B2, C1, and C2) with non-treated infected plants (A0). Before applying this method, primers and probes were tested to demonstrate that the amplification efficiency of the diagnostic methods was approximately the same as the endogenous control (Livak and Schmittgen, 2001) and the absolute value of the slope of each test was determined to be <0.1 (**Supplementary Material**).

Results from the calculation were analyzed by ANOVA (Montgomery, 2012). Mean squares of main effects and interactions were compared by *F*-tests (95% of significance) with error variance estimated by three replicates of test condition. ANOVA was performed for each monitored variable (concentration of biochar, presence/absence of microorganisms). Significant results were analyzed using a *post-hoc* test (*t*-test).

RESULTS

Preliminary Evaluation of Biochar Activity

The split-pot test showed that biochar can positively affect the development of tomato roots 30 days after planting, and the dry weight of the roots grown in biochar at the concentration from 2% to 20% was significantly higher than the control (roots grown in peat only) (**Figures 1A,B**).

Biochar showed a positive effect on the growth of rhizobacteria present in the rhizosphere of the tomato seedlings.

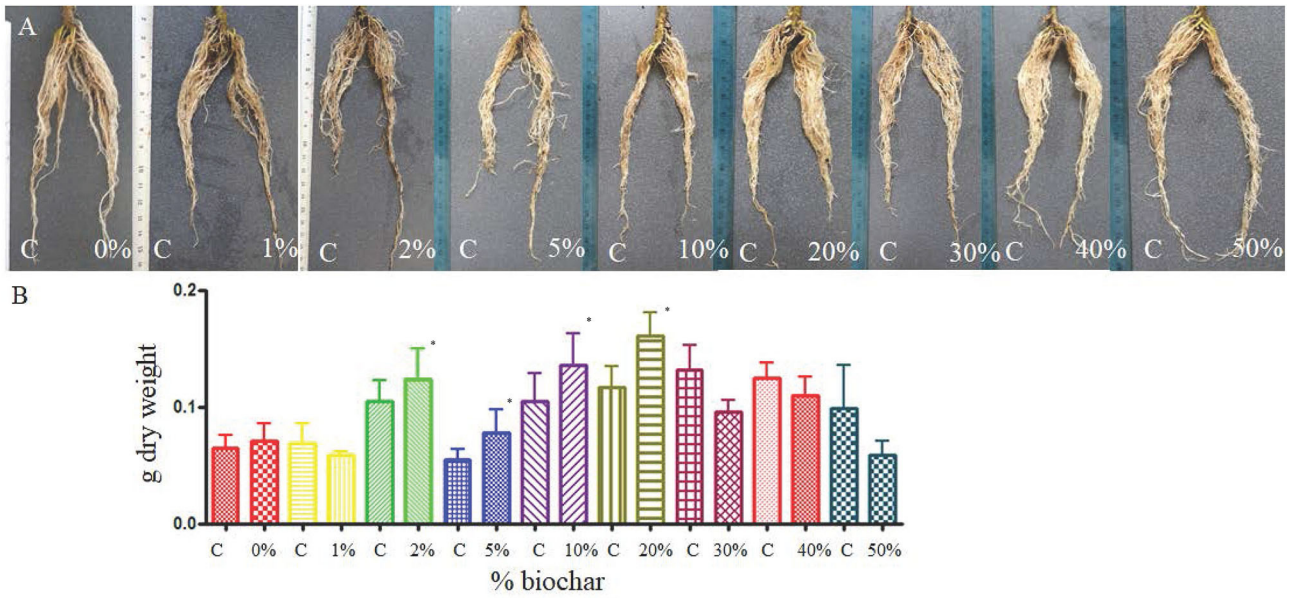

FIGURE 1 | Root of tomato seedlings **(A)** grown half in peat (C, control) and half on a substrate containing different concentrations of biochar (from 0 to 50%) in a split pot test. **(B)** Dry weight of the same roots grown half in peat (C) and half in biochar at different concentrations. *$p < 0.05$.

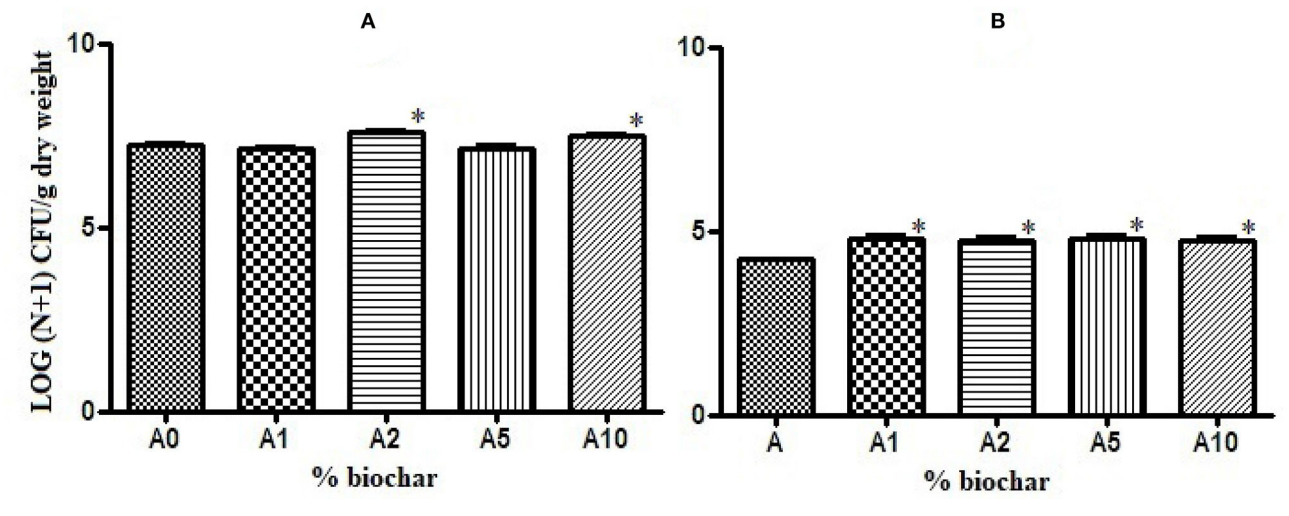

FIGURE 2 | Effect of different concentrations of biochar on the total bacterial load **(A)** and the sporogenic bacteria concentration **(B)** of the rhizobacteria isolated from the tomato roots. *$p < 0.05$.

The total bacterial load was significantly higher in substrates with 2 and 10% of biochar (A2 and A10) than in the control substrate (A0), (**Figure 2A**), and the charge of sporogenic bacteria significantly increased in all the biochar substrates (**Figure 2B**).

Both *Trichoderma* spp. and *Bacillus* spp. were successfully grown in the proper media added with 1, 2, 5, and 10% of biochar, and they were reisolated after keeping the samples for 90 days at room temperature, suggesting that the amendment has no antimicrobial effects (data not shown).

Effect of Biochar on the Response of Tomato Systemically Infected Plants

The effect of the biochar on the plant systemic pathogens was ascertained by both symptom evaluation and virus/viroid quantification with respect to the expression of a stable endogenous control. Primers and probes were tested before to ascertain the comparability of the efficiency of the quantification protocols (see **Supplementary Material**).

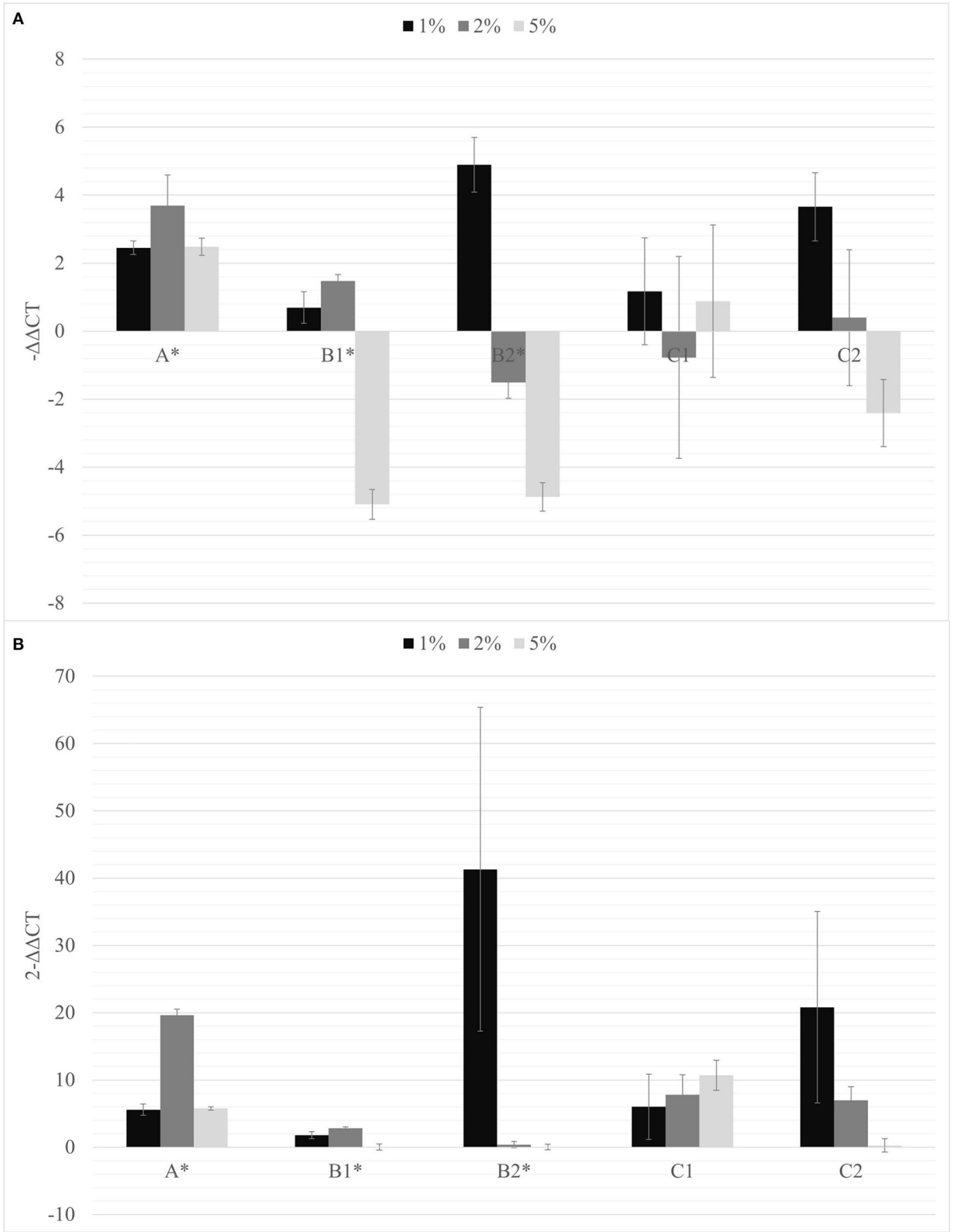

FIGURE 3 | The $-\Delta\Delta Ct$ **(A)** and fold change in PSTVd replication ($2^{-\Delta\Delta Ct}$) **(B)** mean values obtained for all the biochar percentages (1% black; 2% dark gray; 5% light gray) are reported. *$p < 0.05$.

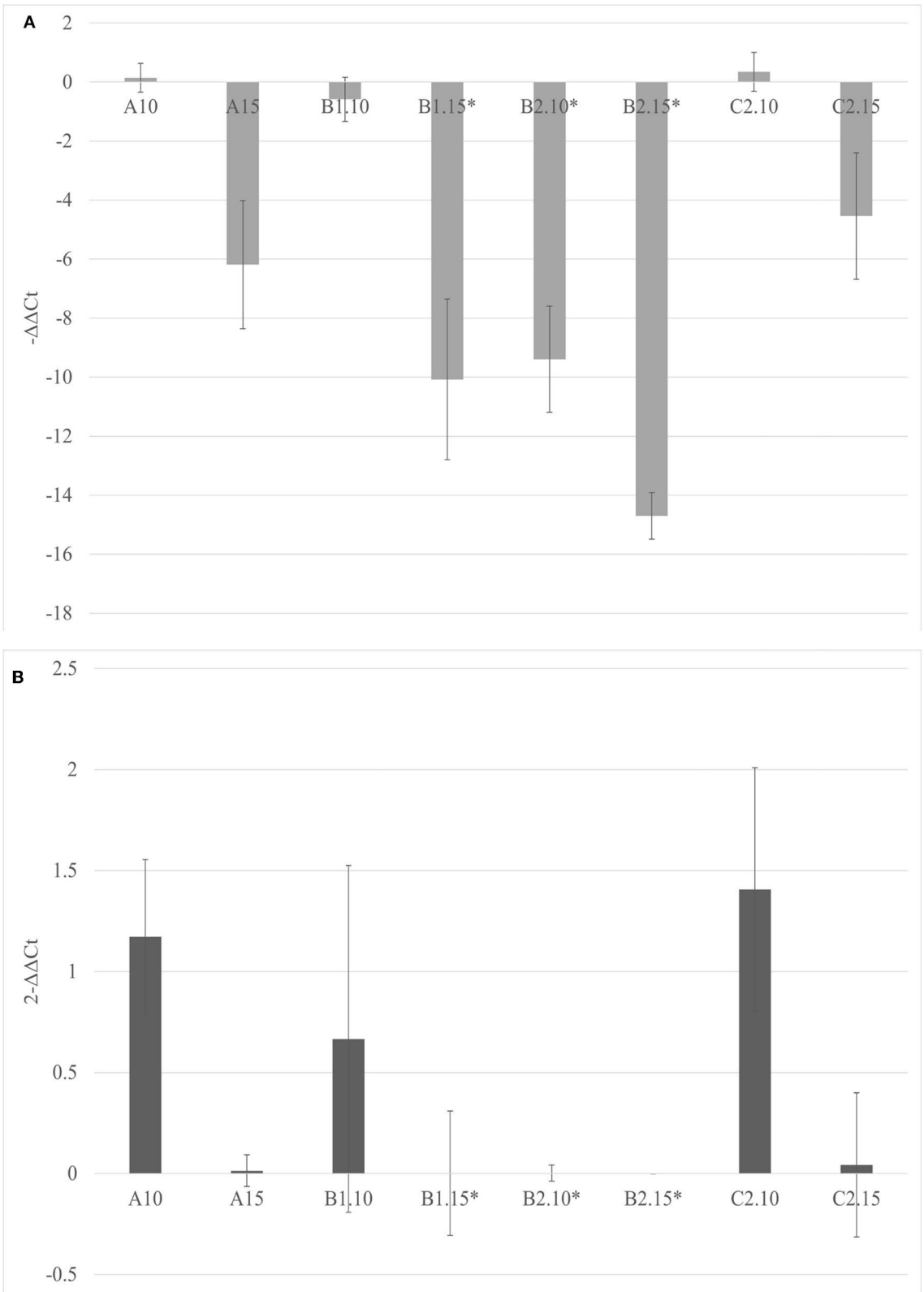

FIGURE 4 | The $-\Delta\Delta Ct$ **(A)** and fold change in PSTVd replication ($2^{-\Delta\Delta Ct}$) **(B)** mean values obtained for all the theses are reported in the left and right, respectively. *$p < 0.05$.

Potato Spindle Tuber Viroid

Considering the effects of biochar observed on the growth of tomato root and on the growth of rhizobacteria and PGPMs, biochar at 1, 2, and 5% was first added to the A, B1, and B2 substrates and the same PGPM concentration used in B1 and B2 was added to peat into C1 and C2 substrates. All the PSTVd-inoculated tomato plants growing onto these different substrates resulted to be symptomatic and positive to the viroid after 30 dpi (data not shown) and were subjected to the viroid titer quantification (**Figure 3**).

The soils containing only *Bacillus* spp. (C1) and *Trichoderma* spp. (C2) were not able to inhibit the viroid's replication, and the soil containing only biochar (A) even promoted the replication of the viroid compared to the control. On the contrary, the soils with 5% of biochar in combination with the PGPMs (B1 and B2) significantly reduced the replication of PSTVd compared to the control (A with 5% biochar). According to this, soils with higher concentrations of biochar, 10 and 15%, were prepared and new tests were made inoculating 9 new healthy tomato plants for each substrate. Also in these trials, all the plants tested positive for PSTVd after 30 dpi (data not shown) and were analyzed for titer quantification. In all the theses, the viroid titer decreased compared to the control, but this reduction was significant only in plants grown in the substrate containing 10% of biochar together with *Trichoderma* spp. (B2.10), as well as in the substrate containing 15% of biochar added with *Bacillus* spp. and *Trichoderma* spp., respectively (B1.15 and B2.15) (**Figure 4**).

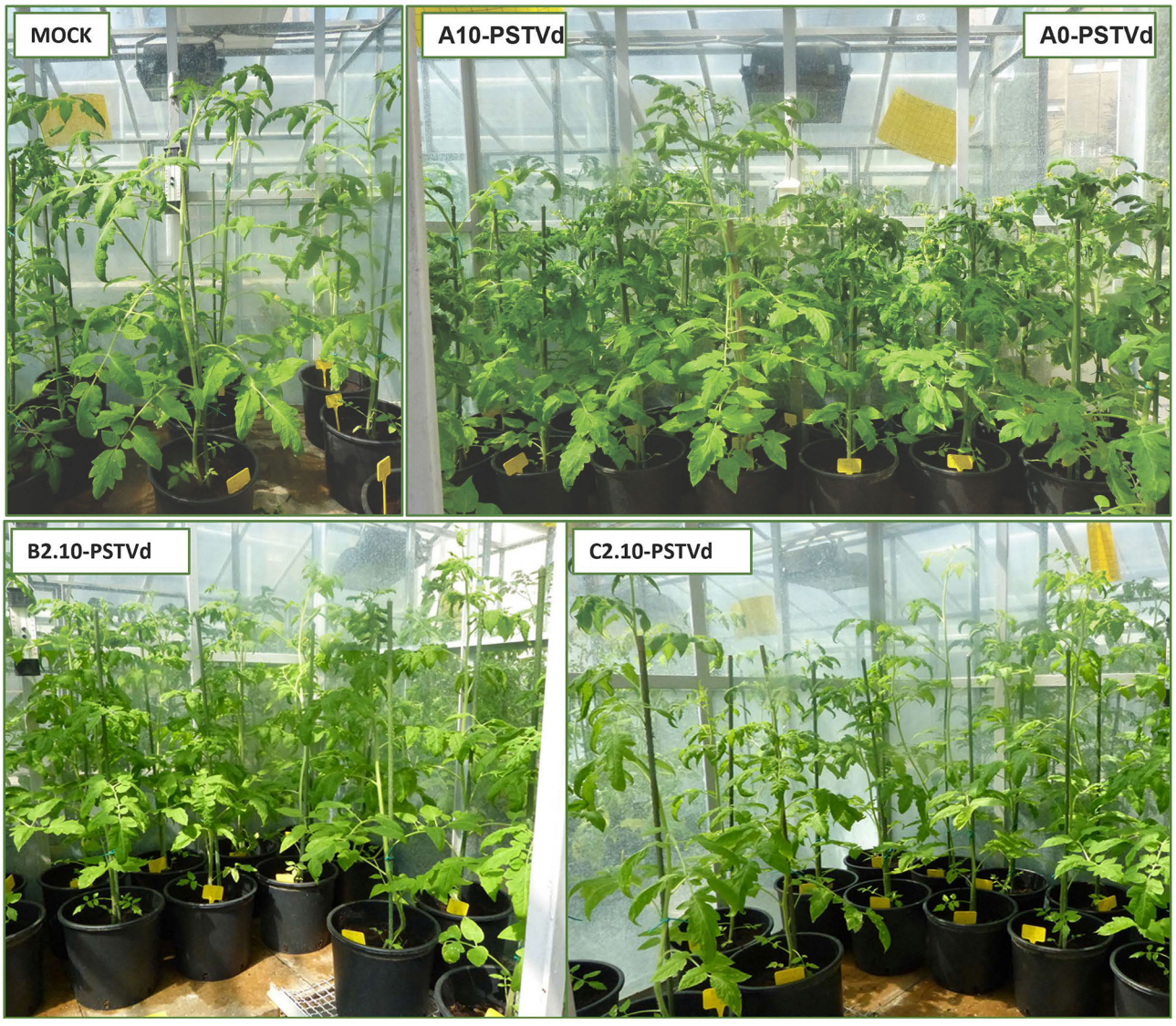

FIGURE 5 | PSTVd symptoms observed on tomato plants growth on different substrates: MOCK-controls inoculated with buffer only; A10-PSTVd, A0-PSTVd showing severe symptoms: shortening of internodes, bunched leaves and shoots on the top of the plants, and stunted growth; B2.10 and C2.10-PSTVd showing mild symptoms: curling leaves and distortion.

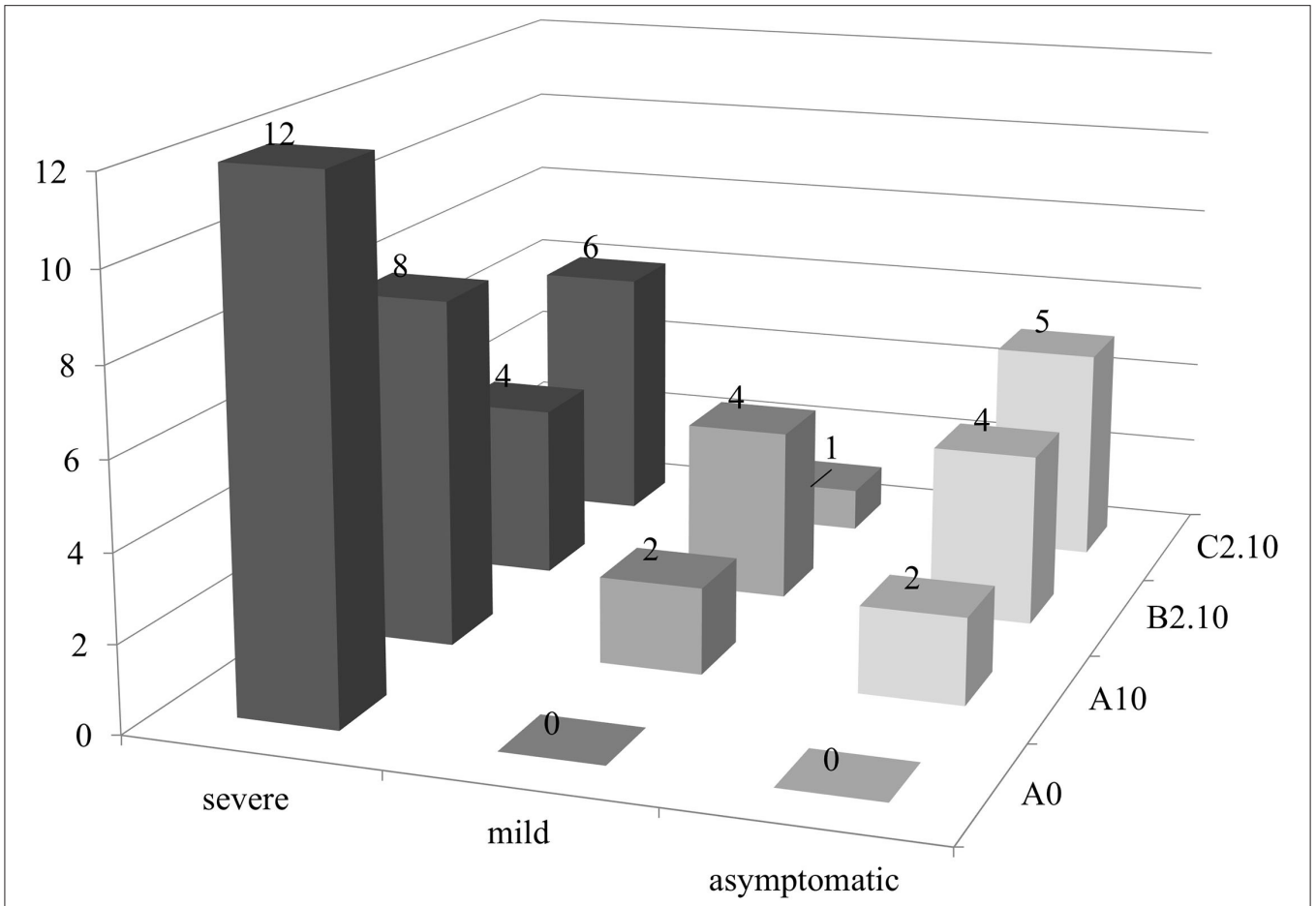

FIGURE 6 | PSTVd symptoms modulation (no. of plants evaluated according to the expression of symptoms for each substrate in this study). Black, severe symptoms; dark gray, mild symptoms; light gray, no symptomatic plants.

A possible effect of biochar and PGPMs on the expression of PSTVd symptoms was inspected growing 12 tomato plants for each substrate for 90 days. The plants were grown on substrate B2.10, which resulted in the best combination to reduce the titer of the viroid, and on substrates A0, A10, and C2.10 as controls. All the inoculated plants tested positive for the viroid, but the symptom modulation varied according to the different substrates (**Figures 5**, **6**). All the plants grown in substrate A0 (only peat) showed severe symptoms (**Figure 5** panel A0-PSTVd) consisting of shortened internodes, bunched lives and shots in the top of the plants, and stunted growth. Similar symptoms were also obtained from the plants transplanted on A.10 substrate (peat and biochar) (**Figure 5**—panel A.10 PSTVd). Plants growing in C2 substrate showed a variability of symptoms, from mild to severe symptoms. Plants grown in the soil containing biochar and *Trichoderma* spp. (B2.10) had the best response to the viroid infection showing mild symptoms, mainly curling and distortion of the leaves, or no symptoms (**Figure 5** panel B2.10). The distribution of the 12 plants per thesis among the three classes of symptoms severity is reported in **Figure 6**.

TABLE 3 | Number of TSWV-infected plants out of the six inoculated plants grown onto the different substrates.

A0	Biochar %	A	B1	B2	C1	C2
3	1	4	2	3	0	4
	2	4	3	0	0	2
	5	4	2	0	5	4

Tomato Spotted Wilt Virus

In the first experiment carried out with the lowest concentrations of biochar (1, 2, and 5%), both symptom observation and virus detection at 30 dpi showed that not all the inoculated plants were infected. The distribution of infection was not uniform among the 6 seedlings of each treatment (**Table 3**) and did not allow a direct comparison to the control A0 (3 infected plants out of 6 inoculated plants). Nevertheless, some differences among substrates are evident (**Table 3**), such as the absence of infected plants in the B2 (biochar plus *Trichoderma* spp.) soil containing 2 and 5% of biochar, and in the C1 soil containing *Bacillus* spp. at

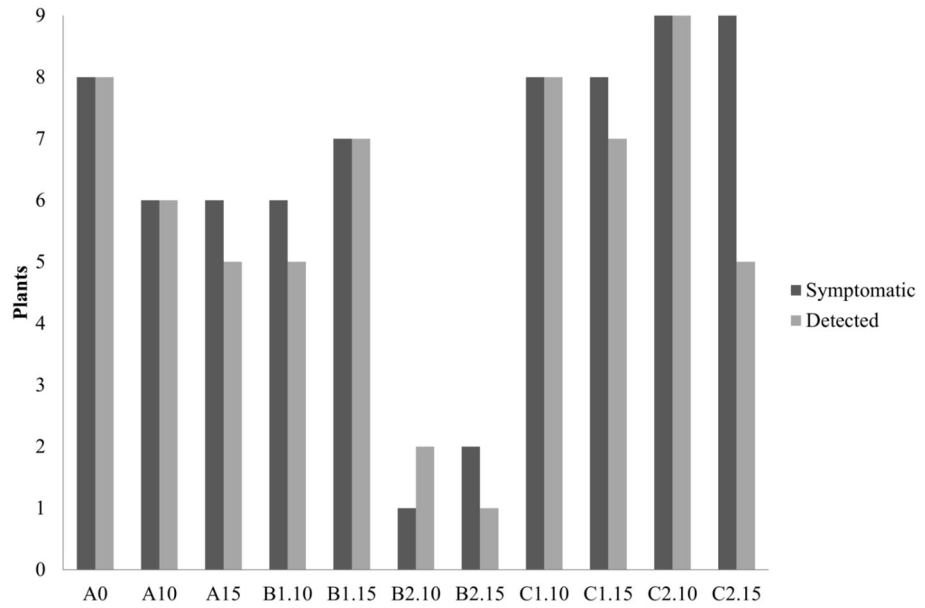

FIGURE 7 | Number of symptomatic and TSWV-positive tomato seedlings grown on different substrates (A0 control-only peat; A, peat combined with biochar; B1, peat combined with biochar and *Bacillus* spp.; B2, peat combined with biochar *Trichoderma* spp.; C1, C2, peat combined only with *Bacillus* spp. or *Trichoderma* spp., respectively), numbers 10 and 15 represent the concentrations. *p-Value < 0.05.

the same concentration used in addition to 1 and 2% of biochar in B1.

In the second trial, again all the substrates were evaluated, increasing the number of seedlings (9 per each treatment) and using higher concentrations of biochar, 10 and 15%. ELISA test at 30th dpi showed a different number of infected plants grown on the different substrates (**Figure 7**). The highest number of the infected plants compared to the inoculated ones (8/9) was obtained in the control substrate (A0-only peat) and in the substrates containing PGPMs only (C1 and C2). In particular, in the C1 substrate (peat and *Bacillus* spp.), the infected plants were 8/9 and 6/9, and in the C2 substrate (peat and *Trichoderma* spp.) the infected plants were 6/9 and 8/9. The number of infected plants decreased (5/9) in substrate A containing biochar at both 10 and 15%, and in substrate B1 (peat, biochar, and *Bacillus* spp.) at 10% concentration. Finally, B2 substrate containing both 10 and 15% of biochar and *Trichoderma* spp. showed a reduction in the number of positive samples that was significant compared to the other substrates (1/9 and 2/9, respectively). Symptom expression at 30th dpi also varied according to the different substrates. The most severe symptoms, consisting of the typical necrotic spots and bronzing of leaves, were observed in treatment A0 (mock control) in all infected plants (**Figure 8**-S1). In the other substrates, the symptoms consisted generally of chlorotic spots or chlorotic leaves (**Figure 8**-M1) without difference in symptoms severity but in the rate of number of symptomatic/infected plants (**Figure 7**). As the number of infected plants obtained in this experiment was higher than in the first one, the real-time RT-PCR analyses for the relative quantification of the viral titer in plants grown on different substrates were possible. The TSWV titer was measured for plants grown in substrate B2 (peat, *Trichoderma* spp., and biochar) at both concentrations 10 and 15% that showed the minor number of infected plants and for the plants grown on the respective substrate controls A10 (peat and biochar) and C2 (peat and *Trichoderma* spp.). The viral titer was lower in plants grown in substrate B2.10 (biochar and *Trichoderma* spp.) compared to plants grown in substrates A10 (peat and biochar) and C2.10 (peat and *Trichoderma* spp.); the titer decreases to about 40,000 times in B2.10 with respect to the infected plants of the control A0 (**Figure 9**).

The third experiment, for symptom evaluation at 90th dpi, was carried out using the A and B2 soil with a biochar concentration of 10%, and A0 and C2 soils served as controls. Again, only a few inoculated plants resulted to be positive to TSWV: 1/10, 3/12, 5/12, and 3/12 for the substrate A0, A10, B2.10, and C2.10, respectively. Severe symptoms, such as stunting of plants, leaf malformation, and necrosis, were observed in the infected plants grown on A0 and C2 substrates, whereas some infected plants grown on biochar substrates were not severely affected by infection and showed good foliage conditions (1/3 and 2/5 plants of A.10 and B2.10, respectively) (**Figure 8**-S2 and M2).

DISCUSSION

The use of biochar as soil amendment can potentially influence the interactions between plant and beneficial microbes, and has a positive impact on the response to pathogen diseases. On the one hand, the enrichment of aromatic molecules originating during biomass pyrolysis makes biochar an organic material capable of stimulating plant growth. On the other hand, the porous

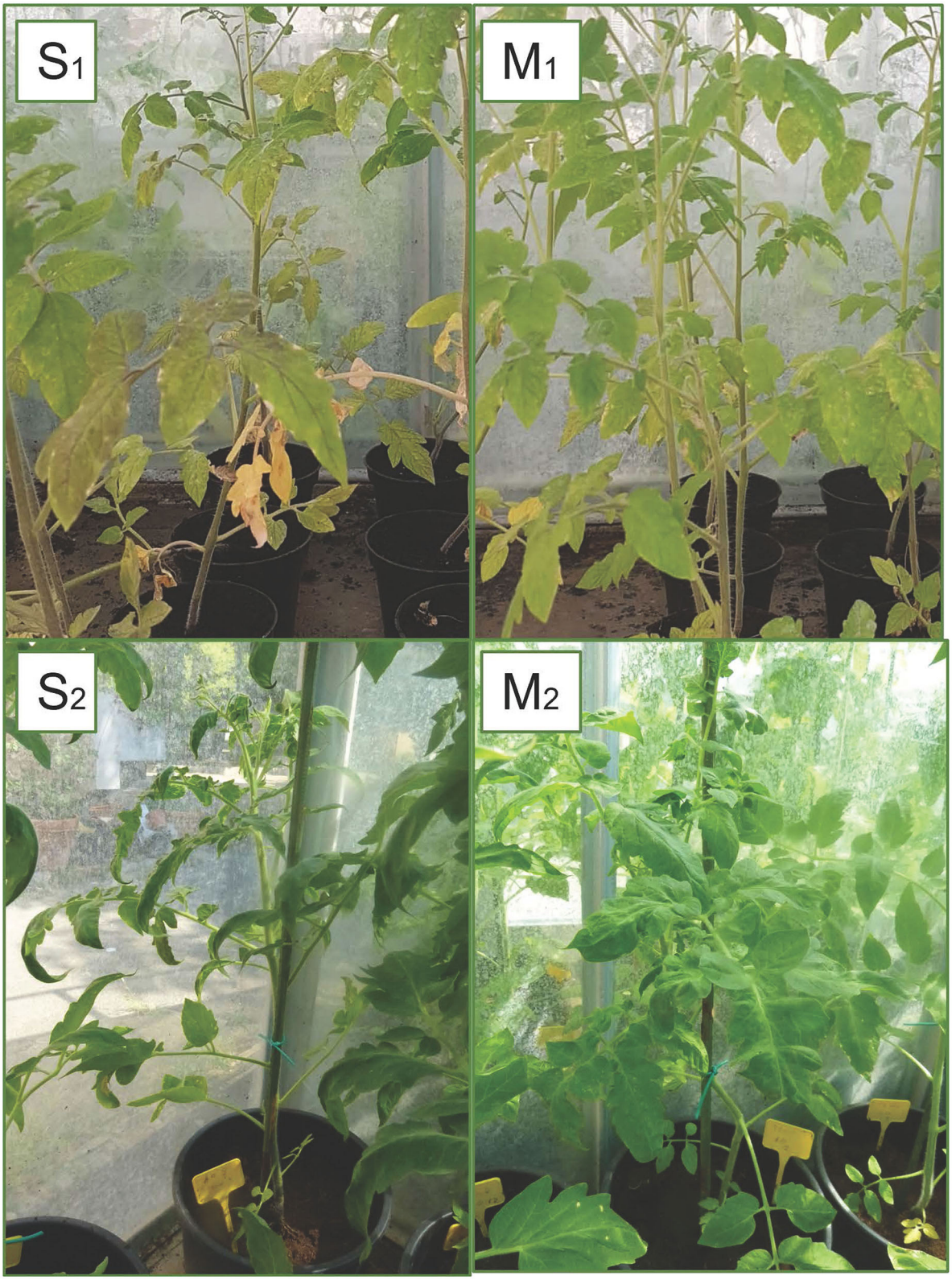

FIGURE 8 | Symptoms of TSWV observed in plants grown on different substrates: severe symptoms with typical necrotic spots and bronzing of leaves **(S1)** and reduction in the plants growth **(S2)** in A0 (only peat); mild symptoms with chlorotic spots or chlorotic leaves **(M1)** and middle symptoms **(M2)** observed in substrates with biochar (A10 and B2.10) (with peat, biochar, and *Trichoderma* spp.).

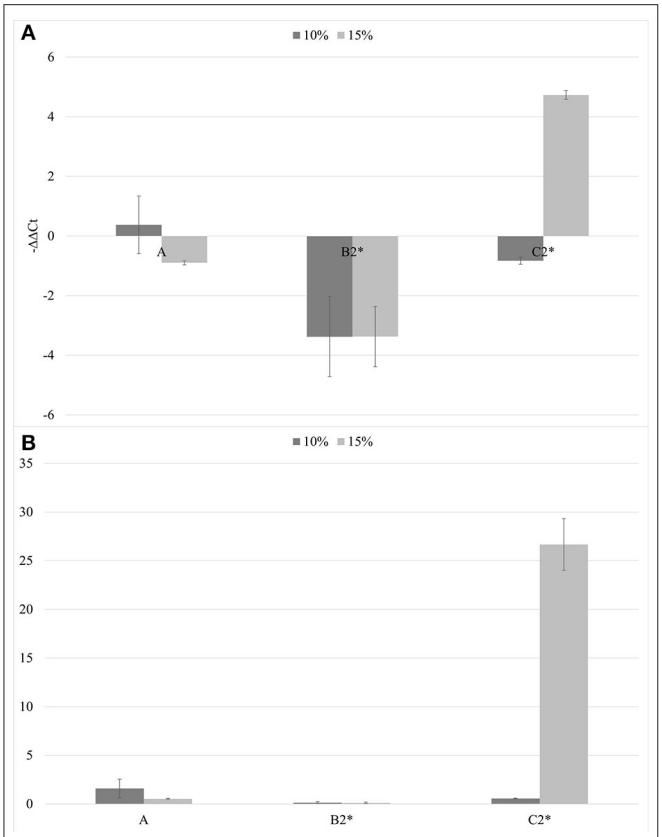

FIGURE 9 | The $-\Delta\Delta$Ct results **(A)** and fold change in TSWV replication ($2^{-\Delta\Delta Ct}$) **(B)** mean values obtained for all the theses (10% in gray and 15% in light gray). *$p < 0.05$.

structure can physically sustain soil microbe colonies in sites that are not reachable by grazers or predators, making biochar a potential carrier for a variety of beneficial microorganisms (Bonanomi et al., 2018).

Positive effects on both plants and soil microbes were observed also with the biochar used in this study. This product was obtained from olive pruning and has all the characteristics to be used as soil amendment, namely, basic pH and low presence of heavy metals and polycyclic aromatic hydrocarbons. The experiments carried out on tomato seedlings confirmed that this biochar is suitable to promote the root growth to the concentration of 20%. Moreover, no antimicrobial effects were observed at the tomato rhizosphere level on the beneficial soil bacteria, whose growth seemed to be even improved. Similarly, biochar did not show any negative effect on PGPMs either on bacteria (*Bacillus* spp.) or fungi (*Trichoderma* spp.), and it promotes the survival of these microorganisms for a long time after the colonization.

The potential role of biochar in enhancing the plant response was tested on tomato plants infected by systemic pathogen agents. The disease suppression activity is already known for soilborne pathogens, mainly fungi, whereas a few studies have been carried out on plants infected by airborne pathogens, and very limited information is available on virus- and viroid-induced diseases (Bonanomi et al., 2020). The results obtained on PSTVd-infected tomatoes showed that the biochar effect is dose-dependent and depends on the presence of PGPMs. The addition of the sole biochar into the soil did not significantly affect the viroid titer and symptoms expression, and even contributed to increase the PSTVd titer at the lowest concentrations. This confirms that, with equal biomass composition and soil chemistry, certain concentrations of biochar can induce a U-shaped dose/response curve and accelerate the plant disease, as already observed for other pathosystems (Frenkel et al., 2017). When proper concentrations of PGPMs were added to biochar, a disease suppression activity was observed. Notably, the addition of *Bacillus* spp. to 15% biochar, as well as the addition of *Trichoderma* spp. to both 10 and 15% biochar, induced a significant reduction in the PSTVd titer in tomato. The presence of *Trichoderma* spp. in the biochar-added soil also contributed to the plant response to infection, inducing only mild or no PSTVd symptoms. Therefore, 10–15% biochar in combination with *Trichoderma* spp. potentially showed a positive activity addressed to the tomato-PSTVd pathosystem since this treatment can sensibly reduce the replication of PSTVd and the expression of symptoms even if it is not able to stop the start of infection.

The data obtained for TSWV were not linear, and the first and third experiments did not provide a significant number of infected plants in the mock treatment without biochar (A0), so the results obtained by comparing the other different substrate combinations could not be considered valid. This extreme variability is probably due to the lability of TSWV that, even if a fresh inoculum was prepared for each thesis within the same experiment, could have a different titer and infection capacity in different theses/trials. Despite only the second experiment being considered valid, according to the controls, the general aspect of the plants treated with biochar yield better results than the others, with an increasing growth rate, even when infected with TSWV. Therefore, biochar could have a role in preventing also the TSWV infection as it did not occur in PSTVd. The experiments suggest that the use of biochar, particularly in combination with *Trichoderma* spp., could induce plants to have a defense response to the virus by blocking or recovering the infection in the first step after inoculation. These positive effects against TSWV confirmed the results obtained by Bonanomi et al. (2020), who tested different organic amendments and showed that biochar combined with alfalfa or manure was among the most effective soil treatments to control the disease caused by this virus in tomato plants.

The beneficial effects of biochar and *Trichoderma* observed on PSTVd- and TSWV-infected tomato plants are consistent with previous studies performed in several stress conditions. It was observed that biochar favors the hyphal growth and elongation of *Trichoderma*, which in turn improves the root system architecture of the tomato plants and contributes to the increase in the foliar area and secondary roots (Chacón et al., 2007). This results in a better uptake of mineral nutrients and photosynthesis efficiency, as demonstrated by the increase in antioxidant contents and minerals in tomato shoots and fruits

as well as by the upregulation of various genes associated with photosynthesis observed after biochar-*Trichoderma* applications on tomato. These beneficial effects on tomato growth and nutrition are more evident when *Trichoderma* and biochar are supplied in combination in the soil rather than either alone. The synergistic action finally results in higher crop yield and fruit quality, as well as in a boosted defense response to several abiotic stresses, parasites, and pathogens, such as *Fusarium oxysporum* (Hasan et al., 2020; Sani et al., 2020 Arshad et al., 2021). Such a virtuous cycle was likely launched also in the PSTVd-infected tomato plants treated with 10–15% biochar and "Remedier," leading to a reduction of both symptom severity and viroid titer.

Similar beneficial effects on tomato were reported also when *Bacillus* spp. were added to biochar (Arshad et al., 2021; Rasool et al., 2021a). For example, the combination of biochar and *B. subtilis* was showed to stimulate not only the plant growth but also the response to the soil-inhabiting fungus *Alternaria solani*, as revealed by the overexpression of defense-associated genes, such as salicylic acid-related PR genes, and the significant reduction of the early blight symptoms (Rasool et al., 2021a,b). Such effect was not so evident in this study since only the addition of *Bacillus* spp. to 15% biochar was effective in reducing the titer but not the symptoms of PSTVd. This may be due to the composition of the soil that included the peat as the main substrate. The presence of peat could have contributed to acidify the pH of the soil and thus create a medium that is not optimal for the growth of *Bacillus* spp. (Gauvry et al., 2021).

This study provides evidence that biochar can promote the root growth and the general fitness of tomato plants and contribute to prime the defense response against systemic pathogens, such as PSTVd and TSWV. The most significant effects on both virus/viroid symptoms and titer were observed when biochar was combined with PGPMs, especially *Trichoderma* spp. This confirms that biochar is an efficient carrier of beneficial microorganisms by playing a protective role and providing nutrients for microbe growth. These promising results have to be confirmed with further experiments, particularly using a more stable and easily transmissible virus as the emerging tomato brown rugose virus (Salem et al., 2016; Luria et al., 2017). The pathogenetic mechanisms that regulate the responses of plants to systemic pathogens in the presence of biochar need to be further elucidated as well. Anyway, the overall results encourage us to develop novel biocontrol products based on the synergistic combination of biochar and PGPMs. A regular supplement of biochar and *Trichoderma* in the soil can likely contribute to the sustainable management of plant viral diseases for which no curative methods are available. As the biochar activity observed in this study resulted to be dose-dependent, different types of biochar with different biomass composition should be tested to identify the most suitable concentration for each crop-pathogen system. The use of biochar in sustainable agriculture is also strongly encouraged because of its involvement in carbon seizing and greenhouse gasses reduction to the point that it has been included in the CO_2-reducing techniques suggested in the G20 meeting of agricultural chief scientists in 2019 (Meeting of Agricultural Chief Scientists (MACS), 2019, Japan).

DATA AVAILABILITY STATEMENT

The raw data supporting the conclusions of this article will be made available by the authors, without undue reservation.

AUTHOR CONTRIBUTIONS

MA, FF, and LT conceived and designed the research. MA and MC prepared all the substrates. ML, AM, and ID conducted experiments. ML, FF, AM, and LT wrote the manuscript. SB, AT, AG, SS, and LV revised the manuscript. All authors approved the publication and have read and agreed to the published version of the manuscript.

FUNDING

This research was done in the frame of the Viva-Biochar project funded by the Italian Ministry of Agricultural, Food and Forestry Policies (MIPAAF).

ACKNOWLEDGMENTS

The authors thank Marina Ciuffio and Massimo Turina of the Institute for Sustainable Plant Protection- National Research Council, Italy for providing the TSWV isolate.

SUPPLEMENTARY MATERIAL

The Supplementary Material for this article can be found online at: https://www.frontiersin.org/articles/10.3389/fmicb.2022.862075/full#supplementary-material

Supplementary Material | Linear regression of the Ct values obtained for the different dilution level. The equations of the obtained curves were reported.

REFERENCES

Ahmad, M., Wang, X., Hilger, T. H., Luqman, M., Nazli, F., Hussain, A., et al. (2020). Evaluating biochar-microbe synergies for improved growth, yield of maize, and post-harvest soil characteristics in a semi-arid climate. *Agronomy* 10, 1055. doi: 10.3390/AGRONOMY10071055

Alves Silva, H. S., Da Silva Romeiro, R., and Mounteer, A. (2003). Development of a root colonization bioassay for rapid screening of rhizobacteria for potential biocontrol agents. *J. Phytopathol.* 151, 42–46. doi: 10.1046/j.1439-0434.2003.00678.x

Bonanomi, G., Alioto, D., Minutolo, M., Marra, R., Cesarano, G., and Vinale, F. (2020). Organic amendments modulate soil microbiota and reduce virus disease incidence in the tswvtomato pathosystem. *Pathogens* 9, 379. doi: 10.3390/pathogens9050379

Bonanomi, G., Ippolito, F., and Scala, F. (2015). A "black" future for plant pathology? Biochar as a new soil amendment for controlling plant diseases. *J. Plant Pathol.* 97, 223–234. doi: 10.4454/jpp.v97i2.3381

Bonanomi, G., Lorito, M., Vinale, F., and Woo, S. L. (2018). Organic amendments, beneficial microbes, and soil microbiota: toward a unified

framework for disease suppression. *Annu. Rev. Phytopathol.* 56, 1–20. doi: 10.1146/annurev-phyto-080615-100046

Boonham, N., González Pérez, L., Mendez, M. S., Lilia Peralta, E., Blockley, A., Walsh, K., et al. (2004). Development of a real-time RT-PCR assay for the detection of Potato spindle tuber viroid. *J. Virol. Methods* 116, 139–146. doi: 10.1016/j.jviromet.2003.11.005

Bronick, C. J., and Lal, R. (2005). Soil structure and management: a review. *Geoderma* 124, 3–22. doi: 10.1016/j.geoderma.2004.03.005

Chacón, M. R., Rodríguez-Galín, O., Benítez, T., Sousa, S., Rey, M., Llobell, A., et al. (2007). Microscopic and transcriptome analyses of early colonization of tomato roots by Trichoderma harzianum. *Int. Microbiol.* 10, 19–27. doi: 10.2436/20.1501.01.4

Chan, K. Y., Dorahy, C., and Tyler, S. (2007). Determining the agronomic value of composts produced from garden organics from metropolitan areas of New South Wales, Australia. *Aust. J. Exp. Agric.* 47, 1377–1382. doi: 10.1071/EA06128

Chan, K. Y., Van Zwieten, L., Meszaros, I., Downie, A., and Joseph, S. (2008). Using poultry litter biochars as soil amendments. *Aust. J. Soil Res.* 46, 437–444. doi: 10.1071/SR08036

Cornelissen, G., Martinsen, V., Shitumbanuma, V., Alling, V., Breedveld, G. D., Rutherford, D. W., et al. (2013). Biochar effect on maize yield and soil characteristics in five conservation farming sites in Zambia. *Agronomy* 3, 256–274. doi: 10.3390/agronomy3020256

De Tender, C., Haegeman, A., Vandecasteele, B., Clement, L., Cremelie, P., Dawyndt, P., et al. (2016). Dynamics in the strawberry rhizosphere microbiome in response to biochar and Botrytis cinerea leaf infection. *Front. Microbiol.* 7, 2062. doi: 10.3389/fmicb.2016.02062

Di Serio, F., Flores, R., Verhoeven, J. T. J., Li, S. F., Pallás, V., Randles, J. W., et al. (2014). Current status of viroid taxonomy. *Arch. Virol.* 159, 3467–3478. doi: 10.1007/s00705-014-2200-6

Dimkić, I., Janakiev, T., Petrović, M., Degrassi, G., and Fira, D. (2022). Plant-associated Bacillus and Pseudomonas antimicrobial activities in plant disease suppression via biological control mechanisms - A review. *Physiol. Mole. Plant Pathol.* 117, 101754. doi: 10.1016/J.PMPP.2021.101754

EBC (2012–2022). 'European Biochar Certificate - Guidelines for a Sustainable Production of Biochar.' European Biochar Foundation (EBC), Arbaz, Switzerland. (http://european-biochar.org). Version 10.1 from 10th Jan 2022. Last website visit 21/03/2022

Elad, Y., Cytryn, E., Meller Harel, Y., Lew, B., and Graber, E. R. (2011). The biochar effect: plant resistance to biotic stresses. *Phytopathol. Mediterr.* 50, 335–349. doi: 10.14601/Phytopathol_Mediterr-9807

EPPO (2022). *A2 List of Pests Recommended for Regulation as Quarantine Pests-Version 2021-09*. Available online at: https://www.eppo.int/ACTIVITIES/plant_quarantine/A2_list (accessed March 21, 2022).

European Commission Directorate-General for Health and Food Safety (2019). Commission Implementing Regulation (EU) 2019/2072. *Official J. Eur. Union* L 319/1. Available online at: https://eur-lex.europa.eu/legal-content/EN/TXT/?uri=CELEX:32019R2072 (accessed March 21, 2022).

Frenkel, O., Jaiswal, A. K., Elad, Y., Lew, B., Kammann, C., and Graber, E. R. (2017). The effect of biochar on plant diseases: what should we learn while designing biochar substrates? *J. Environ. Eng. Landsc. Manage.* 25, 105–113. doi: 10.3846/16486897.2017.1307202

Gauvry, E., Mathot, A. G., Couvert, O., Leguérinel, I., and Coroller, L. (2021). Effects of temperature, pH and water activity on the growth and the sporulation abilities of Bacillus subtilis BSB1. *Int. J. Food Microbiol.* 337, 108915. doi: 10.1016/j.ijfoodmicro.2020.108915

Graber, E. R., Harel, Y. M., Kolton, M., Cytryn, E., Silber, A., David, D. R., et al. (2010). Biochar impact on development and productivity of pepper and tomato grown in fertigated soilless media. *Plant Soil* 337, 481–496. doi: 10.1007/s11104-010-0544-6

Haider, F. U., Coulter, J. A., Cheema, S. A., Farooq, M., Wu, J., Zhang, R., et al. (2021). Co-application of biochar and microorganisms improves soybean performance and remediate cadmium-contaminated soil. *Ecotoxicol. Environ. Safety* 214, 112112. doi: 10.1016/J.ECOENV.2021.112112

Haider, G., Steffens, D., Müller, C., and Kammann, C. I. (2016). Standard extraction methods may underestimate nitrate stocks captured by field-aged biochar. *J. Environ. Qual.* 45, 1196–1204. doi: 10.2134/jeq2015.10.0529

Harel, Y. M., Elad, Y., Rav-David, D., Borenstein, M., Shulchani, R., Lew, B., et al. (2012). Biochar mediates systemic response of strawberry to foliar fungal pathogens. *Plant Soil* 357, 245–257. doi: 10.1007/s11104-012-1129-3

Jaiswal, A. K., Elad, Y., Graber, E. R., and Frenkel, O. (2014). Rhizoctonia solani suppression and plant growth promotion in cucumber as affected by biochar pyrolysis temperature, feedstock and concentration. *Soil Biol. Biochem.* 69, 110–118. doi: 10.1016/j.soilbio.2013.10.051

Jaiswal, A. K., Frenkel, O., Elad, Y., Lew, B., and Graber, E. R. (2015). Non-monotonic influence of biochar dose on bean seedling growth and susceptibility to Rhizoctonia solani: the "Shifted Rmax-Effect." *Plant Soil* 395, 125–140. doi: 10.1007/s11104-014-2331-2

Jeffery, S., Verheijen, F. G. A., van der Velde, M., and Bastos, A. C. (2011). A quantitative review of the effects of biochar application to soils on crop productivity using meta-analysis. *Agric. Ecosyst. Environ.* 144, 175–187. doi: 10.1016/j.agee.2011.08.015

Juriga, M., and Šimanský, V. (2018). Effect of biochar on soil structure - review. *Acta fytotechnica et zootechnica* 21, 11–19. doi: 10.15414/afz.2018.21.01.11-19

Kammann, C. I., Schmidt, H.-P., Messerschmidt, N., Linsel, S., Steffens, D., Müller, C., et al. (2015). Plant growth improvement mediated by nitrate capture in co-composted biochar. *Sci. Rep.* 5, 12378. doi: 10.1038/srep12378

Laird, D. A., Brown, R. C., Amonette, J. E., and Lehmann, J. (2009). Review of the pyrolysis platform for coproducing bio-oil and biochar. *Biofuels Bioproducts Biorefining* 3, 547–562. doi: 10.1002/bbb.169

Livak, K. J., and Schmittgen, T. D. (2001). Analysis of relative gene expression data using real-time quantitative PCR and the 2-△△CT method. *Methods* 25, 402–408. doi: 10.1006/meth.2001.1262

Lorenz, K., and Lal, R. (2018). *Carbon Sequestration in Agricultural Ecosystems*. doi: 10.1007/978-3-319-92318-5

Luria, N., Smith, E., Reingold, V., Bekelman, I., Lapidot, M., Levin, I., et al. (2017). A new israeli Tobamovirus isolate infects tomato plants harboring Tm-22 resistance genes. *PLoS ONE* 12, e0170429. doi: 10.1371/journal.pone.0170429

Meeting of Agricultural Chief Scientists (MACS) (2019). *Communiqué. 8th Meeting of Agricultural Chief Scientists (MACS), G20 Japan*. Available online at: https://www.macs-g20.org/ (accessed March 21, 2022).

Montgomery, D. C. (2012). *Design and Analysis of Experiments Eighth Edition*.

Owens, R. A., and Verhoeven, J., Th, J. (2017). "Potato spindle tuber viroid," in *Viroids and Satellites*, eds A. Hadidi, R. Flores, J. W. Randles, and P. Palukaitis (Boston, MA: Academic Press), 149–158. doi: 10.1016/B978-0-12-801498-1.00014-0

Pietikäinen, J., Kiikkilä, O., and Fritze, H. (2000). Charcoal as a habitat for microbes and its effect on the microbial community of the underlying humus. *Oikos* 89, 231–242. doi: 10.1034/j.1600-0706.2000.890203.x

Poveda, J., and González-Andrés, F. (2021). Bacillus as a source of phytohormones for use in agriculture. *Appl. Microbiol. Biotechnol.* 105, 8629–8645. doi: 10.1007/s00253-021-11492-8

Rajkovich, S., Enders, A., Hanley, K., Hyland, C., Zimmerman, A. R., and Lehmann, J. (2012). Corn growth and nitrogen nutrition after additions of biochars with varying properties to a temperate soil. *Biol. Fertil. Soils* 48, 271–284. doi: 10.1007/s00374-011-0624-7

Rasool, M., Akhter, A., and Haider, M. S. (2021a). Molecular and biochemical insight into biochar and Bacillus subtilis induced defense in tomatoes against Alternaria solani. *Scientia Horticulturae* 285, 110203. doi: 10.1016/j.scienta.2021.110203

Rasool, M., Akhter, A., Soja, G., and Haider, M. S. (2021b). Role of biochar, compost and plant growth promoting rhizobacteria in the management of tomato early blight disease. *Sci. Rep.* 11, 6092. doi: 10.1038/s41598-021-85633-4

Ribera, J., Gandía, M., Marcos, J. F., Bas, M. D. C., Fink, S., and Schwarze, F. W. M. R. (2017). Effect of Trichoderma-enriched organic charcoal in the integrated wood protection strategy. *PLoS ONE* 12, e0183004. doi: 10.1371/journal.pone.0183004

Salem, N., Mansour, A., Ciuffo, M., Falk, B. W., and Turina, M. (2016). A new tobamovirus infecting tomato crops in Jordan. *Arch. Virol.* 161, 503–506. doi: 10.1007/s00705-015-2677-7

Sani, M. N. H., Hasan, M., Uddain, J., and Subramaniam, S. (2020). Impact of application of Trichoderma and biochar on growth, productivity and nutritional quality of tomato under reduced N-P-K fertilization. *Ann Agri Sci.* 65, 107–115. doi: 10.1016/j.aoas.2020.06.003

Shackley, S., Ruysschaert, G., Zwart, K., and Glaser, B. (2016). *Biochar in European soils and Agriculture: Science and Practice*. doi: 10.4324/9781315884462

Stevens, M. R., Scott, S. J., and Gergerich, R. C. (1991). Inheritance of a gene for resistance to tomato spotted wilt virus (TSWV) from Lycopersicon peruvianum Mill. *Euphytica* 59, 9–17. doi: 10.1007/BF00025356

Vicente, I., Baroncelli, R., Hermosa, R., Monte, E., Vannacci, G., and Sarrocco, S. (2022). Role and genetic basis of specialised secondary metabolites in Trichoderma ecophysiology. *Fung. Biol. Rev.* 39, 83–99. doi: 10.1016/J.FBR.2021.12.004

Wardle, D. A., Zackrisson, O., and Nilsson, M. C. (1998). The charcoal effect in Boreal forests: mechanisms and ecological consequences. *Oecologia* 115, 419–426. doi: 10.1007/s004420050536

Weller, S. A., Elphinstone, J. G., Smith, N. C., Boonham, N., and Stead, D. E. (2000). Detection of *Ralstonia solanacearum* strains with a quantitative, multiplex, real-time, fluorogenic PCR (TaqMan) assay. *Appl. Environ. Microbiol.* 66, 2853–2858. doi: 10.1128/AEM.66.7.2853-2858.2000

Yamato, M., Okimori, Y., Wibowo, I. F., Anshori, S., and Ogawa, M. (2006). Effects of the application of charred bark of Acacia mangium on the yield of maize, cowpea and peanut, and soil chemical properties in South Sumatra, Indonesia. *Soil Sci. Plant Nutr.* 52, 489–495. doi: 10.1111/j.1747-0765.2006.00065.x

Zambon, I., Colosimo, F., Monarca, D., Cecchini, M., Gallucci, F., Proto, A. R., et al. (2016). An innovative agro-forestry supply chain for residual biomass: physicochemical characterisation of biochar from olive and hazelnut pellets. *Energies* 9, 526. doi: 10.3390/en9070526

Conflict of Interest: The authors declare that the research was conducted in the absence of any commercial or financial relationships that could be construed as a potential conflict of interest.

Publisher's Note: All claims expressed in this article are solely those of the authors and do not necessarily represent those of their affiliated organizations, or those of the publisher, the editors and the reviewers. Any product that may be evaluated in this article, or claim that may be made by its manufacturer, is not guaranteed or endorsed by the publisher.

frontiers | Frontiers in Microbiology

ORIGINAL RESEARCH
published: 11 May 2022
doi: 10.3389/fmicb.2022.883921

Systematic Comparison of Nanopore and Illumina Sequencing for the Detection of Plant Viruses and Viroids Using Total RNA Sequencing Approach

Anja Pecman[1,2], Ian Adams[3], Ion Gutiérrez-Aguirre[1], Adrian Fox[3], Neil Boonham[4], Maja Ravnikar[1] and Denis Kutnjak[1]**

[1] Department of Biotechnology and System Biology, National Institute of Biology, Ljubljana, Slovenia, [2] Jožef Stefan International Postgraduate School, Ljubljana, Slovenia, [3] Fera Science Ltd., York, United Kingdom, [4] Institute for Agri-Food Research and Innovation, Newcastle University, Newcastle upon Tyne, United Kingdom

OPEN ACCESS

Edited by:
Elvira Fiallo-Olivé,
La Mayora Experimental Station (CSIC), Spain

Reviewed by:
Pasquale Saldarelli,
National Research Council (CNR), Italy
Miguel A. Aranda,
Spanish National Research Council (CSIC), Spain

***Correspondence:**
Anja Pecman
anja.pecman@nib.si
Denis Kutnjak
denis.kutnjak@nib.si

Specialty section:
This article was submitted to Microbe and Virus Interactions with Plants, a section of the journal Frontiers in Microbiology

Received: 25 February 2022
Accepted: 31 March 2022
Published: 11 May 2022

Citation:
Pecman A, Adams I, Gutiérrez-Aguirre I, Fox A, Boonham N, Ravnikar M and Kutnjak D (2022) Systematic Comparison of Nanopore and Illumina Sequencing for the Detection of Plant Viruses and Viroids Using Total RNA Sequencing Approach. Front. Microbiol. 13:883921. doi: 10.3389/fmicb.2022.883921

High-throughput sequencing (HTS) has become an important tool for plant virus detection and discovery. Nanopore sequencing has been rapidly developing in the recent years and offers new possibilities for fast diagnostic applications of HTS. With this in mind, a study was completed, comparing the most established HTS platform (MiSeq benchtop sequencer—Illumina), with the MinION sequencer (Oxford Nanopore Technologies) for the detection of plant viruses and viroids. Method comparisons were performed on five selected samples, containing two viroids, which were sequenced using nanopore technology for the first time and 11 plant viruses with different genome organizations. For all samples, sequencing libraries for the MiSeq were prepared from ribosomal RNA-depleted total RNA (rRNA-depleted totRNA) and for MinION sequencing, direct RNA sequencing of totRNA was used. Moreover, for one of the samples, which contained five different plant viruses and a viroid, three additional variations of sample preparation for MinION sequencing were also used: direct RNA sequencing of rRNA-depleted totRNA, cDNA-PCR sequencing of totRNA, and cDNA-PCR sequencing of rRNA-depleted totRNA. Whilst direct RNA sequencing of total RNA was the quickest of the tested approaches, it was also the least sensitive: using this approach, we failed to detect only one virus that was present in a sample at an extremely low titer. All other MinION sequencing approaches showed improved performance with outcomes similar to Illumina sequencing, with cDNA-PCR sequencing of rRNA-depleted totRNA showing the best performance amongst tested nanopore MinION sequencing approaches. Moreover, when enough sequencing data were generated, high-quality consensus viral genome sequences could be reconstructed from MinION sequencing data, with high identity to the ones generated from Illumina data. The results of this study implicate that, when an appropriate sample and library preparation are selected, nanopore MinION sequencing could be used for the detection of plant viruses and viroids

with similar performance as Illumina sequencing. Taken as a balance of practicality and performance, this suggests that MinION sequencing may be an ideal tool for fast and affordable virus diagnostics.

Keywords: high-throughput sequencing, plant virus/viroid detection, comparison, nanopore MinION sequencing, Illumina MiSeq sequencing

INTRODUCTION

Globalization of agriculture and international trade facilitate the spread of plant viruses and viroids to new geographic regions with unexpected consequences for food production and natural ecosystems (Jones and Naidu, 2019). To decrease the negative impact of viral diseases on crop production and food safety, rapid and generic plant virus or viroid detection technologies (potentially applicable onsite) are needed. Since the first use of high-throughput sequencing (HTS) for generic detection of plant viruses (Adams et al., 2009; Al Rwahnih et al., 2009; Donaire et al., 2009; Kreuze et al., 2009), a range of HTS platforms were developed and became commonly used for plant virus or viroid detection and discovery. The low error rate and relatively "high throughput" of different instruments of the most widely used platforms, such as Illumina, offer many possibilities for plant virus research (Villamor et al., 2019). However, such "high throughput" may not always be necessary, e.g., when analyzing the single or small number of samples in routine diagnostic laboratories, it increases costs. Often, such samples are outsourced to commercial service providers; however, this increases the turnaround time from a couple of days to several weeks and limits the possibilities for quality control of the full process, which might be crucial in some situations. On the other hand, nanopore sequencing implemented by Oxford Nanopore Technologies offers scalable solutions from small flow cells (up to 2.8 Gb of data per run) accessed using a Flongle adapter, through to the MinION flow cells (up to 50 Gb per run) used here to parallel platforms such as the GridION (up to 250 Gb per run) and PromethION (up to 14 Tb per run). MinION sequencing has the potential benefit that the data can be analyzed in real time (Branton and Deamer, 2019). Compared to the established Illumina sequencing, nanopore sequencing enables long-read sequencing (Van Dijk et al., 2018), which can be an advantage for some applications. However, depending on the specific flow cell used, the error rate can reach up to 15% (Ip et al., 2015; Van Dijk et al., 2018), which can limit the potential applications.

One of the first large-scale applications of the MinION sequencer in virology was for real-time genomic surveillance in the Ebola epidemic in West Africa (Quick et al., 2016). The use of MinION for virus detection and investigation is steadily increasing. In human virology and animal virology, MinION has been used to detect dengue (Yamagishi et al., 2017), Zika (Quick et al., 2017) chikungunya, hepatitis C (Greninger et al., 2015), and porcine reproductive and respiratory syndrome virus (Tan et al., 2019) and is at the moment globally utilized for SARS-CoV-2 genomic surveillance (Meredith et al., 2020).

In plant pathology, MinION has been successfully used for the detection of bacteria, fungi, and viruses using RNA or DNA sequencing (Chalupowicz et al., 2019), plum pox virus and *Candidatus* liberibacter asiaticus in plant tissue and insect samples (Bronzato et al., 2018), and viruses in wheat (Fellers et al., 2019) and cassava (Boykin et al., 2019). In several studies (Filloux et al., 2018; Beddoe et al., 2020; Vazquez-Iglesias et al., 2022), both, MinION sequencing and Illumina sequencing, were used for virus detection; however, systematic comparison between established Illumina sequencing and nanopore sequencing for the detection of a wide array of viruses with different genome types is still lacking.

A previous study, comparing the sequencing of small (s)RNA and total (tot)RNA sequencing using the Illumina platform (Pecman et al., 2017), demonstrated that both approaches can be used for the detection of most of the plant viruses and viroids in a sample, and that totRNA sequencing was a better choice for sequencing novel viruses at low titres. In this report, the focus is on testing the performance of the MinION sequencer for a rapid detection of a wide array of plant viruses or viroids using totRNA sequencing. First, a systematic comparison was made of the fastest or simplest approach for this platform involving direct RNA sequencing of total RNA with an established approach based on sequencing ribosomal RNA-depleted total RNA (rRNA-depleted totRNA) using the MiSeq platform (Illumina). Using the methodology described previously (Pecman et al., 2017) several well-characterized samples containing a broad range of plant viruses and viroids with different genome organizations were included in the comparison.

The main advantage of the direct RNA sequencing approach is a simple and fast library preparation protocol (SQK-RNA002) resulting in long reads without PCR bias (Garalde et al., 2018), but unfortunately, a large amount (500 ng) of RNA is required as the input and the error rate is still relatively high (Wongsurawat et al., 2019). Thus, second, a study was completed using one of the samples, which contained five different plant viruses (including one viral species with two different strains) and one viroid which was analyzed using three other approaches: direct RNA sequencing of rRNA-depleted total RNA, cDNA-PCR sequencing of total RNA, and cDNA-PCR sequencing of rRNA-depleted total RNA.

The results obtained using different nanopore sequencing approaches and the Illumina sequencing were compared in terms of suitability for the detection of plant viruses, using complete datasets and rarefied subsets of data. Not all of the nanopore sequencing approaches performed equally well; however, the results demonstrate that some of them can be confidently used for generic detection of different genome types of plant viruses and viroids, since their performance was comparable to the established Illumina sequencing approach.

TABLE 1 | Samples included in the comparison with corresponding results from: HTS (+ virus/viroid detected using pipeline described in section Virus and Viroid Detection Workflow,–virus/viroid not detected using pipeline described in section Virus and Viroid Detection Workflow; NA, not applicable).

Sample number	Host	Virus/viroid present (Baltimore classification)	Initial detection with HTS sequencing using complete datasets					NCBI GenBank accession number	NCBI SRA accession number (MinION direct RNA sequencing of totRNA / MinION direct RNA sequencing of rRNA-depleted totRNA / MinION cDNA-PCR sequencing of totRNA / MinION cDNA-PCR sequencing of rRNA-depleted totRNA / Illumina rRNA-depleted totRNA sequencing)
			MinION direct RNA sequencing of totRNA	MinION direct RNA sequencing of rRNA-depleted totRNA	MinION cDNA-PCR sequencing of totRNA	MinION cDNA-PCR sequencing of rRNA-depleted totRNA	Illumina rRNA-depleted totRNA sequencing		
I	*Solanum lycopersicum*	TYLCV (ssDNA)	+	+	+	+	+	KY810789	SRR17660996/SRR17660995/ SRR17660994/SRR17660993/SRR17319908
		ToCV (ssRNA+)	+	+	+	+	+	KY810786, KY810787	
		PepMV (ssRNA+)	+	+	+	+	+	KF718832.1 (Pep-MV-EU), JX866666.1 (PepMV-CH)	
		ToMV (ssRNA+)	-	+	+	+	+	KY810788	
		STV (dsRNA)	+	+	+	+	+	KY810783	
		CLVd (viroid)	+	+	+	+	+	KY810771	
II	*Brassica oleracea*	CaMV (dsDNA-RT)	+	NA	NA	NA	+	KY810770	SRR17660992/NA/NA/NA/SRR17319907
		CCyV1 (ssRNA-)	+	NA	NA	NA	+	KY810772	
III	*Nicotiana tabaccum*	TSWV (ssRNA-)	+	NA	NA	NA	+	OM112200, OM112201, OM112202	SRR17660991/NA/NA/NA/SRR17319906
IV	*Solanum lycopersicum*	TASVd (viroid)	+	NA	NA	NA	+	KY810784	SRR17660990/NA/NA/NA/SRR17319905
V	*Phaseolus vulgaris*	PVeV1 (dsRNA)	+	NA	NA	NA	+	/	SRR17660989/NA/NA/NA/SRR17319904
		PVeV2 (dsRNA)	+	NA	NA	NA	+	OM112199	
		PVeV3 (dsRNA)	+	NA	NA	NA	+	/	

Virus/viroid names: tomato yellow leaf curl virus (TYLCV, Begomovirus, Geminiviridae), tomato chlorosis virus (ToCV, Crinivirus, Closteroviridae), pepino mosaic virus (PepMV, Potexvirus, Alphaflexiviridae), tomato mosaic virus (ToMV, Tobamovirus, Virgaviridae), southern tomato virus (STV, Amalgavirus, Amalgaviridae), columnea latent viroid (CLVd, Pospiviroid, Pospiviroidae), cauliflower mosaic virus (CaMV, Caulimovirus, Caulimoviridae), cabbage cytorhabdovirus 1 (CCvY1, Cytorhabdovirus, Rhabdoviridae), tomato spotted wilt orthotospovirus (TSWV, Orthotospovirus, Tospoviridae), tomato apical stunt viroid (TASVd, Pospiviroid, Pospiviroidae), and phaseolus vulgaris alphaendornavirus 1, 2, 3 (PVeV1, 2, 3, Alphaendornavirus, Endornaviridae).

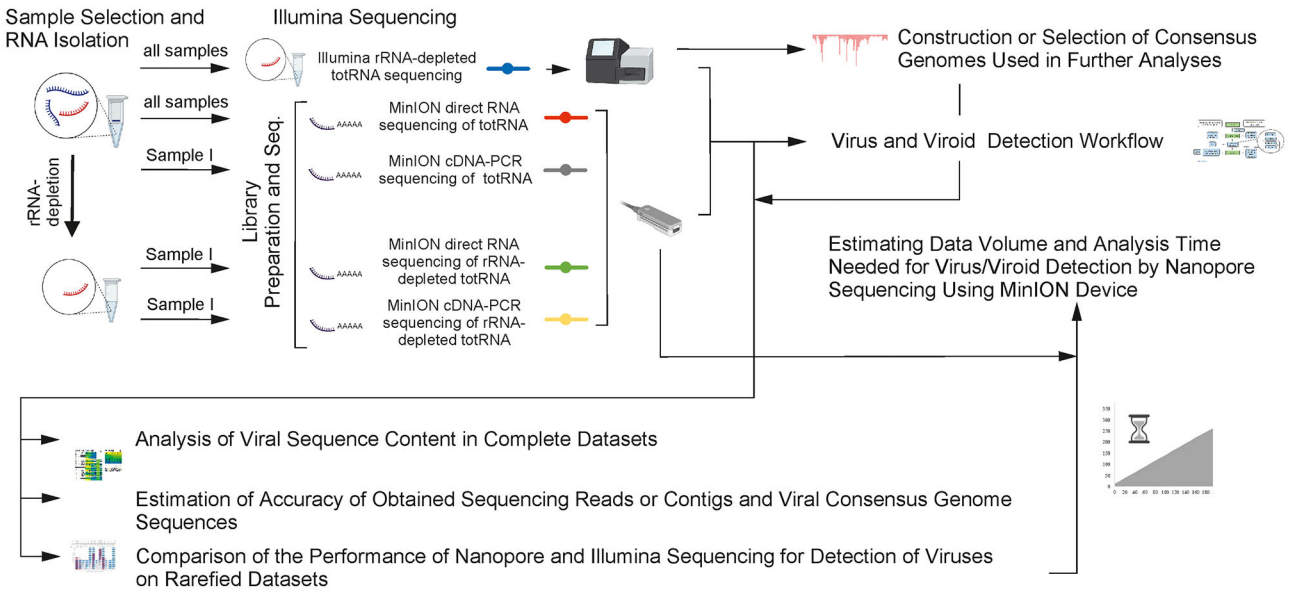

FIGURE 1 | An overview of the conducted study. Listed titles of chapter material and methods are connected with arrows according to the course of work (part of the figure was created with BioRender.com).

MATERIALS AND METHODS

Sample Selection and RNA Isolation

To perform an extensive comparison of the methods on a wide array of plant viruses with different genome types, five plant samples were selected, containing different viruses, most of which (samples I, II, and IV) have already been very well characterized for viruses using HTS and targeted detection methods (Pecman et al., 2017). Either infected plant leaf samples (samples I, II, III, and V) or an infected seed sample (sample IV) were used (**Table 1**; **Supplementary Tables S1**, **S2**). Additionally, leaves of healthy tobacco plants were used as a negative control. RNA was isolated (**Figure 1**) from all leaf samples using the RNeasy Plant Mini Kit (Qiagen) including a DNase step (RNase-Free DNase Set, Qiagen) according to the manufacturer's instructions. From the seed sample (sample IV), RNA was isolated using a combination of CTAB buffer and RNeasy Plant Mini Kit (Qiagen) as described in the study of Adams et al. (2009) with minor modification: incubation with 4 M LiCl was done at 4°C overnight.

A part of the RNA extracted from sample I was further processed: ribosomal RNA was depleted from the extract using the RiboMinusTM Plant Kit for RNA-seq (Invitrogen# A1083808), obtaining two versions of sample I: with and without ribosomal RNA depletion (**Figure 1**, for more details refer to **Supplementary Tables S1, S2**).

Library Preparation and Sequencing

The direct RNA sequencing kit (SQK-RNA002) and cDNA-PCR sequencing kit (SQK-PCS108) required polyA+ RNA as input RNA. Therefore, for each sample, polyA tailing of RNA was performed using E. coli poly(A) polymerase (NEB# M0276). The mixture was incubated at 37°C for 15 min. The reaction was stopped by directly proceeding to the clean-up step with Agencourt® AMPure® XP beads (Beckman Coulter) using 1.8 (AMPure® XP beads): 1 (poly(A) tailing mixture) ratio.

The direct RNA sequencing kit (SQK-RNA002, version DRS_9080_v2_revB_22Nov2018, Oxford Nanopore Technologies) was used to prepare sequencing libraries for all the samples included in the study. The cDNA-PCR sequencing kit (SQK-PCS108, version PCS_9035_v108_revH_26Jun2017, Oxford Nanopore Technologies) was additionally used to prepare libraries from sample I and sample I with ribosomal-depleted RNA.

For all but one library, the recommended amount of RNA input was used (Oxford Nanopore Technologies protocols); however, when preparing the library for direct RNA sequencing of rRNA-depleted totRNA (sample I), 278 ng of RNA, instead of 500 ng of RNA, was used (due to the lower extraction yield). Each library was then sequenced on a separate flow cell (R9.5.1) for 46–48 h using MinION device and MinKNOW software (v18.12.6). The reads were base-called using Guppy v3.1.5 and command: rna_r9.4.1_70bps_hac.cfg / dna_r9.4.1_bps450_hac.cfg –device auto –u_substitution false.

Illumina Sequencing

Sequencing libraries for each sample were prepared using total RNA and the ScriptSeq™ Complete Plant Leaf Kit (production discontinued, Illumina, USA) which included a ribosomal RNA depletion step. The libraries were sequenced on a MiSeq (Illumina, USA) using a 2x300-bp (V3) cartridge.

Virus and Viroid Detection Workflow

In the first part of the data analysis, the aim was to investigate how well different sequencing approaches compare in terms of virus detection from complete datasets (**Figure 1**). To achieve

this, established in-house virus detection workflows were used and virus presence was reported as follows.

Illumina reads were analyzed using a pipeline in CLC Genomic Workbench (v12, v21) and additional Diamond BLASTX analysis, as described below. Quality control was performed, then, adapters were removed from all reads, and additionally, reads were trimmed by quality (quality limit = 0.05) and length (all reads shorter than 30 nts were discarded). Trimmed reads were mapped to viral RefSeq (NCBI database, updated 19.05. 2019) and *de novo* assembled. Contigs (longer than 100 nts) were mapped to viral RefSeq (NCBI database, updated 19.05.2019) and unmapped contigs were further analyzed by searching for conserved protein domains using Pfam analysis (v32) (refer to **Supplementary Tables S3–S6** for details about the used parameters). Additionally, *de novo* assembled contigs were analyzed with Diamond BLASTX (v0.9.22) (Buchfink et al., 2015) against the NCBI nr database (June 2018). Diamond outputs were taxonomically classified and visualized using Megan 6.19.2 (Huson et al., 2007).

To analyse nanopore sequencing data, a similar pipeline was constructed using tools, which enable analysis of long reads. The statistics and quality of MinION reads were checked using the programs NanoQC v0.8.1, NanoStat v1.1.2, and NanoPlot v1.20.1 (De Coster et al., 2018). The read plots generated using the NanoQC v0.8.1 were inspected for each sample individually and were used to determine how to trim them (length of reads, head of reads, and tail of reads) (**Supplementary Table S1**) using program NanoFilt 2.5.0 (De Coster et al., 2018). The trimmed reads were again quality checked with NanoStat v1.1.2 and then mapped to the viral RefSeq (NCBI database, updated 19.05.2019) using minimap2 (v2.16-r922) and the commands: minimap2 -ax splice -uf -k14 for direct RNA reads and minimap2 -ax map-ont for cDNA-PCR reads. Reads were also analyzed using Diamond BLASTX (v0.9.22) (Buchfink et al., 2015) with the –frameshift 15–range-culling–sensitive command option. All reads were *de novo* assembled by combining different programs using a Pomoxis (https://github.com/nanoporetech/pomoxis) inspired approach: after fast mapping (minimap2) (Li, 2018) and *de novo* assembly (Miniasm) (Li, 2016), two rounds of the contig correction using racon (Vaser et al., 2017) were run. The script together with corresponding parameters is shown in **Supplementary Data 1**. The assembled contigs were analyzed using BLASTn against the NCBI nt database and visualized with Megan 6.19.2 (Huson et al., 2007). TASVd (sample V) was not detected by mapping direct RNA MinION reads to the viral RefSeq database, so in the next step, more closely related sequence from NCBI GenBank (KY810784) was used as the reference for reads and contig mapping.

Construction or Selection of Consensus Genomes Used in Further Analyses

To be able to perform comparisons of different sequencing approaches for different viruses or viroids, complete or near complete consensus genomic sequences of viruses in the samples were obtained. Since some of the samples were identical to the ones from a previous study (Pecman et al., 2017), these reference sequences were already available. For phaseolus vulgaris alphaendornavirus 2 (PVeV2, sample V) and tomato spotted wilt orthotospovirus TSWV (sample III), a reference consensus was generated based on the mapping of Illumina reads and contigs, as previously described (Pecman et al., 2017). For pepino mosaic virus (PepMV), two divergent strains (80% nucleotide identity) were detected in the sample I (PepMV-EU and PepMV-Ch2); thus, in this case, the complete genome sequences of KF718832.1 and JX866666.1 were used in subsequent comparisons as described previously (Pecman et al., 2017). For tomato yellow leaf curl virus (TYLCV) (KY810789), tomato chlorosis virus (ToCV) (KY810786), (KY810787), cauliflower mosaic virus (CaMV) (KY810770), and cabbage cytorhabdovirus 1 (CCyV1) (KY810772), the reference sequences described in the study of Pecman et al., (2017) were used in first step, but due to some mismatches after mapping Illumina reads and contigs to those reference sequences, few nucleotides were changed and "new" consensus genome sequences were used for the purpose of the following analysis only (**Supplementary Data 2**). In the case of sample V, only PVeV2 complete genome was covered by reads by both approaches, and thus, only this endornavirus was included in further analyses.

Analysis of Viral Sequence Content in Complete Datasets

To calculate the viral sequence content in the complete datasets, trimmed reads for each dataset were mapped to the corresponding reconstructed or selected viral or viroid reference sequences (Section Construction or Selection of Consensus Genomes Used in Further Analyses). For each sample–virus–sequencing type combination, three parameters were reported: the percentage of mapped reads, average depth (the number of times a nucleotide is covered by a sequencing read averaged across the complete reference genome sequence), and fraction of reference covered by reads.

Estimation of Accuracy of Obtained Sequencing Reads or Contigs and Viral Consensus Genome Sequences

The next step enabled the investigation of (I) average nanopore reads and contig identities (compared to the corresponding reference sequences) and (II) identities of consensus genome sequences generated after mapping the reads to the reference sequence, from now on named "consensus sequence identity". (I) To determine the average identities of nanopore sequencing reads (proxy of error rate), and the identities of *de novo* assembled contigs (generated from those reads), compared to reference sequences, reads and contigs were mapped to corresponding viral genome reference sequences. Identities were calculated using Minimap2 PAF output (Pairwise mApping Format) (Li, 2018). In this way, the average BLAST-like alignment identity was calculated for each mapping of nanopore sequencing data, either with reads or with contigs.

(II) If sequencing errors in nanopore reads are relatively random and if there is a substantial number of reads covering the reference genome sequence after mapping, the resulting

consensus sequence should be "error corrected". To test this, extracted consensus sequences (or their fragments–if whole genomes were not obtained) derived from mapping nanopore or Illumina reads to reference sequences were aligned with original reference sequences and pairwise identities were calculated using CLC Workbench Genomics v12, v21. For this analysis, consensus sequences (or their fragments if whole genomes were not obtained) were used if they had at least 1x average coverage in the read mapping step.

Comparison of the Performance of Nanopore and Illumina Sequencing for Detection of Viruses on Rarefied Datasets

To be able to compare the datasets obtained by different sequencing approaches, complete datasets were rarefied to obtain subsamples with comparable numbers of nucleotides. Depending on the original size (**Supplementary Tables S1, S2**), datasets from different sequencing approaches generated a different number of subsamples. The largest datasets, contained 1,500 million nucleotides, followed by 1,300, 1,100, 900, 700, 500, 300, 200, 100, 50, 30, and 10 millions of nucleotides (**Supplementary Table S7**). Each set of subsampled reads was randomly generated using CLC Genomic Workbench (v12, v21) for Illumina reads and Seqtk Sample for MinION reads. Subsampling was repeated five times for each of the subsample sizes for each sample.

The rarefied subsets were used for further comparative analysis of different sequencing approaches. The read subsamples were mapped to reconstructed or selected reference sequences. The reads were also *de novo* assembled and the resulting contigs were mapped to the selected reference sequences (for nanopore approaches as described above, for Illumina approach refer to **Supplementary Table S3–S5** for details about the used parameters). Finally, the fractions of reference sequences covered by reads or contigs for different subsamples were calculated and visualized as line or bar plots.

Longer reads or contigs mapping to small, circular genomes, could influence mapping efficiency (Visser et al., 2016). All mappings were performed to an artificially constructed viroid sequence, which was made by joining 10 repeated viroid genome sequences. Parameters for mapping contigs from Illumina rRNA-depleted totRNA dataset to viroids were adjusted (for samples I and IV). The length fraction parameter [CLC Genomic Workbench (v12, v21)] was set to 0.5 (50 %) instead of the 0.90 (90 %) used for viruses. Every mapping was individually inspected, and in cases where contigs were longer than the reference sequence, the fraction of reference covered by contig was reported as 100%.

In the case of sample I, in some subsamples, uneven coverage of the two different PepMV strain genome sequences was observed; thus, we performed additional analyses to test whether those observations are the consequence of the presence of two strains of the same virus present in the dataset. For each sequencing approach, one subsample (in which unequal contig coverage was observed for the two viral strains) was chosen (**Figure 4C**, see *). For each of those chosen subsamples, further analyses were implemented: (i) mapping original subsampled reads to the strain better covered by contigs in the original analysis, (ii) *de novo* assembly of the unmapped reads, and (iii) mapping newly assembled contigs to the corresponding reference genome sequence of the other present PepMV strain.

Estimating Data Volume and Analysis Time Needed for Virus/Viroid Detection by Nanopore Sequencing Using MinION Device

To obtain the proxy of the speed of virus or viroid detection and compare different employed MinION sequencing approaches, the sequencing time needed to obtain 50% of viral or viroid genome covered by generated reads was calculated. For this, a script (get_cumulative_yield_table.py, **Supplementary Data 3**) was used to calculate the cumulative yields of reads in gigabases for every 10 min of sequencing from MinION basecalling output files (summary.txt, refer to **Supplementary Table S8**). According to the rarefaction analysis from section Comparison of the Performance of Nanopore and Illumina Sequencing For Detection of Viruses on Rarefied Datasets (the number of nucleotides estimated to cover more than 50% of a reference viral genome) for each virus or sequencing type combination, the time point at which this was reached was calculated according to the cumulative yields of the reads during sequencing.

RESULTS

Nanopore Sequencing Using MinION Device Resulted in Comparable Detection of Plant Viruses/Viroids as Illumina Sequencing

Using the pipeline described above for detection of viral sequences, all viruses except one were detected in the samples employing the MinION direct RNA sequencing approach (**Table 1**). Using this approach, ToMV, which was present in sample I in an extremely low titer (**Figure 2**, **Figure 3A**), was not detected. TASVd (sample IV) was at first not detected by mapping reads to the viral RefSeq database; however, when using a more closely related sequence from NCBI GenBank (KY810784) as the reference, a few reads of this viroid were detected.

When using the three additional MinION sequencing approaches: direct RNA sequencing of rRNA-depleted totRNA, cDNA-PCR sequencing of totRNA, and cDNA-PCR sequencing of rRNA-depleted totRNA, all of the viruses or viroids present in the samples were detected (**Figure 2**).

Performance Comparison of MinION Direct RNA Sequencing and Illumina rRNA-Depleted totRNA Sequencing

The analysis of complete datasets showed that Illumina sequencing of rRNA-depleted totRNA resulted in a markedly higher relative fractions of viral reads compared to MinION direct RNA sequencing of totRNA (**Figure 3A**), which was

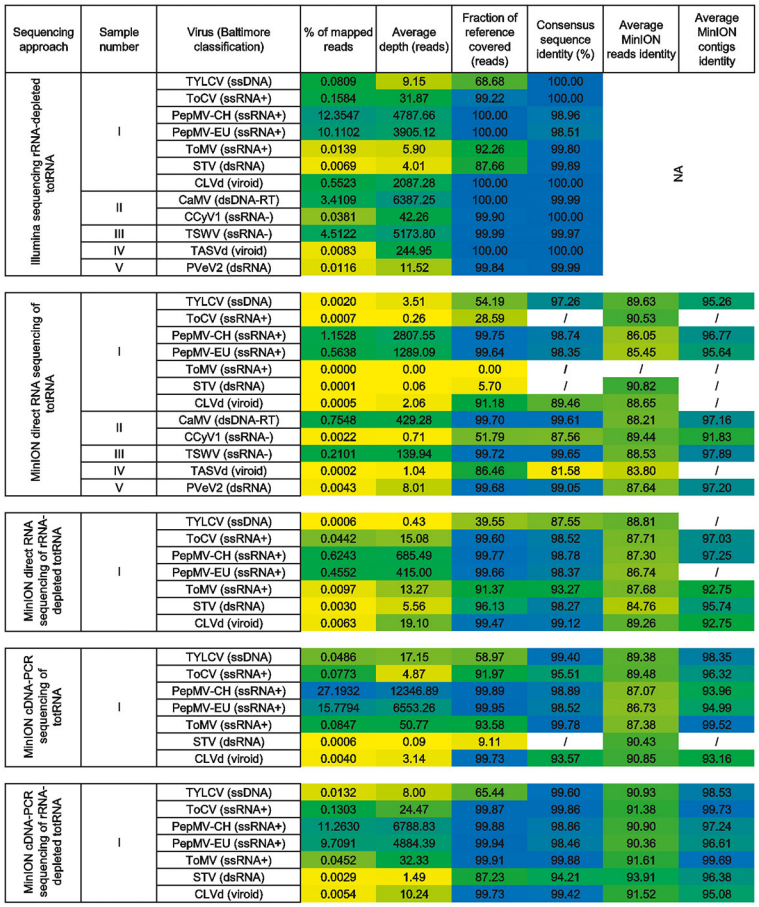

Sequencing approach	Sample number	Virus (Baltimore classification)	% of mapped reads	Average depth (reads)	Fraction of reference covered (reads)	Consensus sequence identity (%)	Average MinION reads identity	Average MinION contigs identity
Illumina sequencing rRNA-depleted totRNA	I	TYLCV (ssDNA)	0.0809	9.15	68.68	100.00	NA	
		ToCV (ssRNA+)	0.1584	31.87	99.22	100.00		
		PepMV-CH (ssRNA+)	12.3547	4787.66	100.00	98.96		
		PepMV-EU (ssRNA+)	10.1102	3905.12	100.00	98.51		
		ToMV (ssRNA+)	0.0139	5.90	92.26	99.80		
		STV (dsRNA)	0.0069	4.01	87.66	99.89		
		CLVd (viroid)	0.5523	2087.28	100.00	100.00		
	II	CaMV (dsDNA-RT)	3.4109	6387.25	100.00	99.99		
		CCyV1 (ssRNA-)	0.0381	42.26	99.90	100.00		
	III	TSWV (ssRNA-)	4.5122	5173.80	99.99	99.97		
	IV	TASVd (viroid)	0.0083	244.95	100.00	100.00		
	V	PVeV2 (dsRNA)	0.0116	11.52	99.84	99.99		
MinION direct RNA sequencing of totRNA	I	TYLCV (ssDNA)	0.0020	3.51	54.19	97.26	89.63	95.26
		ToCV (ssRNA+)	0.0007	0.26	28.59	/	90.53	/
		PepMV-CH (ssRNA+)	1.1528	2807.55	99.75	98.74	86.05	96.77
		PepMV-EU (ssRNA+)	0.5638	1289.09	99.64	98.35	85.45	95.64
		ToMV (ssRNA+)	0.0000	0.00	0.00	/	/	/
		STV (dsRNA)	0.0001	0.06	5.70	/	90.82	/
		CLVd (viroid)	0.0005	2.06	91.18	89.46	88.65	/
	II	CaMV (dsDNA-RT)	0.7548	429.28	99.70	99.61	88.21	97.16
		CCyV1 (ssRNA-)	0.0022	0.71	51.79	87.56	89.44	91.83
	III	TSWV (ssRNA-)	0.2101	139.94	99.72	99.65	88.53	97.89
	IV	TASVd (viroid)	0.0002	1.04	86.46	81.58	83.80	/
	V	PVeV2 (dsRNA)	0.0043	8.01	99.68	99.05	87.64	97.20
MinION direct RNA sequencing of rRNA-depleted totRNA	I	TYLCV (ssDNA)	0.0006	0.43	39.55	87.55	88.81	/
		ToCV (ssRNA+)	0.0442	15.08	99.60	98.52	87.71	97.03
		PepMV-CH (ssRNA+)	0.6243	685.49	99.77	98.78	87.30	97.25
		PepMV-EU (ssRNA+)	0.4552	415.00	99.66	98.37	86.74	/
		ToMV (ssRNA+)	0.0097	13.27	91.37	93.27	87.68	92.75
		STV (dsRNA)	0.0030	5.56	96.13	98.27	84.76	95.74
		CLVd (viroid)	0.0063	19.10	99.47	99.12	89.26	92.75
MinION cDNA-PCR sequencing of totRNA	I	TYLCV (ssDNA)	0.0486	17.15	58.97	99.40	89.38	98.35
		ToCV (ssRNA+)	0.0773	4.87	91.97	95.51	89.48	96.32
		PepMV-CH (ssRNA+)	27.1932	12346.89	99.89	98.89	87.07	93.96
		PepMV-EU (ssRNA+)	15.7794	6553.26	99.95	98.52	86.73	94.99
		ToMV (ssRNA+)	0.0847	50.77	93.58	99.78	87.38	99.52
		STV (dsRNA)	0.0006	0.09	9.11	/	90.43	/
		CLVd (viroid)	0.0040	3.14	99.73	93.57	90.85	93.16
MinION cDNA-PCR sequencing of rRNA-depleted totRNA	I	TYLCV (ssDNA)	0.0132	8.00	65.44	99.60	90.93	98.53
		ToCV (ssRNA+)	0.1303	24.47	99.87	99.86	91.38	99.73
		PepMV-CH (ssRNA+)	11.2630	6788.83	99.88	98.86	90.90	97.24
		PepMV-EU (ssRNA+)	9.7091	4884.39	99.94	98.46	90.36	96.61
		ToMV (ssRNA+)	0.0452	32.33	99.91	99.88	91.61	99.69
		STV (dsRNA)	0.0029	1.49	87.23	94.21	93.91	96.38
		CLVd (viroid)	0.0054	10.24	99.73	99.42	91.52	95.08

% of mapped reads	Average depth (reads)	Fraction of reference covered (reads)	Consensus sequence identity (%)	Average MinION reads identity	Average MinION contigs identity
0	0	0	81	81	81
0.01	1	10	82	82	82
0.025	5	20	83	83	83
0.05	10	30	84	84	84
0.075	15	40	85	85	85
0.1	25	50	86	86	86
1	50	60	87	87	87
3	75	70	88	88	88
6	100	80	89	89	89
9	1000	90	90	90	90
11	1500	91	91	91	91
13	3000	92	92	92	92
15	4500	93	93	93	93
17	6000	94	94	94	94
19	7500	95	95	95	95
21	9000	96	96	96	96
23	10500	97	97	97	97
25	12000	98	98	98	98
27	13500	99	99	99	99
29	15000	100	100	100	100

Heatmap is calculated for every section separately (% of mapped reads / Average depth (reads) / Fraction of reference covered (reads) / Consensus sequence identity (%) / Average MinION reads identity / Average MinION contigs identity) across all sequencing approaches. For every calculation (section - including legend) yellow represents the lowest value in the section, green represents the 50 percentile between the lowes and the highest value, and blue represents the highest value in the section.

FIGURE 2 | Heatmap of the samples included in the comparison with corresponding results: percentage of mapped reads, average depth (reads), fraction of reference covered (reads), consensus sequence identity (%), and average MinION reads/contigs identity (/ no data; NA not applicable).

expected due to the inclusion of the ribosomal RNA depletion step in the Illumina approach. These differences were reflected also when performing additional analyses on rarefied datasets (**Figure 3**); however, they were dependent on the amount of virus reads present in the original dataset.

As noted in section Nanopore Sequencing Using MinION Device Resulted in Comparable Detection of Plant Viruses/Viroids as Illumina Sequencing, no reads of ToMV were detected by MinION direct RNA sequencing of totRNA even in the complete dataset. Comparisons of rarefied subsamples further showed that MinION direct RNA sequencing performed comparably well to Illumina sequencing in cases in which a high fraction of specific viral reads was present in the samples (**Figure 3**). For MinION direct RNA datasets, in which virus sequences were present at more than 0.5% (PepMV in sample I and CaMV in sample II), relatively high fractions of corresponding viral genomes were covered by reads and contigs even in the smallest subsamples (**Figure 3**). Rarefaction analysis also showed very similar performance between the two approaches for PVeV2 (sample V)–in both cases, the fraction of genome covered by reads or contigs dropped correspondingly with the decreased dataset sizes. For TSWV, with 0.2% of the reads mapped to the viral genome, sharp drops in fractions of reference covered by reads or contigs were observed at smaller subsample data sizes for MinION direct RNA sequencing approach. For TYLCV, none of the two approaches enabled reconstruction of the complete genome, and Illumina sequencing approach performed only slightly better considering the two investigated parameters. In this analysis, for the remaining viruses and viroids (ToMV, ToCV, CCyV1, STV, CLVd, and TASVd), the MinION direct RNA sequencing method resulted in lower fraction of the genome covered by reads and contigs when compared to Illumina sequencing. In several cases, *de novo* assembly did not produce any contigs for the corresponding viruses, even for the complete datasets (data not shown).

Choice of a Suitable MinION Sequencing Approach Can Improve Detection of Plant Viruses and Viroids

Direct RNA sequencing using the MinION enabled detection of most of the plant viruses or viroids that were previously confirmed in the same samples with rRNA-depleted totRNA

A

	ssRNA+				ssRNA-		dsRNA		dsDNA -RT	ssDNA	circularRNA	
% of mapped reads	Pep-MV CH (Sample I)	Pep-MV EU (Sample I)	ToMV (Sample I)	ToCV (Sample I)	CCyV1 (Sample II)	TSWV (Sample III)	STV (Sample I)	PVeV2 (Sample V)	CaMV (Sample II)	TYLCV (Sample I)	CLVd (Sample I)	TASVd (Sample IV)
MinION seq. directRNA of totRNA	1.1528	0.5638	0.0000	0.0007	0.0022	0.2101	0.0001	0.0043	0.7548	0.0020	0.0005	0.0002
Illu. rRNA-dep. totRNA seq.	12.3547	10.1102	0.0139	0.1584	0.0381	4.5122	0.0069	0.0116	3.4109	0.0809	0.5523	0.0083

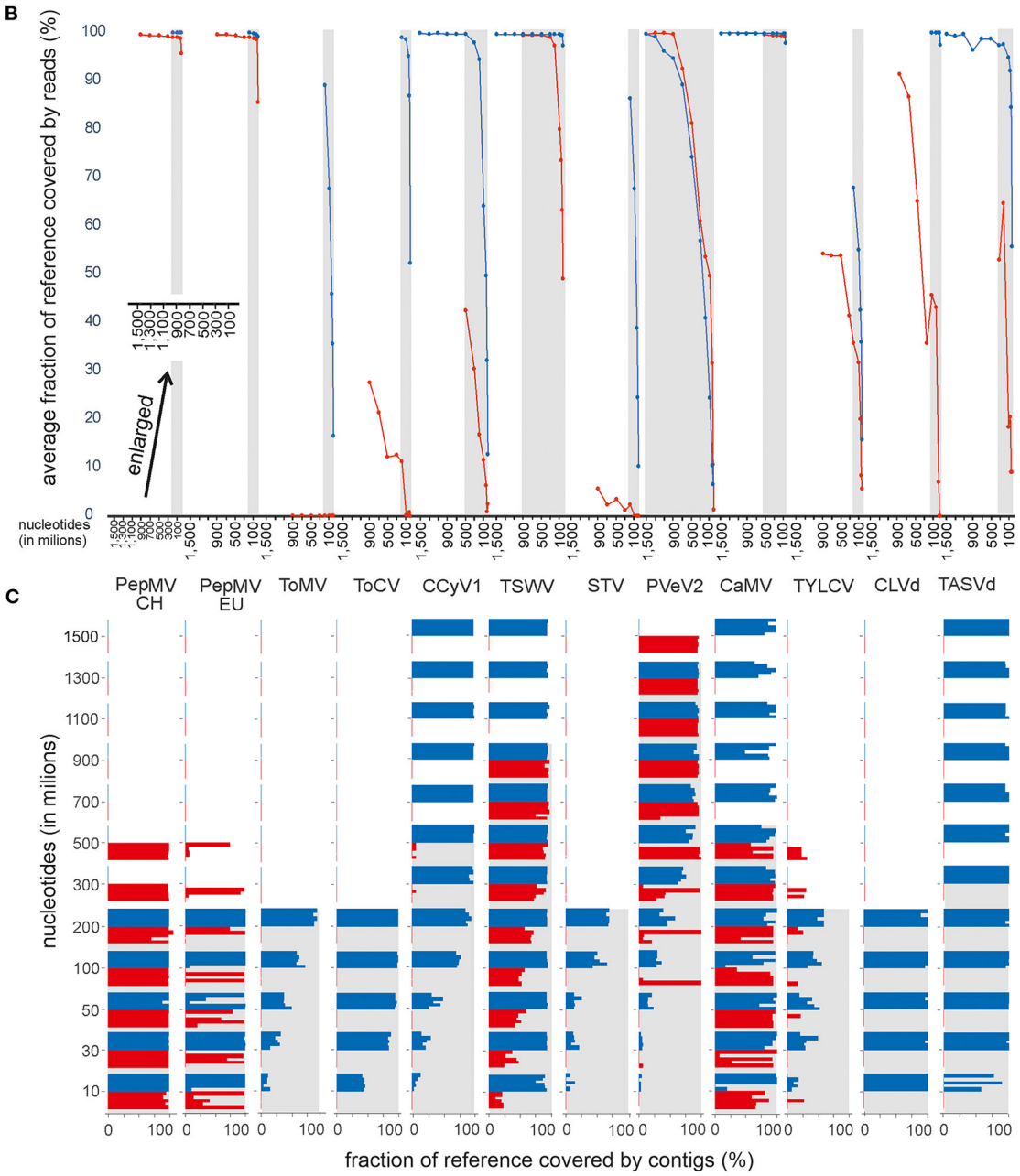

FIGURE 3 | Comparison of MinION direct RNA sequencing of totRNA (represented in red) and Illumina sequencing of rRNA-depleted totRNA (represented in blue) using data size-normalized subsamples. Results for each virus included in the analysis are shown along the x-axis and are grouped according to Baltimore

(Continued)

FIGURE 3 | classification. **(A)** Percentage of specific virus reads in trimmed and filtered complete HTS datasets. **(B)** Average fraction of reference covered by reads (%) at different subsample sizes. Dots represent the average value of analysis of 5 replicate subsamples. Different subsample sizes were used (10, 30, 50, 100, 200, 300, 500, 700, 900, 1,100, 1,300, 1,500 million nts–note the enlarged x-axis in the lower left part of panel 3B for a clearer view). **(C)** Fraction of reference covered by contigs (%) at different subsample sizes. Every bar represents the result of analysis for separate replicate subsamples. In **(B,C)**, gray areas designate the range in which the subsamples were available for both approaches compared.

Illumina sequencing. However, it showed somewhat inferior performance in the systematic comparisons described in a previous section. Thus, a single sample, containing five viruses and one viroid (sample I), was selected and used to further explore the performance of three additional sample preparation or nanopore sequencing library preparation approaches, which included either rRNA depletion, sequencing of PCR-amplified cDNA, or both (**Figure 1**), to investigate how much of the performance deficit is due to the sample preparation or library preparation method and how much is due to the platform.

Of these approaches, the one which is most comparable to the method used for Illumina sequencing (cDNA-PCR sequencing of rRNA-depleted totRNA) resulted in very similar fractions of viral reads in the sequenced datasets (**Figure 4**). This approach resulted in lower fractions of specific virus or viroid reads for almost all viruses than observed for both nanopore cDNA-based sequencing approaches or for the Illumina sequencing approach. Compared to MinION direct RNA sequencing without ribosomal RNA depletion, it resulted in an increased fraction of specific viral reads for four out of 7 viruses or viroids, including the detection of one virus (ToMV), which was not detected using direct RNA sequencing alone.

MinION sequencing of cDNA-PCR without ribosomal RNA depletion also resulted in relatively high fractions of specific viral reads. For four out of seven viruses or viroids, the numbers of corresponding reads were even higher than in the rRNA-depleted dataset sequenced by the same method (**Figure 4**).

Moreover, even though for most viruses, the fractions of viral reads did not increase, when including rRNA depletion to direct RNA sequencing, the rarefaction analysis showed improved performance also in this case, for all but one virus, TYLCV (**Figure 4**).

For viroids, the Illumina rRNA-depleted totRNA sequencing approach resulted in higher fractions of viroid reads than any of the MinION sequencing approaches (**Figures 3A**, **4A**).

De novo assembly of reads from sample I, which contained two strains of PepMV in some subsamples, resulted in an assembly of contigs corresponding only to one strain (**Figures 3C**, **4C**). The effect was observed, when using either Illumina or nanopore sequencing approaches. After the removal of the reads of one or the other PepMV strains and performing *de novo* assembly again (as described in Section Comparison of the Performance of Nanopore and Illumina Sequencing for Detection of Viruses on Rarefied Datasets), the artifact was no longer observed. Additionally, for some subsamples of MinION data, the assembled contigs were longer than the reference genome sequence (**Figure 4C**). Further investigation (visual inspection of nanopore reads mapping to the corresponding contigs) revealed mistakes or artifacts in some mapped reads, which likely led to artifactual *de novo* assembly of the corresponding contigs.

Different Nanopore Sequencing Approaches Using MinION Device Result in Different Accuracy of Reads; However, Generated Consensus Sequences Show Relatively High Accuracies in all Cases, When Sequencing Depths Are High Enough

Closer investigation and comparison of average read identities (proxy of sequencing error rate) for different MinION sequencing approaches for sample I revealed the lowest read identities when using direct RNA sequencing of rRNA-depleted totRNA (minimum 84.67%, average 87.43%). The highest average read identities were observed when using cDNA-PCR sequencing of the rRNA-depleted totRNA approach (minimum 90.36%, average 91.5%). For the same approach, also the highest average contig identities were observed (minimum 95.08%, average 99.73%). Even though the inclusion of the ribodepletion step resulted in a slightly decreased mean quality score (**Supplementary Table S2**), as was already observed in other studies (Wongsurawat et al., 2019), the calculation of average MinION read identity (**Figure 2**) did not show any marked differences.

As expected, the pairwise identities of consensus viral sequences compared to generated or selected references were higher in the case of Illumina sequencing approach for all viruses or viroids for which a calculation was possible (>99.5% in all cases). For MinION sequencing approaches, pairwise identities of consensus viral sequences compared to generated or selected references were higher than 98%, when average sequencing depth values were 5x or more, except in the case of ToMV (sample I), where, despite the sequencing depth of 13.27, this was 93.27%. Upon visual inspection of the mapping files, we observed that this was a consequence of uneven coverage by reads (the 5‘ of the viral genome was covered by very few reads), which contributed to the final lower average pairwise identity of consensus viral genome sequence.

Rapid Generation of MinION Data Needed for Detection of Viruses Present in Plants in Moderate Titres

A relatively short time (>30 min) was needed for retrieving sufficient data (covering at least 50% of viral genomic sequences), in cases, in which fractions of specific viral reads in samples were higher than 0.2% (PepMV, CaMV, TSWV; **Figures 3**, **4**; **Table 2**) using any of the sample preparation approaches. Further, in the case of PVeV2, for which 0.0043% of reads in the sample were mapped to the virus reference sequence, ∼2.5 h was needed to retrieve sufficient amount of data. For cases, in which virus or viroid reads were present in samples in very small fractions, a

A

% of mapped reads	ssRNA+				dsRNA	ssDNA	viroid
	PepMV CH	PepMV EU	ToMV	ToCV	STV	TYLCV	CLVd
MinION directRNA seq. of totRNA	1.1528	0.5638	0.0000	0.0007	0.0001	0.0020	0.0005
MinION directRNA seq. of rRNA-dep. totRNA	0.6243	0.4552	0.0097	0.0442	0.0030	0.0006	0.0063
MinION cDNA- PCR seq. of totRNA	27.1932	15.7794	0.0847	0.0773	0.0006	0.0486	0.0040
MinION cDNA-PCR seq.of rRNA-dep. totRNA	11.2630	9.7091	0.0452	0.1303	0.0029	0.0132	0.0054
Illumina rRNA-dep. totRNA seq.	12.3547	10.1102	0.0139	0.1584	0.0069	0.0809	0.5523

B

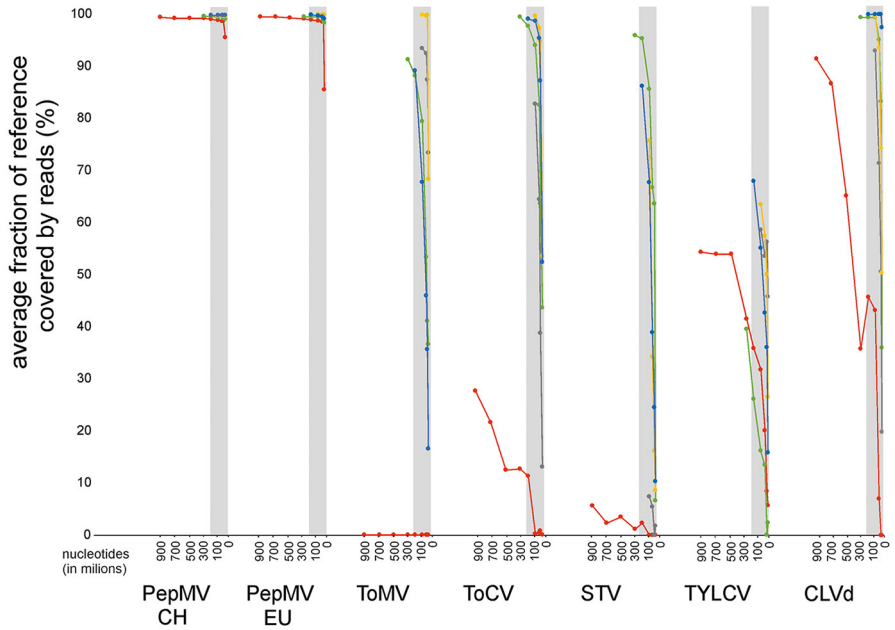

C

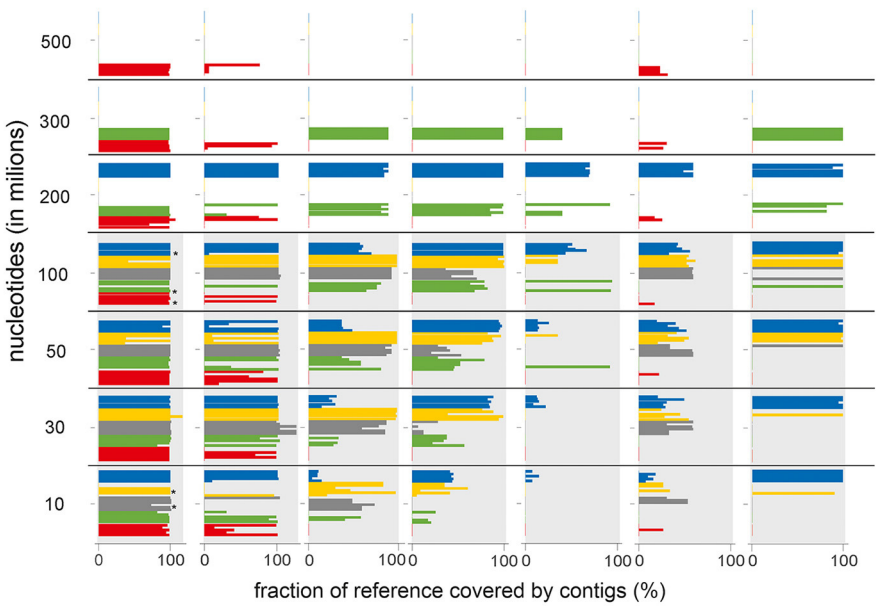

FIGURE 4 | Comparison of MinION sequencing: direct RNA sequencing of totRNA, direct RNA sequencing of rRNA-depleted totRNA, cDNA-PCR sequencing of totRNA, cDNA-PCR sequencing of rRNA-depleted totRNA and Illumina sequencing of rRNA-depleted totRNA using data size-normalized subsamples. Results for

(Continued)

FIGURE 4 | each virus included in the analysis are shown along the x-axis and are grouped according to Baltimore classification. **(A)** Percentage of specific virus reads in trimmed and filtered complete HTS datasets. **(B)** Average fraction of reference covered by reads (%) at different subsample sizes. Dots represent the average value of analysis of 5 replicated subsamples. Different subsample sizes were used (10, 30, 50, 100, 200, 300, 500, 700, 900, 1,100, 1,300, 1,500 million nts). **(C)** Fraction of reference covered by contigs (%) at different subsample sizes. Each bar represents the result of analysis for a separate replicate subsample. Bars with * indicate chosen subsample for additional analysis explained in section Comparison of the Performance of Nanopore and Illumina Sequencing for Detection of Viruses on Rarefied Datasets. In **(B,C)**, red represents MinION direct RNA sequencing of totRNA, green represents direct RNA sequencing of rRNA-depleted totRNA, gray represents cDNA-PCR sequencing of totRNA, yellow represents cDNA-PCR sequencing of rRNA-depleted totRNA, and blue represents the results for Illumina sequencing of rRNA-depleted totRNA. Gray areas designate the range in which the subsamples were available for both compared approaches.

TABLE 2 | Cumulative yield of nucleotides sequenced in time.

Sample number	Virus/viroid present	Nucleotides (millions)	Time (minutes)	Nucleotides (millions)	Time (minutes)	Nucleotides (millions)	Time (minutes)	Nucleotides (millions)	Time (minutes)
		MinION direct RNA sequencing of totRNA		MinION direct RNA sequencing of rRNA-depleted totRNA		MinION cDNA-PCR sequencing of totRNA		MinION cDNA-PCR sequencing of rRNA-depleted totRNA	
I	TYLCV	500	520	/	/	30	50	50	220
	ToCV	/	/	30	80	50	130	10	20
	PepMV	10	10	10	30	10	10	10	20
	ToMV	/	/	50	140	10	10	10	20
	STV	/	/	30	80	/	/	100	600
	CLVd	700	710	30	80	30	50	10	20
II	CaMV	10	10	NA	NA	NA	NA	NA	NA
	CCyV1	/	/	NA	NA	NA	NA	NA	NA
III	TSWV	20	30	NA	NA	NA	NA	NA	NA
IV	TASVd	200	220	NA	NA	NA	NA	NA	NA
V	PVeV2	200	170	NA	NA	NA	NA	NA	NA

Data in table represent the time when enough nucleotides would be sequenced to cover at least 50% of virus/viroid reference sequence by mapping reads. / no data: 50% coverage of virus/viroid reference by reads were not achieved. NA, not applicable.

relatively long time was needed to retrieve sufficient amount of data; e.g., for CLVd (0.0005% of reads were mapped to viroid reference sequence), the sequencing should last at least around 12 h to retrieve enough data. Equivalent observations were made for several other viruses or viroid, sequenced within the sample I (**Table 2**). In some cases, especially when very low fractions of specific viral reads were observed in the samples, retrieving enough data to cover >50% of genome sequence was not achieved even if the sequencing lasted for 46–48 h (**Table 2**).

DISCUSSION

The systematic comparison of different approaches of nanopore and Illumina sequencing performed in this study demonstrated the effectiveness of nanopore sequencing using the MinION platform (Oxford Nanopore Technologies) for fast and sensitive detection of plant viruses, when the most optimal library preparation approach is used. Besides the ability to detect viruses, the accuracy and time efficiency of the approach were evaluated.

All viruses present in investigated samples, except ToMV, which was present in a sample in extremely low titer (Pecman et al., 2017), were identified using all of the employed approaches. ToMV was not detected using direct RNA sequencing of totRNA with the MinION sequencer (**Figure 2**). In general, across all datasets, inferior performance of direct RNA sequencing of totRNA using MinION compared to Illumina-based rRNA-depleted totRNA sequencing for detection of plant viruses is evident: between 10.7 and 1,104.6 (PepMV and CLVd, respectively) times, fewer virus reads (average 244.8) were observed in the complete direct RNA MinION datasets compared to the Illumina datasets. Rarefaction analyses showed a similar picture: the fractions of reference viral genomes covered by viral reads or contigs dropped markedly with reduced dataset sizes for direct RNA MinION for viruses, which were present in the original datasets in low amounts (e.g., below 0.2%) (**Figure 3**). Moreover, in some cases, no contigs were recovered after *de novo* assembly for these viruses (**Figure 3C**), which indicates that the approach would not be very efficient for detection of (new) viruses present in plants in low titres.

We primarily included direct RNA sequencing of totRNA on MinION in this comparative study due to the speed and straightforward nature of this approach (according to SQK-RNA002, only 115 min is needed for library preparation). However, results of this first comparison showed that such an approach has a reduced performance for detection of plant viruses, compared to the Illumina-based sequencing of rRNA-depleted totRNA, which we take as a 'golden standard' in this study. This is likely due to both the high error rate of the sequencing itself and the lack of the rRNA depletion step. Thus, in a second part of the study, we performed analysis of a selected sample (containing a diverse assembly of plant viruses)

using nanopore sequencing MinION device, but with several improvements, which were shown to improve the performance of nanopore sequencing for virus detection.

Including rRNA depletion prior to the direct RNA sequencing approach using the MinION platform resulted in increased fractions of specific virus reads in most of the cases (**Figure 2**). The fractions of specific virus reads changed between 0.3 and 63.1 (TYLCV and ToCV, respectively) times, and on average, the fraction increased by 17.8 times for all viruses tested.

The protocol using cDNA-PCR sequencing of totRNA (with no rRNA depletion) also resulted in improvements in the fractions of specific virus reads in the dataset (**Figure 2**). The fractions of virus reads increased between 6.0 and 110.4 (STV and ToCV, respectively) times compared to direct RNA sequencing of totRNA and on average 33.3 times for all viruses tested. For three viruses (PepMV-EU, PepMV-CH, and ToMV), this approach resulted in a greater proportion (1.5x, 2.2x, and 6.09x, respectively) of virus sequences in the MinION dataset than sequencing rRNA-depleted totRNA using the Illumina platform.

Moreover, incorporating both rRNA depletion and reverse transcription prior to nanopore sequencing using MinION platform (i.e., using cDNA-PCR sequencing of rRNA-depleted totRNA) led to the greatest increases in the observed fractions of specific virus reads. The proportion of virus reads increased between 6.6 and 186.1 (TYLCV and ToCV, respectively) times and on average 43.2 times for all viruses tested compared to direct RNA sequencing. For one virus (ToMV), this approach resulted in a greater proportion (3.2 x) of virus sequences obtained in the respective MinION dataset compared to the dataset generated from rRNA-depleted totRNA using the Illumina platform. Using cDNA-PCR protocol for sequencing rRNA-depleted totRNA also resulted in the highest observed consensus sequence identities, and the comparison of calculated average viral reads identities revealed that this approach resulted in most "accurate" sequencing reads (**Figure 2**).

As mentioned above, in a number of cases, no contigs of the corresponding viruses were generated from complete (data not shown) or near complete MinION direct RNA datasets (**Figures 3**, **4**). This was also observed for two viruses (TYLCV, PepMV-EU) when direct RNA sequencing of rRNA-depleted RNA was used and one virus (STV) when cDNA-PCR sequencing of totRNA was used. This suggests that detection of such viruses could be missed if only contigs are analyzed, and also, that unknown viruses would be missed if present in samples in similarly low titres. Using the cDNA-PCR protocol for sequencing rRNA-depleted totRNA, contigs were assembled for all viruses in the datasets tested and they showed the highest average contig identity of all of the nanopore sequencing approaches compared (**Figures 2**, **4**).

The performance of the direct RNA sequencing of totRNA using MinION was notably poorer for viroids than viruses. Compared to Illumina sequencing, there was 1104,6x and 41,5x smaller proportion of CLVd and TASVd viroid reads when sequencing totRNA directly using the MinION and for both viroids included in the comparison, only partial genomes were obtained. When using either cDNA-PCR sequencing of rRNA-depleted RNA or direct RNA sequencing of rRNA-depleted totRNA, complete viroid genomes were recovered (**Figure 4**). Inferior performance of the direct sequencing of totRNA for the detection of viroids is most likely a consequence of the circular genome which could not be polyadenylated in the first steps of the protocol. Only damaged or intermediate replication forms of viroids could be polyadenylated. Moreover, it is possible that the nanopore sequencing could be adversely affected by the secondary structure of viroid RNA (Flores et al., 2014), and this may be partly overcome by the larger amounts of target present in rRNA-depleted totRNA. This study is the first using nanopore sequencing for viroids, and further improvements in template preparation, such as fragmentation of the input RNA, could be envisaged in this case.

Regardless of the approach used (Illumina or all of the tested template preparation methods using the MinION device), we observed artifacts in an assembly of PepMV genomes. PepMV was present in sample I in a mixed infection of two strains. In several cases, the genome of one of the two strains was not assembled in the process. After subtracting the reads of one of the strains and repeating the *de novo* assembly, the artifact was no longer observed. This suggests that special attention should be applied to analysis pipelines to resolve observed assembly artifacts to ensure detection of multiple strains of the same virus.

Different types of input material could possibly also affect the quality and the amount of the generated sequencing data. Most of the samples used in this study were frozen leaves; however, also, fresh leaves and the dry seed samples were used in some cases. Although in our study, the sample size for different input materials is not large enough to draw any conclusions, we observed the highest amount of generated data when using fresh leaf material (**Supplementary Table S1**). More tests would be needed to study the impact of the input material on the sequencing results and likely specific adaptations of extraction and sample preparation procedures could be implemented to ascertain optimal results for different sample types.

One of the main advantages of the nanopore sequencing is the speed with which sequence data are generated (Bronzato et al., 2018; Fellers et al., 2019). In this study, the libraries for MinION sequencing were prepared and applied to the flow cell within 1 day. Since the data could be analyzed in real time, estimations of the time needed to generate sequences, which would cover 50% or more of a specific viral genome using read mapping were made. The time in which these thresholds were achieved depended on the amount of virus reads present in the complete datasets (a proxy of viral titer). Our estimates suggest the 50% threshold would be achieved in 10–30 min for PepMV using any of the approaches, or on the other end of the spectrum in 11 h and 50 min for CLVd (using MinION direct RNA sequencing of totRNA). This suggests that a diagnostic workflow could be established with <1 day to perform RNA extraction and library preparation, followed by an overnight run on the MinION device and bioinformatic analysis of the following day.

The speed and accessibility of the methodology has led to exploration of the technique as an in-field diagnostic tool (Boykin et al., 2019). Though possible for the detection of high-titer viruses using rapid sample preparation and simplified analysis, this would currently rely on transferring several items

of laboratory equipment to the site where testing is being performed and would also need the end-users to be skilled in molecular biology protocols. For diagnostic applications where potentially low-titer infections are likely, the method would require significantly more time to run the flow cell and analyse the data, making it less practical for in-field use. Furthermore, adoption as a field test is dependent on the time criticality of the actions taken based on the outcome of the test and how these will be improved if the results are generated more quickly. The practical benefits described do make the approach suited to routine diagnostic laboratories, where the larger sequencers may be too expensive and impractical to run, leading laboratories to rely on outsourcing to HTS providers. The speed and scalability of MinION sequencing make it well suited to smaller numbers of samples in diagnostic laboratories and, in particular, where rapid turnaround of results is needed especially, given the results are approaching the quality generated by Illumina sequencing.

One of the challenges for introducing this method into routine laboratory use is the constant and rapid development, introduction and withdrawal of flow cells, kits, protocols, and bioinformatic tools by Oxford Nanopore Technologies. This leads to uncertainty with incorporating nanopore into routine testing protocols, in particular those run within a quality certification scheme (e.g., ISO17025). To overcome this obstacle, the use of internal negative control (healthy plant) and in particular a standardized positive control suited for the entire workflow is needed. For example, *Phaseolus vulgaris*, cv. Black Turtle infected with endornaviruses has been used as a positive control in other studies (Kesanakurti et al., 2016) and was successfully sequenced in this study (Sample V).

Finally, when comparing the costs for sample, library preparation, and sequencing per sample using either MiSeq (Illumina) or MinION flow cell (Oxford Nanopore Technologies), comparable prices can be estimated if using multiplexing of samples. In the case of MiSeq (Illumina) sequencing, the estimated cost is 189 €/sample if sequencing 24 samples in the same run (Vazquez-Iglesias et al., 2022). On the other hand, the estimated cost for barcoding and sequencing 12 or 24 samples on one MinION flow cell using cDNA-PCR barcoding kit and including ribodepletion step is 215 €/sample or 170 €/sample, respectively. Due to the increasing throughput of the MinION flow cells, both multiplexing options should now provide enough data for reliable detection of most of the viruses present in the tested samples. More detailed calculation is described in **Supplementary Data 4**.

To conclude, the results of this study indicate that, when appropriate library preparation and sequencing protocols are selected, nanopore sequencing using the MinION device gave equivalent detection of a range of viruses and viroids than a commonly used Illumina sequencing approach. In this regard, the performance of MinION direct RNA sequencing of totRNA was lower than Illumina sequencing, but improved significantly when rRNA depletion was incorporated or when cDNA amplification or both were incorporated. Whilst these slowed down the sample preparation, they facilitated detection of the lowest titer virus infection included in the study.

DATA AVAILABILITY STATEMENT

The datasets presented in this study can be found in online repositories. The names of the repository/repositories and accession number(s) can be found in the article/**Supplementary Material**.

AUTHOR CONTRIBUTIONS

AP, DK, MR, and NB designed the experiment. AP performed laboratory part of the experiment and analyzed the data with the assistance of IA and DK and wrote the draft of the manuscript. All authors significantly contributed with reviewing and editing the manuscript.

FUNDING

The study was financially supported by Slovenian Research Agency thought project NanoPhyto (L7-2632), core financing (P4-0165, P4-0407), and young researcher grant (AP), Euphresco (VIRFAST) project and by COST Action CA15223, thought STSM (short-term scientific mission).

ACKNOWLEDGMENTS

We thank Sam McGreig for the help with bioinformatic analysis, i.e., sharing tested parameters for *de novo* assembly of MinION reads, Mike Rott for seeds of *Phaseolus vulgaris*, cultivar Black Turtle, in this study analyzed as Sample V, and Wouter De Coster for script: get_cumulative_yield_table.py (**Supplementary Data 3**).

SUPPLEMENTARY MATERIAL

The Supplementary Material for this article can be found online at: https://www.frontiersin.org/articles/10.3389/fmicb.2022.883921/full#supplementary-material

REFERENCES

Adams, I. P., Glover, R. H., Monger, W. A., Mumford, R., Jackeviciene, E., Navalinskiene, M., et al. (2009). Next-generation sequencing and metagenomic analysis: a universal diagnostic tool in plant virology. *Mol. Plant Pathol.* 10, 537–545. doi: 10.1111/j.1364-3703.2009.00545.x

Al Rwahnih, M., Daubert, S., Golino, D., and Rowhani, A. (2009). Deep sequencing analysis of RNAs from a grapevine showing syrah decline symptoms reveals a multiple virus infection that includes a novel virus. *Virology*. 387, 395–401. doi: 10.1016/j.virol.2009.02.028

Beddoe, N., Adams, I. P., McGreig, S., and Forsyth A. (2020). Identification and full genomic sequence of nerine yellow stripe virus. *Arch. Virol.* 16, 2967–2971. doi: 10.1007/s00705-020-04776-3

Boykin, L. M., Sseruwagi, P., Alicai, T., Ateka, E., Mohammed, I.U., Stanton, J.L., et al. (2019). Tree lab: portable genomics for early detection of plant viruses and pests in Sub-Saharan Africa. *Genes*. 10, 632. doi: 10.3390/genes10090632

Branton, D., and Deamer, D. (2019). "The Development of Nanopore Sequencing" in *Nanopore Sequencing*, eds. D. Branton, and D. Deamer (London: World Scientific, Pub Co Inc. doi: 10.1142/10995

Bronzato, B. A., Sherman, D., Stone, A., Gopakumar, A., Wilson, V., Schneider, W., et al. (2018). Nanopore sequencing as a surveillance tool for plant pathogens in plant and insect tissues. *Plant Dis.* 102, 1648–52. doi: 10.1094/PDIS-04-17-0488-RE

Buchfink, B., Xie, C., and Huson, D. H. (2015). Fast and sensitive protein alignment using DIAMOND. *Nat. Methods.* 12, 59–60. doi: 10.1038/nmeth.3176

Chalupowicz, L., Dombrovsky, A., Gaba, V., Luria, N., Reuven, M., Beerman, A., et al. (2019). Diagnosis of plant diseases using the nanopore sequencing platform. *Plant Pathol.* 68, 229–238. doi: 10.1111/ppa.12957

De Coster, W., D'Hert, S., Schultz, D. T., Cruts, M., and Van Broeckhoven, C. (2018). NanoPack: visualizing and processing long-read sequencing data. *Bioinformatics*. 34, 2666–2669. doi: 10.1093/bioinformatics/bty149

Donaire, L., Wang, Y., Gonzalez-Ibeas, D., Mayer, K. F., Aranda, M. A., and Llave, C. (2009). Deep-sequencing of plant viral small rnas reveals effective and widespread targeting of viral genomes. *Virology*. 392, 203–214. doi: 10.1016/j.virol.2009.07.005

Fellers, J. P., Webb, C., Fellers, M. C., Shoup Rupp, J., and Wolf. E. De. (2019). Wheat virus identification within infected tissue using nanopore sequencing technology. *Plant Dis*. 103, 2199–2203 doi: 10.1094/PDIS-09-18-1700-RE

Filloux, D., Fernandez, E., Loire, E., Claude, L., Galzi, S., Candresse, T., et al. (2018). Nanopore-based detection and characterization of yam viruses. *Sci. Rep.* 8. doi: 10.1038/s41598-018-36042-7

Flores, R., Gago-Zachert, S., Serra, P., Sanjuán, R., and Elena, S. F. (2014). Viroids: survivors from the RNA world? *Annu. Rev. Microbiol.* 68, 395–414. doi: 10.1146/annurev-micro-091313-103416

Garalde, D. R., Snell, E. A., Jachimowicz, D., Sipos, B., Lloyd, J. H., Bruce, M., et al. (2018). Highly Parallel Direct RNA Sequencing on an Array of Nanopores. *Nat. Method*. 15, 201–206. doi: 10.1038/nmeth.4577

Greninger, A. L., Naccache, S. N., Federman, S., Yu, G., Mbala, P., Bres, V., et al. (2015). Rapid metagenomic identification of viral pathogens in clinical samples by real-time nanopore sequencing analysis. *Genome Med.* 7, 1–13. doi: 10.1186/s13073-015-0220-9

Huson, D. A., Auch, A. F., Qi, J., and Schuster, S. C. (2007). MEGAN analysis of metagenome data. *Gennome Res.* 17, 377–386. doi: 10.1101/gr.5969107

Ip, C., Loose, M., Tyson, J. R., de Cesare, M., Brown, B. L., Jain, M., et al. (2015). MinION analysis and reference consortium: phase 1 data release and analysis. *F1000Research*. 4, 1075. doi: 10.12688/f1000research.7201.1

Jones, R. A. C., and Naidu, R. A. (2019). Global dimensions of plant virus diseases : current status and future perspectives. *Annu. Rev. Virol.* 6, 387–409. doi: 10.1146/annurev-virology-092818-015606

Kesanakurti, P., Belton, M., Saeed, H., Rast, H., Boyes., I., et al. (2016). Screening for plant viruses by next generation sequencing using a modified double strand RNA extraction protocol with an internal amplification control. *J. Virol. Methods*. 236, 35–40. doi: 10.1016/j.jviromet.2016.07.001

Kreuze, J. F., Perez, A., Untiveros, M., Quispe, D., Fuentes, S., Barker, I., et al. (2009). Complete viral genome sequence and discovery of novel viruses by deep sequencing of small RNAs: a generic method for diagnosis, discovery and sequencing of viruses. *Virology*. 388, 1–7. doi: 10.1016/j.virol.2009.03.024

Li, H. (2016). Sequence analysis minimap and miniasm : fast mapping and de novo assembly for noisy long sequences. *Bioinformatics*. 32, 2103–2010. doi: 10.1093/bioinformatics/btw152

Li, H. (2018). Minimap2 : pairwise alignment for nucleotide sequences. *Bioinformatics*. 34, 3094–3100. doi: 10.1093/bioinformatics/bty191

Meredith, L. W., Hamilton, W. L., Warne, B., Houldcroft, C. J., Hosmillo, M., Jahun, A. S., et al. (2020). Rapid implementation of SARS-CoV-2 sequencing to investigate cases of health-care associated COVID-19: a prospective genomic surveillance study. *Lancet Infect. Dis.* 20, 1263–1272. doi: 10.1016/S1473-3099(20)30562-4

Pecman, A., Kutnjak, D., Gutiérrez-Aguirre, I., Adams, I., Fox, A., Boonham, N., et al. (2017). Next generation sequencing for detection and discovery of plant viruses and viroids: comparison of two approaches. *Front. Microbiol.* 8. doi: 10.3389/fmicb.2017.01998

Quick, J., Grubaugh, N. D., Pullan, S. T., Claro, I. M., Smith, A. D., Gangavarapu, K., et al. (2017). Multiplex PCR method for minion and illumina sequencing of zika and other virus genomes directly from clinical samples. *Nat. Protocols*. 12, 1261–1266. doi: 10.1038/nprot.2017.066

Quick, J., Loman, N. J., Duraffour, S., Simpson, J. T., Severi, E., Cowley, L., et al. (2016). Ebola surveillance. *Nature*. 65, 35–43. doi: 10.1038/nature16996

Tan, S., Dvorak, C. M.T., and Murtaugh, M. P. (2019). Rapid, unbiased PRRSV strain detection using MinION direct RNA sequencing and bioinformatics tools. *Viruses*. 11. doi: 10.3390/v11121132

Van Dijk, E. L., Jaszczyszyn, Y., Naquin, D. and Thermes, C. (2018). The third revolution in sequencing technology. *Trends Genet.* 34, 666–681. doi: 10.1016/j.tig.2018.05.008

Vaser, R., Sović, I., Nagarajan, N., and Šikić, M. (2017). Fast and accurate de novo genome assembly from long uncorrected reads. *Genome Res.* 27, 737–746. doi: 10.1101/gr.214270.116

Vazquez-Iglesias, I., McGreig, S., Pufal, H., Robinson, R., Clover, G. R. G., Fox, A., et al. (2022). A novel high-throughput sequencing approach reveals the presence of a new virus infecting Rosa : Rosa Ilarvirus-1 (RIV-1). *J. Virol. Methods*. 300. doi: 10.1016/j.jviromet.2021.114417

Villamor, D. E.V., Ho, T., Al Rwahnih, M., Martin, R. R. and Tzanetakis, I. E. (2019). High throughput sequencing for plant virus detection and discovery. *Phytopathology*. 109, 716–725. doi: 10.1094/PHYTO-07-18-0257-RVW

Visser, M., Bester, R., Burger, J. T. and Maree, H. J. (2016). Next-generation sequencing for virus detection: covering all the bases. *Virol J.* 13, 85. doi: 10.1186/s12985-016-0539-x

Wongsurawat, T., Jenjaroenpun, P., Taylor, M. K., Lee, J., Tolardo, A. L., Parvathareddy, J., et al. (2019). Rapid sequencing of multiple RNA viruses in their native form. *Front. Microbiol.* 10, 1–8. doi: 10.3389/fmicb.2019.00260

Yamagishi, J., Runtuwene, L. R., Hayashida, K., Mongan, A. E., Nguyen Thi, L. A., Nguyen Thuy, L., et al. (2017). Serotyping dengue virus with isothermal amplification and a portable sequencer. *Sci. Rep.* 7, 1–10. doi: 10.1038/s41598-017-03734-5

Conflict of Interest: IA and AF are employed by Fera Science Ltd.

The remaining authors declare that the research was conducted in the absence of any commercial or financial relationships that could be construed as a potential conflict of interest.

Publisher's Note: All claims expressed in this article are solely those of the authors and do not necessarily represent those of their affiliated organizations, or those of the publisher, the editors and the reviewers. Any product that may be evaluated in this article, or claim that may be made by its manufacturer, is not guaranteed or endorsed by the publisher.

frontiers | Frontiers in Microbiology

ORIGINAL RESEARCH
published: 27 May 2022
doi: 10.3389/fmicb.2022.886331

Ultrastructure of Terpene and Polyphenol Synthesis in the Bark of *Cupressus sempervirens* After *Seiridium cardinale* Infection

Gianni Della Rocca[1], *Alessio Papini*[2], *Isabella Posarelli*[2], *Sara Barberini*[1], *Corrado Tani*[2], *Roberto Danti*[1]* *and Salvatore Moricca*[3]

[1] *Istituto per la Protezione Sostenibile delle Piante, Consiglio Nazionale delle Ricerche (IPSP-CNR), Sesto Fiorentino, Italy,* [2] *Dipartimento di Biologia (BIO), Università di Firenze, Firenze, Italy,* [3] *Dipartimento di Scienze e Tecnologie Agrarie, Alimentari, Ambientali e Forestali (DAGRI), Università di Firenze, Firenze, Italy*

OPEN ACCESS

Edited by:
Marco Scortichini, Council for Agricultural and Economics Research (CREA), Italy

Reviewed by:
Evangelia V. Avramidou, National Agricultural Research Foundation, Greece
Yifan Jiang, Nanjing Agricultural University, China
Ari Mikko Hietala, Norwegian Institute of Bioeconomy Research (NIBIO), Norway

***Correspondence:**
Roberto Danti
roberto.danti@ipsp.cnr.it

Specialty section:
This article was submitted to Microbe and Virus Interactions with Plants, a section of the journal Frontiers in Microbiology

Received: *28 February 2022*
Accepted: *27 April 2022*
Published: *27 May 2022*

Citation:
Della Rocca G, Papini A, Posarelli I, Barberini S, Tani C, Danti R and Moricca S (2022) Ultrastructure of Terpene and Polyphenol Synthesis in the Bark of Cupressus sempervirens After Seiridium cardinale Infection. Front. Microbiol. 13:886331. doi: 10.3389/fmicb.2022.886331

Cypress Canker Disease (CCD) pandemic caused by *Seiridium cardinale* is the major constraint of many *Cupressaceae* worldwide. One of the main symptoms of the disease is the flow of resin from the cankered barks. While inducible phloem axial resin duct-like structures (PARDs) have recently been characterized from an anatomical point of view, their actual resin production is still being debated and has never been demonstrated. Although the involvement of polyphenolic parenchyma cells (PP cells) in the bark of *Cupressus sempervirens* after *S. cardinale* infection was revealed in one of our previous studies using light microscopy, their evolution from the phloem parenchyma cells is yet to be clarified. This study investigated functional and ultrastructural aspects of both PARD-like structures and PP cells by means of more in-depth light (LM) and fluorescence microscopy (FM) combined with histochemical staining (using Sudan red, Fluorol Yellow, NADI Aniline blue black, and Toluidine blue staining), in addition to Transmission Electron Microscope (TEM). Two-year-old stem sections of a *C. sempervirens* canker-resistant clone (var. "Bolgheri"), artificially inoculated with *S. cardinale,* were sampled 5, 7, 14, 21, and 45 days after inoculation, for time-course observations. FM observation using Fluorol yellow dye clearly showed the presence of lipid material in PARD-like structures lining cells of the cavity and during their secretion into the duct space/cavity. The same tissues were also positive for NADI staining, revealing the presence of terpenoids. The cytoplasm of the ducts' lining cells was also positive for Sudan red. TEM observation highlighted the involvement of plastids and endoplasmic reticulum in the production of terpenoids and the consequent secretion of terpenoids directly through the plasma membrane, without exhibiting vesicle formation. The presence of a high number of mitochondria around the area of terpenoid production suggests that this process is active and consumes ATP. The LM observations showed that PP cells originated from the phloem parenchyma cells (and possibly albuminous cells) through the accumulation of phenolic substances in the vacuole. Here, plastids were again involved in their production. Thus, the findings of this work suggest that the PARD-like structures can actually be considered PARDs or even bark traumatic resin ducts (BTRD).

Keywords: cypress, canker, phloem, infectious disease, TEM, resin, terpenoids

INTRODUCTION

Cypress Canker Disease (CCD), also known as cypress bark canker, is a pandemic caused by the invasive necrotrophic fungus *Seiridium cardinale* (Wagener) Sutton and Gibson (Order: Xylariales, Family: Amphisphaeriaceae) affecting many *Cupressaceae* (Danti et al., 2013a). A native of California (Wagener, 1928, 1939; Della Rocca et al., 2011, 2013), this fungal pathogen has spread all around the world mainly through the commerce of infected plants (Della Rocca et al., 2019); this has subsequently caused severe loss and significant limitations to the cultivation of cypresses (genus *Hesperocyparis* and *Cupressus*), especially *Cupressus sempervirens* L. (Graniti, 1998; Danti and Della Rocca, 2017).

A genetic improvement program of *C. sempervirens* for resistance to CCD has been carried out in Europe since the 1970s (Raddi and Panconesi, 1981; Danti et al., 2011), due to this species' valuable role in the landscape and its multifunctionality, especially in Mediterranean countries (Xenopoulos et al., 1990; Della Rocca et al., 2007; Farahmand, 2020). As a result, a series of canker-resistant varieties of *C. sempervirens* have been patented (Panconesi and Raddi, 1990; Danti et al., 2006, 2013b).

In the breeding program of cypress genotypes, it was essential to study the metabolic, molecular, and anatomical mechanisms which underlie the resistance, or susceptibility, to the fungal disease. While the ultrastructural modifications in the phloem, cambium, phloem parenchyma, and ray parenchyma colonized by *S. cardinale* were described by Mutto and Panconesi, 1987, it has been observed that resistance of the common cypress to CCD relies on the tree's ability to produce a barrier that compartmentalizes the bark tissues invaded by the pathogen by building up a ligno-suberized boundary zone (LSZ), which is then followed by the formation of a necrophylactic periderm (NP) (Ponchet and Andreoli, 1990; Spanos et al., 1999). This is the result of the activation of metabolic pathways leading to the synthesis of suberin in bark tissues (Danti et al., 2018). Another host defense reaction against the pathogen (easily visible to the naked eye) is the more or less abundant emission of resin from the cankered bark (Danti et al., 2013a). This was found to be due to increased production of terpenoids and a qualitative change in their mixture in the bark tissues around the *S. cardinale* infection point (Achotegui-Castells et al., 2015, 2016).

Recently, Della Rocca et al. (2021) focused on infection-associated anatomical changes in the phloem of *C. sempervirens*. Specifically, the dynamic accumulation of polyphenolic parenchyma cells (PP cells) and the time course of phloem axial resin duct (PARD)-like structures that form during the initial phase of the infection were documented at the histological level using light microscopy. Notably, a faster and more intense reaction, from a quantitative point of view, occurred a few days after inoculation in a CCD-resistant cypress genotype compared to the susceptible one, in terms of the number of PP cells and PARD-like structures. Danti et al. (2018) showed that the host responses in terms of expression of suberin biosynthesis-related genes differ between bark wounding and bark wounding coupled with pathogen inoculation.

This work intends to increase the understanding of anatomical and cytological changes in the reaction in the bark tissues of common cypress induced by infection with the pathogen *S. cardinale*. Our study investigated the differentiation and genesis of PP cells and PARD-like structures through observations using Light (LM), Fluorescence (FM), and Transmission Electron Microscopes (TEM). Particular attention was paid to the synthesis of polyphenols in the PP cells and of resin in the PARD-like structures. LM investigations employed different dyes to clarify whether PARD-like structures actually synthesize terpenoids inside them and consequently can be considered as induced resin ducts.

MATERIALS AND METHODS

Plants and Stem Inoculation Procedures

The experimental setup was similar to that of Della Rocca et al. (2021). A canker-resistant clone of *C. sempervirens* (PM322, patented with the name "Bolgheri") from the IPSP-CNR clonal collection was used in this study. Forty-five 2-year-old ramets were grafted onto individual 1-year-old *C. sempervirens* seed rootstocks, grown in 4-liter pots containing a mixture of peat, compost, and perlite (3:1:1, v/v/v) under a shading tunnel. The *S. cardinale* isolate used for the stem inoculation was the same standard ATCC 38654 isolate adopted in Della Rocca et al. (2021). This isolate of the pathogen was grown on 2% PDA (Potato Dextrose Agar) Petri dishes for 14 days in the dark at 25 ± 0.7°C. Cypress ramets were stem inoculated in April 2019 following the cork-borer procedure described in Danti et al. (2014). At the beginning of the experiment, plants had a mean height of 80 ± 9 cm and a mean diameter of 1.4 ± 0.2 cm at the base of the stem. For LM, FM, and TEM observations, 30 out of 45 cypress plants were stem inoculated and 6 were only stem injured with the same cork borer (but without inserting the pathogen into the wounds), while 9 others were left intact (as controls).

Sampling and Sample Preparation

Transversal sections, 3–4 mm thick, were sampled from the stems of the 45 ramets of *C. sempervirens* (30 inoculated, 6 wounded + 9 intact) to observe anatomical and cytological changes occurring in the bark tissues (composed of cambium, phloem, and phellogen-derived tissues) after fungal infection or wounding. For TEM observations, sections were sampled at 2 mm (above and below) from the inoculation point (IP), 5 days after being inoculated, and 2 mm (above or below) from the developing external bark necrosis, 21 days after inoculation. For LM and FM viewing, sections were sampled 2 mm above or below the developing bark necrosis, 45 days after the inoculation. Stem sections were also sampled from the intact ramets (the controls) on those same days. The transversal sections used for LM and FM analysis were divided into four to five sectors, whose external part was then soaked in resin (see Section Light Microscope and Fluorescence Microscope Observations). Instead, the TEM-intended sections were processed following the indications in Section Transmission Electron Microscope Observations. Furthermore, from the wounded or inoculated ramets, fresh stem sections were sampled 5 cm from the wound

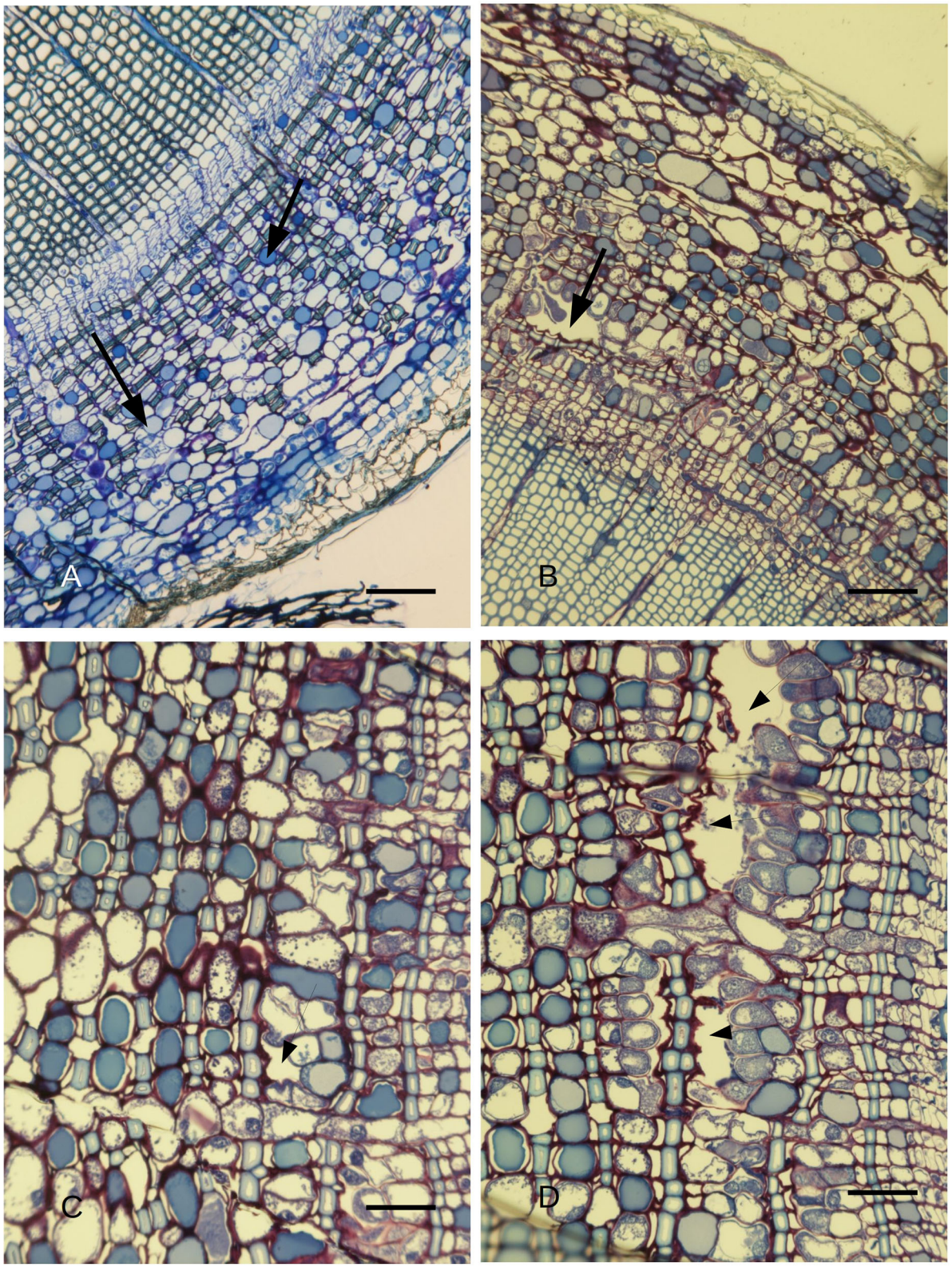

FIGURE 1 | (A) *C. sempervirens* secondary cross-section of an intact stem (control) observed *via* light microscope after toluidine blue staining. No PARD-like structures can be observed in the phloem, while PP cells (two of them indicated with arrows) are numerous. Bar = 50 μm. **(B)** *C. sempervirens* secondary stem cross-section sampled 14 days after the infection with *Seiridium cardinale* observed at LM after toluidine blue staining. A PARD-like structure is formed in the

(Continued)

FIGURE 1 | secondary phloem belt. Bar = 50 μm. **(C)** *C. sempervirens* secondary stem cross-section, cambium zone. Toluidine blue staining. A phloem element degenerated leaving a small cavity (arrow) between a sclerenchymatic fiber and an albuminous cell (asterisk). PP cells are stained in dark blue, while sclerenchymatic fiber walls are light blue. Bar = 50 μm. **(D)** *C. sempervirens* secondary stem cross-section, cambium zone, 12 days after image in **(C)**. Toluidine blue staining. The cavities (arrows) are increasing in dimension due to the degeneration of phloem elements leading to the formation of a PARD. The albuminous cells along the side of the PARD increase their toluidine blue positivity. Bar = 50 μm.

or the IP (above and below), 7 and 14 days after the artificial inoculation or wounding (see Section LM Observations of Fresh Sections for Anatomy Investigation and PARD Occurrence at a Distance From the IP or Wound) to verify the presence of PARD-like structures at a distance from the IP. From the inoculated ramets, 14 days after the inoculation, stem sections were also cut at the IP to verify the presence of the fungal hyphae in the bark tissues.

Light Microscope and Fluorescence Microscope Observations

For LM observations (45 days after inoculation), we used a Leitz DM-RB Fluo Light Microscope equipped with a digital Nikon DS-L1 camera. Cross-sections (one per ramet; six inoculated ramets + three intact) were fixed in FAA (formalin 4%, acetic acid 2%, and alcohol 70%) for 7 days at 4°C. The slides with the sections were washed in 70% alcohol for 2 h and dehydrated in an ethanol series of progressive concentrations (80, 95, and 100% ethanol) twice in each step. Pre-inclusions were done by mixing 100% ethanol and Technovit 7100 resin (Kulzer, Germany) 1:1, and then at a 1:2 ratio for 2 h in each step, at room temperature. Finally, the samples were soaked in a container with pure resin overnight. After 24 h of hardening, the samples were inserted inside sealed polypropylene capsules and embedded in a pure Technovit resin and hardener/catalyst (15:1 ratio) at room temperature. Slides of the resin including the stem were cut with a Heidelberg rotary ultramicrotome (Reichert-Jung OM U3) to produce semi-thin sections (4–6 μm).

These sections were then stained. Fluorol Yellow 088 was used to discern the presence of lipid material (Bundrett et al., 1991, as modified in Giuliani et al., 2020) within the lining cells of PARD-like structures to see whether lipid material had been secreted into the duct space/cavity. Sudan Red 7B (Lison, 1960) confirmed the presence of the fatty acid component of the resin. NADI staining was used to identify the presence of terpenoids (David and Carde, 1964); for this, we used fresh material and sections were produced with a cryostat at −20°C. Finally, we applied Toluidine blue black as a generic stain. However, the latter staining can be used at controlled pH to discriminate between phenols, lignin, cell walls, and resins thanks to metachromasy as reported by Ribeiro and Leitão (2020).

Transmission Electron Microscope Observations

For TEM observations (5 and 21 days after inoculations), we largely followed the method already described in detail in Mosti et al. (2013) and Papini et al. (2014). Stem sections (one per ramet; six inoculated ramets per sampling date + 3 intact as controls for each sampling date) of about 3 mm were fixed in 2.5% glutaraldehyde in 0.1 M phosphate buffer at pH 7.2 for 10 h (overnight) at 4°C. The samples were then post-fixed in 1% OsO4 in the same buffer for 1 h. Washing steps were executed after both the glutaraldehyde and the OsO4 steps. The samples were dehydrated in an ethanol series and then in propylene oxide, which was used to discriminate Spurr resin (Spurr, 1969) until the samples were embedded in pure resin. Subsequently, the samples were sectioned with an ultramicrotome (Reichert-Jung ULTRACUT E). Sections of about 70 nm were stained with uranyl acetate and lead citrate. These sections were then examined with a Philips 201 TEM at 80 kV. TEM was used to assess ultrastructural changes in the phloem's albuminous cells upon their transformation into PP cells and during the PARD-like structures' development. Particular attention was given to plastid and vacuole changes, the accumulation of polyphenols, and terpene production to fill the PARD-like structures.

LM Observations of Fresh Sections for Anatomy Investigation and PARD Occurrence at a Distance From the IP or Wound

Fresh transversal sections of stems (one per ramet; six inoculated ramets per two sampling dates + 3 wounded ramets per date) cut 5 cm above and 5 cm below the IP or the wound were also observed to verify the formation of PARD-like structures at a distance from the lesion (inoculation or wounding). Intact control ramets were not used in this assay, as the recent work by Della Rocca et al. (2021) evidenced the absence of constitutive PARD-like structures in the bark of *C. sempervirens* clones. Stem segments were sampled 7 and 14 days after the treatment (inoculation or wounding) to verify the occurrence of a signal at a distance from the point of inoculation or wound. Semi-thin sections (1–5 μm) were stained with aniline blue black. Samples were observed and digitally imaged with a Leica DMRB Fluo microscope. Three portions of each section were observed at a magnification of 100× for each sampling date (7 and 14 days) and for each of the three sampling sites (IP or wound, 5 cm above the IP or wound, and 5 cm below the IP or wound). For each portion, three pictures were taken to include the cambium (placed parallel to the X-axis) and the number of PARD-like structures (regardless of their developmental phase) was counted.

Statistics

Differences in the number of PARD-like structures counted in the fresh stem sections of *C. sempervirens* ramets at the IP or wound and at 5 cm distance (above and below) after 7 and 14 days were analyzed by one-way ANOVA to evaluate the host's reaction at a distance from the stimulus at different times. Differences among means were compared using Tukey's honestly significant difference (HDS) *post-hoc* test for $p < 0.05$ using STATISTICA 10.0 software.

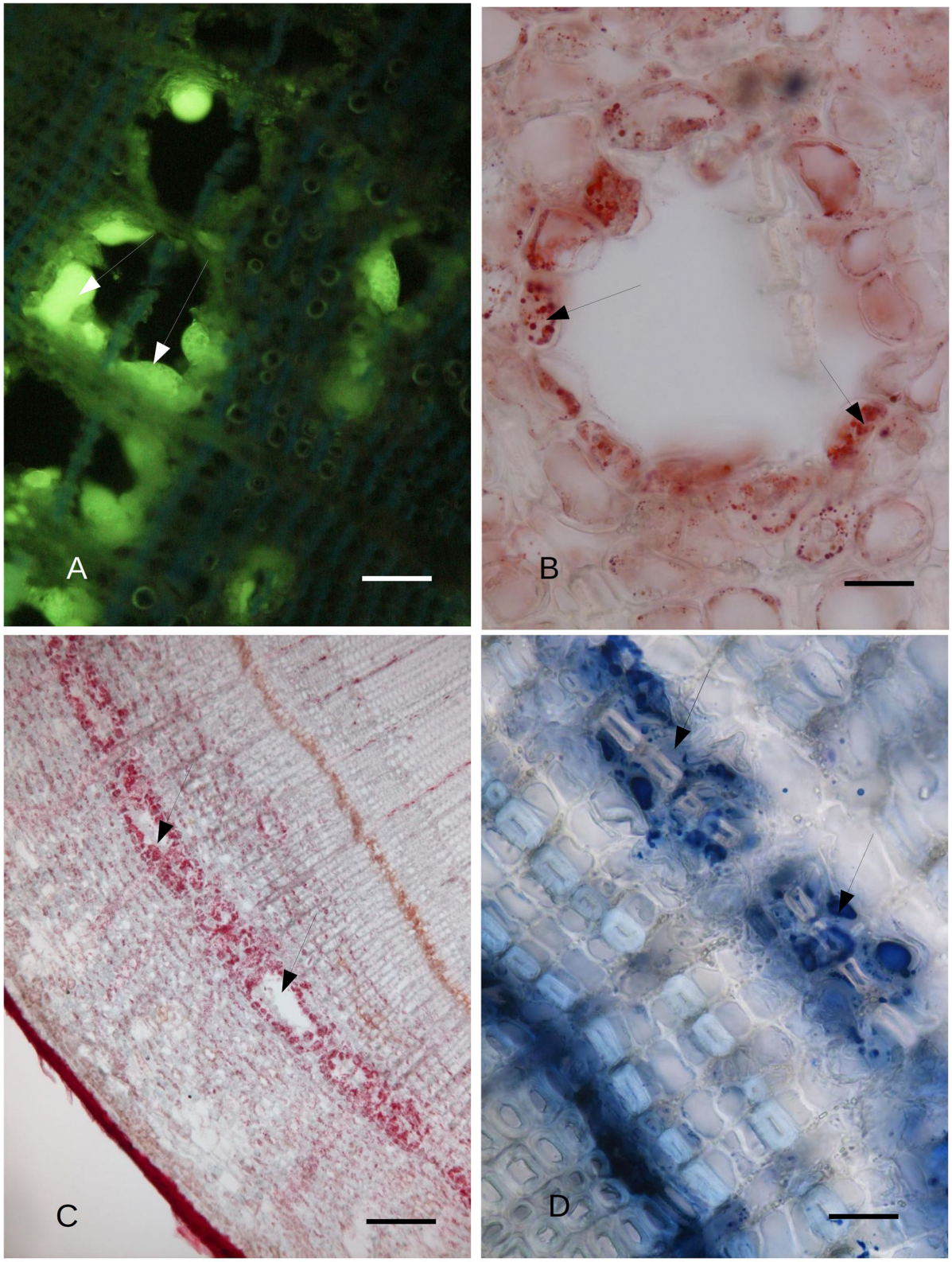

FIGURE 2 | (A) *C. sempervirens* secondary stem cross-section 2 mm from the necrotic lesion caused by the *Seiridium cardinale* fungal pathogen. Bark tissues near the cambium zone were stained with Fluorol Yellow, 45 days after inoculation with the fungal pathogen, as observed by FM. The cells surrounding the cavities of the PARD-like structures react intensely to Fluorol Yellow (arrows), thus showing their lipophilic content. Bar = 40 μm. **(B)** Detail of the cross-section of a PARD-like

(Continued)

FIGURE 2 | structure stained with Sudan red. The cells lining a lacuna react with Sudan red, showing a lipophilic content in droplets. Bar = 20 μm. **(C)** Cavities (arrows) formed by the fusion of multiple PARD-like structures along the cambium in *C. sempervirens* 45 days after artificial inoculation with *S. cardinale*. The stem cross-section was cut 2 mm above the necrotic lesion caused by the fungal pathogen. The cells lining the cavities are strongly positive for Sudan red. Bar = 100 μm. **(D)** The highest NADI positivity was around the forming PARD-like structures (arrows) along the cambium in a stem cross-section of *C. sempervirens* 45 days after artificial inoculation with *S. cardinale*. The newly generated PARD-like structure is still subdivided into two cavities by a sclerenchymatic fiber. The stem section was cut 2 mm above the necrotic lesion induced by the pathogen. Bar = 40 μm.

RESULTS

Anatomy at IP and PARD-Like Structure Formation at a Distance From IP (LM)

At low magnification, a comparison between a secondary intact stem section (**Figure 1A**) and a stem section sampled from an inoculated stem 14 days after infection (**Figure 1B**) showed that the latter had formed a PARD-like structure, while the former was lacking these structures in the phloem. After 7 days from the artificial inoculation with the pathogen, well-developed PARD-like structures were equally observed in stem sections at the IP as well as at 5 cm above and below the IP, with no significant differences in their number between the three sampling points (4.8, 5, and 4.3 PARD-like structures averaged for each picture, respectively). Similarly, PARD-like structures were also observed in wounded ramets, but they were significantly fewer ($p < 0.05$) than in the inoculated ones after 7 days (3.7, 3.3, and 3.5 PARD-like structures on average for each picture at IP, 5 cm over, and 5 cm below the IP, respectively). At 14 days, the number of PARD-like structures was the same as after 5 days in both inoculated or wounded ramets. The formation of PARD-like structures occurred starting with the degeneration of phloem elements between the two rows of sclerenchymatic fibers (**Figure 1C**). Since, between two rows of sclerenchymatic fibers, there are two rows of phloem elements separated by an albuminous cell (**Figure 3**), the degeneration of the phloem element leaves a small cavity. This later grows as the nearby phloem elements continue to disintegrate (**Figure 1D**). Moreover, the albuminous cells adjacent to the PARD-like structure increased their toluidine blue positivity.

PARD-Like Structures: Evidence of Resin Secretion (LM and FM)

The cypress stem sections cut just above and below the pathogen-induced bark necrosis at 45 days after inoculation were stained with Fluorol Yellow; these showed the presence of lipid/lipophilic material within large lacunae of the PARD-like structure in the secondary phloem layer (**Figure 2A**). Part of the Fluorol Yellow positivity was inside the cavity. This result was confirmed by Sudan red staining (**Figures 2B,C**). Sudan red positivity was due to the presence of small particles inside the cells surrounding the cavity (**Figure 2B**). Furthermore, a discontinuous circle of cavities formed around the lacunae outside the cambium (**Figure 2C**). NADI reagent showed that the lipidic material inside the cavities and the cells surrounding the cavity contained terpenoids (**Figures 2D**, **3A**). In **Figure 2B**, the lacuna also contained NADI-positive material and was divided by one sclerenchymatic fiber. The NADI-positive cavities (**Figure 3A**) generally were in the same position as the Sudan red positive cavities seen in **Figure 2C**. The same NADI-positive material also exhibited autofluorescence with UV blue light (**Figure 3B**).

Observations *via* Transmission Electron Microscope

Due to the results obtained with LM, we focused our attention on the ultrastructure of the albuminous cells and the surrounding cells at 5 and 21 days after inoculation (compared to the control and uninoculated plants). Before the infection with *S. cardinale*, the albuminous cells showed plastids with apparently functional thylakoid apparatus containing plastoglobules, whose crystals were forming in the cell wall (**Figure 3C**). The formation of PP cells began with the accumulation of very dense material along the tonoplast of the large vacuole (**Figure 3D**). The nucleus showed condensed chromatin and the plastids contained large granules of starch, while the thylakoid apparatus was arranged in small grana (**Figure 3D**), which were smaller and less organized than those in the albuminous cell seen in **Figure 3C**. Some peroxisomes were visible near the plastids (**Figure 3D**). Five days after the inoculation, the thence-formed PP cells showed vacuoles with abundant electron-dense material along the tonoplast and granular material inside the vacuolar space, while the nucleus seemed to be less active and electron dense (**Figure 4A**) compared to the albuminous and parenchyma cells. In the albuminous cells, for example, the plastids were at the periphery, touching the peroxisomes and mitochondria (**Figure 4B**). Twenty-one days after inoculation, the PARD-like structures (corresponding to the cavities observed with LM) appeared partially occupied by cellular remnants (in particular, cell walls) and granular material (**Figure 4C**). Epithelial cells (around the PARD-like structure) were almost completely occupied by small to medium gray bodies with granular content, apparently derived from small vacuoles, together with even smaller vacuoles with electron transparent content (**Figure 4D**). Also, a larger vacuole was present (**Figure 4D**). The most easily recognizable organelles were mitochondria, which showed rarefied cristae and were arranged around the gray bodies (**Figure 4D**). The plasma membrane appeared detached from the wall at some points (**Figure 4D**). At a later stage, in the epithelial cells, the plastids began to degenerate, losing almost completely their thylakoids, forming internal lipid bodies and granular material (**Figure 5A**). They entered into contact with vacuoles approximately the same size as the plastid, while endoplasmic reticulum (ER) elements began to surround them (**Figure 5A**). In other cells, apparently at a yet later stage of development and secretion, most organelles were no longer recognizable individually in the cytoplasm. Roundish gray bodies formed close to the cell wall and were surrounded by ER (**Figure 5B**). At an even later stage, the PARD-like structure began to fill

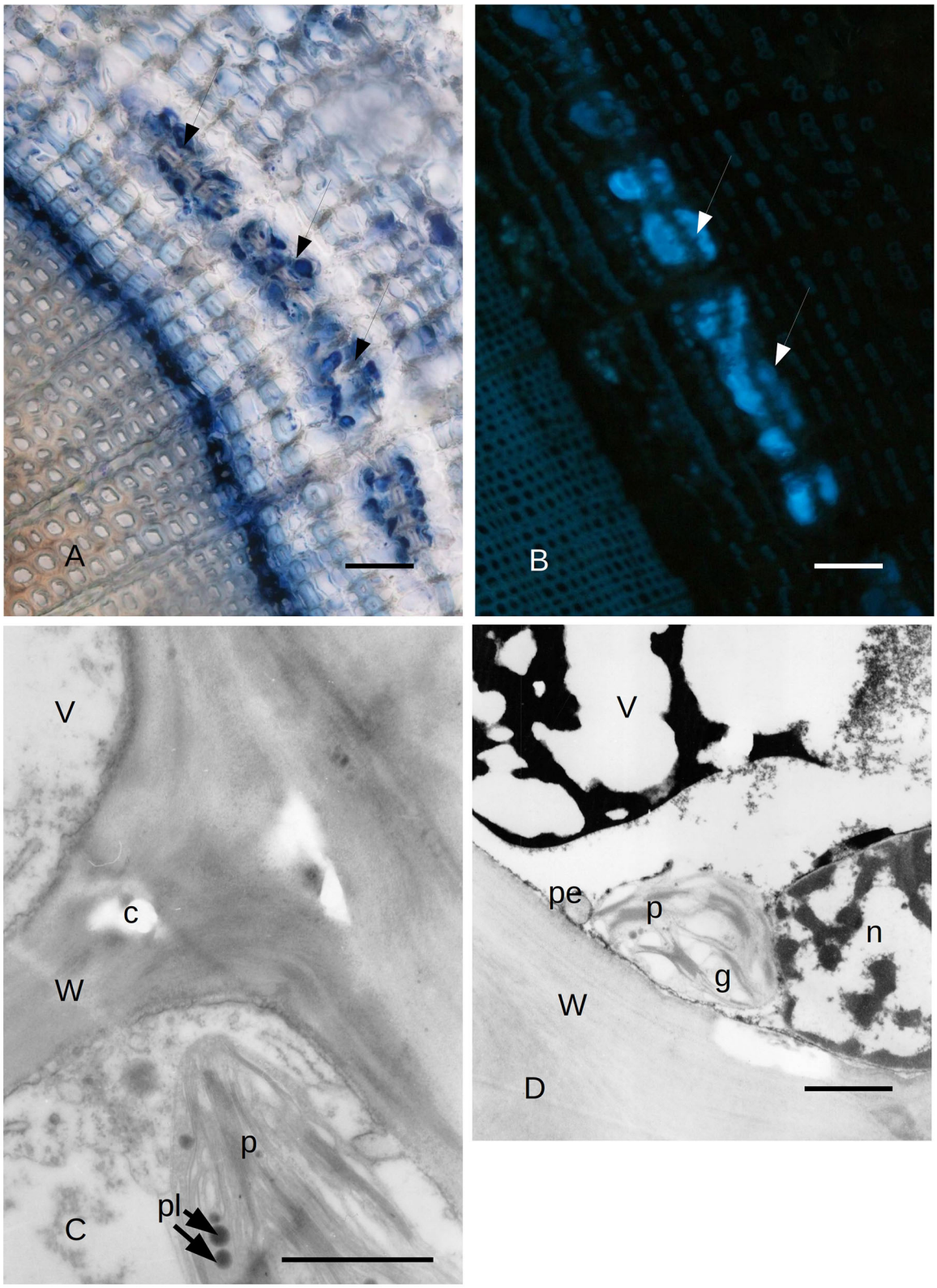

FIGURE 3 | (A) Bark tissues near the cambium zone of *C. sempervirens* secondary stem cross-section, 2 mm from the necrotic lesion developed by the fungal pathogen *S. cardinale* 45 days after artificial inoculation. The NADI positive cells (arrows) are in the same position as those positive to Sudan red in **Figure 5**. Bar = 80 μm. **(B)** Autofluorescent material emitting blue UV light inside the same cells and cavities that were NADI positive in **Figure 2**. Bark tissues near the cambium zone

(Continued)

FIGURE 3 | of *C. sempervirens* (secondary stem cross-section) cut 2 mm from the necrotic lesion developed by the fungal pathogen *S. cardinale* 45 days after artificial inoculation. Bar = 100 μm. **(C)** TEM image of *C. sempervirens* bark tissues of control plants (intact). The albuminous cells in the secondary phloem show active plastids (p) and some plastoglobules (pl). Some crystals (c) are forming in the wall (W) (V, vacuole). Bar = 1 μm. **(D)** TEM image of cross-section of *C. sempervirens* bark tissues of intact plants (controls) (V, vacuole; g, starch granule; n, nucleus; W, cell wall). PP cell in the secondary phloem; a chloroplast (p) appears still active and near peroxisome (pe). Polyphenols are forming inside the vacuole. Bar = 1 μm.

with granular material, while the walls separating different cells forming the PARD-like structure began to collapse (**Figure 5C**). Gray material started forming within the organelles of the epithelial cells, but then was found free in the cytoplasm, and finally outside the epithelial cell in the lumen of the PARD-like structure (**Figure 5D**).

DISCUSSION

This work investigated the genesis and the evolution of PP cells and PARD-like structures in *Cupressus sempervirens* in the phloem tissues after inoculation with the fungal bark pathogen *S. cardinale*. Their developments were examined at intervals, from 7 to 45 days after infection with the pathogen, at both anatomical and cytological levels *via* LM, FM, and TEM using different dyes and techniques. In Della Rocca et al. (2021), the involvement of both PARD-like structures and PP cells in the response of *C. sempervirens* to the necrotrophic bark pathogen *S. cardinale* had been found in both canker-resistant and -susceptible clones. This study evidenced a faster phloem response of the canker-resistant clone in terms of the number of PP cells and PARD-like structures formed 5 and 12 days after infection compared to the susceptible clone.

Resin production is one of the main mechanisms of defense in conifers (Krokene et al., 2008a). Conifer oleoresin is a complex mixture of volatile mono- (C10) and sesquiterpenes (C15), as well as non-volatile diterpene and resin acids. It accumulates at the wound site to counteract invaders (insects and fungi) in several ways: through some antimicrobial activity, by flushing the wound, and by sealing the injury (Phillips and Croteau, 1999; Trapp and Croteau, 2001; Zulak and Bohlmann, 2010).

As reported in Krokene et al. (2008a), *Cupressaceae* do not have pre-formed resin structures, while induced structures appear following a stimulus to the xylem (*Sequoia*, *Sequoiadendron*, *Metasequoia*) or the phloem (*Cupressus*, *Hesperocyparis*, *Chamaecyparis*, *Cryptomeria*). *C. sempervirens* develops PARD-like structures as a reaction to the infection of the bark canker agent *S. cardinale* (Moriondo, 1972; Ponchet and Andreoli, 1990; Della Rocca et al., 2021); its main external symptom is more or less intense resinosis by the cankered bark (Danti et al., 2013a). Although the association between resinosis and infection by pathogenic fungi has been reported (Madar et al., 1995; Spanos et al., 1999; Achotegui-Castells et al., 2015, 2016; Danti et al., 2018), the recent work by Della Rocca et al. (2021) has not definitively clarified the resin production site, perhaps because of the short duration of the experiment. For this reason, one of the goals of this research was to investigate in depth the hypothesis that PARD-like structures are the true sites where resin is produced by the host, whether as a reaction to a fungal pathogen invading the bark tissues or to wounds. Our observation, at first, indicated a quick reaction by the host to the infection/wound signal, after only 7 days from the injury stimulus. The PARD-like structures were produced not only at the IP but also 5 cm above and below the inoculation/wound point, thereby showing a "signal speed" of almost 1 cm per day (at least in the first phase of the stimulus). This is the first case reported of phloematic resin structure being remotely induced in the first days after a "traumatic event" (either pathogen infection or wound) in *Cupressaceae*. The presence of resin ducts in *C. sempervirens* barks affected by *S. cardinale* was previously observed in various works (Moriondo, 1972; Ponchet and Andreoli, 1990; Spanos et al., 1999; Achotegui-Castells et al., 2015, 2016; Danti et al., 2018). Madar and Liphschitz (1989) also reported the formation of traumatic resin ducts in *C. sempervirens* bark upon challenge by *S. cardinale* and *Diplodia cupressi*. The formation of resin ducts in the bark after fungal inoculation was also reported in *C. obtusa* (Yamanaka, 1989; Suto, 1998; Kusumoto and Suzuki, 2003; Fujii et al., 2018) and in *C. macrocarpa*, *Cryptomeria japonica*, *Sequoiadendron giganteum,* after stem treatment with methyl jasmonate (Hudgins and Franceschi, 2004). However, none of these studies reported the formation of traumatic resin ducts in the bark at a distance from the inoculation or wounding site.

Regarding the rapidity of the formation of phloematic resin ducts upon a traumatic event, a timing similar to that observed on *C. sempervirens* in this work is that reported for *C. obtusa* by Yamanaha (1989) and by Kusumoto and Suzuki (2003). In these two studies, the presence of phloematic resin structures was observed 7–15 days after wounding. All the other studies do not allow a direct comparison because they were not based on time series observations but on the detection of phloem resin ducts after arbitrary intervals of time, after infection, wounding, or treatment with methyl jasmonate. In this study, a lower number of PARD-like structures was also observed in the wounded ramets compared to the inoculated ones. Similar results were obtained by Luchi et al. (2005) in *Pinus nigra,* although in that case, they were xylematic traumatic resin ducts (TRDs). In that study, the non-aggressive fungal canker agent, *Diplodia scrobiculata,* artificially inoculated into the stem, induced in 12 days a higher number of TRDs per surface unit compared to those caused by mock inoculations (with sterile agar). In addition, Luchi and fellow authors observed that TRD numbers declined as the sampling distance increased from the IP. One might however speculate that the anatomical modifications (i.e., the induction of resiniferous structures) at the phloematic level (as in *C. sempervirens*) might be a little faster than at the xylematic level (as in *Pinus nigra*). The remote induction of TRDs has been also observed in *Picea abies* by Franceschi et al. (2000), Nagy

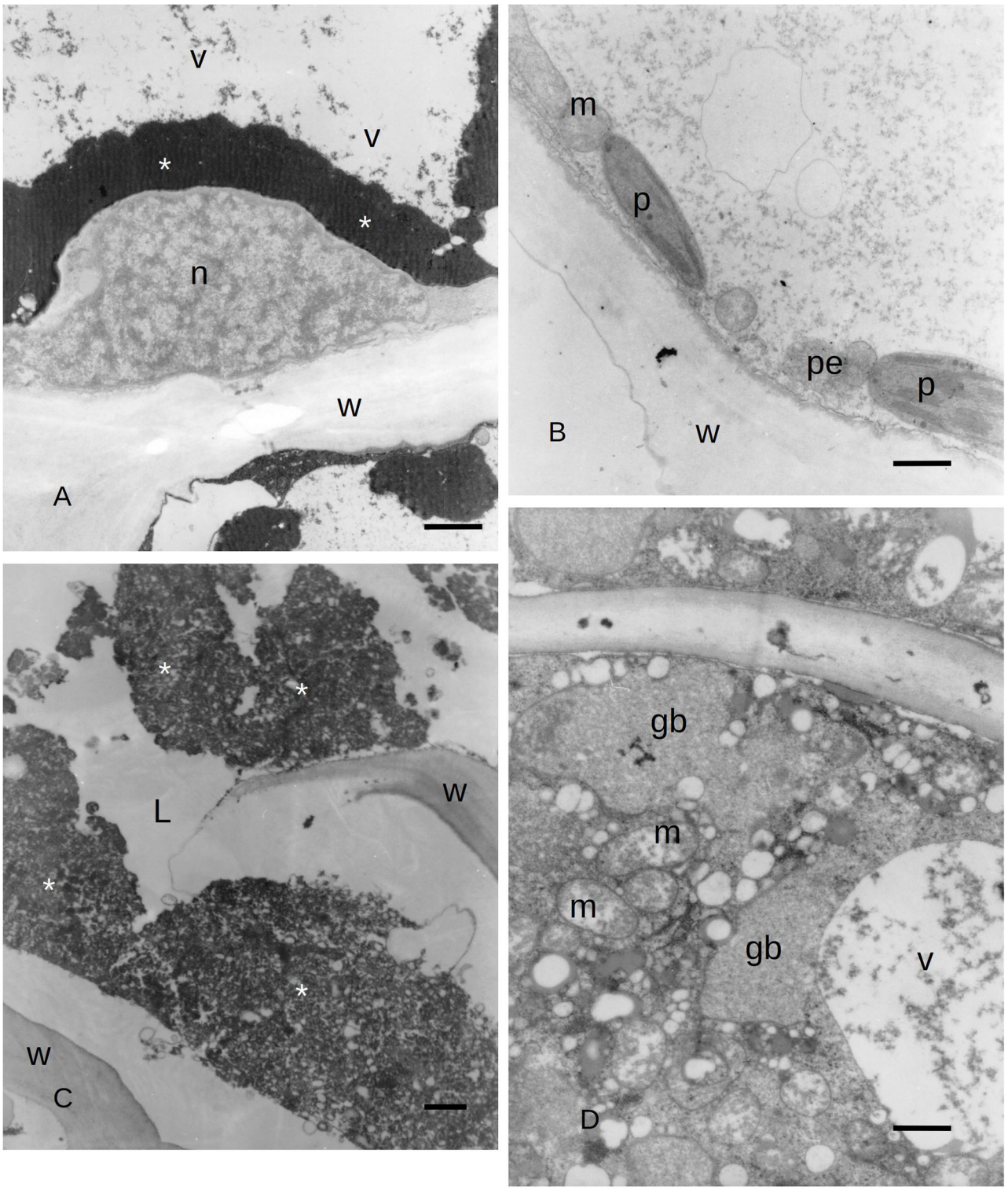

FIGURE 4 | (A) TEM image of PP cells with polyphenols inside (asterisks) the secondary phloem of *C. sempervirens* 5 days after infection with the fungal pathogen *S. cardinale*. (V, vacuole; n, nucleus; W, cell wall) Bar = 1 μm. **(B)** TEM image of an albuminous cell with active plastids (p) near mitochondria (m) and peroxisomes (pe) in the secondary phloem of *C. sempervirens* 5 days after infection with the fungal pathogen *S. cardinale*. (W, cell wall) Bar = 1 μm. **(C)** TEM image of a PARD-like structure with the lumen (L) partially occupied by granular material (asterisks) and remnants of cell walls in bark tissues of *C. sempervirens* 21 days after inoculation with *S. cardinale* (W, cell wall) Bar = 1 μm. **(D)** TEM image of *C. sempervirens* bark tissues 21 days after infection with the pathogen *S. cardinale*. Detail of the epithelial cell of a PARD-like structure with active mitochondria (m) and vacuoles (v) filled with granular material (gb, gray body) Bar = 1 μm.

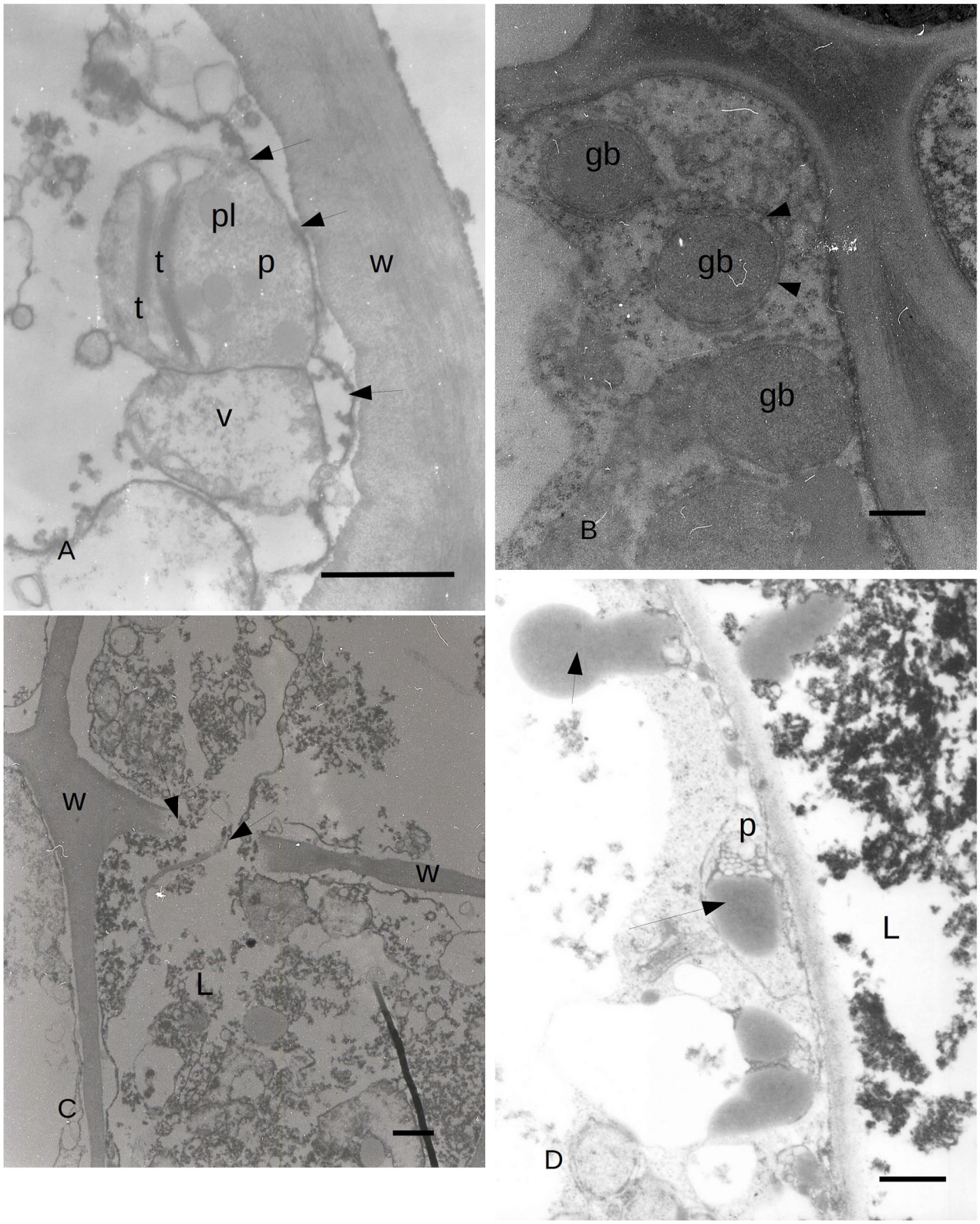

FIGURE 5 | (A) TEM image of *C. sempervirens* bark tissues 21 days after infection with the pathogen *S. cardinale*. PARD-like structure epithelial cells. Plastid (p) degeneration with few thylakoids (t) still intact, with lipid bodies and granular material. Vacuoles (V) are in contact with the plastid, while ER elements (arrows) begin to surround them (W, cell wall; pl, plastoglobules) Bar = 1 μm. **(B)** TEM image of PARD-like structure in *C. sempervirens* bark tissues 21 days after infection with the

(Continued)

FIGURE 5 | pathogen *S. cardinale*. Detail of the epithelial cell with gray bodies (gb) surrounded by endoplasmic reticulum (arrows) and ribosomes as gray dots in the cytoplasm. Bar = 1 μm. **(C)** TEM image of *C. sempervirens* bark tissues 21 days after infection with the pathogen *S. cardinale*. Mature PARD-like structure and activity of the epithelial cell. PARD-like structures are merging, while the wall fractures (arrows) (W, cell wall; L, lumen) Bar = 1 μm. **(D)** TEM image of *C. sempervirens* bark tissues 21 days after infection with the pathogen *S. cardinale*. Production and extrusion of gray material (arrows) from the epithelial cell into the PARD-like structure lumen (L) (p, plastid) Bar = 500 nm. Gb, gray bodies; L, lumen; p, plastid; pl, plastoglobule; t, thylakoid; V, vacuole; W, cell wall.

et al. (2000) and Krekling et al. (2004). Surprisingly, the serious canker agent *Sphaeropsis sapinea* was unable to induce TRD in the xylem of *P. nigra* (Luchi et al., 2005). This might indicate that the induction of TRDs may be a result of a transmittable signal that may relate to perception by the host of fungus or fungal activity.

Due to the degeneration of some phloem elements and ray parenchyma, in this study, we also observed, 45 days after inoculation, a sort of tangential coalescence of neighboring PARD-like structures, which thus formed larger cavities. Coalescence of neighboring PARD-like structures had already been described by Suto in *Chamaecyparis obtusa* 1 month after inoculation with the fungal pathogen *Cistella japonica* (2005). A similar process was found in *Thuja plicata* by Cleary and Holmes (2011), although with the difference that in *T. plicata,* elliptical zones of phellem-like cells in degeneration and necrosis were observed around the longitudinal phloematic resiniferous ducts, which does not occur in the phloem of *Cupressus*.

During the activity of PARD-like epithelial cells, different phases could be observed at the same moment in adjacent cells, which showed a different electron-dense cytoplasm. The increased electron density was probably due to a greater number of ribosomes involved in protein synthesis. Similarly, in *Picea abies,* the epithelial cells of xylem TRD exhibited a greater cytoplasmic density, a high number of plastids, and enlarged nuclei, as observed by Nagy et al. (2000). Apart from the vacuole, the organelle mostly involved in the synthesis of terpenes was the chloroplast which was almost surrounded by a smooth ER; therefore, the formation of terpenes was to be related to the interaction between chloroplast and endoplasmic reticulum. The produced terpenes tended to get out of the cytoplasm by passing through the plasmalemma apparently without the need for specific transport mechanisms. Terpenes in the form of gray bodies were also observed between the plasmalemma and epithelial cell wall. We propose here a possible model of terpenoid formation (**Figure 6**) starting from plastids, with four sequential stages (**Figures 6A–D**), based on the observation of gray bodies *via* TEM. The involvement of the ER in the modification of terpenes had already been proposed by Berthelot et al. (2012), even if without any evidence of an ER-plastid spatial colocalization, while Mehrshahi et al. (2013) showed the importance of ER in modifying the terpenoid tocopherol (with fatty acid desaturation) produced by chloroplasts. The constant presence of mitochondria even in the advanced stages of PARD-like epithelial cell maturation shows that the production of terpenes is an active mechanism that occurs with ATP consumption. Finally, in PARD-like structures, there are also cellular residues derived from the degeneration of fibers and phloem cells, that are being lysed to allow the enlargement of the PARD-like structure lumen *via* wall digestion. The involvement of mitochondria in the last phases of PCD, in general, and in plants, in particular, has been often observed as a consequence of an active PCD process (Adrain and Martin, 2001; Yao et al., 2004; Brighigna et al., 2006).

The content of the PARD-like structure in *C. sempervirens* was confirmed to be lipophilic (*via* Sudan red and Fluorol Yellow positivity) and more specifically composed of terpenoids, as showed by NADI staining positivity and the autofluorescence with UV leading to blue light emission, which may be due to diterpenes and/or oleoresins (Donaldson and Williams, 2018; Donaldson, 2020). About the nature of the terpenes contained in the PARD-like structure, Li et al. (2021) tried to link a specific intensity of NADI staining to a particular class of molecules belonging to terpenes. The topic has not yet been well explored, however, in *Cupressus*, the NADI staining intensity here observed in the PARD-like structures appeared to be more similar to that corresponding to terpenes similar to (E)-β-farnesene found in pyrethrum, even if the exact identification of the specific molecule is not possible with histochemistry.

The PP cells have been identified as another form of defense of *C. sempervirens* as well as a potential proxy of resistance to CCD (Della Rocca et al., 2021), demonstrating that in *C. sempervirens*, new PP cells can originate from albuminous cells through the accumulation of phenolic substances in the vacuole, as noted by Fahn (1990), Krekling et al. (2000), and Krokene et al. (2008b) in *Picea abies*. Their origin, however, had never been investigated before at an ultrastructural level. Although Della Rocca et al. (2021) observed a decrease of PP cells during the formation of the PARD-like structures, probably because some PP cells had lost their vacuolar polyphenol content, similarly to what was observed in *Picea abies* by Nagy et al. (2000). In our study, we observed a few albuminous cells starting a differentiation process 5 days after infection, and then forming what would then become the PARD-like epithelial cells. These cells were very active, with some rounded plastids that formed intra-plastid lipid bodies. Other albuminous cells showed polyphenol accumulations in the middle of the vacuole. TEM observations clarified the ultrastructure of the PP cells in *C. sempervirens*, better distinguishing their genesis. The albuminous cells exhibited low electron-dense cytoplasm; the plastids were located at the periphery of the cytosol, in contact with peroxisomes and mitochondria. In these cells, the plastids were particularly active, showing thylakoids arranged into grana, more plastoglobules (defined as in Van Wijk and Kessler, 2017), and with less accumulated starch compared to PP cells during formation. The constitutive PP cells showed a large vacuole that occupied almost the entire cell volume in which electron-dense material was identified as polyphenols.

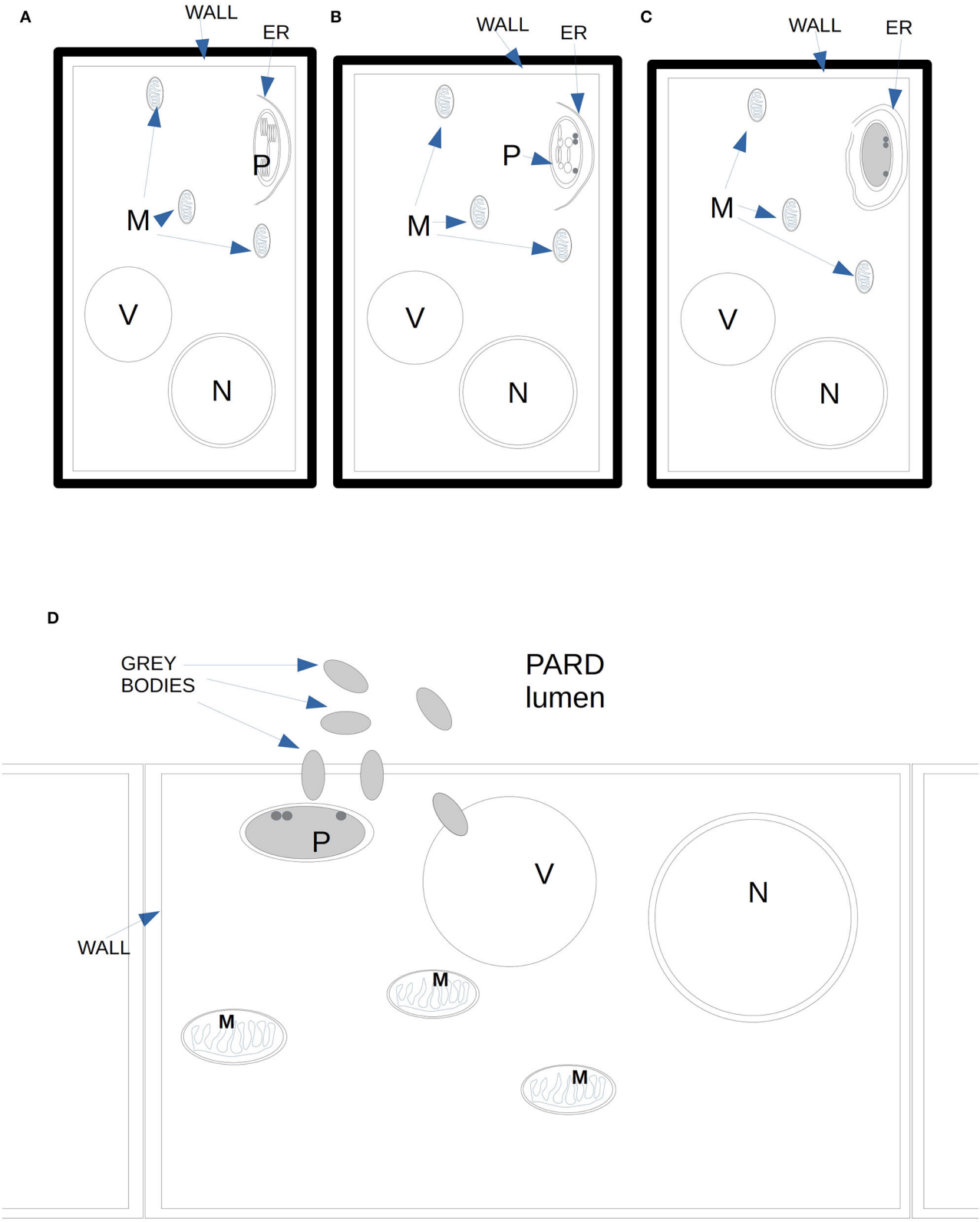

FIGURE 6 | Diagram of the proposed four stages of gray bodies development in an epithelial cell bordering the PARD lumen. **(A)** Close to the plasma membrane on the side of the PARD lumen, a plastid with normal thylakoids starts to enter in contact with ER elements. **(B)** In the plastid, the thylakoids reduce in number and tend to dilate the margins of their cisternae. **(C)** The ER surrounds almost completely the plastid whose stroma is filled with granular content. Some darker globules can be observed on the side of the plasma membrane. No thylakoid is visible anymore. **(D)** Gray bodies start to cross the plastid membranes and even the plasma membrane, ending finally in the PARD lumen.

In the periphery of these cells, the cytoplasm was very dense and we recognized dictyosomes (whose function is to secrete vesicles, which generally contain carbohydrates or glycoproteins, often outside the cell) and plastids with plastoglobules. Plastids are involved in the production of polyphenol precursors, and the key enzyme of their biosynthesis has been localized on the chloroplast starch granules (Grundhöfer et al., 2001). TEM observations showed that the plastids observed in the PP cells of the common cypress contained large starch granules, similarly to what Krekling et al. (2000) observed in PP cells of *Picea abies*. The same authors also detected the presence of lipids, hypothesizing that both compounds constituted an energy reserve for a rapid synthesis of defense compounds (Krokene et al., 2008a). Within PP cells, some peroxisomes, probably involved in lipid metabolism, were also visible. The newly induced PP cells showed vacuoles with a higher electron density and granular material inside compared to the constitutive PP cells. In more advanced stages of maturation, instead, PP cells showed an increased amount of polyphenols in the vacuoles, suggesting that the host defense response against the infection could be related to the total quantity of polyphenols accumulated around the affected area.

CONCLUSIONS

In *C. sempervirens,* both PP cells and resins producing cells in PARD structures can be induced as a response to an attack by a pathogen. Both these cell types develop out of albuminous or parenchyma cells in the secondary phloem layer of the stem's secondary structure.

Plastids appear to be involved in the development of the PP cells, with a phase of starch accumulation and a later stage in which the majority of the cells are filled by a vacuole almost completely occupied by polyphenols.

The resin-producing cells surrounding the PARDs secrete terpenoids toward a large lumen formed by programmed cell death of albuminous cells and parenchyma cells around sclerenchymatous fibers. Terpenoids are produced inside the cells after the ER surrounds the plastids, then the secretion occurs directly through the plasma membrane toward the lumen.

This study showed the production of terpenoids in the lining cells surrounding the lumens which formed in the phloem of *C. sempevirens* following both infections with *S. cardinale* or mechanical injury. These findings suggest that the structures previously defined as PARD-like can be considered traumatic resin ducts of the bark (BTRD).

DATA AVAILABILITY STATEMENT

The raw data supporting the conclusions of this article will be made available by the authors, without undue reservation.

AUTHOR CONTRIBUTIONS

GD, AP, and RD conceived the idea and designed the methodology. CT and AP performed the microscope observations. SB and IP carried out the inoculations, sampling, and preparation of samples for microscope observations. GD, AP, RD, SB, and SM analyzed the data and wrote the manuscript. All authors contributed critically to the drafts and gave final approval for publication.

REFERENCES

Achotegui-Castells, A., Danti, R., Llusià, J., Della Rocca, G., Barberini, S., and Peñuelas, J. (2015). Strong induction of minor terpenes in Italian Cypress, *Cupressus sempervirens*, in response to infection by the fungus *Seiridium cardinale*. *J. Chem. Ecol*. 41, 224–243. doi: 10.1007/s10886-015-0554-1

Achotegui-Castells, A., Della Rocca, G., Llusià, J., Danti, R., Barberini, S., Bouneb, M., et al. (2016). Terpene arms race in the *Seiridium cardinale–Cupressus sempervirens* pathosystem. *Sci. Rep*. 6, 18954. doi: 10.1038/srep18954

Adrain, C., and Martin, S. J. (2001). The mitochondrial apoptosome: a killer unleashed by the cytochrome seas. *Trends Biochem. Sci*. 26, 390–397. doi: 10.1016/S0968-0004(01)01844-8

Berthelot, K., Estevez, Y., Deffieux, A., and Peruch, F. (2012). Isopentenyl diphosphate isomerase: a checkpoint to isoprenoid biosynthesis. *Biochimie*. 94, 1621–1634. doi: 10.1016/j.biochi.2012.03.021

Brighigna, L., Milocani, E., Papini, A., and Vesprini, J. L. (2006). Programmed cell death in the nucellus of Tillandsia (Bromeliaceae). *Caryologia* 59, 334–339. doi: 10.1080/00087114.2006.10797935

Bundrett, M. C., Kendrick, B., and Peterson, C. A. (1991). Efficient lipid staining in plant material with fluorol yellow 088 in polyethylene glycol-glycerol. *Biotech. Histochem*. 66, 111–116. doi: 10.3109/10520299109110562

Cleary, M. R., and Holmes, T. (2011). Formation of traumatic resin ducts in the phloem of western redcedar (*Thuja plicata*) roots following abiotic injury and pathogenic invasion by Armillaria ostoyae. *IAWA J.* 32, 351–359. doi: 10.1163/22941932-90000063

Danti, R., Barberini, S., Pecchioli, A., Di Lonardo, V., and Della Rocca, G. (2014). The epidemic spread of *Seiridium cardinale* on Leyland cypress severely limits its use in the Mediterranean. *Plant Dis*. 98, 1081–1087. doi: 10.1094/PDIS-12-13-1237-RE

Danti, R., and Della Rocca, G. (2017). Epidemiological history of cypress canker disease in source and invasion sites. *Forests* 8, 1–25. doi: 10.3390/f8040121

Danti, R., Della Rocca, G., Di Lonardo, V., Pecchioli, A., and Raddi, P. (2011). "Genetic improvement program of cypress: Results and outlook," in *Status of the Experimental Network of Mediterranean Forest Genetic Resources*, eds. Besacier, C., Ducci, F., Malagnoux, M., and Souvannavong, O. (Silva Mediterranea, Rome: CRA SEL, Arezzo and FAO), 88–96.

Danti, R., Della Rocca, G., and Panconesi, A. (2013a). "Cypress canker," in *Infectious Forest Diseases*, eds. P. Gonthier and G. Nicolotti (Wallingford, CT; Oxfordshire; Boston, MA: CABI), 359–75. doi: 10.1079/9781780640402.0359

Danti, R., Di Lonardo, V., Pecchioli, A., and Della Rocca, G. (2013b). 'Le Crete 1' and 'Le Crete 2': two newly patented *Seiridium cardinale* canker-resistant cultivars of *Cupressus sempervirens*. *For. Pathol*. 43, 204–210. doi: 10.1111/efp.12016

Danti, R., Raddi, P., Panconesi, A., Di Lonardo, V., and Della Rocca, G. (2006). "Italico" and "Mediterraneo": two *Seiridium cardinale* canker resistant cypress cultivars of *Cupressus sempervirens*. *Hortsci*. 41, 1357–1359. doi: 10.21273/HORTSCI.41.5.1357

Danti, R., Rotordam, M. G., Emiliani, G., Giovannelli, A., Papini, A., Tani, C., et al. (2018). Different clonal responses to cypress canker disease based on transcription of suberin-related genes and bark carbohydrates' content. *Trees*. 32, 1707–1722. doi: 10.1007/s00468-018-1745-5

David, R., and Carde, J. P. (1964). Coloration differentielle des inclusions lipidiques et terpeniques des pseudophylles du Pin maritime on moyen du reactif Nadi. *Comptes Rendus de l'Academie des Sciences Paris* 258, 1338–1340.

Della Rocca, G., Danti, R., and Raddi, P. (2007). *Le specie di cipresso nel mondo*. Firenze: CNR-IPP.

Della Rocca, G., Danti, R., Williams, N., Eyre, C., and Garbelotto, M. (2019). Molecular analyses indicate that both native and exotic pathogen populations serve as sources of novel outbreaks of Cypress Canker Disease. *Biol. Invasions*. 21, 1–14. doi: 10.1007/s10530-019-02022-9

Della Rocca, G., Eyre, C. A., Danti, R., and Garbelotto, M. (2011). Sequence and simple-sequence repeat analyses of epidemic for the Mediterranean region. *Phytopathol*. 101, 1408–1417. doi: 10.1094/PHYTO-05-11-0144

Della Rocca, G., Osmundson, T., Danti, R., Doulis, A., Pecchioli, A., Donnarumma, F., et al. (2013). AFLP analyses of California and Mediterranean populations of *Seiridium cardinale* provide insights on its origin, biology and spread pathways. *For. Path*. 43, 211–221. doi: 10.1111/efp.12019

Della Rocca, G., Posarelli, I., Morandi, F., Tani, C., Barberini, S., Danti, R., et al. (2021). Different polyphenolic parenchyma cell and phloem axial resin duct-like structures formation rates in *Cupressus sempervirens* clones infected with *Seiridium cardinale*. *Plant Dis*. 105, 2801–2808. doi: 10.1094/PDIS-01-21-0098-RE

Donaldson, L. (2020). Autofluorescence in plants. *Molecules* 25, 2393. doi: 10.3390/molecules25102393

Donaldson, L., and Williams, N. (2018). Imaging and spectroscopy of natural fluorophores in pine needles. *Plants*. 7, 10. doi: 10.3390/plants7010010

Fahn, A. (1990). *Plant Anatomy*. Oxford: Pergamon Press.

Farahmand, H. (2020). The genus *Cupressus* L. mythology to biotechnology with emphasis on mediterranean cypress (*Cupressus sempervirens* L.). *Hortic. Rev. (Am. Soc. Hortic. Sci.)* 47, 213–287. doi: 10.1002/9781119625407.ch5

Franceschi, V. R., Krokene, P., Krekling, T., and Christiansen, E. (2000). Phloem parenchyma cells are involved in local and distant defense responses to fungal inoculation or bark-beetle attack in Norway spruce (Pinaceae). *Am. J. Bot*. 87, 314–326. doi: 10.2307/2656627

Fujii, T., Osumi, K., and Kubono, T. (2018). Resin canals in "hiwada," bark of hinoki (Chamaecyparis obtusa) as roofing material. *Bull. Forest. Prod. Res. Instit.* 17, 305–316.

Giuliani, C., Pieraccini, G., Santilli, C., Tani, C., Bottoni, M., Schiff, S., et al. (2020). Anatomical investigation and GC-MS analysis of "Coco de Mer", Lodoicea maldivica (JF Gmel.) Pers. (Arecaceae). *Chem. Biodivers*. 17, e2000707. doi: 10.1002/cbdv.202000707

Graniti, A. (1998). Cypress canker: a pandemic in progress. *Annu. Rev. Phytopathol*. 36, 91–114. doi: 10.1146/annurev.phyto.36.1.91

Grundhöfer, P., Niemetz, R., Schilling, G., and Gross, G. G. (2001). Biosynthesis and subcellular distribution of hydrolyzable tannins. *Phytochemistry* 57, 915–927. doi: 10.1016/S0031-9422(01)00099-1

Hudgins, J. W., and Franceschi, V. R. (2004). Methyl jasmonate-induced ethylene production is responsible for conifer phloem defense responses and reprogramming of stem cambial zone for traumatic resin duct formation. *Plant Physiol.* 135, 2134–2149. doi: 10.1104/pp.103.037929

Krekling, T., Franceschi, V. R., Berryman, A. A., and Christiansen, E. (2000). The structure and development of polyphenolic parenchyma cells in Norway spruce (*Picea abies*) bark. *Flora* 195, 354–369 doi: 10.1016/S0367-2530(17)30994-5

Krekling, T., Franceschi, V. R., Krokene, P., and Solheim, H. (2004). Differential anatomical response of Norway spruce stem tissues to sterile and fungus infected inoculations. *Trees (Berl.)* 18, 1–9. doi: 10.1007/s00468-003-0266-y

Krokene, P., Nagy, N. E., and Krekling, T. (2008a). "Traumatic resin ducts and polyphenolic parenchyma cells in conifers", in *Induced Plant Resistance to Herbivory*, ed. A. Schaller (Dordrecht: Springer), 147–169.

Krokene, P., Nagy, N. E., and Solheim, H. (2008b). Methyl jasmonate and oxalic acid treatment of Norway spruce: anatomically based defense responses and increased resistance against fungal infection. *Tree Physiol*. 28, 29–35. doi: 10.1093/treephys/28.1.29

Kusumoto, D., and Suzuki, K. (2003). Spatial distribution and time course of polyphenol accumulation as a defense response induced by wounding in the phloem of Chamaecyparis obtusa. *New Phytol.* 159, 167–173. doi: 10.1046/j.1469-8137.2003.00775.x

Li, N., Dong, Y., Lv, M., Qian, L., Sun, X., Liu, L., et al. (2021). Combined analysis of volatile terpenoid metabolism and transcriptome reveals transcription factors related to terpene synthase in two cultivars of Dendrobium officinale flowers. *Front. Genet.* 12, 661296. doi: 10.3389/fgene.2021.661296

Lison, L. (1960). *Histochimie et cytochimie animales, Vol I*. Paris: Gauthier-Villars.

Luchi, N., Ma, R., Capretti, P., and Bonello, P. (2005). Systemic induction of traumatic resin ducts and resin flow in Austrian pine by wounding and inoculation with Sphaeropsis sapinea and Diplodia scrobiculata. *Planta* 221, 75–84. doi: 10.1007/s00425-004-1414-3

Madar, Z., Gottlieb, H. E., Cojocaru, M., Riov, J., Solel, Z., and Sztejnberg, A. (1995). Antifungal terpenoids produced by cypress after infection by *Diplodia pinea* f. sp. cupressi. *Phytochemistry* 38, 351–354. doi: 10.1016/0031-9422(94)00575-E

Madar, Z., and Liphschitz, N. (1989). Historical studies of Cupressus sempervirens L. affected by *Diplodia pinea* f.sp. *cupressi* and *Seiridium cardinale*. *IAWA J.* 10, 183–192.

Mehrshahi, P., Stefano, G., Andaloro, J. M., Brandizzi, F., Froehlich, J. E., and DellaPenna, D. (2013). Transorganellar complementation redefines the biochemical continuity of endoplasmic reticulum and chloroplasts. *Proc. Nat. Ac. Sci*. 110, 12126–12131. doi: 10.1073/pnas.1306331110

Moriondo, F. (1972). Cancro del cipresso da Coryneum cardinale Wag. I. La progressione del processo infettivo nei tessuti caulinari. *Accad. Ital. Sci. Forest*. XXI, 399–426.

Mosti, S., Ross Friedman, C., Pacini, E., Brighigna, L., and Papini, A. (2013). Nectary ultrastructure and secretory modes in three species of *Tillandsia* L. (Bromeliaceae) that have different pollinators. *Botany*. 91, 786–798. doi: 10.1139/cjb-2013-0126

Mutto, S., and Panconesi, A. (1987). Ultrastructural modifications in *Cupressus sempervirens* tissues invaded by *Seiridium cardinale*. *Eur. J. For. Pathol.* 17, 193–204. doi: 10.1111/j.1439-0329.1987.tb01016.x

Nagy, N. E., Franceschi, V. R., Solheim, H., Krekling, T., and Christiansen, E. (2000). Wound-induced traumatic resin duct development in stems of Norway spruce (Pinaceae): anatomy and cytochemical traits. *Am. J. Bot*. 87, 302–313. doi: 10.2307/2656626

Panconesi, A., and Raddi, P. (1990). Agrimed n. 1 e Bolgheri: due nuove selezioni resistenti al cancro. *Cellulosa e carta*. 42, 47–52.

Papini, A., Mosti, S., and Van Doorn, W. G. (2014). Classical macroautophagy in *Lobivia rauschii* (Cactaceae) and possible plastidial autophagy in *Tillandsia albida* (Bromeliaceae) tapetum cells. *Protoplasma* 251, 719–725. doi: 10.1007/s00709-013-0567-y

Phillips, M. A., and Croteau, R. B. (1999). Resin-based defenses in conifers. *Trends Plant Sci*. 4, 184–190. doi: 10.1016/S1360-1385(99)01401-6

Ponchet, J., and Andreoli, C. (1990). "Compartmentalization and reaction in the host", in: *Progress in EEC Research on Cypress Diseases. Results of the Agrimed Project (1980–88)*, ed J. Ponchet (Luxembourg: Commission of the European Communities EUR 12493), 96–111.

Raddi, P., and Panconesi, A. (1981). Cypress canker disease in Italy: biology, control possibilities and genetic improvement for resistance. *Eur. J. Forest Pathol*. 11, 340–347. doi: 10.1111/j.1439-0329.1981.tb00104.x

Ribeiro, V. C., and Leitão, C. A. E. (2020). Utilisation of Toluidine blue O pH 4.0 and histochemical inferences in plant sections obtained by free-hand. *Protoplasma* 257, 993–1008. doi: 10.1007/s00709-019-01473-0

Spanos, K. A., Pirrie, A., Woodward, S., and Xenopoulos, S. (1999). Responses in the bark of *Cupressus sempervirens* clones artificially inoculated with *Seiridium cardinale* under field conditions. *Eur. J. For. Pathol*. 29, 135–142. doi: 10.1046/j.1439-0329.1999.00136.x

Spurr, A. R. (1969). A low-viscosity epoxy resin embedding medium for electron microscopy. *J. Ultrastruct. Res*. 26, 31–43. doi: 10.1016/S0022-5320(69)90033-1

Suto, Y. (1998). Traumatic resin-canal formation caused by inoculation with Cistella japonica in secondary phloem of Chamaecyparis obtusa. *J. For. Res*. 3, 99–102. doi: 10.1007/BF02760309

Trapp, S., and Croteau, R. (2001). Defensive resin biosynthesis in conifers. *Annu. Rev. Plant Biol*. 52, 689–724. doi: 10.1146/annurev.arplant.52.1.689

Van Wijk, K. J., and Kessler, F. (2017). Plastoglobuli: plastid microcompartments with integrated functions in metabolism, plastid developmental transitions, and environmental adaptation. *Annu. Rev. Plant Biol.* 68, 253–289. doi: 10.1146/annurev-arplant-043015-111737

Wagener, W. W. (1928). Coryneum canker of Cypress. *Science* 67, 584. doi: 10.1126/science.67.1745.584.a

Wagener, W. W. (1939). The canker of Cupressus induced by *Corineum cardinale*. sp. *J. Agric. Res.* 58, 1–46.

Xenopoulos, S., Andréoli, C., Panconesi, A., Pinto Ganhao, J., and Tuset, J. (1990). "Importance of cypress," in: *Progress in EEC Research on Cypress Diseases. Results of the Agrimed Project (1980–88)*, ed J. Ponchet (Luxembourg: Commission of the European Communities EUR 12493), 1–13.

Yamanaka, K. (1989). Formation of traumatic phloem resin canals in Chamaecyparis obtuse. *IAWA J.* 10, 384–394.

Yao, N., Eisfelder, B. J., Marvin, J., and Greenberg, J. T. (2004). The mitochondrion - an organelle commonly involved in programmed cell death in *Arabidopsis thaliana*. *Plant J.* 40, 596–610. doi: 10.1111/j.1365-313X.2004.02239.x

Zulak, K. G., and Bohlmann, J. (2010). Terpenoid biosynthesis and specialized vascular cells of conifer defense. *J. Integr. Plant Biol.* 52, 86–97. doi: 10.1111/j.1744-7909.2010.00910.x

Conflict of Interest: The authors declare that the research was conducted in the absence of any commercial or financial relationships that could be construed as a potential conflict of interest.

Publisher's Note: All claims expressed in this article are solely those of the authors and do not necessarily represent those of their affiliated organizations, or those of the publisher, the editors and the reviewers. Any product that may be evaluated in this article, or claim that may be made by its manufacturer, is not guaranteed or endorsed by the publisher.

Advantages of publishing in Frontiers

OPEN ACCESS
Articles are free to read for greatest visibility and readership

FAST PUBLICATION
Around 90 days from submission to decision

HIGH QUALITY PEER-REVIEW
Rigorous, collaborative, and constructive peer-review

TRANSPARENT PEER-REVIEW
Editors and reviewers acknowledged by name on published articles

Frontiers
Avenue du Tribunal-Fédéral 34
1005 Lausanne | Switzerland

Visit us: www.frontiersin.org
Contact us: frontiersin.org/about/contact

REPRODUCIBILITY OF RESEARCH
Support open data and methods to enhance research reproducibility

DIGITAL PUBLISHING
Articles designed for optimal readership across devices

FOLLOW US
@frontiersin

IMPACT METRICS
Advanced article metrics track visibility across digital media

EXTENSIVE PROMOTION
Marketing and promotion of impactful research

LOOP RESEARCH NETWORK
Our network increases your article's readership